

Pertanika Journal of
**SCIENCE &
TECHNOLOGY**

JST

VOL. 30 (3) JUL. 2022



PERTANIKA
JOURNALS

A scientific journal published by Universiti Putra Malaysia Press

PERTANIKA JOURNAL OF SCIENCE & TECHNOLOGY

About the Journal

Overview

Pertanika Journal of Science & Technology is an official journal of Universiti Putra Malaysia. It is an open-access online scientific journal. It publishes original scientific outputs. It neither accepts nor commissions third party content.

Recognised internationally as the leading peer-reviewed interdisciplinary journal devoted to the publication of original papers, it serves as a forum for practical approaches to improve quality on issues pertaining to science and engineering and its related fields.

Pertanika Journal of Science & Technology is a **quarterly** (*January, April, July, and October*) periodical that considers for publication original articles as per its scope. The journal publishes in **English** and it is open for submission by authors from all over the world.

The journal is available world-wide.

Aims and scope

Pertanika Journal of Science & Technology aims to provide a forum for high quality research related to science and engineering research. Areas relevant to the scope of the journal include: bioinformatics, bioscience, biotechnology and bio-molecular sciences, chemistry, computer science, ecology, engineering, engineering design, environmental control and management, mathematics and statistics, medicine and health sciences, nanotechnology, physics, safety and emergency management, and related fields of study.

History

Pertanika Journal of Science & Technology was founded in 1993 and focuses on research in science and engineering and its related fields.

Vision

To publish a journal of international repute.

Mission

Our goal is to bring the highest quality research to the widest possible audience.

Quality

We aim for excellence, sustained by a responsible and professional approach to journal publishing. Submissions can expect to receive a decision within 90 days. The elapsed time from submission to publication for the articles averages 180 days. We are working towards decreasing the processing time with the help of our editors and the reviewers.

Abstracting and indexing of Pertanika

Pertanika Journal of Science & Technology is now over 27 years old; this accumulated knowledge and experience has resulted the journal being abstracted and indexed in SCOPUS (Elsevier), Clarivate Web of Science (ESCI), EBSCO, ASEAN CITATION INDEX, Microsoft Academic, Google Scholar, and MyCite.

Citing journal articles

The abbreviation for Pertanika Journal of Science & Technology is *Pertanika J. Sci. & Technol.*

Publication policy

Pertanika policy prohibits an author from submitting the same manuscript for concurrent consideration by two or more publications. It prohibits as well publication of any manuscript that has already been published either in whole or substantial part elsewhere. It also does not permit publication of manuscript that has been published in full in proceedings.

Code of Ethics

The *Pertanika* journals and Universiti Putra Malaysia take seriously the responsibility of all of its journal publications to reflect the highest in publication ethics. Thus, all journals and journal editors are expected to abide by the journal's codes of ethics. Refer to *Pertanika's Code of Ethics* for full details, or visit the journal's web link at http://www.pertanika.upm.edu.my/code_of_ethics.php

Originality

The author must ensure that when a manuscript is submitted to *Pertanika*, the manuscript must be an original work. The author should check the manuscript for any possible plagiarism using any program such as Turn-It-In or any other software before submitting the manuscripts to the *Pertanika* Editorial Office, Journal Division.

All submitted manuscripts must be in the journal's acceptable similarity index range:
≤ 20% – PASS; > 20% – REJECT.

International Standard Serial Number (ISSN)

An ISSN is an 8-digit code used to identify periodicals such as journals of all kinds and on all media—print and electronic.

Pertanika Journal of Science & Technology: e-ISSN 2231-8526 (Online).

Lag time

A decision on acceptance or rejection of a manuscript is reached in 90 days (average). The elapsed time from submission to publication for the articles averages 180 days.

Authorship

Authors are not permitted to add or remove any names from the authorship provided at the time of initial submission without the consent of the journal's Chief Executive Editor.

Manuscript preparation

Most scientific papers are prepared according to a format called IMRAD. The term represents the first letters of the words *Introduction, Materials and Methods, Results, And Discussion*. IMRAD is simply a more 'defined' version of the "IBC" (*Introduction, Body, Conclusion*) format used for all academic writing. IMRAD indicates a pattern or format rather than a complete list of headings or components of research papers; the missing parts of a paper are: *Title, Authors, Keywords, Abstract, Conclusions, References, and Acknowledgement*. Additionally, some papers include *Appendices*.

The *Introduction* explains the scope and objective of the study in the light of current knowledge on the subject; the *Materials and Methods* describes how the study was conducted; the *Results* section reports what was found in the study; and the *Discussion* section explains meaning and significance of the results and provides suggestions for future directions of research. The manuscript must be prepared according to the journal's **Instruction to Authors** (http://www.pertanika.upm.edu.my/Resources/regular_issues/Regular_Issues_Instructions_to_Authors.pdf).

Editorial process

Authors who complete any submission are notified with an acknowledgement containing a manuscript ID on receipt of a manuscript, and upon the editorial decision regarding publication.

Pertanika follows a **double-blind peer-review** process. Manuscripts deemed suitable for publication are sent to reviewers. Authors are encouraged to suggest names of at least 3 potential reviewers at the time of submission of their manuscripts to *Pertanika*, but the editors will make the final selection and are not, however, bound by these suggestions.

Notification of the editorial decision is usually provided within 90 days from the receipt of manuscript. Publication of solicited manuscripts is not guaranteed. In most cases, manuscripts are accepted conditionally, pending an author's revision of the material.

As articles are double-blind reviewed, material that may identify authorship of the paper should be placed only on page 2 as described in the first-4-page format in *Pertanika*'s **Instruction to Authors** (http://www.pertanika.upm.edu.my/Resources/regular_issues/Regular_Issues_Instructions_to_Authors.pdf).

The journal's peer review

In the peer-review process, 2 to 3 referees independently evaluate the scientific quality of the submitted manuscripts. At least 2 referee reports are required to help make a decision.

Peer reviewers are experts chosen by journal editors to provide written assessment of the **strengths** and **weaknesses** of written research, with the aim of improving the reporting of research and identifying the most appropriate and highest quality material for the journal.

Operating and review process

What happens to a manuscript once it is submitted to *Pertanika*? Typically, there are 7 steps to the editorial review process:

1. The journal's Chief Executive Editor and the Editor-in-Chief examine the paper to determine whether it is relevance to journal needs in terms of novelty, impact, design, procedure, language as well as presentation and allow it to proceed to the reviewing process. If not appropriate, the manuscript is rejected outright and the author is informed.
2. The Chief Executive Editor sends the article-identifying information having been removed, to 2 to 3 reviewers. They are specialists in the subject matter of the article. The Chief Executive Editor requests that they complete the review within 3 weeks.

Comments to authors are about the appropriateness and adequacy of the theoretical or conceptual framework, literature review, method, results and discussion, and conclusions. Reviewers often include suggestions for strengthening of the manuscript. Comments to the editor are in the nature of the significance of the work and its potential contribution to the research field.

3. The Editor-in-Chief examines the review reports and decides whether to accept or reject the manuscript, invite the authors to revise and resubmit the manuscript, or seek additional review reports. In rare instances, the manuscript is accepted with almost no revision. Almost without exception, reviewers' comments (to the authors) are forwarded to the authors. If a revision is indicated, the editor provides guidelines for attending to the reviewers' suggestions and perhaps additional advice about revising the manuscript.
4. The authors decide whether and how to address the reviewers' comments and criticisms and the editor's concerns. The authors return a revised version of the paper to the Chief Executive Editor along with specific information describing how they have addressed' the concerns of the reviewers and the editor, usually in a tabular form. The authors may also submit a rebuttal if there is a need especially when the authors disagree with certain comments provided by reviewers.
5. The Chief Executive Editor sends the revised manuscript out for re-review. Typically, at least 1 of the original reviewers will be asked to examine the article.
6. When the reviewers have completed their work, the Editor-in-Chief examines their comments and decides whether the manuscript is ready to be published, needs another round of revisions, or should be rejected. If the decision is to accept, the Chief Executive Editor is notified.
7. The Chief Executive Editor reserves the final right to accept or reject any material for publication, if the processing of a particular manuscript is deemed not to be in compliance with the S.O.P. of *Pertanika*. An acceptance letter is sent to all the authors.

The editorial office ensures that the manuscript adheres to the correct style (in-text citations, the reference list, and tables are typical areas of concern, clarity, and grammar). The authors are asked to respond to any minor queries by the editorial office. Following these corrections, page proofs are mailed to the corresponding authors for their final approval. At this point, **only essential changes are accepted**. Finally, the manuscript appears in the pages of the journal and is posted on-line.

Pertanika Journal of

**SCIENCE
& TECHNOLOGY**

Vol. 30 (3) Jul. 2022



A scientific journal published by Universiti Putra Malaysia Press



EDITOR-IN-CHIEF

Luqman Chuah Abdullah
Chemical Engineering

CHIEF EXECUTIVE EDITOR

UNIVERSITY PUBLICATIONS COMMITTEE

CHAIRMAN

Nazamid Saari

EDITORIAL STAFF

Journal Officers:

Kanagamaral Silvarajoo, *ScholarOne*
Siti Zuhaila Abd Wahid, *ScholarOne*
Tee Syn Ying, *ScholarOne*
Umni Fairuz Hanapi, *ScholarOne*

Editorial Assistants:

Ku Ida Mastura Ku Baharom
Siti Juridah Mat Arip
Zulinaardawati Kamarudin

English Editor:

Norhanisah Ismail

PRODUCTION STAFF

Pre-press Officers:

Nur Farrah Dila Ismail
Wong Lih Jiun

WEBMASTER

IT Officer:

Illi Najwa Mohamad Sakri

EDITORIAL OFFICE

JOURNAL DIVISION

Putra Science Park
1st Floor, IDEA Tower II
UPM-MTDC Technology Centre
Universiti Putra Malaysia
43400 Serdang, Selangor Malaysia.

Gen Enquiry

Tel. No: +603 9769 1622 | 1616

E-mail:

executive_editor.pertanika@upm.edu.my

URL: www.journals-jd.upm.edu.my

PUBLISHER

UPM Press

Universiti Putra Malaysia
43400 UPM, Serdang, Selangor, Malaysia.

Tel: +603 9769 8851

E-mail: penerbit@putra.upm.edu.my

URL: <http://penerbit.upm.edu.my>



ASSOCIATE EDITOR

2021-2023

Adem Kilicman

Mathematical Sciences
Universiti Putra Malaysia, Malaysia

Miss Laiha Mat Kiah

Security Services Sn: Digital Forensic, Steganography, Network Security, Information Security, Communication Protocols, Security Protocols
Universiti Malaya, Malaysia

Saidur Rahman

Renewable Energy, Nanofluids, Energy Efficiency, Heat Transfer, Energy Policy
Sunway University, Malaysia

EDITORIAL BOARD

2020-2022

Abdul Latif Ahmad

Chemical Engineering
Universiti Sains Malaysia, Malaysia

Hsiu-Po Kuo

Chemical Engineering
National Taiwan University, Taiwan

Mohd. Ali Hassan

Bioprocess Engineering, Environmental Biotechnology
Universiti Putra Malaysia, Malaysia

Ahmad Zaharin Aris

Hydrochemistry, Environmental Chemistry, Environmental Forensics, Heavy Metals
Universiti Putra Malaysia, Malaysia

Ivan D. Rukhlenko

Nonlinear Optics, Silicon Photonics, Plasmonics and Nanotechnology
The University of Sydney, Australia

Najafpour Darzi Ghasem

Bioprocess Technology, Chemical Engineering, Water and Wastewater Treatment Technology, Biochemical Engineering and Biotechnology, Bioethanol, Biofuel, Biohydrogen, Enzyme and Fermentation Technology
Babol Noshirvani University of Technology, Iran

Azlina Harun@Kamaruddin

Enzyme Technology, Fermentation Technology
Universiti Sains Malaysia, Malaysia

Lee Keat Teong

Energy Environment, Reaction Engineering, Waste Utilization, Renewable Energy
Universiti Sains Malaysia, Malaysia

Bassim H. Hameed

Chemical Engineering: Reaction Engineering, Environmental Catalysis & Adsorption
Qatar University, Qatar

Mohamed Othman

Communication Technology and Network, Scientific Computing
Universiti Putra Malaysia, Malaysia

Nor Azah Yusof

Biosensors, Chemical Sensor, Functional Material
Universiti Putra Malaysia, Malaysia

Biswajeet Pradhan

Digital image processing, Geographical Information System (GIS), Remote Sensing
University of Technology Sydney, Australia

Mohd Sapuan Salit

Concurrent Engineering and Composite Materials
Universiti Putra Malaysia, Malaysia

Norbahiah Misran

Communication Engineering
Universiti Kebangsaan Malaysia, Malaysia

Daud Ahmad Israf Ali

Cell Biology, Biochemical, Pharmacology
Universiti Putra Malaysia, Malaysia

Mohd Shukry Abdul Majid

Polymer Composites, Composite Pipes, Natural Fibre Composites, Biodegradable Composites, Bio-Composites
Universiti Malaysia Perlis, Malaysia

Roslan Abd-Shukur

Physics & Materials Physics, Superconducting Materials
Universiti Kebangsaan Malaysia, Malaysia

Hari M. Srivastava

Mathematics and Statistics
University of Victoria, Canada

Mohd Zulkifly Abdullah

Fluid Mechanics, Heat Transfer, Computational Fluid Dynamics (CFD)
Universiti Sains Malaysia, Malaysia

Wing Keong Ng

Aquaculture, Aquatic Animal Nutrition, Aqua Feed Technology
Universiti Sains Malaysia, Malaysia

INTERNATIONAL ADVISORY BOARD

2021-2024

CHUNG, Neal Tai-Shung

Polymer Science, Composite and Materials Science
National University of Singapore, Singapore

Mohamed Pourkashanian

Mechanical Engineering, Energy, CFD and Combustion Processes
Sheffield University, United Kingdom

Yulong Ding

Particle Science & Thermal Engineering
University of Birmingham, United Kingdom

Hiroshi Uyama

Polymer Chemistry, Organic Compounds, Coating, Chemical Engineering
Osaka University, Japan

Mohini Sain

Material Science, Biocomposites, Biomaterials
University of Toronto, Canada

ABSTRACTING AND INDEXING OF PERTANIKA JOURNALS

The journal is indexed in SCOPUS (Elsevier), Clarivate-Emerging Sources Citation Index (ESCI), BIOSIS, National Agricultural Science (NAL), Google Scholar, MyCite, ISC. In addition, Pertanika JSSH is recipient of "CREAM" Award conferred by Ministry of Higher Education (MoHE), Malaysia.



Pertanika Journal of Science & Technology
Vol. 30 (3) Jul. 2022

Contents

Foreword <i>Chief Executive Editor</i>	i
Modeling and Molecular Dynamics of Aquaporin from an Antarctic <i>Pseudomonas</i> sp. Strain AMS3 <i>Muhairil Sulong Tuah, Wahhida Latip, Ainur Yasmin Ahmad Ridzwan, Samyuktha Balakrishnan, Raja Noor Zaliha Raja Abd. Rahman, Noor Dina Muhd Noor and Mohd Shukuri Mohamad Ali</i>	1755
Mathematical Models for Predicting the Mechanical Properties of Poly(Lactic Acid) for Load-Bearing Applications <i>Abraham Aworinde, Titus Ajewole, Olakunle Olukayode and Joseph Dirisu</i>	1771
Assessment of the Grid Safety Values for Substation Grounding Grid Design Parameters in Vertical Two-Layer Soil Structure <i>Navinesshani Permal, Miszaina Osman, Azrul Mohd Ariffin and Mohd Zainal Abidin Ab Kadir</i>	1789
<i>Review Article</i> External Skeletal Fixator to Stabilize the Orthopedic Conditions in Avian Species: A Systematic Review of Case Reports and Case Series <i>Hossein Taiyari and Jalila Abu</i>	1815
Spectral Gradient Method with Log-determinant Norm for Solving Non- Linear System of Equations <i>Yeong Lin Koay, Hong Seng Sim, Yong Kheng Goh and Sing Yee Chua</i>	1841
Esterification of Acetin Production from By-Products of Biodiesel Industry Using Heterogeneous Catalysts Based on Wetland Commodities <i>Hesty Heryani, Abdul Ghofur and Nursiah Chairunnisa</i>	1861
DFT-Based Reversible Watermarking Method for Image Ownership Protection <i>Ansam Osamah Abdulmajeed and Sundus Abdulmuttalib Mohamed</i>	1883
Vulnerability of Saudi Private Sector Organisations to Cyber Threats and Methods to Reduce the Vulnerability <i>Emad Shafie</i>	1909

Experimental Investigations on Scour Volume Upstream of a Slit Weir <i>Naeem Zaer Nkad, Thamer Ahmad Mohammad and Haider Mohammed Hammoodi</i>	1927
Removal of Remazol Yellow Using SnO ₂ -Co Photocatalyst <i>Muhammad Said, Fahma Riyanti, Poedji Loekitowati Hariani, Sastriani and Widya Twiny Rizki</i>	1949
<i>Review Article</i>	
The Compilation Records of Fireflies (Coleoptera: Lampyridae) Diversity and Distribution and Display Trees Throughout Malaysia <i>Nurhafizul Abu Seri and Azimah Abd Rahman</i>	1963
<i>Review Article</i>	
Trends of Filtration and Adsorption Technology Using Biomaterials from Agricultural Wastes: A Bibliometric Analysis <i>Awang Nasrizal Awang Ali, Jason Lowell Jitolis, Juferi Idris, Ismail Saad and Nurmin Bolong</i>	1989
Validity and Reliability of Typhoid Risk Factors Questionnaire (TRFQ) in Gombe Metropolis, Gombe State, Nigeria <i>Umar Abdullahi Tawfiq, Shamarina Shohaimi, Noor Hisham Mohd Nadzir, Syafinaz Amin Nordin, Abdul Hafiz Ab Rahman and Nader Salari</i>	2007
Leaching of Electric Arc Furnace Slag for Selective Recovery of Iron: Effect of Temperature, H ₂ SO ₄ /HCl Acid, and Oxidant Concentration <i>Faizatul Syazwani Zulkifili, Hawaiah Imam Maarof, Norhaslinda Nasuha and Siti Wahidah Puasa</i>	2023
A Hybrid Technique for Analysis of Low-Frequency Oscillation in Power System <i>Abhinav Pathak and Ratnesh Gupta</i>	2033
<i>Review Article</i>	
Mechanical Properties of Natural Fibre Reinforced Geopolymer Composites: A Review <i>Noor Abbas Al-Ghazali, Farah Nora Aznieta Abdul Aziz, Khalina Abdan and Noor Azline Mohd Nasir</i>	2053
<i>Case Study</i>	
An Unusual Cause of Tenosynovitis by Group B <i>Streptococcus</i> in the Immunocompromised Patient: A Case Report <i>AbdulRahman Muthanna, Nur Afiza Aziz, Mohd Nasir Mohd Desa, Nurul Diana Dzaraly, Nurul Hana Zainal Baharin, Mohammad Noor Amal Azmai and Syafinaz Amin-Nordin</i>	2071

Thermal Performances of Hybrid Pin Fin with Connector Heat Sink Under Natural Convection <i>Rosnadiyah Bahsan, Muhammad Aniq Asyraf Mohd Zamri, Alhassan Salami Tijani, Jeeventh Kubenthiran, Sajith Thottathil Abdulrahman and Ibrahim Kolawole Muritala</i>	2077
Evaluation of Factors Affecting Microbial Growth Inhibition and Optimization Using Pineapple Leaves Juice <i>Norazwina Zainol, Amirah Ya'acob, Putri Nurul Yasmin Mohd Ridza, Siti Hatijah Mortan and Kamaliah Abdul Samad</i>	2097
<i>Short Communication</i> Canarium odontophyllum Miq. (Dabai) Leaf Phytoextracts and Their Medicinal Properties <i>Muhammad Wahizul Haswan Abdul Aziz, Siti Fathiah Masre, Dayang Fredalina Basri and Ahmad Rohi Ghazali</i>	2115
Synthesis, Characterisation, and Electrochemical Impedance Spectroscopy Study of Green and Sustainable Polyurethane Acrylate from Jatropha Oil Using a Three Step Process <i>Kai Ling Chai, Min Min Aung, Hong Ngee Lim, Ikhwan Syafiq Mohd Noor, Luqman Chuah Abdullah and Hiroshi Uyama</i>	2127
<i>Review Article</i> A Review on Soil Erodibility Studies in Malaysia <i>Adnan Derahman, Mohd Fairuz Bachok, Muhamad Fuad Shukor, Farah Wahida Mohd Latib and Rohaya Alias</i>	2139
<i>Review Article</i> Classification of Fault Prediction: A Mapping Study <i>Sasha Farhana Shamsul Anwar, Marshima Mohd Rosli and Nur Atiqah Sia Abdullah</i>	2157
Effect of Khat Chewing on Gingival Health of Patients with Fixed Orthodontic Appliances: A Controlled-Clinical Trial <i>Ahmed Taher Al-Haj, Rami Ishaq, Anas Shamala, Mohammed Al-Wesabi, Khalid Aldhorae, Mohammed Sultan Alakhali and Mohammed Al-Labani</i>	2173
Statistical Analysis of Dry Grinding of Mica in Planetary Mill <i>Ku Esyra Hani Ku Ishak, Shafinaz Saad, Syed Fuad Saiyid Hashim and Hashim Hussin</i>	2191
Water Quality Assessment of Surface Water at the Urban Area of An Giang Province, Vietnam <i>Khanh Tran Thien Nguyen, Chi Thi Dao Vo, An Thuy Ngo, Nghi Thanh Doan, Luyen Phuc Huynh and Dung Huynh Thuy Tran</i>	2205

- The Effectiveness of Workplace Health Promotion Programme in Improving
Sickness Absenteeism, Medical Cost Claims and Work Engagement
Among Manufacturing Workers in Malaysia: A Randomised Control Trial
*Ahmad Fairuz Mohamed, Marzuki Isahak, Mohd Zaki Awg Isa and
Rusli Nordin* 2225
- Facies Mapping of the Holocene Carbonate Complexes in Kepulauan
Seribu Java Basin, Indonesia Using Satellite-Derived Data Set
*Shafiqah Amir, Haylay Tsegab, Grisel Jimenez Soto and
Ali Imran Azman* 2253
- Hybrid Lean Practices Integrated with IR 4.0 and Sustainability in Malaysia
Food and Beverages Companies: Conceptual Framework and Hypothesis
Development
Muslim Diekola Akanmu and Norshahrizan Nordin 2271
- Importance of Transfer of Technology Skills and Human Resource
Development Skills in Work Performance of Extension Agent in Sarawak
Cocoa Industry
Nur Syahirah Abd Halim, Salim Hassan and Ramle Kasin 2295

Foreword

Welcome to the third issue of 2022 for the *Pertanika Journal of Science and Technology (PJST)*!

PJST is an open-access journal for studies in Science and Technology published by Universiti Putra Malaysia Press. It is independently owned and managed by the university for the benefit of the world-wide science community.

This issue contains 30 articles; six review articles, a short communication, a case study and the rest are regular articles. The authors of these articles come from different countries namely India, Indonesia, Iran, Iraq, Malaysia, Nigeria, Saudi Arabia and Vietnam.

Another article that we wish to highlight is “The compilation records of fireflies (Coleoptera: Lampyridae) diversity and distribution and display trees throughout Malaysia” by Nurhafizul Abu Seri and Azimah Abd Rahman from Universiti Sains Malaysia. It indicates that firefly species, especially from the genera *Pteroptyx* (*Pteroptyx tener* species), are widely distributed in Peninsular Malaysia and East Malaysia. Fireflies undergo a complete metamorphosis with four phases in their life cycle: egg, larva, pupa, and adult, all highly dependent on mangrove plants. Based on the records from the study conducted by previous researchers, it was found that the population of fireflies is declining in some areas in Malaysia, and so are their habitats and host/display trees that have suffered the same decline. Detailed information on this study is presented on page 1963.

A review article titled “Soil erodibility studies in Malaysia” was written by Adnan Derahman and co-researchers from Universiti Teknologi MARA, Malaysia. Their review mentioned two widely used soil erodibility approaches in Malaysia, mainly to assess the impacts of soil erosion on washed and transported sediments in water bodies and landslide occurrence in slope areas. The methods are USLE and ROM scale. Both methods had advantages and disadvantages depending on the site’s data availability application. Determination of soil erodibility will lead to soil erosion assessment, whereby this input significantly is one of the key factors in local authorities’ decision-making in determining the safety, impact, and mitigation of any physical development in an area. However, the conventional method of determining soil erodibility involves complicated laboratory work. The analysis would be an obstacle to the holistic assessment of soil erosion, especially for erosion-induced landslide risk. Thus, new approaches are needed which practicality in terms of less artistry, time and cost, and simplicity in analysis so that more soil erodibility for soil samples could be determined. Detailed information on this study can be found on page 2139.

Muslim Diekola Akanmu and Norshahrizan Nordin from Universiti Malaysia Perlis had evaluated the hybrid lean practices integrated with IR 4.0 and sustainability in Malaysia food and beverages companies. This study aims to confirm the future direction of the food industry that is recently employing new technologies in its manufacturing systems. This study is underpinned by the theories of contingency and practice-based view by highlighting the contributions of operations management practices to implement successful strategies in enhancing sustainability performance in food and beverages companies through performance variations. Also, the study provides implications and future direction for industry consultants, practitioners, and academicians. Further details of the article are available on page 2271.

We anticipate that you will find the evidence presented in this issue to be intriguing, thought-provoking and useful in reaching new milestones in your own research. Please recommend the journal to your colleagues and students to make this endeavour meaningful.

All the papers published in this edition underwent Pertanika's stringent peer-review process involving a minimum of two reviewers comprising internal as well as external referees. This was to ensure that the quality of the papers justified the high ranking of the journal, which is renowned as a heavily-cited journal not only by authors and researchers in Malaysia but by those in other countries around the world as well.

We would also like to express our gratitude to all the contributors, namely the authors, reviewers, Editor-in-Chief and Editorial Board Members of PJST, who have made this issue possible.

PJST is currently accepting manuscripts for upcoming issues based on original qualitative or quantitative research that opens new areas of inquiry and investigation.

Chief Executive Editor

executive_editor.pertanika@upm.edu.my

Modeling and Molecular Dynamics of Aquaporin from an Antarctic *Pseudomonas* sp. Strain AMS3

Muhairil Sulong Tuah^{1,2}, Wahhida Latip^{1,2}, Ainur Yasmin Ahmad Ridzwan^{1,2}, Samyuktha Balakrishnan^{1,2}, Raja Noor Zaliha Raja Abd. Rahman¹, Noor Dina Muhd Noor^{1,2} and Mohd Shukuri Mohamad Ali^{1,2*}

¹Enzyme and Microbial Technology Research Centre, Faculty of Biotechnology and Biomolecular Sciences, Universiti Putra Malaysia, 43400 UPM, Serdang, Selangor, Malaysia

²Department of Biochemistry, Faculty of Biotechnology and Biomolecular Sciences, Universiti Putra Malaysia, 43400 UPM, Serdang, Selangor, Malaysia

ABSTRACT

Aquaporins, also known as water channels, are a large family of transmembrane channel proteins present throughout all life domains and are implicated in human disorders. The psychrophilic aquaporin comes to attention because of its specialty in adaptive ability to keep on functioning to maintain water homeostasis under low temperatures, which have an optimal temperature for growth at about 15°C or lower. However, studies regarding aquaporin isolated from psychrophilic *Pseudomonas* sp. are still scattered. Recently, the genome sequence of an Antarctic *Pseudomonas* sp. strain AMS3 revealed a gene sequence encoding for a putative aquaporin designated as PAqpZ2_AMS3. In this study, structure analysis and molecular dynamics (MD) simulation of a predicted model of a fully hydrated aquaporin monomer was embedded in a lipid bilayer and was performed at different

temperatures for structural flexibility and stability analysis. The MD simulation results revealed that the predicted structure could remain stable and flexible at low to medium temperatures. In addition, the important position of water gating amino acids, Phe36 and Asn180 residues were rearranged in -5°C MD simulation, leading to changes in the aquaporin water column size. The information obtained from this psychrophilic aquaporin, PAqpZ2_AMS3, provides new insights into the structural

ARTICLE INFO

Article history:

Received: 08 October 2021

Accepted: 16 December 2021

Published: 20 April 2022

DOI: <https://doi.org/10.47836/pjst.30.3.01>

E-mail addresses:

muhairilst@gmail.com (Muhairil Sulong Tuah)

wahhidalatip@gmail.com (Wahhida Latip)

yasmin97ay@gmail.com (Ainur Yasmin Ahmad Ridzwan)

gs59053@student.upm.edu.my (Samyuktha Balakrishnan)

rnzaliha@upm.edu.my (Raja Noor Zaliha Raja Abd. Rahman)

dina@upm.edu.my (Noor Dina Muhd Noor)

mshukuri@upm.edu.my (Mohd Shukuri Mohamad Ali)

* Corresponding author

adaptation of this protein at low temperatures and could be a useful tool for low-temperature industrial applications and molecular engineering purposes in the future.

Keywords: Antarctica, aquaporin, homology modeling, molecular dynamics, *Pseudomonas* sp. AMS3, water gating

INTRODUCTION

Aquaporin is known as one of the integral membrane channel proteins which belong to the major intrinsic protein (MIP) family responsible for maintaining water homeostasis in a cell by facilitating the water movement across the cell membranes. These channels are highly selective with passively transporting water and other small polar molecules. Previously reported research on aquaporin revealed that the protein structures consist of the conserved structural fold with six transmembrane helices and five loops with a single narrow pore at the center of the structure (Gomes et al., 2009). Aquaporin signature Asparagine-Proline-Alanine (NPA) motif constitutes the center of the channel. Other than that, facing the extracellular side of the protein also contain a conserved constriction region of aromatic/Arginine (ar/R) motif that acts as the selectivity filter in facilitating the water or other small polar molecules movement across the membrane (Aponte- Santamaría et al., 2017; Brown, 2017; Lind et al., 2017; Araya-Secchi et al., 2011).

Another member of the MIP family, the aquaglyceroporin (Glp), is known to have a less pronounced periplasmic protrusion, where it allows the permeation of glycerol alongside the water molecules. This Glp possesses the same NPA motifs as aquaporin, which serve as the crucial structural domain that plays a role in permeation selectivity. The ar/R constriction site impairs the entrance of high molecular weight substrates, which is around 3.4 Å, compared to only 2.8 Å for the aquaporin. This region is composed of a different set of amino acids that will allow the passage of wider compounds such as glycerol. For example, the smaller Glycine residue in aquaglyceroporin could provide a hydrophobic corner that interacts with bigger molecules (Hub et al., 2009; Gomes et al., 2009).

Useful discovery of the aquaporin gating provided by high-resolution aquaporin structures and molecular dynamics (MD) simulations categorized the mechanisms as capping and pinching (Hedfalk et al., 2006). The regulation of water movement across the aquaporin channel is by either gating, which controls the water flow rate through the channel, or by targeting the aquaporin to different membranes, known as trafficking (Sachdeva & Singh, 2014). As studied by Woo et al. (2008), the phosphorylation of Serine or Threonine residues may or may not involve the membrane trafficking mechanism of aquaporin. Besides that, Németh-Cahalan and Hall (2000) mentioned that changes in pH provide a feedback signal which regulates the aquaporin water permeability. Changes in divalent cation concentrations are also common signals utilized as gating for the aquaporin channel (Kourghi et al., 2017). In addition, Sachdeva and Singh (2014) stated that the

involvement of a single or few residues movement that results in small conformational changes of the aquaporin leads to water flow blockage through the channel.

In a low-temperature environment, unfavorable cell water loss is a critical adaptive mechanism for an organism to prevent osmotic shock and injury or cell death from internal ice formation (Goto et al., 2015). The psychrophilic aquaporin comes to attention because of its specialty in adaptive ability to keep on functioning to maintain water homeostasis under the temperatures. So far, functional studies of aquaporin that have been done were for mesophilic organisms (Aponte-Santamaría et al., 2017; Sachdeva & Singh, 2014), thermophilic microorganisms (Araya-Secchin et al., 2011; Mathai et al., 2009; Kozono et al., 2003) and psychrophilic insect (Goto et al., 2015; Cohen, 2012). The recent completion of a genome project of polar bacteria isolated from Antarctic soil revealed the presence of aquaporin in *Pseudomonas* sp. Strain AMS3. With this available genomic dataset, the structure of the bacterial aquaporin was predicted and studied using appropriate computer-aided software, and (MD) simulation was used to study its functional adaptation at various low temperatures. Molecular dynamics have been considered a powerful and useful computational tool as it provides more information and understanding of the molecular mechanism at a molecular scale, especially for the study of aquaporin (Hospital et al., 2015; Hub et al., 2009).

Antarctic habitat proved that staying dehydrated is important to survive under low temperatures and desiccation stress, where this important water metabolism control is ruled by aquaporin (Goto et al., 2015). Aponte-Santamaría et al. (2017) stated that aquaporin gating might influence the rapid change in water transport activity, and various external stimuli may trigger this gating. Tyr31 acts as aquaporin gating residue from the Aqy1 genome, the water transporting aquaporin in *Pichia pastoris* results in the microorganism death after undergoing multiple freeze/thaw cycles. When comparing the position of the residue at room temperature and low temperature, the simulation data of Aqy1 in a freezing environment shows a movement of about 0.5Å towards the cytoplasm. It leads to changes in the size of the pore water column that results in blockage of the channel. Thus, it can be concluded that temperature changes cause this change.

This paper reported for the first time the homology modeling and molecular dynamics studies of aquaporin from an Antarctic *Pseudomonas* sp. AMS3, to the best of the authors' knowledge. The three-dimensional structures of the putative aquaporin were predicted and evaluated using appropriate software. The structural properties of the putative aquaporin at various temperatures were studied using molecular dynamics (MD) simulations and were discussed. More research is needed to understand the psychrophilic aquaporin, which could contribute to biomimetic membrane approaches for water filtration technologies. As a result, industrial wastewater treatment will particularly benefit the food and beverage and pharmaceutical industries.

METHODOLOGY

Sequence Alignment of PAqpZ2_AMS3

Recently, the genome sequence project of an Antarctic isolate, *Pseudomonas* sp. strain AMS3 was completed by Codon Genomics Sdn Bhd. Genome mining for aquaporin revealed the gene encoding for the putative aquaporin. The identified amino acid sequence designated as PAqpZ2_AMS3, consisting of 231 amino acid residues respectively, was used for the sequence analysis and modeling. First, the aquaporin amino acid sequence was named based on its scaffold position identified in the structural annotation. Then, the homologous sequence was identified using the BLAST program (Donkor et al., 2014; Altschul et al., 1990). Next, multiple sequence alignment was carried out using ClustalW open software with the amino acid sequence from the nearest hit in BLAST result and aquaporin crystal structure sequence isolated from *E. coli*.

Homology Modeling and Validation

SWISS-MODEL homology modeling (Bienert et al., 2017) open software was used to identify the most suitable template and build the 3D model for PAqpZ2_AMS3. The template used for the modeling was the 2.5 Å crystal structure of Aquaporin Z obtained from *Escherichia coli* (strain K12) (PDB ID: 1RC2) (Savage et al., 2003) based on the highest percentage of similarity in BLAST. The structure validation was assessed with ERRAT to compare the six types of non-bonded atom-atom interactions (CC, CN, CO, NN, NO, and OO) of the modeled structures with a reliable high-resolution structure database (Kleywegt, 2000; Colovos & Yeates, 1993) and Ramachandran plot to evaluate the structures' geometrical aspects (Mannige et al., 2016; Zhou et al., 2011).

Software

The molecular dynamics (MD) simulations were performed using the Yet Another Scientific Reality Application (YASARA) software program version 10.2.1 on the predicted aquaporin model structure (Krieger & Vriend, 2014). In addition, AMBER03 (Assisted Model Building with Energy Refinement) force field package was used to conduct the simulation as it includes a set of advanced molecular mechanical force fields for a suite of molecular simulation programs (Salomon-Ferrer et al., 2013).

Molecular Dynamics (MD) Simulations at Various Temperature

This study seeks to investigate membrane simulation of the predicted models at the temperatures of -5°C, 0°C, 5°C, 15°C, and 37°C. A 10 ns of membrane simulation was performed with the first nanosecond considered an equilibration period, and the last 10

ns were used for analysis. AMBER03 force field parameter implemented in the YASARA software was employed for the system's proteins, phospholipids, and water molecules.

The initial model was oriented and embedded in the membrane by the software after it scanned for the secondary structure elements with hydrophobic surface residues of the protein. The simulated system consisted of the PAqpZ2_AMS3 monomer embedded in a fully solvated lipid bilayer of approximately 167 phosphatidylethanolamines (PEA). In addition, the bilayer was fully solvated with 8643 (PAqpZ2_AMS3) clear water and NaCl molecules. Subsequently, the initial model was energy-minimized in each simulation. Before the real simulation, 250 ps of restrained equilibration simulation was run to ensure the adaptability of the new embedded protein in the membrane.

Simulation Analysis

PAqpZ2_AMS3 monomer was studied using 400 saved steps for each simulation. The data obtained were analyzed using YASARA tools as the analysis provides a better understanding of the dynamic properties of the protein-embedded membrane in water at different temperatures. Furthermore, the root mean square deviations of C α (C α -RMSD) were computed to measure the magnitude of each amino acid's conformational change to evaluate each residue's stability and flexibility at different temperatures. Besides, the fluctuation of C α (C α -RMSF) was also computed for each aquaporin monomer per residue to study the trajectories' flexibilities.

Further analysis was performed by calculating and estimating the pore radius for the final simulated aquaporin model structures at different temperatures. The channel geometry was monitored by computing the pore radius profile in the z-direction that fits in the channel space without overlapping the van der Waals surfaces of the surrounding residues using the HOLE 2.0 program software (Brezovsky et al., 2013). In addition, a superimposition image of the aquaporin was generated with UCSF Chimera software to compare distinct residues that were influenced by different temperatures during the simulation period.

RESULTS AND DISCUSSION

Sequence and Structure Comparisons

Sequence Analysis. Gene sequence encoding for a putative aquaporin was identified from an Antarctic *Pseudomonas* sp. strain AMS3 and designated PAqpZ2_AMS3. The sequence analysis using BLAST (Donkor et al., 2014) showed that the protein sequence represented members of classical water aquaporin within the classical aquaporin subfamily named AqpZ. All aquaporin consists of an NPA motif which is similar to PAqpZ2_AMS3. Two sets of NPA motifs were identified in sequence alignment Figure 1 box in red color. This agreement with aquaporin isolated from *Methanothermobacter marburgensis* consists of

two NPA motifs in the protein sequence (Colovos & Yeates, 1993). Moreover, the NPA motif was reported to have a significant role in proton exclusion during water movement through the aquaporin pore (Finn & Cerda, 2015).

To distinguish between AqpZ and Glps is the conserved amino acid residue, the ar/R region (Tong et al., 2019), which functions as a selective filter. The AqpZ ar/R region is F(H/I)XR which are F43, H172, R187, and carbonyl of T181 in PAqpZ2_AMS3 protein marked with a blue arrow in Figure 1. The combination of these four residue side chains located at the construction site of the aquaporin determines the pore size of the water channel protein and the protein structural organization (Lind et al., 2017). Moreover, the BLAST result showed that sequence similarity between identified aquaporin scores is 63% from sequence identity, *E. coli* AqpZ (PDB ID: 1RC2). The percentage similarity of 63% was the highest score in the sequence database and is known to be sufficient to compare and confirm the identified aquaporin, PAqpZ2_AMS3. It is supported by the similarity with the sequences having the same important motifs as highlighted in Figure 1.

Modeling and Validation of Aquaporin Structure. The homology modeling pipeline aims for the modeling template which optimally covers the target sequence length to maximize the expected quality of the models and the coverage of the target (Mathai et al., 2009). This study modeled the predicted structure using a crystal structure of aquaporin from *Escherichia coli* strain K12 (PDB ID: 1RC2) (Savage et al., 2003). It is due to its highest quality selected by the SWISS-MODEL homology modeling server for model building with

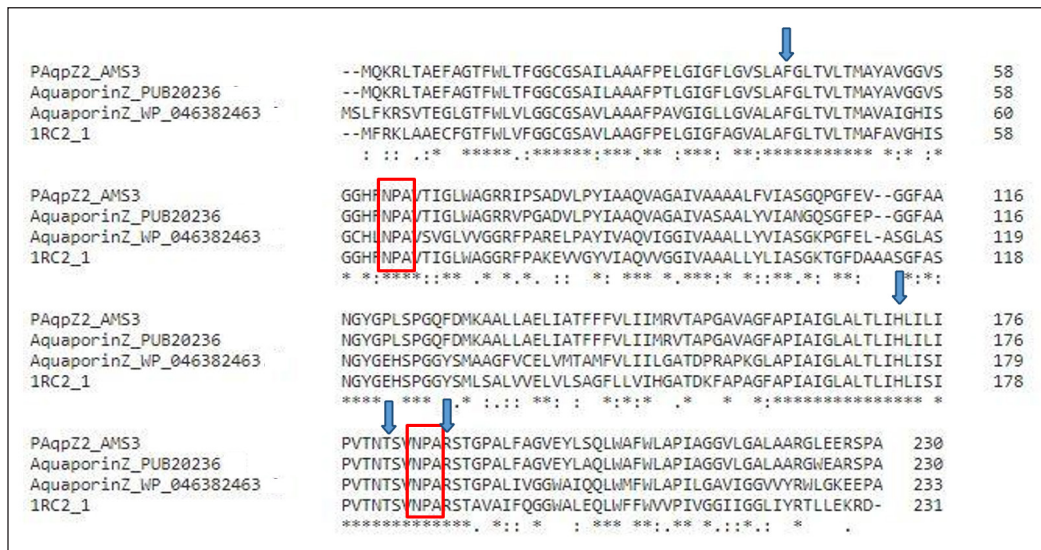


Figure 1. The sequence alignment of both identified putative aquaporins from Antarctic *Pseudomonas sp.* AMS3 (PAqpZ2_AMS3); *Pseudomonas sp.* GV105 (PUB20236); *Pseudomonas sp.* (WP_046382463) and *E. coli* AqpZ (1RC2). The conserved NPA motif regions (red box) and the selectivity filter or ar/R constriction region (blue arrow) are indicated.

a score of 65% for sequence identity of PAqpZ2_AMS3, respectively.

The aquaporin model quality was verified using the Ramachandran plot and ERRAT before MD simulation. It is because to see the reliability of the predicted structure. Figure 2 and Table 1 indicate the score obtained for structure validation of the aquaporin model structure using stated programs. Ramachandran plot provides a way to indicate the quality of a three-dimensional protein structure as it can display the distribution of torsion angles known as Phi (ϕ) and Psi (ψ) angles in a protein structure and an overview of excluded regions that shows which rotation of the polypeptide is not allowed due to the steric hindrance (Zhou et al., 2011). The predicted structure showed a high-quality model where the score is up to 97.8% (PAqpZ2_AMS3) for localization validation. The residues within the select region were 92.1%, and those in the additional allowed region were 5.7%. In addition, amino acids such as Gln 126, Thr 181, and Val 197 contribute to the outer region.

Low-resolution structures generally produce an average overall quality factor of around 91%, and the calculated error value falls below 95% of the rejection limit (Colovos & Yeates, 1993). PAqpZ2_AMS3 structure showed above 95% as in Table 1 for ERRAT validation. The ERRAT program assesses the predicted protein structure by comparing the six types of non-bonded atom-atom interactions (CC, CN, CO, NN, NO, and OO) of

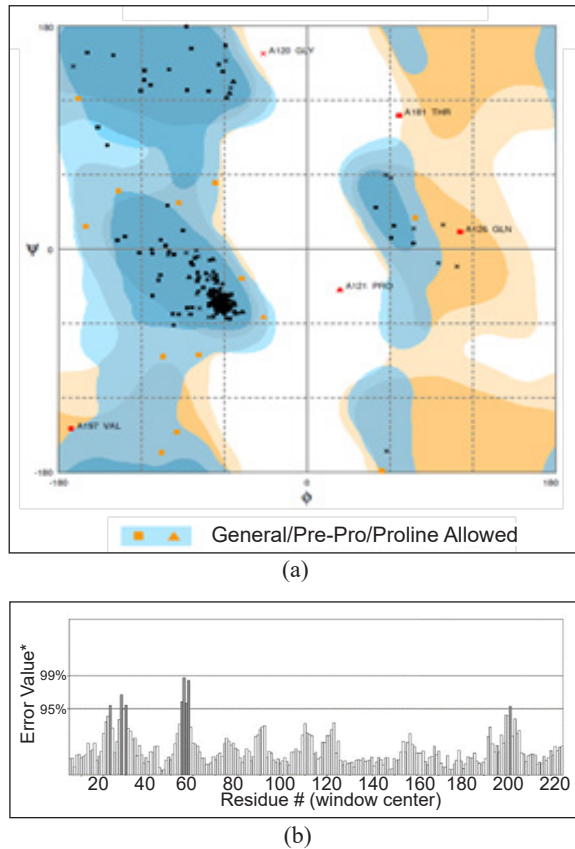


Figure 2. Validation of the predicted aquaporin three-dimensional model: (a) Ramachandran plot; and (b) ERRAT. The predicted 3D aquaporin model structure was of good quality because most residues can be seen clustered at the most favored region and were within an acceptable overall structure quality factor for the lower resolution of structures.

Table 1
Details of Ramachandran plot and ERRAT results

Ramachandran plot statistics	PAqpZ2_AMS3
Residues in favored region	92.1%
Residues in the allowed region	5.7%
Residues in outlier region	2.2%
ERRAT Overall quality factors	96.4%

the modeled structures with a reliable high-resolution structure available in the database (Kleywegt, 2000). In conclusion, the predicted structure is a high-quality structure used for MD simulation.

Structure Analysis. The model structure built was compared and superposed with its template, the crystal structure of AqpZ (PDB ID: 1RC2), using UCSF Chimera (Figure 3). The predicted three-dimensional aquaporins show similar structural properties as Lind et al. (2017) reported research on aquaporin where the protein structures consist of the conserved structural fold with six transmembrane helices and five loops with a single narrow pore at the center of the structure. The structure that showed differences between AqpZ and PAqpZ2_AMS3 is zoomed in the box. Moreover, the center of the channel consists of the aquaporin signature Asparagine-Proline-Alanine (NPA) motif [Figure 4 (b)]. Besides, the aquaporin's conserved constriction region of aromatic/Arginine (ar/R) motif positioned which are Phe; His; Thr, and Arg at the extracellular side of the protein that acts as the selective filter [Figure 4 (a)] (Brown 2017; Araya-Secchin et al., 2011; Goto et al., 2015).

Based on the superimposition of the aquaporin in Figure 3, the overall Root Mean Square Deviation (RMSD) of the protein alpha carbon was calculated using the UCSF Chimera software. The calculated C α -RMSD between the predicted model with its model template is 0.27Å respectively. Comparing the conserved constriction region and the NPA motif of the aquaporins (Figure 4), calculated C α -RMSD is not showing an obvious difference, with an average only of 0.06Å. The highest C α -RMSD can be found at the residues located at the top of the aquaporin structure, as indicated in the box in Figure 3. The

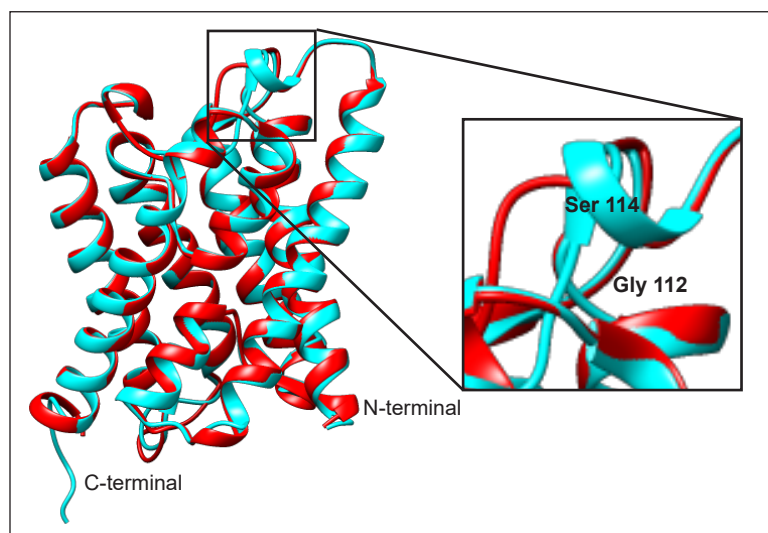


Figure 3. The superimposition of the aquaporin model and its template 3D structure. The aquaporins are red for PAqpZ2_AMS3 and cyan for template AqpZ (PDB ID: 1RC2). The zoomed figure shows the highest C α -RMSD residues calculated by UCSF Chimera between the aquaporin structures.

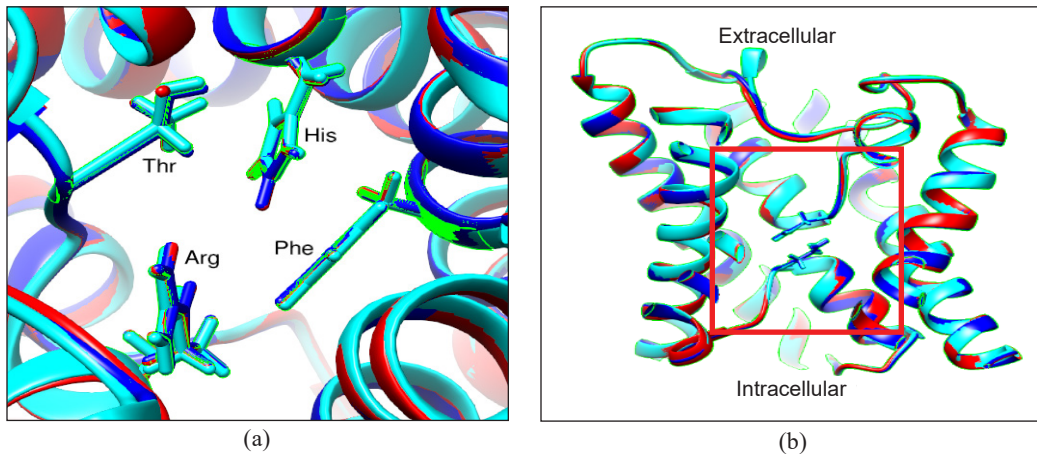


Figure 4. Zoom-in of the superimposition of the aquaporin model and its template 3D structure. The aquaporins are indicated as red for PAqPZ2_AMS3 and cyan for template AqpZ. (a) ar/R region details of superposed models. (b) NPA motif region details are indicated in the red box (Asn63, Pro64, Ala65, Asn184, Pro185, Ala186).

highest difference was between the Gly112 of PAqPZ2_AMS3 and Ser114 of AqpZ with 3.34Å. It indicates that the modeling of putative aquaporin obtained from the *Pseudomonas* sp. AMS3 shows a slight difference in structural properties with its template, which is a solved aquaporin crystal structure, AqpZ.

Other than that, De Maayer et al. (2014) mentioned that a low number of hydrogen bonds could be found in psychrophilic protein as it is important for the protein's conformational flexibility under a cold environment. In agreement with these statements, the hydrogen bond calculated using UCSF Chimera in each predicted aquaporin model and its template, AqpZ, shows a difference of up to hundreds of hydrogen bonds in number. For example, the hydrogen bond calculated in PAqPZ2_AMS3 was 203, respectively. However, compared to the template used, which originates from a mesophilic microorganism (*E. coli*), 307 hydrogen bonds were calculated in the AqpZ.

Molecular Dynamics (MD) Simulation

MD simulation was performed in this study to discover the aquaporin's structural, flexibility, and dynamics changes identified in different temperatures. Theoretically, the density of water varies with temperature as it depends on this parameter (Cho et al., 2002). The monomer of predicted aquaporin was used for the MD simulation. Schmidt and Sturgis (2017) revealed that the tetrameric nature of aquaporins is important to remain stable while integrated within the bilayer membrane and perform its function. However, they added that the monomeric structure of aquaporin in some family members does not affect the protein's role in facilitating the water movement across the membrane. In concurrence with previous studies, the aquaporin monomers used in this study also appear to integrate into

the membrane normally since the secondary structure of the aquaporin monomer contains a lot of hydrophobic residues that can be a part of the transmembrane region of the protein.

The predicted aquaporins were also suggested to be a psychrophilic protein. Increasing the temperature to 37°C may raise the kinetic energy and result in the conformational changes of the psychrophilic aquaporin due to the intermolecular forces disruption, leading to dysfunction of the protein. The coordinates of the last frame from the conformational sampling were saved to analyze its water column structure.

Molecular Dynamics (MD) Simulation Analysis

By calculating the Root Mean Square Deviation values of the C-alpha ($C\alpha$ -RMSD) relative to the coordinates of the energy-minimized initial structures, the overall changes in the model atomic coordinates were monitored during MD simulations as a function of time. For example, the convergence of RMSD values from the minimized predicted aquaporin structure during the simulation at -5°C, 0°C, 5°C, 15°C, and 37°C after a period are shown in Figure 5.

At the first nanosecond of PAqpZ2_AMS3 at -5°C, the RMSD value fluctuates almost to a value of 4.0 Å. This obvious fluctuation by the protein can be considered acceptable. In MD simulation, there is an equilibration phase where the membrane is artificially stabilized to adapt to the newly embedded aquaporin and the right density without being damaged. Overall, the predicted aquaporin model can be deduced as stable simulated in different temperatures throughout the simulation. The protein can maintain its structural stability after the first nanosecond of the simulation. Besides, the protein structure did not diverge more than 3.0 Å towards the end of the simulation at 10 ns, implying that the protein had reached its structural equilibrium with the membrane lipids. In addition, the aquaporin

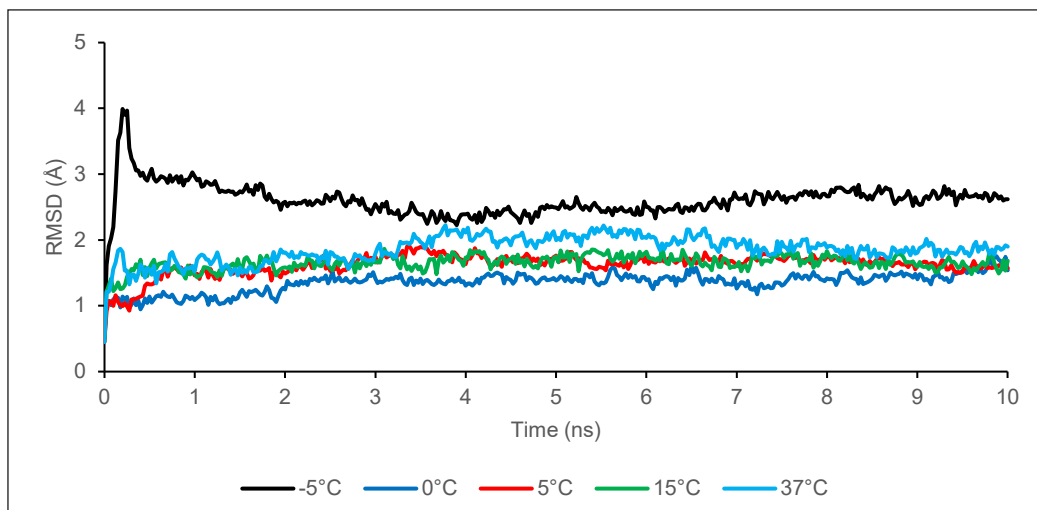


Figure 5. Root Mean Square Deviation (RMSD) of the Carbon alpha as functions of time for PAqpZ2_AMS3

model also showed a stable conformation when simulated at 37°C as structural changes should be seen as the temperature rises.

Figure 6 depicts the Root Mean Square Fluctuation (RMSF) per residue of the predicted aquaporin model simulated at -5°C to 37°C with the initial model secondary structure displayed at the top. The fluctuation with up to 6.0 Å and more than 2.0 Å can be seen in the proteins' C-terminal tail and loop region, respectively. Compared to these loop regions, most of the helical regions of the predicted aquaporin model can be observed with smaller RMSF values. It indicates lower flexibility of the residues in these regions when simulated at different temperatures. The reason may be due to the hydrogen bond that holds the helical conformation of the proteins resulting in less fluctuation of the residues in the regions (Hub et al., 2009).

However, some of the aquaporin helical structures that lose shape can be observed during the MD simulation. It proves the flexibility of the loop regions that face the extracellular and intracellular side and the loss of some of the aquaporin helical structure when simulated in water at various temperatures. Besides that, as compared in Figure 3, the loop region that connects between H3 and H4 of both predicted aquaporin (Figure 6) shows longer length and predominance with more small residue side chains which can be observed in the most secondary structure of psychrophilic proteins for their higher flexibility in low temperature (Schmidt & Sturgis, 2017).

Channel Radius

Due to the selectivity filter formed by Phe43, His172, Arg187, and Thr181 [Figure 4 (a)] of the aquaporin model, the channel diameter is reduced to be very small, sterically excluding

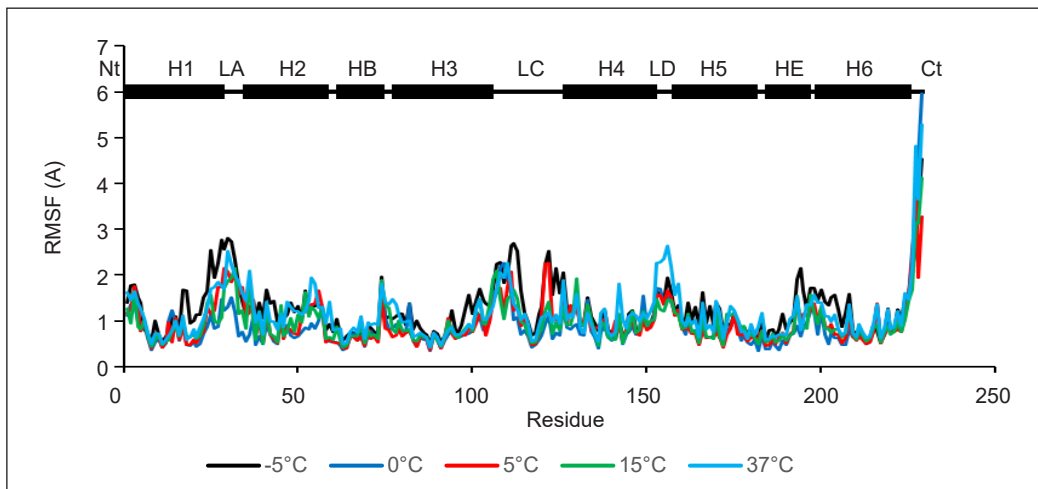


Figure 6. Root Mean Square Fluctuation (RMSF) as functions of time for PaqpZ2_AMS3 atoms. The secondary structure of the proteins was displayed at the top, indicating helices (H1 to H6), half-helices (HB and HE), loops (LA to LD), and termini (Nt and Ct).

the passage of molecules larger than water. This section has the narrowest diameter size in the channel as computed by HOLE 2.0 software (Figure 7) (Brezovsky et al., 2013). In the middle section of the channel, the two conserved Asn-Pro-Ala (NPA) motifs were observed in Asn63 and Asn184 for PAqpZ2_AMS3. The channel radius of each predicted aquaporin monomer was displayed in Figure 7. The program HOLE 2.0 software was used to achieve the pore radius of PAqpZ2_AMS3 monomers along the channel in the z-direction. The pore radius was obtained from configurations of the last frame structure over the 10 ns of the MD simulation. According to Figure 7, the three-dimensional visualization of a monomer pore size was presented as red, which represents the parts that are inaccessible to the water with a pore radius less than 1.15 Å, green for the parts that are accessible to water with a radius between 1.15 Å to 2.30 Å, and blue for the parts that are greater than 2.30 Å (Brezovsky et al. 2013).

The smallest pore radius of PAqpZ2_AMS3 after simulated at -5°C for 10 ns can be seen above in the aquaporin selectivity filter Figure 7. As predicted by the HOLE 2.0 software, the amino acid residues responsible for the narrowest pore radius calculated were Phe36 and Asp180. It shows that the aquaporin Phe36 and Asp180 residues adopted a conformation that more effectively blocks the channel. Its motion was accompanied by a temperature-driven rearrangement of the water molecules inside the channel. A temperature of -5°C induced both residues to populate exclusively deeper positions inside the water channel. It proves the flexibility of the residues when simulated in water at different temperatures.

Figure 8 depicts the superposition of the initial and final structures of PAqpZ2_AMS3 simulated at -5°C after 10 ns. The C α -RMSD calculated between the Phe36 and Asn180

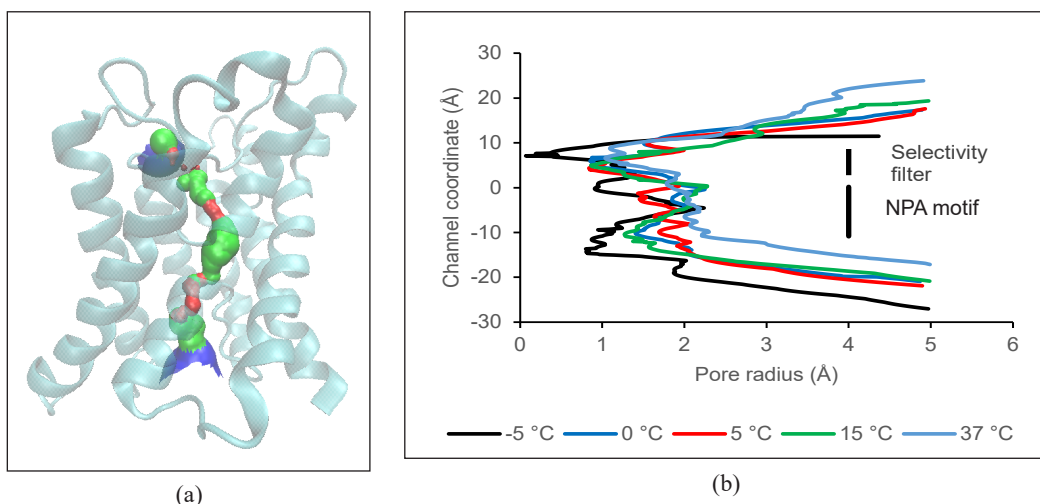


Figure 7. The pore radius of the final structure. The 10 ns of (a) PAqpZ2_AMS3 model simulated in -5°C visualized with the water pore outline. On the extracellular side of PAqpZ2_AMS3, the channel is blocked. The calculated pore diameter versus the z coordinate of each final structure of PAqpZ2_AMS3 is simulated at various temperatures.

residues in initial and final structures of the PAqpZ2_AMS3 that are involved in blocking the water column is 4.63 Å and 0.75 Å, respectively. Asn180 is the amino acid from the NPA motif, and Phe36 is known to be the water-gating amino acid, thus acting as the selectivity filter in PAqpZ2_AMS3. This result led to the hypothesis that the Phe36 and Asn180 residues of PAqpZ2_AMS3 are more flexible as their conformation is rearranged in low temperatures leading to a decrease of the aquaporin water column and next blocking the channel.

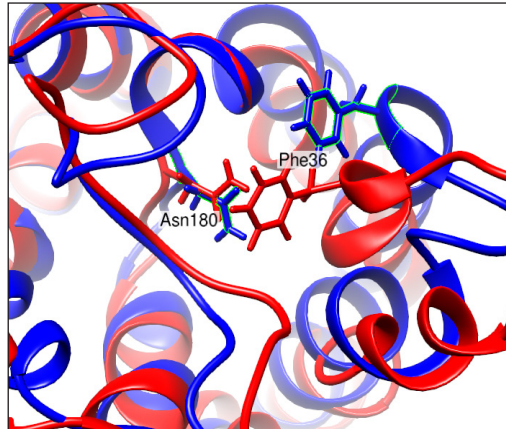


Figure 8. Top view of superposed initial (blue) and final (red) structure of PAqpZ2_AMS3 simulated at -5°C . The Phe36 and Asn180 residues block the water column.

CONCLUSION

This structural and dynamic study of putative aquaporin from Antarctic *Pseudomonas* sp. strain AMS3 provides insights into the mechanistic properties of the water transport protein when simulated in water at various temperatures. The MD simulation results suggest that the aquaporin model can remain stable and flexible throughout the simulation under different temperatures. In addition, the position of Phe36 and Asn180 residues in PAqpZ2_AMS3 were rearranged after 10 ns in -5°C MD simulation, leading to changes in the aquaporin water column size and next blocking the channel. The information obtained from this identified psychrophilic water channel protein provides new information about this protein's structural adaptability at low temperatures, which may be useful tools for cryogenic industrial applications and molecular engineering.

Future studies will be highly interesting to test this *in silico* analyses and its physiological connection to the channel-blocking mechanism. Furthermore, aquaporin should be simulated in its tetrameric form, and its single-channel water permeability constant should be compared to that of other aquaporin family members. In addition, water orientation inside this protein pore should be studied to provide information and understanding of this psychrophilic aquaporin's cold adaptation and structural insights.

ACKNOWLEDGEMENT

The Ministry of Education supported this project through the Fundamental Research Grant Scheme (FRGS/1/2019/STG04/UPM/02/04).

REFERENCES

- Altschul, S. F., Gish, W., Miller, W., Myers, E. W., & Lipman, D. J. (1990). Basic local alignment search tool. *Journal of Molecular Biology*, 215(3), 403-410. [https://doi.org/10.1016/S0022-2836\(05\)80360-2](https://doi.org/10.1016/S0022-2836(05)80360-2)
- Aponte-Santamaría, C., Fischer, G., Báth, P., Neutze, R., & de Groot, B. L. (2017). Temperature dependence of protein-water interactions in a gated yeast aquaporin. *Scientific Reports*, 7(1), 1-14. <https://doi.org/10.1038/s41598-017-04180-z>
- Araya-Secchi, R., Garate, J. A., Holmes, D. S., & Perez-Acle, T. (2011). Molecular dynamics study of the archaeal aquaporin AqpM. *BioMed Central Genomics*, 12(4), 1-13. <https://doi.org/10.1186/1471-2164-12-S4-S8>
- Bienert, S., Waterhouse, A., de Beer, T. A., Tauriello, G., Studer, G., Bordoli, L., & Schwede, T. (2017). The SWISS-MODEL Repository-new features and functionality. *Nucleic Acids Research*, 45, 313-319. <https://doi.org/10.1093/nar/gkw1132>
- Brezovsky, J., Chovancova, E., Gora, A., Pavelka, A., Biedermannova, L., & Damborsky, J. (2013). Software tools for identification, visualization and analysis of protein tunnels and channels. *Biotechnology Advances*, 31(1), 38-49. <https://doi.org/10.1016/j.biotechadv.2012.02.002>
- Brown, D. (2017). The discovery of water channels (aquaporins). *Annals of Nutrition and Metabolism*, 70(1), 37-42. <https://doi.org/10.1159/000463061>
- Cho, C. H., Urquidi, J., Singh, S., Park, S. C., & Robinson, G. W. (2002). Pressure Effect on the density of water. *The Journal of Physical Chemistry A*, 106(33), 7557-7561. <https://doi.org/10.1021/jp0136260>
- Cohen, E. (2012). Roles of aquaporins in osmoregulation, desiccation and cold hardiness in insects. *Entomology, Ornithology & Herpetology*, 1, 1-17. <https://doi.org/10.4172/2161-0983.S1-001>
- Colovos, C., & Yeates, T. O. (1993). Verification of protein structures: Patterns of nonbonded atomic interactions. *Protein Science*, 2(9), 1511-1519. <https://doi.org/10.1002/pro.5560020916>
- De Maayer, P., Anderson, D., Cary, C., & Cowan, D. A. (2014). Some like it cold: Understanding the survival strategies of psychrophiles. *European Molecular Biology Organization Reports*, 15(5), 508-517. <https://doi.org/10.1002/embr.201338170>
- Donkor, E. S., Dayie, N. T., & Adiku, T. K. (2014). Bioinformatics with basic local alignment search tool (BLAST) and fast alignment (FASTA). *Journal of Bioinformatics and Sequence Analysis*, 6(1), 1-6. <https://doi.org/10.5897/IJBC2013.0086>
- Finn, R. N., & Cerda, J. (2015). Evolution and functional diversity of aquaporins. *The Biological Bulletin*, 229, 6-23. <https://doi.org/10.1086/BBLv229n1p6>
- Gomes, D., Agasse, A., Thiébaud, P., Delrot, S., Gerós, H., & Chaumont, F. (2009). Aquaporins are multifunctional water and solute transporters highly divergent in living organisms. *Biochimica et Biophysica Acta (BBA)-Biomembranes*, 1788(6), 1213-1228. <https://doi.org/10.1016/j.bbame.2009.03.009>
- Goto, S. G., Lee Jr, R. E., & Denlinger, D. L. (2015). Aquaporins in the Antarctic midge, an extremophile that relies on dehydration for cold survival. *The Biological Bulletin*, 229(1), 47-57. <https://doi.org/10.1086/BBLv229n1p47>

- Hedfalk, K., Törnroth-Horsefield, S., Nyblom, M., Johanson, U., Kjellbom, P., & Neutze, R. (2006). Aquaporin gating. *Current Opinion in Structural Biology*, 16(4), 447-456. <https://doi.org/10.1016/j.sbi.2006.06.009>
- Hospital, A., Goñi, J. R., Orozco, M., & Gelpi, J. L. (2015). Molecular dynamics simulations: Advances and applications. *Advances and Applications in Bioinformatics and Chemistry*, 8, 37-47. <https://doi.org/10.2147/AABC.S70333>
- Hub, J. S., Grubmüller, H., & De Groot, B. L. (2009). Dynamics and energetics of permeation through aquaporins. What do we learn from molecular dynamics simulations.? *Handbook of Experimental Pharmacology*, 190, 57-76. https://doi.org/10.1007/978-3-540-79885-9_3
- Kleywegt, G. J. (2000). Validation of protein crystal structures. *Acta Crystallographica Section D: Biological Crystallography*, 56(3), 249-265. <https://doi.org/10.1107/S0907444999016364>
- Kourghi, M., Nourmohammadi, S., Pei, J. V., Qiu, J., McGaughey, S., Tyerman, S. D., Byrt, C. S., & Yool, A. J. (2017). Divalent cations regulate the ion conductance properties of diverse classes of aquaporins. *International Journal of Molecular Sciences*, 18(11), Article 2323. <https://doi.org/10.3390/ijms18112323>
- Kozono, D., Ding, X., Iwasaki, I., Meng, X., Kamagata, Y., Agre, P., & Kitagawa, Y. (2003). Functional expression and characterization of an archaeal aquaporin: AqpM from *Methanothermobacter marburgensis*. *Journal of Biological Chemistry*, 278(12), 10649-10656. <https://doi.org/10.1074/jbc.M212418200>
- Krieger, E., & Vriend, G. (2014). YASARA view - Molecular graphics for all devices from smartphones to workstations. *Bioinformatics*, 30(20), 2981-2982. <https://doi.org/10.1093/bioinformatics/btu426>
- Lind, U., Järvå, M., Alm Rosenblad, M., Pingitore, P., Karlsson, E., Wrangé, A. L., Kamdal, E., Sundell, K., Andre, C., Jonsson, P. R., Havenhand, J., Eriksson, L. A., Hedfalk, K., & Blomberg, A. (2017). Analysis of aquaporins from the euryhaline barnacle *Balanus improvisus* reveals differential expression in response to changes in salinity. *Public Library of Science One*, 12(7), 1-33. <https://doi.org/10.1371/journal.pone.0181192>
- Mannige, R. V., Kundu, J., & Whitelam, S. (2016). The Ramachandran number: An order parameter for protein geometry. *Public Library of Science One*, 11(8), 1-14. <https://doi.org/10.1371/journal.pone.0160023>
- Mathai, J. C., Missner, A., Kügler, P., Saparov, S. M., Zeidel, M. L., Lee, J. K., & Pohl, P. (2009). No facilitator required for membrane transport of hydrogen sulfide. *Proceedings of the National Academy of Sciences*, 106(39), 16633-16638. <https://doi.org/10.1073/pnas.0902952106>
- Németh-Cahalan, K. L., & Hall, J. E. (2000). pH and calcium regulate the water permeability of aquaporin 0. *The Journal of Biological Chemistry*, 275(10), 6777-6782. <https://doi.org/10.1074/jbc.275.10.6777>
- Sachdeva, R., & Singh, B. (2014). Insights into structural mechanisms of gating induced regulation of aquaporins. *Progress in Biophysics and Molecular Biology*, 114(2), 69-79. <https://doi.org/10.1016/j.pbiomolbio.2014.01.002>
- Salomon-Ferrer, R., Case, D. A., & Walker, R. C. (2013). An overview of the Amber biomolecular simulation package. *Wiley Interdisciplinary Reviews: Computational Molecular Science*, 3(2), 198-210. <https://doi.org/10.1002/wcms.1121>

- Savage, D. F., Egea, P. F., Robles-Colmenares, Y., O'Connell III, J. D., Stroud, R. M., & Simon, S. (2003). Architecture and selectivity in aquaporins: 2.5 Å X-ray structure of aquaporin Z. *Public Library of Science Biology*, 1(3), 334-340. <https://doi.org/10.1371/journal.pbio.0000072>
- Schmidt, V., & Sturgis, J. N. (2017). Making monomeric aquaporin Z by disrupting the hydrophobic tetramer interface. *American Chemical Society Omega*, 2, 3017-3027. <https://doi.org/10.1021/acsomega.7b00261>
- Tong, H., Hu, Q., Zhu, L., & Dong, X. (2019). Prokaryotic aquaporins. *Cells*, 8(11), Article 1316. <https://doi.org/10.3390/cells8111316>
- Woo, J., Chae, Y. K., Jang, S. J., Kim, M. S., Baek, J. H., Park, J. C., Trink, B., Ratovitski, E., Lee, T., Park, B., Park, M., Kang, J. H., Soria, J. C., Lee, J., Califano, J., Sidransky, D., & Moon, C. (2008). Membrane trafficking of AQP5 and cAMP dependent phosphorylation in bronchial epithelium. *Biochemical and Biophysical Research Communications*, 366(2), 321-327. <https://doi.org/10.1016/j.bbrc.2007.11.078>
- Zhou, A. Q., O'Hern, C. S., & Regan, L. (2011). Revisiting the Ramachandran plot from a new angle. *Protein Science*, 20, 1166-1171. <https://doi.org/10.1002/pro.644>

Mathematical Models for Predicting the Mechanical Properties of Poly(Lactic Acid) for Load-Bearing Applications

Abraham Aworinde^{1*}, Titus Ajewole², Olakunle Olukayode³ and Joseph Dirisu¹

¹Department of Mechanical Engineering, College of Engineering, Covenant University, Ota 112233, Nigeria

²Department of Electrical and Electronic Engineering, Osun State University, Osogbo 230262, Nigeria

³Department of Mechanical Engineering, Osun State University, Osogbo 230262, Nigeria

ABSTRACT

In order to widen the areas of application of poly (lactic acid) (PLA), there has been a multiplicity of experiments. This study attempts to develop mathematical models for predicting the mechanical properties of PLA to reduce the number of experimental runs and material wastage. The melt-cast method produced unreinforced PLA samples with different slenderness ratios (λ) in triplicate using. The samples were subjected to a compression test to obtain the mechanical properties captured at three main points on the stress-strain curve: yield, ultimate stress, and fracture. Regression models were developed from the data obtained at the three points, and their validity was examined by testing them against the previous relevant experimental studies from various authors. The coefficient of determination (R^2) and coefficient of correlation (ρ) was also examined for each model to establish their degree of correctness further. Analyses show that the developed models give reasonable approximations of some of the properties examined. The mass (M) and the modulus of elasticity (E) were the most accurately predictable properties with [R^2 , ρ] of [99.97%, 0.9998] and [91.55%, 0.9568], respectively. Results also show that apart from the melt-cast method, the compressive modulus of PLA (both circular and rectangular cross-sections test samples) produced via injection molding and fused filament fabrication can be predicted with near accuracy using the model developed in this study. This study

gives researchers the tools needed to avoid material wastage by having close-to-real values of the mechanical properties of PLA through prediction before carrying out any experiment.

ARTICLE INFO

Article history:

Received: 18 October 2021

Accepted: 16 December 2021

Published: 20 April 2022

DOI: <https://doi.org/10.47836/pjst.30.3.02>

E-mail addresses:

abraham.aworinde@covenantuniversity.edu.ng (Abraham Aworinde)

titus.ajewole@uniosun.edu.ng (Titus Ajewole)

olakunle.kayode@uniosun.edu.ng (Olakunle Olukayode)

joseph.dirisu@covenantuniversity.edu.ng (Joseph Dirisu)

* Corresponding author

Keywords: Compressive modulus, fused deposition modeling, processing technologies, regression models, sample size effect, slenderness ratio

INTRODUCTION

Poly lactide has become a widely applied biopolymer. Several studies have reported its application in cardiovascular devices (Hadasha & Bezuidenhout, 2018), skeletal tissues (Aworinde et al., 2020a; Ferrer et al., 2018), drug delivery (Li et al., 2018; Tyler et al., 2016), commodities and specialties (Malinconico et al., 2018), sensing (Tajitsu, 2017), and automotive (Bouzouita et al., 2017). Its application is gaining an incredible increase in biomedical recently (Aworinde et al., 2020a; Aworinde et al., 2021a; Deepthi et al., 2016; Wang et al., 2016). Its future applications abound because of its propensity to replace many materials in the near future (Anderson & Shenkar, 2021; Cooper, 2013). It is consistent that, unlike synthetic polymers, biopolymers are generally environmentally benign (Abioye & Obuekwe, 2020; Adegbola et al., 2020; Mansour et al., 2020) and possess structural applications. For instance, a recent consideration has been given to PLA as a replacement for metals as internal bone fixation to avoid problems such as hardware pain, elastic modulus mismatch, temperature sensitivity, and others. Another emerging application of PLA is in the renewable energy field. Wind energy is one of the green energy sources already on a commercial scale and is expected to expand in the future. When the turbine structures reach their end of service life, their fabrication materials must be recyclable to be totally green. The turbine blades are made up of thermosetting fiber-reinforced polymers, which are very difficult to recycle because of the materials' nature and complex composition (Rahimizadeh et al., 2019). A study considered thermal and mechanical recycling methods in reclaiming glass fibers from end-of-life wind turbine blades (Rahimizadeh et al., 2020). It was reported that short glass fibers from blades of decommissioned wind turbines were recovered and mixed with a polylactic acid (PLA) matrix through a double extrusion process to prepare novel composite filaments for Fused Deposition Modeling (FDM).

Successful applications of PLA in various fields require that test samples of different configurations be obtained and tested in the laboratory before it is made available for end-users. In order to obtain these various test samples, a number of processing techniques are employed. These techniques include electrospinning, melt electro-writing, melt casting, and solvent casting (Aworinde et al., 2018; Gbenebor et al., 2018a; Jamshidian et al., 2010). The test samples produced by the techniques mentioned above have been subjected to tests such as hydrophobicity (Aworinde et al., 2020b; Sundar et al., 2021), morphology (Taleb et al., 2021), rheology (Fang & Hanna, 1999; Rokbani & Aji, 2018), and thermal (Taleb et al., 2021). Of all the tests carried out on PLA, its mechanical properties appear to be its most evaluated property (Adeosun et al., 2016; Akpan et al., 2019; Aworinde et al., 2019; Aworinde et al., 2020c; Aworinde et al., 2020a; Aworinde et al., 2021b; Brischetto & Torre, 2020; Deepthi et al., 2016; Wang et al., 2016). The mechanical test becomes necessary whenever PLA is applied as a load-bearing structure by the rule of thumb. The load-bearing samples vary in thickness, length, and shape, as shown in Table 1 and Figures 1-3, depending on the applications.

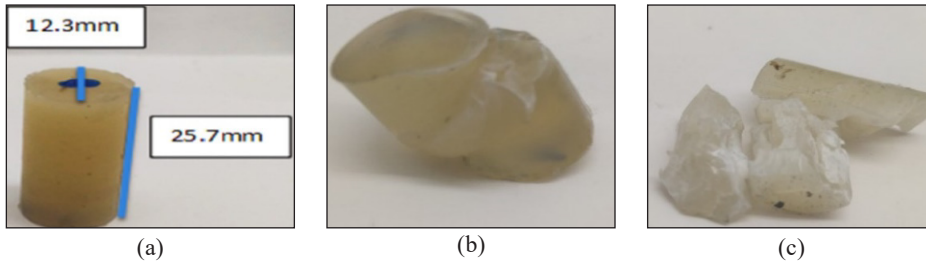


Figure 1. Compression sample of unreinforced PLA: (a) before testing (b) buckled after testing (c) fractured after testing (Barkhad et al., 2020)

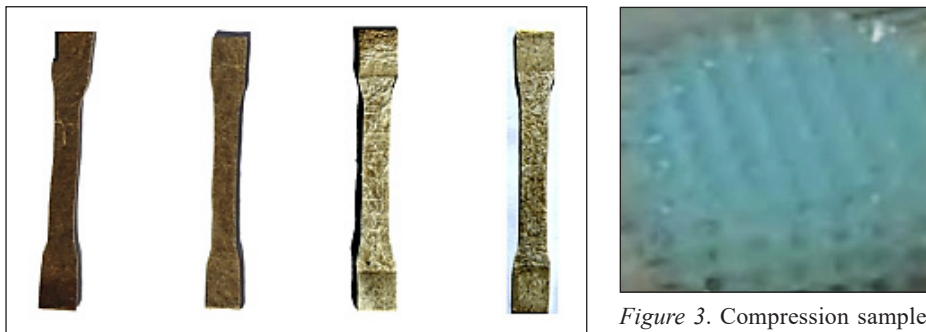


Figure 2. Tensile test samples of PLA composites (Farah et al., 2016)

Figure 3. Compression samples from a laser-cut, 3D printed PLA (Rodrigues et al., 2016)

Table 1
Variations in the sizes of the mechanical test sample

Reference	Method of sample production	Sample's cross-section	Type of mechanical sample	Type of mechanical test	λ
(Aworinde et al., 2020a)	Melt casting	circle	Cylinder	Compression	2.24
(Akpan et al., 2019)	Electrospinning	Rectangle	Fiber mat	Tensile	n/a
(Brischetto & Torre, 2020)	Fused deposition modeling	Rectangle	Rectangular prism	Compression	10.90
(Abbas et al., 2017)	Fused deposition modeling	Rectangle	Rectangular prism	Compression	6.92
(Barkhad et al., 2020)	Injection molding	circle	Cylinder	Compression	8.36
(Gbenebor et al., 2018b)	Electrospinning	Rectangle	Fiber mat	Tensile	n/a
(Oksiuta et al., 2000)	Extrusion	n/a	Dog bone	Tensile	n/a
(Farah et al., 2016)	Hot press	n/a	Dog bone	Tensile	n/a

The compression test is one of the most frequently performed mechanical tests for obtaining the mechanical properties of PLA. Generally, the compression test has several advantages over other mechanical tests. Aside from the fact that various properties can be obtained from its result, compression test samples are very easy to fabricate. In addition, there is no limit to the extent to which the stress/strain relationship can be obtained since

the test sample is usually loaded between two relatively rigid flat platens (Figure 4), which removes the possibility of any constraints in movement until the specimen fractures (Williams & Gamonpilas, 2008). Studies show that the simplicity and versatility of the compression test have attracted researchers to its usage in determining the mechanical properties of PLA and PLA composites (Abbas et al., 2017; Aworinde et al., 2020a; Barkhad et al., 2020). This study, therefore, attempted a means of minimizing material and time wastage by providing regression models that predict some of the properties of PLA, which are obtainable via compression test.

MATERIALS AND METHOD

Poly lactide (PLA) with an overall lactide purity $\geq 99.5\%$ and monomer's molecular weight of 144 g/mol was purchased from NatureWorks, USA. It was pre-dried in an oven at 50 °C for 6 hours to eliminate the possible moisture content to forestall viscosity degradation and possibly significantly impact the mechanical properties (Lawrence et al., 2001). The moisture-free PLA was then processed using melt casting and mold pressing at the pouring temperature of 210 °C. Solid cylinders with a constant diameter of 13.28 mm and arithmetic progressively varying heights according to Equation 1 were developed. In Equation 1, l_n is the length of an n th term of a sample while a is the starting length, i.e., 9.4 mm. c is the positive constant difference between any two successive lengths, and n denotes the n th term. Three samples were produced for each length. Care was taken to keep all lengths within the prescription of ASTM D695 to avoid buckling during the mechanical test. However, there was chipping off of some samples during testing (Figure 4), which possibly impacted the linearisation of the mechanical properties.

$$l_n = a + c(n - 1) \quad (1)$$

The masses of the samples (triplicate) of each length were measured. The samples were afterward subjected to a compression test using a double column Instron universal testing machine with model number 3369 (equipped with Bluehill software for data acquisition) located at the Centre for Energy Research and Development (CERD) at Obafemi Awolowo University, Ile-Ife in Nigeria. The samples were axially loaded as stipulated by ASTM D695 and used in many studies (Abbas et al., 2017; Aworinde et al., 2020a; Bakar et al., 2003). The mean values of the masses, and all the compressive mechanical properties examined via experiment, were reported. The moduli of elasticity were obtained using MATLAB R2019a (9.6) to find the slope within the elastic region. Table 2, in addition to the mass, lists the compressive mechanical properties obtained from the test. These properties were considered at three main regions on the stress-strain curve (i.e., yield, ultimate or maximum stress, and break) to account for the responses of the samples when loaded in compression.

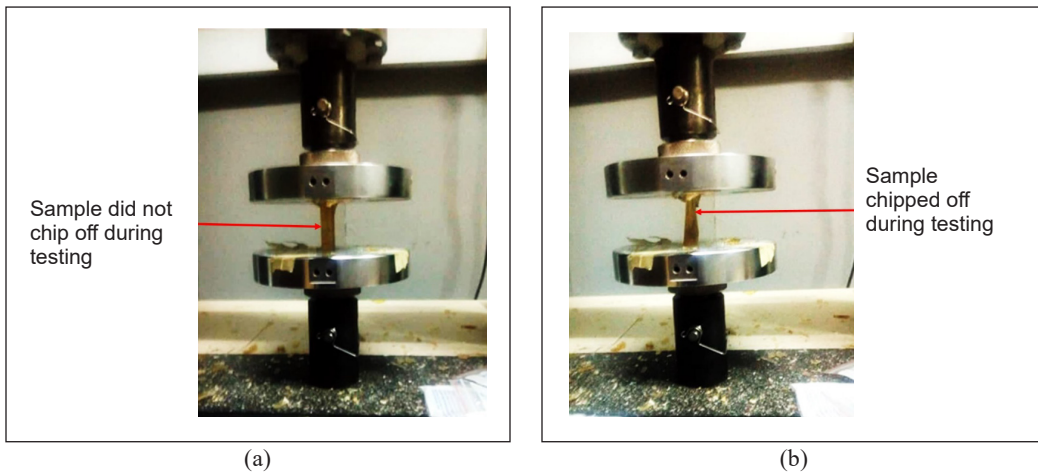


Figure 4. Chipping off of samples during compression test: (a) no chipping (b) sample chipped off

Mathematical functions were generated for each property to examine their dependence on the slenderness ratio, λ . The coefficient of determination, R^2 , was also generated for each property to establish the proportion of the variance in these properties that can be predicted from the independent variable, λ .

RESULTS AND DISCUSSION

Table 2 displays the mechanical and the physical (i.e., mass) properties. The values of R^2 are also shown in Table 2. The R^2 values show that the dependence of all the examined properties on the independent variable, λ , was supported by at least 70% of the experimental data. Mass, modulus of elasticity, compressive extension at the break, ductility, compressive extension at maximum compressive stress, and compressive strain at maximum compressive stress were related to the λ and had 99.97%, 91.55%, 93.66%, 97.38%, 93.14% and 94.38% degree of predictability, respectively, using the experimental values obtained in this study. Compressive stress and load at break were 84.79% predictable. Compressive stress and load at maximum compressive stress were 79.29% predictable, compressive stress and load at yield were 71.29% predictable. In comparison, energies at maximum compressive stress and break had 77.98% and 74.23% predictive extent of accuracy, respectively.

Figure 5 shows changes in length and mass as a function of the slenderness ratio. The length is not the focus here; hence it was not modeled since it was a predetermined factor (Equation 1) and not one of the study's outputs. Mass (M), on the other hand, was modeled by Equation 2. The model showed a fairly linear relationship. The R^2 value of 99.97% and coefficient of correlation of 0.9998 imply a reasonable degree of accuracy of values that can be predicted by Equation 2. The implication of Equation 2 is that the approximate amount of mass of PLA can be reasonably predicted, given λ . It would, in turn, help to know the

Table 2
Mechanical and physical properties of Polylactide obtained from the compression test and direct measurement

Mechanical and physical properties	Unit	Symbol	R ²	correlation (ρ)
Maximum compressive stress	MPa	σ_{UCS}	0.7929	0.7075
Compressive strain at maximum compressive stress	%	ϵ_{UCS}	0.9438	-0.7419
Energy at maximum compressive stress	J	U_{UCS}	0.7798	0.7472
Compressive load at maximum compressive stress	N	F_{UCS}	0.7929	0.7075
Compressive extension at maximum compressive stress	mm	e_{UCS}	0.9314	0.6182
Compressive stress at break	MPa	σ_b	0.8479	0.7933
Compressive load at break	N	F_b	0.8479	0.7933
Compressive strain at break, i.e., ductility	%	ϵ_b	0.9738	-0.8024
Compressive extension at break	mm	e_b	0.9366	0.6067
Energy at break	J	U_b	0.7423	0.7308
Compressive stress at yield	MPa	σ_y	0.7129	0.4492
Compressive load at yield	N	F_y	0.7129	0.4492
Modulus	MPa	E	0.9155	0.9568
Mass	g	M	0.9997	0.9998

financial implication of the mass needed for a known λ to be produced for a compression test. Although melt blending and injection molding processes have been copiously used to fabricate PLA and its composites (Aworinde et al., 2020a; Mofokeng et al., 2012), these processes have not been developed like fused deposition modeling (FDM) in terms of parametric modeling.

$$M = 0.5653\lambda + 0.0228 \tag{2}$$

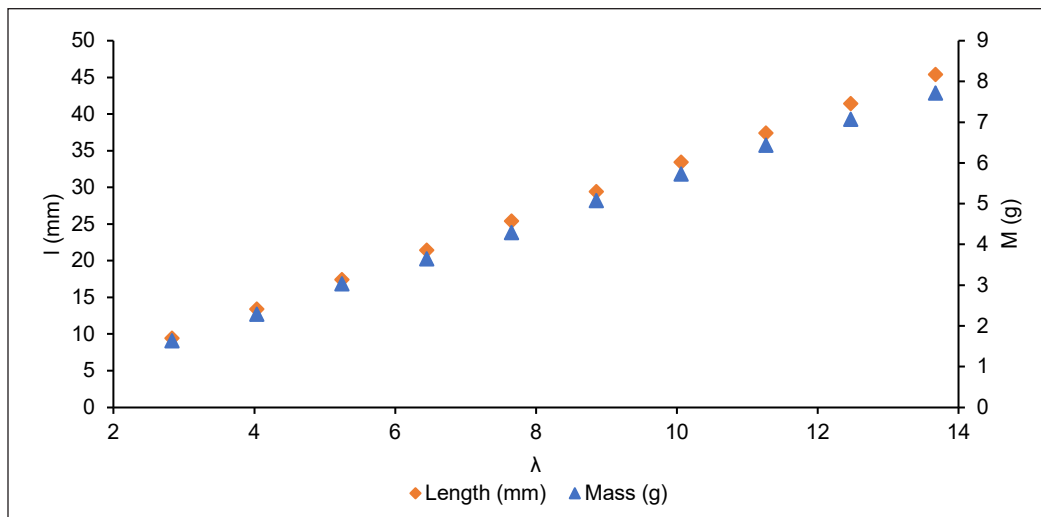


Figure 5. Samples' mass and length as affected by the slenderness ratio

Mechanical Properties at Yield

Figures 6 and 7 capture the mechanical properties of the samples at yield. Figure 6 summarizes the stress-strain responses of the samples to the compressive load within the elastic region. Equations 3 to 5 are the polynomial functions intended for predicting the elastic modulus (E), compressive load (F_y), and compressive stress (σ_y), respectively. These properties are the responses of the axially loaded PLA samples within the region where the deformation was only elastic. For example, with Equation 3, the modulus of elasticity could be predicted with 91.95% accuracy using a polynomial regression model of order one.

$$E = 226.63\lambda + 43.19 \quad (3)$$

$$F_y = 0.9395\lambda^6 - 47.833\lambda^5 + 965.26\lambda^4 - 9812.2\lambda^3 + 52559\lambda^2 - 139070\lambda + 142304 \quad (4)$$

$$\sigma_y = 0.0068\lambda^6 - 0.3453\lambda^5 + 6.9688\lambda^4 - 70.841\lambda^3 + 379.45\lambda^2 - 1004\lambda + 1027.4 \quad (5)$$

The examination of Equation 3 shows some degree of reliance in the light of other studies. Our previous work, for instance, with λ equal to 2.2 for an unreinforced sample of PLA, conforms with the model in Equation 3 (Aworinde et al., 2020a). Equation 3 also reasonably approximates the compressive modulus of elasticity of 3D printed PLA (with $\lambda = 12.6$) reported by other researchers (Brischetto & Torre, 2020). Another study equally corroborates the validity of Equation 3 (Barkhad et al., 2020). The study reports $E = 1.75$ GPa for unreinforced PLA (with $\lambda = 8.36$), while Equation 3 gives $E = 1.94$ GPa for the same value of λ . The validity of Equation 3, as further proven by its coefficient of correlation (ρ) of 0.9568, established a stately model for predicting the modulus of elasticity without any experimental setup and material wastage, given a known value of λ . Interestingly, λ can be easily determined without any recourse to experimental trials. Table 3 summarises the correlation between experimental reports and predicted values by the regression model of Equation 3. The small differences between the experimental and the predicted values could be due to the formation of pores/voids in the fabrication method (i.e., melt casting), especially as the sample's size increased.

Figure 7 shows the compressive load (F_y) and strength (σ_y) at yield. The load at yield heralds the onset of plastic deformation. After the load at yield, the load value ceases to travel in a straight line. Both properties (i.e., load and strength at yield) have the same curve pattern. Equation 4 models the relationships between λ and F_y , while Equation 5 models the relationships between λ and σ_y . The sixth (6th) order that approximates these relationships shows that the polynomial regression models may not be very reliable and that the relationships may not truly exist. The correlation coefficient (Table 2) that linearly

relates F_y and σ_y to λ was 0.4492, indicating a weak correlation. It implies then that, unlike what was obtainable in the prediction of M and E , the linear relationships that connect F_y and σ_y to λ may not be properly predicted by the regression models of Equations 4 and 5. However, Figure 7 shows that the same variational pattern exists between λ and F_y and between λ and σ_y .

Table 3
Extent of the accuracy of Equation 3 in the light of experimental reports

Reference	Method of sample production	Sample's cross-section	Type of mechanical test	λ	Modulus from experiment	Modulus from Equation 3
(Aworinde et al., 2020a)	Melt casting	cylinder	Compression	2.24	522.18 MPa	550.84 MPa
(Barkhad et al., 2020)	Injection molding	cylinder	Compression	8.36	≈1750.00 MPa	1937.82 MPa
(Brischetto & Torre, 2020)	FDM	rectangle	Compression	10.90	2093.00 MPa (100%*)	2513.46 MPa

* = Infill Density

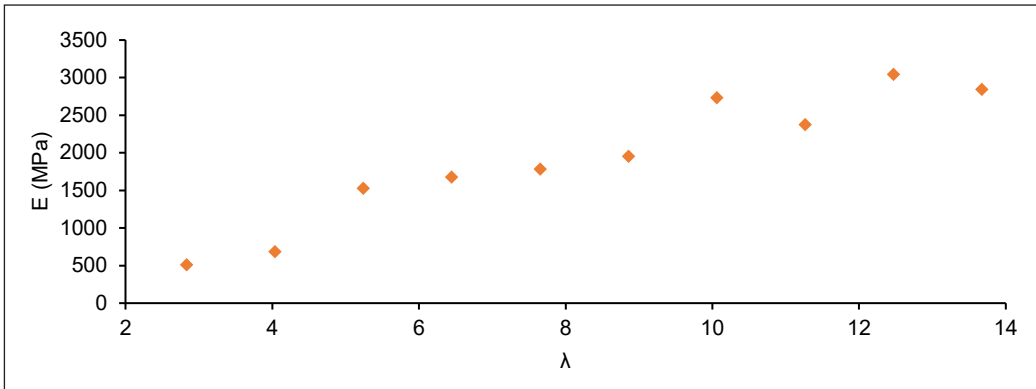


Figure 6. Dependence of modulus of elasticity on slenderness ratio

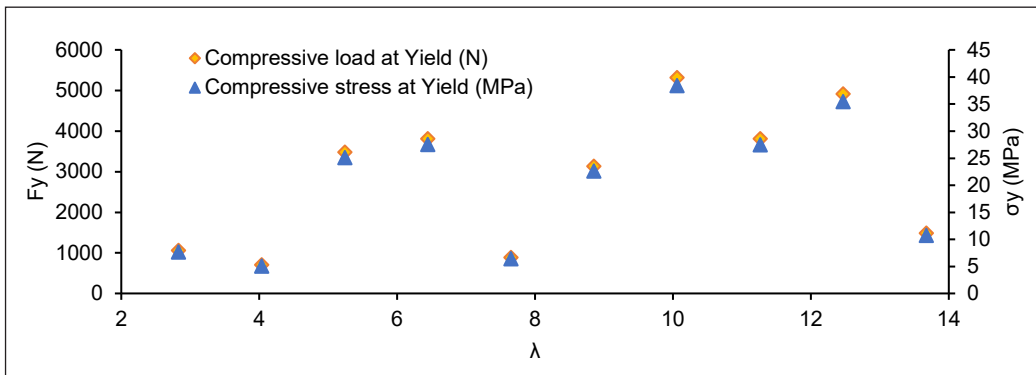


Figure 7. Predictive model of compressive load and stress at yield by slenderness ratio

Mechanical Properties at Ultimate Compressive Strength (UCS)

Figures 8-10 show the variations of the mechanical properties of PLA relative to the λ at maximum compressive strength, i.e., ultimate compressive stress (UCS). Figure 8 and Equations 6 and 7 detail the effect of λ on the compressive load (F_{UCS}) and compressive stress (σ_{UCS}) of PLA at UCS. F_{UCS} , which is the load that produces σ_{UCS} , is usually not the subject of many experimental reports. σ_{UCS} , however, has been reported for various materials (Akpan et al., 2019; Aworinde et al., 2020a; Brischetto & Torre, 2020; Gbenebor et al., 2018b), being the maximum stress any material can withstand before breaking. The values of R^2 (79.29%) and the coefficient of correlation (0.7075) show that the obtained regression model (Equation 7) is a little reliable. In the light of experimental reports, Table 2 shows the extent of accuracy of the regression model for the prediction of σ_{UCS} and the values obtained from various research reports.

$$F_{UCS} = 0.8301\lambda^6 - 42.692\lambda^5 + 873.54\lambda^4 - 9030.3\lambda^3 + 49256\lambda^2 - 132529\lambda + 137624 \quad (6)$$

$$\sigma_{UCS} = 0.006\lambda^6 - 0.3082\lambda^5 + 6.3066\lambda^4 - 65.195\lambda^3 + 355.61\lambda^2 - 956.81\lambda + 993.59 \quad (7)$$

The strain (ϵ_{UCS}) and the extension (e_{UCS}) at the maximum compressive stress in Figure 9 and the energy (U_{UCS}) at maximum compressive stress in Figure 10 are usually not the subjects of intense discussion when it comes to the mechanical properties of PLA. Figure 10 depicts the energy absorbed by the samples when the stress is maximum. It also describes the work done by the uniaxial compressive load as the compressive stress reaches the maximum value. As shown in Table 2, the correlation coefficient between λ and ϵ_{UCS} is negative. It implies a decrease in λ as ϵ_{UCS} increases and vice versa. The extent of reliability of Equations 8, 9, and 10 are 94.38%, 93.14%, and 77.98%, respectively (Table 2). The regression models at maximum compressive stress were evaluated at degree 6 polynomial functions. This degree substantially impacted their degree of accuracy (Sun et al., 2014; Ye & Zhou, 2013), as seen in Table 4.

$$\epsilon_{UCS} = 0.0006\lambda^6 - 0.0336\lambda^5 + 0.719\lambda^4 - 7.846\lambda^3 + 45.541\lambda^2 - 131.8\lambda + 152.75 \quad (8)$$

$$e_{UCS} = 0.0001\lambda^6 - 0.0069\lambda^5 + 0.1471\lambda^4 - 1.5823\lambda^3 + 9.0269\lambda^2 - 25.409\lambda + 27.903 \quad (9)$$

$$U_{UCS} = 0.0003\lambda^6 - 0.0144\lambda^5 + 0.3047\lambda^4 - 3.2328\lambda^3 + 18.024\lambda^2 - 49.392\lambda + 51.873 \quad (10)$$

Table 4
Extent of the accuracy of Equation 7 in the light of experimental reports

Reference	Method of sample production	Type of mechanical test	Sample's cross-section	λ	Ultimate strength from the experiment	Ultimate strength from Equation 7
(Abbas et al., 2017)	3D printing	Compression test	rectangle	6.92	27.5 Mpa (65*)	27.38 MPa
(Aworinde et al., 2020a)	Melt casting	Compression test	circle	2.24	24.75 MPa	44.04 MPa
(Barkhad et al., 2020)	Injection molding	Compression test	circle	8.36	≈58 MPa	24.06 MPa

* = Infill Density

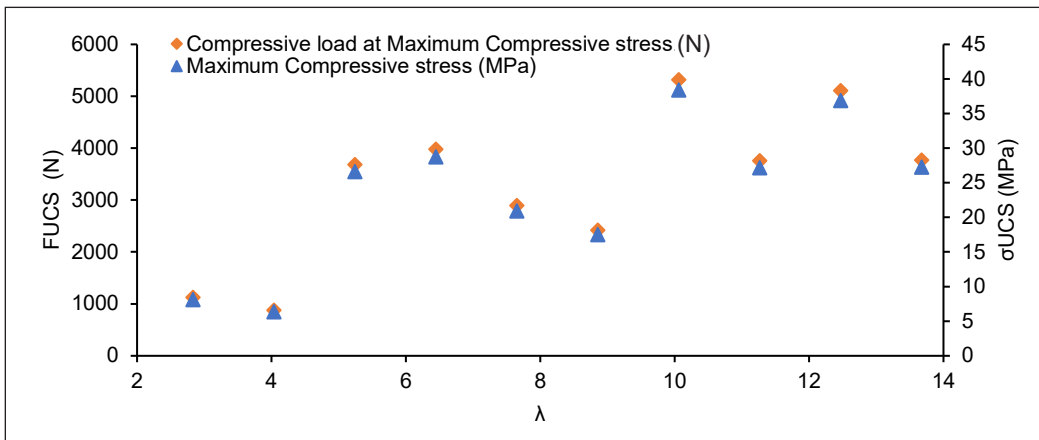


Figure 8. Dependence of compressive load and stress at UCS on slenderness ratio

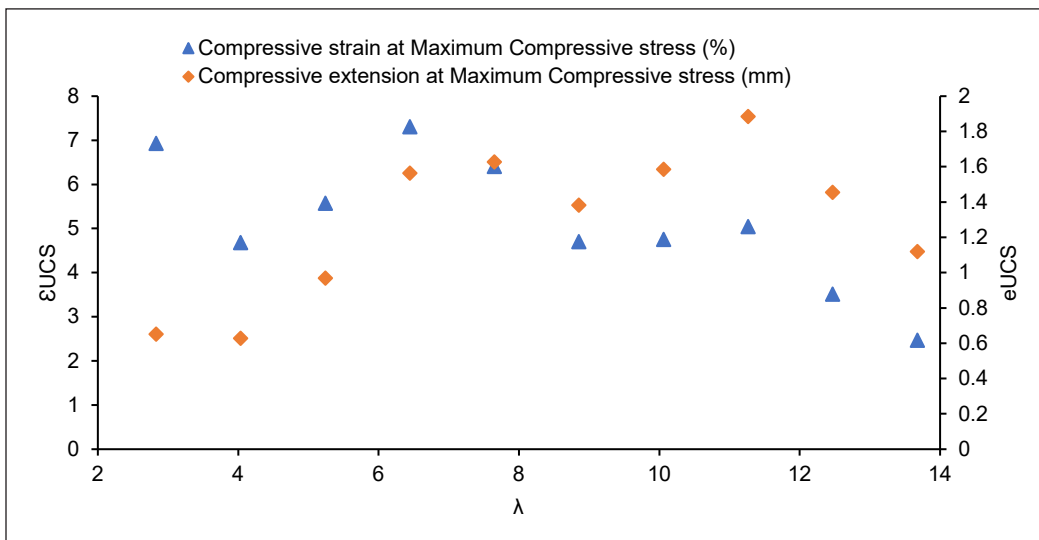


Figure 9. Pattern of compressive strain and extension at UCS as affected by slenderness ratio

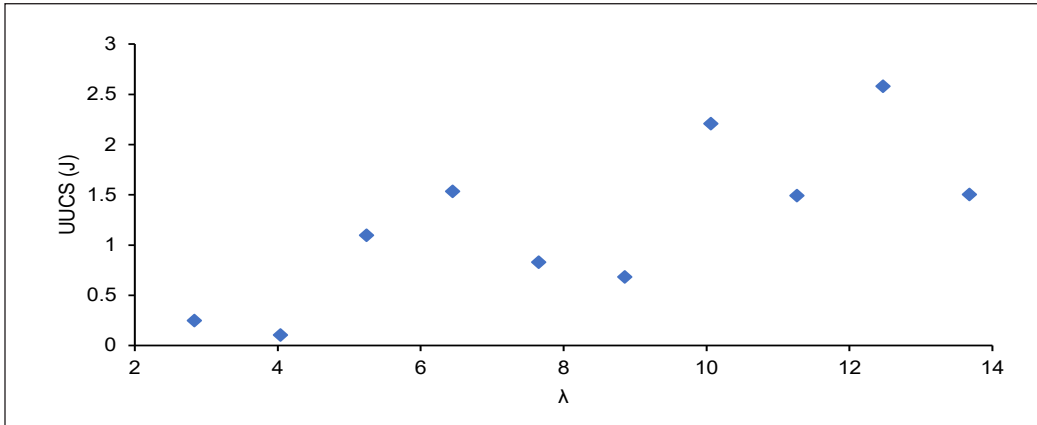


Figure 10. Energy at UCS as affected by the slenderness ratio

Mechanical Properties at Break

Five properties were evaluated at the break. Figure 11 shows the compressive load (F_b) and compressive stress (σ_b) with their regression models in Equations 11 and 12, respectively. In Figure 12, compressive strain (ε_b) and extension (e_b) are displayed, while Equations 13 and 14 model their data. Finally, the variation of energy at the break with λ is shown in Figure 13 with its corresponding regression model in Equation 15.

$$e_b = 0.0002\lambda^6 - 0.0085\lambda^5 + 0.1775\lambda^4 - 1.8896\lambda^3 + 10.696\lambda^2 - 30.002\lambda + 32.954 \quad (11)$$

$$F_b = 0.4872\lambda^6 - 25.653\lambda^5 + 536.83\lambda^4 - 5666.2\lambda^3 + 31469\lambda^2 - 85779\lambda + 89864 \quad (12)$$

$$\sigma_b = 0.0035\lambda^6 - 0.1852\lambda^5 + 3.8757\lambda^4 - 40.908\lambda^3 + 227.19\lambda^2 - 619.29\lambda + 648.78 \quad (13)$$

$$\varepsilon_b = 0.0008\lambda^6 - 0.0428\lambda^5 + 0.9093\lambda^4 - 9.8517\lambda^3 + 56.934\lambda^2 - 164.85\lambda + 191.35 \quad (14)$$

$$U_b = 0.0004\lambda^6 - 0.0198\lambda^5 + 0.4098\lambda^4 - 4.2711\lambda^3 + 23.469\lambda^2 - 63.636\lambda + 66.415 \quad (15)$$

The most relevant mechanical properties at fracture are usually ε_b , also known as ductility, and U_b . Also known as fracture energy, U_b has been researched to expand the application of PLA (Noori, 2019) as it directly reflects the crack resistance of any material (Xu et al., 2018). Also, several reports have been on the ductility of PLA, which detail the outcome of various fabrication methods and the attendant effects on ductility (Adeosun et al., 2016; Akpan et al., 2019; Aworinde et al., 2019). In consonance with various studies, PLA was brittle (Nagarajan et al., 2016; Song et al., 2014). A study reported the ductility of melt-cast PLA with $\lambda=2.24$ to be 13.71% (Aworinde et al., 2019), while Equation 14

gives the ductility of the same sample size as 17.61%. Table 2 shows that Equation 14 is 97.38% reliable with a coefficient of correlation of 0.8024, which implies a strong inverse relationship between sample size and ductility. As a result of this inverse relation, increased ductility leads to decreased strength (Lascano et al., 2019).

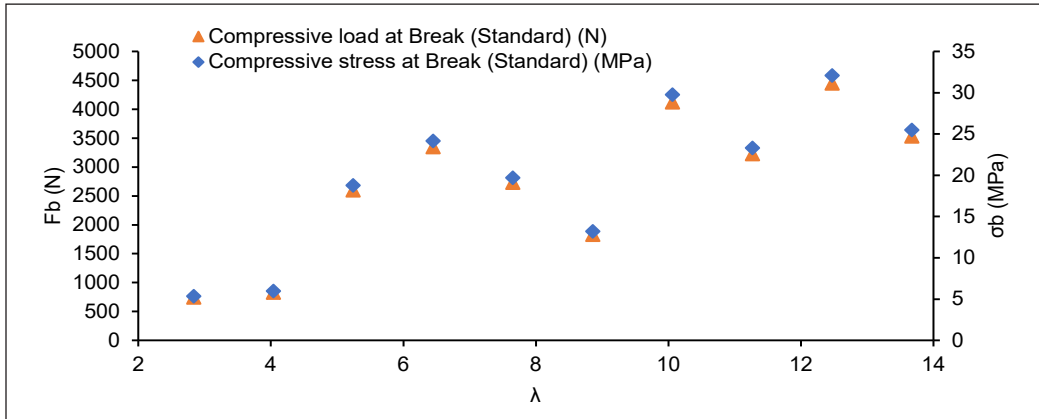


Figure 11. Compressive load and stress dependence on slenderness ratio

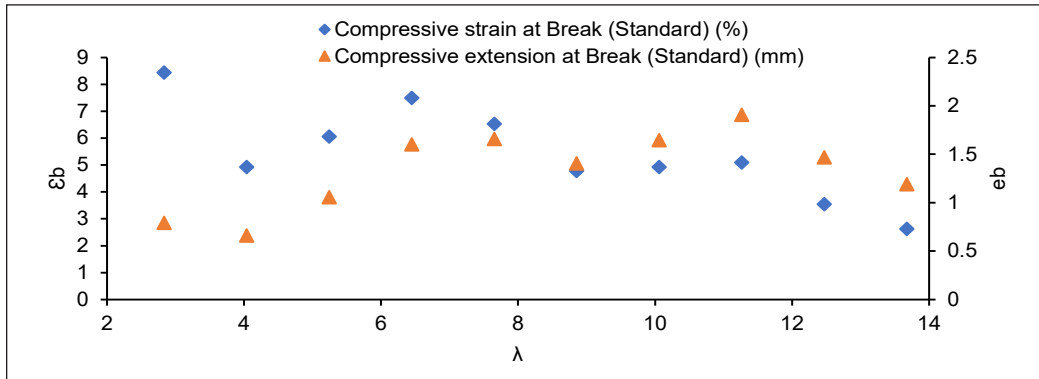


Figure 12. Compressive strain and extension at fracture as affected by slenderness ratio

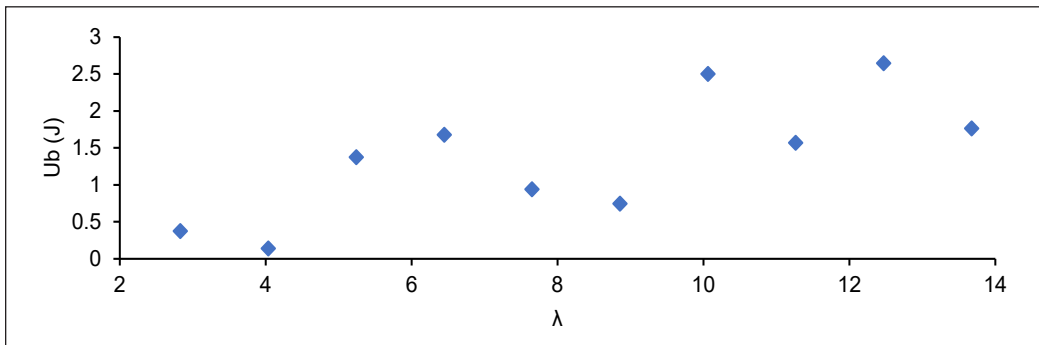


Figure 13. Energy at the break due to the growth in sample size

CONCLUSION

Regression models for predicting the mechanical properties of uniaxially compressed poly(lactic acid) samples have been developed in this study. The study was targeted toward fine-tuning experiments to manage time and resources effectively. Out of all the models developed, regression models for predicting the mass and the modulus of elasticity are the most accurate. The modulus of elasticity's regression model agrees well with the experimental results from the various relevant studies. The study revealed a strong correlational and causal relationship between the slenderness ratio of PLA and the mass of the sample. If the mass of PLA needed for an experiment can be reasonably predicted, the cost of the material can be estimated without any trial-and-error or experimental setup. Also, the study showed that the compressive modulus of elasticity of PLA could be predicted with about 92% accuracy with a known value of the slenderness ratio. In addition, the model for predicting the elastic modulus of PLA samples fabricated via melt casting (as shown in this study) can also predict the compressive modulus of PLA samples obtained via fused deposition modeling (FDM) and injection molding processes. Besides, the models developed in this work can be used to build software that predicts the mechanical properties of PLA obtainable from compression tests, which will help minimize the number of experimental runs, thereby cutting down on time, money, and material wastage.

ACKNOWLEDGEMENT

The authors wish to thank Covenant University for supporting the publication.

REFERENCES

- Abbas, T., Othman, F. M., & Ali, H. B. (2017). Effect of infill parameter on compression property in FDM Process. *International Journal of Engineering Research and Application*, 7(10), 16-19. <https://doi.org/10.9790/9622-0710021619>
- Abioye, A. A., & Obuckwe, C. C. (2020). Investigation of the biodegradation of low-density polyethylene-starch Bi-polymer blends. *Results in Engineering*, 5, Article 100090. <https://doi.org/10.1016/j.rineng.2019.100090>
- Adegbola, T. A., Agboola, O., & Fayomi, O. S. I. (2020). Review of polyacrylonitrile blends and application in manufacturing technology: Recycling and environmental impact. *Results in Engineering*, 7, Article 100144. <https://doi.org/10.1016/j.rineng.2020.100144>
- Adeosun, S. O., Aworinde, A. K., Diwe, I. V., & Olaleye, S. A. (2016). Mechanical and microstructural characteristics of rice husk reinforced polylactide nanocomposite. *The West Indian Journal of Engineering*, 39(2), 63-71.
- Akpan, E. I., Gbenedor, O. P., Igogori, E. A., Aworinde, A. K., Adeosun, S. O., & Olaleye, S. A. (2019). Electrospun porous bio-fibre mat based on polylactide/natural fibre particles. *Arab Journal of Basic and Applied Sciences*, 26(1), 225-235. <https://doi.org/10.1080/25765299.2019.1607995>

- Anderson, G., & Shenkar, N. (2021). Potential effects of biodegradable single-use items in the sea: Polylactic acid (PLA) and solitary ascidians. *Environmental Pollution*, 268, Article 115364. <https://doi.org/10.1016/j.envpol.2020.115364>
- Aworinde, A. K., Adeosun, S. O., Oyawale, F. A., Emagbetere, E., Ishola, F. A., Olatunji, O., Akinlabi, S. A., Oyedepo, S. O., Ajayi, O. O., & Akinlabi, E. T. (2020a). Comprehensive data on the mechanical properties and biodegradation profile of polylactide composites developed for hard tissue repairs. *Data in Brief*, 32, Article 106107. <https://doi.org/10.1016/j.dib.2020.106107>
- Aworinde, A. K., Adeosun, S. O., Oyawale, F. A., Akinlabi, E. T., & Akinlabi, S. A. (2020b). Comparative effects of organic and inorganic bio-fillers on the hydrophobicity of polylactic acid. *Results in Engineering*, 5, 1-3. <https://doi.org/10.1016/j.rineng.2020.100098>
- Aworinde, A. K., Adeosun, S. O., & Oyawale, F. A. (2020c). Mechanical properties of poly(L-Lactide)-based composites for hard tissue repairs. *International Journal of Innovative Technology and Exploring Engineering (IJITEE)*, 9(5), 2152-2155. <https://doi.org/10.35940/ijitee.C8501.039520>
- Aworinde, A. K., Adeosun, S. O., Oyawale, F. A., Akinlabi, E. T., & Akinlabi, S. A. (2019). The strength characteristics of chitosan- and titanium-poly(L-lactic) acid based composites. *Journal of Physics: Conference Series*, 1378(2), Article 022061. <https://doi.org/10.1088/1742-6596/1378/2/022061>
- Aworinde, A. K., Adeosun, S. O., Oyawale, F. A., Akinlabi, E. T., & Emagbetere, E. (2018, October 29 - November 1). Mechanical strength and biocompatibility properties of materials for bone internal fixation: A brief overview. In *Proceedings of the International Conference on Industrial Engineering and Operations Management* (pp. 2115-2126). Pretoria, South Africa.
- Aworinde, A. K., Taiwo, O. O., Adeosun, S. O., Akinlabi, E. T., Jonathan, H., Olayemi, O. A., & Joseph, O. O. (2021a). Biodegradation profiles of chitin, chitosan and titanium reinforced polylactide biocomposites as scaffolds in bone tissue engineering. *Arab Journal of Basic and Applied Sciences*, 28(1), 351-359. <https://doi.org/10.1080/25765299.2021.1971865>
- Aworinde, A. K., Emagbetere, E., Adeosun, S. O., & Akinlabi, E. T. (2021b). Polylactide and its composites on various scales of hardness. *Pertanika Journal of Science and Technology*, 29(2), 1313-1322. <https://doi.org/10.47836/pjst.29.2.34>
- Bakar, M. S. A., Cheang, P., & Khor, K. A. (2003). Mechanical properties of injection molded hydroxyapatite-polyetheretherketone biocomposites. *Composites Science and Technology*, 63, 421-425. [https://doi.org/10.1016/S0266-3538\(02\)00230-0](https://doi.org/10.1016/S0266-3538(02)00230-0)
- Barkhad, M. S., Abu-Jdayil, B., Mourad, A. H. I., & Iqbal, M. Z. (2020). Thermal insulation and mechanical properties of polylactic acid (PLA) at different processing conditions. *Polymers*, 12(9), 1-16. <https://doi.org/10.3390/POLYM12092091>
- Bouzouita, A., Notta-cuvier, D., Raquez, J., Lauro, F., & Dubois, P. (2017). Poly(lactic acid)-based materials for automotive applications. In M. L. Di Lorenzo & R. Androsch (Eds.), *Industrial Applications of Poly(lactic acid)* (pp. 177-219). Springer. <https://doi.org/10.1007/12>
- Brischetto, S., & Torre, R. (2020). Tensile and compressive behavior in the experimental tests for PLA specimens produced via fused deposition modelling technique. *Journal of Composites Science*, 4(3), Article 140. <https://doi.org/10.3390/jcs4030140>

- Cooper, T. A. (2013). Developments in bioplastic materials for packaging food, beverages and other fast-moving consumer goods. In N. Farmer (Ed.), *Trends in Packaging of Food, Beverages and Other Fast-Moving Consumer Goods (FMCG)* (pp. 58-107). Woodhead Publishing Limited. <https://doi.org/10.1533/9780857098979.108>
- Deepthi, S., Sundaram, M. N., Kadavan, J. D., & Jayakumar, R. (2016). Layered chitosan-collagen hydrogel/aligned PLLA nanofiber construct for flexor tendon regeneration. *Carbohydrate Polymers*, *153*, 492-500. <https://doi.org/10.1016/j.carbpol.2016.07.124>
- Fang, Q., & Hanna, M. A. (1999). Rheological properties of amorphous and semicrystalline polylactic acid polymers. *Industrial Crops and Products*, *10*(1), 47-53. [https://doi.org/10.1016/S0926-6690\(99\)00009-6](https://doi.org/10.1016/S0926-6690(99)00009-6)
- Farah, S., Anderson, D. G., & Langer, R. (2016). Physical and mechanical properties of PLA, and their functions in widespread applications - A comprehensive review. *Advanced Drug Delivery Reviews*, *107*, 367-392. <https://doi.org/10.1016/j.addr.2016.06.012>
- Ferrer, G. G., Liedmann, A., Niepel, M. S., Liu, Z. M., & Groth, T. (2018). Tailoring bulk and surface composition of polylactides for application in engineering of skeletal tissues. *Advances in Polymer Science*, *282*, 79-108. https://doi.org/10.1007/12_2017_26
- Gbenebor, O. P., Akpan, E. I., Atoba, R. A., Adeosun, S. O., Olaleye, S. A., Taiwo, O. O., Igoori, E. A., Alamu, O. B., & Aworinde, A. K. (2018). Development and performance analysis of high voltage generator for electrospinning of nano fibres. *Unilag Journal of Medicine, Science and Technology*, *6*(2), 45-58. <https://doi.org/10.1520/acem20170008>
- Gbenebor, O. P., Atoba, R. A., Akpan, E. I., Aworinde, A. K., Adeosun, S. O., & Olaleye, S. A. (2018). Study on polylactide-coconut fibre for biomedical applications. In *Minerals, Metals and Materials Series* (pp. 263-273). Springer. https://doi.org/10.1007/978-3-319-72526-0_24
- Hadasha, W., & Bezuidenhout, D. (2018). Poly(lactic acid) as biomaterial for cardiovascular devices and tissue engineering applications. *Advances in Polymer Science*, *282*, 51-77. https://doi.org/10.1007/12_2017_27
- Jamshidian, M., Tehrani, E. A., Imran, M., Jacquot, M., & Desobry, S. (2010). Poly-lactic acid: Production, applications, nanocomposites, and release studies. *Comprehensive Reviews in Food Science and Food Safety*, *9*(5), 552-571. <https://doi.org/10.1111/j.1541-4337.2010.00126.x>
- Lascano, D., Moraga, G., Ivorra-Martinez, J., Rojas-Lema, S., Torres-Giner, S., Balart, R., Boronat, T., & Quiles-Carrillo, L. (2019). Development of injection-molded polylactide pieces with high toughness by the addition of lactic acid oligomer and characterization of their shape memory behavior. *Polymers*, *11*(12), Article 2099. <https://doi.org/10.3390/polym11122099>
- Lawrence, S. S., Willett, J. L., & Carriere, C. J. (2001). Effect of moisture on the tensile properties of poly(hydroxy ester ether). *Polymer*, *42*(13), 5643-5650. [https://doi.org/10.1016/S0032-3861\(00\)00836-3](https://doi.org/10.1016/S0032-3861(00)00836-3)
- Li, J., Ding, J., Liu, T., Liu, J. F., Yan, L., & Chen, X. (2018). Poly(lactic acid) controlled drug delivery. *Advances in Polymer Science*, *282*, 109-138. https://doi.org/10.1007/12_2017_11
- Malinconico, M., Vink, E. T. H., & Cain, A. (2018). Applications of poly(lactic acid) in commodities and specialties. *Advances in Polymer Science*, *282*, 35-50. https://doi.org/10.1007/12_2017_29

- Mansour, G., Zoumaki, M., Tsongas, K., & Tzetzis, D. (2020). Starch-sandstone materials in the construction industry. *Results in Engineering*, 8, Article 100182. <https://doi.org/10.1016/j.rineng.2020.100182>
- Mofokeng, J. P., Luyt, A. S., Tábi, T., & Kovács, J. (2012). Comparison of injection moulded, natural fibre-reinforced composites with PP and PLA as matrices. *Journal of Thermoplastic Composite Materials*, 25(8), 927-948. <https://doi.org/10.1177/0892705711423291>
- Nagarajan, V., Mohanty, A. K., & Misra, M. (2016). Perspective on polylactic acid (PLA) based sustainable materials for durable applications: Focus on toughness and heat resistance. *ACS Sustainable Chemistry and Engineering*, 4(6), 2899-2916. <https://doi.org/10.1021/acssuschemeng.6b00321>
- Noori, H. (2019). Interlayer fracture energy of 3D-printed PLA material. *International Journal of Advanced Manufacturing Technology*, 101(5-8), 1959-1965. <https://doi.org/10.1007/s00170-018-3031-5>
- Oksiuta, Z., Jalbrzykowski, M., Mystkowska, J., Romanczuk, E., & Osiecki, T. (2000). Mechanical and thermal properties of polylactide (PLA) composites modified with Mg, Fe, and polyethylene (PE) additives. *Polymers*, 12, 1-14. <https://doi.org/10.3390/polym12122939>
- Rahimizadeh, A., Kalman, J., Henri, R., Fayazbakhsh, K., & Lessard, L. (2019). Recycled glass fiber composites from wind turbine waste for 3D printing feedstock: Effects of fiber content and interface on mechanical performance. *Materials*, 12(23), Article 3929. <https://doi.org/10.3390/MA12233929>
- Rahimizadeh, A., Tahir, M., Fayazbakhsh, K., & Lessard, L. (2020). Tensile properties and interfacial shear strength of recycled fibers from wind turbine waste. *Composites Part A: Applied Science and Manufacturing*, 131, Article 105786. <https://doi.org/10.1016/j.compositesa.2020.105786>
- Rodrigues, N., Benning, M., Ferreira, A. M., Dixon, L., & Dalgarno, K. (2016). Manufacture and characterisation of porous PLA scaffolds. *Procedia CIRP*, 49, 33-38. <https://doi.org/10.1016/j.procir.2015.07.025>
- Rokbani, H., & Aji, A. (2018). Rheological properties of poly(lactic acid) solutions added with metal oxide nanoparticles for electrospinning. *Journal of Polymers and the Environment*, 26(6), 2555-2565. <https://doi.org/10.1007/s10924-017-1155-6>
- Song, X., Chen, Y., Xu, Y., & Wang, C. (2014). Study on tough blends of polylactide and acrylic impact modifier. *BioResources*, 9(2), 1939-1952. <https://doi.org/10.15376/biores.9.2.1939-1952>
- Sun, B., Liu, H., Zhou, S., & Li, W. (2014). Evaluating the performance of polynomial regression method with different parameters during color characterization. *Mathematical Problems in Engineering*, 2014(3), 1-8. <https://doi.org/10.1155/2014/418651>
- Sundar, N., Stanley, S. J., Kumar, S. A., Keerthana, P., & Kumar, G. A. (2021). Development of dual purpose, industrially important PLA-PEG based coated abrasives and packaging materials. *Journal of Applied Polymer Science*, 138(21), 1-18. <https://doi.org/10.1002/app.50495>
- Tajitsu, Y. (2017). Poly(lactic acid) for sensing applications. In M. L. Di Lorenzo & R. Androsch (Eds.), *Industrial Applications of Poly(lactic acid)* (pp. 159-176). Springer. <https://doi.org/10.1007/12>
- Taleb, K., Pillin, I., Grohens, Y., & Saidi-Besbes, S. (2021). Polylactic acid/Gemini surfactant modified clay bio-nanocomposites: Morphological, thermal, mechanical and barrier properties. *International Journal of Biological Macromolecules*, 177, 505-516. <https://doi.org/10.1016/j.ijbiomac.2021.02.135>

- Tyler, B., Gullotti, D., Mangraviti, A., Utsuki, T., & Brem, H. (2016). Polylactic acid (PLA) controlled delivery carriers for biomedical applications. *Advanced Drug Delivery Reviews*, 107, 163-175. <https://doi.org/10.1016/j.addr.2016.06.018>
- Wang, Z., Wang, Y., Ito, Y., Zhang, P., & Chen, X. (2016). A comparative study on the *in vivo* degradation of poly(L-lactide) based composite implants for bone fracture fixation. *Scientific Report*, 6, 1-12. <https://doi.org/10.1038/srep20770>
- Williams, J. G., & Gamonpilas, C. (2008). Using the simple compression test to determine Young's modulus, Poisson's ratio and the Coulomb friction coefficient. *International Journal of Solids and Structures*, 45(16), 4448-4459. <https://doi.org/10.1016/j.ijsolstr.2008.03.023>
- Xu, P., Ma, J., Zhang, M., Ding, Y., & Meng, L. (2018). Fracture energy analysis of concrete considering the boundary effect of single-edge notched beams. *Advances in Civil Engineering*, 2018, Article 3067236. <https://doi.org/10.1155/2018/3067236>
- Ye, J. J., & Zhou, J. (2013). Minimizing the condition number to construct design points for polynomial regression models. *Society for Industrial and Applied Mathematics*, 23(1), 666-686. <https://doi.org/10.1137/110850268>



Assessment of the Grid Safety Values for Substation Grounding Grid Design Parameters in Vertical Two-Layer Soil Structure

Navinesshani Permal^{1*}, Miszaina Osman¹, Azrul Mohd Ariffin¹ and Mohd Zainal Abidin Ab Kadir²

¹Institute of Power Engineering, Universiti Tenaga Nasional, 43000 Kajang, Selangor, Malaysia

²Centre for Electromagnetic and Lightning Protection Research (CELP), Advanced Lightning, Power, and Energy Research Centre (ALPER), Universiti Putra Malaysia, 43400 UPM, Serdang, Selangor, Malaysia

ABSTRACT

Typically, the impact of the structure of vertically layered soil on the grounding behavior is not considered while designing a substation grounding system. Therefore, it will result in poor grounding designs due to computed inaccurate grid safety values. Besides, no comparative analysis of the grounding design parameters' impact on the grounding grid systems' behavior and protection level between vertical and horizontal two-layer soil structures is presently available. Computing and analyzing the grounding behavior of apparent soil resistivity installed in a vertical two-layer soil structure is more challenging than in a horizontal two-layer soil. There are many other parameters to consider, such as the distance 'a' between the test electrodes and the angle 'β' between the perpendicular line to the soil boundary and the location of the test electrodes. One of the important findings of the assessment shows that the influence of vertically layered soil on grid impedance, step, and touch voltages of a grounding system is insignificant compared to a homogeneous and horizontally layered soil structure. The current flow is affected by an entire grounding grid placed in a specified layer of soil with a specific resistivity for horizontally layered

soil. In contrast, soil boundaries separate a grounding grid with various resistivities for vertically layered soil. The outcome of this work is crucial in helping the engineers to understand the behavior of grounding systems in diverse soil conditions and tropical climates.

Keywords: Grounding behavior, horizontal soil layers, substation, tropical climate, vertical soil layers

ARTICLE INFO

Article history:

Received: 22 October 2021

Accepted: 04 January 2022

Published: 20 April 2022

DOI: <https://doi.org/10.47836/pjst.30.3.03>

E-mail addresses:

nesshani@yahoo.com (Navinesshani Permal)

miszaina@uniten.edu.my (Miszaina Osman)

azrula@uniten.edu.my (Azrul Mohd Ariffin)

mzk@upm.edu.my (Mohd Zainal Abidin Ab Kadir)

* Corresponding author

INTRODUCTION

The soil characteristics in which the grid will be buried must be reviewed and evaluated when planning an efficient and safe grounding grid system. The substation grounding grid configuration is vital in ensuring the grounding system's safety, which is highly dependent on the soil characteristics in which the grounding system will be installed (IEEE 80, 2013; Gursu & Cevdet, 2019; Moradi, 2020; Nikolovski et al., 2016; Pavel et al., 2020; Sing et al., 2013; Vyas & Jamnani, 2012). Soil resistivity varies greatly depending on the earth's geological structure (Coelho et al., 2018; Nasserredine et al., 2010; Ma & Dawalibi, 2009; Tung & Lim, 2017; Vycital et al., 2017; Yang & Zou, 2020). Due to the variations in soil conditions at each substation, the grounding system design is made with caution to provide the maximum level of protection. Vertical and horizontal soil layers influence the installation site for the grounding system. For example, a grid located in a vertically layered soil structure might have a different safety level than one positioned in a horizontally layered soil structure. When a grounding system is designed based on vertically-layered soil, the grounding system's performance is governed by the proportion of grounding systems in low- and high-resistivity soils. In contrast, if a grounding grid ought to be built in a horizontally layered soil structure, the height and soil resistivity of the top layer will impact the performance of a grounding system as a whole (Mokhtari et al., 2016b; Nahman & Paunovic, 2006; Takahashi & Kawase, 1990). Despite knowing that the soil characteristics in which a grounding grid is installed are non-homogeneous in general, the soil is frequently considered homogeneous due to the challenges of grounding systems assessment in non-homogeneous soil. Thus, the calculation of ground resistance and surface potentials will be inaccurate due to this assumption.

Most substation grounding system safety evaluations and design procedures employ a homogenous soil environment as an input to calculate safety values (grid impedance, step, and touch voltages). However, despite significant studies into grounding behavior in homogenous soil environments (Mokhtari et al., 2016a; Nikolovski et al., 2016; Pavel et al., 2020) and horizontal two-layer soil with varying soil properties such as the upper layer height (Zaini & Ghoneim, 2012) and the soil reflection factors (K) (Gouda et al., 2019; Tong et al., 2019) and varying grid design parameters such as the analysis of single horizontal grounding conductor (de Araujo et al., 2019; Arnautovski-Toseva et al., 2007), the mesh count of a grounding system (Unde & Kushare, 2012), vertical rod length (Anggoro et al., 2018), there is presently no comprehensive study available that assess the grounding behavior in vertical two-layer soil under the impact of design parameters. Furthermore, no simultaneous comparisons or discussions between horizontal and vertical two-layer soil structures are available. The desired study would show the difference in behavior and protection levels of a grounding system when placed in different soil structures and if existing grounding system design procedures are appropriate for designing a grounding grid installed in vertically stratified soil.

Figure 1 depicts the vertical soil structure, while Equation 1 depicts its apparent resistivity. The first-layer soil resistivity is represented as ρ_1 (Ωm), the soil resistivity of the second layer is shown as ρ_2 (Ωm), the distance between 4 electrodes is represented as 'a' (m), K is the reflection factor between soil layer 1 and 2, the normal distance between the first electrode and boundary between soil layers 1 and 2 is represented as 'd' and ' β ' is the angle between the straight line where 4 electrodes are located and perpendicular line to the boundary between soil layer 1 and 2. The varying electrode spacing 'a', the distance from the two-layer soil interface 'd' and the angle ' β ' between a perpendicular line to the soil border and the line where 4 electrodes are positioned have different effects on the apparent resistivity which have been presented in Nayel (2014) and Nayel et al. (2012).

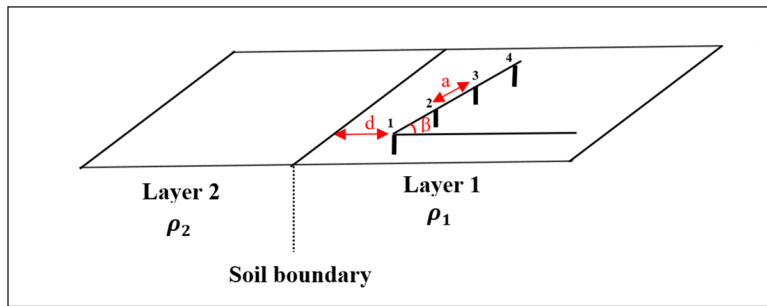


Figure 1. Vertical two-layer soil structure

$$\rho_a = a\rho_1 \left(\frac{1}{a} + \frac{K}{\sqrt{4d^2 + 4da \cos \beta + a^2}} + \frac{K}{\sqrt{4(d+3a \cos \beta)(d+2a \cos \beta) + a^2}} - \frac{K}{\sqrt{4d^2 + 8da \cos \beta + 4a^2}} - \frac{K}{\sqrt{4(d+3a \cos \beta)(d+a \cos \beta) + 4a^2}} \right) \quad [1]$$

Where

ρ_1 = Layer 1/right-layer soil resistivity ($\Omega\text{.m}$)

ρ_2 = Layer 2/left-layer soil resistivity ($\Omega\text{.m}$)

K = reflection factor between soil layers 1 and 2

a = distance between 4 electrodes Wenner's test (m)

d = the normal distance between the first electrode and boundary between soil layers 1 and 2

β = angle between line where 4 electrodes are located and perpendicular line to the boundary between soil layers 1 and 2.

A detailed discussion on the impact of the soil resistivity in vertically-layered soil on the grounding behavior will be given in the Results and Discussions section. The low soil resistivity is assumed to be 100 $\Omega\text{.m}$ on layer 2 and 1000 $\Omega\text{.m}$ for high resistivity on layer 1 of the soil structure.

INPUT PARAMETERS AND METHODOLOGY

Design Parameters for Substation Grounding Grids

An analysis of grounding grid performance for different grid designs was conducted at a power frequency response of 50 Hz with a centrally energized fault current of 30 kA, as shown in Figure 2. The fault current is maintained constant in the middle of the grid because the maximal Ground Potential Rise (GPR) and grounding resistance at the current injection location at the grid's center are significantly lower than at the grounding grid's periphery. The inductance of grounding conductors will prevent the fault current from dispersing in other directions if the fault current is injected into a corner. However, the grounding conductors will be effective for a modest inductive effect when the current injection location is in the middle. Figure 2 shows the methodology of the grounding design analysis process.

The grounding behavior analysis was conducted using grid sizes ranging from 30 m × 30 m to 130 m × 130 m. The dimensions chosen for the grounding grid are based on assumptions intended for research purposes, but the fundamental grid size is based on the Tenaga Nasional Berhad substation. The grounding grid size is based on a 132/33/11 kV Main Intake Substation as specified in the Tenaga Nasional Berhad Substation Design Manual (Asset Management Department, 2012; TNB, 2019), which was throughout the analysis apart from the analysis on the grid sizes. Then, the analysis was continued by varying the mesh sizes from 5 m × 5 m to 21.7 m × 21.7 m. A 130 m × 130 m grounding grid with a mesh size of 10 m × 10 m is shown in Figure 2. The mesh size of 5 m × 5 m is made up of equally spaced 27 horizontal and 27 vertical grid conductors; a 10 m × 10

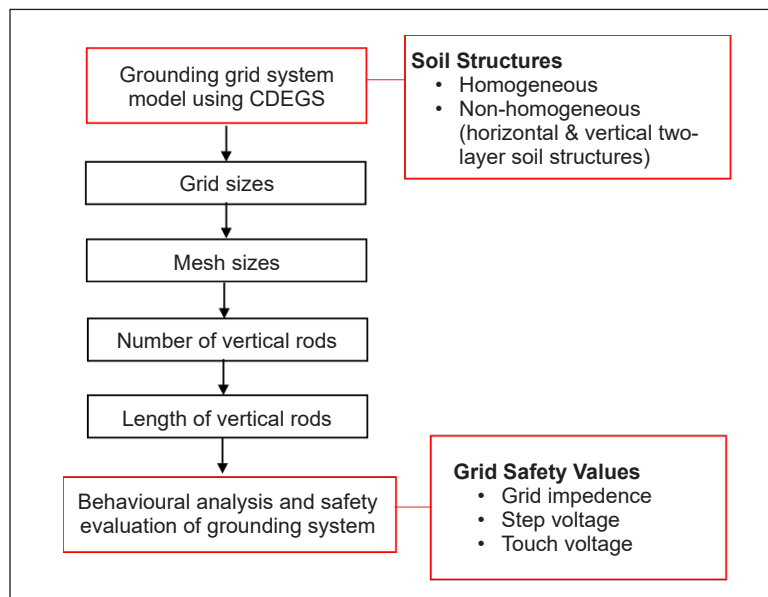


Figure 2. Methodology of grounding system design analysis

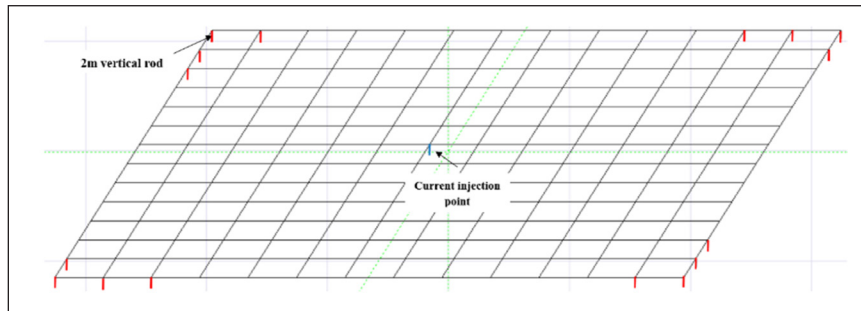


Figure 3. The grounding grid comprises 16 vertical rods attached

m has 14 horizontal and 14 vertical grid conductors; a $16.3 \text{ m} \times 16.3 \text{ m}$ has 9 horizontal and 9 vertical grid conductors while mesh size of $21.7 \text{ m} \times 21.7 \text{ m}$ has 7 horizontal and 7 vertical grid conductors.

The analysis is followed by varying the number of vertical rods from 4 rods to 16 rods. At the grid's perimeter, the vertical rods connecting to the grid conductors are varied from 4 to 16 rods once the grounding mesh size analysis is completed. The rods are placed on the grid's perimeter throughout the analysis because most fault current is discharged through the bottom section of vertical rods, making them efficient in controlling the high current densities that occur in grounding conductors at the perimeter. In addition, due to the increasing shielding effect between both grounding conductors and vertical rods when the vertical rods are positioned in the middle of the grid, the impact of the potential gradient of the vertical rod placed on the grid's perimeter has less influence than the rod placed in the middle. Figure 3 shows 16 rods placed at the grounding grid's perimeter. Each rod is 2 meters in length.

The analysis of the different lengths of vertical rods was then continued. The vertical rod helps in discharging more current into the earth than the grid conductor for a given length of grid conductor. The lengths of 4 rods placed at the grounding grid's edges range from 2 to 6 meters. The summary of the grounding design process with grids buried 0.5 m into the soil is shown in Table 1. Each design is classified into different case numbers.

Table 1

Analysis of grounding design parameters with constant grid depth at 0.5 m

Design Parameters	Case number
Grounding grid size	
30 m × 30 m	A1
50 m × 50 m	A2
130 m × 130 m	A3
Grounding mesh size	
5 m × 5 m	B1
10 m × 10 m	B2
16.3 m × 16.3 m	B3
21.7 m × 21.7 m	B4
Number of electrodes	
4 rods	C1
8 rods	C2
13 rods	C3
16 rods	C4
Length of electrodes	
2 m	D1
4 m	D2
6 m	D3

Computation of Soil Boundary in Vertical Soil Structure

The proportions of the grounding grid in a vertically layered soil utilized in CDEGS simulation are shown in Figure 4. The percentage of soil ratio (%) indicates the proportions of the grounding grid placed on the soil border's left side (layer 2) compared to the right side (layer 1). The soil ratios are ranged between 25%, 50 %, and 75%. The soil ratio of 25% refers to the location of the majority of the grounding grid in high resistivity soil, with just 25% of the grounding grid in low resistivity soil. A 50% soil ratio means that the soil resistivity on both layers 1 and 2 of the grounding grid is equal; with low resistivity (layer 2) and high resistivity (layer 1), and a 75% soil ratio means that most of the grid on the right is located in low resistivity soil. The Trace Angle (θ), between the soil boundary with the positive direction of the x-axis of the coordinate system, is assumed at 90°.

The grounding system's performance and safety level computation in the vertical soil layer is not straightforward compared to the horizontal soil layer. Since grounding behavior is modeled and analyzed in CDEGS, three main parameters, as indicated in Figure 5 (red box), must be addressed: the Trace Angle (θ), X Reference, and Y Reference. The test electrodes in the vertical soil layer are assumed to parallel the vertical soil boundary. Therefore, the Trace Angle (θ) in CDEGS computation and the 'β' value from the vertical soil layer Equation 1 is presumed to be similar.

The X and Y References, which define the soil boundary in the vertical soil model, require some computations depending on the grounding grid dimensions, as in Figure 6.

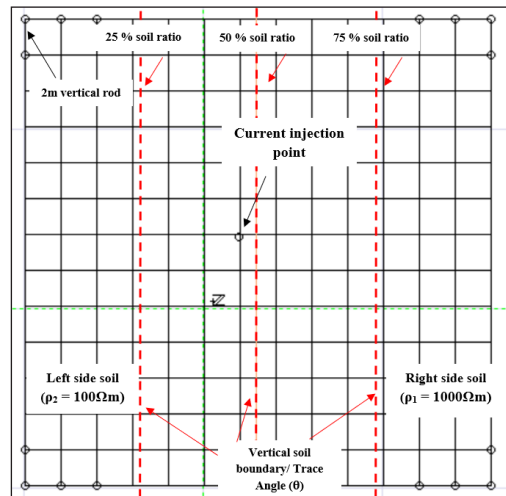


Figure 5. Vertical soil model in CDEGS

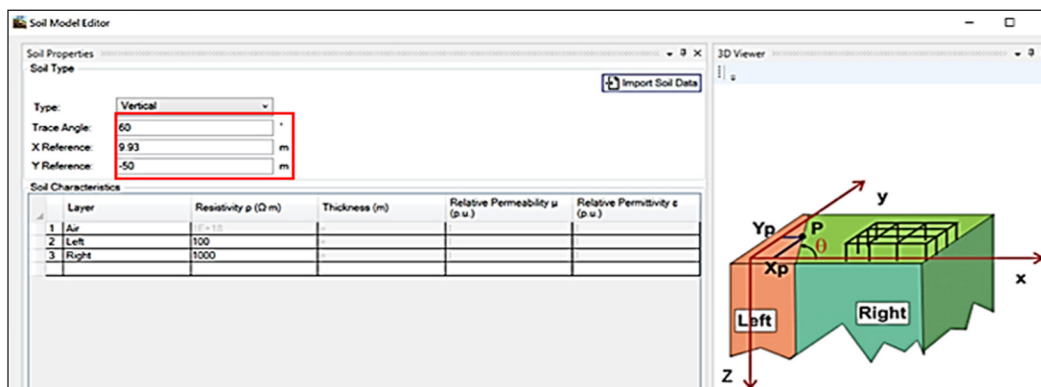


Figure 4. The proportion of grounding grid in vertically layered soil

The dark red letters represent the known quantities (given by the user): (I) c and d are the edges of the grounding grid, (II) k is the ratio of the left area (S_1) to the right area (S_2) and (III) θ is the Trace Angle assuming the grounding grid is parallel to the x-axis. Again, there are two equations, Equations 2 and 3, with two unknowns.

$$S_1 = \frac{1}{2} \times (2a + c \cot\theta) \times c \quad [2]$$

$$S_2 = \frac{1}{2} \times (2b - c \cot\theta) \times c \quad [3]$$

$$a + b = d \quad [4]$$

$$\frac{S_1}{S_2} = k \quad [5]$$

Putting the Equations 4 and 5 in matrix form:

$$\begin{bmatrix} 1 & 1 \\ 2 & -2k \end{bmatrix} \begin{bmatrix} a \\ b \end{bmatrix} = \begin{bmatrix} d \\ -c \times \cot\theta \times (1 + k) \end{bmatrix} \quad [6]$$

Where

θ = Trace Angle ($^\circ$)

' c ' and ' d ' = edges of the grid (m)

S_1 = left area (m^2)

S_2 = right area (m^2)

' k ' = ratio of the left area to the right area

The ratio of ' k ' is 25/75 for 25 % soil ratio, 50/50 for 50 % soil ratio, and 75/25 for 75 % soil ratio in this paper. By solving the 2 by 2 system from Equation 6 for the Trace Angle, θ , the ratio of the left area to the right area ' k ' and edges of the grid ' c ' and ' d ', one of the points belonging to the boundary line by solving ' a ' or ' b ' is (X Reference, Y Reference) = (-50 + a , -50) m. The coordinate of the bottom-left corner of the grid is (-50, -50). Then, the x-coordinate is shifted by adding ' a '.

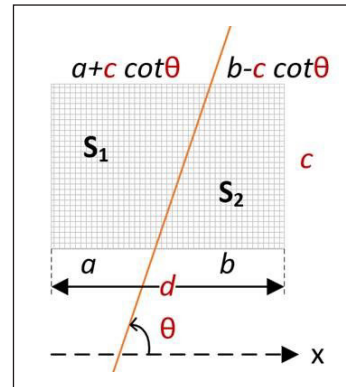


Figure 6. Soil proportion of two-layer vertical soil

RESULTS AND DISCUSSIONS

Comparison of Percentage Difference in Grid Impedance in Different Soil Structures for Various Design Parameters

This section represents the percentage difference in grid impedance for various design parameters of grounding, such as the sizes of grounding grids, the mesh sizes of a grid, the length and number of vertical rods in a grounding system placed in different soil structures. Since there are many results in analyzing the grounding behavior, only a few examples

were presented in this study. An example of the percentage difference calculation in grid impedance of 30 m × 30 m grid size, which is placed in low resistive homogeneous soil and low resistive upper layer of horizontal two-layer soil structure, is shown in Table 2. For the horizontal two-layer soil model, the top layer soil with the resistivity of 1000 Ω.m and the lower layer resistivity of 100 Ω.m with infinite depth is denoted as Top (1000 Ω.m), while the top layer soil with the resistivity of 100 Ω.m and the lower layer resistivity of 1000 Ω.m with infinite depth is denoted as Top (100 Ω.m). The top layer thickness of a horizontal two-layer soil structure is 5 m.

Table 2

Grid impedance for grounding design parameters in homogeneous and horizontal two-layer soil structure

Grid size	Homogeneous soil		Horizontal two-layer soil	
	Uni (100 Ωm)	Uni (1000 Ωm)	Top (100 Ωm)	Top (1000 Ωm)
30 m × 30 m	1.66 Ω	16.55 Ω	5.33 Ω	7.82 Ω
50 m × 50 m	0.96 Ω	9.60 Ω	3.92 Ω	3.51 Ω
130 m × 130 m	0.35 Ω	3.52 Ω	2.06 Ω	0.80 Ω

$$\begin{aligned} \text{Grid impedance percentage difference (\%)} &= [(1.66 \Omega - 5.33 \Omega) / (5.33 \Omega)] \times 100 \\ &= 68.95 \% \end{aligned}$$

Figure 7 presents the percentage difference in grid impedance when a grid is positioned in a low resistive homogenous soil (Uni (100 Ωm)) and high resistive homogenous soil (Uni (1000 Ωm)), and vertical two-layer soil structure with various soil ratios (25%, 50%, and 75%).

Figure 8 presents the percentage difference in impedance when the grid is positioned in a low resistive top soil layer of a horizontal two-layer soil structure, denoted as Top (100 Ωm), and the high resistive top soil layer denoted as Top (1000 Ωm), and vertical two-layer soil structures with different soil ratios.

Figures 7 and 8 demonstrate that the impedance value for different soil conditions varies significantly. It indicates the potential for errors if the soil structure of which a grounding grid will be installed is presumed as homogeneous. Figure 9 shows the impedances differences for varied vertical rods lengths placed in various soil structures. The findings demonstrate that the length of vertical rods has a major impact on the performance of a grounding system, especially in horizontally layered soil. The vertical rods of 2 m and 4 m are located before the soil border, while the 6 m vertical rods have passed through the soil boundary with different soil resistivity from the top soil layer's resistivity, which is absent in homogenous and vertical two-layer soil structure. As a result, when compared to homogenous and vertically layered soil structures, a significant difference can be seen, particularly for 6 m vertical rods at the high resistive bottom layer.

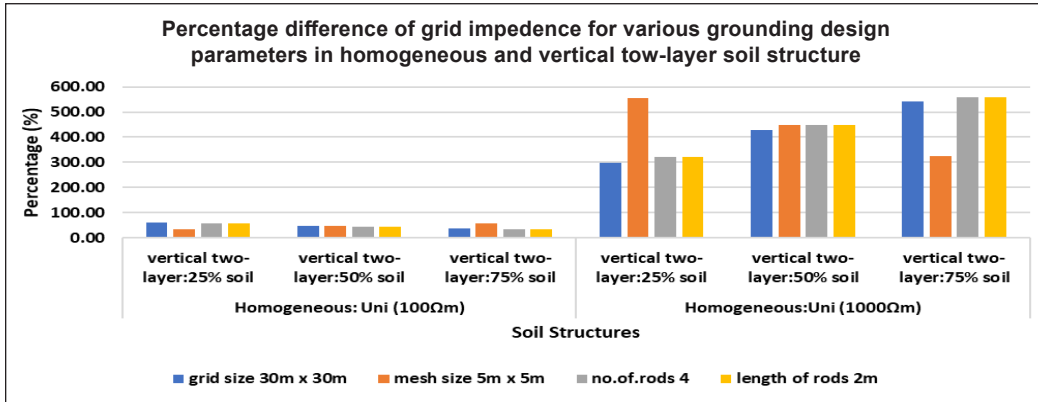


Figure 7. Percentage difference of grid impedance for grounding design parameters in homogeneous and vertical two-layer soil structure

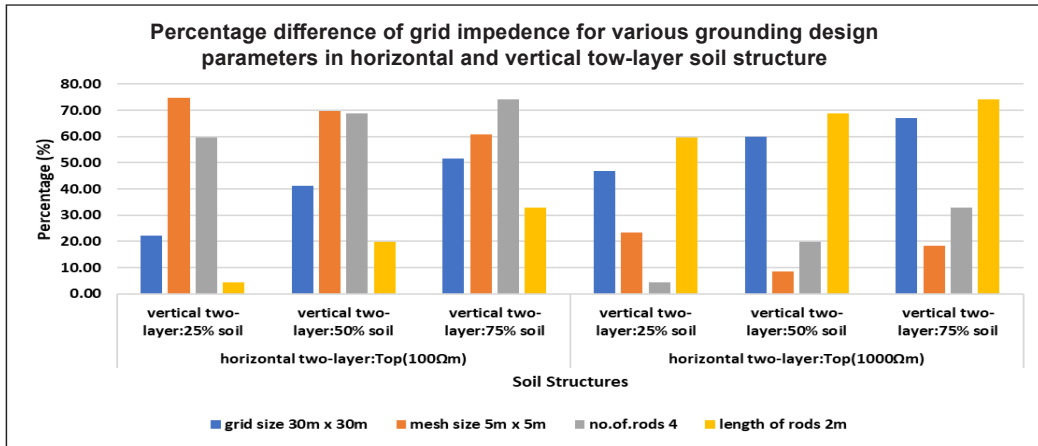


Figure 8. Percentage difference of grid impedance for grounding design parameters in horizontal and vertical two-layer soil structure

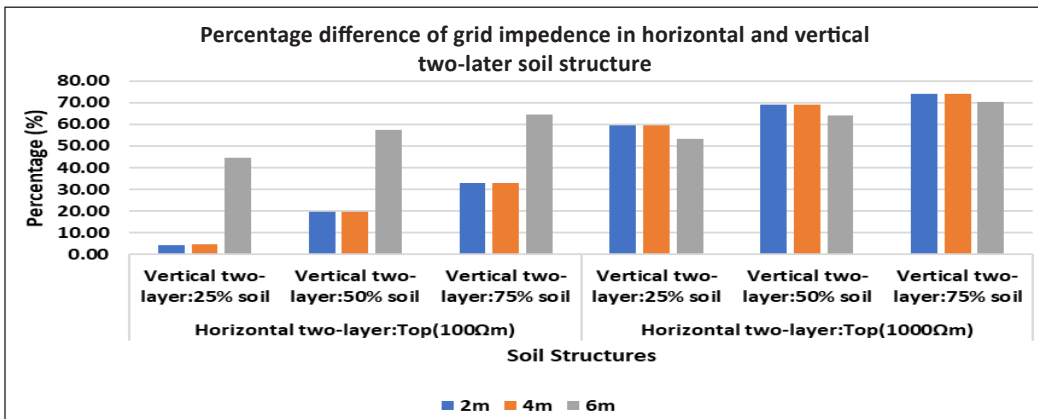
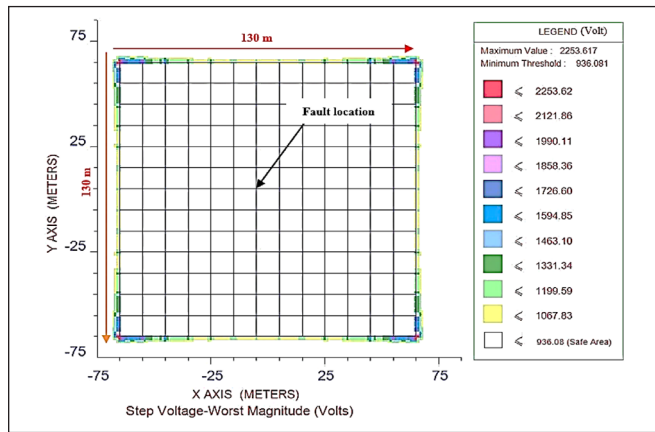


Figure 9. Percentage difference of grid impedance for different vertical rod lengths in horizontal and vertical two-layer soil structure

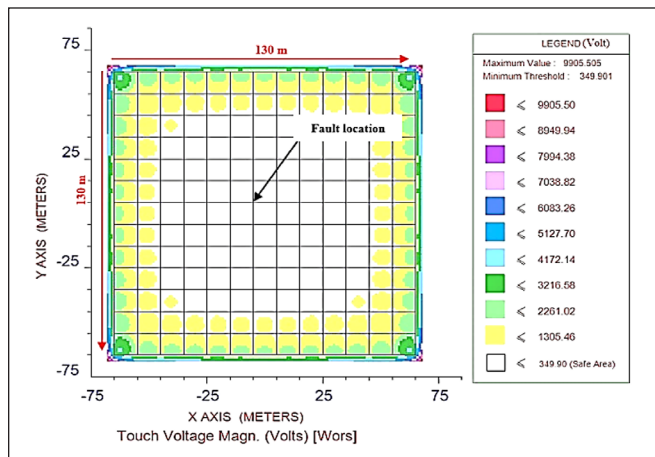
Grounding Behavior in Vertical Two-Layer Soil: Effects of Grid Design Parameters

Based on horizontal two-layer soil data given in Permal et al. (2021), comparisons of grounding behavior between vertical and horizontal two-layer soil structures are presented. The safety threshold for vertically layered two-layer soil is 1120 V and 399.2 V for step and touch voltage correspondingly for all soil ratios (25%, 50%, and 75%) calculated based on equations available in IEEE 80 (2013) for a bodyweight of 50 kg. According to IEEE 80 (2013) and the Malaysian Utility standard (Asset Management Department, 2012), the grid impedance threshold value is 1Ω .

Figures 10(a) and 10(b) illustrate the examples of step and touch voltages using Current Distribution, Electromagnetic Fields, Grounding, and Soil Structure Analysis (CDEGS) simulation software as reported by Permal et al. (2021) for the horizontal two-layer soil model. Figures 10(a) and 10(b) illustrate that the highest voltages are found to be at the



(a)



(b)

Figure 10. Grounding grid safety voltages for a 130 m × 130 m grid. (a) step voltage (b) touch voltage (Permal et al., 2021)

edges of the profile boundaries of the grounding grid. The propagations of fault current injected into the grid to the nearby conductors result in this condition. Being bare, the conductors will allow the current to leak into the soil. By doing so, the conductors will acquire a potential rise. The current dispersion between the middle and corner grounding conductors is significantly different, resulting in a substantially greater step and voltage at the edges than in the middle of the grid (He et al., 2013). A grounding grid is regarded as reliable and protected in this study if all the values of grid impedance, step, and touch voltages fall under the safety threshold mentioned before.

The Number of Vertical Rods. This section examines the effect of varying numbers of vertical rods placed on a 130 m × 130 m grounding grid with a 10 m × 10 m mesh size. Two meters of a varying number of vertical rods are positioned around the grid's periphery. The graphs of grid impedance, step, and touch voltage reduction percentages as the number of vertical rods rise from 4 to 16 in various soil ratios are shown in Figures 11 to 13. When the rods are added, safety values' magnitudes reduce for all soil ratios, similar to grounding behavior in different mesh sizes.

The percentage of impedance reduction in Figure 11 as the vertical rods increases from 4 rods to 16 rods (C1 to C4) is around 0.31% for grounding placed in 25%, 0.56% for 50% soil ratio, and 0.78% for 75% soil ratios. Compared to the horizontal two-layer soil, the overall impedance percentage reduction is much lower in the vertical soil layer when vertical rods are added (less than 1%). In contrast, the step voltage reduction in horizontal two-layer soil is reduced by about 21%, as seen in Figure 14. Similar to grid sizes, this may be attributable to the impact of two different soil resistivities on a grounding grid in the vertical soil layer, while an entire grounding grid in the horizontal soil layer is influenced by a top soil layer with a specific resistivity.

For step voltages in Figure 12, the reduction percentage as the vertical rods increases from 4 rods to 16 rods (C1 to C4) is the highest at 75% soil ratio and lowest at 25% ratio with 5.0% and 2.8% of reduction, respectively. For touch voltage in Figure 13, the reduction percentage as vertical rods increases from 4 rods to 16 rods (C1 to C4) is 3.7% for 75% soil ratio, 2.5% for 50% soil ratio, and 1.5% for 25% soil ratio.

As previously stated, the number of vertical rods differs depending on the soil ratios. Therefore, increasing the number of rods by adding 8 rods on the left of the grid on low resistive soil, as shown in Figure 15, helps lower the grid impedance. For example, adding the number of rods (adding 8 rods, a total of 16 vertical rods) on layer 1 (low resistive soil) for a 25% soil ratio, while at layer 2, the number of rods remains 8 rods, helps in reducing the grid impedance further by dissipating more current into the soil.

The percentage of impedance reduction in Figure 16 shows that although most of the grid is placed in a high resistivity soil, a significant reduction from the initial total of 16

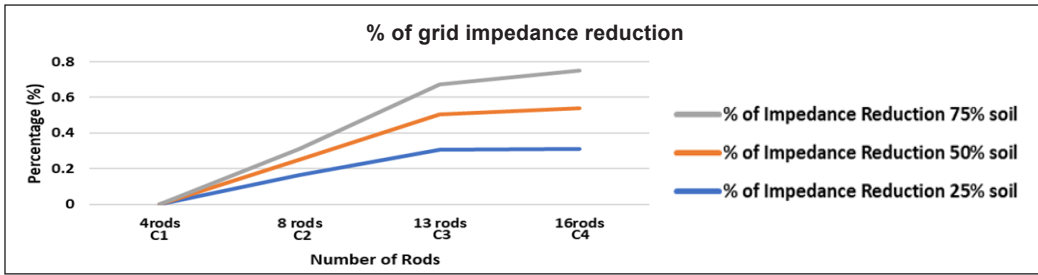


Figure 11. Percentage of grid impedance reduction for an increasing number of vertical rods in the vertical soil layer

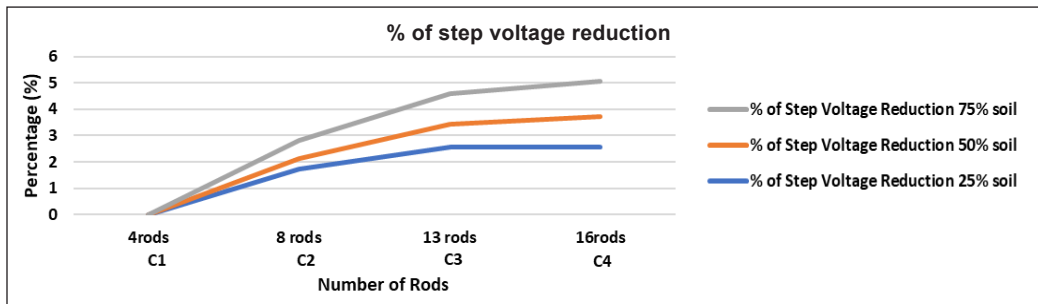


Figure 12. Percentage of step voltage reduction for an increasing number of vertical rods in the vertical soil layer

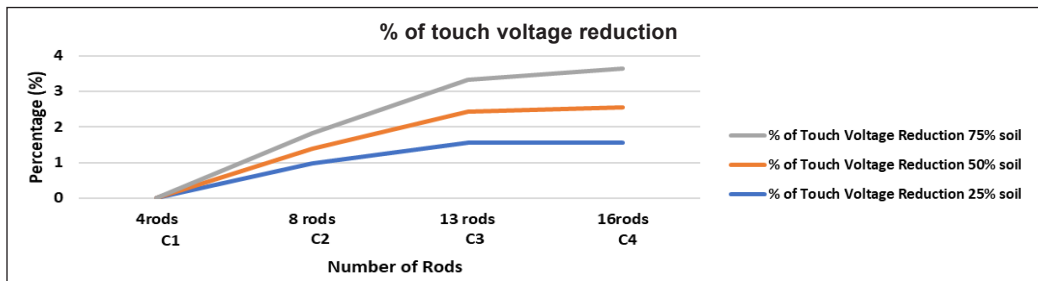


Figure 13. Percentage of touch voltage reduction for an increasing number of vertical rods in the vertical soil layer

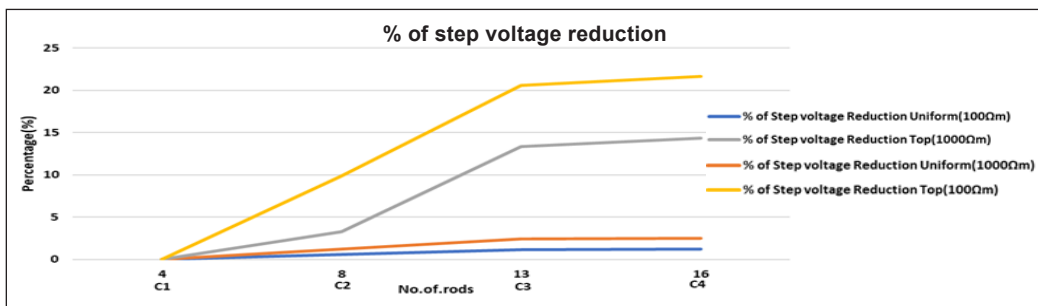


Figure 14. Percentage reduction for step voltage as the number of vertical rods rises in horizontal two-layer soil (Permal et al., 2021)

rods can be seen by adding 8 rods to the low resistivity soil in a 25% soil ratio compared to 50% and 75% soil ratio. It demonstrates that adding more vertical rods in low resistive soil would help in reducing the grid impedance.

Given that the magnitudes of the safety parameters (impedance, step, and touch voltages) drop as the number of vertical rods rises, a grounding system must have a sufficient number of vertical rods to enhance the safety of a grounding system. For example, Table 3 shows that a grounding system with 16 vertical rods is not safe in all vertical two-layer soil structure soil ratios. However, an additional 8 rods on layer 1, which is on the low resistive soil layer, helped enhance the grounding system’s safety. Although Figure 16 shows that the percentage of impedance reduction is the highest for grounding placed in a 25% soil ratio, however, it is not sufficient to improve the grounding’s safety compared to a 75% soil ratio.

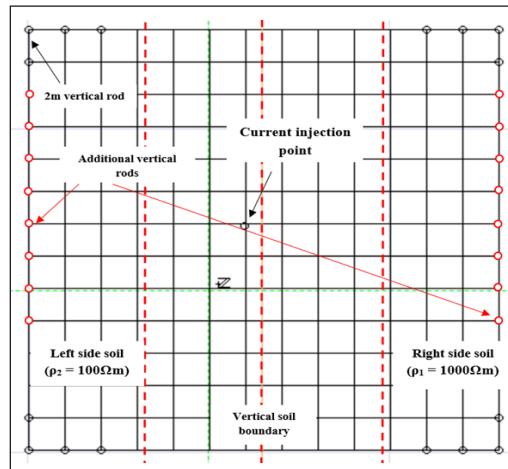


Figure 15. Illustrations of the additional number of rods on layer 1 and layer 2 of vertically layered soil

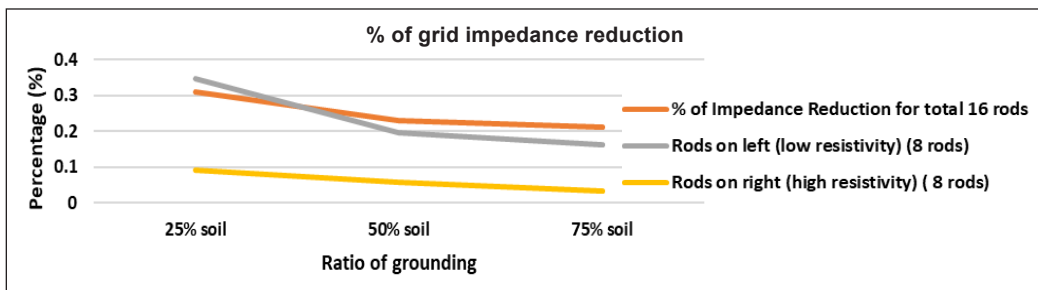


Figure 16. Percentage of grid impedance reduction for adding more vertical rods to the main grounding grid in the vertical soil layer

Table 3
A grounding system’s safety assessment for the varying number of vertical rods

Number of vertical rods	The ratio of vertical two-layer soil		
	25 % soil	50 % soil	75 % soil
4 rods	Unsafe	Unsafe	Unsafe
8 rods	Unsafe	Unsafe	Unsafe
13 rods	Unsafe	Unsafe	Unsafe
16 rods	Unsafe	Unsafe	Unsafe
8 rods (left)	Unsafe	Unsafe	Safe
8 rods (right)	Unsafe	Unsafe	Unsafe

Length of Vertical Rods. This section investigates the effect of the varying length of four vertical rods placed on a 130 m × 130 m grounding grid with a mesh size of 10 m × 10 m. Figures 17 to 19 depict a graph of grid impedance, step, and contact voltage reduction percentages as the length of vertical rods increases from 2 m to 6 m in various soil ratios. Similar to the number of rods, the magnitudes of safety parameters in the vertical soil layer continue to lower for all soil ratios when the length of rods is increased. This behavior contrasts with the grounding grid behavior in a horizontally layered soil structure. As

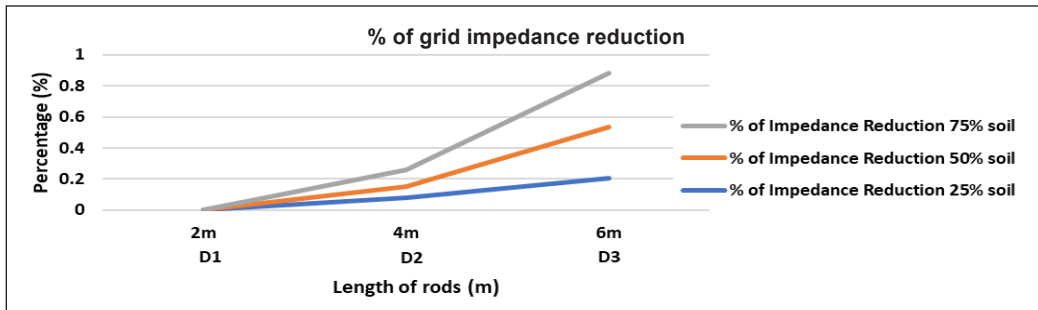


Figure 17. Percentage of grid impedance reduction for increasing length of 4 vertical rods in the vertical soil layer

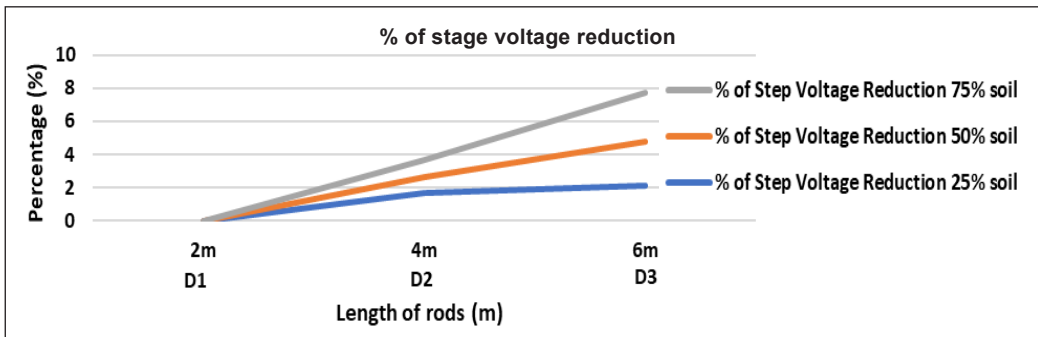


Figure 18. Percentage of step voltage reduction for increasing length of 4 vertical rods in the vertical soil layer

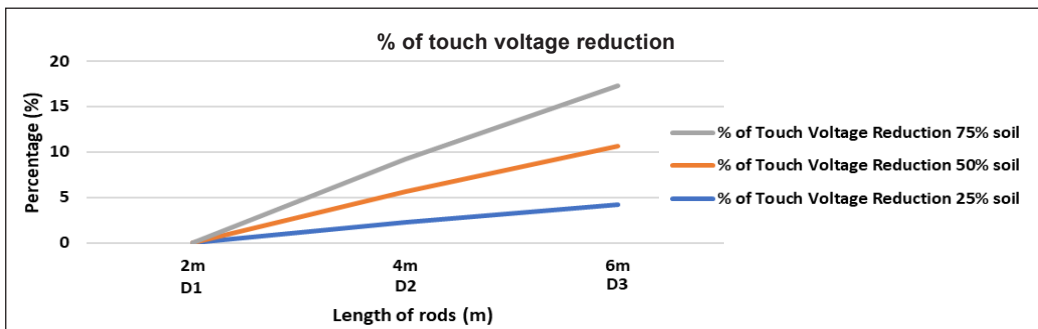


Figure 19. Percentage of touch voltage reduction for increasing length of 4 vertical rods in the vertical soil layer

illustrated in Figure 20, grid impedance may increase when the vertical rods cross beyond the two-layer soil border with a high resistive bottom layer for a low resistive top layer of the horizontal two-layer soil.

The percentage of impedance reduction in Figure 17 as the length of vertical rods increases from 2 m to 6 m (D1 to D3) is around 0.13% for grounding placed in 25% soil ratio, and 0.38% for 50% soil ratio, and 0.63% for 75% soil ratios.

For step voltages in Figure 18, the percentage of reduction as the length of vertical rods increases from 2 m to 6 m (D1 to D3) is the highest at 75% soil ratio and lowest at 25% ratio with 7.84% and 2.24% of reduction respectively. For the 75% soil ratio, most of the grid is placed in a low resistive soil layer, allowing more current to disperse into the soil and lowering the safety parameters, and vice versa for the grid placed in the 25% soil ratio.

For touch voltage in Figure 19, the highest percentage of reduction as the length of vertical rods increases from 2 m to 6 m (D1 to D3) can be seen at 16.09% for a 75% soil ratio and the lowest at around 3.66% of reduction for 25% soil ratios.

Similar to the number of rods, the magnitudes of safety parameters in the vertical soil layer continue to lower for all soil ratios when the length of rods is increased. This behavior is similar to grounding behavior in homogeneous soil but in contrast to the grounding grid behavior in a horizontally layered soil structure. For horizontal two-layer soil with a low resistive top layer, as illustrated in Figure 20, there is an increase in grid impedance, step, and touch voltages when the length of rods passes through a soil boundary with a high resistive bottom soil layer.

The difference in behavior between horizontal and vertical two-layer soil structures is caused by the effect of two distinct soil resistivity on each vertical rod in the horizontal soil layer. In contrast, a single soil layer influences every vertical rod in the vertical soil layer with a specific resistivity (either left or right). Therefore, adding the length of vertical rods as shown in Figure 21 (adding 8 m, 14 m length of each vertical rod) on layer 2 for low resistive soil in 25% soil ratio, and each rod length on layer 1 remains at 6 m, helps in reducing the grid impedance further, as shown in Figure 22.

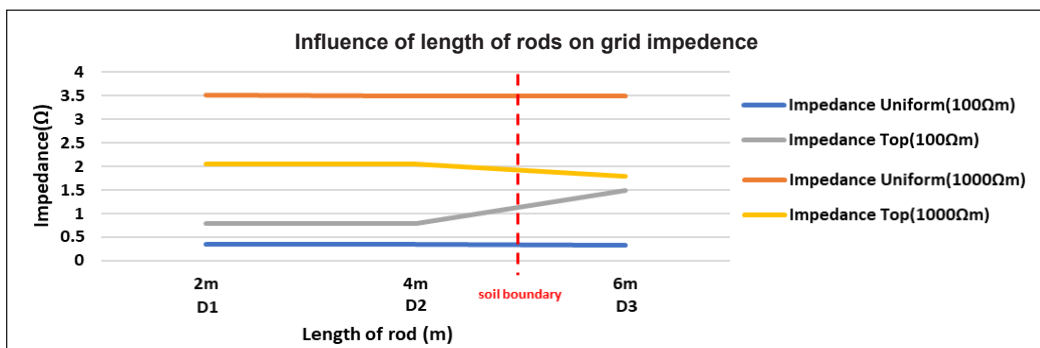


Figure 20. Grid impedance graph for increasing vertical rod length in horizontal two-layer soil (Permal et al., 2021)

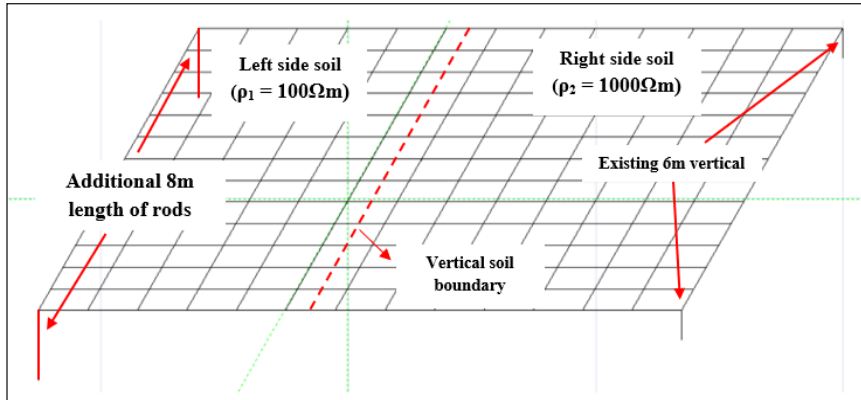


Figure 21. Illustrations of the additional length of rods on layer 2 and layer 1 of vertically layered soil

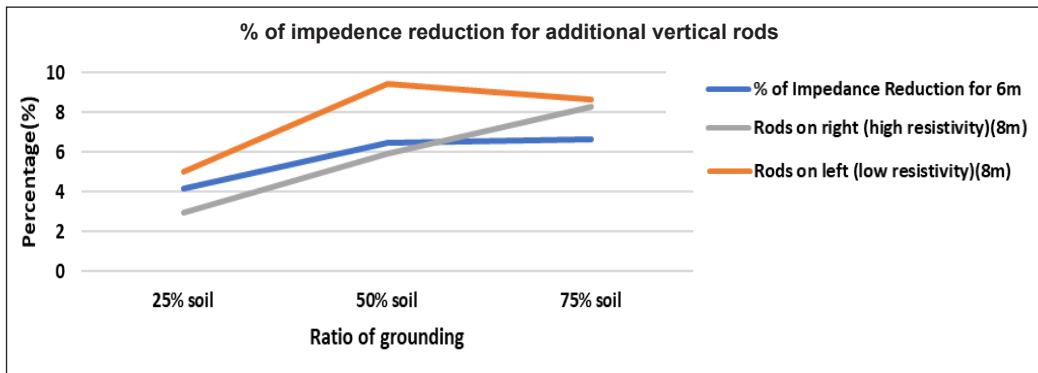


Figure 22. Percentage of grid impedance reduction for extending the length of vertical rods to the primary grounding grid in the vertical soil layer

Longer rods are only effective in less resistive soil layers. Therefore, more current will spread over a longer rod, reducing the grid safety values and securing the grounding system, as shown in Table 4. Increasing the length of rods on low-resistance soil also helps to dissipate more current into the soil, lowering grounding grid impedance in all soil ratios. Thus, it is important to make a vertical rod sufficiently long to disperse more current

Table 4
A grounding system's safety assessment for different vertical rods' lengths

Length of rods	The ratio of vertical two-layer soil		
	25 % soil	50 %	75 %
2 m	Unsafe	Unsafe	Unsafe
4 m	Unsafe	Unsafe	Unsafe
6 m	Unsafe	Unsafe	Unsafe
8 m (left)	Unsafe	Unsafe	Safe
8 m (right)	Unsafe	Unsafe	Unsafe

through a longer rod and help enhance the grid's safety. However, it can also be seen that the grounding system is still not safe even when the length of vertical rods is added in the 25% and 50% soil ratio. It can be resolved by further increasing the length of rods or adding more numbers of vertical rods on the low resistive soil layer.

Grounding Grid Size. The magnitudes of impedance, touch, and step voltage for various grid sizes in varied soil ratios of vertically layered soil are presented. The grid impedance, step, and touch voltages in Figures 23 to 25 show that all groundings behave the same way, decreasing magnitudes as the grid size expands. The results show that the grid safety parameters (impedance, step, and touch voltage) in 25%, 50%, and 75% soil ratios of vertical two-layer soil are higher than a high resistive top layer of horizontal two-layer soil. It is because the current density at the grid's perimeter is high, which is caused by the flow of the current outward from a high resistive soil layer. On the other hand, the grid safety parameters are lower in vertical two-layer soil than in a high resistive top layer of horizontal two-layer soil because of the current dispersion into the lower resistivity layer.

Figure 23 shows the impedance reduction of 61% from 50 m × 50 m to 130 m × 130 m grid size (A2 and A3) in a 75% soil ratio of a vertical two-layer soil is lower compared to the percentage of impedance reduction of 77% of the same grounding grid placed in a horizontal soil layer with a high soil resistivity top layer as can be seen for grid impedance in Figure 26 (Permal et al., 2021). The difference in the percentage of impedance reduction in horizontal and vertical two-layer soil shows that the soil structure impacts the grounding system's behavior. For horizontally layered soil, an entire grounding grid is positioned in a specific layer with a specific resistivity (normally the first layer of soil). A grounding grid is divided by a soil boundary with different resistivities for vertically two-layered soil.

Figure 24 shows that the step reduction percentage from 50 m × 50 m to 130 m × 130 m grid size (A2 and A3) in a 75% soil ratio is higher than grid placed in 25% and 50% soil ratios of a vertical two-layer soil. Figure 25 shows the touch reduction percentage of

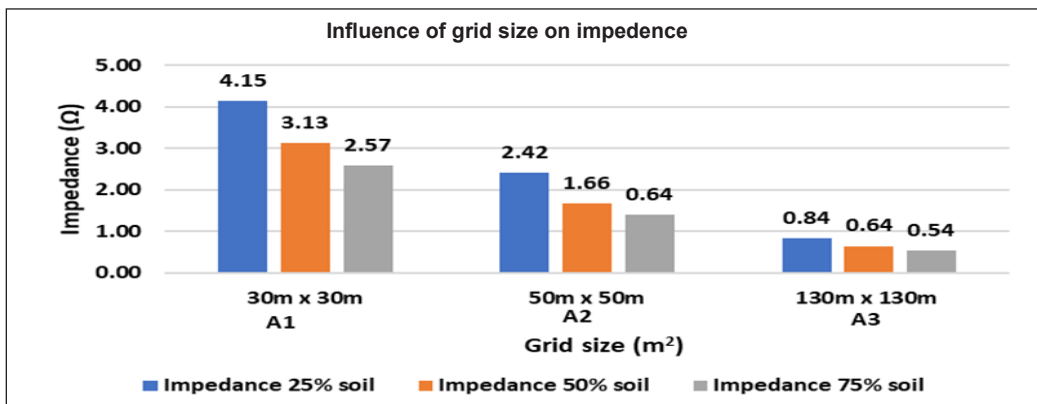


Figure 23. Grid impedance in the vertical soil layer for increasing grid size

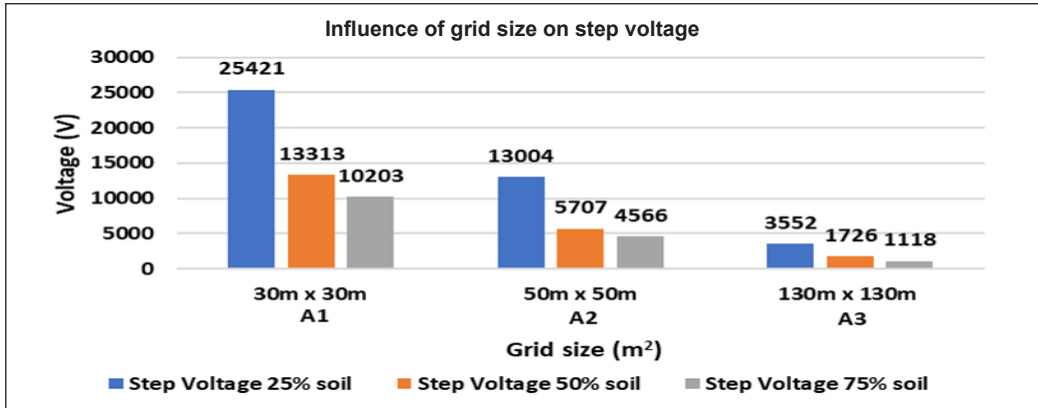


Figure 24. Step voltages in the vertical soil layer for increasing grid size

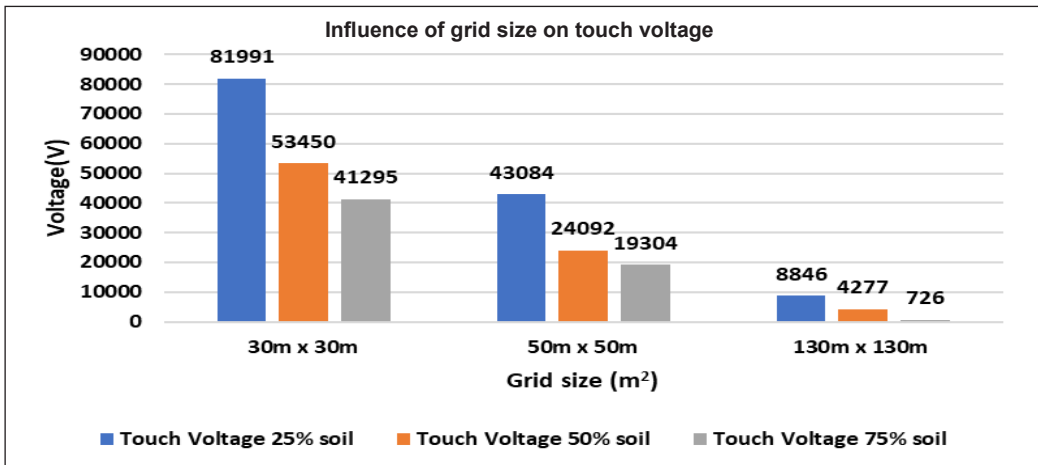


Figure 25. Touch voltages in the vertical soil layer for increasing grid size

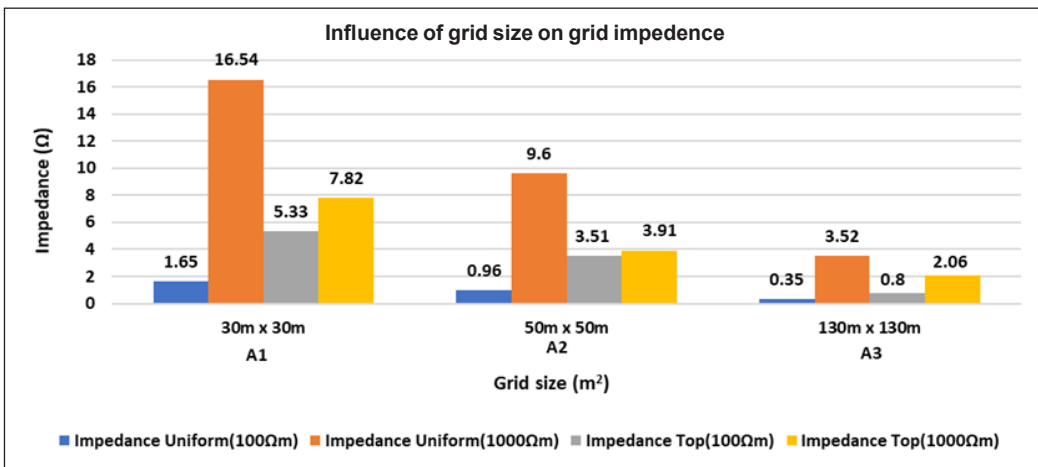


Figure 26. Grid impedance for increasing grid sizes in horizontal two-layer soil (Permal et al., 2021)

Table 5
A grounding system's safety assessment for varied grid sizes

Grid size	The ratio of vertical two-layer soil		
	25 % soil	50 % soil	75 % soil
30 m × 30 m	Unsafe	Unsafe	Unsafe
50 m × 50 m	Unsafe	Unsafe	Unsafe
130 m × 130 m	Unsafe	Unsafe	Unsafe

47% from 50 m × 50 m to 130 m × 130 m grid size (A2 and A3) in a 75% soil ratio of a vertical two-layer soil.

When placed in a vertical soil structure with varied soil ratios, the grounding grid's size affects its behavior and safety. As known, a grounding system must be large enough to keep the impedance and safety voltages (step and touch) within the allowable limit. Even when a substantial portion of a grounding grid is placed in a low resistive, vertically layered two-layer structure, a large grid does not ensure safety. Table 5 illustrates the grounding system's overall safety evaluation, which meets all three acceptable levels (impedance, step, and touch voltages). When placed in varied soil ratios, it can be observed that all three grid sizes are unsafe. Further adjustments such as decreasing the mesh size or connecting vertical rods to the primary grounding grid are necessary to produce a safe grounding grid.

Grounding Mesh Size. The impact of varying mesh sizes of a 130 m × 130 m grounding grid will be discussed in this part. Figures 27 to 29 demonstrate a similar behavior pattern for varying mesh sizes to grounding behavior in varying grid sizes. Figure 30 shows how the impedance, touch, and step voltage increase as the mesh size increases in horizontally layered soil. The percentage of impedance increment in Figure 27 as the mesh size increases from 5 m × 5 m to 16.3 m × 16.3 m (B1 to B3) is around 3.8 % for grounding placed in 25%, 4.2% for 50% soil ratio, and 4.7% for 75% soil ratios.

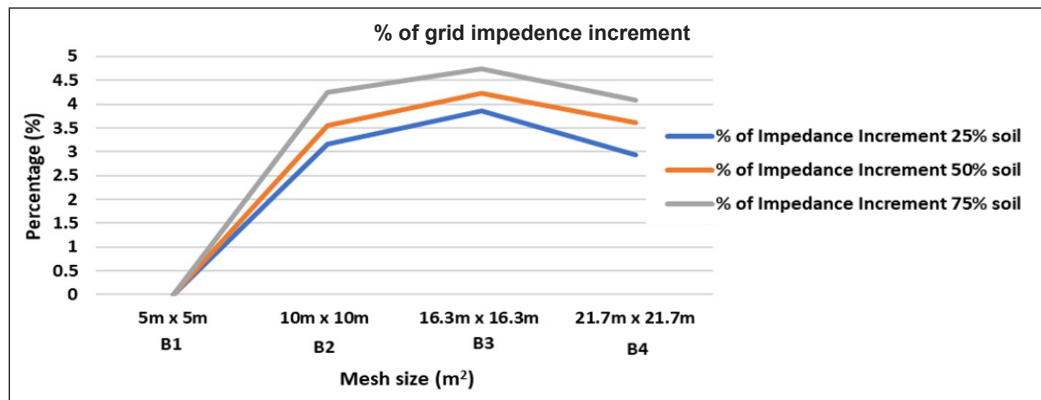


Figure 27. Percentage of grid impedance increment for increasing mesh sizes in the vertical soil layer

The percentage of step voltage increment in Figure 28 as the mesh size increases from 5 m × 5 m to 16.3 m × 16.3 m (B1 to B3) is around 3.22% for grounding placed in 25%, 8.7% for 50% soil ratio, and 11.01% for 75% soil ratios.

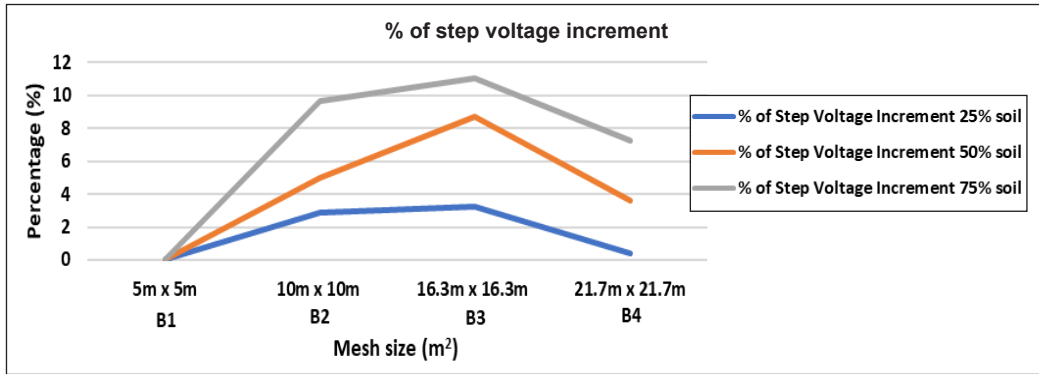


Figure 28. Percentage of step voltage increment for increasing mesh sizes in the vertical soil layer

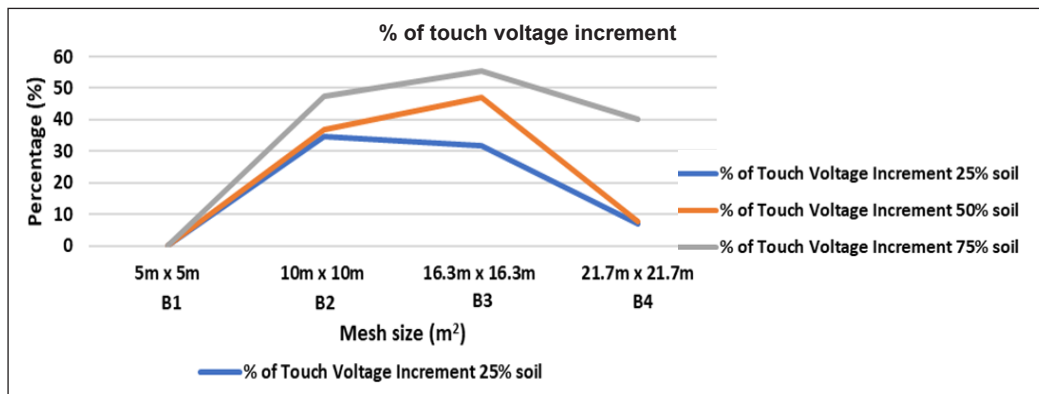


Figure 29. Percentage of touch voltage increment for increasing mesh sizes in the vertical soil layer

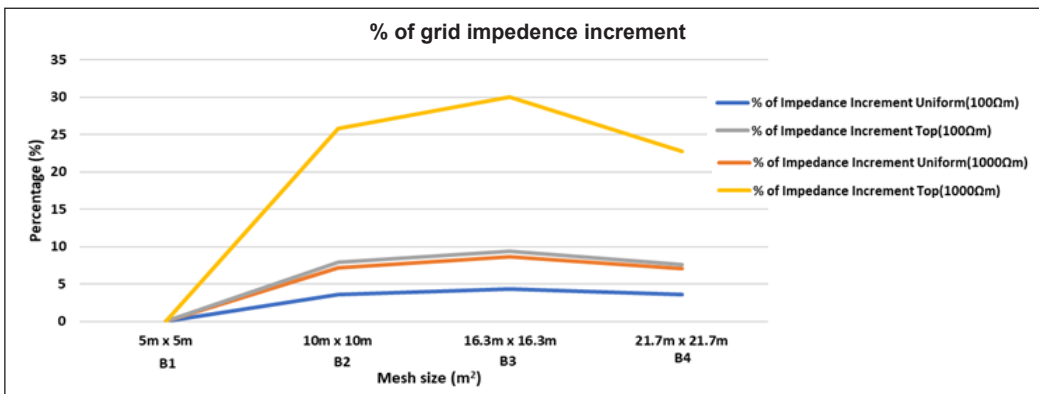


Figure 30. Percentage of grid impedance increment as mesh sizes increase in horizontal two-layer soil (Permal et al., 2021)

The percentage of touch voltage increment in Figure 29 as the mesh size increases from 5 m × 5 m to 16.3 m × 16.3 m (B1 to B3) is around 31.74% for grounding placed in 25%, 47% for 50% soil ratio, and 55.59% for 75% soil ratios.

Identical to grid size, the highest percentage of impedance, step, and touch voltages increment overall could be found for grounding in a 75% soil ratio. Conversely, the lowest increment percentage could be seen at a 25% soil ratio for increasing mesh sizes because of the proportion of the grid in different soil layers.

The percentage of grid impedance increment from 10 m × 10 m to 16.3 m × 16.3 m mesh sizes are small for all soil ratios and begins to drop at 16.3 m × 16.3 m mesh size, similar to horizontal two-layer. It indicates that the mesh size has attained its effective size. Varying the grid's mesh size has little influence on behavior when installed in soil structures with varying ratios of soil resistivity. However, it has an impact on the grounding's safety level.

Regardless of soil conditions with different resistivity values, the impedances for all analyzed mesh sizes are under the allowed value. Nevertheless, the step and touch voltages vary for every soil environment. For example, Table 6 indicates only a 130 m × 130 m grounding grid with a 5 m × 5 m mesh size is considered safe in 75% soil ratio but unsafe when placed in 25% and 50% soil ratios of a vertical two-layer soil. As a result, more changes are needed to ensure that the grounding is secure in all soil ratios.

Table 6
A grounding system's safety assessment for different mesh sizes

Mesh size	The ratio of vertical two-layer soil		
	25 % soil	50 % soil	75 % soil
5 m × 5 m	Unsafe	Unsafe	Safe
10 m × 10 m	Unsafe	Unsafe	Unsafe
16.3 m × 16.3 m	Unsafe	Unsafe	Unsafe
21.7 m × 21.7 m	Unsafe	Unsafe	Unsafe

The Effect of Surface Layer Resistivity on the Grounding Behavior. Figure 31 shows the influence of surface resistivity on the allowable step voltages in different soil ratios. The allowable step voltage is calculated using the IEEE 80 (2013) equation. Similar to homogeneous soil, the findings show that the allowable limits of safety voltages increase as surface resistivity increases. Without surface resistivity, step and touch voltage values will be lower. A comparison of allowable step voltage between high resistive and low resistive ρ_1 is shown in Table 7. The allowable step voltage in vertical two-layer soil trailed the allowable step voltage in the high resistive homogeneous soil when the ρ_1 value at layer 1 of the vertical two-layer soil is highly resistive. This grounding behavior can be related to the influence of high soil resistivity, ρ_1 (1000 Ω .m), on layer 1 from the apparent soil resistivity in Equation 1.

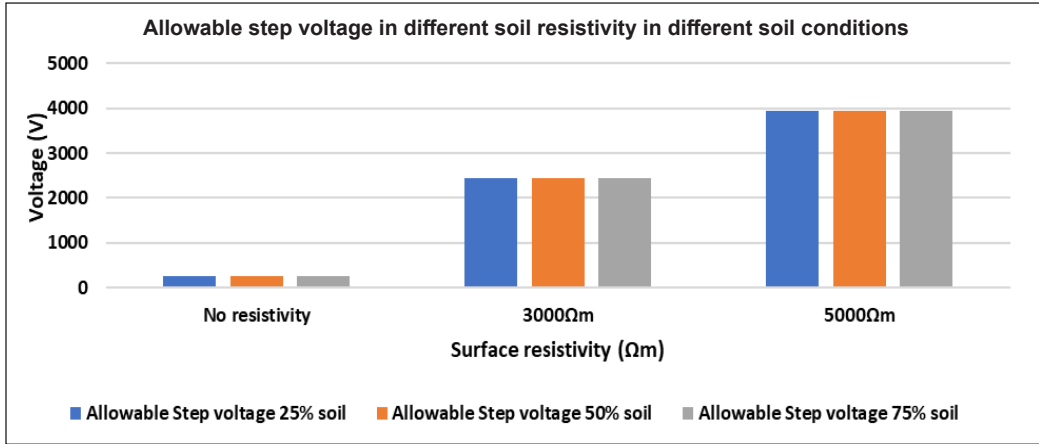


Figure 31. Allowable step and step and touch voltages for different soil ratios of vertical two-layer soil

Table 7

Comparison of ρ_1 value in vertical and horizontal two-layer soil on the allowable step voltage

	Allowable Step voltage (V)			
	Vertical	Homogeneous	Vertical	Homogeneous
Surface resistivity	Right soil (100Ω.m)	Uni (100Ω.m)	Right soil (1000Ω.m)	Uni (1000Ω.m)
1000Ω.m	936.1	936.1	1120	1120
3000Ω.m	2442	2442	2676	2676
5000Ω.m	3948	3948	4195	4195

The overall findings indicate that the effect of vertically layered soil on the reduction or increment of impedance, step, and touch voltages of the grid is small compared to horizontally layered soil. An entire grounding grid is installed in a particular layer of soil (usually the first soil layer) with a specific resistivity for horizontally layered soil. A grounding grid is divided by soil boundaries with different soil resistivities for vertically layered soil. Increasing the vertical rods' length has insignificant effects on the grounding behavior for vertical two-layer soil differs from the horizontal soil layer. Suppose the vertical rod is longer than the soil boundary. In that case, the current flow through two soil layers with different resistivity affects each vertical rod in the horizontal soil layer. In contrast, each vertical rod in the vertical soil layer is influenced by a single soil layer with a certain resistivity left or right.

In vertical two-layer soil, the grid safety values gradually reduce as the length of vertical rods increases. However, in horizontal two-layer soil, the safety values are governed by the height of the top soil layer and its corresponding soil resistivity. Besides, the location to place the number of vertical rods to be added in vertically layered soil structure is crucial compared to horizontally layered soil structure. For a horizontal two-layer soil,

placing the vertical rods at any point on the grid's perimeter while increasing the number of vertical rods is acceptable. However, for a vertical two-layer soil structure, adding the number of vertical rods is recommended at the low resistive layer as it helps in reducing the grid impedance.

CONCLUSION

This study describes and compares the performance of the grounding system in varied design parameters placed in horizontal and vertical two-layer soil structures. According to the results, the grounding system's performance pattern in a vertical soil structure is identical to that of a horizontally layered soil structure as the grounding design parameters vary. However, as an overall comparison to the horizontal soil layer, the percentage of increase or decrease is much lower in the vertical soil layer because of the impact of two different soil resistivity as a grounding grid is divided by a soil boundary. Furthermore, in contrast to horizontally layered soil, installing a grounding grid in a vertical soil layer is more complicated because of the difficulty of the safety parameter computations required to design a safe grounding system.

In terms of grounding behavior, a noticeable increase/decrease can be seen more in the 75% soil ratio of the vertical soil layer, where most of the grid is located in a low resistivity soil layer. It indicates the importance of the grid's proportion placed in different soil layers. For the 75% soil ratio, most of the grid is placed in a low resistive soil layer, allowing more current to disperse into the soil and lowering the safety parameters, and vice versa for the grid placed in the 25% soil ratio.

The results also show that increasing the number of vertical rods in vertical two-layer soil has the smallest reduction percentages compared to the horizontal two-layer soil structures. The effect of vertically layered soil on the reduction or increment of grid impedance, step, and touch voltages of the grounding system is small compared to horizontally layered soil. For horizontally layered soil, an entire grounding grid is placed in a specific layer of soil (normally the top soil layer) with a specific resistivity. A grounding grid is divided by soil boundaries with different soil resistivities for vertically layered soil. Increasing the vertical rods' length has insignificant effects on the grounding behavior for vertical two-layer soil differs from the horizontal soil layer. Suppose the vertical rod is longer than the soil boundary. In that case, the current flow through soil layers with different resistivity affects each vertical rod in the horizontally layered soil. In contrast, each vertical rod in the vertically layered soil is influenced by a single soil layer with a certain resistivity on the left or right.

Thus, the magnitudes of safety parameters gradually reduce as the length of vertical rods increases in vertical two-layer soil. In contrast, the safety parameters are dependent on the soil resistivity and height of the top soil layer for horizontal two-layer soil. Therefore,

increasing the number of vertical rods in vertically layered soil structures is crucial compared to horizontally layered soil structures. For a horizontal two-layer soil, placing the vertical rods at any point on the grid's perimeter with increasing the number of vertical rods is acceptable. However, for a vertical two-layer soil structure, an increase in the number of vertical rods is recommended at the low resistive layer as it helps in reducing the grid impedance significantly even if most of the grid is placed in a high resistive soil layer.

This work would add to the branch of knowledge by identifying and anticipating the behavior of the grounding system impacted by the design parameters in non-homogeneous soil conditions, more precisely on the vertical two-layer soil structure. Besides, comparing the grounding behavior between different soil conditions would help eliminate the misinterpretations of grounding behavior.

ACKNOWLEDGEMENT

The authors want to thank the Ministry of Higher Education (MOHE) Malaysia for supporting this research through the Fundamental Research Grant Scheme (FRGS) 2020 under FRGS/1/2020/TK0/UNITEN/02/13 and Uniten BOLD Grant.

REFERENCES

- Anggoro, B., Dharmawanwas, R. H., Ningrum, H. N. K., Burhan, J., & Tamjis, M. R. (2018). Grounding impedance characteristics for two-layer soil of vertical rod configuration with variation of length and diameter. *International Journal on Electrical Engineering and Informatics*, 10(4), 799-815. <https://doi.org/10.15676/ijeei.2018.10.4.12>
- Arnautovski-Toseva, V., Greev, L., & El Khamlichi Drissi, K. (2007). High frequency electromagnetic analysis of horizontal grounding conductor and near-by passive parallel conductor within two-layer soil. In *2007 15th International Conference on Software, Telecommunications and Computer Networks* (pp. 111-115). IEEE Publishing. <https://doi.org/10.1109/SOFTCOM.2007.4446077>
- Asset Management Department. (2012). *Substation design manual*. Tenaga Nasional Berhad. <https://pdfcoffee.com/substation-design-manualpdf-pdf-free.html>
- Coelho, R. R. A., Pereira, A. E. C., & Neto, L. M. (2018). A high-performance multilayer earth parameter estimation rooted in Chebyshev polynomials. *IEEE Transactions on Power Delivery*, 33(3), 1054-1061. <https://doi.org/10.1109/TPWRD.2017.2664738>
- de Araujo, A. R. J., Colqui, J. S. L., Seixas, C. M., Kurokawa, S., Salarieh, B., Filho, J. P., & Kordi, B. (2019). Computing tower- footing grounding impedance and GPR curves of grounding electrodes buried in multilayer soils. In *International Symposium on Lightning Protection (XIV SIPDA)* (pp. 1-8). IEEE Publishing. <https://doi.org/10.1109/SIPDA47030.2019.8951559>
- Gouda, O. E., El-Saied, T., Salem, W. A. A., & Khater, A. M. A. (2019). Evaluations of the apparent soil resistivity and the reflection factor effects on the grounding grid performance in three-layer soils. *IET Science, Measurement and Technology*, 13(4), 469-477. <https://doi.org/10.1049/iet-smt.2018.5336>

- Gursu, B., & Cevdet, M. (2019). Limiting GPR in a two-layer soil model via genetic algorithms Limiting GPR in a two-layer soil model via genetic algorithms. *Journal of the Franklin Institute*, 346(8), 768-783. <https://doi.org/10.1016/j.jfranklin.2009.07.003>
- He, J., Zeng, R., & Zhang, B. (2013). *Methodology and technology for power system grounding*. John Wiley & Sons. <https://doi.org/10.1002/9781118255001>
- IEEE 80 (2013). *IEEE guide for safety in AC substation grounding Std 80-2013*. IEEE Power and Energy Society. <https://standards.ieee.org/ieee/80/4089/>
- Ma, J., & Dawalibi, F. P. (2009). Computerized analysis of grounding plates in multilayer soils. *IEEE Transactions on Power Delivery*, 24(2), 650-655. <https://doi.org/10.1109/TPWRD.2008.2005887>
- Mokhtari, M., Abdul-Malek, Z., & Gharehpetian, G. B. (2016). A critical review on soil ionisation modelling for grounding electrodes. *Archives of Electrical Engineering*, 65(3), 449-461. <https://doi.org/10.1515/aee-2016-0033>
- Mokhtari, M., Abdul-Malek, Z., & Wooi, C. L. (2016). Integration of frequency dependent soil electrical properties in grounding electrode circuit model. *International Journal of Electrical and Computer Engineering*, 6(2), 792-799. <https://doi.org/10.11591/ijece.v6i1.9527>
- Moradi, M. (2020). Analysis of transient performance of grounding system considering frequency-dependent soil parameters and ionization. *IEEE Transactions on Electromagnetic Compatibility*, 62(3), 785-797.
- Nahman, J., & Paunovic, I. (2006). Resistance to earth of earthing grids buried in multi-layer soil. *Electrical Engineering*, 88(4), 281-287. <https://doi.org/10.1007/s00202-004-0282-y>
- Nassereddine, M., Rizk, J., Nagrial, M., & Hellany, A. (2010). Estimation of apparent soil resistivity for two-layer soil structure. *International Journal of Energy and Environment*, 1(3), 427-446.
- Nayel, M. (2014). Study apparent grounding resistivity in vertical-layer soil. *Electric Power Components and Systems*, 42(8), 845-851. <https://doi.org/10.1080/15325008.2014.896432>
- Nayel, M., Lu, B., Tian, Y., & Zhao, Y. (2012). Study of soil resistivity measurements in vertical two-layer soil model. In *2012 Asia-Pacific Power and Energy Engineering Conference* (pp. 1-5). IEEE Publishing. <https://doi.org/10.1109/APPEEC.2012.6307337>
- Nikolovski, S., Knežević, G., & Baus, Z. (2016). Assessment of step and touch voltages for different multilayer soil models of complex grounding grid. *International Journal of Electrical and Computer Engineering*, 6(4), 1441-1455. <https://doi.org/10.11591/ijece.v6i4.10637>
- Pavel, S. G., Maier, V., Ciorca, C., Beleiu, H. G., & Birou, I. (2020). Optimal design of the vertical earthing with electrodes arranged in line. *Applied Sciences*, 10(3), 5-8. <https://doi.org/10.3390/app10031177>
- Permal, N., Osman, M., Ariffin, A. M., & Kadir, M. Z. A. A. (2021). The impact of substation grounding grid design parameters in non-homogenous soil to the grid safety threshold parameters. *IEEE Access*, 9, 37497-37509. <https://doi.org/10.1109/ACCESS.2021.3063018>
- Sing, L. K., Yahaya, N., Othman, S. R., Fariza, S. N., & Noor, N. M. (2013). The relationship between soil resistivity and corrosion growth in tropical region. *Journal of Corrosion Science and Engineering*, 16, 1-11.

- Takahashi, T., & Kawase, T. (1990). Analysis of apparent resistivity in a multi-layer earth structure. *IEEE International Transactions on Power Delivery*, 5(2), 604-612. <https://doi.org/10.1109/61.53062>
- TNB. (2019). *Electricity supply application handbook* (Version 3.1). Tenaga Nasional Berhad. https://www.mytnb.com.my/themes/user/mytnb/pdf/2020_ESAH_Complete_v3.1.pdf
- Tong, X., Dong, X., & Tan, B. (2019). High current field test of impulse transient characteristics of substation grounding grid. *The Journal of Engineering*, 2019(16), 2018-2021. <https://doi.org/10.1049/joe.2018.8826>
- Tung, C. C., & Lim, S. C. (2017). Performance of electrical grounding system in soil at low moisture content condition at various compression levels. *Journal of Engineering Science and Technology*, 12(Special Issue 1), 27-47.
- Unde, M. G., & Kushare, B. E. (2012). Grounding grid performance of substation in two layer soil - A parametric analysis. *International Journal of Engineering Science and Emerging Technologies*, 1(2), 69-76. <https://doi.org/10.7323/ijeset/v1>
- Vyas, K. A., & Jamnani, J. G. (2012). Optimal design of grounding system for HV/EHV substations in two layered soil. *International Journal of Emerging Technology and Advanced Engineering*, 2(5), 383-392.
- Vycital, V., Topolanek, D., Toman, P., & Ptacek, M. (2017). Sensitivity analysis of earthing system impedance for single and multilayered soil. *CIREN - Open Access Proceedings Journal*, 2017(1), 428-431. <https://doi.org/10.1049/oap-cired.2017.1108>
- Yang, J., & Zou, J. (2020). Parameter estimation of a horizontally multilayered soil with a fast evaluation of the apparent resistivity and its derivatives. *IEEE Access*, 8, 52652-52662. <https://doi.org/10.1109/ACCESS.2020.2980875>
- Zaini, H. G., & Ghoneim, S. S. (2012). Earth surface potential and grounding resistance for grounding grid in two-layer model soil. In *2012 IEEE International Conference on Power System Technology (POWERCON)* (pp. 1-5). IEEE Publishing. <https://doi.org/10.1109/PowerCon.2012.6401396>

Review Article

External Skeletal Fixator to Stabilize the Orthopedic Conditions in Avian Species: A Systematic Review of Case Reports and Case Series

Hossein Taiyari and Jalila Abu*

Department of Veterinary Clinical Studies, Faculty of Veterinary Medicine, Universiti Putra Malaysia, 43400 UPM, Serdang, Selangor, Malaysia

ABSTRACT

Orthopedic conditions are among the most frequent avian emergency cases admitted to veterinary hospitals and clinics. An external skeletal fixator is commonly used as surgical treatment in avian orthopedics. This review aimed to systematically evaluate the use of external skeletal fixator (ESF) in published cases of avian orthopedics. Four electronic databases were searched to identify all relevant case reports and case series. Altogether, 24 primary reports met the inclusion criteria. Of those, 16 reports were case reports; and eight were case series. In total, 166 avian patients with different orthopedic conditions were undergone ESF stabilization techniques; and raptor species formed the majority of the patients. The characteristics of the fractured bone were the key factor in the suitability of different ESF techniques. In addition, other factors such as type, location, and severity of the orthopedic condition should be considered. ESF implants are promising techniques for treating avian orthopedic conditions, as the complications related to the fixators were few, and the percentage of successfully released raptors was high. Unfortunately, there are so many cases of avian orthopedics that were not published. Considering this caveat, it is not easy to draw a firm conclusion on this topic. However, this paper can serve as a guiding principle for clinicians.

Keywords: Avian orthopedics, external skeletal fixator, fracture, luxation, raptor species, systematic review

ARTICLE INFO

Article history:

Received: 23 October 2021

Accepted: 03 February 2022

Published: 20 April 2022

DOI: <https://doi.org/10.47836/pjst.30.3.04>

E-mail addresses:

hosseintaiyari@gmail.com (Hossein Taiyari)

jalila@upm.edu.my (Jalila Abu)

* Corresponding author

INTRODUCTION

Orthopedic disorders in avian patients are mainly inclusive of fractures and luxations. These conditions are of great importance in avian medicine practice, especially when it comes to the admissions of birds of prey to veterinary clinics and hospitals (Harcourt-

Brown, 2002; Buttle, 2004; Helmer & Redig, 2006). Raptors are sensitive to changes in their surroundings and are susceptible to trauma caused by crashing into cars or artificial obstacles (Fix & Barrows, 1990). A gunshot is also a common cause of fractures and can cause nerve damage through lead toxicity, which may worsen the prognosis of the injured birds (Bennett, 1994). The main goals in fracture management are stabilization and length maintenance after achieving fragments alignment (Ponder & Redig, 2016; Carrasco, 2019). Both internal and external skeletal fixator provides a substantial reduction in the movement of the injured site, which ultimately enhances the recovery of both fractures and luxations (Redig & Ponder 2016). Although most of the techniques and principles used in fracture management in birds are similar to mammals, anatomic and physiologic particularities lead to different preferences for surgical approaches between avian and non-avian species (Tully Jr., 2002; Carrasco, 2019). One of the main differences is the more favorable outcome of using an external skeletal fixator (ESF) in avian orthopedic cases (Carrasco, 2019). An external skeletal fixator (ESF) is commonly used in two-dimensional space where its holding pins pass through both cortices. If the pins extend to the other side and attach to the second external bar, it is called ESF type 2. Otherwise, it is called ESF type 1 (Carrasco, 2019). Recently, a novel multidimensional ESF technique, namely key ring or circular fixator, has been developed to stabilize the avian long bone fractures (Katogiritis et al., 2019). The combination of ESF with an intramedullary (IM) pin is called a tie-in fixator (TIF) which is considered one of the most rigid and commonly used stabilization techniques in the treatment of avian orthopedic conditions (Bueno et al., 2015; Van Wettere et al., 2009; Carrasco et al., 2017). In addition, ESF can be practical for applying for recent advances in the avian orthopedic field like bone grafts and bone matrix (Jones & Redig, 2001; Jalila et al., 2004).

This paper aims to summarize and critically evaluate the published studies that used ESF to stabilize and ultimately promote the recovery of avian orthopedic conditions.

MATERIALS AND METHODS

This systematic review followed the principles of both PRISMA (Preferred Reported Items for Systematic Review and Meta-Analyses) guideline and the Cochrane Handbook for Systematic Reviews of Interventions (Liberati et al., 2009; Moher et al., 2009).

Search Methods and Inclusion Criteria

Literature has been explored using the electronic search of the keywords in the following databases: Scopus, PubMed, Veterinary Information Network (VIN), and Google Scholar. In order to reduce the possibility of missing the relevant studies, a wider category of keywords was used. The details of the electronic search can be found in Appendices A and B.

The inclusion criteria of the primary studies were based on PICOS (Population, Intervention, Comparison, Outcomes, Study design).

All species of birds that participated in avian orthopedics case reports (CRs) or case series (CSs) were considered the study population.

The primary outcome was shown by describing the different ESF used to stabilize various avian orthopedic conditions. These include the percentage of each type of ESF used in different orthopedic conditions, the release percentage of raptors, and the mean time spent for each type of ESF to stabilize the fractures and luxations.

The secondary outcome was mainly related to the healing failures and consisted of complications of external fixation (major, minor, the effect of these complications on the fracture healing).

Only studies written in English and published in indexed, peer-reviewed Journals were reported. No restriction was set on the date of publication.

Selection of Studies and Data Collection

Two independent reviewers assessed the primary studies after excluding the duplicates identified from one or more search databases. Studies were screened based on a two steps assessment. The first step was the assessment of both titles and abstracts of the studies. The unsuitable studies were excluded, and then the second step of the assessment continued with a full-text screening. The eligible studies were then classified as suitable for the systematic review and presented in Table 1. The following data were extracted from each of the eligible studies. The collected data are summarized in Appendix C.

- 1) Study characteristics (first author's name, year of publication, study design);
- 2) Avian species characteristics (number, species);
- 3) Orthopedic conditions characteristics (involved bone, location, type, severity)
- 4) Intervention characteristics (type of ESF, fracture reduction, removal time, clinical findings, complications);
- 5) Main results of the included studies.

Table 1
Included studies based on the alphabetical order of the first author

Author (year)	Study design	No. of patient	Bird species
Ackermann & Redig (1997)	CS	4	Raptors (Wild)
Arias et al. (2015)	CR	1	Slender-billed Parakeet (Wild)
Bueno et al. (2015)	CS	37	Raptors (Wild, Captive)
Bueno et al. (2019)	CR	2	Raptors (Wild)
Burdeaux & Wade (2018)	CR	1	Snowy owl (Wild)
Carrasco et al. (2017)	CS	35	Pet birds
Folland et al. (2016)	CR	1	Bald eagle (Wild)

Table 1 (continue)

Author (year)	Study design	No. of patient	Bird species
Hatt et al. (2007)	CS	18	Psittacine, Raptor, Passerine (Captive, Pet, Wild)
Hoybergs et al. (2008)	CR	1	Harris's hawk (Captive)
Jones & Redig (2001)	CR	1	Red-tailed hawk (Wild)
Katogiritis et al. (2019)	CR	2	Psittacines (Pet)
Kavanagh (1997)	CR	1	Scarlet macaw (Pet)
Kaya & Özsoy (2017)	CS	19	Chukar partridges and Domestic pigeons (Captive)
Kinney et al. (2015)	CR	1	African sacred ibis (Captive)
Martin et al., (1993)	CS	8	Raptors
Meij et al. (1996)	CS	12	Psittacines, Peacock, Domestic fowl, Racing pigeons (Pet, Captive)
Montgomery et al. (2011)	CR	1	Bald eagle (Wild)
Rahal et al. (2008)	CR	1	Toco toucan (Captive)
Rochat et al. (2005)	CR	1	Bald eagle (Wild)
Rosenthal et al. (1994)	CR	2	Moluccan cockatoo & barn owl
Rui et al. (2017)	CR	1	Rock pigeon (Free flying)
Sample et al. (2008)	CR	1	Whooping crane (Captive)
Vergneau-Grosset et al. (2019)	CS	14	Raptors (Wild)
Vergneau-Grosset et al. (2020)	CS	24	Raptors (Wild)
Van Wettere & Redig (2004)	CR	2	Raptors (Wild)
Yoon et al. (2008b)	CR	1	Great Horned Owl (Wild)
Yoon et al. (2008a)	CS	19	Raptors (Wild)

CR: case report, CS: case series.

RESULTS

Descriptive Statistics of ESF Implants Used

In comparison to mammals, the healing of orthopedic conditions in avian patients requires additional challenges. These challenges are mostly related to thin cortices and low soft tissue support, including blood vessels and nerves. These challenges have made the stabilization of fractures more difficult. Moreover, some features of the fractured bone can pose additional difficulty to the stabilization of avian orthopedic conditions (Helmer & Redig, 2006). For instance, the relatively small medullary cavity of the tibiotarsus is making the fixation of tibiotarsal orthopedic conditions more difficult (Kinney et al., 2015). In this regard, various types of ESF have been developed to provide a practical tool to stabilize the avian orthopedic condition to fulfill the specific need of certain orthopedic conditions. Figure 1 presents the percentage of different types of ESF used in different avian orthopedic conditions. Results showed that tie-in was mainly used for humeral, femoral, and tibiotarsal fractures. For tarsometatarsal and carpometacarpal fractures, ESF type2 was used mainly.

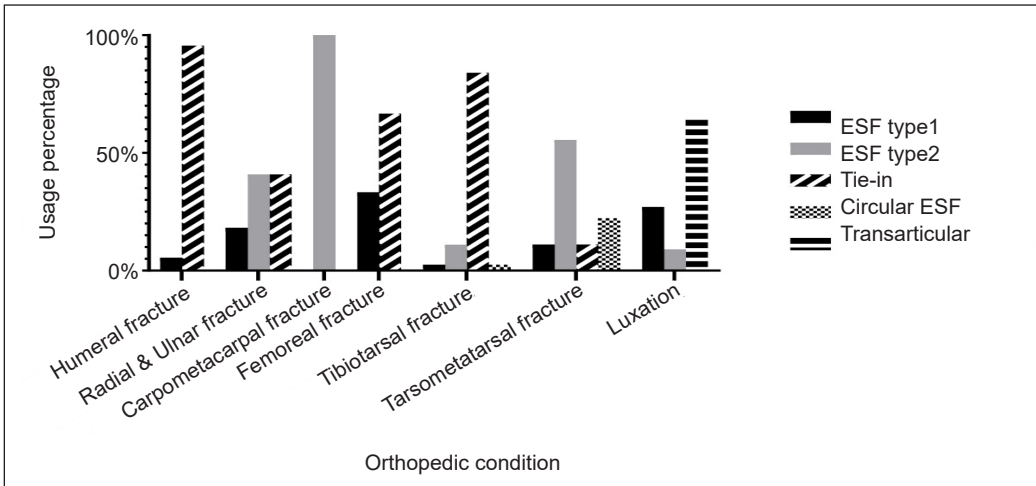


Figure 1. Percentage of different types of ESF used in different avian orthopedic conditions

Transarticular ESF was the main choice to stabilize luxation in the studies. Both type2 and tie-in were equally used to stabilize the fractures for radial and ulnar fractures.

Release Percentage of Raptors

Release percentage can indicate the suitability of each ESF technique for different avian orthopedic cases, especially in injured raptors. The decision on releasing injured raptors into the wild requires a complete healing of the orthopedic condition without any complications and comorbidities. The percentage of the injured raptors released for each type of ESF used to stabilize different orthopedic conditions of raptors can be found in Figure 2. Results

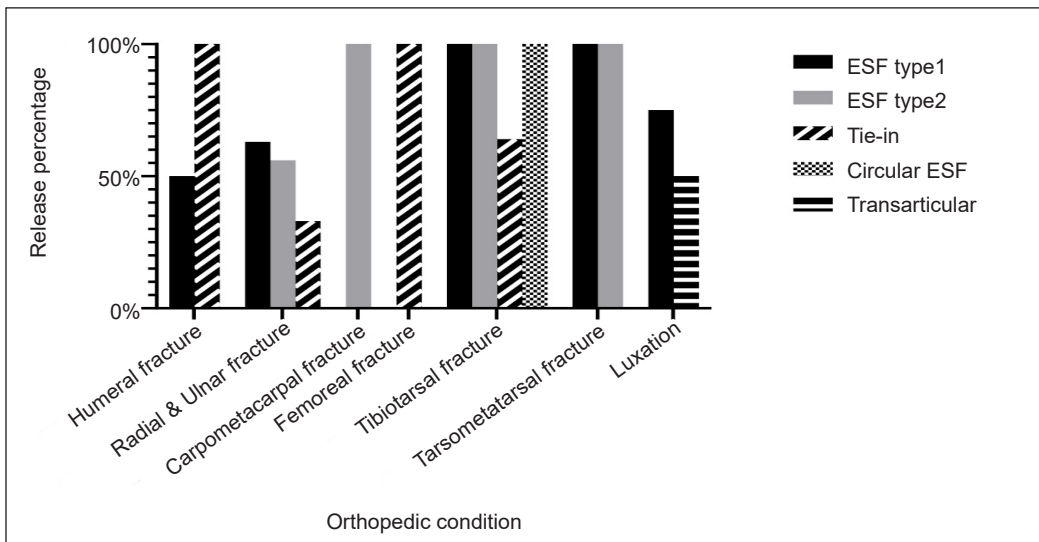


Figure 2. Release percentage of injured raptors with different orthopedic conditions

showed that tie-in ESF for the humeral and femoral fractures led to a more successful release rate of raptors. For carpometacarpal fracture, ESF type 2 had a more successful release rate. For luxation and radial and ulnar fracture, ESF type 1 was more successful. In tarsometatarsal fracture, ESF type 1 and type 2 showed an equal successful release rate of injured raptors. ESF type 1, type 2, and circular ESF had equal success in the release of injured raptors. Falconry techniques can be very useful in flight assessment and recovery of these raptors' flight strength before the injury. These techniques were used in 10% of the raptor cases. The birds recovered their flight potency in all of these cases and were successfully released to the wild.

Required Stabilization Period

One of the key factors in the treatment of avian orthopedic conditions is the period required for the ESF implant to stabilize the fracture or luxation. In other words, the lesser the time required for ESF, the better the stabilization. This period can also indicate the suitability of the ESF technique used. This period started when the ESF implant was employed during the surgery and usually ends when radiography findings approved firm callus bridging at the fracture site. This period is more highlighted for wild raptors, as they need to be released to the wild as soon as possible. Fracture severity, fracture type, and fracture location can influence the ESF implant usage period, especially by looking at this period from the fracture's perspective only. Therefore, these factors affect the type of ESF considered to be used. Table 2 shows the average time required for different ESF types to stabilize different orthopedic conditions. The ESF removal times reported in the studies with negative outcomes were excluded from this calculation.

Table 2
Average time spent for different types of ESF to stabilize different orthopedic conditions

Orthopedic condition	Average time required for ESF (week(s) after surgery)					
	Type 1	Type 2	Tie-in		Circular	Transarticular
			IM	ESF pins		
Load sharing fracture	6	9	5	8	5	-
Non-load sharing fracture	8.5	7	5	6.5	9	-
Open fracture	10	6	5	6.5	7	-
Close fracture	6	8.5	5.5	7.5	8.5	-
Proximal fracture	-	8	6	8	12	-
Midshaft fracture	8	8	5	7	6.5	-
Distal fracture	6	7	3	5	5	-
Osteotomy	9	8	2	5	5	-
Arthrodesis	12	13	-	-	-	-
Luxation	7.5	-	-	-	-	1

Complications of External Fixation

Complications associated with external fixation can delay the removal of the ESF implant, which ultimately may fail in the fracture to heal. These complications can be categorized into major and minor. In major complications, there is a high risk of fracture healing failure. Minor complications, however, cause discomfort for the patients and seldom result in healing failure (Egger, 1991). Failure of apparatus to provide adequate stability, failure of the bone-fixation pin interface, and healing problems of fracture or luxation are considered major complications. On the other hand, minor complications include pin-tract drainage, poor limb use, injury to musculotendon structures, and neurovascular damage (Egger, 1991; Marti & Miller, 1994). Thirty-eight complications were reported among the 166 avian patients with orthopedic conditions (38/166, 22%). Major complications have formed the majority of the 29/38 (76%). These include 21/29 (72%) reports of fracture or luxation healing problems, six reports on the failure of the bone-fixation pin interface, and two reports of failure of the apparatus to provide adequate stability. Forty-two percent of major complications lead to failure in healing. Failure in healing led to 11 cases of euthanasia, three cases of amputation, two cases of significant shortening, and two cases of arthrodesis. In addition, two cases of aspergillosis and one case of plasmodium infestation resulted in the death of patients prior to the healing of the orthopedic condition.

DISCUSSION

This systematic review aimed to summarize and evaluate the use of ESF as the most common stabilizer in the treatment of avian orthopedic conditions. Compared with mammals, treatment of avian orthopedic conditions faces additional challenges. Avian bones have lower soft tissue support, contain a higher proportion of hydroxyapatite, and have thinner and more brittle cortices (Bennett & Kuzma, 1992; Degernes et al., 1998). External skeletal fixators can provide fracture reduction without impairing the vascularization of the fracture site (Bush et al., 1976). Detailed information on different techniques of ESF and their suitability to stabilize different types of fractures has been reported (Harcourt-Brown, 2002; Orosz, 2002). Apart from summarizing the frequency of each ESF technique used to stabilize different orthopedic conditions in a larger number of cases, this paper also provides additional information on two major factors involved in ESF; required fixation time and complications. One of the main variables that should be considered when choosing the proper type of ESF is fractured bone. For instance, humeral fractures are prone to comminuted fractures and hard to stabilize (Bennett & Kuzma, 1992; MacCoy, 1992). Consistent results were observed in the data in which the majority (80%) of the humeral fractures were comminuted, and all the healed humeral fractures were stabilized by tie-in ESF. Fractures of tarsometatarsus also inhere additional challenges mainly related to the small medullary cavity and being hard to stabilize (Helmer & Redig, 2006). Six

tarsometatarsal fractures were stabilized with either type 2 or tie-in ESF, and most of the tie-in cases had major or minor complications causing delayed healing or amputation.

This might indicate the unsuitability of tie-in ESF for stabilization of tarsometatarsal fractures. On the other hand, Circular ESF has been deemed a more proper fixation method for tarsometatarsal fractures. Circular ESF can also provide distraction osteogenesis, especially in cases where tibiotarsal shortening happened due to the malunion of the two fracture ends stabilized by unsuitable fixators (Bueno et al., 2019). Speaking of bones with a relatively small medullary cavity, radial and ulnar (antebrachial) fractures are the most complex challenges in avian orthopedics. These bones are always under torsional forces, making them more susceptible to complex fractures than other forelimb bones (De Margerie, 2002). Since these bones play a key role in the circumduction of wings, any impairment in the healing of antebrachial fractures can prevent the pronation and supination movements of the wing required for adequate flight (Beaufreire, 2009). Tie-in and type 1 ESF techniques are the recommended fixation methods for antebrachial fractures (Orosz, 2002). This study showed that tie-in ESF was slightly more preferable than type 1 ESF. Synostosis is a common sequela to antebrachial fractures. This complication is common for external coaptation of antebrachial fractures and can reduce the flight capability of recovered birds (Orosz et al., 1992). Two cases of synostosis were reported in the included studies.

Consistent findings can be seen in the successful release of raptors statistics, whereby the fracture of large bones requires a higher stabilization force, which can be found in tie-in. However, tie-in might be less suitable for the bones with a small medullary cavity. It can be noticed by looking at the release percentage of raptors according to which higher release was seen when type 1 ESF was used for antebrachial fractures. Various factors such as complications, comorbidities, captivity stress, and species specificity can cause failure to release raptors into the wild (Bueno et al., 2015; Vergneau-Grosset et al., 2019). Altogether, 31 complications and 12 cases with comorbidities were reported for the injured raptors. Thirteen cases were recovered from complications and comorbidities, but the rest of the birds were either euthanized or became captive for various purposes. Species distribution is the main factor in the frequent representation of a species. However, it is notable that bald eagle, great horned owl, and red-tailed hawk were the most common admitted raptors.

The severity and type of fracture can also affect bone healing substantially. In this regard, the average time required for each type of ESF to treat different kinds of orthopedic conditions with different severity and type can be practical factors to show each ESF technique's suitability. A previous study found that none of the severity and type of fracture were significantly affected the required time for each type of ESF to successfully stabilize the fracture (Bueno et al., 2015). Clinical trials showed that less than six weeks is required for the type 1 ESF to stabilize the healing of the experimental transverse fractures of

ulna in pigeon models (Hatt et al., 2007; Tunio et al., 2014). Using a lightweight external fixator in a system called Fixateur Externe du Service de Santé des Armées (FESSA) can reduce the fixation time to 4 weeks in the same type of fracture using both types 1 and tie-in ESF (Hatt et al., 2007). The adjustable feature of FESSA allows veterinarians to create numerous construct configurations. For example, one uses hinges to connect two FESSA tubes as a transarticular fixator to stabilize the luxation. This system can fix the joint at a desirable angle and makes physical therapy possible without removing the fixator (Azmanis et al., 2014).

When it comes to extremely complex bone fractures in which there is a need to replace bone defects, common orthopedic techniques alone might not provide a good prognosis as the bone itself can only regenerate the small fracture defects. However, different techniques of bone grafting can provide a practical way to treat bone defects in animal orthopedic practices (Nunamaker & Rhinelander, 1985). Osteoinductive, osteoconductive, and osteogenic properties of bone grafts will allow the fractured bone to regenerate the bone defects feasibly.²² Various techniques of bone grafting have been introduced in avian orthopedics. These include the use of callus graft, cortical graft, bone morphogenetic proteins, bone marrow, and hydroxyapatite (HA) (MacCoy & Haschek, 1988; Jones & Redig, 2001; Sample et al., 2008; Sanaei et al., 2011; Sanaei et al., 2015; Tunio et al., 2015). Most of these studies used an external skeletal fixator (ESF) as the stabilizer to expedite fracture healing. Four of the included studies used bone grafting techniques, two of which are case reports, and the other two are clinical control trials.

Case reports were used autogenous callus and recombinant human bone morphogenetic protein-2 to treat the humeral bone defects in a red-tailed hawk and a whooping crane, respectively (Jones & Redig, 2001; Sample et al., 2008). The red-tailed hawk had a close midshaft comminuted fracture, and healing was achieved within five weeks after surgery-based radiography findings. On the other hand, the whooping crane suffered an open proximal comminuted fracture that healed within fourteen weeks after surgery. Autogenous bone grafts are considered the gold treatment for repairing bone defects. However, alternative bone graft materials are needed in avian patients due to the limitation of autogenous bone grafts (Bennett & Kuzma, 1992; Jalila et al., 2004). In a recent study, it has been found that the allogenic tubular demineralized bone marrow, along with the application of tie-in ESF, can be a promising alternative to autogenous bone grafts in the treatment of the critical bone defect of the ulna (Sanaei et al., 2015).

CONCLUSION

The implications of the summarized data suggest that each avian orthopedic condition requires a specific way of fixation. In the bigger picture, the involved bone or joint, type of fracture or luxation, and the fracture location are the main factors that should be

considered when an ESF technique is decided to be employed. This review also provides guiding principles for choosing a suitable ESF, highlighted more when dealing with the raptor's emergency orthopedic cases. However, this systematic review has several important limitations. These limitations pertain to the incompleteness of the outcome. Complications and the implementations taken were underreported. Several reports lacked ESF implant removal time, and some reports lacked sufficient radiographic assessments before and after the removal of ESF implants. Some studies did not report whether the recovered birds were returned to their formal status. Given such incompleteness of data, this review cannot suggest the best ESF technique for different avian orthopedic conditions, making this review less conclusive than it had hoped. However, it provides clinicians with guiding principles for choosing suitable ESF techniques and the ESF-related complications they should know.

ACKNOWLEDGEMENT

The authors give special thanks to Dr. Claire Vergneau-Grosset for providing supplementary data on her works and her valuable comments and guidance. In addition, the authors are grateful to Dr. Jean-Michel Hatt and Dr. Irene Bueno for sharing the supplementary data of their works.

REFERENCES

- Ackermann, J., & Redig, P. (1997). Surgical repair of elbow luxation in raptors. *Journal of Avian Medicine and Surgery*, 11(4), 247-254.
- Arias, J. I., Beato, C., & Espinoza, A. (2015). Epoxy putty external skeletal fixation in a tibiotarsal fracture of a wild choroy parakeet (*Enicognathus leptorhynchus*). *Arquivo Brasileiro de Medicina Veterinária e Zootecnia*, 67, 671-678. <https://doi.org/10.1590/1678-4162-7474>
- Azmanis, P. N., Voss, K., & Hatt, J. M. (2014). Evaluation of short-term outcomes of experimental stifle luxation in feral pigeons (*Columba livia domestica*) treated with a hinged transarticular external skeletal fixator and physical therapy. *International Journal of Applied Research in Veterinary Medicine*, 12(2), 157-166.
- Beaufre, H. (2009). A review of biomechanic and aerodynamic considerations of the avian thoracic limb. *Journal of Avian Medicine and Surgery*, 23(3), 173-185. <https://doi.org/10.1647/2007-023.1>
- Bennett, R. A. (1994). Neurology. In B. W. Ritchie, G. J. Harrison, & L. R. Harrison (Eds.), *Avian Medicine: Principles and Application* (pp. 721-747). Wingers Publishing.
- Bennett, R. A., & Kuzma, A. B. (1992). Fracture management in birds. *Journal of Zoo and Wildlife Medicine*, 23(1), 5-38.
- Bueno, I., Anderson, G., Willette, M., Redig, P. T., & Ponder, J. (2019). Distraction osteogenesis in two wild raptors. *Journal of Avian Medicine and Surgery*, 33(4), 427-436. <https://doi.org/10.1647/2018-384>

- Bueno, I., Redig, P. T., & Rendahl, A. K. (2015). External skeletal fixator intramedullary pin tie-in for the repair of tibiotarsal fractures in raptors: 37 cases (1995-2011). *Journal of the American Veterinary Medical Association*, 247(10), 1154-1160. <https://doi.org/10.2460/javma.247.10.1154>
- Burdeaux, R. R., & Wade, L. (2018). Successful management of open, contaminated metacarpal fractures in an adult snowy owl (*Bubo scandiacus*) with a minimal type II external skeletal fixator. *Journal of Avian Medicine and Surgery*, 32(3), 210-216. <https://doi.org/10.1647/2017-280>
- Bush, M., Montali, R. J., Novak, G. R., & James, A. E. (1976). The healing of avian fractures: A histological xeroradiographic study. *Journal of the American Animal Hospital Association*, 12(6), 768-773.
- Buttle, E. P. (2004). Concomitant leg injuries in raptors with wing damage: To the editor. *Journal of the South African Veterinary Association*, 75(4), Article 154. <https://doi.org/10.4102/jsava.v75i4.473>
- Carrasco, D. C. (2019). Fracture management in avian species. *Veterinary Clinics: Exotic Animal Practice*, 22(2), 223-238. <https://doi.org/10.1016/j.cvex.2019.02.002>
- Carrasco, D. C., Shimizu, N., Zoller, G., Huynh, M., & Forbes, N. A. (2017, March 25-29). Retrospective study on 35 tibiotarsal fracture repairs with external skeletal fixator-intramedullary pin tie-in in pet birds. In *3rd International Conference on Avian Herpetological and Exotic Mammal Medicine (ICARE)*. Venice, Italy.
- De Margerie, E. (2002). Lamellar bone as an adaptation to torsional loads in flapping flight. *Journal of Anatomy*, 201(6), 521-526. <https://doi.org/10.1046/j.1469-7580.2002.00118.x>
- Degernes, L. A., Roe, S. C., & Abrams Jr, C. F. (1998). Holding power of different pin designs and pin insertion methods in avian cortical bone. *Veterinary Surgery*, 27(4), 301-306. <https://doi.org/10.1111/j.1532-950X.1998.tb00131.x>
- Egger, E. L. (1991). Complications of external fixation: A problem-oriented approach. *Veterinary Clinics of North America: Small Animal Practice*, 21(4), 705-733. [https://doi.org/10.1016/S0195-5616\(91\)50080-2](https://doi.org/10.1016/S0195-5616(91)50080-2)
- Fix, A. S., & Barrows, S. Z. (1990). Raptors rehabilitated in Iowa during 1986 and 1987: A retrospective study. *Journal of Wildlife Diseases*, 26(1), 18-21. <https://doi.org/10.7589/0090-3558-26.1.18>
- Folland, D. W., Echols, M. S., & Wallace, M. (2016). Elbow arthrodesis in a bald eagle (*Haliaeetus leucocephalus*). *Journal of Exotic Pet Medicine*, 25(3), 203-207. <https://doi.org/10.1053/j.jepm.2016.05.003>
- Harcourt-Brown, N. H. (2002). Orthopedic conditions that affect the avian pelvic limb. *The Veterinary Clinics of North America. Exotic Animal Practice*, 5(1), 49-81. [https://doi.org/10.1016/S1094-9194\(03\)00046-X](https://doi.org/10.1016/S1094-9194(03)00046-X)
- Hatt, J. M., Christen, C., & Sandmeier, P. (2007). Clinical application of an external fixator in the repair of bone fractures in 28 birds. *Veterinary Record*, 160(6), 188-194. <https://doi.org/10.1136/vr.160.6.188>
- Helmer, P., & Redig, P. T. (2006). Surgical resolution of orthopedic disorders. In J. G. Harrison, & L. T. Lightfoot (Eds.), *Clinical Avian Medicine* (pp. 761-773). Spix Publishing.
- Hoybergs, Y., Bosmans, T., Risselada, M., Van Caelenberg, A., & Polis, I. (2008). General anesthesia for the surgical repair of a tarsometatarsal fracture in a Harris's Hawk (*Parabuteo unicinctus*). *Vlaams Diergeneeskundig Tijdschrift*, 77(5), 309-314.
- Jalila, A., Redig, P. T., Wallace, L. J., Ogema, T. R., Bechtold, J. E., & Kidder, L. (2004). The effect of chicken, pigeon, and turkey demineralized bone matrix (DBM) implanted in ulnar defects fixed with

- the intramedullary-external skeletal fixator (IM-ESF) tie-in in pigeons (*Columba livia*): Histological evaluations. *The Medical Journal of Malaysia*, 59, 125-126.
- Jones, R., & Redig, P. T. (2001). Autogenous callus for repair of a humeral cortical defect in a red-tailed hawk (*Buteo jamaicensis*). *Journal of Avian Medicine and Surgery*, 15(4), 302-309. [https://doi.org/10.1647/1082-6742\(2001\)015\[0302:ACFROA\]2.0.CO;2](https://doi.org/10.1647/1082-6742(2001)015[0302:ACFROA]2.0.CO;2)
- Katogiritis, A., Barry, S. L., & Finch, N. (2019). Key ring fixator: A novel external fixation technique for avian long bone stabilization. *Journal of Avian Medicine and Surgery*, 33(2), 161-170. <https://doi.org/10.1647/2018-355>
- Kavanagh, M. (1997). Tibiotarsal fracture repair in a scarlet macaw using external skeletal fixation. *Journal of Small Animal Practice*, 38(7), 296-298. <https://doi.org/10.1111/j.1748-5827.1997.tb03469.x>
- Kaya, D. A., & Özsoy, S. (2017). Repair of tibiotarsal rotation in 7 chukar partridges (*Alectoris chukar*) and 12 domestic pigeons (*Columba livia domestica*) with type-2 external skeletal fixator intramedullary pin tie-in. *Journal of Avian Medicine and Surgery*, 31(3), 206-212. <https://doi.org/10.1647/2016-160>
- Kinney, M. E., Gorse, M. J., & Anderson, M. A. (2015). Circular external fixator placement for repair of an open distal tarsometatarsal fracture in an African sacred ibis (*Threskiornis aethiopicus*). *Journal of Zoo and Wildlife Medicine*, 46(4), 957-960. <https://doi.org/10.1638/2015-0154.1>
- Liberati, A., Altman, D. G., Tetzlaff, J., Mulrow, C., Gøtzsche, P. C., Ioannidis, J. P. A., Clarke, M., Devereaux, P. J., Kleijnen, J., & Moher, D. (2009). The PRISMA statement for reporting systematic reviews and meta-analyses of studies that evaluate health care interventions: Explanation and elaboration. *Journal of Clinical Epidemiology*, 62(10), e1-e34. <https://doi.org/10.1016/j.jclinepi.2009.06.006>
- MacCoy, D. M. (1992). Treatment of fractures in avian species. *Veterinary Clinics of North America: Small Animal Practice*, 22(1), 225-238. [https://doi.org/10.1016/S0195-5616\(92\)50016-X](https://doi.org/10.1016/S0195-5616(92)50016-X)
- MacCoy, D. M., & Haschek, W. M. (1988). Healing of transverse humeral fractures in pigeons treated with ethylene oxide-sterilized, dry-stored, onlay cortical xenografts and allografts. *American Journal of Veterinary Research*, 49(1), 106-111.
- Marti, J. M., & Miller, A. (1994). Delimitation of safe corridors for the insertion of external fixator pins in the dog 1: Hindlimb. *Journal of Small Animal Practice*, 35(1), 16-23. <https://doi.org/10.1111/j.1748-5827.1994.tb03576.x>
- Martin, H., Bruecker, K., Herrick, D., & Scherpelz, J. (1993). Elbow luxation in raptors: A review of eight cases. In P. T. Redig, J. E. Cooper, J. D. Remple, & D. B. Hunter (Eds.), *Raptor Biomedicine* (pp. 199-206). University of Minnesota Press.
- Meij, B. P., Hazewinkel, H. A., & Westerhof, I. (1996). Treatment of fractures and angular limb deformities of the tibiotarsus in birds by type II external skeletal fixation. *Journal of Avian Medicine and Surgery*, 10(3), 153-162.
- Moher, D., Liberati, A., Tetzlaff, J., Altman, D. G., & Prisma Group. (2009). Preferred reporting items for systematic reviews and meta-analyses: The PRISMA statement. *PLoS Medicine*, 6(7), Article e1000097. <https://doi.org/10.7326/0003-4819-151-4-200908180-00135>

- Montgomery, R. D., Crandall, E., & Bellah, J. R. (2011). Use of a locking compression plate as an external fixator for repair of a tarsometatarsal fracture in a bald eagle (*Haliaeetus leucocephalus*). *Journal of Avian Medicine and Surgery*, 25(2), 119-125. <https://doi.org/10.1647/2009-016.1>
- Nunamaker, D. M., & Rhinelander, F. W. (1985). Bone grafting. In C. D. Newton, & D. M. Nunamaker (Eds.), *Textbook of Small Animal Orthopaedics* (pp. 261-286). JB Lippincott.
- Orosz, S. E. (2002). Clinical considerations of the thoracic limb. *The Veterinary Clinics of North America. Exotic Animal Practice*, 5(1), 31-48. [https://doi.org/10.1016/S1094-9194\(03\)00045-8](https://doi.org/10.1016/S1094-9194(03)00045-8)
- Orosz, S. E., Ensley, P. K., & Haynes C. J. (1992). Considerations for avian surgery. In S. E. Orosz, P. K. Ensley, & C. J. Haynes (Eds.), *Avian Surgical Anatomy: Thoracic and Pelvic Limbs* (pp. 111-120). WB Saunders.
- Ponder, J. B., & Redig, P. (2016). Orthopedics. In B. Speers (Ed.), *Current Therapy in Avian Medicine and Surgery* (pp. 657-667). Elsevier Health Sciences.
- Rahal, S. C., Teixeira, C. R., Pereira-Junior, O. C., Vulcano, L. C., Aguiar, A. J., & Rassy, F. B. (2008). Two surgical approaches to fracture malunion repair. *Journal of Avian Medicine and Surgery*, 22(4), 323-330. <https://doi.org/10.1647/2007-058.1>
- Redig, P. T., & Ponder, J. (2016). Orthopedic surgery. In J. Samour (Ed.), *Avian Medicine* (pp. 312-358). Elsevier. <https://doi.org/10.1016/B978-0-7234-3832-8.00012-2>
- Rochat, M. C., Hoover, J. P., & DiGesualdo, C. L. (2005). Repair of a tibiotarsal varus malunion in a bald eagle (*Haliaeetus leucocephalus*) with a type 1A hybrid external skeletal fixator. *Journal of Avian Medicine and Surgery*, 19(2), 121-129. <https://doi.org/10.1647/2004-003>
- Rosenthal, K., Hillyer, E., & Mathiessen, D. (1994). Stifle luxation repair in a *Moluccan cockatoo* and a barn owl. *Journal of the Association of Avian Veterinarians*, 8(4), 173-178. <https://doi.org/10.2307/30135077>
- Rui, L. A., Viana, D. C., Dora, A. B., & Fratini, P. (2017). External fixation to correct tarsal-metatarsal fracture in rock pigeon (*Columba livia*). *Revista Ceres*, 64, 25-30. <https://doi.org/10.1590/0034-737x201764010004>
- Sample, S., Cole, G., Paul-Murphy, J., Hartup, B. K., Clyde, V., Seeherman, H. J., & Schaefer, S. (2008). Clinical use of recombinant human bone morphogenic protein-2 in a Whooping Crane (*Grus americana*). *Veterinary Surgery*, 37(6), 552-557. <https://doi.org/10.1111/j.1532-950X.2008.00419.x>
- Sanaei, M. R., Abu, J., Nazari, M., Faiz, N. M., Bakar, M. Z. A., & Allaudin, Z. N. (2011). Heterotopic implantation of autologous bone marrow in rock pigeons (*Columba livia*): Possible applications in avian bone grafting. *Journal of Avian Medicine and Surgery*, 25(4), 247-253. <https://doi.org/10.1647/2010-035.1>
- Sanaei, R., Abu, J., Nazari, M., Zuki, M. A., & Allaudin, Z. N. (2015). Evaluation of osteogenic potentials of avian demineralized bone matrix in the healing of osseous defects in pigeons. *Veterinary Surgery*, 44(5), 603-612. <https://doi.org/10.1111/vsu.12292>
- Tully Jr, T. N. (2002). Basic avian bone growth and healing. *The Veterinary Clinics of North America. Exotic Animal Practice*, 5(1), 23-30. [https://doi.org/10.1016/S1094-9194\(03\)00044-6](https://doi.org/10.1016/S1094-9194(03)00044-6)
- Tunio, A., Jalila, A., & Goh, Y. M. (2015). Histologic evaluation of critical size defect healing with natural and synthetic bone grafts in the pigeon (*Columba livia*) ulna. *Journal of Avian Medicine and Surgery*, 29(2), 106-113. <https://doi.org/10.1647/2013-047>

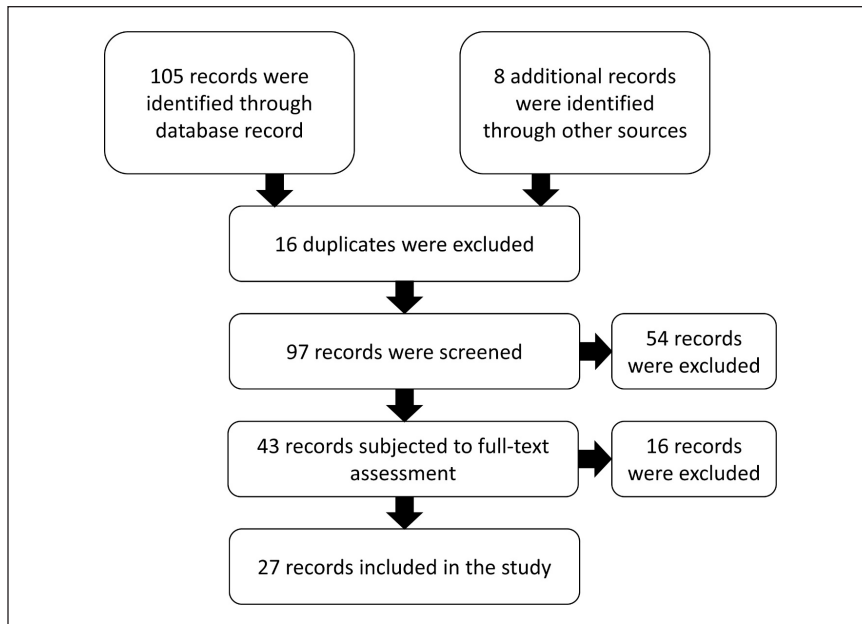
- Tunio, A., Jalila, A., Meng, C. Y., & Shameha, I. (2014). Experimental fracture healing with external skeletal fixation in a pigeon ulna model. *Journal of Advanced Veterinary and Animal Research*, 1(2), 58-64. <https://doi.org/10.5455/javar.2014.a14>
- Van Wettere, A. J., & Redig, P. T. (2004). Arthrodesis as a treatment for metacarpophalangeal joint luxation in 2 raptors. *Journal of Avian Medicine and Surgery*, 18(1), 23-29. <https://doi.org/10.1647/2003-002>
- Van Wettere, A. J., Redig, P. T., Wallace, L. J., Bourgeault, C. A., & Bechtold, J. E. (2009). Mechanical evaluation of external skeletal fixator-intramedullary pin tie-in configurations applied to cadaveral humeri from red-tailed hawks (*Buteo jamaicensis*). *Journal of Avian Medicine and Surgery*, 23(4), 277-285. <https://doi.org/10.1647/1082-6742-23.4.277>
- Vergneau-Grosset, C., Dubé, C., Fitzgerald, G., & Lair, S. (2020). Characteristics of antebrachial fractures associated with a successful outcome among free-ranging birds of prey that received treatment in a rehabilitation program. *Journal of the American Veterinary Medical Association*, 256(5), 580-589. <https://doi.org/10.2460/javma.256.5.580>
- Vergneau-Grosset, C., Kapatkin, A. S., Paul-Murphy, J., Guzman, D. S. M., & Hawkins, M. G. (2019). Release rates and complications for birds of prey with antebrachial fractures at a veterinary teaching hospital. *Journal of Avian Medicine and Surgery*, 33(4), 388-397. <https://doi.org/10.1647/2018-394>
- Yoon, H. Y., Fox, D. B., & Jeong, S. W. (2008). Long bone fractures in raptors: 28 cases (2004-2007). *Journal of Veterinary Clinics*, 25(3), 215-217.
- Yoon, H. Y., Fox, D. B., & Jeong, S. W. (2008). Tibiotarsal and ulnar fracture repair in a great horned owl (*Bubo virginianus*). *Journal of Veterinary Clinics*, 25(3), 218-220.

APPENDIX A

The keywords and how Boolean characters (AND, OR) are used for the electronic search. (((("external skeletal fixator") OR ("ESF") OR ("external fixator") OR ("external fixation") OR ("external skeletal") OR ("tie-in") OR ("hybrid external fixator") OR ("hybrid external fixation"))) AND (("fracture") OR ("luxation") OR ("bone") OR ("bone fracture") OR ("osteosynthesis") OR ("osteogenic") OR ("osseous defects") OR ("tarsometatarsal") OR ("tibiotarsal") OR ("femoral") OR ("humeral") OR ("rotation") OR ("dislocation") OR ("arthrodesis") OR ("radial") OR ("ulnar") OR ("antebrachial"))) AND (("avian") OR ("bird") OR ("pigeon") OR ("goose") OR ("raptor") OR ("exotic bird") OR ("owl") OR ("eagle") OR ("duck") OR ("chicken") OR ("turkey") OR ("poultry") OR ("fowl") OR ("hawk") OR ("partridges") OR ("macaw") OR ("pheasant") OR ("parrot") OR ("psittacine") OR ("pet bird") OR ("wild bird") OR ("hobby bird") OR ("game bird") OR ("birds of prey") OR ("falcon") OR ("kestrel")))

APPENDIX B

PRISMA flow diagram to select the included studies.



APPENDIX C

Data summary table

Author	Year	Species	Orthopedic condition	ESF type	Complications	Radiography & clinical findings	Remarks
Van Wetteere & Redig	2004	Prairie falcon	Closed metacarpophalangeal joint luxation	Type 1	No complications	Week 4: periosteal and medullary bridging. Week 6: bridging was complete, and the distal external skeletal fixator pin was loose).	19 weeks later, the bird was released into the wild (falconry techniques were used).
		Great horned owl	Open metacarpophalangeal joint luxation	Type 1	No complications	Week 4: periosteal and medullary fusion. Week 6: periosteal bridging. Week 9: complete healing.	17 weeks later, the bird was released into the wild (falconry techniques were used).
Kinney et al.	2015	African sacred ibis	Open distal comminuted tarsometatarsal fracture	Circular ESF			58 days after fracture diagnosis, the bird was recovered completely.
Sample et al.	2008	Whooping crane	Open proximal comminuted humeral fracture	Tie-in	Aspergillosis (itraconazole was administered)	Week 4: callus formation. Week 8: callus bridging. Week 11: further callus remodeling. Week 14: both cortices re-established.	Recombinant human bone morphogenic protein-2 was used.
Folland et al.	2016	Bald eagle	Elbow joint malfunctioning (possibly due to the osteomyelitis developed during previous humeral fracture healing) (arthrodesis)	Type 1 (the first attempt failed, then modified with lag screws)	Osteomyelitis, severe wing drooping	Week 9: significant bony fusion	The second attempt for the arthrodesis was successful
Arias et al.	2015	Slender-billed parakeet	Closed distal transverse tibiotarsal fracture	Type 1		Week 4: initial callus formation with the osseous union. Week 6: mature and well-organized callus.	Eight weeks after surgery, the bird was released
Rui et al.	2017	Rock pigeon	Open midshaft tarsometatarsal fracture	Type 2		Day 15: no presence of callus or disappearance of fracture. Day 60: bone healing was confirmed	

Data summary table (continue)

Author	Year	Species	Orthopedic condition	ESF type	Complications	Radiography & clinical findings	Remarks
Bueno et al.	2015	American kestrel			Broken ESF pin at 14 days. The bird was healed and released		
		Bald eagle (x11)					
		Barred owl					
		Broad-winged hawk (x2)					
		Eastern screech owl					
		Great gray owl (x2)	Tibiotarsal Fracture (35 closed, 2 open)	Tie-in	ESF pin loosening in one case (the bird was euthanized).	Week 2-3: sufficient callus was formed (IM pin was removed). Week 4-5: continuous callus formation and weight-bearing on the affected limb (ESF implant was removed).	20/34 birds were healed completely and returned to their former status. Five fracture healing complications. One case of aspergillosis and one case of plasmodium died.
		Great horned owl (x6)					
		Harris hawk					
		Osprey					
		Peregrine falcon (x3)					
Red-tailed hawk (x7)				ESF pin loosening in one case (the bird was completely healed and released).			
		Turkey vulture					
Hoybergs et al.	2008	Harris's hawk	Open midshaft transverse tarsometatarsal fracture	Type 2	Osteolysis	Week 6: good healing with low and medium osteolysis around the pins.	Osteolysis was cured, and the fracture was healed.

Data summary table (*continue*)

Author	Year	Species	Orthopedic condition	ESF type	Complications	Radiography & clinical findings	Remarks
Katogiritis et al.	2019	Amazon parrot	Open comminuted midshaft tarsometatarsal fracture		Slight shortening	One month: bridging callus formation. Two months: Progressive osseous bridging & healing of the fracture line.	Both tarsometatarsi had a fracture. The left one was treated with coaptation and lost three fingers. The right one got circular ESF. Both fractures healed.
		Catalina macaw	Closed oblique proximal tibiotarsal fracture	Circular ESF	Slight shortening	Day 1: poor apposition of the fracture ends & misalignment of fragments. Week 12: healed fracture & slight shortening of the left tibiotarsus	
Rochat et al.	2005	Bald eagle	Malunion in tibiotarsus (osteotomy)	Type 1 hybrid (4/circular)	Fracture in ulna	Day 27: pins were stable, and healing progress was good. Day 47: good callus formation. Day 63: osteotomy healed, and ESF removed.	Falconry techniques were used.
Kaya & Özsoy	2017	Chukar partridges (x7) Domestic pigeons (x12)	Tibiotarsal rotation (osteotomy)	Tie-in	No complications	Day 22: sufficient callus formation.	The mean time for complete recovery was 46 and 47 days for pigeons and partridges, respectively.
Burdeaux & Wade	2018	Snowy owl	Open transverse midshaft Metacarpal fracture	Type 2 (minimal): 2/2 on one side 1/1 on the other side	Synostosis	Day 25: callus formation. Day 42: periosteal callus at the fracture site and no sign of osteomyelitis.	Severe feather louse infestation. Delayed skin closure (day 25). The bird was recaptured in poor body condition. The birds were maintained and released again.
Ackermann & Redig	1997	Long-eared owl		Transarticular ESF	Aspergillosis		Luxation healed, but the bird died two weeks after removal of ESF due to severe aspergillosis.
		Sharp-shinned hawk	Closed elbow luxation	Transarticular ESF	low motion range of the joint		Luxation healed, but its extension was not enough for optimum flight (the bird was not released).

Data summary table (*continue*)

Author	Year	Species	Orthopedic condition	ESF type	Complications	Radiography & clinical findings	Remarks
		Peregrine falcon		Transarticular ESF	No complications		The bird was released into the wild after falconry training.
		Eastern screech owl		Transarticular ESF	No complications		Removing the ESF caused a transverse fracture in the ulna. The bird was released into the wild two weeks after the removal of ESF.
Kavanagh	1997	Scarlet macaw	Close transverse proximal tibiotarsal fracture	Type 2 (2/2)		Week 6: callus bridging. Week 11: callus remodeling with the osseous union.	The bird had full use of the limb.
		Hyacinth macaw	Closed transverse midshaft tibiotarsal fracture		No complications		
		Blue and gold macaw	Closed transverse midshaft tibiotarsal fracture		No complications		
		Blue and gold macaw	Closed transverse midshaft tibiotarsal fracture	Type 2 (2/2)	No complications		
		Sulfur-crested cockatoo	Closed spiral midshaft tibiotarsal fracture		No complications		
		African grey parrot	Closed transverse midshaft tibiotarsal fracture		No complications		
Meij et al.	1996	Peacock	Closed comminuted proximal tibiotarsal fracture	Type 2 (3/3)	No complications		
		Domestic fowl	Closed comminuted distal tibiotarsal fracture	Type 2 (2/2)	No complications		
		Racing pigeon	Closed comminuted proximal tibiotarsal fracture	Type 2 (1/2)	Malunion		The fracture was not healed (the bird was euthanized)

Data summary table (continue)

Author	Year	Species	Orthopedic condition	ESF type	Complications	Radiography & clinical findings	Remarks
		African grey parrot	Tibiotarsal angular deformity (osteotomy)		No complications		
		Racing pigeon	Tibiotarsal angular deformity (osteotomy)	Type 2 (2/2)	Malunion		The deformity was not healed
		African grey parrot	Tibiotarsal angular deformity (arthrodesis)		No complications		
		Amazon parrot	Tibiotarsal angular deformity (arthrodesis)		No complications		
Rahal et al.	2008	Toco toucan	Tarsometatarsal malunion (osteotomy)	2/2 type 2	Pin tract drainage	Day 15: periosteal callus formation. Day 62: healing of the osteotomy.	
Montgomery et al.	2011	Bald eagle	Open comminuted midshaft tarsometatarsal fracture	3/3 type 1	Pin loosening		falconry techniques were used
Jones & Redig	2001	Red-tailed hawk	Closed comminuted midshaft humeral fracture	Tie-in		Week 2: increase the defect's radiodensity at the fracture site and incorporate the graft material into the callus. Week 3: periosteal, intercortical, and medullary bridging was evident radiographically. Week 5: bridging was complete, and remodeling was evident.	The humerus had a defect: autologous callus was used to fill the defect (falconry techniques).
Yoon et al.	2008b	Great Horned Owl	Close comminuted midshaft tibiotarsus & ulnar fracture	Tie-in	No complications	Week 6: smooth callus formation. Week 13: bridging callus was formed over cortices of the fracture area.	
Yoon et al.	2008a	Raptor species (x19)	Humeral fracture (x12) Tibiotarsal fracture (x4) Ulnar fracture (x2) Femoral fracture	Tie-in	No complications		All the birds were released or returned to their former status.
Vergneau-Grosset et al.	2019	Raptor species	Ulnar fracture (x6)	Type 1	Osteomyelitis (one case) Malunion (two cases)		Eight of 14 birds were released.

Data summary table (continue)

Author	Year	Species	Orthopedic condition	ESF type	Complications	Radiography & clinical findings	Remarks
		Peregrine falcon	ulnar	Tie-in	Osteomyelitis (one case) Malunion (two cases)		Eight of 14 birds were released.
			ulnar & radial (x2)	Tie in & IM			
			ulnar & radial	Tie in & type 1			
			ulnar & radial (x2)	Tie-in			
			ulnar & radial	Type 1			
			ulnar	Type 1			
Bueno et al.	2019	Great horned owl	Open distal oblique tibiotarsal fracture. Shortening happened (osteotomy to distract osteogenesis)	Tie-in (shortening happened). Circular ESF (distract osteogenesis).	Shortening, pododermatitis		falconry techniques were used
			Closed fracture midshaft tibiotarsal fracture	Type I (shortening happened). Circular ESF (distract osteogenesis).	Shortening, malunion		
Hatt et al.	2007	Blue-fronted amazon	Closed comminuted midshaft humeral fracture	Tie-in	IM pin loosening		Delayed healing
			Cockatiel	Closed comminuted midshaft humeral fracture	Tie-in		
		Wild-caught hobby	Open comminuted midshaft humeral fracture	Tie-in	No complication		
			Wild-caught tawny owl	Open comminuted midshaft ulnar & radial fracture	Type 1		
		Wild-caught tawny owl	Open comminuted midshaft ulnar & radial fracture	Type 1	No complication		

Data summary table (continue)

Author	Year	Species	Orthopedic condition	ESF type	Complications	Radiography & clinical findings	Remarks
		Grey parrot	Open comminuted proximal ulnar & radial fracture	Type 1	Non-union		Amputation
		Grey parrot	Closed comminuted midshaft femoral fracture	Tie-in	No complication		
		Wild-caught red kite	Closed comminuted midshaft femoral fracture	Type 1	Minor instability		
		Grey parrot	Tibiotarsal deformity (osteotomy)	Type 2	No complication		
		Goshawk	Closed proximal oblique tibiotarsal fracture	Type 2	No complication		
		Hawk-headed parrot	Closed distal oblique tibiotarsal fracture	Type 2	No complication		
		Grey parrot	Closed distal oblique tibiotarsal fracture	Type 2	No complication		
		White cockatoo	Closed comminuted midshaft tibiotarsal fracture	Tie-in	No complication		
		Grey parrot	Closed comminuted midshaft tibiotarsal fracture	Type 1	Slow callus formation		
		Blue-fronted amazon	Closed transverse midshaft tibiotarsal fracture	Type 2	Malunion		Delayed healing
		Bali starling	Open simple midshaft tarsometatarsal fracture	Type 2	Osteomyelitis, soft tissue infection		Amputation
		Bodin's amazon	Open simple distal tarsometatarsal fracture	Tie-in	Non-union		Amputation
		Wild-caught barn owl	Open comminuted midshaft tarsometatarsus	Type 2	Osteolysis around one pin		

Data summary table (*continue*)

Author	Year	Species	Orthopedic condition	ESF type	Complications	Radiography & clinical findings	Remarks	
Vergneau-Grosset et al.	2020	Merlin (x3)	Open transverse midshaft radial & ulnar fracture	Type 1				
			Closed comminuted radial & ulnar fracture	Tie-in			Ulnar fracture healed only (not released)	
			Closed distal radial & ulnar fracture	Tie-in				
		Snowy owl (x3)	Open oblique midshaft radial & ulnar fracture	Type 1				Died during anesthesia
			Open proximal radial & ulnar fracture (x2)	Type 1				Both radial & ulnar fractures healed (died)
			Open comminuted midshaft radial & ulnar fracture	Tie-in				
		Sharp-shinned hawk (x5)	Open oblique midshaft radial & ulnar fracture	Tie-in				Released
			Open transverse midshaft radial & ulnar fracture	Type 1				
			Open oblique proximal radial & ulnar fracture	Type 1				
		Red-tailed hawk	Closed proximal radial & ulnar fracture	Tie-in				Ulnar fracture healed only (not released)
			Closed transverse midshaft radial & ulnar fracture	Tie-in	Low motion range of carpal joint			Ulnar fracture healed only (euthanized)
			Closed transverse proximal radial & ulnar fracture	Tie-in				Ulnar fracture healed only, with a low carpal joint extension (not released). Ulna radiectomy (not released)
Short-eared owl (x3)	Open proximal radial & ulnar fracture	Tie-in				Ulnar fracture healed only (not released)		
	Open distal radial & ulnar fracture	Tie-in				Ulnar fracture healed only (not released)		

Data summary table (continue)

Author	Year	Species	Orthopedic condition	ESF type	Complications	Radiography & clinical findings	Remarks			
Vergneau-Grosset et al.	2020	American kestrel	Open proximal radial fracture	Type 1			Ulnar fracture healed only (not released)			
			Open comminuted midshaft radial & ulnar fracture	Type 1			Released			
			Broad-winged hawk (x3)	Open proximal radial & ulnar fracture (x2)	Tie-in			Ulna radiectomy (not released)		
			Peregrine falcon	Closed oblique distal radial & ulnar fracture	Tie-in			Both radial & ulnar fractures healed (not released)		
			Cooper's hawk	Open comminuted midshaft radial & ulnar fracture	Tie-in			Ulnar fracture healed only (not released)		
			Barred Owl	Closed transverse distal radial & ulnar fracture	Tie-in			Ulnar fracture healed only (not released)		
			Turkey vulture	Closed transverse proximal radial & ulnar fracture	Tie-in	Malunion		Both radial & ulnar fractures healed malunion occurred (not released)		
			Great horned owl	Closed midshaft radial & ulnar fracture	Tie-in			Released		
			Rosenthal et al.	1994	Moluccan cockatoo	Open stifle joint luxation (arthrodesis)	Type 1	Severe derangement, secondary cartilage damage	Day 26: signs of bony fusion of femur to tibiotarsus. Day 47: bony remodeling at the arthrodesis site. Day 90: continuation of bony remodeling. Month 7: increase in bony fusion.	The luxation was closed, but the distal femur had perforated the skin.
						Closed stifle joint luxation	Type 1	50% reduction in motion range of elbow		Five weeks after surgery the joint recovered its motion range.
Martin et al.	1993	Great horned owl	Closed elbow luxation	Transarticular	20% reduction in motion range of elbow		With physical therapy motion range of the elbow recovered, and the bird was released.			

Data summary table (*continue*)

Author	Year	Species	Orthopedic condition	ESF type	Complications	Radiography & clinical findings	Remarks
		Prairie falcon	Open elbow luxation	Transarticular	The motion range of the elbow joint was restricted to 90 degrees		There was a proximal radial fracture on the same wing. The fracture was treated with an IM pin (bird kept for teaching purposes)
		Prairie falcon	Closed elbow luxation	Type 2	Decrease in elbow's range of motion		With physical therapy motion range of the elbow recovered, and the bird was released
Carrasco et al.	2017	Pet birds (x35)	Tibiotarsal fracture	Tie-in	Osteolysis (x3) New fracture during removal of IM pin (x2) Minor malunion (x1)		27/35 fractures healed



Spectral Gradient Method with Log-determinant Norm for Solving Non-Linear System of Equations

Yeong Lin Koay¹, Hong Seng Sim^{1*}, Yong Kheng Goh¹ and Sing Yee Chua²

¹Department of Mathematical and Actuarial Sciences, Lee Kong Chian Faculty of Engineering and Science, Universiti Tunku Abdul Rahman, 43000 Selangor, Malaysia

²Department of Electrical and Electronic Engineering, Lee Kong Chian Faculty of Engineering and Science, Universiti Tunku Abdul Rahman, 43000 Selangor, Malaysia

ABSTRACT

Solving a system of non-linear equations has always been a complex issue whereby various methods were carried out. However, most of the methods used are optimization-based methods. This paper has modified the spectral gradient method with the backtracking line search technique to solve the non-linear systems. The efficiency of the modified spectral gradient method is tested by comparing the number of iterations, the number of function calls, and computational time with some existing methods. As a result, the proposed method shows better performance and gives more stable results than some existing methods. Moreover, it can be useful in solving some non-linear application problems. Therefore, the proposed method can be considered an alternative for solving non-linear systems.

Keywords: Jacobian, log-determinant norm, nonlinear systems, optimization, spectral gradient method

INTRODUCTION

Solving a system of non-linear equations has always been a complex issue whereby various methods were carried out. The scenario becomes challenging if the system does not show good linear or polynomial characteristics. Non-linear equation systems exist in various fields, such as chemistry, engineering, and medicine.

Let $F : R^n \rightarrow R^n$ be a continuously differentiable function, and then the non-linear equation systems can be expressed as Equation 1:

$$F(x) = 0, \quad x \in R^n \quad (1)$$

ARTICLE INFO

Article history:

Received: 30 October 2021

Accepted: 27 January 2022

Published: 20 April 2022

DOI: <https://doi.org/10.47836/pjst.30.3.05>

E-mail addresses:

koayyeonglin@gmail.com (Yeong Lin Koay)

simhs@utar.edu.my (Hong Seng Sim)

gohyk@utar.edu.my (Yong Kheng Goh)

sychua@utar.edu.my (Sing Yee Chua)

* Corresponding author

In solving a system of non-linear Equation 1, some iterative methods exist. Most of the methods used are optimization-based. There is a close relationship between solving a series of non-linear equations and finding a local minimum. A local minimum of an objective function corresponds to the point where derivatives of the objective function are zero. If one considers a system of non-linear equations as the derivatives of a particular objective function, then seeking a solution to the non-linear system is equivalent to minimizing the objective function. Such equations satisfied at the current point are considered constraints at each stage, whereas others are considered objective functions.

This paper proposes modifying the spectral gradient method in solving the non-linear systems under a modified backtracking line search strategy. The paper is organized as follows: the section materials and methods introduce standard optimization methods that compare with the proposed method and the modified spectral gradient method to solve non-linear systems. Then, the section “Result and Discussion” shows the numerical results of the test problems and some real-life applications. Finally, conclusions will be presented in the last section of the paper.

MATERIALS AND METHODS

Standard Optimization Methods

The standard way of solving a non-linear system of Equation 1 is to assume an initial approximation x_0 and then perform an iterative formula in the form of Equation 2

$$x_{k+1} = x_k + \mu_k d_k, \text{ for } k \geq 0 \quad (2)$$

where x_k is the current solution approximation and x_{k+1} is the next approximation of the solution for the non-linear system. The vector d_k represents the search direction, and the scalar μ_k defines the step length. At each step, the results of the current iteration are used as the initial point for the next iteration. To generate x_{k+1} closer to the solution, we will need to choose an appropriate form of d_k and μ_k .

The steepest descent (SD) method was first raised by Cauchy (1847). It is one of the simplest and most well-known methods for minimizing non-linear functions. SD method updates the current point μ_k in the opposite direction of the gradient, g_k of the function (Equation 3).

$$d_k = -g_k \quad (3)$$

Apart from well-conditioned problems, the traditional SD approach performs poorly. Raydan and Svaiter (2002) noted that the bad behavior of the SD approach is not related to the choice of search direction. Instead, poor behavior is related to the optimal selection of step length by Cauchy. Despite the small storage capacity and very low computational

expense per execution, the SD approach has been known as extremely poor and inefficient due to the slow convergence speed and oscillatory behavior. Therefore, the SD method is not often used in practice.

The convergence of the Cauchy traditional SD method has been deeply studied. It has been found that it is related to the spectral properties of the Hessian matrix. De Asmundis et al. (2013) recommended a way to improve the SD method. The purpose of the modification is to force the gradients into a one-dimensional subspace as the iterations progress. It may avoid the key reason for the SD method's slow convergence, which is the classical zigzag pattern.

Hestenes and Stiefel (1952) published the first paper on the conjugate gradient (CG) method for solving linear systems. Currently, the CG method is a commonly used method to solve non-linear problems of large-scale systems. It performs the update by combining the previous and new directions to approximate the optimal solutions. The search direction d_k and the scalar β_{k-1} are defined as Equations 4 and 5

$$d_k = -g_k + \beta_{k-1}d_{k-1}, \quad (4)$$

where

$$\beta_{k-1} = \frac{g_k^T g_k}{g_{k-1}^T g_{k-1}}. \quad (5)$$

CG method has a small space requirement and good properties for global convergence. CG method is characterized to carry out a learning approach that falls between SD and Newton's method (Marini, 2009). The method aims to speed up the convergence rate of the classic SD method while minimizing the computational load associated with Newton's method's processes, such as storage requirement and computation of the inverse Hessian.

One of the methods that can be used to solve non-linear equations is Newton's method, also known as the Newton-Raphson method. The method was first published by Wallis (1095). Simpson (1740) defined Newton's method as an iterative approach used to solve general non-linear equations using calculus. In addition, Simpson claimed that Newton's method could also be used to solve optimization problems by setting the slope to zero.

However, the weakness of Newton's approach is that it often fails to converge and might be stuck in a repeating cycle. Even the convergence requirements of this approach are well understood, but still, this approach depends on the assumption that the initial solution is reasonably good. Thus, this method is not considered a successful practical procedure. Broyden (1965) also noted another disadvantage: the difficulty of measuring the Jacobian matrix. Even though the functions are extremely straightforward to obtain their partial derivatives, the efforts needed to determine the matrix may be excessive. The execution of Newton's method will become expensive.

Therefore, quasi-Newton approaches have developed. Martinez (2000) has mentioned that the quasi-Newton method is a static Newton method and a discrete Newton method. If the Jacobian matrix is large for the discrete Newton method, it is not comparable with the inexpensive linear algebra models. Nevertheless, discrete Newton algorithms are successful in many large sparse problems. Here a large sparse problem means a problem involving a high dimensional sparse matrix. In such situations, the limited difference method allows us to use a small number of functional calculations to measure the estimated Jacobian. The matrix form is not expensive to be factorized.

Quasi-Newton approaches are used for solving unconstrained optimization problems. Some quasi-Newton approaches are popular because many linear algebra iterations are avoided. Martinez (2000) stated that before 1990, there had been many published articles on numerical analysis research of the quasi-Newton method for solving non-linear systems. However, the study might be out of practice after the method involved in the usual practice of problem solvers in other fields, such as engineering and manufacturing. While the users know these benefits and weaknesses, quasi-Newton methods can be used to solve large-scale non-linear problems. There are some common quasi-Newton algorithms such as symmetric rank-one, Davidon-Fletcher-Powell (DFP), Broyden-Fletcher-Goldfarb-Shanno (BFGS), and Berndt-Hall-Hall-Hausman.

BFGS method is part of the quasi-Newton methods. BFGS method can be used to solve unconstrained non-linear optimization problems. Instead of directly computing the exact Hessian matrix, the BFGS method approximates the Hessian matrix by using a full rank matrix. It is an efficient method to deal with small or medium-scale problems. However, the BFGS method requires many iterations and function calls in solving large-scale problems. When the Hessian matrix is ill-conditioned, an inappropriate initial approximation of the Hessian matrix or a poorly defined search direction will result in the inefficiency of the method (Cheng & Li, 2010).

The approximation of Hessian B_{k+1} is defined by Equation 6

$$B_{k+1} = \begin{cases} B_k - \frac{B_k s_k s_k^T B_k}{s_k^T B_k s_k} + \frac{y_k y_k^T}{y_k^T s_k}, & \text{if } s_k^T y_k > 0 \\ B_k, & \text{otherwise} \end{cases} \tag{6}$$

where s_k and y_k are defined as Equations 7 and 8

$$s_k = x_{k+1} - x_k \tag{7}$$

$$y_k = F_{k+1} - F_k \tag{8}$$

and F is the non-linear equation system.

The presence of Jacobian matrix computation during the selection of the step length might increase the difficulty. Hence, the modified BFGS approach has been proposed with

the backtracking line search techniques that avoid computing the Jacobian matrix. Yuan and Lu (2008) introduced a new backtracking inexact BFGS method for solving symmetric non-linear equations. The modified BFGS method has a descent property norm, where under appropriate circumstances, the global and superlinear convergence will be guaranteed. The authors have shown that the modified BFGS method with the new backtracking line search is more efficient than the Jacobian matrix computation technique.

Spectral gradient (SG) methods for minimization originated from Barzilai-Borwein. Barzilai and Borwein (1988) proposed a two-point step size gradient method. Raydan (1993) has developed the convergence for quadratics of the spectral gradient method. One unique way of dealing with large-scale problems is the spectral gradient method. This method is a nonmonotone step length associated with the gradient approach to overcome the Cauchy method's weaknesses. Different techniques have been proposed since there are many variations when choosing the effective step length along the negative gradient direction (Biglari & Solimanpur, 2013). This method is obtained by approximation of the secant equation for the SD method. At each iteration, a descent in the objective function is not guaranteed in the SG method; however, it outperforms the traditional SD method in practice (Raydan, 1997). This method delivers better efficiency and low-cost computations than the traditional SD method since it needs a small number of storage locations. By combining the classical SG method with better nonmonotone line search strategies, the method's effectiveness can be greatly increased (Xiao et al., 2010).

If the Hessian matrix of the objective function is ill-conditioned, it will lead to the inefficiency of the gradient methods. The gradient methods have a fixed condition in selecting the step length to reduce the function value. Therefore, it will cause the slow convergence of a stable complex system. Dealing with the problem of inefficiency, Sim et al. (2019) have modified the SG method. This method is proposed to improve the slow convergence issues. It operates separately on the gradient vector norm and the objective function simultaneously. Furthermore, this method is combined with some line search strategies. The line search reduces the function evaluation, whereas an individual adaptive parameter damps the gradient vector. The proposed method is developed under the backtracking and nonmonotone line search. Finally, the comparison is made between the proposed method and some well-known CG-based methods since the CG methods have extremely good convergence properties. Sim et al. (2019) proved that the proposed spectral gradient method is a comparative alternative for solving large-scale problems.

The modification of SG methods and their applications have been studied in recent years (Abubakar et al., 2020; Antonelli et al., 2016; Ibrahim et al., 2020). For example, Raydan (1997) combined the Barzilai and Borwein technique with a nonmonotone line search strategy that ensures global convergence. The results show that using the global Barzilai and Borwein technique might reduce the gradient evaluations and the number of line searches. Besides, the SG method can be accelerated by using an alternating strategy

that cycles between the SD and SG steps (Xiao et al., 2010). The Barzilai–Borwein (CBB) approach (Dai et al., 2006) contributed significantly to this scheme.

Cruz and Raydan (2003) developed a method for solving non-linear systems of equations using the spectral method. The authors present an approach for ensuring global convergence based on nonmonotone line search techniques and details of the implementation for handling large-scale problems. Zhang and Zhou (2006) have proposed an approach for solving non-linear monotone equations. A modified spectral gradient approach and a projection method (Solodov & Svaiter, 1998) are combined in this method. If the non-linear equations to be solved are monotone and Lipschitz continuous, it has been proven to be globally convergent to a solution of the system. This method is also able to solve non-smooth equations.

In recent years, there has been a significant increase in the application of optimization techniques. Due to the advantages and disadvantages of different classical optimization methods, many modifications have been made. Modifying those methods aims to improve the overall performance, such as efficiency, computational time, and convergence rate. In a nutshell, various optimization methods are proposed to solve the non-linear system, and the SG method has been modified to solve non-linear systems in this paper.

Line Search Strategy

The backtracking Armijo algorithm (BTA) is a line search strategy to select the best step length. The BTA algorithm begins with a large approximation of the step length. Then, depending on the local gradient of the objective function, it will gradually reduce the step length, known as “backtracking,” until a satisfactory reduction is detected in the objective function. The algorithm for modified backtracking line search strategy with Armijo condition is given as Equation 9:

Step 0: Given constants $\delta \in (0,1)$.

Step 1: Set $k = 0$ and $\mu = 1$.

Step 2: Test the relation

$$\|F(x_k + \mu_k d_k)\|_2^2 \leq \|F(x_k)\|_2^2 + \delta \mu_k^2 F_k^T d_k \tag{9}$$

where $d_k = -B_k^{-1} g_k$.

Step 3: If Equation 9 does not satisfy, choose a new $\mu \rightarrow \frac{1}{2} \mu$ and set $k = k + 1$, then go

to Step 2. Otherwise, set $\mu_k = \mu$ and $x_{k+1} = x_k + \mu_k d_k$.

Spectral Gradient Method with Log-Determinant Norm

In order to derive an updated scheme for B_k , a restriction for components of B_k under some measures is imposed by minimizing the log-determinant norm and allowing them to satisfy

the secant equation. Hence, for any positive matrix B , the solution is given by the updated B_{k+1} (Equations 10 & 11):

$$\min tr(B_{k+1}) - \ln(\det(B_{k+1})) \quad (10)$$

$$\text{s.t. } s_k^T B_{k+1} s_k = s_k^T y_k \quad (11)$$

where tr is the trace of a square matrix, defined as the sum of elements on the main diagonal of the matrix; \det is the determinant of a matrix. Note that B_k is a symmetric matrix; for simplicity, this paper only consider the case B_k is diagonal.

Let $B_{k+1} = \text{diag}(B_{k+1}^{(1)}, \dots, B_{k+1}^{(n)})$ and $s_k^T = (s_k^{(1)}, \dots, s_k^{(n)})$, the minimization Equations 10 and 11 become Equations 12 and 13:

$$\min \left(\sum_{i=1}^n B_{k+1}^{(i)} \right) - \ln \left(\prod_{i=1}^n B_{k+1}^{(i)} \right) \quad (12)$$

$$\text{s.t. } \left(\sum_{i=1}^n (s_k^{(i)})^2 B_{k+1}^{(i)} \right) - \sum_{i=1}^n s_k^{(i)} y_k^{(i)} = 0 \quad (13)$$

By applying the Lagrange method to the minimization, Equations 12 and 13 become Equation 14:

$$L(\omega) = \left(\sum_{i=1}^n B_{k+1}^{(i)} \right) - \ln \left(\prod_{i=1}^n B_{k+1}^{(i)} \right) + \omega \left[\sum_{i=1}^n (s_k^{(i)})^2 (B_{k+1}^{(i)}) - s_k^T y_k \right] \quad (14)$$

where ω is the Lagrange multiplier.

Differentiate Equation 14 with respect to $B_{k+1}^{(i)}$ and set the derivatives to zero (Equation 15):

$$\frac{\partial L}{\partial B_{k+1}^{(i)}} = 1 - \frac{1}{B_{k+1}^{(i)}} + \omega (s_k^{(i)})^2 = 0, i = 1, 2, \dots, n \quad (15)$$

then gives Equation 16

$$B_{k+1}^{(i)} = \frac{1}{1 + \omega (s_k^{(i)})^2}, i = 1, 2, \dots, n \quad (16)$$

By substituting Equation 16 into constraint Equation 13 and rewriting the left-hand side of Equation 13 as a function of ω (Equation 17):

$$F(\omega) = \sum_{i=1}^n \frac{(s_k^{(i)})^2}{1 + \omega (s_k^{(i)})^2} - s_k^T y_k \quad (17)$$

where the Lagrange multiplier ω can be obtained by solving the non-linear equation $F(\omega) = 0$. It can be approximated by applying only one iteration of Newton-Raphson,

with $\omega = 0$. When $s_k^T s_k > s_k^T y_k$, Equation 17 has a unique positive solution and hence, the Lagrange multiplier ω_k can be approximated by using Equation 18:

$$\begin{aligned} \omega_k &\approx \omega - \frac{F(\omega)}{F'(\omega)} \\ &= \frac{s_k^T s_k - s_k^T y_k}{\sum_{i=1}^n (s_k^{(i)})^4} \end{aligned} \tag{18}$$

Lastly, the updating formula for B_{k+1} is given as Equation 19

$$B_{k+1} = \begin{cases} \text{diag}(B_{k+1}^{(1)}, \dots, B_{k+1}^{(n)}), & \text{if } s_k^T s_k > s_k^T y_k \\ \frac{s_k^T y_k}{s_k^T s_k} I, & \text{otherwise} \end{cases} \tag{19}$$

Where $\frac{s_k^T y_k}{s_k^T s_k}$ exactly the Oren-Luenberger scaling (Luenberger and Ye, 1984), B_{k+1} as

defined in Equation 19 and ω is defined in Equation 18.

The algorithm for modified spectral gradient method is shown below:

- Step 0: Set $k = 0$. Given initial guessing point x_0 , tolerance $\in (0,1)$ and B_0 .
- Step 1: If $\|F_k\|_2 = 0$, then stop.
- Step 2: Calculate $y_k = F_{k+1} - F_k$, $y_k = F_{k+1} - F_k$ and ω based on Equation 18.
- Step 3: Calculate B_{k+1} from Equation 19.
- Step 4: Obtain μ_k through the modified BTA algorithm.
- Step 5: Compute $x_{k+1} = x_k + \mu_k d_k$, for $k \geq 0$, where $d_k = -B_k^{-1} F_k$.
- Step 6: Set $k = k + 1$ and go to Step 1.

Convergence Analysis

This section briefly discusses the convergence of the modified spectral gradient method. The detailed proofs can be referred to Sim et al. (2019).

Assumption 1.

- a. The objective function f is twice continuously differentiable.
- b. The level set $D = \{x \in R^n : f(x) \leq f(x_0)\}$ is convex.
- c. There exist positive constants M_1 and M_2 such that

$$M_1 \|z\|_2^2 \leq z^T G(x) z \leq M_2 \|z\|_2^2,$$

for $\forall z \in D$ and $\forall x \in D$. It implies that the objective function f has a unique minimize x^* in x_0 .

Lemma 1. Let x_0 be a starting point and $B_0 = I$, where I is the $n \times n$ identity matrix.

Then for C_1 defined by Equation 19, the sequence $\{\|B_k\|_2\}$ is bounded by some positive constants c_1 and c_2 , i.e. $0 < c_1 < B_0 < B_1 < \dots < B_k < \dots < c_2$.

The proof of Lemma 1 is based on the assumptions provided by Byrd and Nocedal (1989). The next lemma is a direct result of Lemma 1.

Lemma 2. Suppose that the assumptions in Lemma 1 hold, then there exist positive constants c_3 and c_4 such that

$$d_k^T g_k \leq -c_3 \|F_k\|_2^2 \text{ and } \|d_k\|_2^2 \leq -c_4 \|F_k\|_2^2,$$

where $d_k = -B_k^{-1} F_k$ where c_1 is defined by Equation 19.

The convergence of the spectral gradient method using the BTA line search algorithm is presented in the next theorem.

Theorem 1. Under assumption by Bryd and Nocedal (1989), there exist positive constants c_1 and c_2 such that, for any x_k and any d_k with $F_k^T d_k < 0$, the step length μ_k produced by the BTA Algorithm will satisfy either

$$\|F(x_k + \mu_k d_k)\|_2^2 - \|F(x_k)\|_2^2 \leq -c_1 \frac{(F_k^T d_k)^2}{\|d_k\|_2^2}$$

or

$$\|F(x_k + \mu_k d_k)\|_2^2 - \|F(x_k)\|_2^2 \leq -c_2 F_k^T d_k$$

Furthermore, if d_k satisfies the following conditions:

$$F_k^T d_k \leq c_3 \|F(x_k)\|_2^2,$$

$$\|d_k\|_2 \leq -c_4 \|F_k\|_2$$

for some positive constants c_3 and c_4 , then

$$\lim_{k \rightarrow \infty} \|F_k\|_2 = 0.$$

In the next section, numerical experiments are conducted to compare the efficiency of the proposed method.

RESULTS AND DISCUSSIONS

Numerical Experiments and Discussion

This section applies the modified SG method to solve some non-linear systems. The comparison is made between the modified SG method and three other methods under the modified BTA line search strategy. The following methods are taken into consideration:

1. Modified Spectral Gradient Method (Modified SG)

2. Broyden-Fletcher-Goldfarb-Shanno Method (BFGS)
3. Steepest Descent Method (SD)
4. Conjugate Gradient Method (CG)

The step lengths μ_k are generated by the BTA algorithm with the parameter $\delta = 0.1$. The step length $\mu = 1$ is used as the initial step length and reduced if the Armijo condition does not satisfy. The minimum value for step length is set as 2^{-7} . Since the modified SG method and BFGS method require the computation of matrix B_k , the matrix B_0 is initialized to an identity matrix with dimension n .

There are two termination criteria for these methods: the norm of the non-linear functions and the number of iterations. The first termination criterion is $\|F_k\|_2 \leq 10^{-4}$ and the maximum number of iterations is set to be 10^4 . If the number of iterations exceeds 10^4 , the tested problem will be considered “fail to converge.” The codes are written in Python 3.7.9.

A total of 31 problems given by Fang et al. (2018) and Andrei (2008) have been used to test the performance of these methods. The dimensions of the tested problems are set as $n = 10, 100, 200$ and 500 , if the dimensions are not provided in the tested problems.

Using Dolan and Moré’s (2002) performance profile, the performance of the modified SG, BFGS, SD, and CG methods can be evaluated clearly. The performance of problem p by solver s is defined as Equation 20:

$$P(t \leq \tau) = \frac{1}{|\mathbf{P}|} \text{size}\{p \in \mathbf{P} : t_{p,s} \leq \tau\} \tag{20}$$

where the function $P(t \leq \tau)$ is the cumulative distribution function for the performance ratio, \mathbf{P} is a set of test problems, $|\mathbf{P}|$ denotes the cardinality of \mathbf{P} and $t_{p,s}$ represents the performance ratio within a factor τ which is a real number (Equation 21)

$$t_{p,s} = \frac{m_{p,s}}{\min\{m_{p,s} : s \in S\}} \tag{21}$$

where $m_{p,s}$ represents the performance measure of interest accordingly. It is obtained for each pair (p, s) of solver s in a set S of optimization solvers and problem p in a set P of test problems.

Figures 1, 2, and 3 are the performance profiling graphs for these methods, based on the number of iterations, function calls, and computational time. Figures 1 to 3 show that the BFGS method performs the best among these methods in terms of the number of iterations, function calls, and computational time. The modified SG method indicates a better performance compared to SD and CG methods. Besides, SD and CG methods exhibit a similar pattern, which shows a poorer performance than the modified SG and BFGS methods.

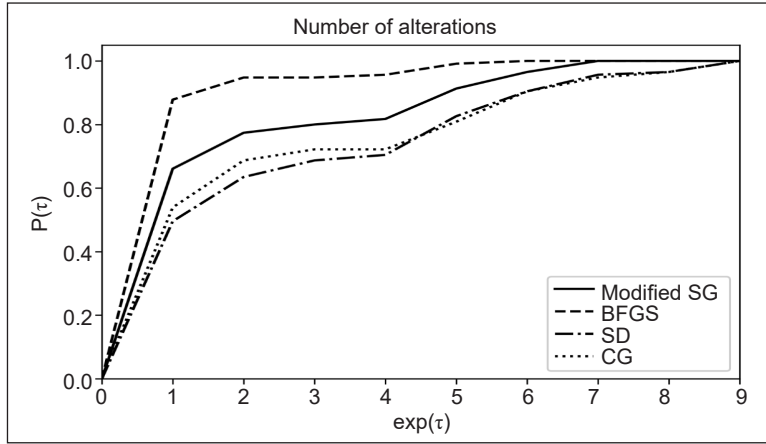


Figure 1. Comparison of methods in terms of the number of iterations

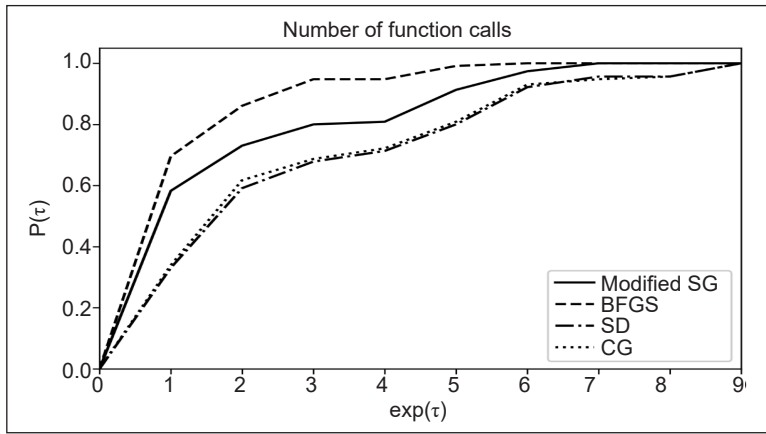


Figure 2. Comparison of methods in terms of the number of function calls

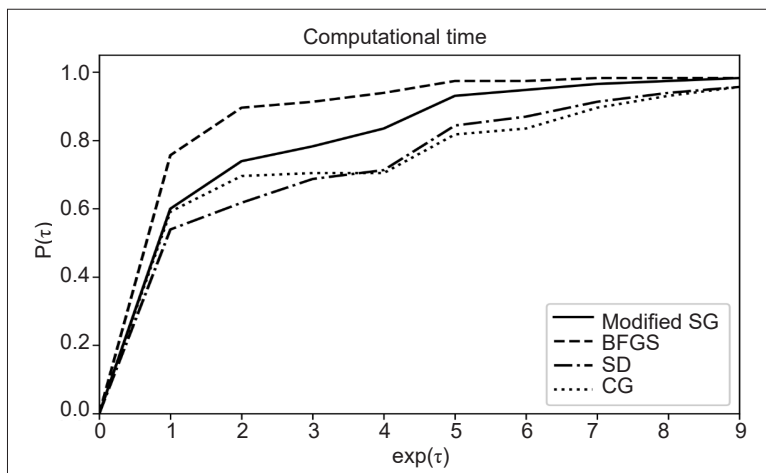


Figure 3. Comparison of methods in terms of CPU time in seconds

For the BFGS method, some of the tested problems require an extremely high number of iterations, number of function calls, and computational time compared to the modified SG method. Therefore, this study concludes that the modified SG method gives a more stable result than the BFGS method. One of the reasons the BFGS method gives better performance is that it uses the full rank matrix for B_k , while the modified SG method uses the diagonal matrix in the updating formula of B_k . Numerous researchers have suggested that the BFGS method is not appropriate for solving large-scale problems since high storage is required. Although the modified SG method is not showing the best performance among these methods, it is still considered an alternative to solve the non-linear tested problems.

Applications

Systems of non-linear equations occur in many areas of practical importance, such as engineering. In order to evaluate the performance of the modified SG method, six systems of nonlinear equations are considered. The application problems are provided by Chen et al. (2017), Grosan and Abraham (2008), Buzzi-Ferraris and Manenti (2013), and Turgut et al. (2014). These problems [(a) - (f)] are applied in both the engineering and science fields.

(a) Kinematic Application

$$\begin{cases} x_i^2 + x_{i+1}^2 - 1 = 0 \\ a_{1i}x_1x_3 + a_{2i}x_1x_4 + a_{3i}x_2x_3 + a_{4i}x_2x_4 + \\ a_{5i}x_2x_7 + a_{6i}x_5x_8 + a_{7i}x_6x_7 + a_{8i}x_6x_8 + \\ a_{9i}x_1 + a_{10i}x_2 + a_{11i}x_3 + a_{12i}x_4 + a_{13i}x_5 + \\ a_{14i}x_6 + a_{15i}x_7 + a_{16i}x_8 + a_{17i} = 0 \\ 1 \leq i \leq 4 \end{cases}$$

The initial guessing point used is

$$x^{(0)} = [-0.06, 0.78, -0.05, 0.38, -0.56, -0.70, 0.40, 0.09]^T$$

and the coefficients a_{ki} , $1 \leq k \leq 17, 1 \leq i \leq 4$, are given in Table 1.

Table 1
Coefficients a_{ki} for the Kinematic Application

a_{ki}	a_{k1}	a_{k2}	a_{k3}	a_{k4}
a_{1i}	- 0.249150680	+ 0.125016350	-0.635550070	+ 1.48947730
a_{2i}	+ 1.609135400	- 0.686607360	- 0.115719920	+ 0.23062341
a_{3i}	+ 0.279423430	- 0.119228120	- 0.666404480	+ 1.32810730
a_{4i}	+ 1.434801600	- 0.719940470	+ 0.110362110	- 0.25864503

Table 1 (continue)

a_{ki}	a_{kl}	a_{k2}	a_{k3}	a_{k4}
a_{5i}	+ 0.000000000	- 0.432419270	+ 0.290702030	+ 1.16517200
a_{6i}	+ 0.400263840	+ 0.000000000	+ 1.258776700	- 0.26908494
a_{7i}	- 0.800527680	+ 0.000000000	- 0.629388360	+ 0.53816987
a_{8i}	+ 0.000000000	- 0.864838550	+ 0.581404060	+ 0.58258598
a_{9i}	+ 0.074052388	- 0.037157270	+ 0.195946620	- 0.20816985
a_{10i}	- 0.083050031	+ 0.035436896	- 1.228034200	+ 2.68683200
a_{11i}	- 0.386159610	+ 0.085383482	+ 0.000000000	- 0.69910317
a_{12i}	- 0.755266030	+ 0.000000000	- 0.079034221	+ 0.35744413
a_{13i}	+ 0.504201680	- 0.039251967	+ 0.026387877	+ 1.24991170
a_{14i}	- 1.091628700	+ 0.000000000	- 0.057131430	+ 1.46773600
a_{15i}	+ 0.000000000	- 0.432419270	- 1.162808100	+ 1.16517200
a_{16i}	+ 0.049207290	+ 0.000000000	+ 1.258776700	+ 1.07633970
a_{17i}	+ 0.049207290	+ 0.013873010	+ 2.162575000	- 0.69686809

(b) Interval Arithmetic Benchmark Application

$$\left\{ \begin{array}{l} x_1 - 0.25428722 - 0.18324757x_4x_3x_9 = 0 \\ x_2 - 0.37842197 - 0.16275449x_1x_{10}x_6 = 0 \\ x_3 - 0.27162577 - 0.16955071x_1x_2x_{10} = 0 \\ x_4 - 0.19807914 - 0.15585316x_7x_1x_6 = 0 \\ x_5 - 0.44166728 - 0.19950920x_7x_6x_3 = 0 \\ x_6 - 0.14654113 - 0.14654113x_8x_5x_{10} = 0 \\ x_7 - 0.42937161 - 0.21180486x_2x_5x_8 = 0 \\ x_8 - 0.07056438 - 0.17081208x_1x_7x_6 = 0 \\ x_9 - 0.34504906 - 0.19612740x_{10}x_6x_8 = 0 \\ x_{10} - 0.42651102 - 0.21466544x_4x_8x_1 = 0 \end{array} \right.$$

The initial guessing point used is $x^{(0)} = [1, 1, 1, 1, 1, 1, 1, 1, 1, 1]^T$.

(c) Chemical Equilibrium

$$\left\{ \begin{array}{l} x_1 + x_4 - 3 = 0 \\ 2x_1 + x_2 + x_4 + x_7 + x_8 + x_9 + 2x_{10} - R = 0 \\ 2x_2 + 2x_5 + x_6 + x_7 - 8 = 0 \\ 2x_3 + x_9 - 4R = 0 \\ x_1x_5 - 0.193x_2x_4 = 0 \\ x_6\sqrt{x_1} - 0.002597\sqrt{x_2x_4 \cdot \sum_{i=1}^{10} x_i} = 0 \\ x_7\sqrt{x_4} - 0.003448\sqrt{x_1x_2 \cdot \sum_{i=1}^{10} x_i} = 0 \\ x_4x_8 - 1.799 \times 10^{-5} x_1 \cdot \sum_{i=1}^{10} x_i = 0 \\ x_4x_9 - 2.155 \times 10^{-4} x_1 \sqrt{x_3 \cdot \sum_{i=1}^{10} x_i} = 0 \\ x_{10}x_4^2 - 3.846 \times 10^{-5} x_4^2 \cdot \sum_{i=1}^{10} x_i = 0 \end{array} \right.$$

where R is 4.056734.

The initial guessing point used is

$$x^{(0)} = [0.15884, 0.89358, 8.11340, 2.84116, 3.08473, \\ 0.04039, 0.00300, 0.00002, 0.00013, 0.00058]^T$$

(d) Neurophysiology application

$$\left\{ \begin{array}{l} f_1 = x_1^2 + x_3^2 - 1 = 0 \\ f_2 = x_2^2 + x_4^2 - 1 = 0 \\ f_3 = x_5x_3^3 + x_6x_4^3 = 0 \\ f_4 = x_5x_1^3 + x_6x_2^3 = 0 \\ f_5 = x_5x_1x_3^2 + x_6x_4^2x_2 = 0 \\ f_6 = x_5x_1^2x_3 + x_6x_2^2x_4 = 0 \end{array} \right.$$

The initial guessing point used is $x^{(0)} = [0.446, -0.446, 0.895, 0.367, 0.367]^T$.

(e) Combustion application

$$\begin{cases} f_1 = x_2 + 2x_6 + x_9 + 2x_{10} - 10^{-5} = 0 \\ f_2 = x_3 + x_8 - 3 \cdot 10^{-5} = 0 \\ f_3 = x_1 + x_3 + 2x_5 + 2x_8 + x_9 + x_{10} - 5 \cdot 10^{-5} = 0 \\ f_4 = x_4 + 2x_7 - 10^{-5} = 0 \\ f_5 = 0.5140437 \cdot 10^{-7} x_5 - x_1^2 = 0 \\ f_6 = 0.100632 \cdot 10^{-6} x_6 - 2x_2^2 = 0 \\ f_7 = 0.7816278 \cdot 10^{-15} x_7 - x_4^2 = 0 \\ f_8 = 0.1496236 \cdot 10^{-6} x_8 - x_1 x_3 = 0 \\ f_9 = 0.6194411 \cdot 10^{-7} x_9 - x_1 x_2 = 0 \\ f_{10} = 0.2089296 \cdot 10^{-14} x_{10} - x_1 x_2^2 = 0 \end{cases}$$

The initial guessing point used is

$$x^{(0)} = [-5.9286 \cdot 10^{-8}, -6.9428 \cdot 10^{-5}, -0.2980, -8.8526 \cdot 10^{-5}, -0.4127, \\ -0.0547, 4.9253 \cdot 10^{-5}, 0.2981, 0.9453, -0.4179]^T.$$

(f) Experimental Test

$$\begin{cases} f_1(x_1, x_2) = \cos(2x_1) - \cos(2x_2) - 0.4 = 0 \\ f_2(x_1, x_2) = 2(x_2 - x_1) + \sin(2x_2) - \sin(2x_1) - 1.2 = 0 \end{cases}$$

The initial guessing point used is $x^{(0)} = [0.15, 0.49]^T$.

The results of the application problems are listed in Table 2. According to Table 2, it can be concluded that the modified SG method serves as another option to solve different systems of non-linear equations in real-life applications. Although the modified SG method gives a higher number of iterations, function calls, and computation time than the SD method in problems a and f, it performs better than CG and BFGS methods since they fail to converge in these two problems. Generally, the modified SG method indicates comparable results with the other three existing methods. In certain situations, the modified SG method exhibits more robust convergence properties than CG and BFGS.

CONCLUSION

This paper proposes a modified spectral gradient method for solving non-linear systems. The modification is performed since the actual Hessian is unavailable or requires large

Table 2
Numerical results for application problems

Number of Iteration					
Problem	Dim	Modified SG	BFGS	SD	CG
a	8	169	-	152	-
b	10	4	4	4	3
c	10	2	2	2	2
d	6	2	2	2	2
e	10	2	2	2	2
f	2	8171	-	881	-
Number of Function Call					
Problem	Dim	Modified SG	BFGS	SD	CG
a	8	3450	-	2644	-
b	10	18	26	18	14
c	10	19	41	25	37
d	6	52	56	52	52
e	10	10	14	10	13
f	2	193489	-	21241	-
Computational Time					
Problem	Dim	Modified SG	BFGS	SD	CG
a	8	1.8066	-	1.2886	-
b	10	0.0100	0.0139	0.0096	0.0070
c	10	0.0091	0.0107	0.0087	0.0069
d	6	0.0070	0.0091	0.0082	0.0072
e	10	0.0060	0.0110	0.0060	0.0060
f	2	16.3163	-	1.5309	-

Note: The symbol ‘-’ represents that the method failed to converge.

storage when handling large-scale problems. The proposed method uses a diagonal matrix to approximate the actual Hessian matrix instead of the full rank matrix.

It uses the eigenvalues of the actual Hessian matrix as the diagonal entries to approximate the inverse of Hessian. The proposed method is derived based on the log-determinant norm, where the Lagrange multiplier is approximated by using only one step of the Newton-Raphson method. The standard line search strategy with the Armijo condition is modified to solve the non-linear systems. The proposed method is compared with the common existing methods regarding the number of iterations, function calls, and computational time. The numerical results show that the proposed method can be an alternative in solving systems of non-linear equations in research-tested problems and real-life applications, therefore, justifying the contribution of the modified spectral gradient method.

ACKNOWLEDGEMENTS

The Ministry of Higher Education (MoHE) Malaysia supported this research through the Fundamental Research Grant Scheme (FRGS/1/2019/STG06/UTAR/02/4). In addition, the research was also supported by Universiti Tunku Abdul Rahman (UTAR) through Universiti Tunku Abdul Rahman Research Fund (UTARRF) project IPSR/RMC/UTARRF/2020-C2/S05.

REFERENCES

- Abubakar, A. B., Kumam, P., & Mohammad, H. (2020). A note on the spectral gradient projection method for nonlinear monotone equations with applications. *Computational and Applied Mathematics*, 39(2), 1-35. <https://doi.org/10.1007/s40314-020-01151-5>
- Andrei, N. (2008). An unconstrained optimization test functions collection. *Advanced Modeling and Optimization*, 10(1), 147-161.
- Antonelli, L., De Simone, V., & Di Serafino, D. (2016). On the application of the spectral projected gradient method in image segmentation. *Journal of Mathematical Imaging and Vision*, 54(1), 106-116. <https://doi.org/10.1007/s10851-015-0591-y>
- Barzilai, J., & Borwein, J. M. (1988). Two-point step size gradient methods. *IMA Journal of Numerical Analysis*, 8(1), 141-148. <https://doi.org/10.1093/imanum/8.1.141>
- Biglari, F., & Solimanpur, M. (2013). Scaling on the spectral gradient method. *Journal of Optimization Theory and Applications*, 158(2), 626-635. <https://doi.org/10.1007/s10957-012-0265-5>
- Broyden, C. G. (1965). A class of methods for solving nonlinear simultaneous equations. *Mathematics of Computation*, 19(92), 577-593.
- Buzzi-Ferraris, G., & Manenti, F. (2013). *Nonlinear systems and optimization for the chemical engineer: Solving numerical problems*. John Wiley & Sons.
- Byrd, R. H., & Nocedal, J. (1989). A tool for the analysis of quasi-Newton methods with application to unconstrained minimization. *SIAM Journal of Numerical Analysis*, 26, 727-739. <https://doi.org/10.1137/0726042>
- Cauchy, A. (1847). Méthode générale pour la résolution des systèmes d'équations simultanées [General method for solving systems of simultaneous equations]. *Comptes rendus de l'Académie des Sciences*, 25(1847), 536-538.
- Chen, X., Liu, Y., Zhou, W., & Peng, X. (2017). Simplex-fruit fly optimization algorithm for solving systems of non-linear equations. In *2017 13th International Conference on Natural Computation, Fuzzy Systems and Knowledge Discovery (ICNC-FSKD)* (pp. 615-620). IEEE Publishing. <https://doi.org/10.1109/FSKD.2017.8393341>
- Cheng, W. Y., & Li, D. H. (2010). Spectral scaling BFGS method. *Journal of Optimization Theory and Applications*, 146(2), 305-319. <https://doi.org/10.1007/s10957-010-9652-y>
- Cruz, W. L., & Raydan, M. (2003). Nonmonotone spectral methods for large-scale nonlinear systems. *Optimization Methods and Software*, 18(5), 583-599. <https://doi.org/10.1080/10556780310001610493>

- Dai, Y. H., Hager, W. W., Schittkowski, K., & Zhang, H. (2006). The cyclic Barzilai-Borwein method for unconstrained optimization. *IMA Journal of Numerical Analysis*, 26(3), 604-627. <https://doi.org/10.1093/imanum/drl006>
- De Asmundis, R., di Serafino, D., Riccio, F., & Toraldo, G. (2013). On spectral properties of steepest descent methods. *IMA Journal of Numerical Analysis*, 33(4), 1416-1435. <https://doi.org/10.1093/imanum/drs056>
- Dolan, E. D., & Moré, J. J. (2002). Benchmarking optimization software with performance profiles. *Mathematical Programming*, 91(2), 201-213. <https://doi.org/10.1007/s101070100263>
- Fang, X., Ni, Q., & Zeng, M. (2018). A modified quasi-Newton method for nonlinear equations. *Journal of Computational and Applied Mathematics*, 328, 44-58. <https://doi.org/10.1016/j.cam.2017.06.024>
- Grosan, C., & Abraham, A. (2008). A new approach for solving nonlinear equations systems. *IEEE Transactions on Systems, Man, and Cybernetics-Part A: Systems and Humans*, 38(3), 698-714. <https://doi.org/10.1109/TSMCA.2008.918599>
- Hestenes, M. R., & Stiefel, E. (1952). Methods of conjugate gradients for solving linear systems. *Journal of Research of the National Bureau of Standards*, 49(6), 409-436.
- Ibrahim, S. M., Yakubu, U. A., & Mamat, M. (2020). Application of spectral conjugate gradient methods for solving unconstrained optimization problems. *An International Journal of Optimization and Control: Theories & Applications (IJOCTA)*, 10(2), 198-205. <https://doi.org/10.11121/ijocta.01.2020.00859>
- Luenberger, D. G., & Ye, Y. (1984). *Linear and nonlinear programming* (Vol. 2). Addison-Wesley.
- Marini, F. (2009). Neural networks. In R. Tauler & B. Walczak (Eds.), *Comprehensive Chemometrics: Chemical and Biochemical Data Analysis* (pp. 477-505). Elsevier. <https://doi.org/10.1016/B978-044452701-1.00128-9>
- Martinez, J. M. (2000). Practical quasi-Newton methods for solving nonlinear systems. *Journal of Computational and Applied Mathematics*, 124(1-2), 97-121. [https://doi.org/10.1016/S0377-0427\(00\)00434-9](https://doi.org/10.1016/S0377-0427(00)00434-9)
- Raydan, M. (1993). On the Barzilai and Borwein choice of steplength for the gradient method. *IMA Journal of Numerical Analysis*, 13(3), 321-326. <https://doi.org/10.1093/imanum/13.3.321>
- Raydan, M. (1997). The Barzilai and Borwein gradient method for the large scale unconstrained minimization problem. *SIAM Journal on Optimization*, 7(1), 26-33. <https://doi.org/10.1137/S1052623494266365>
- Raydan, M., & Svaiter, B. F. (2002). Relaxed steepest descent and Cauchy-Barzilai-Borwein method. *Computational Optimization and Applications*, 21(2), 155-167. <https://doi.org/10.1023/A:1013708715892>
- Sim, H. S., Leong, W. J., & Chen, C. Y. (2019). Gradient method with multiple damping for large-scale unconstrained optimization. *Optimization Letters*, 13(3), 617-632. <https://doi.org/10.1007/s11590-018-1247-9>
- Simpson, T. (1740). Essays on several curious and useful subjects, in speculative and mix'd mathematics. *London, 1740*, Article 81.
- Solodov, M. V., & Svaiter, B. F. (1998). A globally convergent inexact Newton method for systems of monotone equations. In *Reformulation: Nonsmooth, piecewise smooth, semismooth and smoothing methods* (pp. 355-369). Springer. https://doi.org/10.1007/978-1-4757-6388-1_18

- Turgut, O. E., Turgut, M. S., & Coban, M. T. (2014). Chaotic quantum behaved particle swarm optimization algorithm for solving nonlinear system of equations. *Computers & Mathematics with Applications*, 68(4), 508-530. <https://doi.org/10.1016/j.camwa.2014.06.013>
- Wallis, J. (1095). A treatise of algebra, both historical and practical. *Philosophical Transactions of the Royal Society of London*, 15(173), 1095-1106. <https://doi.org/10.3931/e-rara-8842>
- Xiao, Y., Wang, Q., & Wang, D. (2010). Notes on the Dai–Yuan–Yuan modified spectral gradient method. *Journal of Computational and Applied Mathematics*, 234(10), 2986-2992. <https://doi.org/10.1016/j.cam.2010.04.012>
- Yuan, G., & Lu, X. (2008). A new backtracking inexact BFGS method for symmetric nonlinear equations. *Computers & Mathematics with Applications*, 55(1), 116-129. <https://doi.org/10.1016/j.camwa.2006.12.081>
- Zhang, L., & Zhou, W. (2006). Spectral gradient projection method for solving nonlinear monotone equations. *Journal of Computational and Applied Mathematics*, 196(2), 478-484. <https://doi.org/10.1016/j.cam.2005.10.002>



Esterification of Acetin Production from By-Products of Biodiesel Industry Using Heterogeneous Catalysts Based on Wetland Commodities

Hesty Heryani^{1*}, Abdul Ghofur² and Nursiah Chairunnisa³

¹Department of Agro-industrial Technology, University of Lambung Mangkurat, Banjarbaru 70714, Indonesia

²Department of Mechanical Engineering, University of Lambung Mangkurat, Banjarbaru 70714, Indonesia

³Department of Civil Engineering, University of Lambung Mangkurat, Banjarbaru 70714, Indonesia

ABSTRACT

The peculiarities of wetland commodities are unique and can produce new materials which function as catalysts. The objective was to determine the best catalyst components, crystalline properties, pore size, catalyst morphology, and selectivity in producing acetin. The research started with sampling, sorting, purification, extraction, catalyst synthesis, characterization, and determining the molar ratio between glycerol sourced from biodiesel industry by-products and CH₃COOH. Determination of catalyst components by XRF spectrometry, crystallinity by XRD, pore size by Brunauer-Emmett-Teller, and morphology of the resulting catalyst used SEM/EDS. Selectivity of the target compound in the form of acetin, either monoacetin, diacetin, or triacetin, used GC-MS. The catalyst of orange peels obtained silica 29.201% and alumina 4.115%, pineapple leaves obtained silica 34.072% and alumina 0.074%, and sugar palm peels obtained silica 40.017% and alumina 0.953%. The diffractogram results showed that all heterogeneous catalysts had sharp-narrow peaks, meaning the crystallinity of the sample was high according to the typical peak

of SiO₂. The pore size of the orange peel catalyst was 4.328 nm with a surface area of 263.475 m² g⁻¹, the pineapple leaf catalyst was 4.850 nm and 35.983 m² g⁻¹, and the sugar palm peel catalyst was 5.658 nm and 10.884 m² g⁻¹. The results of the morphological test of orange peels were composed of a very heterogeneous dense porous structure; pineapple leaves were amorphous, while sugar palm peels were composed of small, irregular pores. All the

ARTICLE INFO

Article history:

Received: 05 November 2021

Accepted: 03 February 2022

Published: 20 April 2022

DOI: <https://doi.org/10.47836/pjst.30.3.06>

E-mail addresses:

hheryani@ulm.ac.id (Hesty Heryani)

ghofur70@ulm.ac.id (Abdul Ghofur)

nursiah.chairunnisa@ulm.ac.id (Nursiah Chairunnisa)

* Corresponding author

resulting heterogeneous catalysts met the characteristics of standard SiO₂ silica catalysts. The best acetin selectivity result is a 1:9 molar ratio.

Keywords: Acetin, biodiesel, catalyst, esterification, selectivity

INTRODUCTION

Most of the processes done by developing countries in manufacturing industry activities involve homogeneous and heterogeneous catalysts, reaching 80% (Hermann et al., 2016; Bravo-Suárez et al., 2013). Along with technology and innovation development to reduce environmental degradation, agricultural biomass sources have potential as new basic materials for heterogeneous catalysts in replacing commercial catalysts to meet industrial needs, including biodiesel, biogas, bioethanol, and biosorbents to remove heavy metals in water (Heryani & Yanti, 2020). In recent years, agricultural waste has been considered and has proven to be an excellent source of solid catalysts and catalyst supports (Sharma et al., 2012; Sadh et al., 2018; Khan et al., 2021). Sources of biomass come from the agro-industry, which is categorized into two types, namely agricultural waste and industrial waste. Agricultural waste as field residue is in the form of the waste left in the field, such as stems, leaf stems, and seed pods. Process waste after harvesting is residue up to the point where the crop is converted into another valuable resource. These remains consist of leaf straw, stems, husks, bagasse, the bark of stem shells, and roots. Meanwhile, industrial waste can be generated from food processing plants, such as potato chips, juice, candy, and fruit industries, producing large organic residue every year (Sadh et al., 2018).

Agricultural waste material has been identified to contain high levels of potassium produced as a by-product of the combustion of agricultural biomass waste. It is a potential source of alkali, which can be used as an alternative to inorganic alkalis such as KOH and NaOH. Research shows that the high catalytic potential of this waste ash can be attributed to the high content of metal oxides, especially potassium and other metals such as calcium, sodium, and magnesium, which are important sources of alkali production (Betiku & Ajala, 2014; Abdullah et al., 2017b; Etim et al., 2020). Potassium derived from agricultural waste is chemically pure and poses no threat to its development and use (Khan et al., 2021). However, millions of tons of this waste biomass are found in various world regions. Therefore, proper waste management is needed for optimal utilization, especially in reducing environmental pollution and will reduce pollution. Various sources of agricultural waste which have been studied are plantain peels (Betiku & Ajala, 2014; Onoji et al., 2016), banana peels (Betiku et al., 2016; Gohain et al., 2017), orange peels (Lathiya et al., 2018), cocoa pod husks (Syamsiro et al., 2012; Betiku et al., 2017; Campos-Vega et al., 2018; Ofori-Boateng & Lee, 2013), coconut shell (Endut et al., 2017), rubber seed shell (Onoji et al., 2016), oil palm trunk (Zulkefli et al., 2017) and rice husk (Chen et al., 2015).

Agricultural waste has not been used, especially in rural areas, due to the lack of knowledge and technology (Marshall & Farahbakhsh, 2013). The utilization of pineapple, sugar palm, and orange plants so far has only been limited to fruit, while the leaves or peels of each plant have not been widely used. According to the Food and Agriculture Organization, citrus production, which dominates the global fruit market, reaches 68 million tons, with orange peel waste accounting for 44% of the weight of citrus fruits (Widmer et al., 2010). Then the pineapple, whose leaves are only removed by burning or left to rot (Yusof et al., 2015). Waste from pineapple plants is rich in lignocellulosic materials, especially the pineapple leaves. Many studies show that pineapple leaves are rich in insoluble fiber-rich fractions, wherein cellulose generally accounts for 20%–25% of dry weight (Huang et al., 2011). Similarly, pineapple leaf fiber has a high content of lignin and cellulose, most of which are in the crystalline structure and hemicellulose (6%–19%). The remainder consists of lignin (4%–15%), wax (4%), and ash (1%–5%) (Huang et al., 2011; Hemalatha & Anbuselvi, 2013). Meanwhile, orange waste has 2.34% ash content, 42.7% carbon, 6.4% hydrogen, 1% nitrogen, and 47.6% oxygen. Furthermore, the pectin content is 35.3%, hemicellulose is 16.6%, cellulose is 17.1%, and the remaining 28.7% is lignin, protein and dissolved sugars, and some fats (Alvarez et al., 2018). The chemical composition of sugar palm peels is fiber consisting of 43.88% cellulose, 33.24% lignin, 7.24% hemicellulose, 51.12% holocellulose, 1.01% ash, and 8.36% moisture content (Ilyas et al., 2019). The three commodities above have biomass waste which can be processed to produce new or smart materials, apart from the fact that their availability is continuous and does not depend on the season.

In South Kalimantan, the well-known waste of pineapple leaves is from the Tamban Pineapple Varieties, sugar palms growing well on land near swamps, have sap, sugar palm fruit, and sugar palm peels which can be used as new materials. Marabahan Oranges or Madang Oranges, also known in Malaysia and Saudi Arabia, compete with Bali Oranges for their sweet taste. Remnants are fully utilized before they are converted into other valuable resources. One of them is unconventional catalysts as a viable alternative to chemical catalysts, and it has received considerable attention because it comes from biogenic/biomass waste sources. It is renewable, non-toxic, biodegradable, easy and safe to develop, non-corrosive, does not produce used water, is abundantly available and can be recovered and reused (Güleç et al., 2019; Chakraborty et al., 2016). Heterogeneous catalysts derived from biomass materials (sugarcane bagasse, wood ash, *Lemna perpusilla* Torrey, palm kernel shell, banana peduncle, *Enterolobium cyclocarpum* pod husk, kola nut pod husk, and tucuma peels) is effective and very efficient in biodiesel production. Transesterification can catalyze oil with a high Free Fatty Acid (FFA) content of up to 3% or more and can operate under mild conditions with a short residence time. The final product is pure and does not cause any difficulties during the separation and purification process. There has

been a great increase in the discovery of new biomass materials with effective catalytic power, but most of them have not been studied. It is, therefore, necessary to develop a database of biomass waste materials with the effective catalytic potential to exploit waste biomass sources for the development of heterogeneous catalysis for biodiesel synthesis (Sharma et al., 2012; Chouhan & Sarma, 2013; Abdullah et al., 2017a; Balajii & Niju, 2019; Falowo et al., 2019; Betiku et al., 2019; Mendonça et al., 2019; Etim et al., 2020).

Biodiesel is a potential option among existing biofuel production technologies. It has renewable nature, low toxicity, and environmental impact if it is compared to petroleum-based diesel (Daud et al., 2015). The biodiesel process is a production to process Refined Bleached Deodorized Palm Oil (RBDPO) into Fatty Acid Methyl Ester (biodiesel). There are several benefits of biodiesel for the environment, such as reducing CO₂ emissions, particulates, and unburned hydrocarbons. These benefits make it promising (Mahmudul et al., 2017). However, industrial developments, especially in South Kalimantan, have generated waste of fatty matter and crude glycerol, which amounts to 10% of the daily biodiesel production capacity of 1100 metric tons (mt).

Crude glycerol is a by-product of the biodiesel industry, which has begun to develop in research in recent years. It is triggered by the development of the search for alternative energy to meet energy needs in the future. The increasing target for biodiesel production from year to year will also increase the crude glycerol produced as a by-product (Monteiro et al., 2018; Chong et al., 2020). The source of glycerol comes from crude glycerol from the biodiesel industry waste, which is previously purified. Crude glycerol can be used as a starting material to produce valuable products such as mono, di and triacylglycerols and through the esterification process.

It is estimated that in 2027 the annual production of crude glycerol globally will reach 3.9 billion liters (Ciriminna et al., 2014; Ardi et al., 2015). One solution for converting glycerol into acetin derivative products is the esterification of glycerol with acetic acid using a catalyst to obtain monoacetin, diacetin, and triacetin (Rastegari & Ghaziaskar, 2015; Oliverio et al., 2016; Nda-Umar et al., 2019). The group of acetin compounds such as monoacetin (MAG), diacetin (DAG), and triacetin (TAG) are compounds that are widely needed in the industry. Monoacetin and diacetin have applications in the food industry, cryogenics for biodegradable polymers, and solvents (Kale et al., 2015; Gorji & Ghaziaskar, 2016). In addition, diacetin and triacetin can act as additives in various fuels to reduce engine knocking, namely the ability to increase engine performance, octane rating, and are used as an additive for biodiesel (Malaika & Kozłowski, 2019; Herrada-Vidales et al., 2020; Tasuna et al., 2021).

Several researchers have carried out the use of solid catalysts in the production of acetin due to the ease in the product purification process, including ion exchange resins (Dosuna-Rodríguez & Gaigneaux, 2012; Mufrodi et al., 2018; Caballero et al., 2019), heteropoly acids, HPAs (Ferreira et al., 2011; de Abreu Dessimoni et al., 2018), clays

(Dill et al., 2019; Yanti et al., 2019). The target is to reduce the import of chemicals, especially new materials such as catalysts, by replacing the source of materials based on wetland biomass which is very potential in South Kalimantan. From an eco-friendly point of view, functionalized clay and activated carbon (Sulphonated Hydrothermal Carbon (SHTC)) have been used in glycerol acetylation reactions to synthesize glycerol esters (mono, di, and triacetin) (Ferreira et al., 2011; Khayoon & Hameed, 2011; de la Calle et al., 2015). Studies that have been conducted (Ferreira et al., 2011; Khayoon & Hameed, 2011) using carboxylic acid reported that sulfonated carbon obtained by mild hydrothermal carbonization of D-glucose achieved a combined selectivity of DAG of 74% and TAG of 64% at 120°C with a reaction time of 3 hours.

Optimizing the by-product and waste industry must become industrial supporting materials and pioneering materials for future hopes (Kemenristekdikti RIRN 2017-2045, 2017). Therefore, the opportunity to be upgraded into applied research with Micro and Small Enterprises and then into development research for commercialization in partnership with the industry has a very big opportunity. The study aims to obtain the best catalyst of the three types of wetland biomass by using catalyst characterization tests, including catalyst components using X-Ray Fluorescence spectrometry (XRF), crystallinity using X-ray Diffraction (XRD), pore size using Brunauer-Emmett-Teller (BET), and morphology of the resulting catalyst using Scanning Electron Microscopy- Energy Dispersive X-Ray (SEM-EDX). Furthermore, testing the performance of heterogeneous catalysts produced to produce acetin (monoacetin, diacetin, and triacetin) used glycerol as a by-product of the biodiesel industry purification.

MATERIALS AND METHODS

Materials

The raw material for biomass waste comes from sugar palm peels, Tamban pineapple leaves, and Madang orange peels located in wetlands or swamps. Furthermore, crude glycerol was a by-product of industrial biodiesel sourced from the palm oil agro-industry in Kotabaru Regency, South Kalimantan. The materials used include active carbon, CH_3COOH , H_2SO_4 , NaOH , NaIO_4 , KOH , $\text{C}_2\text{H}_6\text{O}_2$, $\text{C}_2\text{H}_5\text{OH}$, HCl , bromthymol blue (BTP), and phenolphthalein indicator, had a pre-analysis degree. Meanwhile, all heterogeneous catalysts were sourced from orange peels, pineapple leaves, and sugar palm peels.

Preparation of Catalyst Source Material

The stage of providing catalyst material began with taking it at the source and sorting it to ensure it was not mixed with other materials or biomass. Furthermore, washing, drying, and drying in the sun are done until the water content is 10% (Moni et al., 2016). Furthermore, the samples were mashed with a porcelain mortar and pestle and sieved using an 80 mesh

sieve. The refined sample was then put into the NaberthErm brand furnace from Germany for the calcination process. The furnace process was carried out for 4 hours at a temperature of 800°C at a heating rate of 15°C min⁻¹ and below a nitrogen flow rate of 150 ml min⁻¹ for an inert atmosphere. Furthermore, the charcoal was pulverized to 200 mesh by sifting using an ASTM sieve measuring 200 mesh until a uniform size was obtained (Ogungbenro et al., 2018; Yanti et al., 2019).

Synthesis of Wetland Biomass-Based Heterogeneous Catalyst

Sources of biomass that had gone through the preparation stage and calcined were extracted using 3M NaOH solution in a ratio of 1:4 (w/t) from the weight of the biomass used. It referred to previous research done by Heryani and Yanti (2020), which had produced silica (SiO₂) from the hydrolysis process with the addition of NaOH under alkaline conditions so that the concentration of NaOH set to 3M could dissolve silica in biomass and produced a gel-shaped solid. The leaching process was then carried out at 90°C for 12 hours, at a speed of 300 rpm, using a magnetic stirrer. Furthermore, the extracted filtrate and residue were separated with filter paper. The filtrate was then added with 1M HCl drop by drop until the pH reached neutral (pH 7), and a white precipitate was formed. The precipitate obtained was then washed with distilled water and baked in an oven at a temperature of 110°C for 6 hours for the drying process to form dry silica gel. The dry silica gel was then ground into powder. Its final calcination was carried out at 700°C for 3 hours to obtain a heterogeneous catalyst (silica) at a heating rate of 15°C min⁻¹ and below a nitrogen flow rate of 150 ml min⁻¹ for an inert atmosphere (Ogungbenro et al., 2018; Yanti et al., 2019).

Glycerol Crude Refining

The distillation process was carried out among by-products of glycerol from the biodiesel industry and added with distilled water in a ratio of 2: 3 (v/v). Furthermore, 5% (v/v) activated carbon was added after washing. The sample mixture and activated carbon were stirred for 30 minutes, then allowed to stand for 24 hours. After 24 hours, the sample was filtered using filter paper. Next, the sample was put into a rotary evaporator set at a vacuum pressure and a temperature of 60°C. To increase the purity of glycerol, the bottom product of the rotary evaporator was distilled for 4 hours. Then the physical properties were analyzed, including glycerol content, water content, ash content, and density or density (Tan et al., 2013; Domingos et al., 2019).

Characterization of Wetland Biomass-Based Heterogeneous Catalyst Synthesis

The characterization of the synthesis of heterogeneous biomass-based catalysts could be carried out using the X-Ray Fluorescence (XRF) method with the PANalytical Epsilon 3 apparatus, which was used to determine the composition of the elements in the sample.

The instrument was equipped with a Benchtop tube under a dispersive X-ray fluorescence spectrometer. Then, characterization using the X-Ray Diffraction (XRD) method was carried out with a Shimadzu XRD 7000 apparatus. The XRD pattern was measured at 30 mA and 40 kV under Cu-K α radiation conditions at $k = 1.54$. The diffraction pattern was observed at an angle of 2θ from 10 to 90° with a step time of 0.5 s. The data obtained were then processed using match software (Match Copyright 2003–2016 Crystal Impact, Bonn, Germany-Phase Analysis Report) to find the peak intensity component. Furthermore, the Brunauer Emmett–Teller (BET) method was used to estimate the sample's surface area. Characterization was carried out using the ChemBET PULSAR Quantachrome apparatus using the Nitrogen adsorption-desorption method at 195.8°C (77.35 K). The samples were degassed at 300°C (573.15 K) for 5 hours under vacuum (6.58×10^{-5} 1Torr $^{-1}$) before adsorption. Finally, to determine the surface structure (morphology) and catalyst components using Scanning Electron Microscopy-Energy Dispersive of X-ray Spectroscopy (SEM-EDX) with the Hitachi SEM S-4700 tool (Buchori et al., 2020; Yanti et al., 2019)

Production of Acetin Additive

There were three types of acetin produced in this research: monoacetin, diacetin, and triacetin. The production principle started from glycerol material derived from the crude glycerol biodiesel industry. First, glycerol with a certain volume was put into a three-neck flask, then heated to a temperature close to 100°C. Second, the acetic acid with a certain volume was heated to a temperature of 100°C in an Erlenmeyer. Third, the acetic acid was put into a three-neck flask, then heated to maintain the temperature while the magnetic stirrer continued to run; the stirring speed was constant at 600 rpm. Next, put the heterogeneous catalyst as much as 3% by weight of glycerol; the reaction process ran at a temperature of 115°C for 180 minutes. Finally, the solution resulting from acetic acid and glycerol reaction with a biomass-based silica catalyst was analyzed using Gas Chromatography-Mass Spectrometry (GC-MS) from the Shimadzu (GCMS QP2010 Plus). The column oven temperature is set to 100.0°C, with the split mode injection temperature of 250.00°C. The flow control mode linear velocity is set to 107.2 kPa pressure, the total flow of 433.8 mL min $^{-1}$, column flow of 1.43 mL min $^{-1}$, the linear velocity of 44.5 cm sec $^{-1}$, purge flow of 3.0 mL min $^{-1}$, a split ratio of 300.0 and injection volume of 1 microliter. The mixture of compounds containing glycerol, acetic acid, monoacetin, diacetin, and triacetin could be easily separated in gas chromatography so that GC identified all compounds.

RESULTS AND DISCUSSIONS

Characterization of Heterogeneous Catalyst Extract Yield

X-Ray Spectroscopy (XRF) showed that the highest Si element content was from sugar palm peels at 40.017%, followed by Si element content from pineapple leaves at 34.072%

and Si element content from orange peels at 29.201%. It showed that the calcination process at 700°C in the catalyst extract of SiO₂ sugar palm peel was able to remove dissolved impurities to increase the crystallinity of high-purity SiO₂. In addition, according to Ilyas et al. (2019), components contained in sugar palm peel, namely cellulose, lignin, hemicellulose, holocellulose, were a constituent of fiber in a plant. Furthermore, the highest Al content based on XRF results from orange peels was at 4.115%, followed by the content of Al elements from sugar palm peels at 0.953%, and the catalyst extract from pineapple leaves at 0.074%, as could be seen in Figure 1.

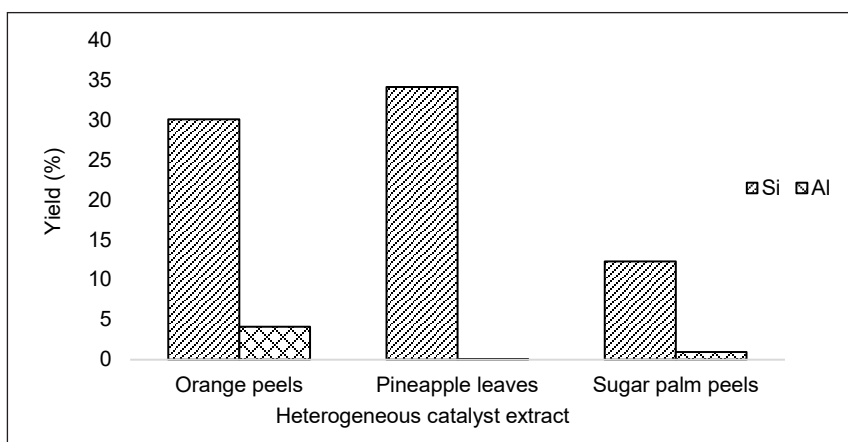


Figure 1. Yield of wetland biomass-based heterogeneous catalyst extract

From Figure 1, it could be seen that the silica produced from the extraction of wetland commodity sources contained Si elements having a high level of purity and was an element that made up SiO₂ in plants. The results of previous research showed that the content of Si elements from calcined pineapple leaves was 34.131%, orange peels were 30.102%, and sugar palm peels were 12.281% (Heryani & Yanti, 2020). NaOH concentration, leaching process, and temperature would affect the Si/Al content in silica sources obtained from wetland-based plants. The higher the Si/Al ratio, the lower the crystallinity was. It was known that citrus Si/AL is 7.10%, Pineapple Si/AL was 460.43%, sugar palm rind Si/AL was 41.99%, and the catalyst was amorphous when the Si/AL ratio was 75%. After adding acid, a clear glassy [Si(OH)₄] hydrogel was formed in the gelling stage. It was then dried at 110°C to a constant weight. Drying was carried out to remove the water content in the sample by evaporating water from its surface, obtaining dry silica gel by removing the liquid present in the gel's pores, and obtaining a white silica powder.

Characterization of Wetland Biomass-Based Heterogeneous Catalyst Synthesis

The characterization using X-ray diffraction (XRD) determined the crystallinity of the heterogeneous catalyst synthesis material based on wetland biomass produced. The

material's crystallinity could be observed from the peak intensity generated on the diffractogram. The results of the X-ray diffraction pattern using a long angle of 2θ were between 10° and 90° . The hump formed from the X-ray diffraction pattern showed that all synthesis of heterogeneous catalysts based on wetland biomass was a combination of amorphous and crystalline. Peaks that were clearly visible, high, sharp, and had high intensity indicated an increasingly regular crystal arrangement so that it had a high level of crystallinity. Then, if the material had low regularity (amorphous), the peak intensity appearing on the diffractogram looked low, less clear, and wide.

The hump indicated that the amorphous structure was sloping and wide. In the synthesis of sugar palm peel catalyst extract, the highest amorphous structure was at 2θ at 10.17° , while the highest amorphous structure in the synthesis of orange peel catalyst extract was at 2θ at 10.27° , and the highest amorphous structure in the synthesis of pineapple leaf catalyst extract was at 2θ at 10.09° . It showed that when the sample was calcined at a temperature of 700°C with a holding time of 3 hours, a change began to occur, namely the appearance of crystal peaks. The amorphous structure had enough energy to transform into a crystalline structure, as shown in Figure 2. These broad peaks indicated that the heterogeneous catalyst synthesis material based on wetland biomass had a crystalline structure, meaning an orderly arrangement of particles.

From that Figure 2, it was obtained data in the form of distance among planes, intensity, and angle (2θ), which was then matched with data on the JCPDS (Joint Committee for Powder Diffraction) X-ray diffraction pattern. It was done so that the compounds contained in the sample could be identified, as presented in Table 1.

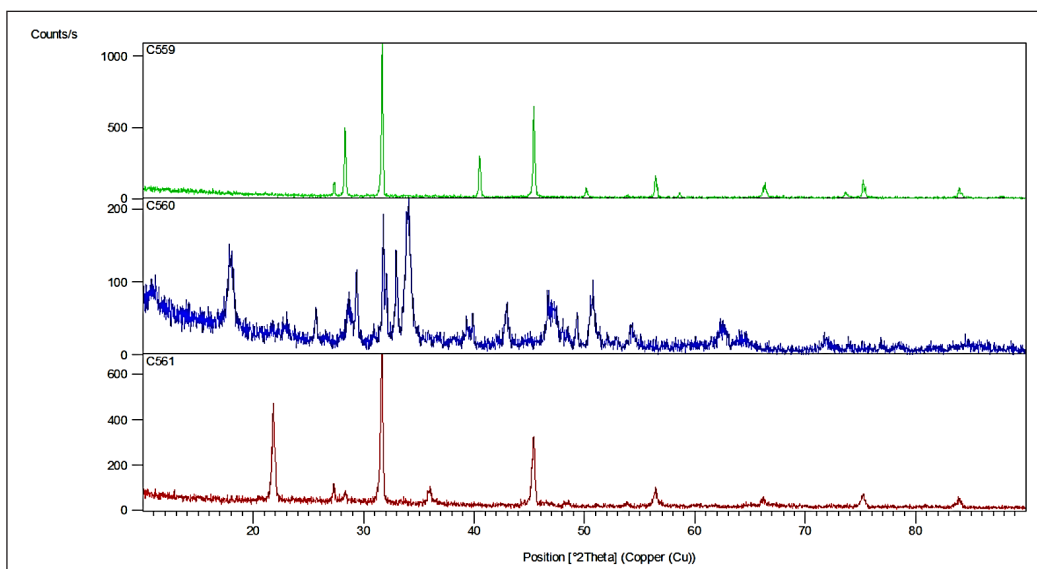


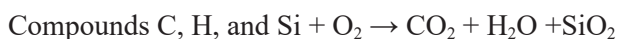
Figure 2. X-ray diffraction pattern of silica synthesized from wetland biomass-based heterogeneous catalyst extract

Table 1
Diffraction peaks for the synthesis of wetland biomass-based heterogeneous catalysts

Silica Source	Peak of Difactogram			Information
	2 θ	2 θ	2 θ	
SiO ₂ standard	26,640°	45,793°	50,139°	JCPDS No. 46-1045
SiO ₂ orange peel extract	25,664°	46,715°	50,727°	Research
SiO ₂ pineapple leaf extract	27,302°	45,410°	53,861°	Research
SiO ₂ sugar palm peel extract	28.331°	45.421°	50,183°	Research

From Table 1, the diffractogram showed that all the results of the wetland biomass-based synthesis of heterogeneous catalyst extracts identified the quartz SiO₂ form with a sharp peak typical of silicon oxide (SiO₂). Similar XRD resulted in the catalysts of orange peels and sugar palm peels because they had close Si/Al ratios. It was following the XRD standard for the structure of silicon oxide (SiO₂) JCPDS card No. 46-1045 in the ICDD database. The wetland biomass-based synthesis of silica catalyst extract, whose process ended with calcination at a temperature of 700°C, was able to form a fairly high intensity of the crystalline and reduce the amorphous form. The results of previous research conducted by Heryani and Yanti, 2020 were also following the XRD standard for the structure of silicon oxide (SiO₂) JCPDS card No. 46-1045 at 2 θ in the range of 25.917°-45.660° at a temperature of 700°C that the product had a crystallinity which met the standard of silicon oxide (SiO₂).

Furthermore, the pore size measurement of the catalyst of the wetland biomass-based synthesis obtained from the adsorption isotherm describes the type of adsorption of the solid produced using the Brunauer Emmett Teller (BET) method. The pore size of the material was classified into three according to its range: the microporous (<2 nm), mesoporous (2–50 nm), and macropore (>50 nm) areas. The pore size of the synthesis of orange peel extract was 4.328 nm, that of pineapple leaf extract was 4.850 nm, and that of sugar palm peel extract was 5.658 nm. The organic matter content of large sugar palm peels reached 69.59%, with the calcination process reaching a temperature of 700°C, causing the loss of these components to open the previously closed pores due to the complex composition. It was higher than orange peels and pineapple leaves. It was in line with research (Trisunaryanti et al., 2018) which successfully synthesized mesoporous silica with a pore size diameter of 3.43 nm. It showed that the final leaching and calcination process at 700°C for 3 hours was able to open the pores of the catalyst surface so that water evaporation occurred on the porous catalyst surface. Pore size without calcination ranged from 0.04 nm to 0.05 nm. The reaction for the formation of biomass-based silica through the calcination process was as follows:



According to ALOthman (2012), this reaction produced silica in the form of a solid such as a gel. The gel-shaped solid was then heated to remove the water content on the silica surface and pulverized to obtain white silica powder. It was for various applications such as gas and liquid separation, optical coatings, protective films, membranes, and catalysis.

Furthermore, the Brunauer Emmett–Teller (BET) results showed that silica synthesized catalyst of orange peels had a surface area of $263.475 \text{ m}^2 \text{ g}^{-1}$. This result was in line with research (Zhang et al., 2010), showing that SBET nano-silica catalyst synthesized surface area was 120 to $288 \text{ m}^2 \text{ g}^{-1}$. The surface area of the catalyst of the synthesis of silica from sugar palm peels was $10.884 \text{ m}^2 \text{ g}^{-1}$, and that from pineapple leaves was $35.983 \text{ m}^2 \text{ g}^{-1}$. This result was in line with the silica catalyst research done by Putra et al. (2017), which had a surface area of $39.7 \text{ m}^2 \text{ g}^{-1}$. Silica nanoparticles took an important role in scientific research due to their easy preparation methodology and wide use in various applications. The results of XRF analysis showed the presence of different ratios of Si and Al. The ratio of Si and Al on the orange peel catalyst of 7.10% gave a sharper and narrower XRD diffractogram meaning that the surface area of SiO_2 was much larger than the other two catalysts. This phenomenon meant that there was high sample crystallinity. It showed that the catalyst produced from biomass waste had the potential as a supporting catalyst in the production process.

The characterization of the synthesis of wetland biomass-based heterogeneous catalysts on orange peels, sugar palm, and pineapple leaves using *Scanning Electron Microscopy-Energy Dispersive X-Ray* to determine the morphology and elemental content can be seen in Figure 3.

Figure 3 shows the shape and size of the solids of the synthesis of wetland biomass-based heterogeneous catalysts at a magnification of 10000x. The morphology of the orange peel catalyst synthesis showed the presence of large lumps, but it had pores on the surface. The pineapple leaf catalyst synthesis results showed that the morphology of the solid surface filled with the pores was very dense, relatively small. The synthesis results of the

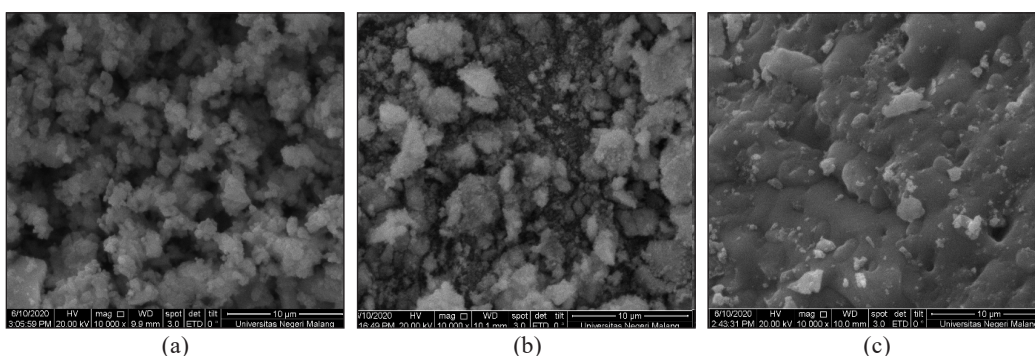


Figure 3. SEM morphology of catalyst solids of (a) orange peels, (b) pineapple leaves, and (c) sugar palm peels

sugar palm peel catalyst showed that the surface morphology of the solids was irregular, denser, and perforated on the surface. In addition, it showed that the silica particles were not evenly distributed; some formed small particles, and some formed uneven lumps. In line with the research results conducted (Heryani & Yanti, 2020), the SiO₂ catalyst of orange peel extract was composed of a very heterogeneous dense porous structure. The SiO₂ catalyst of pineapple leaf extract was composed of round lumps, and the SiO₂ catalyst of sugar palm peel extract was composed of small pores orderly.

The solid morphological results of the catalyst using SEM supported the diffractogram data in the International Center for Diffraction Data database. The catalysts synthesized from extracts of orange peels, pineapple leaves, and sugar palm peels had peaks already representing the SiO₂ diffractogram with high crystallinity. In the SiO₂ catalyst of orange peel extract and the pineapple leaf extract, there was an increase in fiber crystallinity caused by the removal of non-cellulose fiber compounds (lignin and hemicellulose) by chemical treatment and calcination. The process caused the SiO₂ catalyst of sugar palm peel extract, pineapple leaf extract, and orange peel extract to crystallize more with open pores so that the surface area increased.

Then in the analysis of the Energy Dispersive X-Ray test, the results of the content contained in the wetland biomass-based catalyst solids in Figure 4 showed that the composition of the orange peel element was O by 28.86%, Na by 21.83%, Al by 05.46%, Cl of 40.66% and K of 11.19%. The elemental composition of pineapple leaves was 38.44% O, 17.46% Na, 10.97% Al, 17.50% Cl, and 15.62% Si. Meanwhile,

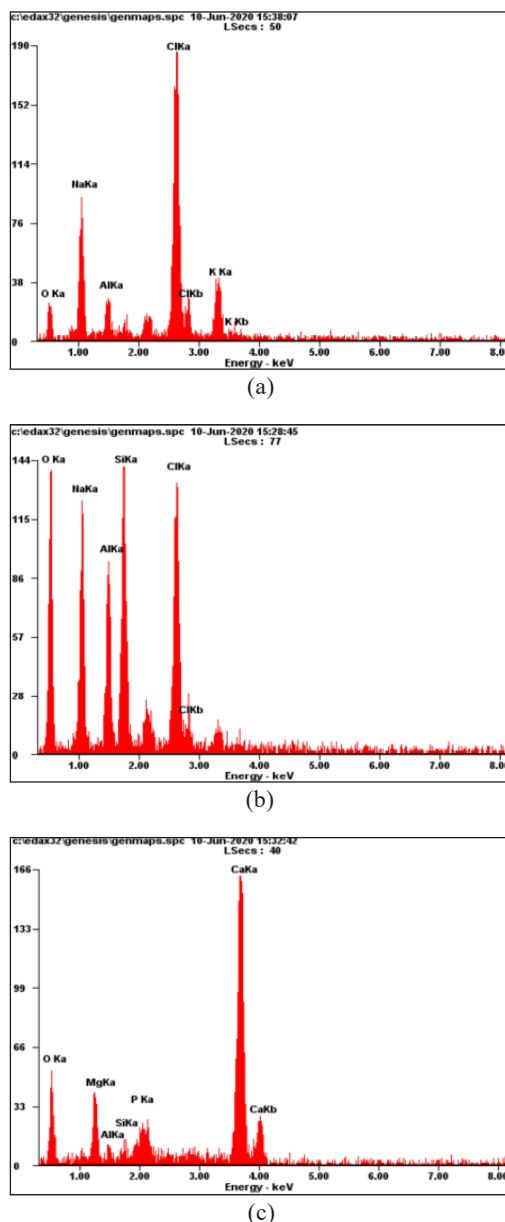


Figure 4. EDX elemental composition of solid catalysts of (a) orange peels, (b) pineapple leaves, and (c) sugar palm peels

the composition of the sugar palm peel elements was O by 43.36%, Mg by 0.816%, Al by 01.39%, Si by 01.17%, P by 03.70%, and Ca by 42.22%. It showed that the ratio of Si and AL indicated a high crystallinity process. It could increase the percentage of silica purity due to the increasing number of impurities in the form of volatile compounds released, and organic compounds can be degraded by heat. In addition, it meant that the catalyst had a high selectivity. The elements contained in the wetland biomass-based catalyst solids were micro and macronutrients which were very important for the growth process and productivity of a plant.

Analysis of Acetin Products from Glycerol Esterification Results By-Products from the Biodiesel Industry with Acetic Acid

Glycerol Crude Refining. The crude glycerol used came from the by-product of the biodiesel industry in South Kalimantan. Before being used as a raw material to manufacture acetin products, the impurities of crude glycerol needed to be removed using activated carbon and purified using the evaporation method to remove water, methanol, and residual acid. After purification, the yield obtained was 57.5% glycerol, while 42.5% impurities such as water, residual methanol, catalysts, and others were lost. Therefore, the area was 57.5%, whereas the selectivity of triacetin was 100% when it was calculated. The total area produced was only 57.5% because, in the esterification process, the main product was triacetin. However, there were also by-products in the form of water and residual acetic acid.

Based on the chemical properties analysis carried out on the purified crude glycerol and glycerol, it was known that the water content of crude glycerol before purification was 13.52%, and crude glycerol purified was 2.33%. The evaporation process influenced the decrease during purification. According to Wu et al. (2020), the decrease in water content was due to some of the water absorbed by the adsorbent (activated carbon). For the ash content, the ash content of crude glycerol before purification was 4.54% and crude glycerol purified was 4.35%. It showed that the low inorganic compounds in the form of metal and mineral remnants contained therein. In terms of color, the crude glycerol turns from reddish yellow to yellowish clear after purification. It was caused by the adsorption process using activated carbon. According to Babayemi et al. (2021), activated carbon was a bleaching agent that could adsorb color on glycerol. The activated carbon adsorption process could separate glycerol from various impurities, including beta carotene dyes, MONG (non-glycerin organic matter), and other compounds.

Furthermore, it was known that the pH of crude glycerol was 3.9 and the purified crude glycerol obtained was a pH of 3.7. For crude glycerol before purification, it was known that the glycerol content was 32.23%, and the glycerol content of the purified crude glycerol was 99.5%. Then, the density of crude glycerol, having not gone through the purification stage of 1.255 g ml^{-1} , looked lower than the density of crude glycerol after purification of 1.265

g ml⁻¹. However, it followed the pro analysis glycerol standard, which was 1.260 g ml⁻¹, due to other compounds present in crude glycerol before purification, such as methanol, catalyst, water, gum, and others affecting its density. In this study, glycerol from crude glycerol, a by-product of the biodiesel industry, which had been purified, was used as a raw material to manufacture acetin products.

Testing the Performance of Heterogeneous Catalysts on Acetin Products

The products resulting from the esterification of glycerol and acetic acid with a heterogeneous catalyst based on biomass waste were analyzed using Gas Chromatography-Mass Spectrometry GC-MS. This treatment used variations in moles of reactants, namely the formulation of moles of reactants 1:7, 1:8, 1:9, 1:10, 1:12 with a heterogeneous catalyst ratio of 3% by weight of glycerol. A ratio of 12 acetic acids could produce a glycerol conversion of 100% with a selectivity of 99.9% (Souza et al., 2017) and 75% glycerol conversion with 91% selectivity (Chamack et al., 2018).

According to the attached journal, in general, it could be said that there was no significant difference between 3% and 5% catalyst concentrations; thus, it could be

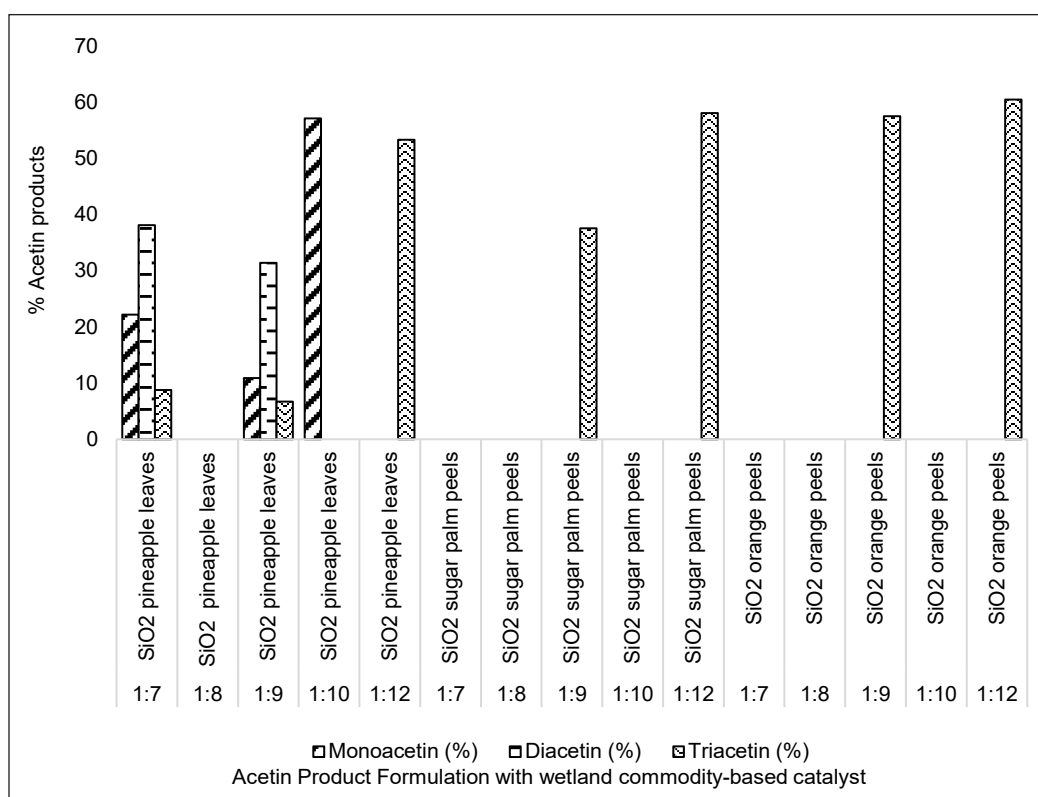


Figure 5. The products of the esterification of glycerol and acetic acid with heterogeneous catalysts based on biomass waste

concluded that 3% catalyst concentration was the optimum concentration. The products obtained were monoacetin, diacetin, and triacetin, presented in Figure 5.

From Figure 5, the results of the GC-MS analysis of acetin products showed at a temperature of 115°C with a mole ratio of glycerol reagent with acetic acid 1:7; 1:8; 1:9; 1:10; and 1:12 resulted in different compositions of monoacetin, diacetin and triacetin formed in the esterification reaction, some of which were formed but some were not. This condition was because heterogeneous catalysts involved several reaction steps on the catalyst surface, such as external and internal diffusion, the adsorption of molecules, surface reactions, desorption, internal diffusion away from the catalyst surface, and external diffusion. Therefore, variations in the molar ratio and catalyst concentration of 3% were used, referring to the preliminary study using the same glycerol source as the esterification process. It was in line with Arsyad et al. (2015) research.

The mole formulation of reactants at 1:7 and 1:9 with heterogeneous catalyst SiO₂ derived from pineapple leaf extract resulted in acetin with the composition of monoacetin, diacetin, and triacetin in the esterification reaction. The presence of Si and Al with a ratio of 1.42 indicated the crystallinity of the X-Ray Diffraction test, which aimed at characterizing the crystal structure, crystal size of a solid material. An increase in crystallinity could be seen from the peak formed by sharp and narrow X-ray diffraction, which showed the high crystallinity of the sample. Each crystal gave a specific pattern so that the peaks' position in the diffractogram indicated the presence of a particular compound. The good selectivity of pineapple leaves was shown by the results of XRF analysis on the characterization of components, especially the difference between Si and Al ratios of 1.42. It showed the high crystallinity of the sample and meaning each crystal gave a special pattern at the peak position indicating the presence of the target compound, namely acetin.

At a mole ratio of 1:10, reactants with a heterogeneous catalyst SiO₂ pineapple leaf extract formed the highest monoacetin composition of 57.14% at Mass Spectrometry Peak 8 with a retention time of 4.86 minutes. It was due to the difference in temperature of the monoacetin production process.

Furthermore, the composition of diacetin formed at the ratio of moles of reactants to moles of 1:7 with heterogeneous catalyst SiO₂ pineapple leaf extract was highest at 38.16% at Mass Spectrometry Peak 6 with a retention time of 8.23 minutes. Then for the composition of triacetin formed at the ratio of moles of reactants to moles of reactants 1:12 with a heterogeneous catalyst SiO₂ orange peel extract, the highest was 60.54% at Mass Spectrometry Peak 26 with a retention time of 13.232 minutes, which could be seen in Figure 6. Selectivity was a measure of the catalyst in accelerating the reaction in forming a product. In this study, the difference in the molar ratio used in producing acetin was a determining factor for selectivity.

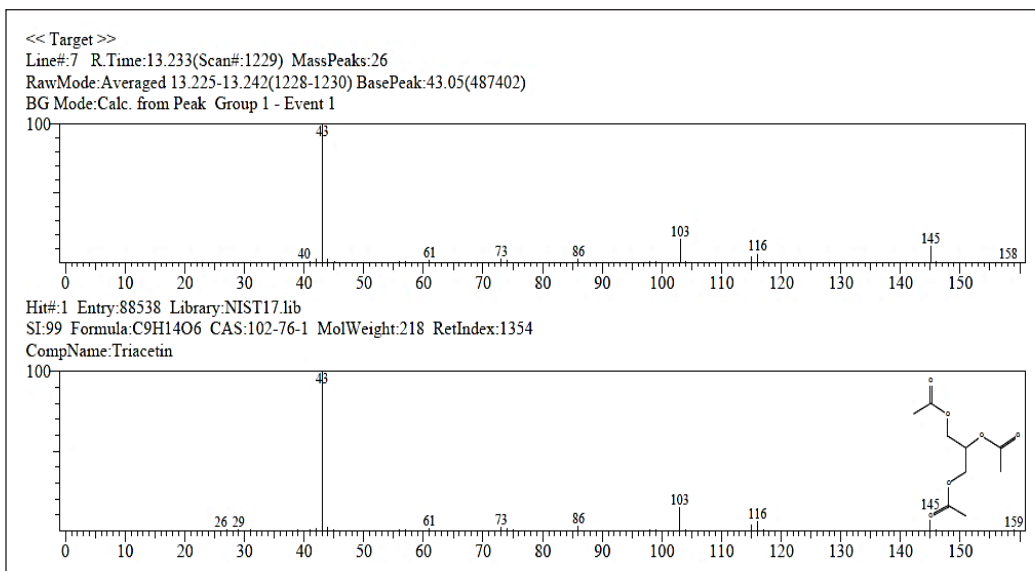


Figure 6. Results of GC-MS analysis of Acetin products

CONCLUSION

The study results show that the three types of catalysts originating from wetland biomass, namely Madang Orange peels, Tamban pineapple leaves, and sugar palm peels, are heterogeneous catalysts that can produce acetin from biodiesel industry products in the esterification process. The results of XRF analysis were on orange peels obtained silica 29.201% and alumina 4.115%, pineapple leaves obtained silica 34.072% and alumina 0.074%, and sugar palm peels obtained silica 40.017% and alumina 0.953%. The diffractogram from XRD analysis showed that all heterogeneous catalysts had sharp and narrow peaks, meaning that the crystallinity of the sample was high according to the typical peak of silicon oxide (SiO₂). The results of the BET analysis showed that the pore size of the catalysts of orange peels was 4.328 nm with a surface area of 263.475 m² g⁻¹, pineapple leaves had a pore size of 4.850 nm, and a surface area of 35.983 m² g⁻¹ and sugar palm peels was 5.658 nm with a surface area of 10.884 m² g⁻¹. Morphological tests using SEM-EDX found that the catalyst of orange peels was composed of a very heterogeneous dense porous structure, that of pineapple leaves was amorphous. In contrast, sugar palm peels were composed of small, irregular pores. All the resulting heterogeneous catalysts met the characteristics of standard SiO₂ silica catalysts. The ratio used in the esterification process for acetin production was 1:7; 1:8; 1:9; 1:10; and 1:12. The molar ratio which gave the best acetin product selectivity was 1:9. In fulfillment in the industry, acetin can be used for the food and non-food industries.

ACKNOWLEDGEMENTS

The authors want to thank the Ministry of Education and Culture, Research and Technology, Directorate of Resources, for the funding provided through the National Competitive Basic Research with SK KPA of the Directorate of Resources No. 1867/E4/AK.04/2021, dated on the 07th of June 2021.

REFERENCES

- Abdullah, Sianipar, R. N. R., Ariyani, D., & Nata, I. F. (2017). Conversion of palm oil sludge to biodiesel using alum and KOH as catalysts. *Sustainable Environment Research*, 27(6), 291-295. <https://doi.org/10.1016/j.serj.2017.07.002>
- Abdullah, S. H. Y. S., Hanapi, N. H. M., Azid, A., Umar, R., Juahir, H., Khatoon, H., & Endut, A. (2017). A review of biomass-derived heterogeneous catalyst for a sustainable biodiesel production. *Renewable and Sustainable Energy Reviews*, 70, 1040-1051. <https://doi.org/10.1016/j.rser.2016.12.008>
- ALothman, Z. A. (2012). A review: Fundamental aspects of silicate mesoporous materials. *Materials*, 5(12), 2874-2902. <https://doi.org/10.3390/ma5122874>
- Alvarez, J., Hooshdaran, B., Cortazar, M., Amutio, M., Lopez, G., Freire, F. B., Haghshenasfard, M., Hosseini, S. H., & Olazar, M. (2018). Valorization of citrus wastes by fast pyrolysis in a conical spouted bed reactor. *Fuel*, 224, 111-120. <https://doi.org/10.1016/j.fuel.2018.03.028>
- Ardi, M. S., Aroua, M. K., & Hashim, N. A. (2015). Progress, prospect and challenges in glycerol purification process: A review. *Renewable and Sustainable Energy Reviews*, 42, 1164-1173. <https://doi.org/10.1016/j.rser.2014.10.091>
- Arsyad, A., Sulistyono, H., & Sarto. (2015). Kinetics of esterification reaction of glycerol monoacetin from glycerol by-products of biodiesel and acetic acid industry with passive monophasic catalyst. *Process Engineering Journal*, 9(2), 51-57
- Babayemi, A. K., Onukwuli, O. D., Eluno, E. E., & Otolorin, J. A. (2021). Optimizing process parameters of palm oil bleaching on locally prepared animal bone-based activated carbon using response surface methodology. *Environmental Quality Management*, 30(3), 43-51. <https://doi.org/10.1002/tqem.21729>
- Balajii, M., & Niju, S. (2019). A novel biobased heterogeneous catalyst derived from *Musa acuminata* peduncle for biodiesel production - Process optimization using central composite design. *Energy Conversion and Management*, 189, 118-131. <https://doi.org/10.1016/j.enconman.2019.03.085>
- Betiku, E., & Ajala, S. O. (2014). Modeling and optimization of *Thevetia peruviana* (yellow oleander) oil biodiesel synthesis via *Musa paradisiacal* (plantain) peels as heterogeneous base catalyst: A case of artificial neural network vs. response surface methodology. *Industrial Crops and Products*, 53, 314-322. <https://doi.org/10.1016/j.indcrop.2013.12.046>
- Betiku, E., Akintunde, A. M., & Ojumu, T. V. (2016). Banana peels as a biobase catalyst for fatty acid methyl esters production using Napoleon's plume (*Bauhinia monandra*) seed oil: A process parameters optimization study. *Energy*, 103, 797-806. <https://doi.org/10.1016/j.energy.2016.02.138>

- Betiku, E., Etim, A. O., Pereo, O., & Ojumu, T. V. (2017). Two-step conversion of neem (*Azadirachta indica*) seed oil into fatty methyl esters using a heterogeneous biomass-based catalyst: An example of cocoa pod husk. *Energy & Fuels*, *31*(6), 6182-6193. <https://doi.org/10.1021/acs.energyfuels.7b00604>
- Betiku, E., Okeleye, A. A., Ishola, N. B., Osunleke, A. S., & Ojumu, T. V. (2019). Development of a novel mesoporous biocatalyst derived from kola nut pod husk for conversion of kariya seed oil to methyl esters: A case of synthesis, modeling and optimization studies. *Catalysis Letters*, *149*(7), 1772-1787. <https://doi.org/10.1007/s10562-019-02788-6>
- Bravo-Suárez, J. J., Chaudhari, R. V., & Subramaniam, B. (2013). Design of heterogeneous catalysts for fuels and chemicals processing: An overview. In *Novel Materials for Catalysis and Fuels Processing* (pp. 3-68). American Chemical Society. <https://doi.org/10.1021/bk-2013-1132.ch001>
- Buchori, L., Widayat, W., Muraza, O., Amali, M. I., Maulida, R. W., & Prameswari, J. (2020). Effect of temperature and concentration of zeolite catalysts of geothermal solid waste in biodiesel production from used cooking oil by esterification–transesterification process. *Processes*, *8*(12), Article 1629. <https://doi.org/10.3390/pr8121629>
- Caballero, K. V., Guerrero-Amaya, H., & Baldovino-Medrano, V. G. (2019). Revisiting glycerol esterification with acetic acid over amberlyst-35 via statistically designed experiments: Overcoming transport limitations. *Chemical Engineering Science*, *207*, 91-104. <https://doi.org/10.1016/j.ces.2019.06.003>
- Campos-Vega, R., Nieto-Figueroa, K. H., & Oomah, B. D. (2018). Cocoa (*Theobroma cacao* L.) pod husk: Renewable source of bioactive compounds. *Trends in Food Science & Technology*, *81*, 172-184. <https://doi.org/10.1016/j.tifs.2018.09.022>
- Chakraborty, R., Chatterjee, S., Mukhopadhyay, P., & Barman, S. (2016). Progresses in waste biomass derived catalyst for production of biodiesel and bioethanol: A review. *Procedia Environmental Sciences*, *35*, 546-554. <https://doi.org/10.1016/j.proenv.2016.07.039>
- Chamack, M., Mahjoub, A. R., & Akbari, A. (2018). Zirconium-modified mesoporous silica as an efficient catalyst for the production of fuel additives from glycerol. *Catalysis Communications*, *110*, 1-4. <https://doi.org/10.1016/j.catcom.2018.02.021>
- Chen, G. Y., Shan, R., Shi, J. F., & Yan, B. B. (2015). Transesterification of palm oil to biodiesel using rice husk ash-based catalysts. *Fuel Processing Technology*, *133*, 8-13. <https://doi.org/10.1016/j.fuproc.2015.01.005>
- Chong, C. C., Aqsha, A., Ayoub, M., Sajid, M., Abdullah, A. Z., Yusup, S., & Abdullah, B. (2020). A review over the role of catalysts for selective short-chain polyglycerol production from biodiesel derived waste glycerol. *Environmental Technology & Innovation*, *19*, Article 100859. <https://doi.org/10.1016/j.eti.2020.100859>
- Chouhan, A. P. S., & Sarma, A. K. (2013). Biodiesel production from *Jatropha curcas* L. oil using *Lemna perpusilla* Torrey ash as heterogeneous catalyst. *Biomass and Bioenergy*, *55*, 386-389. <https://doi.org/10.1016/j.biombioe.2013.02.009>
- Ciriminna, R., Pina, C. D., Rossi, M., & Pagliaro, M. (2014). Understanding the glycerol market. *European Journal of Lipid Science and Technology*, *116*(10), 1432-1439. <https://doi.org/10.1002/ejlt.201400229>
- Daud, N. M., Abdullah, S. R. S., Hasan, H. A., & Yaakob, Z. (2015). Production of biodiesel and its wastewater treatment technologies: A review. *Process Safety and Environmental Protection*, *94*, 487-508. <https://doi.org/10.1016/j.psep.2014.10.009>

- de Abreu Dessimoni, A. L., de Oliveira Pereira, L., Penido, E. S., Veiga, T. R. L. A., de Barros Fernandes, R. V., Teixeira, M. L., de Resende Bonésio, M., & Bianchi, M. L. (2018). Characterization of catalysts for glycerol ester production with various acetylating agents. *Analytical Letters*, *51*(11), 1705-1717. <https://doi.org/10.1080/00032719.2017.1385620>
- de la Calle, C., Fraile, J. M., García-Bordejé, E., Pires, E., & Roldán, L. (2015). Biobased catalyst in biorefinery processes: Sulphonated hydrothermal carbon for glycerol esterification. *Catalysis Science & Technology*, *5*(5), 2897-2903. <https://doi.org/10.1039/C5CY00059A>
- Dill, L. P., Kochepek, D. M., Melinski, A., Wypych, F., & Cordeiro, C. S. (2019). Microwave-irradiated acetylation of glycerol catalyzed by acid activated clays. *Reaction Kinetics, Mechanisms and Catalysis*, *127*(2), 991-1004. <https://doi.org/10.1007/s11144-019-01594-w>
- Dosuna-Rodríguez, I., & Gaigneaux, E. M. (2012). Glycerol acetylation catalysed by ion exchange resins. *Catalysis Today*, *195*(1), 14-21. <https://doi.org/10.1016/j.cattod.2012.04.031>
- Domingos, A. M., Pitt, F. D., & Barros, A. A. C. (2019). Purification of residual glycerol recovered from biodiesel production. *South African Journal of Chemical Engineering*, *29*(1), 42-51. <https://doi.org/10.1016/j.sajce.2019.06.001>
- Endut, A., Abdullah, S. H. Y. S., Hanapi, N. H. M., Hamid, S. H. A., Lananan, F., Kamarudin, M. K. A., Umar, R., Juahir, H., & Khattoon, H. (2017). Optimization of biodiesel production by solid acid catalyst derived from coconut shell via response surface methodology. *International Biodeterioration & Biodegradation*, *124*, 250-257. <https://doi.org/10.1016/j.ibiod.2017.06.008>
- Etim, A. O., Musonge, P., & Eloka-Eboka, A. C. (2020). Effectiveness of biogenic waste-derived heterogeneous catalysts and feedstock hybridization techniques in biodiesel production. *Biofuels, Bioproducts and Biorefining*, *14*(3), 620-649. <https://doi.org/10.1002/bbb.2094>
- Falowo, O. A., Oloko-Oba, M. I., & Betiku, E. (2019). Biodiesel production intensification via microwave irradiation-assisted transesterification of oil blend using nanoparticles from elephant-ear tree pod husk as a base heterogeneous catalyst. *Chemical Engineering and Processing - Process Intensification*, *140*, 157-170. <https://doi.org/10.1016/j.cep.2019.04.010>
- Ferreira, P., Fonseca, I. M., Ramos, A. M., Vital, J., & Castanheiro, J. E. (2011). Acetylation of glycerol over heteropolyacids supported on activated carbon. *Catalysis Communications*, *12*(7), 573-576. <https://doi.org/10.1016/j.catcom.2010.11.022>
- Gohain, M., Devi, A., & Deka, D. (2017). *Musa balbisiana* Colla peel as highly effective renewable heterogeneous base catalyst for biodiesel production. *Industrial Crops and Products*, *109*, 8-18. <https://doi.org/10.1016/j.indcrop.2017.08.006>
- Gorji, Y. M., & Ghaziaskar, H. S. (2016). Optimization of solketalacetin synthesis as a green fuel additive from ketalization of monoacetin with acetone. *Industrial & Engineering Chemistry Research*, *55*(25), 6904-6910. <https://doi.org/10.1021/acs.iecr.6b00929>
- Güleç, F., Sher, F., & Karaduman, A. (2019). Catalytic performance of Cu-and Zr-modified beta zeolite catalysts in the methylation of 2-methylnaphthalene. *Petroleum Science*, *16*(1), 161-172.

- Huang, X., Yin, Z., Wu, S., Qi, X., He, Q., Zhang, Q., Yan, Q., Boey, F., & Zhang, H. (2011). Graphene-based materials: Synthesis, characterization, properties, and applications. *Small*, 7, 1876-1902. <https://doi.org/10.1002/sml.201002009>
- Hemalatha, R., & Anbuselvi, S. (2013). Physicochemical constituents of pineapple pulp and waste. *Journal of Chemical and Pharmaceutical Research*, 5(2), 240-242.
- Herrada-Vidales, J. A., García-González, J. M., Martínez-Palou, R., & Guzmán-Pantoja, J. (2020). Integral process for obtaining acetins from crude glycerol and their effect on the octane index. *Chemical Engineering Communications*, 207(2), 231-241. <https://doi.org/10.1080/00986445.2019.1578758>
- Hermann, M., Pentek, T., & Otto, B. (2016). Design principles for industrie 4.0 scenarios. In *Proceedings of the Annual Hawaii International Conference on System Sciences* (pp. 3928-3937). IEEE Publishing. <https://doi.org/10.1109/HICSS.2016.488>
- Heryani, H., & Yanti, N. R. (2020). Potentials of biomass waste sources for heterogeneous catalyst production. In *IOP Conference Series: Earth and Environmental Science* (Vol. 472, No. 1, p. 012035). IOP Publishing. <https://doi.org/10.1088/1755-1315/472/1/012035>
- Ilyas, R. A., Sapuan, S. M., Ibrahim, R., Abrial, H., Ishak, M. R., Zainudin, E. S., Asrofi, M., Atikah, M. S. N., Huzaifah, M. R. M., Radzi, A. M., Azammi, A. M. N., Shaharuzaman, M. A., Nurazzi, N. M., Syafri, E., Sari, N. H., Norrahim, M. N. F., & Jumaidin, R. (2019). Sugar palm (*Arenga pinnata* (Wurmb.) Merr) cellulosic fibre hierarchy: A comprehensive approach from macro to nano scale. *Journal of Materials Research and Technology*, 8(3), 2753-2766. <https://doi.org/10.1016/j.jmrt.2019.04.011>
- Kale, S., Umbarkar, S. B., Dongare, M. K., Eckelt, R., Armbruster, U., & Martin, A. (2015). Selective formation of triacetin by glycerol acetylation using acidic ion-exchange resins as catalyst and toluene as an entrainer. *Applied Catalysis A: General*, 490, 10-16. <https://doi.org/10.1016/j.apcata.2014.10.059>
- Khan, H. M., Iqbal, T., Yasin, S., Ali, C. H., Abbas, M. M., Jamil, M. A., Hussain, A., M. Soudagar, M. E., & Rahman, M. M. (2021). Application of agricultural waste as heterogeneous catalysts for biodiesel production. *Catalysts*, 11(10), Article 1215. <https://doi.org/10.3390/catal11101215>
- Khayoon, M. S., & Hameed, B. H. (2011). Acetylation of glycerol to biofuel additives over sulfated activated carbon catalyst. *Bioresource Technology*, 102(19), 9229-9235. <https://doi.org/10.1016/j.biortech.2011.07.035>
- Lathiya, D. R., Bhatt, D. V., & Maheria, K. C. (2018). Synthesis of sulfonated carbon catalyst of waste orange peel for cost effective biodiesel production. *Bioresource Technology Reports*, 2, 69-76. <https://doi.org/10.1016/j.biteb.2018.04.007>
- Mahmudul, H. M., Hagos, F. Y., Mamat, R., Adam, A. A., Ishak, W. F. W., & Alenezi, R. (2017). Production, characterization and performance of biodiesel as an alternative fuel in diesel engines - A review. *Renewable and Sustainable Energy Reviews*, 72, 497-509. <https://doi.org/10.1016/j.rser.2017.01.001>
- Malaika, A., & Kozłowski, M. (2019). Glycerol conversion towards valuable fuel blending compounds with the assistance of SO₃H-functionalized carbon xerogels and spheres. *Fuel Processing Technology*, 184, 19-26. <https://doi.org/10.1016/j.fuproc.2018.11.006>
- Marshall, R. E., & Farahbakhsh, K. (2013). Systems approaches to integrated solid waste management in developing countries. *Waste Management*, 33(4), 988-1003. <https://doi.org/10.1016/j.wasman.2012.12.023>

- Monteiro, M. R., Kugelmeier, C. L., Pinheiro, R. S., Batalha, M. O., & da Silva César, A. (2018). Glycerol from biodiesel production: Technological paths for sustainability. *Renewable and Sustainable Energy Reviews*, 88, 109-122. <https://doi.org/10.1016/j.rser.2018.02.019>
- Mendonça, I. M., Paes, O. A. R. L., Maia, P. J. S., Souza, M. P., Almeida, R. A., Silva, C. C., Duvoisin, S., & de Freitas, F. A. (2019). New heterogeneous catalyst for biodiesel production from waste tucumã peels (*Astrocaryum aculeatum* Meyer): Parameters optimization study. *Renewable Energy*, 130, 103-110. <https://doi.org/10.1016/j.renene.2018.06.059>
- Moni, M. N. Z., Sulaiman, S. A., Raja, Y. S., Karunamurthy, K., Inayat, M., & Bou-Rabee, M. A. (2016). Investigation of the relationship between moisture content and density of selected Malaysian biomass. *Journal of Mechanical Engineering and Sciences*, 10(2), 2112-2126. <https://doi.org/10.15282/jmes.10.2.2016.15.0199>
- Mufrodi, Z., Astuti, E., Aktawan, A., & Purwono, S. (2018). The effect of recycle stream on the selectivity and yield of the formation of triacetin from glycerol. In *IOP Conference Series: Earth and Environmental Science* (Vol. 175, No. 1, p. 012013). IOP Publishing. <https://doi.org/10.1088/1755-1315/175/1/012013>
- Nda-Umar, U. I., Ramli, I., Taufiq-Yap, Y. H., & Muhamad, E. N. (2019). An overview of recent research in the conversion of glycerol into biofuels, fuel additives and other bio-based chemicals. *Catalysts*, 9(1), Article 15. <https://doi.org/10.3390/catal9010015>
- Ofori-Boateng, C., & Lee, K. T. (2013). The potential of using cocoa pod husks as green solid base catalysts for the transesterification of soybean oil into biodiesel: Effects of biodiesel on engine performance. *Chemical Engineering Journal*, 220, 395-401. <https://doi.org/10.1016/j.cej.2013.01.046>
- Ogunbenro, A. E., Quang, D. V., Al-Ali, K. A., Vega, L. F., & Abu-Zahra, M. R. M. (2018). Physical synthesis and characterization of activated carbon from date seeds for CO₂ capture. *Journal of Environmental Chemical Engineering*, 6(4), 4245-4252. <https://doi.org/10.1016/j.jece.2018.06.030>
- Oliverio, M., Costanzo, P., Nardi, M., Calandrucchio, C., Salerno, R., & Procopio, A. (2016). Tunable microwave-assisted method for the solvent-free and catalyst-free peracetylation of natural products. *Beilstein Journal of Organic Chemistry*, 12(1), 2222-2233.
- Onoji, S. E., Iyuke, S. E., Igbafe, A. I., & Nkazi, D. B. (2016). Rubber seed oil: A potential renewable source of biodiesel for sustainable development in sub-Saharan Africa. *Energy Conversion and Management*, 110, 125-134. <https://doi.org/10.1016/j.enconman.2015.12.002>
- Putra, M. D., Ristianingsih, Y., Jelita, R., Irawan, C., & Nata, I. F. (2017). Potential waste from palm empty fruit bunches and eggshells as a heterogeneous catalyst for biodiesel production. *RSC Advances*, 7(87), 55547-55554. <https://doi.org/10.1039/c7ra11031f>
- Rastegari, H., & Ghaziaskar, H. S. (2015). From glycerol as the by-product of biodiesel production to value-added monoacetin by continuous and selective esterification in acetic acid. *Journal of Industrial and Engineering Chemistry*, 21, 856-861. <https://doi.org/10.1016/j.jiec.2014.04.023>
- Sadh, P. K., Duhan, S., & Duhan, J. S. (2018). Agro-industrial wastes and their utilization using solid state fermentation: A review. *Bioresources and Bioprocessing*, 5(1), Article 1. <https://doi.org/10.1186/s40643-017-0187-z>

- Sharma, M., Khan, A. A., Puri, S. K., & Tuli, D. K. (2012). Wood ash as a potential heterogeneous catalyst for biodiesel synthesis. *Biomass and Bioenergy*, *41*, 94-106. <https://doi.org/10.1016/j.biombioe.2012.02.017>
- Souza, T. F. C., Ferreira, N. L., Marin, M., & Guardani, R. (2017). Glycerol esterification with acetic acid by reactive distillation using hexane as an entrainer. *International Journal of Chemical Engineering and Applications*, *8*(6), 344-350.
- Syamsiro, M., Saptoadi, H., Tambunan, B. H., & Pambudi, N. A. (2012). A preliminary study on use of cocoa pod husk as a renewable source of energy in Indonesia. *Energy for Sustainable Development*, *16*(1), 74-77. <https://doi.org/10.1016/j.esd.2011.10.005>
- Tan, H. W., Aziz, A. R. A., & Aroua, M. K. (2013). Glycerol production and its applications as a raw material: A review. *Renewable and Sustainable Energy Reviews*, *27*, 118-127. <https://doi.org/10.1016/j.rser.2013.06.035>
- Tasuna, N., Hidayatillah, K. H., Marwan, & Zuhra. (2021). Selective esterification of glycerol diacetin and triacetin over rice husk biosilica catalyst with microwave heating. In *IOP Conference Series: Materials Science and Engineering* (Vol. 1087, No. 1, p. 012063). IOP Publishing. <https://doi.org/10.1088/1757-899x/1087/1/012063>
- Trisunaryanti, W., Triyono, T., Falah, I. I., Siagian, A. D., & Marsuki, M. F. (2018). Synthesis of Ce-mesoporous silica catalyst and its lifetime determination for the hydrocracking of waste lubricant. *Indonesian Journal of Chemistry*, *18*(3), 441-447.
- Widmer, W., Zhou, W., & Grohmann, K. (2010). Pretreatment effects on orange processing waste for making ethanol by simultaneous saccharification and fermentation. *Bioresource Technology*, *101*(14), 5242-5249. <https://doi.org/10.1016/j.biortech.2009.12.038>
- Wu, L., Dong, Z., Cai, Z., Ganapathy, T., Fang, N. X., Li, C., Yu, C., Zhang, Y., & Song, Y. (2020). Highly efficient three-dimensional solar evaporator for high salinity desalination by localized crystallization. *Nature Communications*, *11*(1), Article 521. <https://doi.org/10.1038/s41467-020-14366-1>
- Yanti, N. R., Heryani, H., Putra, M. D., & Nugroho, A. (2019). Triacetin production from glycerol using heterogeneous catalysts prepared from peat clay. *International Journal of Technology*, *10*(5), 291-319. <https://doi.org/10.14716/ijtech.v10i5.2685>
- Yusof, N., Iranmanesh, M., & Awang, H. (2015). Pro-environmental practices among Malaysian construction practitioners. In *Advances in Environmental Biology* (pp. 117-120). American-Eurasian Network for Scientific Information.
- Zhang, H., Zhao, X., Ding, X., Lei, H., Chen, X., An, D., Li, Y., & Wang, Z. (2010). A study on the consecutive preparation of d-xylose and pure superfine silica from rice husk. *Bioresource Technology*, *101*(4), 1263-1267. <https://doi.org/10.1016/j.biortech.2009.09.045>
- Zulkefli, S., Abdulmalek, E., & Rahman, M. B. A. (2017). Pretreatment of oil palm trunk in deep eutectic solvent and optimization of enzymatic hydrolysis of pretreated oil palm trunk. *Renewable Energy*, *107*, 36-41. <https://doi.org/10.1016/j.renene.2017.01.037>

DFT-Based Reversible Watermarking Method for Image Ownership Protection

Ansam Osamah Abdulmajeed* and Sundus Abdulmuttalib Mohamed

College of Computer Science and Mathematics, University of Mosul, Almajmoa, 41002, Mosul, Iraq

ABSTRACT

The Performance of Discrete Fourier Transform (DFT)-based watermarking methods has been carefully examined in the literature. Although the watermark in most of the literature was embedded in the DFT magnitudes using bit plane embedding, it was recently embedded in the Direct Current (DC) coefficient in the spatial domain. However, data loss due to rounding and replacement operations are still evident. Therefore, the objective of the method proposed here was to combine previous literature designs to implement a reversible DFT-based watermarking method for image ownership protection using bit plane embedding in the DC coefficient. The watermark was embedded in a middle bit plane of the DC coefficient for each DFT-transformed image block. In order to ensure reversibility and improve the security level, a combination of double Feynman and XOR gates was used to shuffle the watermark bits. The results revealed that the 8th (PSNR/SSIM = 32dB/0.8826), the 9th (PSNR/SSIM = 38dB/0.0.9587), and the 10th (PSNR/SSIM = 44dB/0.9917) bit planes for block sizes of 4×4, 8×8, and 16×16, respectively, were the best bit planes showing good imperceptibility and resistance to compression, filtering, and noise attacks. In conclusion, embedding the DC coefficients rather than all the magnitudes has influentially increased the watermarking robustness. In contrast, embedding the DC coefficients in the frequency domain rather than the spatial domain reduced the image's structural contents distortion.

Furthermore, the proposed method for grayscale images is effective in applications where reversibility is desired. However, further studies to find colored images' reversible methods are recommended.

Keywords: Bit plane, DC coefficient, digital watermarking, discrete Fourier transform, Feynman gate, reversible watermarking

ARTICLE INFO

Article history:

Received: 6 November 2021

Accepted: 31 January 2022

Published: 20 April 2022

DOI: <https://doi.org/10.47836/pjst.30.3.07>

E-mail addresses:

ansam_osamah@uomosul.edu.iq (Ansam Osamah Abdulmajeed)

sundus_abid7@uomosul.edu.iq (Sundus Abdulmuttalib Mohamed)

*Corresponding author

INTRODUCTION

Protection of intellectual rights has recently become crucial due to the huge amounts of digital media being increasingly transmitted throughout the internet. Watermarking is one of the most powerful techniques to protect digital media from intentional or unintentional tampering behaviors (Feng et al., 2019). It is widely used in applications of ownership pretensions and confirming copyrights (Luo et al., 2021). Digital watermarking embeds watermark information in the host media in some way that prevents it from being destroyed and being matched later with those of the owners (Feng et al., 2019). The basic requirements that must be taken into consideration in designing a digital watermarking system are imperceptibility, payload, and robustness, where imperceptibility means the amount of perceptual effect of an embedded watermark on the quality of the host media, while payload refers to the amount of information that can be embedded in the host media without affecting the quality (Qasim et al., 2018). Robustness denotes the ability of a watermarking method to resist attacks. However, not all watermarking methods can resist all types of attacks. For instance, fragile watermarking methods cannot resist slight tampering of host media. On the other hand, robust watermarking methods can resist intentional and malicious attacks. There are semi-fragile methods that can withstand only unintended attacks, such as noise attacks and JPEG compression (Menendez-Ortiz et al., 2019). There is a trade-off between payload and both robustness and imperceptibility. A large payload can be acquired by compromising either robustness or imperceptibility (Ansari et al., 2018).

In some critical applications, such as medical applications, reversible watermarking methods are required to restore the original copy of the host media. Indeed, reversible watermarking methods recover the host media without any loss if the channel is noise-free. In contrast, a complete recovery of the host media cannot be guaranteed if there are attacks (Menendez-Ortiz et al., 2019).

Watermarking methods can be divided into three categories according to the extraction process. Blind extraction does not require additional information other than the secret key to retrieve the watermark. Non-blind extraction, on the other hand, necessitates both the watermark and the original media, whereas semi-blind extraction necessitates the watermark to extract the embedded watermarks (Khalilidan et al., 2020). A watermark is embedded either in the spatial or frequency domain. In the frequency domain, the most commonly used transforms are the Discrete Cosine Transform (DCT), Discrete Wavelet Transform (DWT), and Discrete Fourier Transform (DFT) (Jimson & Hemachandran, 2018). The performance of DFT-based digital watermarking methods has been carefully examined in various studies (Table 1). For instance, Ahmed and Moskowitz (2004) proposed a bit plane embedding method to embed the watermark in the middle bit plane of the rounded magnitude. This study found that the 13th bit plane was the optimum plane for embedding. In additional work, Ahmed and Moskowitz (2006) proposed a semi-reversible method where the bit plane

(i-1) was replaced with the embedding bit plane (i) prior to the embedding process to recover the most impact bit plane on image quality during the extraction process.

In another study, Zhu et al. (2007) examined the fragility of the method proposed by Ahmed and Moskowitz (2004) against malicious attacks. This study found that the embedding in the 9th bit plane did not resist any unintended or malicious attacks but reserved good image quality. In contrast, embedding in the 13th bit plane showed good resistance to JPEG compression; however, it was very fragile against tampering. On the other hand, Su et al. (2019) embedded the watermarking bits by modifying the pixels of colored image blocks based on the Direct Current (DC) coefficients, which were calculated in the spatial domain, and their optimal boundary values. Finally, Zhang et al. (2020) proposed a blind color image watermarking algorithm in the spatial domain. The embedding strategy in this study was designed based on the similarity between the values of the DC coefficients of adjacent blocks.

Table 1

The design of the related DFT-based watermarking method

Method	Domain	Host image	Watermark image	Embedding technique	Place of embedding	Reversibility
Ahmed and Moskowitz (2004)	Frequency	512×512 grayscale	512×512 Binary	Bit plane embedding	Real magnitudes	Irreversible
Ahmed and Moskowitz (2006)	Frequency	512×512 grayscale	512×512 Binary	Bit plane embedding	Real magnitudes	Semi-reversible
Zhu et al. (2007)	Frequency	512×512 grayscale	512×512 Binary	Bit plane embedding	Real magnitudes	Irreversible
Su et al. (2019)	Spatial	512×512 RGB	32×32 RGB	Quantization technique	DC coefficient	Irreversible
Zhang et al. (2020)	Spatial	512×512 RGB	32×32 RGB	Quantization technique	DC coefficient	Irreversible

Previous studies, however, suffered from data loss due to rounding and replacement operations which made them irreversible. Therefore, the objective of the proposed method here was to implement a reversible watermarking method. The current method combines the designs of the abovementioned studies listed in Table 1. It implemented a bit plane embedding in the DC coefficient in the frequency domain. The watermark was embedded in a middle bit plane of the DC coefficient for each DFT-transformed image block (Figure 1). In order to ensure reversibility and improve the security level, the proposed method used a combination of double Feynman and XOR gates to shuffle the watermark bits with both the secret key and the original bit of the selected bit plane.

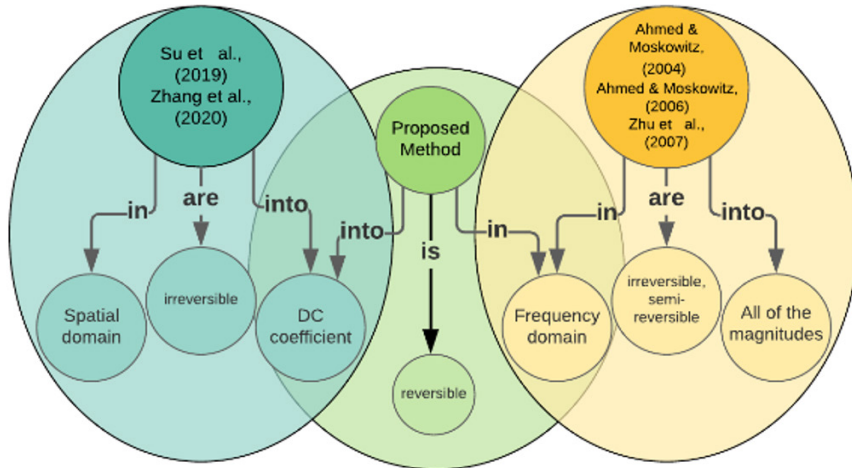


Figure 1. Proposed method framework

MATERIALS AND METHOD

Discrete Fourier Transform (DFT)

DFT is one of the most widely used transforms in the digital watermarking algorithm. For example, the digital image can be transformed into the DFT domain by Equation 1 below (Qasim et al., 2018):

$$F(u, v) = \sum_{x=0}^{N-1} \sum_{y=0}^{M-1} f(x, y) e^{-j2\pi(\frac{ux}{N} + \frac{vy}{M})} \quad [1]$$

where M and N are the image dimensions, and $f(x, y)$ is the image's pixel. DFT coefficients, $F(u, v)$, are complex numbers. In polar form, the real $R(u, v)$ and imaginary $I(u, v)$ parts of the coefficients are expressed as the magnitude and phase, which can be computed by Equations 2 and 3, respectively (Qasim et al., 2018):

$$|F(u, v)| = [R^2(u, v) + I^2(u, v)]^{\frac{1}{2}} \quad [2]$$

$$\theta(u, v) = \tan^{-1} \left[\frac{I(u, v)}{R(u, v)} \right] \quad [3]$$

The phase is more significant than the magnitude since the magnitude includes fewer pieces of information (Jimson & Hemachandran, 2018). $F(0, 0)$ is often called the DC coefficient, representing the image's average brightness (Zhang et al., 2020). The Inverse Discrete Fourier Transform (IDFT) can be computed by the following Equation 4 (Qasim et al., 2018):

$$f(x, y) = \frac{1}{NM} \sum_{u=0}^{N-1} \sum_{v=0}^{M-1} F(u, v) e^{j2\pi(\frac{ux}{N} + \frac{vy}{M})} \quad [4]$$

Feynman Gate

The reversible logical gate maps one input to one output without data loss, e.g., NOT and XOR gates. Feynman gate is a reversible logical gate of two inputs and two outputs. The first input is the control and the second one is the target. The Feynman gate negates the target input only if the control input is set. Therefore, it is known as the ‘‘Controlled NOT’’ gate. The Double Feynman gate comprises two Feynman gates (Figure 2) (Krishna & Ramesh, 2019).

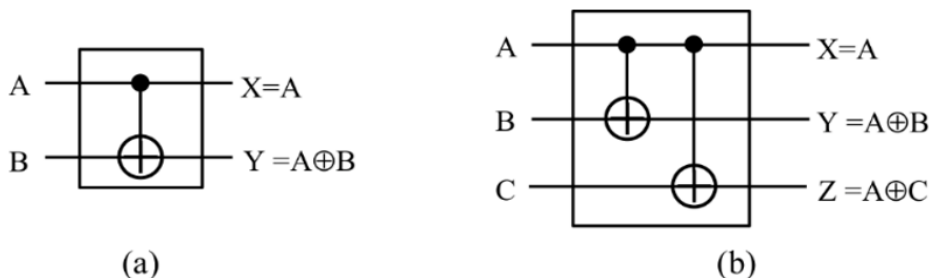


Figure 2. (a) Feynman gate (b) Double Feynman gate (Krishna & Ramesh, 2019)

Proposed Method

Embedding Process. The in-detail steps of the embedding process included the following (Figure 3):

Step-1: The host image I , of size $M \times M$, was subdivided into non-overlapping blocks of size $N \times N$.

Step-2: Each block was transformed to the frequency domain using DFT.

Step-3: The original watermark W was shuffled with the secret key K and the selected middle bit plane BP of the DC coefficient of each block using a combination of double Feynman and XOR gates. Both W and K were binary images of size $M/N \times M/N$.

Step-4: Every bit of the shuffled watermark W_s was embedded in the selected middle bit plane BP of the DC coefficients.

Step-5: IDFT was applied to produce the watermarked image I_w .

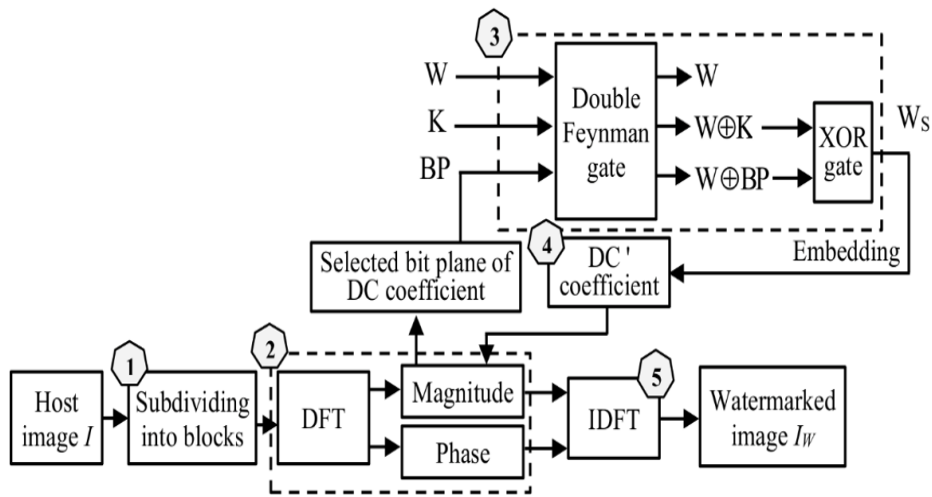


Figure 3. The embedding process of the proposed method

Extraction Process. The extraction process required the original watermark to extract the hidden watermark because the proposed method was a semi-blind watermarking method. The extraction process included the following steps (Figure 4):

Step-1: The watermarked image I_w was subdivided into non-overlapping blocks of size $N \times N$.

Step-2: Each block was transformed to the frequency domain using DFT.

Step-3: The hidden watermark W_s was extracted from the selected bit plane of the DC coefficients of each block.

Step-4: The original watermark W was re-initialized using the secret key K , such that $W_{RE} = W \oplus K$.

Step-5: W_s was passed to XOR gate along with W_{RE} .

Step-6: The result of Step 5 was passed to XOR twice with the following:

1st. The original watermark W to recover the original bit plane of the DC coefficient, replaced by those of each block.

2nd. The recovered bit plane of the DC coefficient to extract the watermark.

Step-7: The magnitude and the unchanged phase were passed to IDFT to recover an identical copy of the host image.

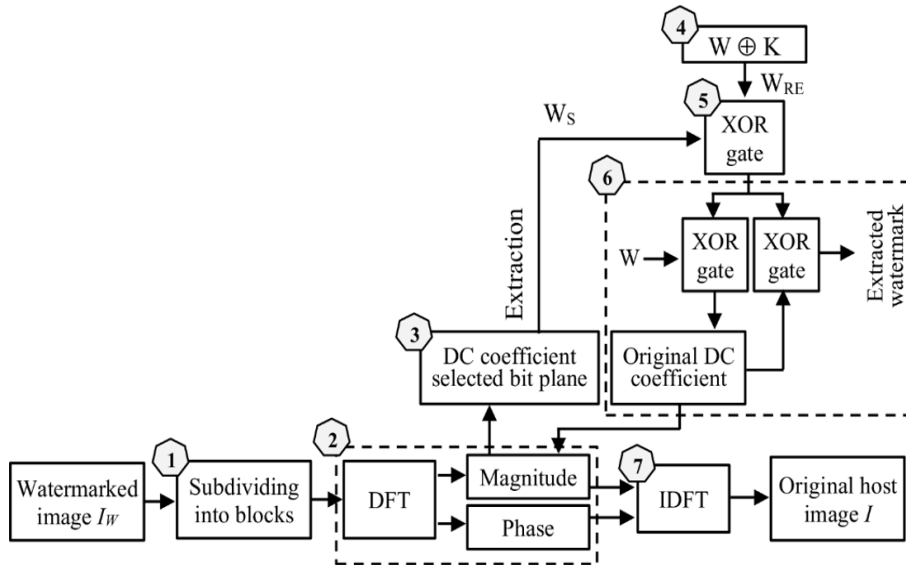


Figure 4. The extraction process of the proposed method

Analysis of the Performance

Several metrics can ensure that the digital watermarking methods achieve the most important requirements of secure watermarking. Peak Signal-to-Noise Ratio (PSNR) is the most widely measure used to test the method’s imperceptibility. PSNR can be computed according to the following Equation 5 (Qasim et al., 2018):

$$PSNR(I, I_w) = 10 \times \log_{10} \frac{MAX_I^2}{MSE} \tag{5}$$

where I and I_w are the host and watermarked images, respectively. MAX denotes the value of the maximum sample, and MSE , the Mean Square Error (Equation 6) (Qasim et al., 2018):

$$MSE(I, I_w) = \frac{1}{MN} \sum_{i=0}^{M-1} \sum_{j=0}^{N-1} (I(i, j) - I_w(i, j))^2 \tag{6}$$

The main component of PSNR is the squared error values that refer to the difference between the co-located pixel values. The accepted value of PSNR is greater than 30 dB (Setiadi, 2021). When the two images are identical, the value of the corresponding PSNR is infinite. Accordingly, the value of PSNR must be sufficiently large to assert that the watermarking methods are imperceptible (Begum & Uddin, 2021). Structural Similarity Index (SSIM) is a more recent measurement than PSNR that measures the similarity between two images based on the luminance, contrast, and correlation coefficients (Setiadi,

2021). The SSIM between the host image I and the watermarked image I_w can be computed as the following Equation 7 (Qasim et al., 2018):

$$SSIM(I, I_w) = \frac{(2\mu_I\mu_{I_w} + c_1)(2cov + c_2)}{(\mu_I^2 + \mu_{I_w}^2 + c_1)(\sigma_I^2 + \sigma_{I_w}^2 + c_2)} \quad [7]$$

where μ , σ , and cov are the mean, standard deviations, and covariance, which measure the luminance, the contrast, and the structure, respectively. $c_1 = (0.01L)^2$ and $c_2 = (0.03L)^2$ where $L = 2^8 - 1$.

The value of SSIM is between -1 and 1 (Qasim et al., 2018), where one is for the structurally identical images. Therefore, the closer the SSIM value is to 1, the more imperceptibility is (Begum & Uddin, 2021).

Normalized Cross-Correlation (NCC) was used to evaluate the robustness of the watermarking method. First, it is computed between the extracted watermark W' and the original watermark W according to the following Equation 8 (Su et al., 2019):

$$NCC = \frac{\sum_{i=1}^M \sum_{j=1}^N W(i, j)W'(i, j)}{\sqrt{\sum_{i=1}^M \sum_{j=1}^N W(i, j)^2} \sqrt{\sum_{i=1}^M \sum_{j=1}^N W'(i, j)^2}} \quad [8]$$

where M and N are the image dimension (Su et al., 2019). The optimal value of NCC is 1. Thus, the closer the NCC value to the optimal value, the more robust the method is (Begum & Uddin, 2021). On the other hand, Accuracy Ratio (AR) is the ratio of the correctly extracted bits C_b to the original watermark bits N_b . It can be computed as the following Equation 9 (Qasim et al., 2018):

$$AR = C_b / N_b \quad [9]$$

RESULT AND DISCUSSION

Inclusive experiments have been performed using MATLAB to evaluate the performance of the proposed method. These experiments have been conducted on a set of both colored and grayscale standard images of size 512×512 as host images and a binary image of size $512/N \times 512/N$ as a watermark image where $N = \{4, 8, 16\}$. N also represents the dimension of the host image's squared blocks (Figure 5). Because the image's blocks are square, N will be used throughout the rest of this paper to represent block size.

The strategy of the experiments included the following sequential steps:

1. Investigate the appropriate bit planes for embedding for each block size.
2. Investigate the suitable block size among those blocks.
3. Compare the proposed method to other related works.



Figure 5. The dataset used in the experiments (a) the host images (b) the watermark image

Experiments on Grayscale Images

The grayscale image of “Lena.bmp” was used to investigate the appropriate bit plane for embedding to fulfill the requirements of digital watermarking methods and achieve reversibility. The experiments were performed for $N = \{4, 8, 16\}$ and $BP = \{4, \dots, 15\}$. PSNR and SSIM were computed between the original and watermarked images to measure the imperceptibility. Furthermore, they were computed again between the original and recovered host images to check the reversibility (Figures 6 & 7). The NCC and AR were calculated for the same N and BP values to assess the robustness (Figure 8).

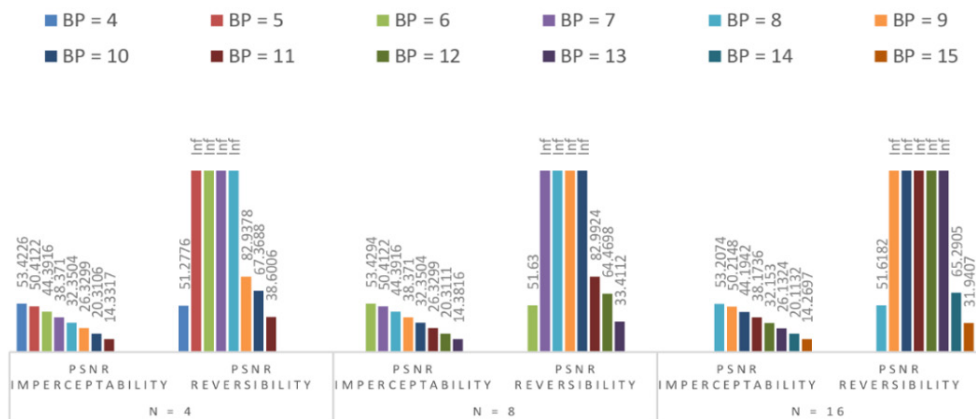


Figure 6. The PSNR of the proposed method uses different bit planes BP and block size N of the grayscale image of "Lena.bmp"

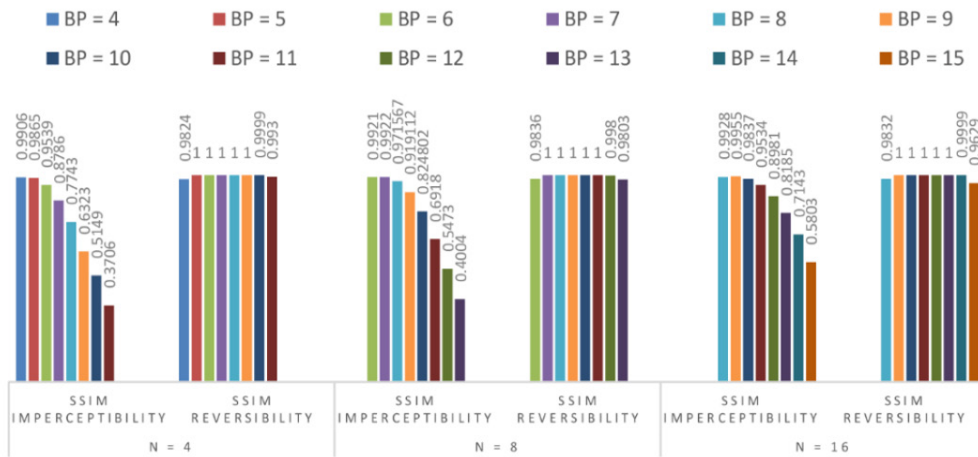


Figure 7. The SSIM of the proposed method uses different bit planes BP and block size N of the grayscale image of “Lena.bmp”

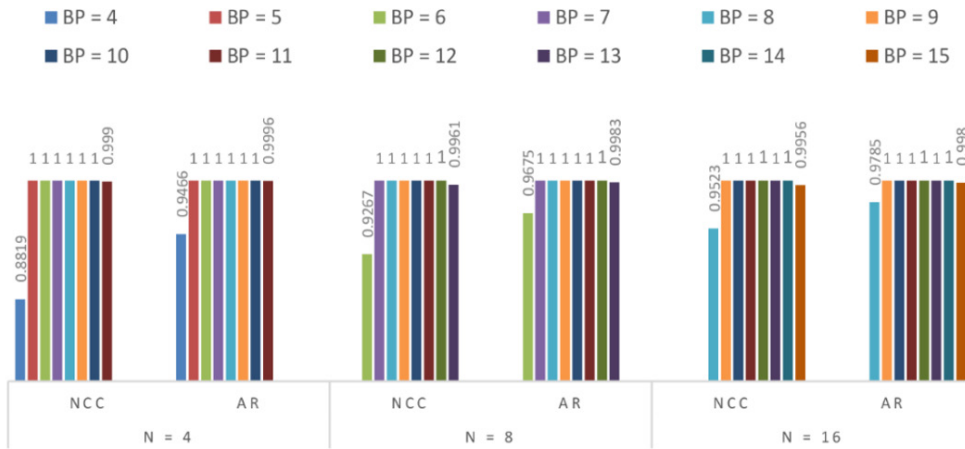


Figure 8. The robustness of the proposed method using different bit planes BP and block size N of the non-attacked grayscale image of “Lena.bmp”

Equation 10 represents the relationship between block size N and the bit plane BP.

$$BP_j = BP_i + 2 \times (\log_2(N_j) - \log_2(N_i)) \quad [10]$$

According to Equation 10, the difference between the original and the watermarked images was almost constant for different N values. The PSNR in the case of embedding in BP = 6 for N = 8 was almost the same as the PSNR of embedding in BP = 4 and BP = 8 for

$N=4$ and $N=16$, respectively. However, this relationship did not apply clearly to the values of SSIM. Figures 6, 7, and 8 show that, for each value of N , there is a set of bit planes BP that fulfills good imperceptibility ($PSNR > 32$ dB) and reversibility ($PSNR = Inf$) as well as full robustness when no attacks ($NCC = 1$). These sets were $BP = \{5, 6, 7, 8\}$, $BP = \{7, 8, 9, 10\}$, and $BP = \{9, 10, 11, 12\}$ for $N=4$, $N=8$, and $N=16$, respectively. Accordingly, further tests have been performed to decide the embedding bit plane among those ranges that could achieve the highest robustness against JPEG compression 50%, filtering attack (Median filter 3×3 , and Low pass filter 3×3), and noise attack (Gaussian noise, Poisson noise, Salt & pepper noise, and Speckle noise) (Figures 9, 10, & 11).

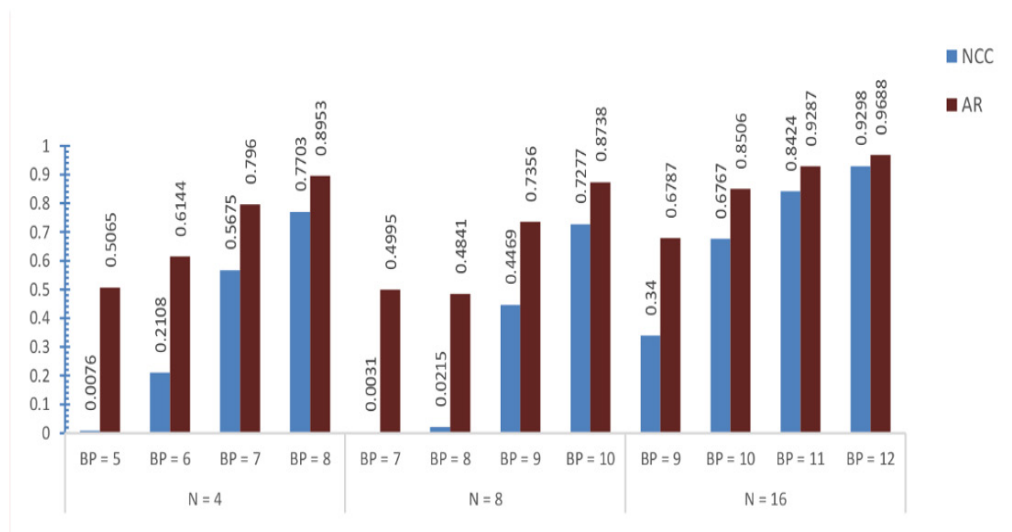


Figure 9. The robustness of the proposed method against JPEG compression 50% using the grayscale image of “Lena.bmp”

Figures 9, 10, and 11 show that the greater the value of BP , the lower the imperceptibility (Figure 12) but the higher the resistance to attacks conversely (Table 2). Therefore, the appropriate bit planes are $BP = 8$, $BP = 9$, and $BP = 10$ for $N = 4$, $N = 8$, and $N = 16$, respectively. However, the embedding in bit plane $BP = 9$ in the case of $N = 8$ could be considered a suitable choice that fulfills the tradeoff between the basic digital watermarking requirements. Finally, it is worth noting that the payloads of the proposed method are 0.0625 bit/pixel, 0.0156 bit/pixel, and 0.0039 bit/pixel for $N = 4$, $N = 8$, and $N = 16$, respectively.

Additional grayscale images were used to test the efficiency of the proposed method in the case of embedding in the bit plane $BP = 9$ for block size $N = 8$ (Table 3).

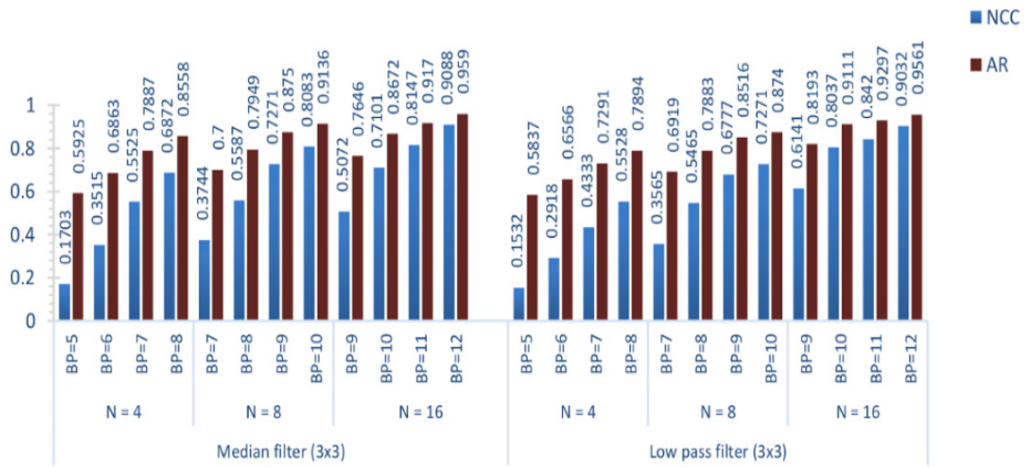
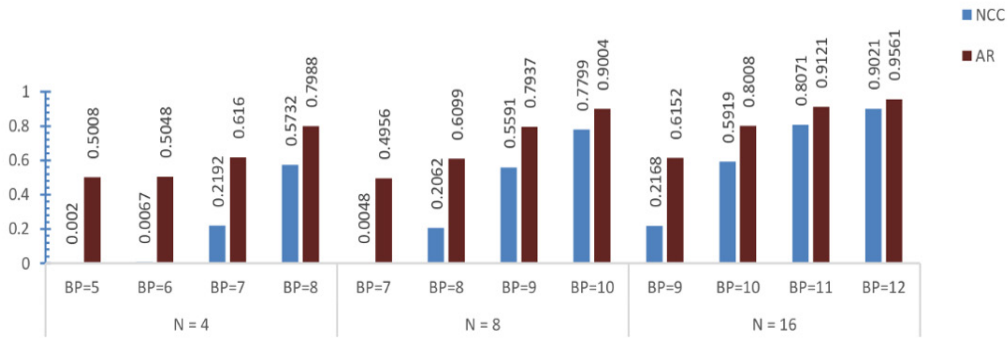
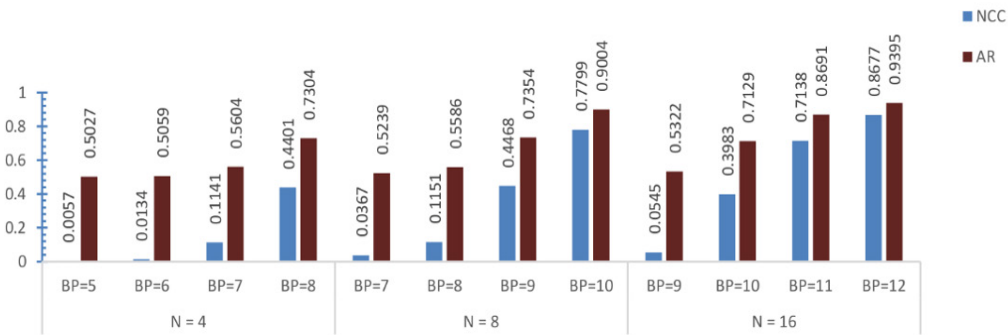


Figure 10. The robustness of the proposed method against filtering attacks using the grayscale image of “Lena.bmp”

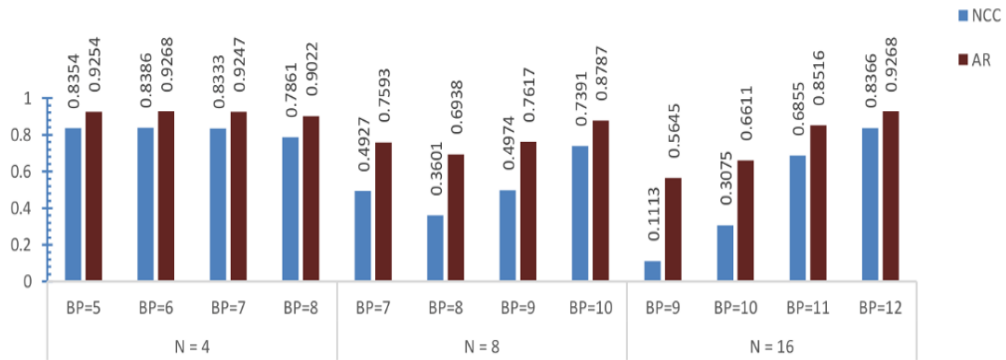


(a) Robustness against Gaussian noise 0.001

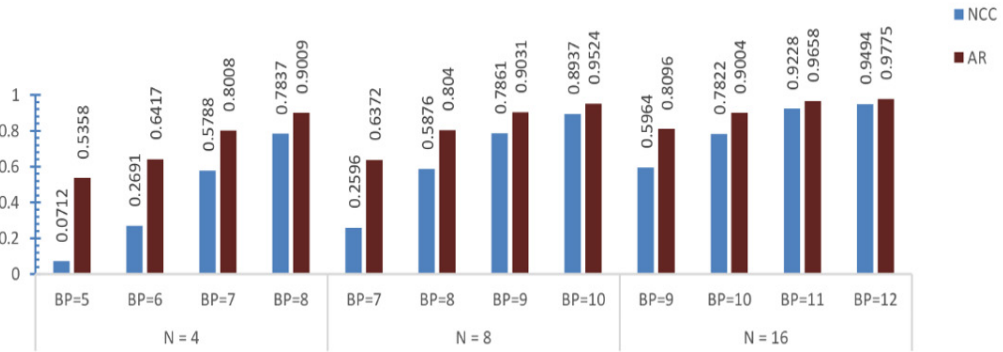


(b) Robustness against Poisson noise

Figure 11. The robustness of the proposed method against noise attacks using the grayscale image of “Lena.bmp”



(c) Robustness against salt & pepper noise 0.01



(d) Robustness against speckle noise 0.001

Figure 11. (Continue)



Figure 12. The imperceptibility of the proposed method using the grayscale image of “Lena.bmp”



Figure 12. (Continue)

Table 2

The NCC/AR of the proposed method on the attacked grayscale image of "Lena.bmp"

Attack	N = 4		N = 8		N = 16		
	BP = 7	BP = 8	BP = 9	BP = 10	BP = 10	BP = 11	BP = 12
JPEG compression 50%	 0.5675/ 0.7960	 0.7703/ 0.8953	 0.4469/ 0.7356	 0.7277/ 0.8738	 0.6767/ 0.8506	 0.8424/ 0.9287	 0.9298/ 0.9688
Gaussian noise 0.001	 0.2192/ 0.6160	 0.5732/ 0.7988	 0.5591/ 0.7937	 0.7799/ 0.9004	 0.5919/ 0.8008	 0.8071/ 0.9121	 0.9021/ 0.9561
Poisson noise	 0.1141/ 0.5604	 0.4401/ 0.7304	 0.4468/ 0.7354	 0.7799/ 0.9004	 0.3983/ 0.7129	 0.7138/ 0.8691	 0.8677/ 0.9395
Salt and Pepper noise 0.001	 0.8333/ 0.9247	 0.7861/ 0.9022	 0.4974/ 0.7617	 0.7391/ 0.8787	 0.3075/ 0.6611	 0.6855/ 0.8516	 0.8366/ 0.9268
Speckle noise 0.001	 0.5788/ 0.8008	 0.7837/ 0.9009	 0.7861/ 0.9031	 0.8937/ 0.9524	 0.7822/ 0.9004	 0.9228/ 0.9658	 0.9494/ 0.9775
Median filter	 0.5525/ 0.7887	 0.6872/ 0.8558	 0.7271/ 0.8750	 0.8083/ 0.9136	 0.7101/ 0.8672	 0.8147/ 0.9170	 0.9088/ 0.9590
Low pass filter	 0.4333/ 0.7291	 0.5528/ 0.7894	 0.6777/ 0.8516	 0.7271/ 0.8740	 0.8037/ 0.9111	 0.8420/ 0.9297	 0.9032/ 0.9561

Table 3
The efficiency of the proposed method using grayscale images, BP =9 for N=8

Image Name	Robustness NCC / AR												
	Compression					Noise					Filtering		
	Imperceptibility	PSNR/SIM	Reversibility	No attack	JPEG 30	JPEG 60	JPEG 80	Gaussian noise 0.002	Poisson noise	Salt and Pepper noise 0.01	Speckle noise 0.001	Median filter	Low pass filter
Airplane	38.1192	Inf/1	1/1	1/1	0.5408	0.7206	0.7454	0.4031	0.3236	0.5222	0.6515/0.8367	0.6577	0.6032
	/	0.8419	Inf/1	1/1	0.7834	0.8716	0.8845	0.7102	0.6692	0.7695	0.8251	0.8406	0.8145
Barbara	38.0090	Inf/1	1/1	1/1	0.5587	0.8037	0.8914	0.4124	0.4543	0.5076	0.8251	0.6326	0.6380
	/	0.9310	Inf/1	1/1	0.7922	0.9109	0.9514	0.7156	0.7397	0.7668	0.9204	0.8306	0.8311
Boat	38.1556	Inf/1	1/1	1/1	0.5074	0.7744	0.8821	0.4070	0.4188	0.4899	0.7618	0.6326	0.6371
	/	0.91101	Inf/1	1/1	0.7659	0.8967	0.9473	0.7148	0.7200	0.7568	0.8911	0.8318	0.8325
Elaine	38.2998	Inf/1	1/1	1/1	0.5255	0.7670/0.8933	0.8784	0.4012	0.4076	0.5137	0.7407	0.6961	0.6992
	/	0.9576	Inf/1	1/1	0.7749	0.9456	0.9456	0.7158	0.7148	0.7708	0.8811	0.8594	0.8604
Goldhill	38.0090	Inf/1	1/1	1/1	0.5662	0.7695	0.8872	0.4165	0.4666	0.4889	0.8082	0.6255	0.6586
	/	0.9585	Inf/1	1/1	0.7944	0.8938	0.9492	0.7202	0.7446	0.7544	0.9124	0.8245	0.8398
House	38.0459	Inf/1	1/1	1/1	0.5432	0.7380	0.8607	0.4226	0.3479	0.4945	0.7069	0.6436	0.6156
	/	0.9020	Inf/1	1/1	0.7820	0.8804	0.9370	0.7224	0.6858	0.7590	0.8638	0.8374	0.8220
Sailboat	38.4416	Inf/1	1/1	1/1	0.5766	0.7440	0.7369	0.3793	0.4229	0.4988	0.6927	0.5363	0.5378
	/	0.9240	Inf/1	1/1	0.7986	0.8833	0.8787	0.7021	0.7253	0.7639	0.8596	0.7795	0.7798

The efficiency of the proposed method in the case of embedding in bit planes BP = 9 and BP =13 for N = 8 was compared with the bit plane embedding method proposed by Ahmed & Moskowitz (2004) (Figure 13). Despite the high capacity and imperceptibility of the method proposed by Ahmed and Moskowitz (2004), which involved all the magnitudes in the embedding process, it showed low robustness compared to the current method. The proposed method utilized only the DC coefficients in the embedding. Furthermore, according to the proposed method, embedding in the 9th bit plane showed higher imperceptibility and robustness than the embedding in the 13th bit plane, according to Ahmed and Moskowitz (2004).

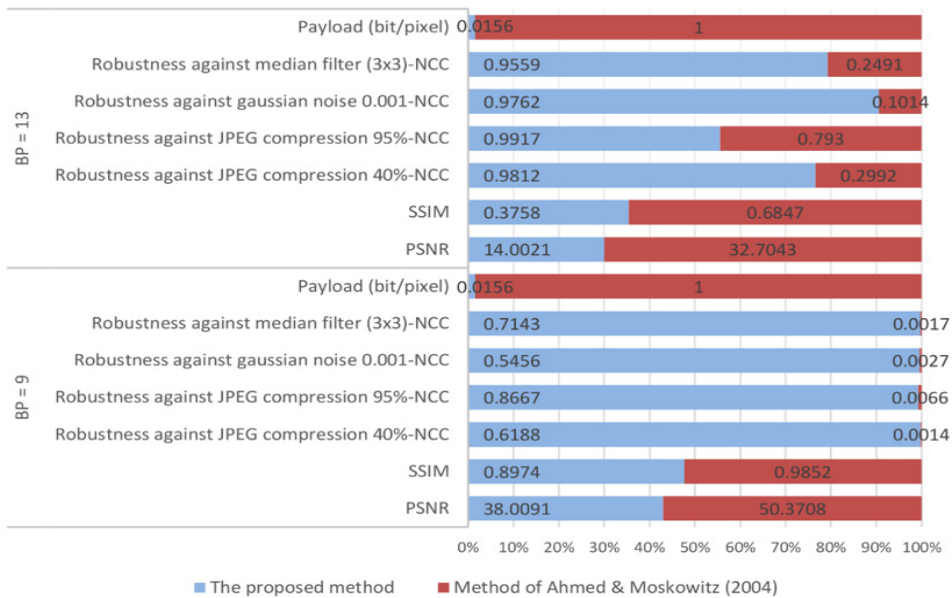


Figure 13. The comparison between the proposed method and the method of Ahmed and Moskowitz (2004)

Experiments on Colored Images

For the colored images, the same steps of the proposed method were carried out on the luminance components (Y) after converting the host image into YUV color space. The previous experiments were performed again on the colored image of “Lena.bmp” to investigate the appropriate bit planes for embedding (Figures 14, 15, & 16). It should be pointed out that the PSNR of the colored images was computed for only the luminance channel.

Figures 14 and 15 show that reversibility was not achieved for the colored images using the embedding into any bit plane (PSNR ≠ Inf) regardless of the block size despite the high

corresponding SSIM values. However, the set of bit planes that fulfill good imperceptibility and some levels of robustness (Figure 16) were $BP = \{5, 6, 7, 8\}$, $BP = \{7, 8, 9, 10\}$, $BP = \{9, 10, 11, 12\}$ for $N = 4$, $N = 8$, and $N = 16$, respectively.

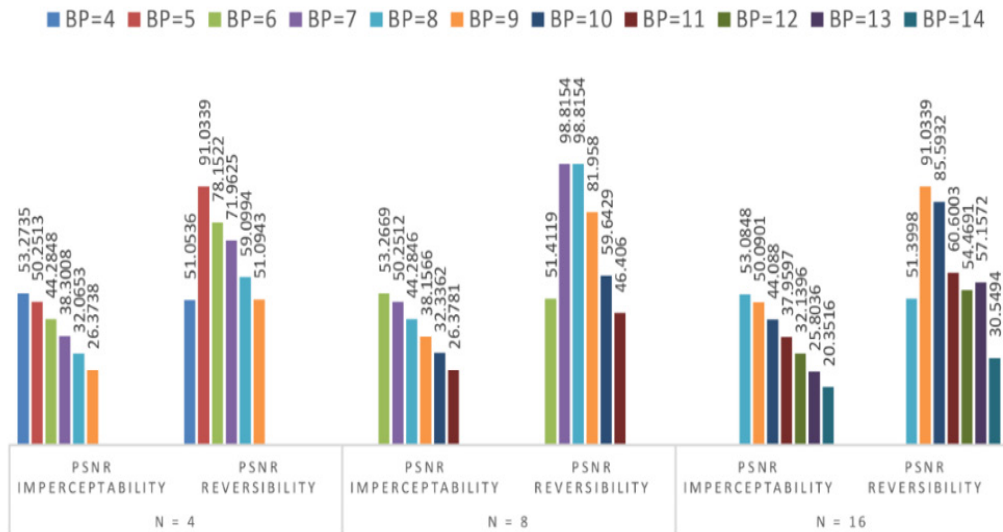


Figure 14. The PSNR of the proposed method using different bit planes BP and block size N of the colored image of “Lena.bmp”

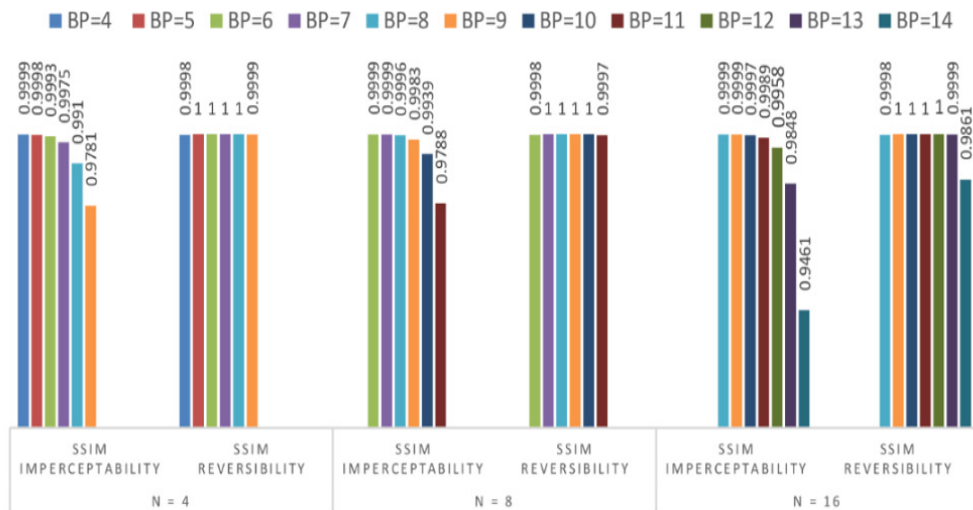


Figure 15. The SSIM of the proposed method using different bit planes BP and block size N of the colored image of “Lena.bmp”

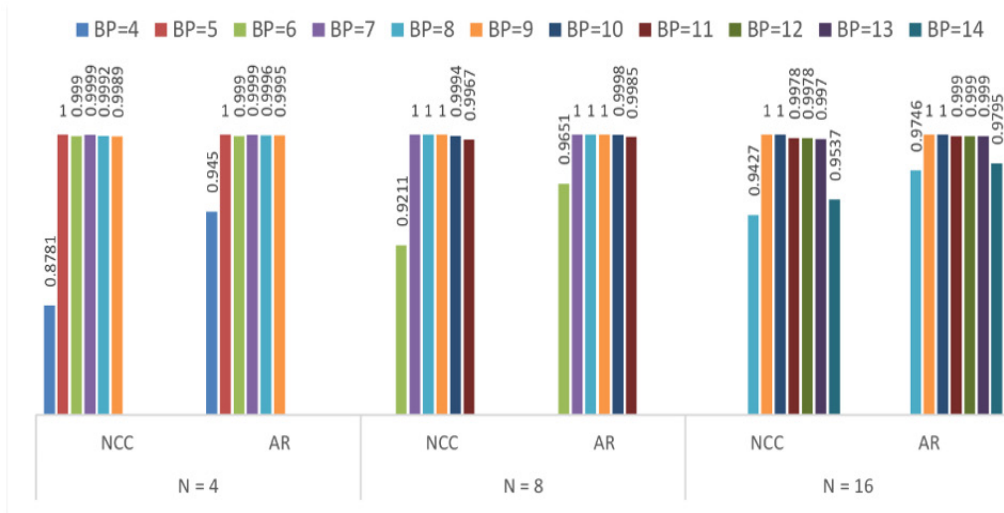


Figure 16. The robustness of the proposed method using different bit planes BP and block size N of the non-attacked colored image of “lena.bmp”

Figures 17, 18, and 19 show the robustness of the proposed method against attacks. In addition, Figures 17, 18, and 19 reveal that the bit planes BP = 8, PB = 9, BP = 10 for N = 4, N = 8, and N = 16, respectively, could be used for semi-fragile watermarking depending on the system requirement (Table 4) (Figure 20).

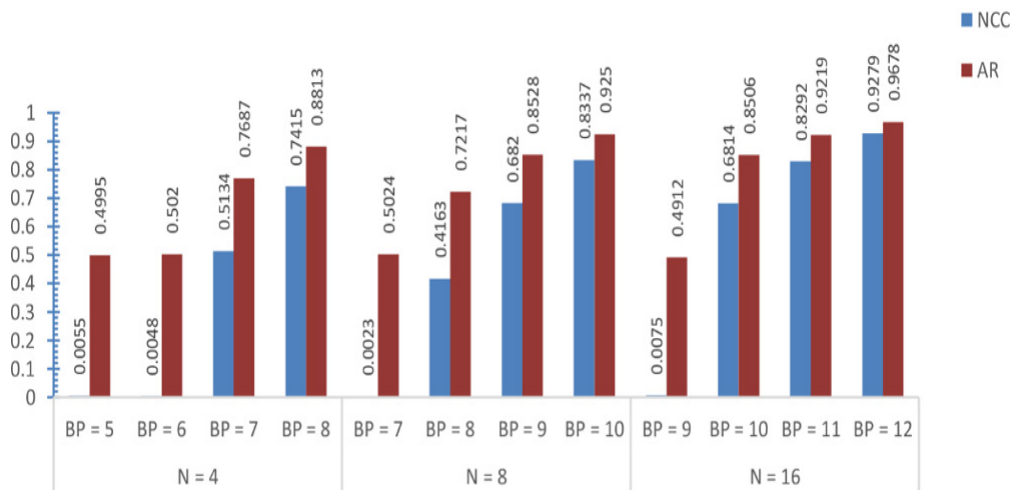


Figure 17. The robustness of the proposed method against JPEG compression 50% using the colored image of “Lena.bmp”

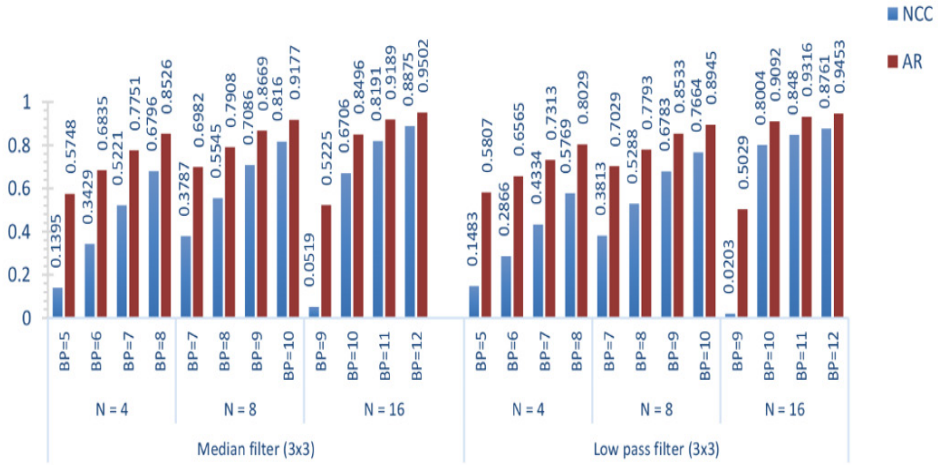
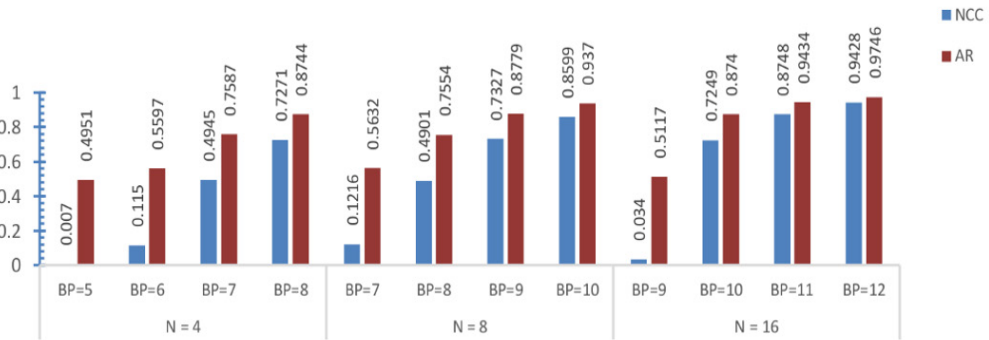
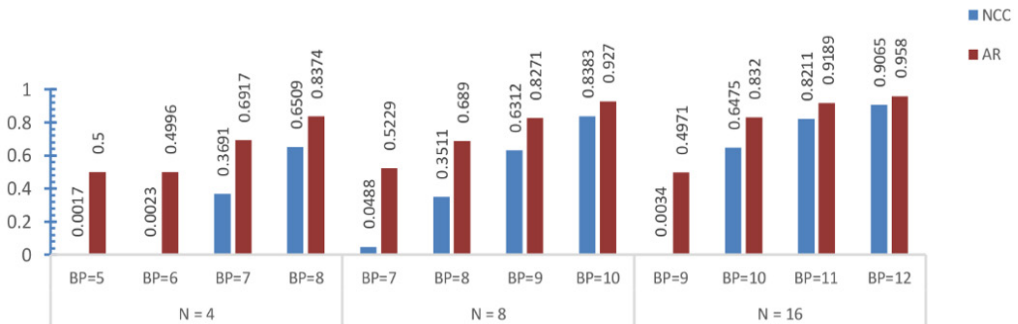


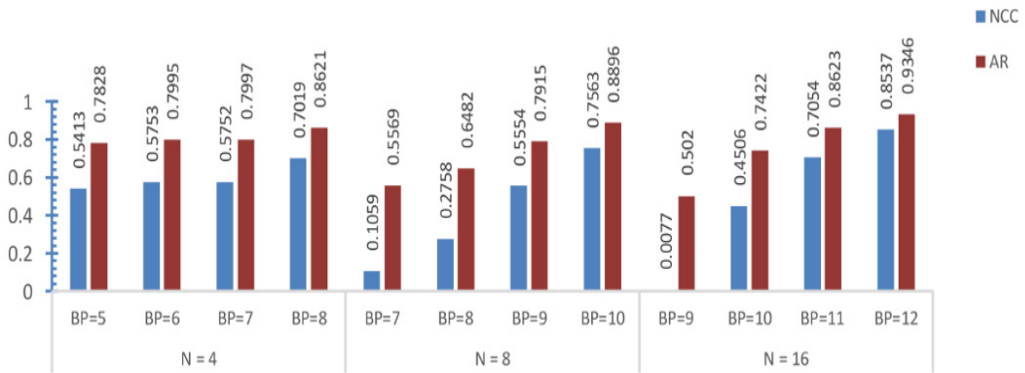
Figure 18. The robustness of the proposed method against filtering attacks using the colored image of “Lena. bmp”



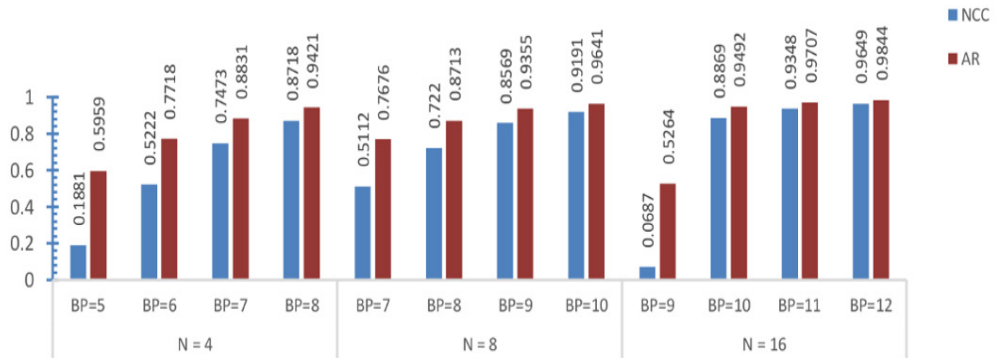
(a) Robustness against Gaussian noise 0.001



(b) Robustness against Poisson noise



(c) Robustness against salt & pepper noise 0.01



(d) Robustness against speckle noise 0.001

Figure 19. The robustness of the proposed method against noise attacks using the colored image of “Lena.bmp”

Table 4

The NCC/AR of the proposed method on the attacked colored image of "Lena.bmp"

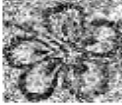
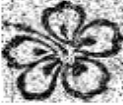
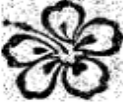
Attack	N = 4		N = 8		N = 16		
	BP = 7	BP = 8	BP = 9	BP = 10	BP = 10	BP = 11	BP = 12
JPEG compression 50%	 0.5134/ 0.7687	 0.7415/ 0.8813	 0.682/ 0.8528	 0.8337/ 0.925	 0.6814/ 0.8506	 0.8292/ 0.9219	 0.9279/ 0.9678
Gaussian noise 0.001	 0.4945/ 0.7587	 0.7271/ 0.8744	 0.7327/ 0.8779	 0.8599/ 0.937	 0.7249/ 0.874	 0.8748/ 0.9434	 0.9428/ 0.9746
Poisson noise	 0.3691/ 0.6917	 0.6509/ 0.8374	 0.6312/ 0.8271	 0.8383/ 0.927	 0.6475/ 0.832	 0.8211/ 0.9189	 0.9065/ 0.958
Salt and Pepper noise 0.001	 0.5752/ 0.7997	 0.7019/ 0.8621	 0.5554/ 0.7915	 0.7563/ 0.8896	 0.4506/ 0.7422	 0.7054/ 0.8623	 0.8537/ 0.9346
Speckle noise 0.001	 0.7473/ 0.8831	 0.8718/ 0.9421	 0.8569/ 0.9355	 0.9191/ 0.9641	 0.4506/ 0.7422	 0.9348/ 0.9707	 0.9649/ 0.9844
Median filter	 0.5221/ 0.7751	 0.6796/ 0.8526	 0.7086/ 0.8669	 0.816/ 0.9177	 0.6706/ 0.8496	 0.8191/ 0.9189	 0.8875/ 0.9502
Low pass filter	 0.4334/ 0.7313	 0.5769/ 0.8029	 0.6783/ 0.8533	 0.7664/ 0.8945	 0.8004/ 0.9092	 0.848/ 0.9316	 0.8761/ 0.9453



Figure 20. The imperceptibility of the proposed method using the colored image of “Lena.bmp”

Additional colored images were used to test embedding efficiency in the bit plane BP = 9 for block size N = 8 (Table 5).

The efficiency of the proposed method was compared with both methods of Zhang et al. (2020) and Su et al. (2019) (Figure 21). In this comparison, the embedding was performed on the colored image of “Lena.bmp” in RGB color space. The watermark was embedded in the DC coefficients of red, green, and blue components in the bit plane BP = 8, and BP=10 for block sizes N = 4, and N = 8, respectively. Despite the high PSNR of Zhang et al. (2020) and Su et al. (2019), the proposed method outperformed these two methods in terms of SSIM values regardless of the payload. It means that the distortion in the structural contents of the image due to embedding was less in the currently proposed method. Figure 21 shows that both Zhang et al. (2020) and Su et al. (2019) methods were more robust against JPEG compression. In contrast, the level of robustness against salt & pepper noise was very close in all the methods, despite the high payload of the proposed method in the case of N = 4, which reached double the payload of both Zhang et al. (2020) and Su et al. (2019) methods. On the other hand, the robustness of the median filter was less robust in the proposed method when N = 4.

Table 5
The efficiency of the proposed method using colored images, BP = 9 for N=8

Image Name	Robustness NCC / AR											
	Compression					Noise					Filtering	
	JPEG 30	JPEG 60	JPEG 80	Gaussian noise 0.002	Poisson noise	Salt and Pepper noise 0.01	Speckle noise 0.001	Median filter	Low pass filter	Reversibility PSNR/SSIM	No attac	
Airplane	37.8621 /	65.2868 /	0.9994 /	0.4852 /	0.7562 /	0.8327 /	0.6433 /	0.5698 /	0.5171 /	0.8160 /	0.6969 /	0.6533 /
	0.9388	0.9999	0.9998	0.7571	0.8867	0.9243	0.8335	0.7961	0.7676	0.9153	0.8606	0.8408
Barbara	37.8222 /	98.6221 /	1/1	0.5058 /	0.7662 /	0.8665 /	0.6369 /	0.6723 /	0.5542 /	0.8964 /	0.6423 /	0.6318 /
	0.9935	1		0.7676	0.8933	0.9399	0.8306	0.8464	0.7876	0.9539	0.8333	0.8279
House	37.9797 /	59.3828 /	0.9978 /	0.4985 /	0.7322 /	0.8447 /	0.5566 /	0.5212 /	0.5214 /	0.7690 /	0.6916 /	0.6774 /
	0.9922	1	0.9990	0.7617	0.8774	0.9299	0.7900	0.7722	0.7727	0.8945	0.8562	0.8486
Mandrill	37.7094 /	75.4084 /	1/1	0.4956 /	0.7550 /	0.8587 /	0.6341 /	0.6302 /	0.5771 /	0.8629 /	0.3306 /	0.5105 /
	0.9975	1		0.7644	0.8889	0.9365	0.8308	0.8289	0.8025	0.9287	0.6665	0.7703
Sailboat	38.0943 /	60.4602 /	1/1	0.5052 /	0.7530 /	0.8667 /	0.6117 /	0.6455 /	0.5347 /	0.8604 /	0.5850 /	0.6122 /
	0.9948	1		0.7646	0.8875	0.9402	0.8186	0.8342	0.7834	0.9373	0.7998	0.8186
Koala	38.7242 /	71.6941 /	1/1	0.5058 /	0.7350 /	0.8708 /	0.6199 /	0.6804 /	0.5605 /	0.8887 /	0.6547 /	0.6582 /
	0.9911	0.9999		0.7642	0.8779	0.9424	0.8193	0.8528	0.7917	0.9502	0.8401	0.8420
Goldhill	38.7394 /	60.7647 /	0.9967 /	0.5493 /	0.6083 /	0.8596 /	0.5098 /	0.5218 /	0.5526 /	0.7607 /	0.5727 /	0.6341 /
	0.9088	0.9972	0.9985	0.7915	0.8188	0.9370	0.7603	0.7627	0.7886	0.8877	0.8020	0.8313

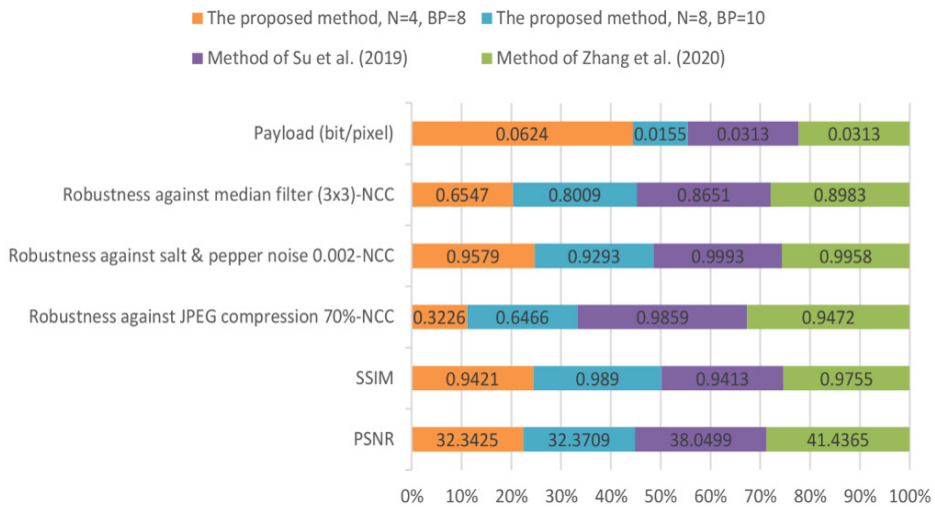


Figure 21. The comparison between the proposed method and the methods of Zhang et al. (2020) and Su et al. (2019)

CONCLUSION

This paper proposed a semi-fragile, semi-blind watermarking method for image ownership protection. The watermark was embedded in a middle bit plane of the DC coefficients of the DFT magnitudes. The proposed method used a combination of double Feynman and XOR reversible gates to shuffle the watermark with the secret key and original bit plane of the DC coefficients to improve the security level and ensure reversibility. The experimental results on grayscale and colored images show that the greater the bit plane of DC coefficients, the more robust but less imperceptible the watermarking method is. However, the best bit planes used for semi-fragile embedding were BP = 8, PB = 9, BP = 10 for block sizes N = 4, N = 8, and N = 16, respectively. Compared to related works, it was discovered that utilizing only the DC coefficients rather than all the DFT magnitudes has a significant impact on increasing robustness. In addition, embedding a watermark in the DC coefficients in the frequency domain rather than the spatial domain reduces the structural content’s distortion of the image. Furthermore, the proposed method using grayscale images is particularly effective in applications where reversibility is desired. However, further studies are recommended to find a reversible embedding method for colored images.

ACKNOWLEDGEMENT

The authors acknowledge the support of the University of Mosul for this manuscript completion.

REFERENCES

- Ahmed, F., & Moskowitz, I. S. (2004). Correlation-based watermarking method for image authentication applications. *Optical Engineering*, 43(8), 1833-1838. <https://doi.org/10.1117/1.1763589>
- Ahmed, F., & Moskowitz, I. S. (2006). A semi-reversible watermark for medical image authentication. In *1st Transdisciplinary Conference on Distributed Diagnosis and Home Healthcare* (pp. 59-62). IEEE Publishing. <https://doi.org/10.1109/DDHH.2006.1624797>
- Ansari, A., Hong, S., Saavedra, G., Javidi, B., & Martinez-Corral, M. (2018). Ownership protection of plenoptic images by robust and reversible watermarking. *Optics and Lasers in Engineering*, 107, 325-334. <https://doi.org/10.1016/j.optlaseng.2018.03.028>
- Begum, M., & Uddin, M. S. (2021). Implementation of secured and robust DFT-based image watermark through hybridization with decomposition algorithm. *SN Computer Science*, 2, Article 221. <https://doi.org/10.1007/s42979-021-00608-6>
- Feng, B., Li, X., Jie, Y., Guo, C., & Fu, H. (2019). A novel semi-fragile digital watermarking scheme for scrambled image authentication and restoration. *Mobile Networks and Applications*, 25, 82-94. <https://doi.org/10.1007/s11036-018-1186-9>
- Jimson, N., & Hemachandran, K. (2018). DFT based digital image watermarking: A survey. *International Journal of Advanced Research in Computer Science*, 9(2), 540-544. <https://doi.org/10.26483/ijarcs.v9i2.5747>
- Khalilidan, S., Mahdavi, M., Balouchestani, A., Moti, Z., & Hallaj, Y. (2020) A semi-blind watermarking method for authentication of face images using autoencoders. In *2020 6th International Conference on Web Research (ICWR)* (pp. 229-233). IEEE Publishing. <https://doi.org/10.1109/ICWR49608.2020.9122276>
- Krishna, K. B., & Ramesh, A. P. (2019). Implementation of sequential circuit using feynman and fredkin reversible logic gates. In *Journal of Physics: Conference Series (Vol. 1228, No. 1, p. 012047)*. IOP Publishing. <https://doi.org/10.1088/1742-6596/1228/1/012047>
- Luo, Y., Li, L., Liu, J., Tang, S., Cao, L., Zhang, S., Qiu, S., & Cao, Y. (2021). A multi-scale image watermarking based on integer wavelet transform and singular value decomposition. *Expert Systems with Applications*, 168, Article 114272. <https://doi.org/10.1016/j.eswa.2020.114272>
- Menendez-Ortiz, A., Feregrino-Uribe, C., Hasimoto-Beltran R., & Garcia-Hernandez, J. J. (2019). A survey on reversible watermarking for multimedia content: A robustness overview. *IEEE Access*, 7, 132662-132681. <https://doi.org/10.1109/ACCESS.2019.2940972>
- Qasim, A. F, Meziane, F., & Aspin, R. (2018). Digital watermarking: Applicability for developing trust in medical imaging workflows state of the art review. *Computer Science Review*, 27, 45-60. <https://doi.org/10.1016/j.cosrev.2017.11.003>
- Setiadi, D. R. I. (2021). PSNR vs SSIM: Imperceptibility quality assessment for image steganography. *Multimedia Tools and Applications*, 80, 8423-8444. <https://doi.org/10.1007/s11042-020-10035-z>
- Su, Q., Liu D., Yuan, Z., Wang, G., Zhang, X., Chen, B., & Yao, T. (2019). New rapid and robust color image watermarking technique in spatial domain. *IEEE Access*, 7, 30398-30409. <https://doi.org/10.1109/ACCESS.2019.2895062>

- Zhang, X., Su, Q., Yuan Z., & Liu, D. (2020). An efficient blind color image watermarking algorithm in spatial domain combining discrete Fourier transform. *Optik*, 219, Article 165272. <https://doi.org/10.1016/j.ijleo.2020.165272>
- Zhu, X., Wu, J., & Sang, J. (2007). On the fragility of the binary phase-only filter based digital image watermarking. In *MIPPR 2007: Remote Sensing and GIS Data Processing and Applications; and Innovative Multispectral Technology and Applications* (Vol. 6790, pp. 1367-1372). SPIE Publishing. <https://doi.org/10.1117/12.751141>.

Vulnerability of Saudi Private Sector Organisations to Cyber Threats and Methods to Reduce the Vulnerability

Emad Shafie

Department of Computer and Applied Science, Applied College, Umm Al-Qura University, 715 Saudi Arabia

ABSTRACT

The Middle Eastern region has witnessed many cyber-attacks in recent years, especially in Saudi Arabia. Saudi Arabian organisations face problems anticipating, detecting, mitigating, or preventing cyber-attacks despite policies and regulations. The reasons for this have not been investigated adequately. This research aims to study the methods used to address cyber security issues in the private sector. A survey of IT managers of private organisations yielded 230 usable responses. The data were analysed for descriptive statistics and frequency estimations of responses, and the results are presented in this paper. Poor awareness of cyber security issues is reflected in the survey responses. The expenditure on cyber security, especially by large firms, was inadequate. There was a greater tendency to outsource many aspects of cyber security without concern about the risks. A very small percentage of IT managers considered the certainty of a cyber threat within the next year. It is important from the point of proactive strategies to prevent attacks. The findings highlight a lack of required knowledge and skills in performing their expected roles well. Additionally, many weaknesses have been detected in cyber security management in Saudi private organisations, and there is room to improve the quality of computer security systems. The published literature largely supported this. The findings from this study have implications for the stakeholders, especially IT managers working in the private sector of

Saudi Arabia. The learnings from this study may be used to address the vulnerabilities identified. The findings clearly show the need to train IT managers of Saudi private organisations.

Keywords: Awareness survey, computer security, database systems, quality improvement, Saudi Arabia

ARTICLE INFO

Article history:

Received: 6 November 2021

Accepted: 7 February 2022

Published: 20 April 2022

DOI: <https://doi.org/10.47836/pjst.30.3.08>

E-mail address:

eashafie@uqu.edu.sa (Emad Shafie)

INTRODUCTION

The occurrence of cybercrimes has increased in recent years. In 2020, Interpol reported that the global health crisis due to Covid-19 had been further complicated by cyber-attacks related to the pandemic, thereby causing a considerable strain on healthcare and law enforcement authorities worldwide. It is estimated that approximately 907,000 spam messages, 737 incidents related to the malware, and 48,000 malicious URLs, all related to Covid-19, were identified between January and April 2020. The attacks have increasingly been aimed at big corporations, governments, and critical infrastructure, all of which have a significant role in dealing with the pandemic. Out of 194 countries, 48 participated in an Interpol survey from April to May 2020. Thirteen private partners provided additional data. The results showed Europe sharing 42% of the attacks and the MENA region sharing 10% of the attacks. The types of attacks were online phishing and scams (most frequent), disruptive malware such as DDoS, data harvesting malware, malicious domains, and misinformation (Stock, 2020).

The global costs of cybercrime increased from \$3 trillion in 2015 to \$6 trillion in 2021 and are expected to increase further to over \$10.5 trillion by 2025. These estimates do not include non-monetary cybercrimes like violence, stalking, and sexual exploitation through the internet (Hawdon, 2021).

Most cyber-attacks occur due to a lack of awareness and vigil when dealing with the internet leading to inadvertent actions which attract cyber-attackers. Therefore, the main issue arising from the above trends is creating awareness to reduce vulnerability to cyberattacks at all levels.

Saudi Arabia continues to be a key target for cyberattacks due to its oil resources and its location in the geopolitically tense Middle East. The International Data Corporation's (IDC) most recent Chief Information Officer (CIO) Survey conducted in Saudi Arabia revealed that about 60% of Saudi CIOs perceive their biggest technological challenge as cyber security management. The impact of this perception may be on about 46% of Saudi CIOs. An estimated 75% of them have their highest priority business objective as investments in privacy and cybersecurity, especially with their digital transformation agendas. Cyber security readiness is becoming an important performance indicator of Saudi Arabian firms for addressing the country's goals for achieving its Vision 2030 (Wright & Allan, 2020). These observations show that lack of awareness by internet users leads to increased vulnerability to cyber-attacks. The global observation of creating increased awareness to reduce vulnerability is equally important to Saudi Arabia.

Hence, this research investigates the awareness and the methods used to address cyber security issues in the Saudi private sector. It is the opportune moment for such a study because Saudi Arabia, as in the case of the rest of the world, is during the new waves of delta and Omicron variants of the covid pandemic, providing cybercriminals with an

excellent opportunity for their nefarious activities. The intention is to use the survey findings to recommend improvements in the current database systems of Saudi private sectors for enhanced cyber security.

The findings show that IT managers of Saudi private organisations are not adequately aware of the issues related to cyber security and how to protect and mitigate cyber security breaches. These observations stress the need to train them on possible types of cyber security breaches, proactive and mitigation strategies.

The rest of this paper is organised in the following manner. The next section reviews the published literature related to the topic to justify this study. It is followed by the Methodology section describing the procedure adopted for collecting and analysing data to achieve the aim of this study. The results obtained from the collected and analysed data are presented in the Results section. These results are discussed, interpreted and explained with the literature support in the Discussion section. The Conclusion section captures the main points of this research. Some recommendations to improve cyber security in Saudi private organisations are derived from the findings listed in the Recommendations section. Finally, some limitations of the study are enumerated with explanations.

LITERATURE REVIEW

The vulnerability to cyber-attacks increases with the increasing use of the internet. The rapid increase in internet and social media use by Saudi people makes them increasingly vulnerable. According to the statistics published by ITU (2021), 4.9 billion people (63% of the population) were using the internet in 2021 worldwide. About 66% of the Arab population was using the internet this year. More male and young population in urban areas was using the internet than the female and older population in rural areas. The Middle East and specifically Saudi Arabia, have witnessed a surge in the number of internet users, reaching approximately 22.4 million in 2016 (Alzarhani & Alomar, 2016) and 33.58 million out of an estimated population of 35.08 million (95% of the population are internet users) in 2021, spending an average of 7 hrs and 45 minutes on the internet (The Global Statistics, 2022). There is also a substantial increase in different internet services in Saudi Arabia. According to GMI (2021), 27.8 million (79.25% of the population) use and spend about three hours daily on social media. More than 25 million (70%) of the population uses YouTube, Instagram, Facebook, and Twitter. Most people send and receive messages on WhatsApp (80%), followed by Facebook and Snapchat (about 54%). Men and the younger generation see social media ads more than women and the older generation. It has meant that the number of internet users has increased over the years, and the variety of services utilising the internet and providing their services online has also risen. The Saudi population's increased vulnerability due to increased internet and online services usage is compounded by a lack of Information Security Awareness (ISA) found in Saudi Arabia (Alzarhani & Alomar, 2016).

Cybercrimes include a host of different activities such as hacking, identity theft, virus dissemination, denial of service attack, phishing, spamming, cyberstalking, and cyber terrorism, to name a few (Elnaim, 2013). In Saudi Arabia, the largest cyber-attack took place on the Aramco oil plant in August 2012. A Shamoon virus attack damaged an estimated 30,000 computers to stop oil and gas production at the biggest OPEC exporter. Aramco had been the prime target for repeated cyber-attacks with malware like Emotet. Increased frequency of attacks was noted even as late as the final quarter of 2019 (Hydrocarbon Processing, 2020). However, Aramco had been able to survive these attacks through methodical strategies. Many other companies in Saudi Arabia may not have had the resources and know-how to do so. The Aramco incidences show how awareness helps to devise strategies against cyber-attacks.

According to Perlroth and Krauss (2018), the August 2012 attack was meant to trigger an explosion. Instead, it represented the threatening intensification of international hacking by anonymous operatives who possessed the drive and the ability to cause severe physical damage. The incident also posed a similar threat to other countries.

In 2017 there was a string of hacking attacks on petrochemical plants in Saudi Arabia. Computer screens went blank at the National Industrialization Company (Tasnee), one of the very few privately owned Saudi petrochemical companies leading to the hard drives being destroyed and data erased to appear the image of a Syrian child who had drowned off the Turkey coast when the family was fleeing civil war. Thus, a political message was also intended. Simultaneously, about 15 miles away, computers crashed at Sadara Chemical Company, a joint venture between Saudi Aramco and Dow Chemical. These attacks thwart Crown Prince Mohammed bin Salman's aim to accelerate Saudi Arabia's economic growth through private participation and diversification from oil. The attack on a private oil processing firm was interpreted as an indication. This attack compromised the computerised controllers, which are also used for many worldwide applications. The official website of King Saud University, too, suffered a hack by unknown entities, which led to a data dump of users' information (Alzarhani & Alomar, 2016). Therefore, these attacks exposed the vulnerability of even the most dependable systems in the country. The success of cyber-attacks on private firms shows how the lack of awareness can prevent implementing strategies to protect vital installations.

It is even more alarming when the study by Kaspersky Lab states that approximately 60% of institutions in Saudi Arabia have experienced virus and malware attacks from August 2016 to August 2017 (Alshammari & Singh, 2018). Another alarming statistic is that from 2012, 40% of social media users in the country fell victim to some cybercrime. In the same year, such cybercrimes cost the country approximately \$693 million (Alshammari & Singh, 2018). Therefore, it is evident that cybercrime is on the rise in Saudi Arabia and requires strict and effective measures to prevent them from reducing the cost burden.

In the wider context of the region, poor preparedness against cyber-attacks in Muslim countries could be the cause of recent increased incidences of grave impacts in Saudi Arabia and a few other Muslim countries (Basamh et al., 2014). The need for organisational efforts to enhance the awareness and skills to deal with cyber threats was highlighted by AlMindeel and Martins (2020) through a single case study of a Saudi public organisation. The required knowledge involves an awareness of information security, knowledge, and behaviour at individual levels. Customisation to the needs of stakeholders, the organisational needs, integration of both electronic and physical learning resources, and a range of other factors all facilitate this.

Cyber Security Awareness in Saudi Arabia

Some recent findings on the cyber security awareness of Saudi people are reviewed here. Earlier works have been cited and discussed already in the discussed works (Alotaibi et al., 2016; Alsmadi & Zarour, 2018; Alotaibi, 2019; AlMindeel & Martins, 2020; Alzubaidi, 2021).

Very limited awareness was noted among Saudi people about cyber security and the role of the government and other organisations in ensuring cyber safety, despite their good knowledge about IT, from an online survey by Alotaibi et al. (2016). A low level of awareness leading to high-risk internet behaviour among Saudi people was also reported by Alzubaidi (2021), with the second-highest cyber security breachers attracting cyber-attacks due to its wealth and high level of active internet and social media uses. Many researchers observed this lack of awareness among regions, industry sectors, types of internet services, attacks, and specific demographic groups. A low level of cyber security awareness and a preference for mobile applications for learning about cyber security was observed among a sample of the Saudi population in a survey by Alotaibi (2019). The need for information security awareness among employees was highlighted using a case study of a government organisation by AlMindeel and Martins (2020). Alsmadi and Zarour's (2018) survey results showed that many Saudi Arabian people knew security tools, but many did not know or use them. Employers had provided no awareness or training programmes on cyber security or mitigating methods. As a result, most Saudis did not know how to or did not report cybercrimes. Healthcare, financial, technology, multiple, individual/private, and public sectors were particularly vulnerable to cyber-attacks; hence, these sectors need to be given priority for awareness training programmes.

Saudi Government Initiatives to Solve the Problems

The government has taken several initiatives to address the growing risk of cyber-attacks in Saudi Arabia. The Communications and Information Technology Commission (CITC) initiative was set up in 2005. It is equipped with the responsibility of regulating 'the

necessary organisational procedures and implementing policies and laws enacted by the government in the sphere of IT' (Quadri & Khan, 2019). In addition, the Commission grants licenses and upholds Saudi statutes about IT and cybersecurity. This Commission also has the power to identify and block websites that it mandates as being inappropriate or dangerous.

Another step the government took in tackling cybersecurity was the setting up the Computer Emergency Response Team (CERT) in 2006. This team works under the CITC to spread awareness about cybersecurity threats in the country and how to mitigate them.

In 2007, Saudi Arabia issued a cybercrime law known as the Anti-Cyber Crime Law or ACCL. The law aims to protect information security and protect against identity theft, piracy, and other cybercrimes (Alshammari & Singh, 2018).

In addition to this, the National Cybersecurity Authority (NCA) was established in 2017 with the aim 'to boost the state cybersecurity and defend the national infrastructure' (Quadri & Khan, 2019). The NCA is mandated to achieve this goal by analysing, drafting, mandating, and regulating 'cybersecurity policies, frameworks, criteria, and guidelines' (Quadri & Khan, 2019). Furthermore, as per Saudi Vision 2030, the NCA must create 'a national cybersecurity industry' to enable Saudi Arabia to become a 'leader in cybersecurity in the region' (Quadri & Khan, 2019). Hence, it is evident that the government has taken steps in the right direction to address the threats posed by the spate of cyber-attacks and further enhance its cybersecurity infrastructure.

It must be mentioned here that although the relevant laws exist in Saudi Arabia to address cybersecurity, there is a corresponding need to raise awareness among citizens regarding safe usage of the internet. Spreading awareness about the financial impact of cybercrimes may be a step in the right direction.

The literature review reveals, therefore, the vulnerability of Saudi Arabia's cybersecurity infrastructure. The government has enacted certain laws and made provisions that treat cybercrimes as punishable offences to address this vulnerability. While this is a step in the right direction, simultaneous efforts must also be made to spread awareness about cyberattacks' nature, types, and impact. It is essential to ensure that people remain vigilant and avoid falling into traps laid out by criminals online. It is even more relevant in Covid-19, which has seen an escalation in online services, especially for education, shopping, financial services, and health. Many people access goods and services online and may be vulnerable to cyberattacks. While effective laws must be in place to punish those who perpetrate such crimes, they must go hand in hand with raising awareness levels.

Based on the observation that the Saudi people preferred mobile applications for cyber security tools, Alotaibi (2019) developed two mobile-based game applications to enhance cyber security awareness. In a detailed discussion, Alshammari and Singh (2018) observed that to solve the cyber security issues, Saudi Arabia enacted the anti-cybercrimes law in

2007. Anti-cybercrimes law covers important areas to fight against cybercrimes and states their penalties. However, it is deficient in protecting against identity theft and invasion of privacy. As a result, the country is among the top ranks in cyber security measures. The Global Cyber-Security Index of 2017 placed Saudi Arabia in the maturing stage behind the leading nations. Thus, Saudi Arabia may be considered a semi-prepared nation concerning the capability to defend itself against cybercrimes. To improve its GCI ranking to the top levels, Saudi Arabia needs to strengthen its cybercrimes law, cyber-security regulations and authorities. Also, it is important to develop clear cyber-security strategies, standards, metrics, and R&D programs. Furthermore, the domestic cyber-security industry needs to be promoted by incentivising them and encouraging them into multi-lateral agreements.

Talib et al. (2018) proposed an ontology-based cyber security policy for Saudi Arabia. The ontological approach aims to arrive at a desirable cyber security strategic environment by identifying and suggesting a formal, encoded description. A multi-layered protection strategy specifying their roles, responsibilities, and obligations was the core of the strategic environment.

Three models, derived from the basic model of NIST, for the cyber security of Saudi SMEs in the education, healthcare, and commercial sectors were developed by Ajmi et al. (2019). These models help to identify cyber threats of different types based on the structure of the SMEs.

METHODOLOGY

This study uses quantitative methods, relying on data collection and analysis. Quantitative methods may be understood as scientific and precise, relying on statistical analysis to draw inferences. These inferences may then inform the results drawn. It may be said that quantitative methods emphasise measurable data. Quantitative research can best be understood as being data-oriented. Adopting such methods has several advantages. It is possible to arrive at a definitive and precise answer to the research question through quantitative research. The results may be generalised to a larger target group depending on the sample. However, these methods also have their disadvantages. While it is possible to arrive at a clear solution through quantitative methods, they do not provide the 'why' or 'how' behind the data collected.

Quantitative methods are different from qualitative methods. Qualitative research seeks to understand the 'how' and 'why' behind the phenomenon and data; those are less tangible and difficult to quantify. Studies may choose to adopt qualitative, quantitative, or mixed methods.

For this study, it was determined that choosing quantitative methods would be useful.

Several tools may be adopted while conducting a quantitative study. Examples of such tools include surveys, interviews, and questionnaires. Once the sample is determined for

the study, data is collected. This data is then analysed using statistical tools through which the results may be interpreted.

A study conducted a computer security awareness survey on Saudi private sector firms. A simple questionnaire was designed to capture the basic characteristics of the company and the computer security awareness of its employees. The questionnaires were adapted from the literature to the Saudi context. The objective was to understand the extent and factors affecting cyber security awareness among the Saudi public, which can facilitate the recommendation of protection strategies.

The IT managers of the companies participated in the survey. The participants were contacted via email, and their contact information was obtained from private sector business directories (e.g., <https://www.eyeofriyadh.com/directory>) in Saudi Arabia. The survey was deployed in Survey Monkey and contained a cover letter describing the purpose of the research and the voluntary nature of participation. The cover letter also advised the potential participants that they were free to withdraw at any point, and their private details were not being collected. The link to the survey questionnaire in Survey Monkey was emailed to more than 1000 people, from which 230 usable responses were obtained, giving an overall response rate of 23%. The results of this survey are presented in the following section.

All ethical requirements of conducting research using human beings have complied with university regulations. The required permissions were obtained. The privacy and confidentiality of participants were ensured. The hard copies and electronic data of the research were fully protected from theft, malware attacks on the laptop, and other likely losses.

RESULTS

Industry Profile of Survey Participants

The profile of industries sampled for this survey is given below in Table 1. It depicts that more than half (53%) of the participants were from the construction sector. Manufacturing (approximately 15%) and retail (about 8%) were the next two sectors of highest participation. All the others were <5%.

Table 1
Sample distribution by industry

Industry	Number of participants	Percentage
Construction	122	53.0%
Manufacturing	34	14.8%

Table 1 (Continue)

Industry	Number of participants	Percentage
Electricity, Gas, Water and Waste Services	7	3.0%
Mining, Oil and Gas	11	4.8%
Retail Trade	19	8.3%
Accommodation and Food Services	6	2.6%
Transport, Postal and Warehousing	9	3.9%
Information Media and Telecommunications	3	1.3%
Financial and Insurance Services	5	2.2%
Administrative and Support Services	5	2.2%
Public Administration and Safety	2	0.9%
Education and Training	3	1.3%
Health Care and Social Assistance	4	1.7%
Total	230	100.0%

Cyber Security Expenditure

The seriousness attached to the issue of cyber security will be evident from the amount spent by any company to ensure the security and privacy of their data and transactions. Figure 1 provides the amounts spent by the sampled companies on cyber security every year.

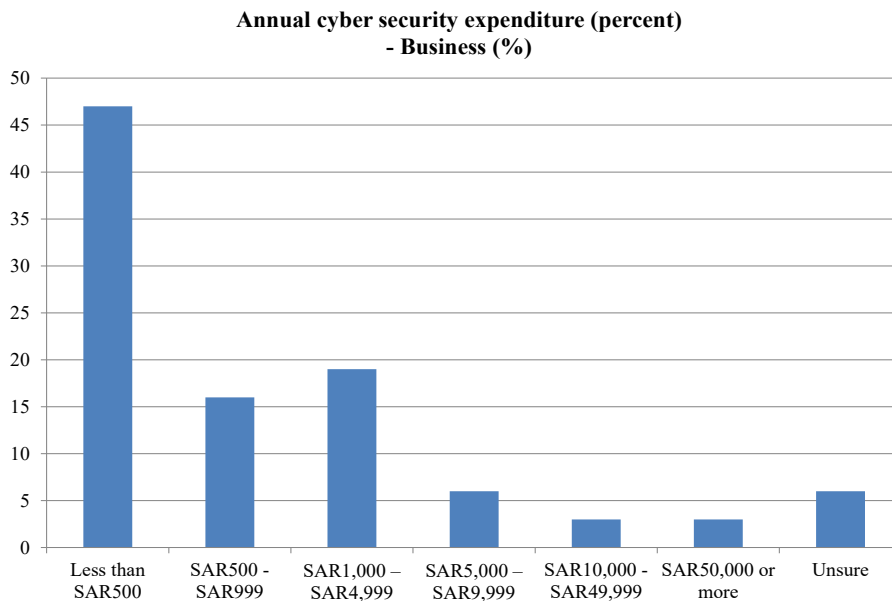


Figure 1. Annual cyber security expenditure of Saudi private organisations

About 82% of the firms spent less than SAR 5000/ per annum. Nearly half (47%) spent a nominal SAR 500 or less on this. Only 6% of the companies spent SAR 10000 or more. The amounts spent may reflect their unawareness of the seriousness of cyber security, no record of such instances, or just the risk-taking behaviour of the management.

Gross Income of the Participating Firms

Relative cyber security threats and the need to spend on cyber security may be related to the company’s gross income. Cyber attackers may not be interested in the small stakes of low-income firms. However, the threat may be real in the case of high-income firms. However, no cut-off income can be placed on the probability of cyber threats. Figure 2 below provides the frequency of firms in different gross income ranges.

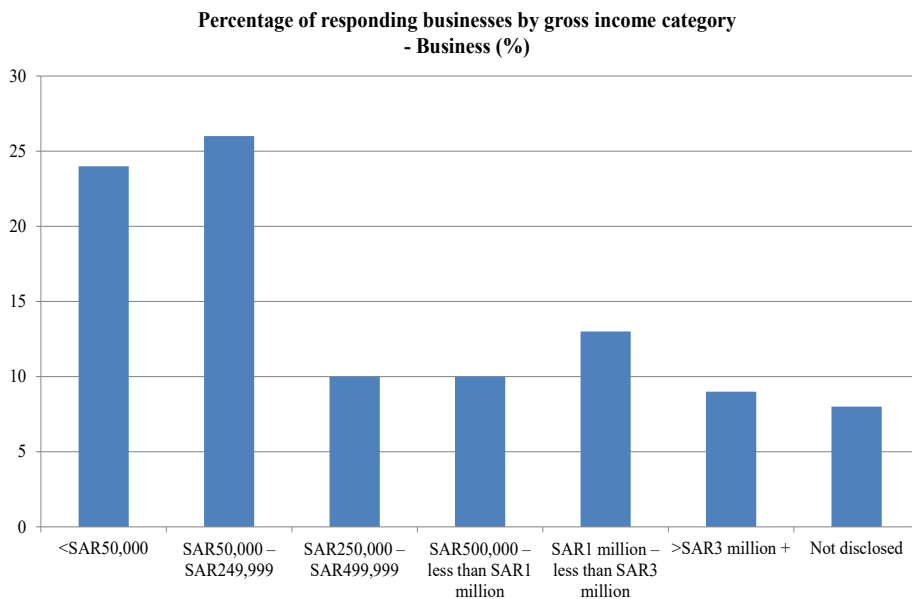


Figure 2. Percentage of businesses based on their gross income ranges

According to data in Figure 2, the gross income of approximately 70% of the firms is less than a million SAR. Cyber attackers may not be interested in these firms. However, cyber threat is a strong possibility for the remaining 30 firms with higher than 1 million SAR. In this respect, the study assumes that the 8% not disclosed belongs to the high-income group, so they do not want to disclose. Sizeable expenditure on cyber security (10000 or more SAR) in Table 2 was seen only by 12% of the firms sampled. Suppose this 12% represents the high-income firms (as low-income firms cannot afford it), leaving about 18% of high-income firms doing nothing to protect their data and transactions. The stakeholders with whom they are in contact may also be vulnerable due to this reason.

IT Security Outsourcing

A firm may outsource security as a management strategy or out of compulsion like lack of resources or expertise or being too small to have a separate system. In Table 2, the scenario related to outsourcing based on the size of the business in terms of employee size is presented.

Table 2

Responsibility for IT security management by business size (per cent)

Business size	Internal and outsourced IT response (per cent)	
	Internal IT security	Outsourced sourced IT security
1 person company	98	2
2–4 employees	90	10
5–19 employees	60	40
20–199 employees	55	45

The general trend in Table 2 is the tendency of bigger firms to outsource their cybersecurity responsibility. The threat is real and big for them, and they may like experts to handle this issue. Smaller firms may not have to face cyber threats due to their unattractiveness. Single-person companies may not be too concerned about it or may not be aware of these issues. Hence, the requirement and outsourcing of cyber security are very low in their cases.

Security Aspects Outsourced

Within outsourcing, not all aspects are outsourced as a complete package in most cases. The company may prefer to handle smaller problems by themselves. For example, where outsourcing involves compromising business secrets or sensitive data, such aspects may not be outsourced. Thus, many times, only certain aspects of cyber security may be selectively outsourced due to a lack of expertise or resources. This picture is clear from the data presented in Figure 3.

Restricted admin access, disabling macros, and daily backups could be handled by them, as they do not involve the use of complicated protection systems. However, allowlisting, patching applications, system operations, and hardening applications require sufficient expertise even for daily management. So, these were best outsourced.

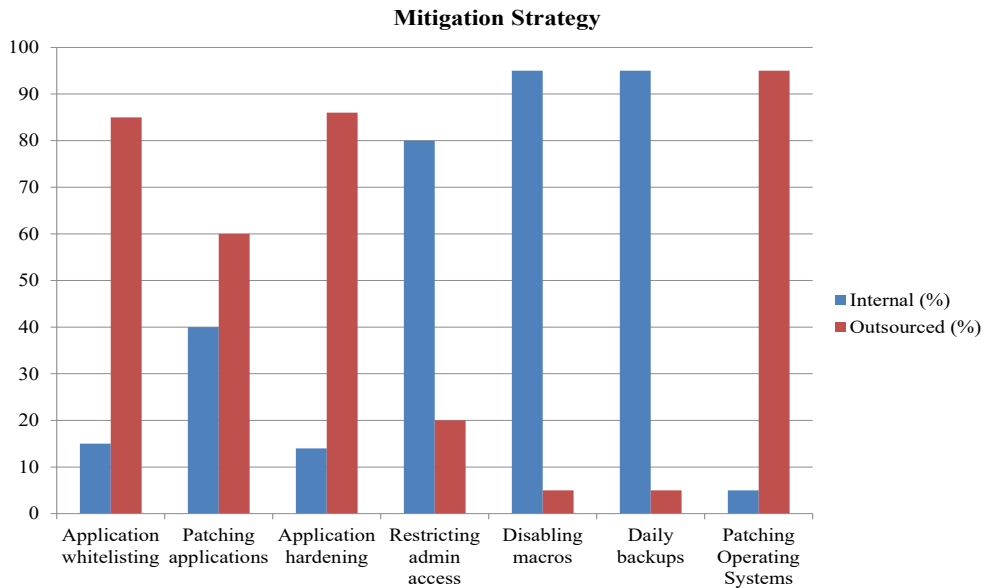


Figure 3. IT security aspects outsourced

Risk Assessment

One of the duties of IT managers is to assess and manage the cyber security risks of the company. Table 3 provides the data on how these managers did this in their firms.

Table 3
Self-assessed risk of experiencing a cyber incident in the next year

Category	Risk of experiencing a cyber incident	
	n	%
Almost certain	10	4.3%
Likely	16	7.0%
Possible	137	59.6%
Unlikely	56	24.3%
Highly unlikely	6	2.6%
Don't know	5	2.2%

In these days of almost uncontrolled internet traffic of various types and equally frequent attacks on even highly protected countries' defence systems, it is prudent to expect a major cyber threat at any time. Therefore, expecting at least one such major instance every year makes sense. It will enable us to prepare for such instances well in advance so that they can be prevented, managed with the least impact, or mitigated. Unfortunately, only <5% of the IT managers thought such a possibility to be certain. Overall, nearly 60% of IT managers thought that it was possible. Approximately 70% of all IT managers thought cyberattacks were

possible or more than possible or more than possible. That leaves the rest, 30% of highly vulnerable firms, which is very serious.

Understanding Cyber Security

It should be noted that IT managers participated in this survey. So, they are expected to understand and explain the phenomenon of cyber security risks of various types. To what extent this is true is known from the data presented in Figure 4.

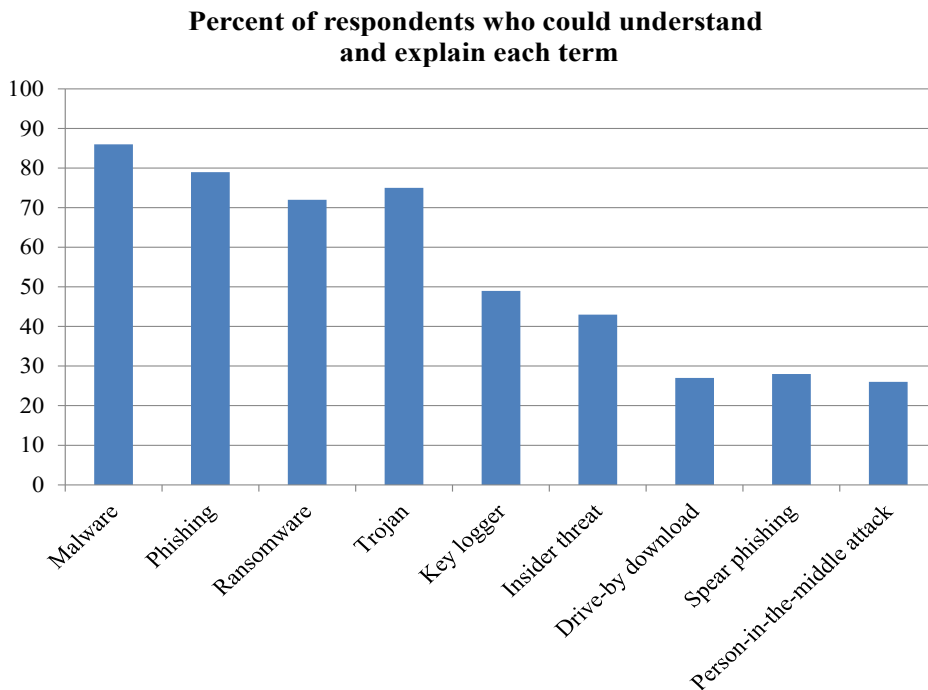


Figure 4. Percentage of survey respondents who understood and explained terms related to cyber threats

About 70–80% of the participants knew and could explain malware, phishing, ransomware, and Trojan, which are the most common types. Surprisingly, insider threat was known only to less than half of them. If an insider threat occurs in their own company, they may not be able to detect it and take countermeasures. These IT managers need to be educated and equipped to handle all types of cyber security risks to make them effective in their organisations.

DISCUSSION

Overall, in the case of Saudi private firms, there is much to be desired for near-perfect prevention/management of cyber-attacks in the future. Gaps were seen inadequate expenditure on cyber security even by high-income firms. Outsourcing may be a suitable strategy in many ways.

Equally, the security dimensions which can be outsourced and the parties to whom these are entrusted are critically important. Just to save money, outsourcing to unreliable parties may be self-defeating and even dangerous. Improvements in risk assessment are possible only if the current and future IT managers are equipped with the required knowledge and skills, which are highly inadequate at present.

One reason for this state of affairs may be awareness itself. In this study, the level of awareness, even among IT managers of private firms, was inadequate and quite serious in the case of certain types of security threats. There is a poor status of cyber security and its awareness at the public level, as was noted by Alarifi et al. (2012) through a survey. The highly censored, patriarchal, and tribal cultures were attributed as the reasons for the poor information security rating of the country. Even where awareness needs to exist at operational levels, intentional and deliberate security breaches of computerised accounting information systems (CAIS) could happen in Saudi organisations, as Abu-Musa (2006) reported. The types of security breaches identified were the accidental or intentional entry of bad data, accidental destruction of data by employees, unauthorised sharing of passwords among employees, the introduction of computer viruses to CAIS deliberately or accidentally, suppression and destruction of output; unauthorised document visibility and directing prints and distributed information to people who are not empowered to receive them.

A security culture should lead to sound information security management systems at the organisational level. Alnatheer and Nelson (2009) reported Saudi Arabian firms to lack in both these aspects. Although Saudi Arabia started promoting a National Commissions and IT Plan (NCITP) in 2005, cyber security does not find any place in that plan but only in the Ministry documents. Even in these documents, there is no adequate description of policies and strategies related to information security management. Security culture includes social, cultural, and ethical measures to improve the security-related behaviour by the organisational members as an organisational subculture. The earlier cited paper of Abu-Musa (2006) demonstrates the absence of such a culture in Saudi organisations. As measured by Hofstede (2019), the national cultural dimensions of Saudi Arabia show high power distance, uncertainty avoidance, and collectivism, which indicates that Saudi society is hesitant in adopting and implementing new practices that do not fit in their culture. As could be expected, Saudi organisations reflect the national culture. Overall, it means poor security culture and management in Saudi organisations (Alnatheer & Nelson, 2009).

In the studies of Alzamil (2018), most of the surveyed Saudi organisations had established an information security policy and deployed adequate levels of technology. However, ineffective and inefficient enforcement and publication and inadequate comprehensibility and clarity of these policies affected the level of cyber protection, even with the best systems. The use of the phrase ‘fair technology’ is important. These organisations did not have the best systems, but only good ones, which still provided enough room for malware attacks, affecting protection levels seriously. The results of this study also confirm these trends. Organisations are hesitant to spend money on cyber security and prefer to outsource a large part of their security components. In addition, IT managers are not adequately knowledgeable or equipped with risk assessment and analysis skills. These observations are borne out by the fact that, even after implementing information security and enforcement policies for data security management in many organisations, some critical issues were identified by Almutairi et al. (2020) for the attention of the national information security management authority.

According to the cyber security maturity model proposed in SAMA (2017), most Saudi organisations can be included in the first three levels (0,1,2) of non-existent, ad hoc, or repeatable but informal. These levels do not require high levels of knowledge. The observation of a low level of knowledge possessed by IT managers in this study is adequate for these three maturity levels. In a survey study of Saudi private organisations, similar to this study, Al-Harethi and Al-Amoodi (2019) observed that about 70% of IT managers were not aware of the security standards of Saudi Arabia. About two-thirds of the firms surveyed experienced different types of information security breaches. This finding reiterates the observation in the current study of poor risk perceptions of various types of cyber-attacks on their firms. Companies gave inadequate attention to proper security policy, access control, communications and operation management, personnel security, and organisational security. IT managers must explain these things to the top management.

Unfortunately, they lack awareness and knowledge on this subject. A strategy for business continuity management needs to be in place to restore economically important operations soon after any cyber-attack is countered. Outsourcing should be determined based on a risk assessment compared to internal development or different options of outsourcing. These findings support the observations of this study. The need for Saudi IT workers to develop their skills in many areas of cyber threat was noted by Al-Ghamdi (*In Press*). The gap in the knowledge between the Security Operation Team and other IT experts also needs to be narrowed down. This study showed that IT managers themselves do not have the required knowledge, narrowing the said gap will be a problem.

The findings point out the need to train the IT managers of Saudi private organisations on the possible cyber security breaches and the proactive strategies of protection and mitigating strategies when an attack occurs. IT managers need more than awareness to do their jobs effectively.

CONCLUSION

This study shows that Saudi private organisations do not invest adequately in cyber security. The tendency for outsourcing security management needs to be reviewed because of its risks. IT managers do not possess adequate knowledge or skills to anticipate the possibility of cyber-attacks and risk assessment procedures for proactive and mitigation strategies. They do not even possess the skills to identify internal security threats. Saudi private organisations need to take steps to rectify the organisational problems. IT managers can be sent to attend useful courses and workshops to acquire adequate knowledge and skills offered by various international organisations.

ACKNOWLEDGEMENT

The author wants to thank Umm Al-Qura University for the constant support and encouragement of research activities.

REFERENCES

- Abu-Musa, A. A. (2006). Exploring perceived threats of CAIS in developing countries: The case of Saudi Arabia. *Managerial Auditing Journal*, 21(4), 387-407. <https://doi.org/10.1108/02686900610661405>
- Ajmi, L., Alqahtani, N., Rahman, A. U., & Mahmud, M. (2019). A novel cybersecurity framework for countermeasure of sme's in Saudi Arabia. In *2019 2nd International Conference on Computer Applications & Information Security (ICCAIS)* (pp. 1-9). IEEE Publishing. <https://doi.org/10.1109/CAIS.2019.8769470>
- Alarifi, A., Tootell, H., & Hyland, P. (2012). A study of information security awareness and practices in Saudi Arabia. In *International Conference on Communications and Information Technology (ICCIT)* (pp. 6-12). IEEE Publishing. <https://doi.org/10.1109/ICCITechnol.2012.6285845>
- Al-Ghamdi, M. I. (In Press). Effects of knowledge of cyber security on prevention of attacks. *Materials Today: Proceedings*. <https://doi.org/10.1016/j.matpr.2021.04.098>
- Al-Harethi, A. A., & Al-Amoodi, A. H. (2019). Organisational factors affecting information security management practices in private sector organisations. *International Journal of Psychology and Cognitive Science*, 5(1), 9-23.
- AlMindeel, R., & Martins, J. T. (2020). Information security awareness in a developing country context: insights from the government sector in Saudi Arabia. *Information Technology & People*, 34(2), 770-788. <https://doi.org/10.1108/itp-06-2019-0269>
- Almutairi, M. M., Halikias, G., & Yamin, M. (2020). An overview of security management in Saudi Arabia. In *7th International Conference on Computing for Sustainable Global Development (INDIACom)* (pp. 261-265). IEEE Publishing. <https://doi.org/10.23919/INDIACom49435.2020.9083725>
- Alnathair, M., & Nelson, K. (2009, December 1-3). Proposed framework for understanding information security culture and practices in the Saudi context. In *Proceedings of the 7th Australian Information Security Management Conference* (pp. 6-12). Queensland University of Technology, Perth, Western Australia. <https://doi.org/10.4225/75/579850d331b4d>

- Alotaibi, F. F. (2019). *Evaluation and enhancement of public cyber security awareness* (PhD Thesis). University of Plymouth, England. <https://pearl.plymouth.ac.uk/bitstream/handle/10026.1/14209/2019ALOTAIBI10392328PhD.pdf?sequence=1>
- Alotaibi, F., Furnell, S., Stengel, I., & Papadaki, M. (2016). A survey of cyber-security awareness in Saudi Arabia. In *11th International Conference for Internet Technology and Secured Transactions (ICITST)* (pp. 154-158). IEEE Publishing. <https://doi.org/10.1109/ICITST.2016.7856687>
- Alshammari, T., & Singh, H. (2018). Preparedness of Saudi Arabia to defend against cyber crimes: An assessment with reference to anti-cyber crime law and GCI index. *Archives of Business Research*, 6, 131-146. <https://doi.org/10.14738/abr.612.5771>.
- Alsmadi, I., & Zarour, M. (2018). Cybersecurity programs in Saudi Arabia: Issues and recommendations. In *1st International Conference on Computer Applications & Information Security (ICCAIS)* (pp. 1-5). IEEE Publishing. <https://doi.org/10.1109/ICIT52682.2021.9491711>
- Alzahrani, A., & Alomar, K. (2016). Information security issues and threats in Saudi Arabia: A research survey. *International Journal of Computer Science Issues*, 13(6), 129-135. <https://doi.org/10.20943/01201606.129135>
- Alzamil, Z. A. (2018). Information security practice in Saudi Arabia: Case study on Saudi organisations. *Information & Computer Security*, 26(5), 568-583. <https://doi.org/10.1108/ICS-01-2018-0006>
- Alzubaidi, A. (2021). Measuring the level of cyber-security awareness for cybercrime in Saudi Arabia. *Heliyon*, 7(1), Article e06016. <https://doi.org/10.1016/j.heliyon.2021.e06016>
- Basamh, S. S., Qudaih, H. A., & Ibrahim, J. B. (2014). An overview on cyber security awareness in Muslim countries. *International Journal of Information and Communication Technology*, 4(1), 21-24.
- Elnaim, B. (2013). Cyber crime in Kingdom of Saudi Arabia: The threat today and the expected future. *Information and Knowledge Management*, 3(12), 14-19.
- GMI. (2021). *Saudi Arabia social media statistics 2021*. Global Media Insight. <https://www.globalmediainsight.com/blog/saudi-arabia-social-media-statistics/>
- Hawdon, J. (2021). Cybercrime: Victimization, perpetration, and techniques. *American Journal of Criminal Justice*, 46, 837-842. <https://doi.org/10.1007/s12103-021-09652-7>
- Hofstede, G. (2019). *National culture*. Hofstede Insights. <https://www.hofstede-insights.com/models/national-culture/>
- Hydrocarbon Processing. (2020). *Saudi Aramco sees increase in attempted cyber-attacks*. Hydrocarbon Processing. <https://www.hydrocarbonprocessing.com/news/2020/02/saudi-aramco-sees-increase-in-attempted-cyber-attacks#:~:text=Aramco%2C%20which%20pumps%2010%25%20of,at%20the%20biggest%20OPEC%20exporter>
- ITU. (2021). *Measuring digital development facts and figures 2021*. International Telecommunication Union. <https://www.itu.int/en/ITU-D/Statistics/Documents/facts/FactsFigures2021.pdf>
- Perlroth, N., & Krauss, C. (2018, March 15). *A cyberattack in Saudi Arabia had a deadly goal. Experts fear another try*. The New York Times: <https://www.nytimes.com/2018/03/15/technology/saudi-arabia-hacks-cyberattacks.html>

- Quadri, A., & Khan, M. K. (2019). *Cybersecurity challenges of the Kingdom of Saudi Arabia: Past, present and future*. Global Foundation for Cyber Studies and Research.
- SAMA. (2017). *Cyber security framework*. Saudi Arabian Monetary Authority. <https://www.sama.gov.sa/en-US/Laws/BankingRules/SAMA%20Cyber%20Security%20Framework.pdf>
- Stock, J. (2020). *INTERPOL report shows alarming rate of cyberattacks during COVID-19*. Interpol. <https://www.interpol.int/en/News-and-Events/News/2020/INTERPOL-report-shows-alarming-rate-of-cyberattacks-during-COVID-19>
- Talib, A. M., Alomary, F. O., Alwadi, H. F., & Albusayli, R. R. (2018). Ontology-based cyber security policy implementation in Saudi Arabia. *Journal of Information Security*, 9(4), Article 88030. <https://doi.org/10.4236/jis.2018.94021>
- The Global Statistics. (2022). *Saudi Arabia social media statistics 2021: Internet & mobile statistics*. The Global Statistics. <https://www.theglobalstatistics.com/saudi-arabia-social-media-users/>
- Wright, B., & Allan, K. (2020). *Saudi CIOs consider security their toughest tech challenge*. IDG Communications Inc. <https://www.cio.com/article/3445225/saudi-arabias-cybersecurity-concerns-increase-as-threats-evolve.html>

Experimental Investigations on Scour Volume Upstream of a Slit Weir

Naeem Zaer Nkad¹, Thamer Ahmad Mohammad^{2*} and Haider Mohammed Hammoodi²

¹Ministry of Water Resources, State Enterprise for Operation and Maintenance of Irrigation and Drainage Projects, Baghdad, Iraq

²Department of Water Resources Engineering, College of Engineering, University of Baghdad, 10070 Jadriyah, Baghdad, Iraq

³Department of Civil Engineering, College of Engineering, University of Baghdad, 10070 Jadriyah, Baghdad, Iraq

ABSTRACT

The frequent removal of sediment accumulation from reservoirs by dredging requires interruption of power generation. Alternatively, this can be avoided by using a slit weir. In the present study, the impact of sediment nonuniformity, slit weir dimensions, weir slit position, and discharge on the effectiveness of sediment removal was experimentally investigated using a flume with a length of 12 m, a width of 0.30 m, and a depth of 0.30 m. In the flume, a slit weir was tightly fixed at the end of a 2 m working section filled with nonuniform sediments up to 110mm. Results showed that using coarser sediment ($d_{50} = 0.70$ mm) reduces the scour volume by 22-folds compared to finer sediment ($d_{50} = 0.30$ mm). This study tested five different slit weir dimensions using two weir slit positions (slit positioned in the center and slit positioned on the side). The maximum scour volume was recorded when the crest level, z of the slit weir, was 0 cm from the mobile bed. The study concluded that a 3-fold increase in discharge corresponds to a 10-fold increase in scour volume regardless of bed material nonuniformity. The existing model for estimating scour volume for uniform sediments was validated using

the data of this study, and it was observed that the model predicts the scour volume in nonuniform sediments with sufficient accuracy. Thus, the model can determine the scour volume, and maximum scour depth occurring upstream of a slit weir near a hydropower intake in reservoirs.

Keywords: Nonuniform sediment, scour volume, slit weir, uniform flow

ARTICLE INFO

Article history:

Received: 7 November 2021

Accepted: 6 January 2022

Published: 20 April 2022

DOI: <https://doi.org/10.47836/pjst.30.3.09>

E-mail addresses:

naemzaer@gmail.com (Naeem Zaer Nkad)

tthamer@gmail.com (Thamer Ahmad Mohammad)

hydmekk@yahoo.com (Haider Mohammed Hammoodi)

*Corresponding author

INTRODUCTION

Erosion in river basins increases sediment loading in surface water runoff from the basins during a rainfall event. The runoff with the high sediment load will eventually reach rivers and storage reservoirs. In reservoirs, the sediments carried by the inflow water usually settle at different locations, including near the hydropower intake. The continuous accumulation of sediments in reservoirs reduces storage capacity and hence hydropower production. In addition, the passage of sediments through the hydropower intake can damage the turbine blades. Generally, the removal of sediments accumulation from reservoirs by dredging is a costly and time-consuming process and causes interruption to the hydropower generation process. Ota et al. (2017a) proposed an economical method by discharging the sediments utilizing flowing water through a slit weir.

However, the amount of water used to carry the sediment accumulation away from the hydropower intake should be controlled to minimize the wastage of water storage in reservoirs. The design and operation of the slit weir are essential for evaluating the volume of released sediment and temporal variation in scouring depth since it affects the structure's safety. Thus, the accurate estimation of sediment volume and temporal variation in scour depth at the site of the slit weir requires intensive research. However, the phenomena of scouring at slit weirs have not been researched sufficiently, and hence few solutions are available. In addition, studies on sediment removal by scouring near a hydropower intake are also limited. The major studies on scouring upstream of a slit weir were conducted by Ota and Sato (2015), Ota et al. (2016), Ota et al. (2017a), and Ota et al. (2017b). In order to simulate the scouring process around the slit weir, Ota and Sato (2015) proposed a numerical model based on solving the Reynolds-averaged Navier Stokes equation coupled with the Volume of Fluid Method, VOF, and the $k-\omega$ turbulence closure model. The concept of the above model was later utilized by Zhang et al. (2016) to predict the clear water scour depth below a submarine pipeline for a range of steady flow conditions.

Ota et al. (2016) modified the three-dimensional (3D) numerical model that was proposed by Ota and Sato (2015) and used it to produce a scour geometry around a slit weir. Also, Ota et al. (2017a) proposed another numerical model based on an ordinary differential equation that can compute the time variation of scouring volume and maximum scour depth upstream of a slit weir for steady and unsteady flow conditions. The data from experimental runs in a laboratory utilizing a mobile bed with uniform sediments were used by Ota et al. (2017a) to produce the following relationship between the scour volume, V_s , maximum scour depth, d_s , slit weir width, b_{sl} , and channel width, B for uniform flow (Equation 1):

$$d_s/(V_s)^{1/3}=0.39(b_{sl}/B)^{-0.383} \quad [1]$$

A hybrid Euler-Lagrange numerical model that considers the interaction between the suspended sediment transport and bedload to reproduce temporal variation of the three-

dimensional bed geometry around a weir-type structure with sufficient accuracy was proposed by Ota et al. (2017b).

Based on intensive experimental investigations on fine uniform sand, Wang et al. (2018) concluded that no upstream clear water scour depth was observed at a sloped submerged weir and that the downstream scour depth was independent of the upstream weir slope. In addition, Guan et al. (2019) used coarse uniform sand to study the time evolution of scouring downstream of submerged weirs. The analysis of sediment passage over a piano key weir (PKW) with different configurations was studied by Nosedá et al. (2019). The impact of W-weir configuration and height on scour depth occurring downstream of the weir location were studied by Abdollahpour et al. (2017), while Khalili and Honar (2017) studied the impact of height and radius of a semi-circular labyrinth side weir on discharge. Muller et al. (2011) studied the impact of weir height and discharge on the size of the dunes formed in an open channel. Finally, Lauchlan (2004) undertook experimental investigations to model the bedload transport and suspended-load sediments over steep-sloped weirs.

Other experimental investigations on uniform mobile beds were carried out by Powell and Khan (2012) and Wang et al. (2019) where the former work was focused on scouring upstream of an orifice while the latter focused on the effectiveness of local scour countermeasure by using “anti-scour collar” around physical pier model.

Moreover, many soft computing methods were employed to predict the scour depths occurring in various hydraulic structures. For example, Azamathulla et al. (2008) used the neuro-fuzzy scheme for predicting scour depth downstream of ski-jump spillways, while Sayed et al. (2019) utilized genetic expression programming (GEP) and multivariate adaptive regression splines (MARS) to estimate clear-water local scour depth at pile groups while Rajkumar et al. (2016) utilized published data in the literature to demonstrate the efficiency of artificial neural network (ANN) and genetic algorithm (GA) in predicting scour depth within channel contractions.

In summary, the studies covered in the literature were experimental, numerical, and statistical. The numerical and statistical studies proposed models for scouring prediction, and these models were validated using experimental data. However, most studies were related to scouring downstream of weirs with different configurations and flow conditions. By reviewing the published literature, it is noted that the experimental studies on scouring upstream of a slit weir were limited, and studies that used numerical simulation models for estimation of scouring volume upstream of a slit weir have underestimated the experimental scour volume by up to 30% (Ota & Sato, 2015). The above findings highlighted the need for more experimental studies.

In addition, other cases covered in the literature were related to scouring upstream of a circular orifice, scour depth within channel contractions, scouring around a circular pier, scour depth below a submarine pipeline and scour depth for ski-jump type of spillways.

However, the findings of all the studies were mainly related to scouring mobile beds with uniform sediments.

In this study, extensive experimental work was conducted on the occurrence of scouring upstream of a slit weir in a nonuniform mobile bed. The combined effect of slit weir location, dimensions, sediment coarseness, and flow intensity was studied. Thus, the present study aims to contribute to the gap currently found in the literature.

MATERIALS AND METHODS

A series of experimental investigations were conducted in a glass-sided tilting flume 0.30m wide, 12 m long, and 0.30 m deep. The flume is located at the hydraulics laboratory of the College of Engineering, University of Baghdad, Iraq. The slit weirs used in the trials were made up of Plexiglas with a thickness of 6mm. In this study, two different positions for the slit of the weir were tested, as shown in Figure 1. Table 1 shows the dimensions and positions of the weir slit used in this study.

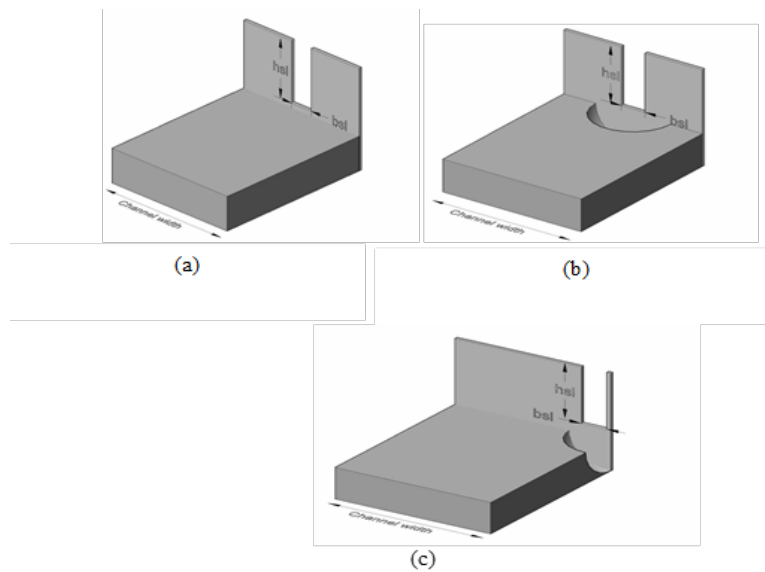


Figure 1. Diagrammatic sketch for the experimental investigations; (a) The working section before scouring; (b) The formation of scour hole (weir slit positioned in the center); (c) The formation of scour hole (the weir slit positioned in the side)

The slit weir was located at 9m from the flume inlet and was fixed and sealed at the end of the working section to eliminate leakage from the weir bottom and sides. The working section of the weir is 2 m long and 0.3 cm wide (the same width as the flume). The section was filled with sediments up to a depth of 11 cm. In a real-world scenario and according to Subramanya (2015), sediments have a nonuniform size distribution, and hence it is a

common practice to use the median size, d_{50} , as a representative size of sediments. In this study, two types of nonuniform sand were used in the working section of the flume, and these types were obtained by mixing sand with differing grading. The percentage finer and size of the sediments, which were determined from sieve analysis, are shown in Figure 2 and 3. The median size, d_{50} for the first type of sediments, was 0.30 mm (Figure 2), while the d_{50} for the second type of sediments was 0.70 mm. In addition, the values of geometric standard deviation, σ_g for the first type and the second type of the sediments were found to be 1.58 and 1.60, respectively. Therefore, the geometric standard deviation for nonuniform sediments should be more than 1.30, and it was calculated using the following Equation 2 (Melville & Coleman 2000):

$$\sigma_g = \sqrt{\frac{d_{84}}{d_{16}}} \tag{2}$$

where sediment sizes with diameters of d_{84} and d_{16} were determined from the grading curve of each sediment type.

Table 1
Dimensions and locations of the slit weirs

Slit location	Dimensions ($h_{sl} \times b_{sl}$)	z^*
Center	11x6 cm	0cm
Center	10x6 cm	1cm
Center	9x6 cm	2cm
Center	8x6 cm	3cm
Center	7x6 cm	4cm
Side	10x6cm	1cm

z^* is the distance in cm between the crest of the weir and the bed of the working section before the commencement of the experiments

From the grading curves of nonuniform sediments (Figures 2 & 3), d_{max} and d_{min} can be determined. While the values of d_{50a} for the sediment used in the working section were calculated using the following Equation 3 (Melville & Coleman 2000):

$$d_{50a} = \frac{d_{max}}{1.8} \tag{3}$$

where the d_{max} is the largest sediment size for the nonuniform sediments.

In practice, d_{90} can be used instead of d_{max} , which is unlikely to be known (Melville & Coleman 2000). However, in this study, the largest size of the sediment was taken as

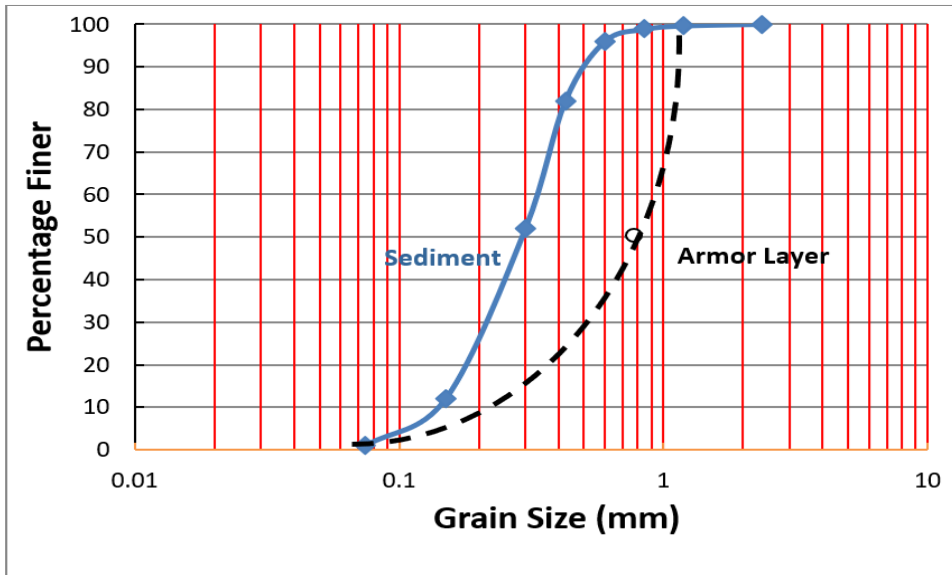


Figure 2. Grain size distribution curves for the sediments ($d_{50}=0.30\text{mm}$) and armor layer

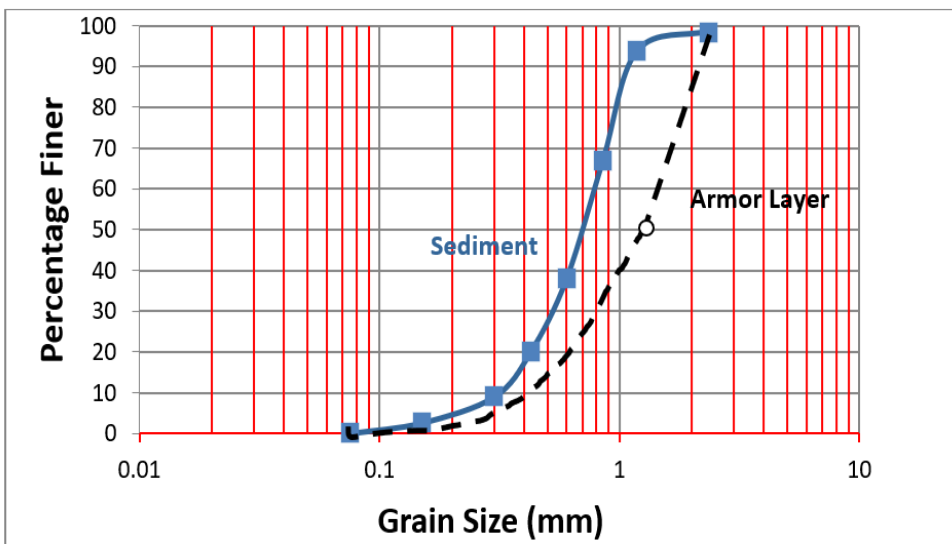


Figure 3. Grain size distribution curves for the sediments ($d_{50}=0.70\text{mm}$) and armor layer

d_{\max} , while the smallest size was taken as d_{\min} . The values of d_{\max} , d_{50a} , and d_{\min} were used to plot the grading curves for the armor layers of the nonuniform sediments used in the working section (Figures 2 & 3). In the present study, the shapes of the plotted grading curves for the armor layer are similar to the typical grading curves for the armor layer

presented by Melville and Coleman (2000). All experimental runs were carried out for 300 minutes under clear water scour conditions. The clear water scours conditions usually exist when the flow intensity $v/v_c < 1$ (the approach velocity, v /critical velocity, v_c is less than one). The clear water scour conditions exist for both uniform and nonuniform sediments when flow intensity, $v/v_c < 1$ or $[v - (v_a - v_c)]/v_c < 1$ respectively. In this study, the maximum value of the flow intensity was 0.80. However, v_a is called the armor peak velocity (Melville & Coleman 2000). A general view of the working section before and after the experiments are shown in Figure 4.

The weir was calibrated before the experiments were carried out; the calibration was conducted by measuring the discharge and head above the weir crest. The head over the weir was measured at 50 cm upstream of the weir, while a volumetric method was used to measure the discharge. The discharge in the flume ranged from a minimum of 2.6 l/s to a maximum of 8 l/s. At the flume entrance, a honeycomb flow straightener was used to eliminate the effect of flow turbulence on the sediment within the working section. In addition, a ramp with a slope of 1:10 was used to make a smooth flow transition from the original flume bed to the mobile bed of the working section. Although all the flows in the flume were steady and subcritical, the flow types were defined by the Froude number after measuring the approach velocity in the flume. The water depth was measured using a point gauge with an accuracy of ± 1 mm. After each trial, the scour depth upstream of the slit weir was measured, as shown in Figure 4. Scour depth measurements were carried out on a 5mm grid basis around the scour hole.



a. Before the experiment fore

b. After four hours (Experiment was completed)

Figure 4. The measurements of scour depth upstream of the slit weir; (a) Before the experiment; (b) after the experiment

After each run, the scouring data upstream of the slit weir were measured manually using a calibrated point gauge which was later fed into the Surfer® program. The Surfer® program was used to calculate the scouring volume and represent the contours of the areas affected by scouring.

RESULTS AND DISCUSSION

The velocity, v_a , is called armor peak velocity, which marks the transition from clear water scour to live bed conditions for nonuniform sediments, and it is equivalent to v_c in the uniform sediment. For nonuniform sediment, the geometric standard deviation of the particle size distribution, σ_g , should be more than 1.30. In this case, armoring occurs on the mobile bed of the working section and in the scour hole. Armor layer formation within the scour hole reduces the scour volume around the weir. The ratio v/v_a is a measure of flow intensity for the scouring that occurred within the nonuniform mobile bed, and it is equivalent to v/v_c for the uniform sediment. Therefore, the armor peak velocity, v_a , marks the transition from clear water scours to live bed conditions for nonuniform sediments. In this study, two types of sediments were used in the working section; the first sediments type were with $d_{50} = 0.30\text{mm}$ and geometric standard deviation, $\sigma_g = 1.60$, while the second sediments type were with $d_{50} = 0.70\text{mm}$ and $\sigma_g = 1.58$. It showed that both sediments were nonuniform, and Equations 4 and 5 were used to calculate the v_c and v_a , and these equations are based on a shields diagram or quartz sand in the water at 20°C. Equation 4 can be applied to determine the critical mean approach flow velocity for entrainment of bed sediment, v_c when $0.10\text{mm} < d_{50} < 1\text{mm}$. However, Equation 5 can be applied to determine the armor peak velocity, v_a when $0.10\text{mm} < 0.55d_{90} < 1\text{mm}$.

$$v_c = 0.049 + 0.053(d_{50})^{1.4} + \{0.066 + 0.072(d_{50})^{1.4}\} \log(y/d_{50}) \quad [4]$$

$$v_a = 0.039 + 0.018(d_{90})^{1.4} + \{0.052 + 0.025(d_{90})^{1.4}\} \log(y/d_{90}) \quad [5]$$

where y is approach flow depth, and d_{90} is used in place of d_{\max} , which is unlikely to be known (Melville and Coleman 2000).

In this study, laboratory measurement showed that the maximum value of the flow intensity, $[v - (v_a - v_c)]/v_c$, was 0.80, which is less than 1 and confirms that clear-water conditions for nonuniform sediments occurred during the experimental runs. Ota et al. (2017a) mathematically simulated the local scour upstream of a slit weir using an ordinary differential equation and laboratory data for scour holes formed in uniform sediments. In addition, Ota et al. (2017a) recommended researching the influence of sediment nonuniformity on the scour volume and scouring depth upstream of a slit weir. Based on

this recommendation, two types of nonuniform sediments were tested in the present study. However, the temporal variation of scour volume, V_s and scour depth, d_s of nonuniform sediments recorded upstream of the slit weir were compared with that of uniform sediments, as shown in Figures 5 and 6. The comparison was made to demonstrate the difference in behavior between uniform and nonuniform sediments, and the temporal scour data ($t = 3000$ seconds) were taken from Ota et al. (2017a). Since the objective of this study is to compare the data with Ota et al. (2017a), the comparison between the two studies can only be carried out on the scour data up to 3000 seconds. After $t = 3000$ seconds, the scour volumes and depths occurring in uniform sediments and nonuniform sediments upstream of a slit weir were 20 folds and 4 folds, respectively. The difference between them can be attributed to forming an armor layer within the scour hole of the nonuniform sediments, which did not occur in the scour hole of uniform sediments.

However, previous experimental works on local scour around hydraulic structures indicate that the scour depth tends to decrease with the increase in the nonuniformity of the sediments (Ota et al., 2017a). In addition, Figures 5 and 6 demonstrate the impact of σ_g for uniform and nonuniform sediments on scour volume and scour depth upstream of a slit weir. In the present study, the median size, d_{50} , and geometric standard deviation, σ_g , for the nonuniform sediments were 0.70 mm and 1.60, respectively, while Ota et al. (2017a) used uniform sediments with $d_{50} = 0.77$ mm and $\sigma_g = 1.30$. Therefore, a comparison was made between uniform and nonuniform sediments of approximate d_{50} . In addition, the bed shear stress in a scour hole decreases as the scour hole develops over time; this contributes to the expansion in the flow area as the scour develops (Ota et al., 2017a).

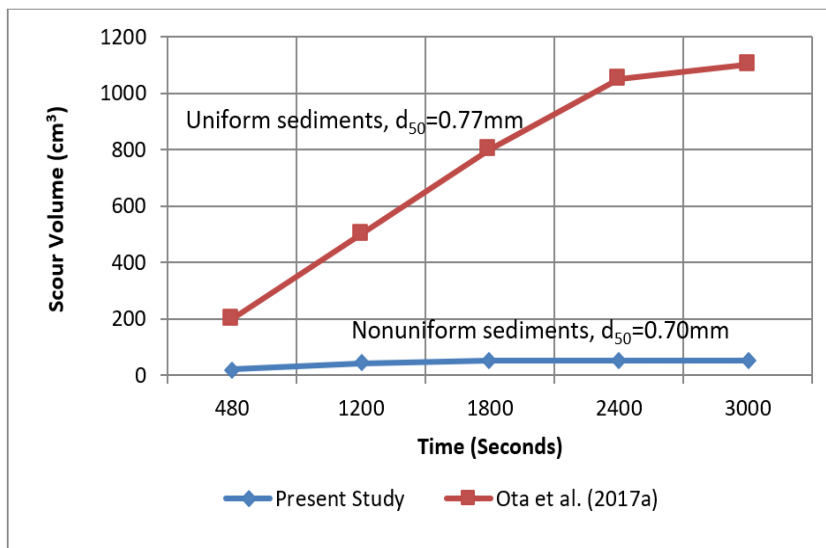


Figure 5. Impact of sediment nonuniformity on scour volume

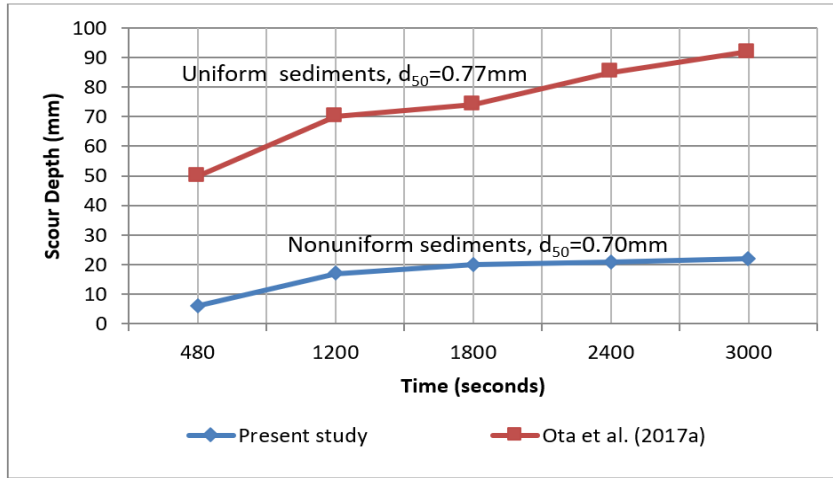


Figure 6. Impact of sediment nonuniformity on scour depth

In this study, it was observed that the increment in scour volume after 300 minutes was not significant, although it is recommended that future studies extend the experimental runs beyond 300 minutes. Figure 7 shows temporal scour data for both types of nonuniform sediments ($d_{50} = 0.70$ mm and $d_{50} = 0.30$ mm), slit weir positioned in the center, slit weir crest level, $z = 1$ cm, and $Q = 8$ l/s. In this study, the coarseness of nonuniform sediments was also investigated. Two sediments were used for this objective; the first sediment had a median size, $d_{50} = 0.30$ mm, while the second type had $d_{50} = 0.70$ mm. Table 2 shows the behavior of the nonuniform sediments under low and high discharges. For weir dimensions of 50 mm x 110 mm (slit positioned at the center), $z = 0$ cm, and the same sediment size, when the discharge increased by three folds, the scour volume increased by 10 folds.

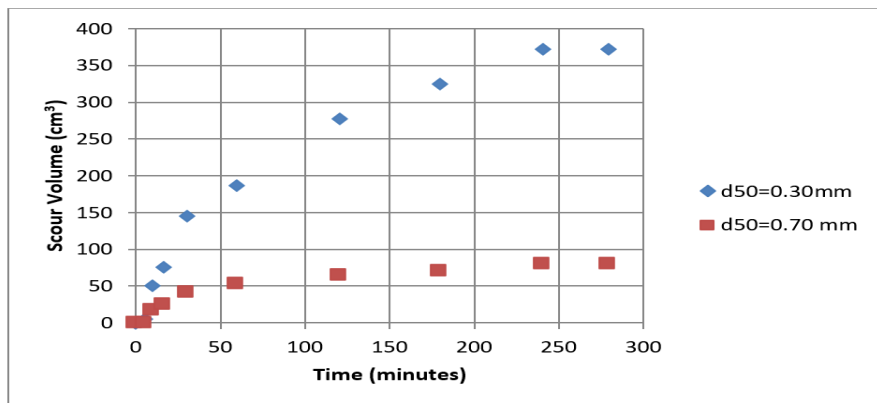


Figure 7. The temporal scour data for $Q = 8$ l/s, $z = 1$ cm, and weir with slit located in the center

Table 2

The behavior of different sediment sizes used in the working section

Slit location	Discharge (l/s)	d_{50} (mm)	z (mm)	Scour depth (mm)	Scour Volume (mm^3)	Scour Time (hour)
center	2.60 l/s	0.30	0	28	34894	4
center	8 l/s	0.30	0	42	371532	4
center	2.60 l/s	0.70	0	6	1560	4
center	8 l/s	0.70	0	30	16340	4

d_{50} is the median size, and z is the weir crest level from the mobile bed

On the contrary, when the sediments in the working section of the flume were changed from $d_{50} = 0.30$ mm to $d_{50} = 0.70$ mm, the scour volume was reduced by 22 folds. The reduction in the scour volume can be attributed to the armoring layer that develops at the top of the nonuniform sediments and requires greater shear stresses for particles' incipient motion.

However, the incipient motion for nonuniform sediments with $d_{50} = 0.70$ mm requires greater shear stress than that for nonuniform sediments with $d_{50} = 0.30$ mm. All the above laboratory trials were conducted under steady flow conditions. Steady and unsteady flow may be encountered in real-world scenarios. This study demonstrated the time variation of V_s and d_s under steady and unsteady flow conditions for engineering applications. The behavior of the nonuniform sediments under unsteady flow conditions was achieved when the flow rate was increased step-wise from 3 to 5 l/s and decreased in a step-wise manner. This used step-wise procedure matches the procedure used by Ota et al. (2017a) to demonstrate the behavior of uniform sediments under unsteady flow conditions. In addition, the flow ranges and time duration in this study for unsteady flow were similar to that used by Ota et al. (2017a). Figures 8 and 9 show the time-varying flow rate with scouring volume and depth. The peak scour volume was observed at the peak flow rate (5 l/s) and decreased afterward. The scour volume continued to develop after the peak flow rate until it reached a value of 150 cm^3 for the sediments with $d_{50} = 0.30$ mm, while it reached a value of 54 cm^3 for sediment with $d_{50} = 0.70$ mm. For unsteady flow, when the median size of the sediments was changed from 0.30 mm to 0.70 mm, the scour volume was decreased by three folds, while the scour depth was decreased by 60%. However, for the same gradual increment in flow rate (from 3-5 l/s) and time, the scour volume obtained by Ota et al. (2017a) for uniform sediments was approximately 20 folds greater than scour volume occurred in the nonuniform sediments. So, in this study, the behavior of nonuniform and uniform sediments was demonstrated under steady and unsteady flow conditions.

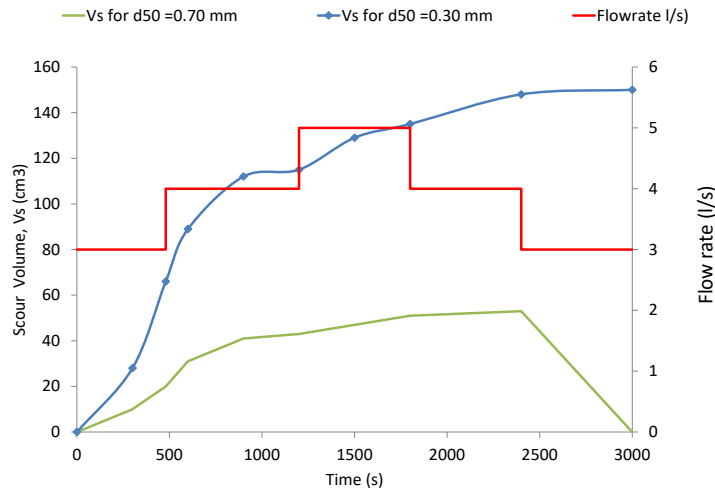


Figure 8. Temporal variation of scouring volume under stepwise unsteady flow

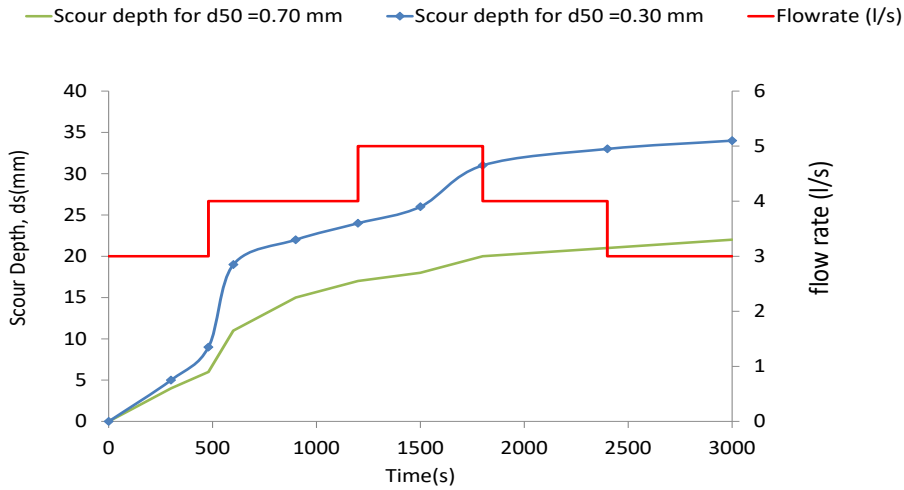


Figure 9. Temporal variation of scour depth under stepwise unsteady flow

Ota et al. (2017a) proposed Equation 1 based on multi regression analysis by considering the geometric features of the scour hole formed upstream of the slit weir for different flows and noncohesive uniform sediments. In addition, they recommend applying Equation 1 without calibration for uniform sediment when $0.10b_{sl}/B < 0.40$, $q_{sl}/q < 8.70$, and $v/v_c < 1$, where b_{sl} is the width of the weir notch, B is the channel width, q_{sl} is the flow rate passing through the slit per unit slit width and q is the flow rate per unit width of the channel.

In this study, although the sediment used was nonuniform but values of $b_{sl}/B = 0.20$, $q_{sl}/q=5$, and $[v-(v_a-v_c)]/v_c < 1$, the slope between V_s and d_s was found to be approximately equal to 3 (Figure 10). The maximum scour depth for the flow conditions of the present study were predicted using Equation 1, and the results were compared with the measured values, as shown in Figure 11. The accuracy of the prediction was tested using the coefficient of determination, R^2 , and the model efficiency, ME, which is described by the following Equation 6:

$$ME=1-[\sum d_{s,e}-d_{s,p})^2/(d_{s,e}-d_{s,a})^2] \tag{6}$$

where the $d_{s,e}$ is the measured experimental maximum scour depth for n experiments, $d_{s,p}$ is the predicted scour depth for n number of cases, $d_{s,a}$ is the mean of measured scours depth for n number of experiments. The value of R^2 between $d_{s,e}$ and $d_{s,p}$ was found to be 0.87, reflecting the accuracy of the prediction since it is closer to 1. In statistics, ME compares calculated values with measured values to indicate the model prediction accuracy or efficiency. A value of 1 means a perfect fit between measured and predicted data, and this value can be negative. The ME value was calculated and found to be 0.87, which confirms the efficiency of Equation 1.

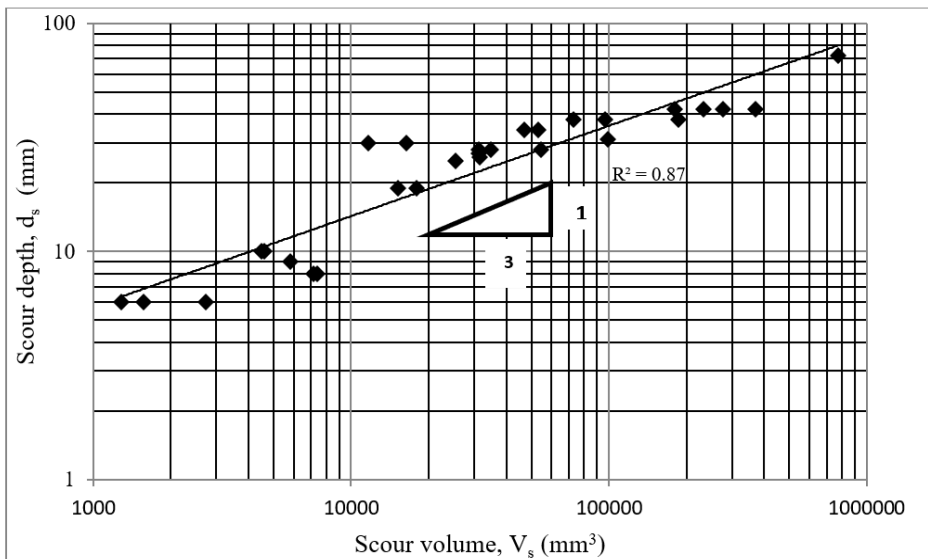


Figure 10. Relationship between maximum scour depth and scour volume for nonuniform sediments

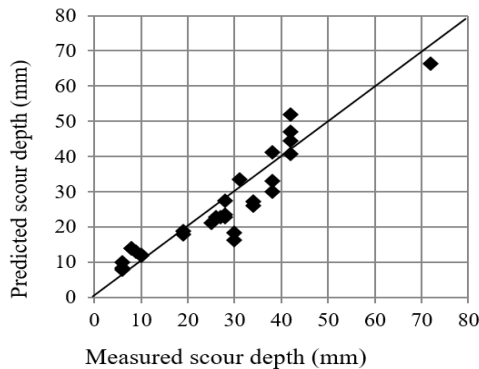


Figure 11. Validation of Equation 1

In addition, Ota et al. (2017a) recommended the application of Equation 1 for uniform sediments only; however, the authors of this study recommend the application of Equation 1 for nonuniform sediments as well the impact of slit weir crest level from the mobile bed upstream, z and the location of the slit weir in the flume on scouring volume were investigated. The temporal variation of scouring volume was monitored for slit weirs with fixed width ($b_{sl} = 6$ cm) and different crest levels ($z = 0, 1, 2, 3,$ and 4 cm) or different slit heights, h_{sl} ($h_{sl} = 11, 10, 9, 8$ and 7 cm). The maximum scours volume was recorded in a slit weir with crest level, $z = 0$ cm or $h_{sl} = 11$ cm (i.e., the crest was at the same level of the mobile bed before the commencement of scouring) and for maximum flow intensity. Figure 12 shows the recorded scour volume after 2 and 4 hours from the commencement of the scour for a flow rate of 8 l/s and different slit weir crest levels. In addition, the maximum scour depth for the scour hole resulted from using slit weirs with different crest levels or different slit height was recorded, and the results are shown in Figure 13. For nonuniform sediments with a median size of 0.30 mm, it was observed that the crest level or slit height influenced the size of the scour hole and scour depth. The maximum volume of scour occurred when the crest level, z , was 0 cm from the mobile bed (when $h_{sl} = 11$ cm). Therefore, the efficiency of sediment removal from the mobile bed was greatly affected by the location of the slit weir (at the side or the center), crest weir level, z or slit height, h_{sl} . From the present study results, it can be concluded that the maximum efficiency of the slit weir in sediment removal was obtained when the slit weir is positioned at the center and when the weir crest level is minimum ($z = 0$ cm).

When the flowing water impinges the right and left wings of the slit weir, a flow vortex develops near the slit weir and causes a circulating flow. Later, the circulating flow caused the sediment particles to entrain into suspension, and the flowing water carried the sediments through the weir notch or slit. At the initial stage, two small scour holes were formed on the left and right of the slit, and with time, the scour holes grew, as shown in Figure 14(a). Finally, the scour holes extended and merged with time to form one larger scour hole, as shown in Figure 14(b). The scour hole reached its maximum volume when the sediment entrained within the scour hole decreased as the scour developed temporally. It can be explained by the increase in flow area and hence a reduction in shear stress. The above explanation of the scour mechanism is based on continuous observation throughout the laboratory work.

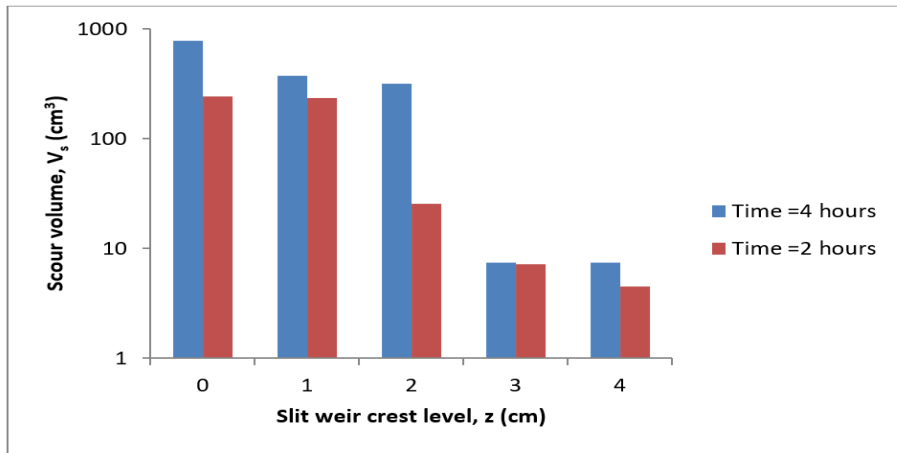


Figure 12. Variation of scour volume with slit weir crest level for a flow rate of 8 l/s and sediment size of 0.30mm

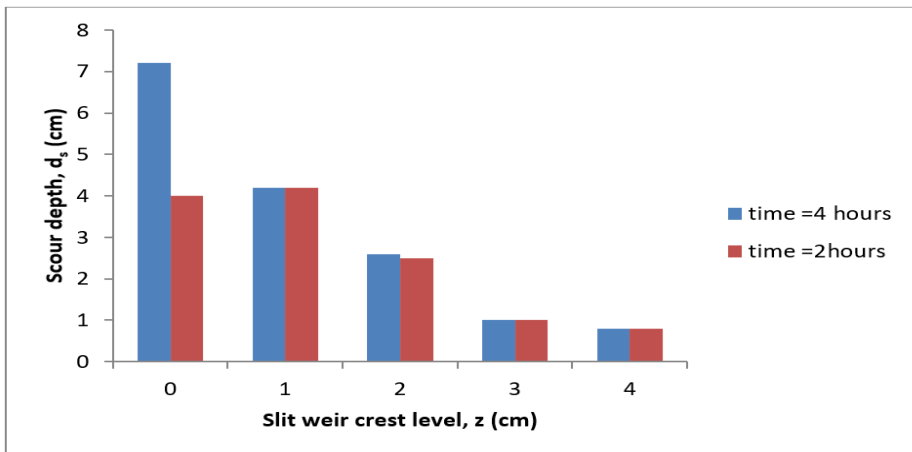


Figure 13. Variation of maximum scour depth with slit weir crest level for a flow rate of 8 l/s and sediment size of 0.30mm

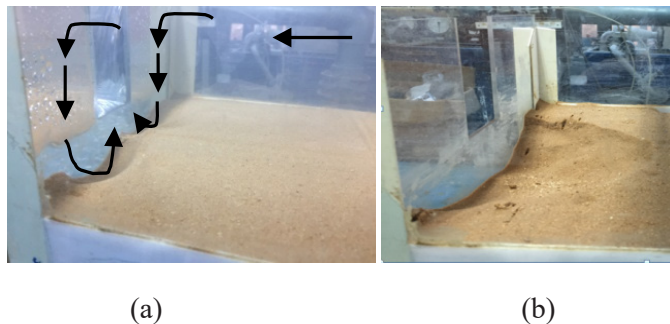


Figure 14. The mechanism of scour hole development upstream of slit weir; (a) The formation of two holes; (b) the final resulting hole

Ota et al. (2017a) also observed the above-described phenomena. The circulating flows were stretched by the contracting flow, accompanied by the overfalling nappe. As a result, the bed shear stresses were amplified around the weir; hence, the occurrence of local scour at the weir site. In this case, vortices caused more sediments entrainment, and these sediments passed over the slit weir downstream. However, when the crest was at a higher level from the flume bed, fewer sediment particles crossed over the slit weir downstream. It is because sediment particles require strong vortices to overcome the effect of gravity to be entrained and carried by the flowing water through the slit weir. Figure 15 illustrates how the flow intensity was affected by the crest level of the slit weir, which is presented in dimensionless form, z/b_{sl} (z is the vertical distance between the slit weir crest and the mobile bed while b_{sl} is the width of the slit weir). Figure 16 shows a sample of contours for scour holes measured after 2 hours and 4 hours from the commencement of the experiments for slits weirs with $z = 1$ cm, $Q = 8$ l/s and slit positioned in the center and the side of the channel. For example, when a slit weir with a dimension of 60 mm x 100 mm ($z = 1$ cm) was positioned in the center of the flume, the scour volume in the working section with sediments of $d_{50} = 0.30$ mm after 4 hours was found to be approximately 6.80 folds greater than the scour occurring in a slit weir with the same conditions but with the weir slit positioned in the side of the flume.

In open channel flow, the maximum velocity occurs in the center of the channel in both longitudinal and transverse sections, while the minimum velocity occurs to the sides of the open channel. Therefore, it justifies why the maximum scour volume was observed when the slit of the weir was positioned within the center of the channel. In this study, it was observed that when the weir's slit was positioned near the side of the flume, the formed vortices were weaker, which generated a smaller scour hole. Reservoir sedimentation endangers the sustainability of all types of hydropower plants located in impoundments and/or rivers. For impoundment hydropower plants, sedimentation of reservoirs is causing various issues such as increasing flood risk of infrastructure and decreasing the active water capacity of reservoirs, leading to a loss of power generation. Many hydropower reservoirs worldwide exhibit sedimentation issues and the loss of power generation associated with it.

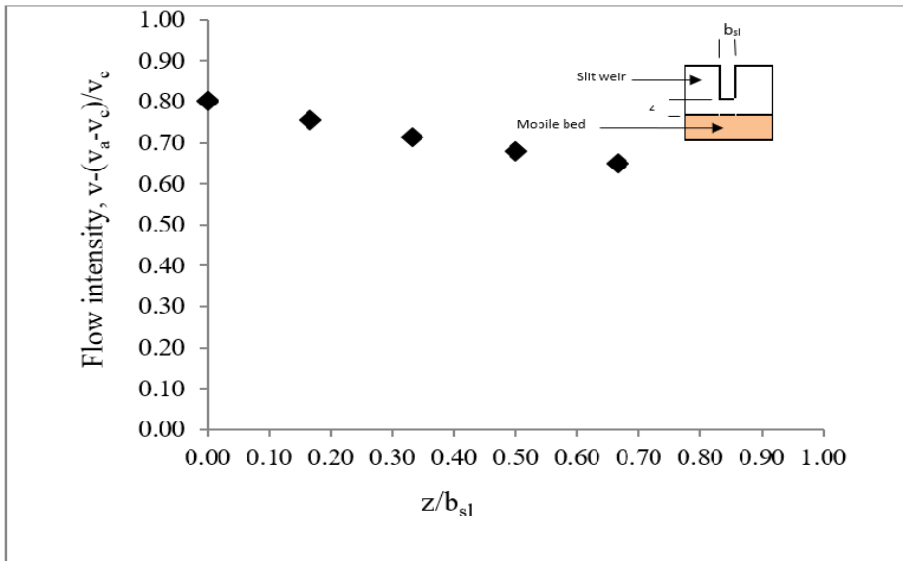


Figure 15. Variation of flow intensities with slit weir crest level for nonuniform sediment with $d_{50}=0.30\text{mm}$

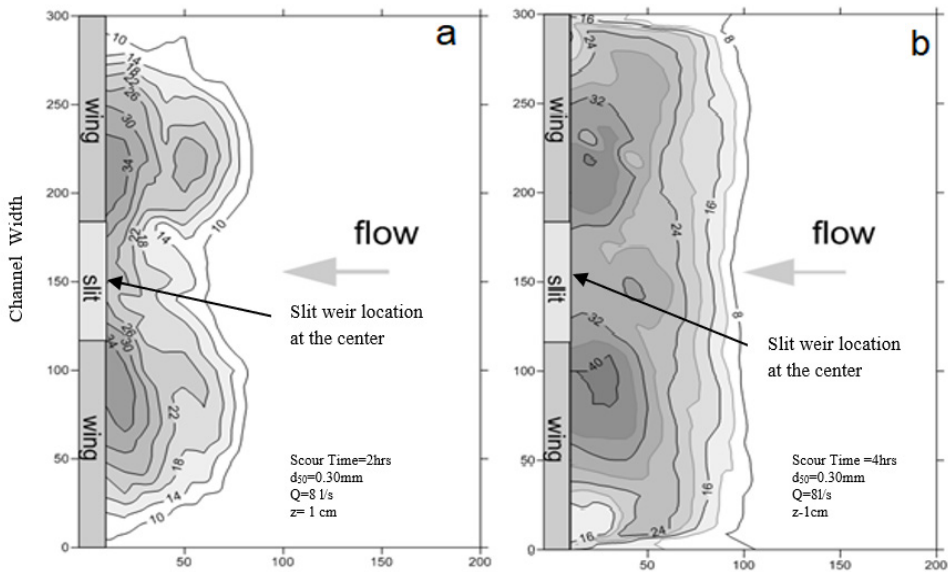


Figure 16. Contours of scour holes for different weir notch locations

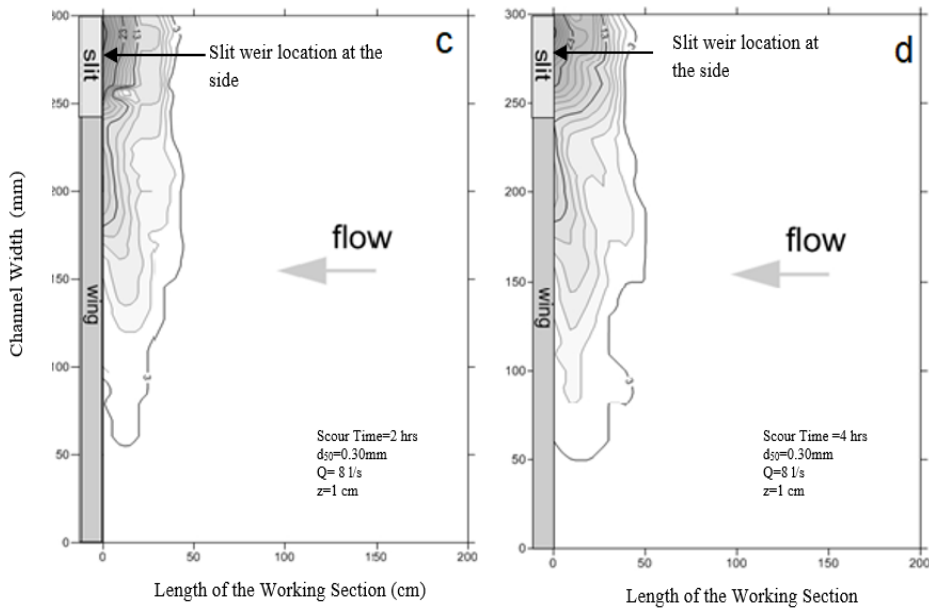


Figure 16. (Continue)

According to Okumura and Sumi (2012), reservoirs of hydropower plants in Japan were affected by increasing sedimentation and flood risk. Boroujeni (2012) estimated the volume of sediments accumulation in the Dez Dam hydropower reservoir, Iran, for 50 years, and it was estimated at approximately 840 million cubic meters (million m^3). Kamarudin et al. (2018) discussed the sedimentation problem in the lake of Kenyir dam, Terengganu, Malaysia, which affected the production of the Sultan Muhmud hydroelectric power station. Reisenb uchler et al. (2020) warned that the run of a river hydropower plant located on the Saalach River in southeastern Germany was subjected to sedimentation. Given the above issues, the results of this study can be used by design engineers, project operators, and other stakeholders doing business in hydropower production. Using a slit weir to cause scouring upstream in or around a hydropower intake is a sustainable method for sedimentation management. The results of scouring depth upstream of the slit weir can be used in the design of the weir floor. On the one hand, fine sediments are causing erosion of turbine blades, and this can be mitigated by conveying more fine sediments from upstream to downstream by utilizing structures such as a slit weir.

CONCLUSION

In this study, a 2 m working section with a mobile bed and Plexiglass slit weir models have been arranged in a glass-sided tilting flume (12 m in length, 0.30 m in width, and 0.30 m deep) to be used for investigating the impact of sediment nonuniformity, slit weir crest

level, slit weir location, and flow intensity on the scour volume upstream of the slit weir location. Nonuniform sediments with median diameters of 0.30 mm and 0.70 mm were tested. For a discharge of 8 l/s, the scour volume upstream of the weir with the slit at the center was reduced by 22 folds when the median size of sediments in the working section, d_{50} , was increased from 0.30mm to 0.70mm. In addition, the temporal variation of scours volume was monitored and compared with the published data of uniform sediments ($d_{50} = 0.77\text{mm}$) with similar flow conditions. Comparisons show that the scour volume and maximum scour depth in uniform sediments of $d_{50} = 0.77 \text{ mm}$ were 20 folds and 4 folds, respectively, greater than those used in this study in nonuniform sediments with a $d_{50} = 0.7\text{mm}$.

In addition, the experimental results revealed that the scour volume was affected significantly by the level and location of the weir's slit. For the same flow conditions, slit level from the mobile bed, z , and sediment median size, d_{50} , the scour volume was much higher when the slit of the weir was positioned at the center than that position at the side. For $Q = 8 \text{ l/s}$, $z = 1 \text{ cm}$, and $d_{50} = 0.30 \text{ mm}$, the scour volume was 14 folds greater when the slit was positioned at the center compared to a slit position at the side. The strength of the formed vortices is affected by slit location, which eventually affects the size of the scour hole. Therefore, maximum efficiency of the slit weir in removing sediments can be obtained when the slit weir is positioned in the center of the flume in conjunction with the weir crest level is at the same level as the mobile bed before the commencement of the scouring phenomena ($z = 0 \text{ cm}$).

ACKNOWLEDGEMENT

The authors wish to acknowledge the support given by the Hydraulic Laboratory, Department of Water Resources Engineering, College of Engineering, the University of Baghdad for the assistance given during the research.

REFERENCES

- Abdollahpour, M., Ali, H. D., David, F., & Carlo, G. (2017). Experimental study on erosion and sedimentation patterns downstream of a W-weir in a sinusoidal mild bend. *Water*, 9(638), Article 638. <https://doi.org/10.3390/w9090638>
- Azamathulla, H. M., Deo, M. C., & Deolalikar, P. B. (2008). Alternative neural networks to estimate the scour below spillways. *Advances in Engineering Software*, 39(8), 689-698. <https://doi.org/10.1016/j.advengsoft.2007.07.004>
- Boroujeni, H. S. (2012). *Hydropower - Practice and application*. InTech Rijeka Publisher.
- Guan, D., Liu, J., Chiew, Y. M., & Zhou, Y. (2019). Scour evolution downstream of submerged weirs in clear water scour conditions. *Water*, 11(1746), Article 1746. <https://doi.org/10.3390/w11091746>

- Kamarudin, A. M. K., Wahab, N. A., Mamat, A. F., Juahir, H., Toriman, M. E., Wan, N. F. N., Ata, F. M., Ghazali, A., Anuar, A., & Saad, M. H. M. (2018). Evaluation of annual sediment load production in Kenyir Lake Reservoir, Malaysia. *International Journal of Engineering and Technology*, 7(3), 55-60.
- Khalili, M., & Honar, T. (2017). Discharge coefficient of semi-circular labyrinth side weir in subcritical flow. *Water*, 43(3), 433-441. <https://doi.org/10.4314/wsa.v43i3.08>
- Lauchlan, C. (2004). Experimental investigation of bed-load and suspended-load transport over weirs. *Journal of Hydraulic Research*, 42(5), 551-558. <https://doi.org/10.1080/00221686.2004.9641224>
- Melville, W. B., & Coleman, S. (2000). *Bridge scour*. Water Resources Publication.
- Muller, S., Guiraud, P., & Line, A. (2011). Particle bed deformation in front of a weir induced by subcritical laminar flow. *Journal of Hydraulic Research*, 4 (2), 194-204. <https://doi.org/10.1080/00221686.2011.552460>
- Nosedá, M., Ivan, S., Michael, P., & Anton, J. S. (2019). Upstream erosion and sediment passage at piano key weirs. *Journal of Hydraulic Engineering*, 145(8), 1-9. [https://doi.org/10.1061/\(ASCE\)HY.1943-7900.0001616](https://doi.org/10.1061/(ASCE)HY.1943-7900.0001616)
- Okumura, H., & Sumi, T. (2012, June 5). Reservoir sedimentation management in hydropower plant regarding flood risk and loss of power generation. In *Proceedings of International Symposium on Dams for Changing World* (pp. 1-6). Kyoto, Japan.
- Ota, K., Sato, T., Arai, R., & Nakagawa, H. (2017a). Local scour upstream of a slit weir: Ordinary differential equation-based model under steady and unsteady flow conditions. *Journal of Hydraulic Engineering*, 143(1), Article 04016073. [https://doi.org/10.1061/\(ASCE\)HY.1943-7900.0001215](https://doi.org/10.1061/(ASCE)HY.1943-7900.0001215)
- Ota, K., Sato, T., Nakagawa, H., & Kawaike, K. (2017b). Three-dimensional simulation of local scour around a weir-type structure: Hybrid Euler LaGrange model for bed-material load. *Journal of Hydraulic Engineering*, 143(4), 1-15. [https://doi.org/10.1061/\(ASCE\)HY.1943-7900.0001263](https://doi.org/10.1061/(ASCE)HY.1943-7900.0001263)
- Ota, K., & Sato, T. (2015). Experimental and numerical study of the local scour caused by sediment releasing through a dam gate. *Journal of Japan Society of Civil Engineers*, 3(1), 184-190. https://doi.org/10.2208/journalofjsce.3.1_184
- Ota, K., Sato, T., Arai, R., & Nakagawa, H. (2016). 3D numerical model of sediment transport considering transition from bed-load motion to suspension-application to a scour upstream of a cross-river structure. *Journal of Japan Society of Civil Engineers*, 4(1), 173-180. https://doi.org/10.2208/journalofjsce.4.1_173
- Powell, D. N., & Khan, A. A. (2012). Scour upstream of a circular orifice under constant head. *Journal of Hydraulic Research*, 50(1), 28-34. <https://doi.org/10.1080/00221686.2011.637821>
- Rajkumar, V. R., Wang, C., Shih, H., & Hong, J. (2016). Prediction of contraction scour using ANN and GA. *Flow Measurement and Instrumentation*, 50, 26-34. <https://doi.org/10.1016/j.flowmeasinst.2016.06.006>
- Reisenbüchler, M., Bui, M. D., Skublics, D., & Rutschmann P. (2020). Sediment management at run-of-river reservoirs using numerical modelling. *Water*, 12(1), Article 249. <https://doi.org/10.3390/w12010249>
- Sayed, B., Vosoughifar, H., Truce, B., & Jeng, D. S. (2019). Estimation of clear-water local scour at pile groups using genetic expression programming and multivariate adaptive regression splines. *Journal of*

Waterway Port Coastal and Ocean Engineering, 145(1), 1-11. [https://doi.org/10.1061/\(ASCE\)WW.1943-5460.0000488](https://doi.org/10.1061/(ASCE)WW.1943-5460.0000488)

Subramanya, K. (2015). *Flow in open channels*. McGraw Hill.

Wang, L., Melville, B. W., Whittaker, C. N., & Guan, D. (2018). Scour estimation downstream of submerged weirs. *Journal of Hydraulic Engineering*, 144(3), 1-9. [https://doi.org/10.1061/\(ASCE\)HY.1943-7900.0001431](https://doi.org/10.1061/(ASCE)HY.1943-7900.0001431)

Wang, S., Wei, K., Shen, Z., & Xiang, Q. (2019). Experimental investigation of local scour protection for cylindrical bridge piers using anti-scour collars. *Water*, 11(7), Article 1515. <https://doi.org/10.3390/w11071515>

Zhang, Z., Bing, S., Yakun, G., & Daoyi, C. (2016). Improving the prediction of scour around submarine pipelines. *Proceedings of the Institution of Civil Engineers-Maritime Engineering*, 169(4), 163-173. <https://doi.org/10.1680/jmaen.2015.22>



Removal of Remazol Yellow Using SnO₂-Co Photocatalyst

Muhammad Said^{1,2*}, Fahma Riyanti^{1,2}, Poedji Loekitowati Hariani^{1,2}, Sastriani¹ and Widya Twiny Rizki³

¹Department of Chemistry, Faculty of Mathematics and Natural Science, Sriwijaya University, 30662, South Sumatra, Indonesia

²Research Centre of Advanced and Nanocomposite, Sriwijaya University, 30662, South Sumatra, Indonesia

³Magister Program of Chemistry, Faculty of Mathematics and Natural Science, Sriwijaya University, 30662, South Sumatra, Indonesia

ABSTRACT

Remazol yellow is a synthetic dye that pollutes the environment and causes disease because it is carcinogenic and mutagenic. Photocatalyst is one of the technologies to remove the dye concentration, and tin oxide (SnO₂) with cobalt (Co) dopant has the potential to be a good semiconductor in the process. Therefore, this study aims to synthesize SnO₂/Co composites as a photocatalyst to degrade Remazol yellow dye. The photodegradation process was carried out with several variables, including the effect of time and the initial concentration of the dye and conditions under pH_{pzc}. Furthermore, the composites were made with SnO₂ to Co mass ratios of (2:1), (2:2), (2:3), and were characterized using X-Ray Diffraction (XRD), Scanning Electron Microscope-Energy Dispersive X-Ray (SEM-EDX), and Ultraviolet-Visible Diffuse Reflectance Spectroscopy (UV-Vis DRS) instruments. Based on the results, the SnO₂/Co (2:3) composite was selected as a photocatalyst to degrade the dye as the XRD characterization showed the formation of a typical peak of 2θ at 33°. The energy bandgap of SnO₂ is 3.05 eV, while the (2:3) composite had a value of 2.8eV. Moreover, the SEM characterization showed a non-uniform surface with pores

and elements composition of Sn, O, and Co with the values 61.24, 24.67, and 14.09 wt%, respectively. The optimum condition for photodegradation was obtained at a contact time and concentration of 180 minutes and 10 ppm, respectively, while the removal of the dye reached 65-80%.

Keywords: Concentration, contact time, photocatalyst, Remazol yellow, SnO₂/Co

ARTICLE INFO

Article history:

Received: 12 November 2021

Accepted: 14 February 2022

Published: 20 April 2022

DOI: <https://doi.org/10.47836/pjst.30.3.10>

E-mail addresses:

msaidusman@unsri.ac.id (Muhammad Said)

sastriani542@gmail.com (Sastriani)

widyatwinirizki@gmail.com (Widya Twiny Rizki)

fatechafj@yahoo.com (Fahma Riyanti)

puji_lukitowati@mipa.unsri.ac.id (Poedji Loekitowati Hariani)

* Corresponding author

INTRODUCTION

Azo compounds and their derivatives in the form of benzene groups are one of the main sources of environmental pollution caused by dyes. One of these compounds is Remazol yellow FG, a synthetic dye often used in the batik industry (Handayani et al., 2016). However, it pollutes the environment and potentially causes disease due to its carcinogenic and mutagenic properties. Several studies have been carried out on the processing of color wastes using the adsorption method (Guezzen et al., 2018), with the bacteria *Pseudomonas sp* (Shah et al., 2013) and the photocatalyst method (Ba-Abbad et al., 2017). Photocatalyst utilizes semiconductor materials and light energy, from sunlight and UV lamps, to degrade dye waste. Light energy is used to activate a catalytic process on the surface of semiconductor materials to produce free electrons and holes (Bouaine et al., 2007). The electron-holes formed will migrate to the semiconductor surface and then react with O_2 and H_2O to form reactive oxidation species (O_2^- and $\cdot OH$), capable of oxidizing the organic molecules (Mohammed et al., 2017). The photocatalytic degradation process can be operated under room temperature and atmospheric pressure and mineralize organic molecules into environment-friendly products (Akti, 2018).

Different studies on semiconductor materials as photocatalysts have been reported, including Sudha and Sivakumar (2015), which used ZnO, TiO_2 , WO_3 , and SnO_2 as semiconductors. Tin oxide (SnO_2) is a semiconductor oxide material with good potential as a photocatalyst as it has good optical properties and electrical conductivity, wide surface area, high physicochemical stability, small energy bandgap, environmentally friendly, and non-destructive (Mani et al., 2016). Meanwhile, SnO_2 photocatalytic ability to degrade dye is increased by modification, such as the addition of metal dopants (Malvankar et al., 2020). Generally, the metal commonly used as a dopant is cobalt (Co) with various concentrations, as Pirmoradi et al. (2011) reported, which used the sol-gel method in the doping process. The result showed a decrease in the energy bandgap from 3.19 eV to 2.97 eV. The addition of dopant Co to SnO_2 was also carried out by Wan et al. (2016), and a homogeneous distribution of the metal particles on the semiconductor surface was found. Moreover, this process affects the crystal size of SnO_2 -Co. The smaller the crystal size, the larger the surface area, thereby increasing the degradation and adsorption performance of the crystals (Attar, 2018). SnO_2 -Co composites are widely used for various purposes such as gas sensor applications (Rukkumani et al., 2017), antibacterial studies (Qamar et al., 2017), and dye degradation (Naje et al., 2013).

The photocatalytic degradation of synthetic dyes was carried out by Sivakarthish et al. (2016), which used SnO_2 -Co to degrade methyl violet and obtained 60–70% degradation with the optimum time of 200–225 minutes using sunlight irradiation. The photocatalytic degradation using SnO_2 -Co was also used by Ragupathy and Ramamoorthy (2021) to degrade methylene blue dye and obtained an efficiency degradation of 95.38%. Furthermore, Remazol yellow photocatalytic degradation studies using various photocatalysis have been

reported. Purnawan et al. (2021) used TiO₂ doped Cd, Co, and Mn. The highest percentages degradation for 30 minutes (74.61%) was achieved using TiO₂-Co. Bhuiyan et al. (2020) used iron oxide extracted from *Carica papaya* leaf. The optimum conditions were obtained at a catalyst dose of 0.8 g/L, pH of 2, for 6 hours with a maximum color degradation of 76.6%. Akti (2018) used Polyaniline doped SnO₂-diatomite. It was found that the use of a catalyst dose of 1 g/L in 1 hour resulted in a degradation achieved of 96%. Akti and Balci (2022) used APTES (3-aminopropyl triethoxysilane) and ethyl alcohol modified Sn/SBA-15. The study showed that the Remazol yellow degradation was obtained up to 58.2%. According to the literature review, studies on photocatalytic degradation of Remazol red using SnO₂-Co semiconductor have not been well reported. Therefore, this study aims to synthesize and modify the semiconductor of SnO₂ doped with cobalt (SnO₂-Co) for Remazol red photodegradation. It was conducted with several variables, including the effect of degradation time and the initial concentration of the dye, while the characterizations used to test the material were XRD (X-ray diffraction), SEM (scanning electron microscopy), and UV-Vis DRS (UV-vis diffuse reflectance spectroscopy).

METHODS

SnO₂ Preparation

3 g of SnCl₂ was dissolved in 150 mL of distilled water and stirred for 1 hour, then NH₄OH solution was added dropwise with constant stirring until it reached pH 7. The gel produced was filtered and dried in an oven at 80°C for 24 hours to remove water molecules (Naje et al., 2013). The powder obtained was characterized using XRD, SEM, and DRS instruments.

Synthesis of SnO₂-Co with Variation in the Concentration of Doping Materials

2 g of SnO₂ powder was added with Co(NO₃)₂ with various concentration ratios of 2:1; 2:2, 2:3, and then dissolved in 100 mL of distilled water with constant stirring for 1 hour. Furthermore, NaOH solution was added dropwise with constant stirring until a pH of 7 was reached. The solution was filtered, while the filtrate was mixed with ethanol, precipitated, and then filtered. The precipitate was washed and dried in an oven at 400°C for 1 hour, while the powder obtained was used for characterization and photocatalytic examination (Saravanakumar et al., 2016). The characterization was carried out using XRD, DRS, and SEM instruments. The material from the best characterization results was used to degrade the dye.

Degradation of Remazol Yellow

Effect of Degradation Time. The effect of time on the degradation process was determined using a sample solution of 25 ppm Remazol yellow FG. 0.50 g of SnO₂-Co was added into 1000 mL of beaker glass and 10 mL of Remazol yellow sample solution. The mixture was

stirred with a magnetic stirrer and exposed to a UV lamp (20 watts) with an irradiation time of 30, 60, 90, 120, 150, and 180 minutes in the radiation box. Furthermore, the degraded dye solution was centrifuged for 20 minutes at a speed of 3000 rpm to separate SnO₂-Co from the solution. 1 mL of the solution was then taken, and the absorbance was measured using a UV-Vis spectrophotometer at the maximum wavelength with distilled water. The concentration calculation was carried out by entering the absorbance obtained into the standard curve equation for Remazol yellow. As a control, Remazol yellow degradation process was also carried out without UV lamp irradiation with the same variation of contact time.

Effect of Initial Concentration of Remazol Yellow. The effect of Remazol yellow dye initial concentration was determined using a standard solution of 10 mL of 10, 15, 20, 25, 30 ppm, respectively. Five beakers of 100 mL were added with 0.50 g of SnO₂-Co and a standard solution of Remazol yellow FG. The mixture was stirred with a magnetic stirrer and then exposed to a UV lamp (20 watts) in a radiation box to determine the optimum exposure time. The degraded dye solution was centrifuged for 20 minutes at a speed of 3000 rpm to separate SnO₂-Co from the solution. Furthermore, 1 mL of the solution was taken, and the absorbance was measured using a UV-Vis spectrophotometer at the maximum wavelength with distilled water. The initial concentration was calculated by entering the absorbance obtained into the standard curve equation for the Remazol yellow. As a control, Remazol yellow degradation process was also carried out without UV lamp irradiation with the same variation of initial concentration.

Data Analysis. The percent decrease in Remazol yellow FG concentration was calculated using Equation 1 with the triple measurement as follows:

$$P = \frac{C_o - C_t}{C_o} \times 100\% \quad (1)$$

Where,

P = Percentage decrease in solution concentration.

C_o = Initial concentration of solution before degradation (ppm).

C_t = concentration of solution after degradation at time t (ppm).

RESULTS AND DISCUSSIONS

Characterization of X-Ray Diffraction (XRD)

Characterization using XRD was carried out to identify the crystal's phase, structure, and size type. The results were identified by comparing the formed peaks with data from the

JCPDS card No. 41-1445. SnO₂ and the SnO₂-Co composite XRD characterization results are shown in Figure 1.

Figure 1(a) shows the results of the SnO₂ material diffractogram, and the 2 θ angle characterization was compared with the JCPDS card data No.41- 1445. Based on the data, the angle characteristic of 2 θ SnO₂ is 26.6°; 33.8°; 37.9°; 51.8° 57.9° and 62.0° with field indexes (110), (101), (200), (211), (002) and (310) (Bhagwat et al., 2015). The SnO₂ result showed similarities with JCPDS card No.41-1445 data with a slight shift of the peaks, in angles 26.52°, 32.1°, and 51.8°. Meanwhile, Figure 1(b) shows the result of the SnO₂-Co (2:1) composite diffractogram with peaks at 2 θ angles of 33.510°; 37.22°; 57.50°, and 62.38° while the (2:2) composite diffractogram showed peaks at an angle of 2 θ 26.9°; 33,516°; 37.32°; 57.61° and 62.41° as shown in Figure 1(c). Furthermore, the SnO₂-Co (2:3) sample diffractogram, as presented in Figure 1(d), indicated peaks at angles of 2 θ 26.60°; 33.40°; 37.26°; 51.0°; 57.61° and 62.54°.

The XRD diffractogram results in Figure 1 showed the type of phase produced by the nanocrystalline. The crystal size was below 100 nm with a tetragonal crystal structure as indicated by the formed peaks at a typical angle of 26°, 33°, and 51° (Saravanakumar et al, 2016). Based on Figure 1, in each SnO₂-Co composite, the highest peak intensity was at 30° 2 θ angle. According to Lokhand (2015), the diffraction pattern of cobalt doping peaks generally appears at a 2 θ angle between 20 to 50° with a characteristic diffraction peak at 30°. The highest intensity of the peak at 30° is due to an incomplete reaction which causes excessive reactants and by-products in each of the composite synthesis processes. Another problem Ibarguen et al. (2007) reported was that the formation of a peak at a 30° in the diffraction pattern is caused by the excess amount of NH₄OH, which makes the pH of

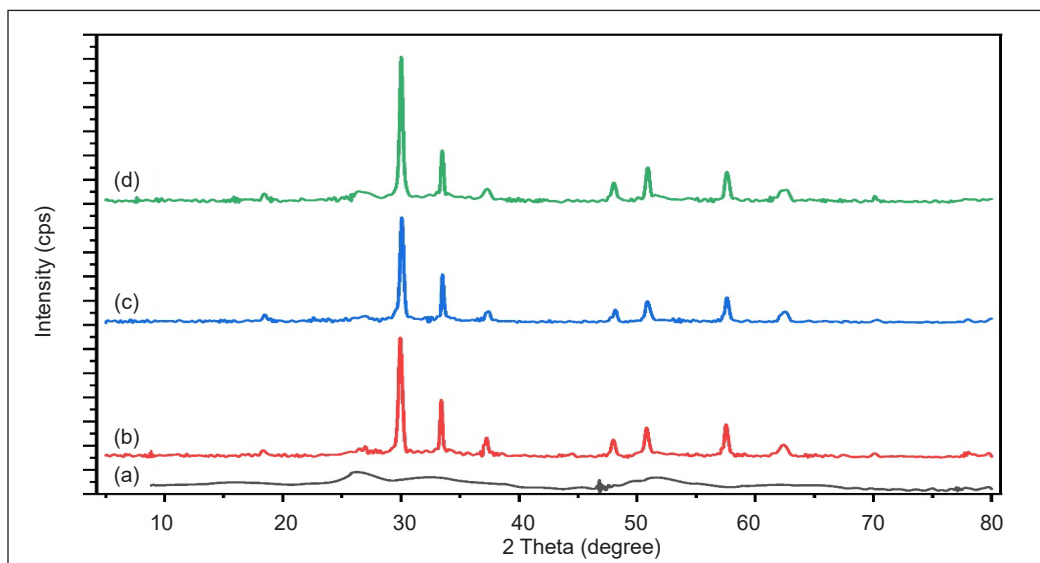


Figure 1. XRD Spectra of (a) SnO₂ (b) SnO₂-Co (2:1) (c) SnO₂-Co(2:2) (d) SnO₂-Co (2:3)

the solution to be alkaline. Therefore, the best XRD characterization from each SnO₂-Co composite was selected for the photodegradation process. One of the factors to determine the best composite for photodegradation applications is the crystal size. Sharma et al. (2014) reported that crystal size affects photodegradation. As the crystal size increases, the degradation efficiency decreases due to the reduction of the surface area and active sites on the surface of the photocatalyst, which in turn decreases the number of hydroxyl radicals and superoxide. A similar finding has also been reported by Peng et al. (2005) that the small crystal size of the photocatalyst indicated high photocatalytic activity. The SnO₂-Co crystal size was calculated using the Debye-Scherrer formula, and the (2:1) (2:2) and (2:3) composites have a value of 48.87 nm, 48.80 nm, and 39.61 nm, respectively. Based on the diffractogram and crystal size data, the SnO₂-Co (2:3) composite was selected for the photodegradation of Remazol yellow because its peaks have a typical angle of 26, 33, and 51°, which are similar to the JCPDS card No.41-1445 data and has the smallest crystal size.

Characterization of UV-Visible Diffuse Reflectance Spectrophotometer (UV-Vis DRS)

The DRS UV-Vis characterization was carried out to determine the energy bandgap value of SnO₂ and the SnO₂-Co composite (2:3). In general, semiconductor materials have two energy bands: valence, and conduction. The distance between the valence to the conduction band is called the energy bandgap. The standard value of the energy bandgap of SnO₂ is 3.6 eV (Pirmoradi et al., 2011). The measurement in the SnO₂ and SnO₂-Co (2: 3) composite with UV-Vis DRS characterization was carried out by providing energy at a wavelength of 200–800 nm. When the electrons in the valence band absorb the appropriate photon energy, then the conduction band is excited. The electrons also transmit some energy back to the ground state, while the transmitted energy by the material is equal to the width of the energy bandgap.

The UV-Vis DRS measurement results of the energy bandgap value of the SnO₂ and SnO₂-Co composite (2:3) are shown in Figure 2. The energy bandgap of SnO₂ was 3.05 eV, while for SnO₂-Co was 2.8 eV. The energy bandgap of SnO₂-Co composite was smaller than SnO₂ due to the influence of doping with Co. This phenomenon was also reported by Mani et al. (2016), which stated that Co metal has a smaller value than Sn; therefore, Co acts as an electron acceptor and decreases the energy bandgap value. The addition of dopant Co to SnO₂ reduced the energy required for electrons to excite from the valence to the conduction band, reducing the bandgap value. Furthermore, Pirmoradi et al. (2011) stated that the addition of cobalt as doping to semiconductors reduces the bandgap energy. Therefore, its application as a photocatalyst was carried out in visible light to reduce energy efficiency. It is caused by cobalt, which acts as an absorber to collect the photoelectrons produced from the semiconductor conduction band.

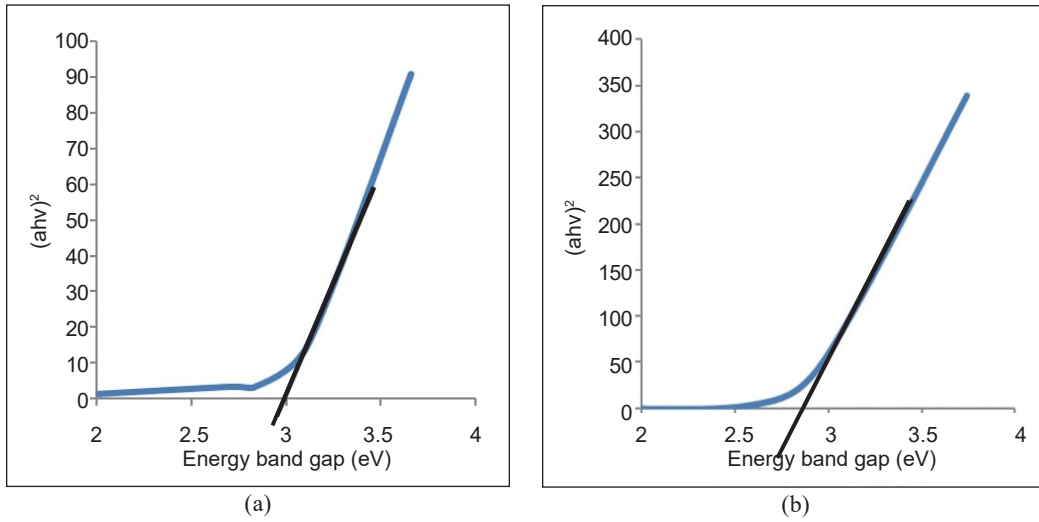


Figure 2. UV-Vis DRS of (a) SnO₂ (b) SnO₂-Co (2:3)

Characterization of Scanning Electron Microscopy (SEM)

SEM characterization was carried out to determine the morphological shape of the SnO₂ semiconductor and SnO₂-Co (2:3) composite to determine the constituent elements. It was performed at 3000x magnification, as shown in Figure 3. The surface morphology presented in Figure 3 (a) showed that the SnO₂ obtained was in the amorphous/crystalline phase. Meanwhile, Yehia et al. (2019) reported that amorphous/crystalline SnO₂ has a distinct porous surface with uneven particles. Furthermore, the surface morphology of the SnO₂-Co composite demonstrated in Figure 3 (b) showed that the particle size of SnO₂-Co was bigger than SnO₂. The SnO₂-Co composite has a round morphology with an uneven surface. It is due to Co doping which aggregates on the surface of SnO₂ and forms pores, as previously

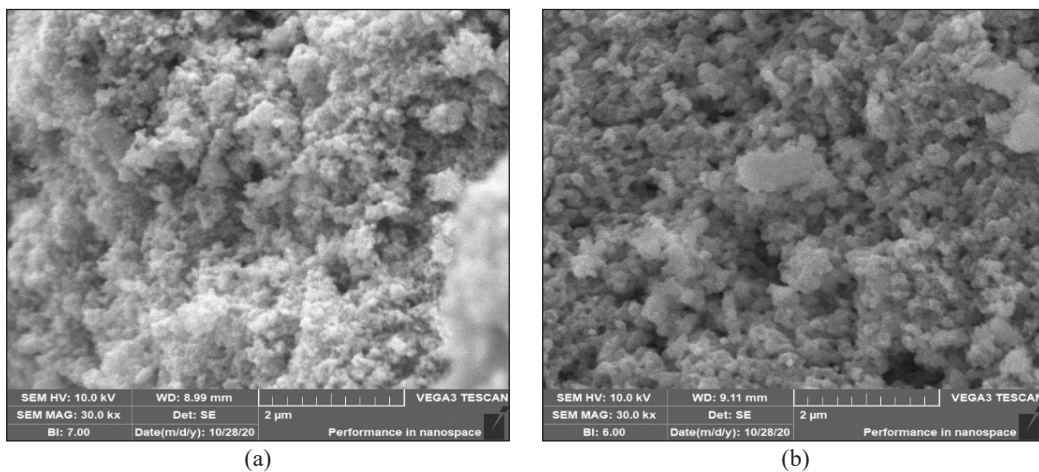


Figure 3. SEM morphology at $\times 3000$ magnification of (a) SnO₂ surface (b) SnO₂-Co (2:3)

reported by Sivakhartik et al. (2016). The analysis results of the constituent elements of SnO₂ and SnO₂-Co composites (2:3) are shown in Table 1.

Based on Table 1, the success of the SnO₂-Co composite (2:3) was indicated by the presence of Sn, O, and Co elements. The Sn composition, namely 61.24 wt%, was higher than the Co, which was only 14.09 wt% and the presence of O at 24.67 wt% indicates that the composite was successfully synthesized. Meanwhile, the Sn and O percentages in the SnO₂ semiconductor were 62.62 wt% and 29.78 wt%, respectively, which indicates successful synthesis with only a few impurities such as carbon (5.61 wt%) and nitrogen (1.98 wt%).

Table 1
Composition of the constituent SnO₂ and composite elements SnO₂/Co (2:3)

	SnO ₂ (wt%)	Composite SnO ₂ /Co (2:3) (wt%)
Sn	62.63	61.24
O	29.78	24.67
Co	-	14.09
C	5.61	-
N	1.98	-

pH Point Zero Charge (pHpzc) SnO₂-Co (2:3) Composite

The pH point zero charges (pH pzc) is the meeting point between the straight lines from the initial to the final pH curve of the solution in a neutral charge state. It is also the point between the initial and final pH after immersion for 24 hours. The pHpzc data is used to determine the appropriate pH conditions for the photodegradation process, as shown in Figure 4.

Figure 4 shows that the pHpzc for the SnO₂/Co (2:3) was 5.18, which indicates the composite is in a neutral charge. Qin et al. (2015) reported that at a pH value below pHpzc, the composite surface charge tends to be positive, degrading anionic dyes. In contrast, when the pH value is above pHpzc, the surface charge tends to be negative for degrading cationic dyes. Since the dye used in the photodegradation process was anionic, namely Remazol yellow, the photodegradation will be favorable if the pH of the solution is adjusted below pHpzc.

Remazol Yellow Photodegradation Effect of Variation in Photodegradation Time. The curve showing the effectiveness of reduction in the concentration of the Remazol yellow dye with variation in time is shown in Figure 5.

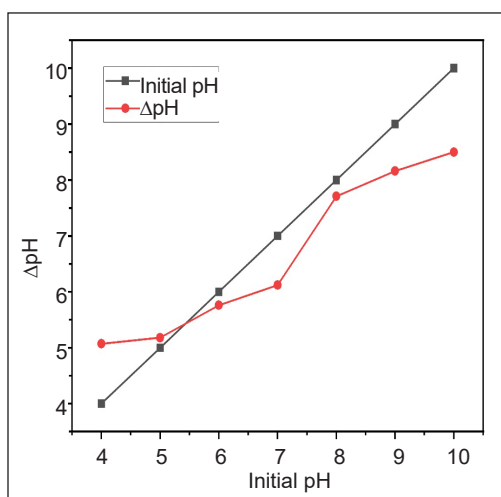


Figure 4. pHpzc SnO₂-Co (2:3)

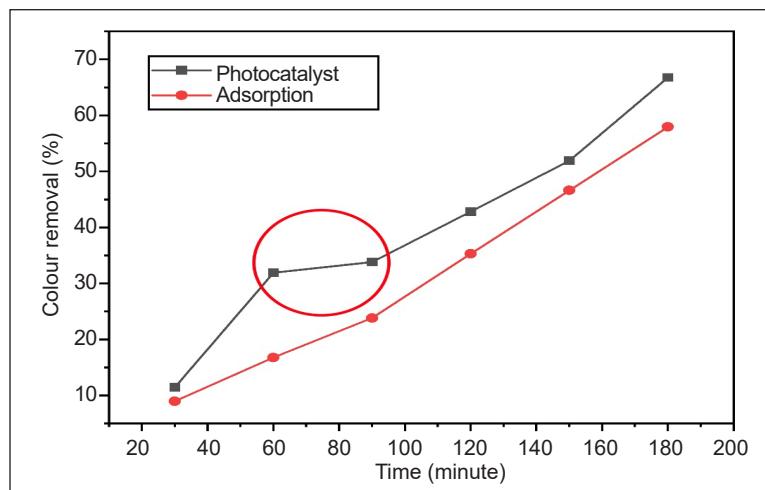


Figure 5. Effect of time on Remazol yellow removal

Based on the curve obtained in Figure 5, at 30 to 180 minutes, there was an increase in the percentage of effectiveness from 11.46 to 66.78%. This percentage shows the degraded dye; hence, the greater the value, the more degraded the Remazol yellow dye. The most effective percentage increase in reducing the dye concentration was found at 30 minutes of irradiation time. Furthermore, at 60 to 180 minutes, the percentage effectiveness of decreasing the concentration was relatively low. The ability of photocatalysts to excite electrons from the valence to the conduction band does not increase; hence, the free electrons produced are widely used to degrade intermediates in the photodegradation process (Kumar & Pandey, 2017). The irradiation time in the photodegradation process describes the length of interaction between the photocatalyst and UV light to produce free electrons (e^-) with holes (h^+) and form a redox reaction that ultimately degrades the dye (Alshabanat & AL-Anazy, 2018). As shown in Figure 5, the highest percentage was at 180 minutes; therefore, it was concluded that the best time for the photodegradation of Remazol dye is at 180 minutes. Moreover, controls as a comparison were also carried out through the adsorption process of Remazol yellow or without UV light irradiation. Based on the curve in Figure 5, there was also an increase in the percentage of effectiveness in decreasing the dye concentration over time. The percentage was smaller without UV light irradiation compared to UV light irradiation of 57.94%. Therefore, the percentage difference in the effectiveness of reducing the concentration with or without UV light irradiation was not significant. The dye and the composite undergo an adsorption process before interacting with UV light during the photodegradation process. Besides, the SnO₂ photocatalyst is also widely used as an adsorbent in dye absorption. Abdelkader et al. (2016) reported that SnO₂ is applicable as a dye adsorbent because it has a wide and dense surface; hence, its ability to absorb dye is relatively large. Paramarta et al. (2016) combined the SnO₂ with graphene

and nanographene to increase the adsorption capacity to degrade the Methylene blue. The results show that the SnO₂ composite with graphene achieves a higher adsorption capacity of about 20% than the composite with NGP. Meanwhile, a SnO₂/CeO₂ Nano-Composite Catalyst was used to adsorb the Alizarin Dye. The removal efficiencies of Alizarin-3-methylimino-diacetic acid, alizarin yellow, and alizarin red S dyes were showed 95.0%, 95.3%, and 87.8%, respectively (Hassan et al., 2020).

Effect of Variation in Initial Concentration of Remazol Yellow. The effectiveness of decreasing Remazol yellow concentration with variations in the initial concentration of the dye is shown in Figure 6.

Based on the curve obtained in Figure 6, the lowest reduction of Remazol yellow is at a concentration of 10 ppm, namely 74.41%. The most effective percentage, which ranged from 10 to 20 ppm, decreased from 74.41 to 64.46%, but at 25 to 30 ppm, the percentage increased from 67.57 to 71.04%. Wahyuningsih et al. (2017) stated that the higher the concentration of the dye used, the larger the number of the molecules, affecting the interaction between the catalyst and UV light. Dyes with large concentrations tend to have a darker color, thereby blocking UV rays for the catalyst. The minimum interaction between UV light and the catalyst produced less photon energy; hence, the catalyst tends to act as an adsorbent at a large dye concentration. Comparative control was also carried out on the effect of variations in the initial concentration of the dye using adsorption or without UV light irradiation. Based on the curve in Figure 6, the largest reduction in the dye concentration was at 30 ppm, with a percentage of 58.96%. This composite is potential in dye removal, and it can be compared with other methods, as Purnawan et al. (2021). Meanwhile, Shu et al. (2015) stated that the higher the concentration, the greater the amount of dye adsorbed on the composite surface.

It is consistent with the data obtained in the adsorption process of Remazol yellow using the SnO₂/Co composite with or without UV light irradiation. Based on the results, the reduction effectiveness with UV light irradiation or photodegradation was greater than that of adsorption without UV light irradiation. It is because the light from the UV lamp interacts with the photocatalysts, which in turn degrades the Remazol yellow solution. Therefore, the decrease in concentration is greater compared to the use of SnO₂-Co, which only absorbs particles on the surface.

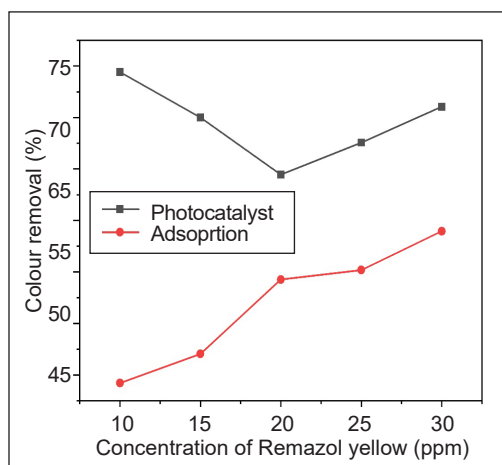


Figure 6. Effect of initial dye concentration of Remazol yellow removal

CONCLUSION

SnO₂/Co composites with mass ratios of (2:1), (2:2), and (2:3) were successfully synthesized, and the characterization results using XRD showed similarities with the typical peak of the JCPDS card No. data. 41-1445 at 2θ of 33°. The UV-Vis DRS characterization results for SnO₂ showed an energy bandgap of 3.05 eV, while the SnO₂/Co composite (2:3) was 2.8 eV. Furthermore, the surface morphology of the SnO₂/Co composite (2:3) determined using SEM characterization showed an uneven round surface and forms pores caused by an aggregate of Co doping on the surface of SnO₂ with the constituent percentage of 61.24, 24.67, and 14.09% for Sn, O, and Co respectively. Therefore, the optimal condition for the reduction in the concentration of Remazol yellow was at 180 minutes contact time and 10 ppm for the initial concentration with the highest percentage of 66.78 and 74.41%, respectively.

ACKNOWLEDGMENT

The author is grateful to Universitas Sriwijaya for the financial support through Hibah Unggulan Kompetitif 2020 Contract No. 0216.050/UN9/SB3.LPPM.PT/2020.

REFERENCES

- Abdelkader, E., Nadjia, L., & Rose-Noelle, V. (2016). Adsorption of Congo red azo dye on nanosized SnO₂ derived from Sol-gel method. *International Journal of Industrial Chemistry*, 7, 53-70. <https://doi.org/10.1007/s40090-015-0061-9>
- Akti, F. (2018). Photocatalytic degradation of remazol yellow using polyaniline-doped tin oxide hybrid photocatalysts with diatomite support. *Applied Surface Science*, 455, 931-939. <https://doi.org/10.1016/j.apsusc.2018.06.019>
- Akti, F., & Balci, S. (2022). Synthesis of APTES and alcohol modified Sn/SBA-15 in presence of competitive ion: Test in degradation of remazol yellow. *Materials Research Bulletin*, 145, Article 111496. <https://doi.org/10.1016/j.materresbull.2021.111496>
- Alshabanat, M. N., & AL-Anazy, M. M. (2018). An experimental study of photocatalytic degradation of Congo red using polymer nanocomposite films. *Journal of Chemistry*, 2018, Article 9651850. <https://doi.org/10.1155/2018/9651850>
- Attar, A. S. (2018). Efficient photocatalytic degradation of methylene blue dye by SnO₂ nanotubes synthesized at different calcination temperatures. *Solar Energy and Solar Cell*, 183, 16-24. <https://doi.org/10.1016/j.solmat.2018.03.046>
- Ba-Abbad, M. M., Takriff, M. S., Said, M., Benamor, A., Nasser, M. S., & Mohammad A.W. (2017). Photocatalytic degradation of pentachlorophenol using ZnO nanoparticles: Study of intermediates and toxicity. *International Journal of Environmental Research*, 11, 461-473. <https://doi.org/10.1007/s41742-017-0041-3>

- Bhagwat, A. D., Sawant, S. S., Ankamwar, B. G., & Mahajan, C. M. (2015). Synthesis of nanostructured tin oxide (SnO₂) Powder and tin films by sol-gel method. *Journal of Nano and Electronic Physics*, 7(4), 1-4.
- Bhuiyan, M. S. H., Miah, M. Y., Paul, S. C., Aka, T. D., Saha, O., Rahaman, M. M., Sharif, M. J. I., Habiba, O., & Ashaduzzaman, M. (2020). Green synthesis of iron oxide nanoparticle using Carica papaya leaf extract: Application for photocatalytic degradation of remazol yellow RR dye and antibacterial activity. *Heliyon*, 6(8), Article e04603. <https://doi.org/10.1016/j.heliyon.2020.e04603>
- Bouaine, A., Brihi, N., Schmeber, G., Ulhaq-Bouillet, C., Colis, S., & Dinia, A. (2007). Structural, optical and magnetic properties of co-doped SnO₂ powders synthesized by the coprecipitation technique. *Journal of Physical Chemistry C*, 111(7), 2924-2928. <https://doi.org/10.1021/jp066897p>
- Guezzen, B., Didi, M. A., & Medjahed, B. (2018). Sorption of Congo red from aqueous solution by surfactant-modified bentonite: Kinetic and factorial design study. *International Journal of Chemical and Molecular Engineering*, 12(3), 149-156. <https://doi.org/10.5281/zenodo.1316193>
- Handayani, D. S., Purnawan, C., Pranoto., Hastuti, S., & Hilmiyana, D. (2016). Adsorption of remazol yellow from aqueous solution on chitosan-linked P-T-Butylcalix[4]Arene. In *IOP Conference Series: Materials Science and Engineering* (Vol. 107, Issue 1, Article 012011). IOP Publishing Limited. <https://doi.org/10.1088/1757-899X/107/1/012011>
- Hassan, S. S. M., Kamel, A. H., Hassan, A. A., Amr, A. E. E., Naby H. A., & Elsayed, E. A. (2020). A SnO₂/CeO₂ nano-composite catalyst for alizarin dye removal from aqueous solutions. *Nanomaterials*, 10(2), Article 254. <https://doi.org/10.3390/nano10020254>
- Ibarguen, C. A., Mosquera, A., Parra, R., Castro, M. S., & Rodríguez-Páez, J. E. (2007). Synthesis of SnO₂ nanoparticles through the controlled precipitation route. *Material Chemistry and Physics*, 101(2-3), 433-440. <https://doi.org/10.1016/j.matchemphys.2006.08.003>
- Kumar, A., & Pandey, G. (2017). A review on the factors affecting the photocatalytic degradation of hazardous materials. *Material Science & Engineering International Journal*, 1(3), 106-114. <https://doi.org/10.15406/mseij.2017.01.00018>
- Lokhand, P. E., & Panda, H. S. (2015). Synthesis and characterization of CoNi(OH)₂ material for supercapacitor application. *International Advanced Research Journal in Science*, 2(9), 10-14.
- Malvankar, S., Doke, S., Gahlaut, R., Martinez-Teran, E., El-Gendy, A.A., Deshpande, U., & Mahamuni, S. (2020). Co-doped SnO₂ nanocrystals: XPS, raman, and magnetic studies. *Journal of Electronic Materials*, 49, 1872-1880. <https://doi.org/10.1007/s11664-019-07865-5>
- Mani, R., Vivekanandan, K., & Vallalperuman, K. (2016). Synthesis of pure and cobalt (Co) doped SnO₂ nanoparticles and its structural optical and photocatalytic properties. *Journal of Materials Science: Material in Electronics*, 28, 4396-4402. <https://doi.org/10.1007/s10854-016-6067-z>
- Mohammed, H. A., Sanaullah, K., Soh, F. L., Andrew Ragai, H. R., Hamza, A., & Khan, A. (2017). Modeling and optimization of photocatalytic treatment of pre-treated palm oil mill effluent (POME) in a UV/TiO₂ system using response surface methodology (RSM). *Cogent Engineering*, 4(1), Article 1382980. <https://doi.org/10.1080/23311916.2017.1382980>
- Naje, A. N., Norry, A. S., & Suhail, A. M. (2013). Preparation and characterization of SnO₂ nanoparticles. *International Journal of Innovative Research in Science Engineering and Technology*, 2(12), 7068-7072.

- Paramarta, V., Taufik, A., & Saleh, R. (2016). Better adsorption capacity of SnO₂ nanoparticles with different graphene addition. *Journal of Physics: Conference Series*, 776(1), Article 012039. <http://dx.doi.org/10.1088/1742-6596/776/1/012039>
- Peng, T., Zhao, D., Dai, K., Shi, W., & Hirao, K. (2005). Synthesis of titanium dioxide nanoparticles with mesoporous anatase wall and high photocatalytic activity. *Journal of Physical Chemistry B*, 109(11), 4947-4952. <https://doi.org/10.1021/jp044771r>
- Pirmoradi, H., Malakootikhah, J., Karimipour, M., Ahmadpour, A., Shahtahmasebi, N., & Koshky, E. F. (2011). Study of cobalt-doped SnO₂ thin films. *Middle-East Journal of Scientific Research*, 8(1), 253-256.
- Purnawan, C., Wahyuningsih, S., Aniza, O. N., & Sari, O. P. (2021). Photocatalytic degradation of remazol brilliant blue R and remazol yellow FG using TiO₂ doped Cd, Co, Mn. *Bulletin of Chemical Reaction Engineering & Catalysis*, 16(4), 804-815. <https://doi.org/10.9767/bcrec.16.4.11423.804-815>
- Qamar, M. A., Shahid, S., Khan, S. A., Zaman, S., & Sarwar, M. N. (2017). Synthesis characterization optical and antibacterial studies of co-doped SnO₂ nanoparticles. *Digest Journal of Nanomaterials and Biostructures*, 12(4), 1127-1135.
- Qin, X., Liu, F., Wang, G., & Huang, G. (2015). Adsorption of humic acid from aqueous solution by hematite: Effect of pH and ionic strength. *Environmental Earth Sciences*, 73, 4011-4017. <https://doi.org/10.1007/s12665-014-3686-7>
- Ragupathy, S., & Ramamoorthy, M. (2021). A study on Co doped SnO₂ loaded corn cob activated carbon for the photocatalytic degradation of methylene blue dye. *Research Square*, 40(1), 1-20. <https://doi.org/10.21203/rs.3.rs-168313/v1>
- Rukkumani, V., Devarajan, N., & Saravanakumar, M. (2017). Fabrication of sram memory devices using co-doped SnO₂ nanoparticles. *Journal of Ovonic Research*, 13(1), 1-5.
- Saravanakumar, M., Jeevitha, N., & Prabakaran, K. (2016). Structural and luminescence characteristics of nanocrystalline SnO₂ doped with Co²⁺. *Journal of Ovonic Research*, 12(4), 209-214.
- Shah, M. P., Patel, K. A., Nair, S. S., & Darji, A. M. (2013). Microbial decolorization of methyl orange dye by *Pseudomonas Sp.* *OA Biotechnology*, 2(1), Article 10. <https://doi.org/10.13172/2052-0069-2-1-497>
- Sharma, J., Vashishtha, M., & Shah, D. O. (2014). Crystallite size dependence on structural parameters and photocatalytic activity of microemulsion mediated synthesized ZnO nanoparticles annealed at different temperatures. *Global Journal of Science Frontier Research: B Chemistry*, 14(5), 18-32.
- Shu, J., Wang, Z., Huang, Y., Huang, N. R. C., & Zhang, W. (2015). Adsorption removal of Congo red from aqueous by polyhedral Cu₂O nanoparticles: Kinetics, isotherms dan thermodynamics mechanism analysis. *Journal of Alloys and Compounds*, 633, 338-346. <https://doi.org/10.1016/j.jallcom.2015.02.048>
- Sivakarthik, P., Thangraj, V., Perumalraj, K., & Balaji, J. (2016). Synthesis of co-doped tin oxide nanoparticles for photocatalytic degradation of synthetic organic dyes. *Digest Journal of Nanomaterials and Biostructures*, 11(3), 935-943.
- Sudha, D., & Sivakumar, P. (2015). Review on the photocatalytic activity of various composite catalysts. *Chemical Engineering and Processing: Process Intensification*, 97, 112-133. <https://doi.org/10.1016/j.cep.2015.08.006>

- Wahyuningsih, S., Estiningsih, P., Anjani, V., Saputri, L. N. M. Z., Purnawan, C., & Pramo, E. (2017). Enhancing remazol yellow FG decoloration by adsorption and photoelectrocatalytic degradation. *Molekul*, *12*(2), 126-132. <http://dx.doi.org/10.20884/1.jm.2017.12.2.321>
- Wan, N., Lu, X., Wang, Y., Zhang, W., Bai, Y., Hu, Y. S., & Dai, S. (2016). Improved Li storage performance in SnO₂ nanocrystals by a synergetic doping. *Scientific Reports*, *6*(1), Article 18978. <https://doi.org/10.1038/srep18978>
- Yehia, M., Labib, S., & Ismail, S. M. (2019). Structural, optical and magnetic properties of co-doped SnO₂ nanoparticles. *Journal of Electronic Materials*, *48*, 4170-4178. <https://doi.org/10.1007/s11664-019-07179-6>

Review Article

The Compilation Records of Fireflies (Coleoptera: Lampyridae) Diversity and Distribution and Display Trees Throughout Malaysia

Nurhafizul Abu Seri and Azimah Abd Rahman*

GeoInformatic Unit, Geography Section, School of Humanities, Universiti Sains Malaysia, 11800 USM, Pulau Pinang, Malaysia

ABSTRACT

The populations of fireflies (Coleoptera: Lampyridae) are increasingly being threatened, and it is, thus, a significant problem in Southeast Asia, particularly Malaysia. Fireflies and their habitat must immediately be protected before they go extinct. Simpson's Diversity Index used in this paper review to measure the diversity of firefly species across Malaysia. The Simpson's Diversity Index showed that the richness and evenness of firefly species in Malaysia is infinite diversity with $D = 0.2255$. The authors compiled and reviewed the studies on the firefly species to incorporate available information/data and emphasised their preferred habitat/display trees in response to the issue. Therefore, this paper was also able to track down records of fireflies' species' distribution through the previous studies in eight states in West Malaysia (Peninsula), namely Johor, Kelantan, Kuala Lumpur, Pahang, Perak, Negeri Sembilan, Selangor, and Terengganu, as well as two states in East Malaysia (Borneo), namely Sabah and Sarawak. It indicates that firefly species, especially from the genera *Pteroptyx* (*Pteroptyx tener* species), are widely distributed in Peninsular Malaysia and East Malaysia. Based on the records from the study conducted by previous researchers, it was found that the population of fireflies is declining in some areas in Malaysia, and so are their habitats and host/display trees that have suffered the same decline. Perhaps,

this paper will help broaden human beings' geographical understanding/knowledge and create awareness which eventually leads to conservation actions of firefly species and their host/display trees.

ARTICLE INFO

Article history:

Received: 16 November 2021

Accepted: 11 February 2022

Published: 20 April 2022

DOI: <https://doi.org/10.47836/pjst.30.3.11>

E-mail addresses:

nurhafizul.abuseri97@gmail.com (Nurhafizul Abu Seri)

azimahrahman@usm.my (Azimah Abd Rahman)

* Corresponding author

Keywords: Coleoptera, distribution, fireflies, Lampyridae, population

INTRODUCTION

Fireflies are categorised in the beetle family Lampyridae. They are made up of ten subfamilies, with around 2200 species described worldwide (Martin et al., 2019). Fireflies are from the Lampyridae family and are not classified as “flies” since flies have only one pair of wings while all other winged insects have two or four wings (Mahadimenakbar & Saikim, 2016). Fireflies have four growth stages: eggs, larvae, pupae, and adults. Within 24 to 48 hours post-mating, adult female fireflies will lay 80 to 150 eggs. Adult female fireflies will die two to three hours after oviposition. After that, the eggs will be incubated for two to four weeks. The newly emerged larvae will feed on the mangrove snail (*Cyclotropis carinata*) (Nallakumar, 2003). If these snails are not found in the area, the larvae will eat any species of snail that is available. Lastly, the larvae prepare for pupation by making a soiled space in the soil, where they will dwell for six to ten days until they emerge as adult fireflies (Nallakumar, 2003).

Luciola pupilla, *Pteroptyx malacca*, and *Pteroptyx tener* are three species found predominantly in Southeast Asian countries, including Malaysia (Razak & Sulaiman, 2016), and this region is home to a wide range of *Pteroptyx* fireflies (Ballantyne et al., 2019; Jusoh et al., 2018). The most common species of fireflies in Malaysia are *Pteroptyx tener* and *Pteroptyx bearni* (Jusoh et al., 2018). The fireflies from the genus *Pteroptyx* are mainly linked with the aquatic-terrestrial ecotone near the edge of mangrove forests, where they congregate (Foo & Mahadimenakbar, 2017). *Pteroptyx tener* congregates in large colonies every night in certain mangrove trees along tidal rivers, providing a stunning bioluminescent flash (Jusoh et al., 2010b), ranking them among the fascinating insects due to their spectacular bioluminescent flash (Oba et al., 2011). Male and female fireflies have distinct flashes of light to help them find mates (Buck & Buck, 1968).

In certain regions, it is reported that habitat loss and degradation have led to the reduction of firefly populations (Khoo et al., 2012; Wong & Yeap, 2012). For example, in Malaysia, the mangrove *Pteroptyx tener* have already experienced a significant decline (Jusoh & Hashim, 2012). A recent global survey has identified three major threats to firefly species in Australia, Central America, East Asia, North America, South America, South Asia, Southeast Asia and the United Kingdom and Europe that include habitat loss and fragmentation, adult dating disorders due to the artificial light at night (ALAN) and excessive use of pesticides (Lewis et al., 2020). It is critical to address this issue since there is a possibility that fireflies are a vital natural pollinator in ecosystems (Sulaiman et al., 2020). As well known, insects are vital pollinators, and many plants rely exclusively on insects for reproduction (Ollerton, 2017; Paudel et al., 2015). Furthermore, fireflies feed primarily on nectar (Nallakumar, 2003).

For the effective conservation of firefly populations, a thorough understanding of their range, abundance, and habitat requirements is needed (Takeda et al., 2006). Cheng

et al. (2020) mentioned that fireflies in the genus *Pteroptyx* are designated as a potential flagship group, umbrella species or indicator species for biodiversity conservation and environmental health in Southeast Asia. It is based on several characteristics, such as adult fireflies in estuarine ecosystems in areas of the region are easier to spot and quantify because of their synchronised flashing behaviour. The *Pteroptyx tener* larvae reside in the topsoil horizon/organic layer, daily inundated by the tidal river. They spend most of their time in this area hunting for their host (*Cyclotropis carinata*; Assimineidae); Finally, their eggs and pupae that also live in the topsoil horizon can be used as effective gauges/indicators of environmental health. Settling on the topsoil horizon makes them extremely sensitive to water and soil quality changes.

Looking at the problems faced by this insect species (fireflies) as well as the lack of studies conducted in some areas, for example, Jusoh et al. (2020) mentioned that although synchronous flashing fireflies of the genus *Pteroptyx* are found across Southeast Asia, very little is known about their biodiversity. Abdullah et al. (2021) also stated that in Malaysia, the records of firefly populations in Sarawak are still lacking compared to Malaysia Peninsula and Sabah. Then according to Chung (2007), a body of research on the diversity of beetles has been conducted in Malaysia; however, due to the high diversity of beetles, the understanding of taxonomy, diversity, species groupings, and ecology is still insufficient. Therefore, the primary purpose of this paper is to compile the records of congregating firefly distribution throughout Malaysia. By knowing the areas that have not yet been covered in the study related to the biodiversity of this species, the researchers and those responsible for wildlife management and forestry can do better planning. Meanwhile, the second objective of this paper is to identify the display tree species favoured by fireflies in Malaysia. Listing the types of tree species chosen by fireflies as host/display trees will help preserve and conserve the tree species.

FIREFLY LIST AND SPECIES DIVERSITY IN MALAYSIA

Bassot and Polunin (1967) were the first to study congregating fireflies in Peninsular Malaysia (Benut River mangrove on the west coast of Johore). *Colophotia*, *Luciola*, *Lychnuris*, and *Pteroptyx* are the four groups of fireflies found in Peninsular Malaysia (Nada & Kirton, 2004; Nallakumar, 2003). The *Pteroptyx* population size changed over time is very concerning (Jusoh et al., 2010a) because one of these species, *Pteroptyx tener*, was a widespread species in Malaysia (Foo & Mahadimenakbar, 2017). If there is a reduction in the number of these species, then it will affect the number of fireflies species found throughout Malaysia. The *Pteroptyx tener* is found at various locations in Peninsular Malaysia, such as in Sungai Sepetang, Perak (Hazmi & Sagaff, 2018; Norela et al., 2017), Sungai Bernam, Selangor (Shahara et al., 2017), Sungai Johor, Johor (Norela et al., 2016) and Chukai River, Kemaman (Mahmod et al., 2018). The Malaysian Nature Society (MNS)

performed a nationwide survey on Congregating Firefly Zones (CFZs) in Malaysia between 2009 and 2010. The goal of the survey was to determine the status of land use, hazards, ecotourism potential, and other features in 28 main CFZs. The majority of CFZs have one to four congregating firefly species, with the east coast having a larger concentration of CFZs. Figure 1 below shows the 58 Congregating Firefly Zones (CFZs) in Peninsular Malaysia (Wong & Yeap, 2012), while Figure 2 shows the location of firefly species that have been found throughout Peninsular Malaysia and Borneo (Sabah and Sarawak).

In Rembau River, a total of 87 colonies of *Pteroptyx* were detected, while in Linggi (two colonies), Ramuan China Besar (13 colonies), and Ramuan China Kechil (20 colonies) (Jusoh et al., 2010a). Hazmi and Sagaff (2018) carried out a study in March, May, and June 2014, successfully collecting 3044 individuals of adult *Pteroptyx tener* fireflies along the Sungai Sepetang in Kampung Dew Perak. The study found that the abundance of the firefly population in Sungai Sepetang dropped as the concentration of heavy metals in the river water increased where the Water Quality Index (WQI) was acquired with polluted status (59%). Meanwhile, firefly eggs and larvae have been discovered to survive on soil with a high percentage of silt (Hazmi & Sagaff, 2018). Mahmud et al. (2018) collected 505 fireflies in Chukai River Kemaman, Terengganu, between November 2017 and April 2018, representing three species: *Pteroptyx tener* Olivier (503 individuals, 99.6%), *Pteroptyx malacca* Gorham, and *Pteroptyx valida* Olivier (1 individual, 0.2% respectively). In addition, *Pteroptyx valida* is very uncommon in the Klias Peninsula, Sabah (Mahadimenakbar et al., 2007).

In the meantime, a study conducted by Foo and Mahadimenakbar (2017) in the eastern part of Malaysia in three locations in Sabah (Garama River, Teratak River and Weston River) recorded about 1,750 individuals representing four species (namely *Pteroptyx bearni* Ballantyne, *Pteroptyx malacca* Gorham, *Pteroptyx tener* Olivier, and *Pteroptyx valida* Olivier). *Pteroptyx tener* (344 individuals) and *Pteroptyx malacca* (306 individuals) were the most common species in Weston River. In contrast, *Pteroptyx tener* (187 individuals) was the most common in Garama River and *Pteroptyx bearni* (255 individuals) was most common in Teratak River. In addition, Foo and Mahadimenakbar (2016) reported that the *Pteroptyx bearni* was also a dominant firefly species found in the mangrove forest of Kawang in Sabah, Malaysia.

Pteroptyx bearni was documented in Miri, Sarawak (Niah River, Sibuti River and Raan River), Terengganu (Kerteh River) on the East Coast of Peninsular Malaysia (Jusoh et al., 2011; Abdullah et al., 2021). In Sarawak, *Pteroptyx bearni* has also been recorded in various locations, including Balingian, Bintulu, Kadulit, and Raan, indicating that both species are widespread in Sarawak (Jusoh et al., 2018). Two hundred ninety-six individual fireflies were reported in Miri, Sarawak, Malaysia, notably *Pteroptyx bearni* Olivier 1909 and *Pteroptyx malacca* Gorham 1880. Both species were found in the Niah River (146 individuals), the

Sibuti River (97 individuals), and the Raan River (53 individuals) (Abdullah et al., 2021). The population of *Pteroptyx bearni* in Likas, Sabah, recorded a very alarming decline triggered by the loss of mangroves. Most worrying is when *Pteroptyx bearni* is found to no longer exist in Likas, and it can be concluded that it is likely that the species is going to extinct (Mahadimenakbar & Saikim, 2016). At the same time, *Pteroptyx gelasina* also suffered the same fate as *Pteroptyx bearni* when the species was no longer found in Likas, Sabah (Mahadimenakbar & Saikim, 2016). Therefore, a study needs to be done in the Likas area, Sabah, to determine the actual situation of these two species, whether they are entirely extinct, and the cause of the loss of the species there.

In the work of Jusoh et al. (2018), there was only one record of *Pteroptyx malaccae* in Sarawak, which is in Limbang. Meanwhile, Abdullah et al. (2021) have successfully recorded the first presence of this species in Niah River, Miri, Sarawak. In 2014 this species was also found in Teratak River, Sabah (Foo & Mahadimenakbar, 2015). Apart from Sabah and Sarawak, this species has also been recorded in Rembau, Negeri Sembilan (Jusoh et al., 2010a), then in Muar, Johor, Chukai, Terengganu and Sungai Pahang Tua, Pahang (Jusoh et al., 2018). However, due to urbanisation and resettlement, fireflies in the Rembau-Linggi River are almost gone (Jusoh & Hashim, 2012). At the same time, *Pteroptyx asymmetria* has only been found in the western region of Peninsular Malaysia (Jusoh et al., 2018). *Pteroptyx* fireflies are known to flash synchronously but not the *Pteroptyx asymmetria* males. Instead of perching on the display trees, *Pteroptyx asymmetria* males are likely to fly about the tops of their trees (Jusoh et al., 2018).

In October 2018, a new record of three species, *Pygoluciola wittmeri*, *Luciola* sp., and eleven out of 17 larvae, was discovered in Kangkawat Research Station, Imbak Canyon, Sabah (genus *Pyrocoelia* sp.). There were 33 solitary fireflies (3 adult males; 13 adult females), and 17 larvae were collected (Mobilim & Mahadimenakbar, 2020). Ballantyne and Lambkin (2006) and Nada and Ballantyne (2018) also stated that the species of *Pygoluciola* fireflies was found in Malaysia, which proves that other species of fireflies other than *Pteroptyx* also exist in Malaysia. It suggests that there is a possibility that there are not many studies done concerning the species that are still not widely covered. Perhaps *Pteroptyx* is somewhat synonymous with its habitat in mangrove areas, but other species inhabit the non-mangrove areas. These species are not as well known as *Pteroptyx* because they can only be found in a few places. For example, *Luciola* sp. in the Maliau Basin (Muslim et al., 2010); *Lychnuris opaca* in Tabin Wildlife Reserve (Chung & Binti, 2008); *Pygoluciola dunguna* Nada sp. nov in Dungun, Jengai Forest Reserve (Nada & Ballantyne, 2018); *Pygoluciola guigliae* and *Pygoluciola wittmeri* in Mahua, Sabah (Ballantyne & Lambkin, 2006); *Pygoluciola kinabalua* found in Mesilau, Sabah (Ballantyne & Lambkin, 2001) and *Pygoluciola wittmeri* in Kionsom, Sabah (Chey, 2008). Three non-synchronised firefly genera were found from December 2011 until January 2013 in UNESCO Chini Lake

Biosphere Reserve, namely *Colophotia* sp., *Pygoluciola* sp. and *Pyrocoelia* sp. (Roslan & Sulaiman, 2015). However, no further studies have been done to prove the existence of fireflies except *Pteroptyx* in non-mangrove areas.

To conclude the findings of this paper review, the authors have utilised Simpson's Diversity Index to highlight the diversity of firefly species found throughout Malaysia. Simpson's Diversity Index showed that the richness and evenness of firefly species in Malaysia is infinite diversity with $D = 0.2255$ (Table 2).

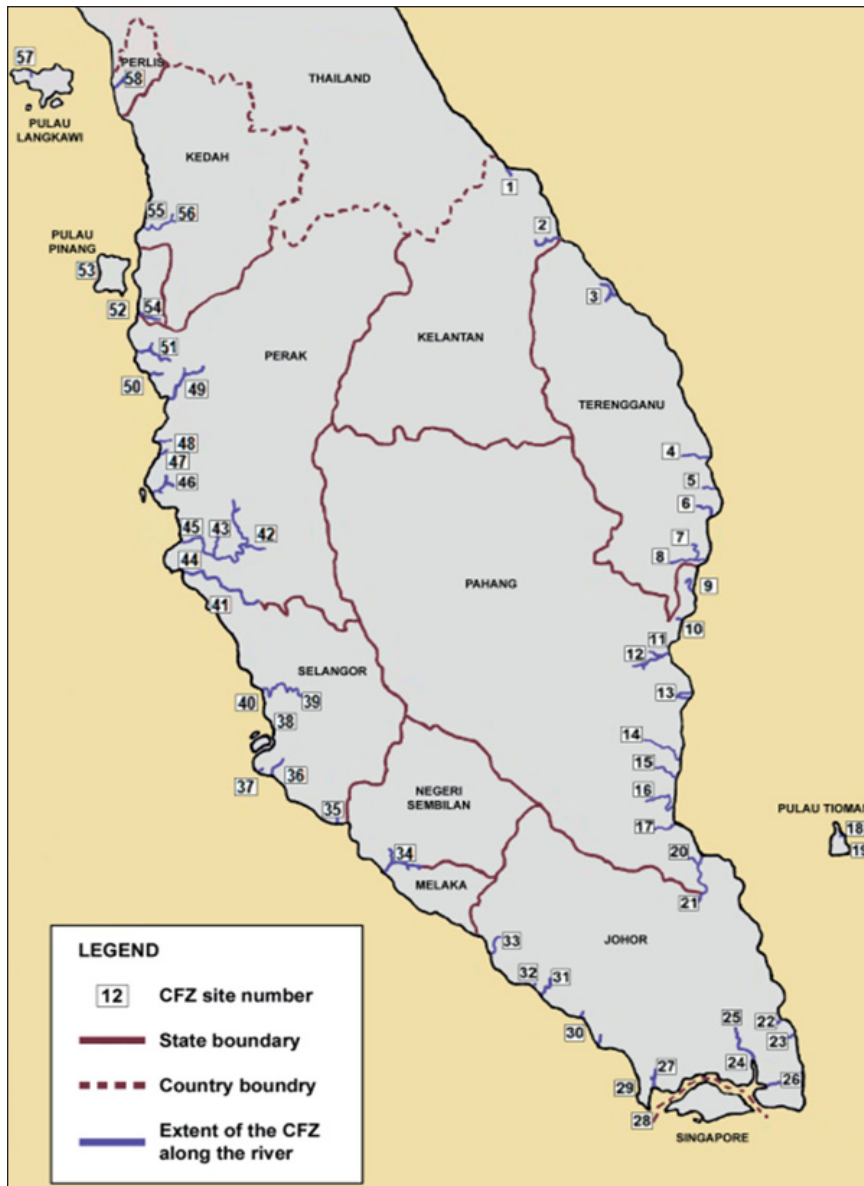


Figure 1. The 58 congregating firefly zones (CFZs) in Peninsular Malaysia (Wong and Yeap, 2012)

Table 1
The compilation of firefly species recorded in Malaysia

No.	Species	Location	References
1	<i>Abscondita berembun</i> Nada sp. nov.	<ul style="list-style-type: none"> Negeri Sembilan (Mount Berembun) Pahang (Fraser's Hill) Perak (Mount Liang) 	Ballantyne et al. (2019)
2	<i>Abscondita jerangau</i> Nada sp. nov.	<ul style="list-style-type: none"> Terengganu (Jerangau Forest Reserve; Pasir Raja Selatan Forest Reserve) 	Ballantyne et al. (2019)
3	<i>Abscondita pallescens</i> (Gorham 1880) comb. nov.	<ul style="list-style-type: none"> Kelantan (Banjaran Titi Wangsa Kampong Lawa) Kuala Lumpur Negeri Sembilan (Mount Berembun; Mount Besar Hantu) Pahang (Cameron Highlands Tanah Rata; Fraser's Hill; Mager Trail; Kuala Tahan National Park) Penang (Penang Hills) Perak (Mount Kledang; Mount Liang; Larut Hills) Sarawak (Mount Mulu National Park; Matang; Mount Dempo; Mount Dulit; Mount Merinjak; Quop) Selangor (Canopy Walkway Trail; Forest Research Institute Malaysia; Gombak Valley; Mount Nuang; Mersawa Trail; Selangor Museum near L gardens) Terengganu (Besul Forest Reserve; Hulu Terengganu Tambahan Forest Reserve; Jengai Forest Reserve; Jerangau Forest Reserve; Pasir Raja Barat Forest Reserve; Pasir Raja Selatan Forest Reserve) 	Ballantyne et al. (2019)
4	<i>Atripennis</i> Pic 1934	<ul style="list-style-type: none"> Malaysia Peninsula (Specific location not stated) 	Ballantyne et al. (2019)
5	<i>Baolacus lajoyei</i> Pic, 1915	<ul style="list-style-type: none"> Malaysia (Specific location not stated) 	Janisova and Bocakova (2013)
6	<i>Colophotia brevis</i>	<ul style="list-style-type: none"> Malaysia Peninsula (Specific location not stated) 	Jusoh et al. (2018)
7	<i>Colophotia brevis</i> Olivier	<ul style="list-style-type: none"> Pahang (Chini Lake) Negeri Sembilan (Mount Besar Hantu) Selangor (Mount Nuang) Terengganu (Besul Forest Reserve; Jengai Forest Reserve; Jerangau Forest Reserve) 	Ballantyne et al. (2019)

Table 1 (continue)

No.	Species	Location	References
8	<i>Colophotia miranda</i> Olivier 1886	Sarawak (Specific location not stated)	Ballantyne et al. (2019)
9	<i>Colophotia praeusta</i>	East Malaysia (Specific location not stated)	Jusoh et al. (2018)
10	<i>Colophotia</i> sp.	Pahang (Chini Lake)	Roslan and Sulaiman (2015)
11	<i>Drilaster axillaris</i> Kiesenwetter, 1879	Malaysia (Specific location not stated)	Janisova and Bocakova (2013)
12	<i>Emasia</i> gen. nov.	Borneo (Specific location not stated)	Bocakova and Janisova (2010)
13	<i>Emasia dentata</i> sp. n.	Borneo (Specific location not stated)	Bocakova and Janisova (2010)
14	<i>Kuantana menayah</i> Ballantyne sp. nov.	Selangor (Selangor River)	Ballantyne et al. (2019)
15	<i>Luciola chapaensis</i> Pic 1923	<ul style="list-style-type: none"> • Kelantan (Banjaran Titiwangsa Kampong Lawa) • Pahang (Cameron Highlands) 	Ballantyne et al. (2019)
16	<i>Luciola jengai</i> Nada sp. nov.	<ul style="list-style-type: none"> • Pahang (Fraser's Hill) • Perak (Mount Liang) • Negeri Sembilan (Mount Besar Hantu) • Terengganu (Jengai Forest Reserve; Pasir Raja Barat Forest Reserve) 	Ballantyne et al. (2019)
17	<i>Luciola lata</i> Olivier 1883	<ul style="list-style-type: none"> • Sabah (Danum Valley) • Sarawak (4th division Grn. Mulu NP; Quop) 	Ballantyne et al. (2019)
18	<i>Luciola niah</i> Jusoh sp. nov.	Sarawak (Kapit; Lambir Hill; Long Aton; Ulu Baram; Niah National Park Forest track)	Ballantyne et al. (2019)
19	<i>Luciola pallidipes</i> Pic 1928	<ul style="list-style-type: none"> • Pahang (Fraser's Hill; Bishop Trail; Taman Negara: Kuala Tahan) • Perak (Banjaran Bintang Bukit Berapit) 	Ballantyne et al. (2019)
20	<i>Luciola Pygoluciola</i> kinabalu	Sabah (Kundasang; Mesilau; Mount Kinabalu)	Ballantyne and Lambkin (2001)
21	<i>Luciola</i> sp.	Sabah (Kangkawat Research Station)	Mobilim and Mahadimenakbar (2020)
22	<i>Luciola tiomana</i> Ballantyne sp. nov.	<ul style="list-style-type: none"> • Johor (Tioman Island Jungle track) • Terengganu (Pasir Raja Selatan Forest Reserve) 	Ballantyne et al. (2019)
23	<i>Luciola</i> WFA	East Malaysia (Specific location not stated)	Jusoh et al. (2018)

Table 1 (continue)

No.	Species	Location	References
24	<i>Luciolinae maculipennis</i> Olivier	Malaysia (Borneo) (Specific location not stated)	Ballantyne et al. (2016)
25	<i>Medeopteryx fraseri</i> Nada sp. nov.	Pahang (Fraser's Hill Bishop Trail)	Ballantyne et al. (2019)
26	<i>Ototreta subvittata</i> Pic, 1943	Malaysia (Specific location not stated)	Janisova and Bocakova (2013)
27	<i>Ototreta weyersi</i> E. Olivier, 1900	Malaysia (Specific location not stated)	Janisova and Bocakova (2013)
28	<i>Potuninius selangoriensis</i> (<i>Pteroptyx testacea</i>)	East Malaysia (Specific location not stated)	Jusoh et al. (2018)
29	<i>Pteroptyx asymmetria</i>	Perak (Sungai Sepetang)	Abdullah et al. (2019); Jusoh et al. (2018)
30	<i>Pteroptyx asymmetria</i> Ballantyne	Negeri Sembilan (Rembau River)	Asri et al. (2020)
31	<i>Pteroptyx balingiana</i>	East Malaysia (Specific location not stated)	Jusoh et al. (2018)
32	<i>Pteroptyx bearni</i> Ballantyne	Sabah (Garama River; Teratak River; Weston River)	Foo and Mahadimenakbar (2017)
33	<i>Pteroptyx bearni</i> or <i>Pteroptyx similis</i>	<ul style="list-style-type: none"> • Pahang (Cherating River) • Sabah (Binsulok River; Kawang River; Kudat Bay; Likas; Paitan River; Sakar Island, Garama River; Kawang River; Klias River; Sungai Sepilok Besar; Sungai Sepilok Kecil; Teratak River; Trayong) 	Ballantyne (2001); Chey (2006); Chey (2008); Chey (2009); Chey (2010); Chey (2011); Faudzi et al. (2021); Foo and Mahadimenakbar (2015); Foo and Mahadimenakbar (2016); Foo et al. (2017); Jusoh et al. (2018); Mahadimenakbar et al. (2007); Mahadimenakbar et al. (2018)
34	<i>Pteroptyx bearni</i> (Olivier, 1909)	Sarawak (Niah River; Sibuti River; Raan River)	Abdullah et al. (2021)
35	<i>Pteroptyx galbina</i> Jusoh sp. nov.	Sarawak (Niah; Suria Timon; Ulu Baram)	Ballantyne et al. (2015); Jusoh et al. (2018)
36	<i>Pteroptyx gelasina</i>	Sabah (Binsulok River; Likas; Paitan River; Sakar Island; Sipitang River; Sungai Sepilok Kecil)	Ballantyne (2001); Chey (2006); Chey (2008); Chey (2011); Mahadimenakbar et al. (2018)

Table 1 (continue)

No.	Species	Location	References
37	<i>Pteroptyx gombakia</i> sp. nov.	Selangor (Kuala Lumpur Gombak Valley)	Ballantyne et al. (2015)
38	<i>Pteroptyx malacca</i>	<ul style="list-style-type: none"> • Perak (Sungai Sepetang) • Negeri Sembilan (Rembau River) • Sabah (Binsulok River; Garama River; Sipitang; Kawang River; Klias River; Teratak River; Trayong) 	Abdullah et al. (2019); Ballantyne (2001); Chey (2009); Chey (2010); Foo and Mahadimenakbar (2015); Foo and Mahadimenakbar (2016); Mahadimenakbar et al. (2018)
39	<i>Pteroptyx malacca</i> Gorham	<ul style="list-style-type: none"> • Sabah (Garama River; Weston River) • Negeri Sembilan (Rembau River) • Terengganu (Chukai River) 	Asri et al. (2020); Foo and Mahadimenakbar (2017); Mahadimenakbar et al. (2007); Mahmood et al. (2018)
40	<i>Pteroptyx malacca</i> (Gorham, 1880)	<ul style="list-style-type: none"> • Sarawak (Niah River) 	Abdullah et al. (2021)
41	<i>Pteroptyx malacca</i> Group 2	Peninsular Malaysia (Specific location not stated)	Jusoh et al. (2018)
42	<i>Pteroptyx malacca</i> Group 3	Peninsular Malaysia (Specific location not stated)	Jusoh et al. (2018)
43	<i>Pteroptyx malacca</i> Group 4	Peninsular Malaysia (Specific location not stated)	Jusoh et al. (2018)
44	<i>Pteroptyx sayangia</i> sp. nov.	Malaysia (Specific location not stated)	Ballantyne et al. (2015)
45	<i>Pteroptyx tener</i>	<ul style="list-style-type: none"> • Perak (Sepetang estuary; Sepetang River) • Negeri Sembilan (Linggi River; Rembau River) • Sabah (Abai; Binsulok River; Garama River; Klias River; Teratak River) • Selangor (Bernam River; Kg. Kuantan; Selangor River) • Terengganu (Chukai River) 	Abdullah et al. (2019); Ballantyne (2001); Cheng et al. (2017); Cheng et al. (2020); Chey (2010); Foo and Mahadimenakbar (2015); Hazmi and Sagaff (2018); Jusoh et al. (2010b); Jusoh et al. (2018); Khoo et al. (2012); Mahadimenakbar et al. (2018); Othman et al. (2018); Shahara et al. (2017)
46	<i>Pteroptyx tener</i> Olivier	<ul style="list-style-type: none"> • Sabah (Garama River; Teratak River; Weston River) • Selangor (Selangor River) • Negeri Sembilan (Rembau River) • Terengganu (Chukai River) 	Asri et al. (2020); Foo and Mahadimenakbar (2017); Mahadimenakbar et al. (2007); Mahmood et al. (2018); Salleh et al. (2019)

Table 1 (continue)

No.	Species	Location	References
47	<i>Pteroptyx valida</i>	<ul style="list-style-type: none"> Sabah (Binsulok River; Teratak River) Terengganu (Chukai River) 	Foo and Mahadimenakbar (2015); Mahadimenakbar et al. (2018)
48	<i>Pteroptyx valida</i> Group 2	Malaysia (Specific location not stated)	Jusoh et al. (2018)
49	<i>Pteroptyx valida</i> Olivier	<ul style="list-style-type: none"> Sabah (Garama River; Teratak River; Weston River) Terengganu (Chukai River) 	Foo and Mahadimenakbar (2017); Mahadimenakbar et al. (2007); Mahmood et al. (2018)
50	<i>Pyrocoelia analis</i>	Peninsular Malaysia (Specific location not stated)	Jusoh et al. (2018)
51	<i>Pygoluciola dunguna</i> Nada sp. nov.	<ul style="list-style-type: none"> Banjarian Titiwangsa Negeri Sembilan (Mount Besar Hantu; Mount Berembun) Perak (Mount Liang) Selangor (Bukit Kutu; Mount Nuang) Terengganu (Besul; Besul Tambahan; Dungun Timber Complex; Hulu Terengganu Tambahan; Jengai; Jerangau; Pasir Raja Barat; Pasir Raja Selatan) 	Ballantyne et al. (2019); Nada and Ballantyne (2018)
52	<i>Pygoluciola nitescens</i> (Olivier 1903b) comb. nov.	Sabah (Ranau)	Ballantyne et al. (2019)
53	<i>Pygoluciola</i> sp.	Pahang (Chini Lake)	Roslan and Sulaiman (2015)
54	<i>Pygoluciola witimeri</i>	Sabah (Kangkawat Research Station)	Mobilim and Mahadimenakbar (2020)
55	<i>Pyrophanes semilimbata</i> (Olivier)	Sabah (Likas; Sandakan)	Ballantyne et al. (2015)
56	<i>Pyrocoelia</i> sp.	<ul style="list-style-type: none"> Pahang (Chini Lake) Sabah (Kangkawat Research Station) 	Mobilim and Mahadimenakbar (2020); Roslan and Sulaiman (2015)

Simpson's Diversity Index

D = Diversity index

N = The total number of organisms of a particular species

N = The total number of organisms of all species

$$D = 1 - \left(\frac{\sum n(n-1)}{N(N-1)} \right)$$

Table 2
Simpson's Diversity Index of firefly species in Malaysia

Species	Number of Adult Fireflies (n)	n(n-1)	References
<i>Luciola</i> sp.	2	2	Mobilim and Mahadimenakbar (2020)
<i>Pteroptyx asymmetria</i> Ballantyne	2	2	Asri et al. (2020)
<i>Pteroptyx bearni</i> Ballantyne	1750	3,060,750	Foo and Mahadimenakbar (2017)
<i>Pteroptyx bearni</i> or <i>Pteroptyx similis</i>	2655	7,046,370	Faudzi et al. (2021); Foo et al. (2017); Foo and Mahadimenakbar (2016); Mahadimenakbar et al. (2007); Mahadimenakbar et al. (2018)
<i>Pteroptyx bearni</i> (Olivier, 1909)	277	76,452	Abdullah et al. (2021)
<i>Pteroptyx gelasina</i>	2	2	Mahadimenakbar et al. (2018)
<i>Pteroptyx malaccae</i>	9	72	Mahadimenakbar (2015); Mahadimenakbar et al. (2018)
<i>Pteroptyx malaccae</i> Gorham	375	140,250	Asri et al. (2020); Foo and Mahadimenakbar (2017); Mahadimenakbar et al. (2007); Mahmud et al. (2018)
<i>Pteroptyx malaccae</i> (Gorham, 1880)	19	342	Abdullah et al. (2021)
<i>Pteroptyx tener</i>	3051	9,305,550	Foo and Mahadimenakbar (2015); Hazmi and Sagaff (2018); Mahadimenakbar et al. (2018)
<i>Pteroptyx tener</i> Olivier	2594	6,726,242	Asri et al. (2020); Mahadimenakbar et al. (2007); Foo and Mahadimenakbar (2017); Mahmud et al. (2018)
<i>Pteroptyx valida</i>	10	90	Foo and Mahadimenakbar (2015); Mahadimenakbar et al. (2018)
<i>Pteroptyx valida</i> Olivier	28	756	Foo and Mahadimenakbar (2017); Mahadimenakbar et al. (2007); Mahmud et al. (2018)
<i>Pygoluciola dunguna</i> Nada sp. nov.	37	1,332	Nada and Ballantyne (2018)
<i>Pygoluciola wittmeri</i>	1	0	Mobilim and Mahadimenakbar (2020)

Total N = 10812 $\sum n(n - 1) = 26,358,212$

Simpson's Diversity Index = 0.2255

*Notes. D = 0 represents infinite diversity and 1, no diversity

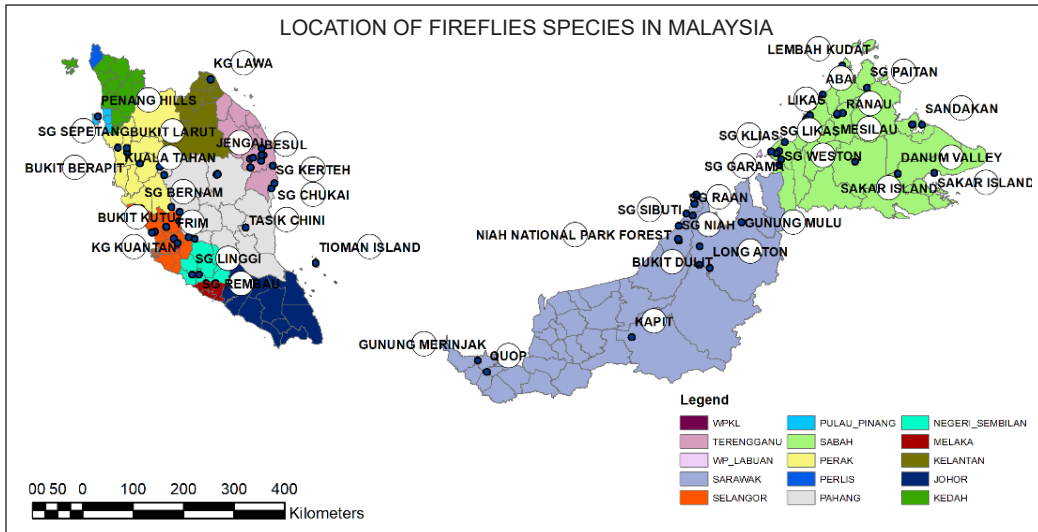


Figure 2. Location of firefly species throughout Malaysia

FIREFLY HABITAT AND HOST/DISPLAY TREES IN MALAYSIA

Firefly habitat is typically situated near the water areas, particularly in mangroves. They lay their eggs near the *Nypa* tree on the riverbanks, and their larvae eat tiny river snails and insects (Hazmi & Sagaff, 2018). According to Ballantyne and McLean (1970), fireflies of the species *Pteroptyx* live in wetlands, estuaries, and brackish water environments. *Pteroptyx* fireflies have been recorded in various mangrove species as display trees (Chey, 2004); however, they are most seen congregating in *Sonneratia caseolaris* (L.) Engl. Trees (Cheng et al., 2017; Jusoh et al., 2010b; Ohba & Wong, 2004) (see figure 3). In conformity with Mahmud et al. (2018), most synchronous fireflies in Chukai River, Terengganu, inhabit *Sonneratia caseolaris* (L.) Engl, which are 432 individuals (85%). Forty-four individuals (9%) inhabit *Hibiscus tiliaceus* L., and 29 individuals (6%) inhabit *Nypa fruticans* Wurm. They also detected fireflies in different vegetation types, such as *Guilandina bonduc* L. and *Barringtonia* sp. However, it does not demonstrate the best synchronisation.

According to Nallakumar (2003), adult fireflies only occupy the young berembang tree (*Sonneratia caseolaris*) associated with *nectaries*. This nectar is a vital nutrient for adult fireflies and a catalyst for the chemical processes that result in synchronised photon flashes. It was also found that this tree is a food source for *Pteroptyx tener* because it contains some amount of sucrose in the sap (Jaafar et al., 2010; Juliana et al., 2012; Nada et al., 2009). The density of firefly larvae was significantly higher in Sago palm groves than in oil palm stands (Kirton et al., 2006). Streambank palms (*Nypa fruticans* and *Metroxylon sago*) are essential food sources for the snail predators the firefly larvae feed (Nada & Kirton, 2004). It is in line with the work of Juliana et al. (2012), who found that the fireflies in Selangor

River are found in Sago's palms (*Metroxylon sago*) and Rengas air (*Gluta velutina*). Kirton et al. (2006) have made a preliminary study to determine firefly larval habitat requirements that show that *Pteroptyx tener* larval densities were high in sago patches (*Metroxylon* spp.), They are low in orchards (mixed fruit tree species) and low in all but one of five oil palm plantation locations (*Elaeis guineensis*).

Pteroptyx tener and *Pteroptyx bearni* adults in Kerteh River, Terengganu, in 2009 were found to select 170 trees from 27 different species located 2–15 km from the estuary as display trees. For instance, most of these fireflies congregated on *Sonneratia caseolaris* (L.) Engl. (22%) of total display sections. Then, this is followed by *Gluta velutina* Blume (15%), *Hibiscus tiliaceus* L. (13%), *Xylocarpus granatum* J. König (9%), *Avicennia alba* Blume (8%), *Rhizophora apiculata* Blume (6%) whilst the remaining individuals were found on other display tree species such as *Brownlowia argentata* Kurtz, *Barringtonia racemosa* (L.) Spreng., *Bruguiera gymnorrhiza* (L.) Lam., *Ceriops decandra* (Griff.) Ding Hou, *Derris trifoliata* Lour, *Excoecaria agallocha* L., and *Nypa fruticans* Wurm (Jusoh et al., 2011).

In contrast to *Sonneratia caseolaris*, fireflies are also reported to be mainly congregating on *Heritiera littoralis* (the dominant trees found in Klias River, Sabah) (Chey, 2004) durian and bachang trees (Nada & Kirton, 2004). In a study conducted by Abdullah et al. (2021), it was found that fireflies were detected to be present in *Pandanus* sp. as a display tree in Sibuti River Sarawak for the first time it was recorded. Meanwhile, fireflies in Bako National Park Sarawak (Sibuti River and Raan River) prefer *Avicennia marina* trees as their display tree (Buck & Buck, 1966). The study conducted by Abdullah et al. (2021) found that *Rhizophora apiculata* was the most preferred display tree for the firefly population in Miri, Sarawak. Aside from that, *Derris* sp., in Raan River, was previously identified as a good display tree for the firefly population in Kerteh River, Terengganu (Jusoh et al., 2011). *Pteroptyx* and its display trees in the Rembau-Linggi Estuary have been studied and found to have the highest abundance percentage (6%) in November and December, while the lowest abundance percentage was observed in January and March (2%). It was also discovered that firefly colonies for two display trees (no. 7 and 10; species unspecified) had disappeared for two months, namely January and March.

Furthermore, one of the display trees died, and the colony that occupied it was relocated to another tree nearby. A tree 50 metres away from the dead tree has around 3% firefly cover (Jusoh et al., 2010a). It concludes that fireflies can inhabit different display trees, and they will need to adapt to the tree species if their original display tree dies or is destroyed. It also proves that fireflies can live or choose display trees other than their common display trees.

Pteroptyx tener is found in estuary ecosystems in Peninsular Malaysia's coastal areas, and it is particularly well-known in Selangor (Selangor River), Rembau, Negeri Sembilan (Sungai Linggi), Kuala Sepetang, Perak (Sungai Sepetang), Johore (Sungai Muar), and Chukai, Terengganu (Chukai River) (Jusoh et al., 2013). In Peninsular Malaysia's

mangrove forests, *Pteroptyx tener* Olivier congregated on several mangrove species, notably *Sonneratia* sp. (Ohba & Wong, 2004). They also suggested that several factors influence firefly species' selection of display trees, including a) the display tree should be at the water's edge, as this allows fireflies to communicate more easily; b) each display tree's leaf arrangement must be ideal for mating (see Figure 3); c) the display tree must be in a healthy condition; d) display trees must have nectar or rubber for adult fireflies if they eat; and e) the larval prey food plant must be closer to the display tree (Ohba & Wong, 2004). Meanwhile, Jusoh et al. (2010b) proposed that favourable display trees for *Pteroptyx* include those that are: a) near the water's edge; b) strong trees; c) near larval food sources; d) supply nectar or rubber for the adults' diet; and e) have an easy-to-communicate leaf arrangement.

According to Cheng et al. (2017), adult *Pteroptyx tener* dietary requirements were unknown, except the suggestion that these insects feed on the nectar and rubber of mangrove trees. In the same investigation, they found only plant DNA and fireflies DNA in extracts of *Pteroptyx tener* gut content DNA fragments which used adult samples of *Pteroptyx tener* fireflies collected from the wild from Selangor, Sepetang (Perak) and Rembau Rivers (Negeri Sembilan) along the west coast of Peninsular Malaysia. The study analysis did not detect *Sonneratia caseolaris* and *Hibiscus tiliaceus* in their gut DNA extracts, although these species relied on the plant for most of their adult lives. In contrast, the analysis discovered a single plant DNA sequence from *Pteroptyx tener* that was similar to the *rbcL* sequences of *Heritiera littoralis* (Malvaceae), *Lawsonia inermis* (Lythraceae), *Aquilaria* sp. and *Gonystylus bancanus* (Thymelaeaceae). All these plants are cultivated and natural, and they may have originated either in hamlets or isolated freshwater swamps located further inland. Thus, with the identification of these four plant DNA sequences in *Pteroptyx tener* gut DNA extracts, possible that the insect species went deep inland to find this host (Cheng et al., 2017).

Pteroptyx mangrove forest habitats are currently jeopardised by urbanisation, industrialisation, and firefly tourism activities (Wong & Yeap, 2012). The destruction of firefly habitats is due to ecotourism activities and local socioeconomic activities (Jaafar et al., 2010). One of the most famous areas for firefly population distribution was around Cherating River in Pahang, Malaysia (Mohd et al., 2019). According to Jusoh and Hashim (2012), 14 of 122 tree species utilised as firefly display trees in 2008 were destroyed in 2010. Based on their mapping, the number of trees inhabited by fireflies has reduced by more than half, from 122 to 57, and no new trees have been used for displays (Figure 4). The decrease and destruction of these trees occurred over a two-decade period due to the Rembau River's mangrove forest being altered. This mangrove forest has also been extensively converted to various land uses like agriculture, aquaculture, and urban areas (Jusoh & Hashim, 2012). According to Kirton et al. (2006), there are three contributors

to the reduction in the total population of fireflies in Kuala Selangor, namely: a) the loss of riverbank vegetation near firefly habitat for development and agricultural activities; b) pesticide usage in oil palm plantations that can affect firefly larvae survival; and c) changes in river water quality caused by pollution or the development of dams and barrages further upstream will also affect the survival of snails and riverside plants on which the fireflies depend. The map in Figure 5 illustrates the distribution of fireflies' display trees in Peninsular Malaysia and Malaysia Borneo (Sabah and Sarawak).

Table 3
Display trees of fireflies in Malaysia

No.	Scientific Name	Location	References
1	<i>Acrostichum aureum</i>	<ul style="list-style-type: none"> Teratak River, Sabah Sepetang Estuary Selangor River, Kampung Kuantan 	Foo and Mahadimenakbar (2015); Jusoh et al. (2010b); Juliana et al. (2012)
2	<i>Aegiceras floridum</i>	<ul style="list-style-type: none"> Kawang River, Sabah 	Foo and Mahadimenakbar (2016)
3	<i>Avicennia alba</i>	<ul style="list-style-type: none"> Teratak River, Sabah Paitan River, Sabah Klias Peninsula, Sabah 	Chey (2006); Foo and Mahadimenakbar (2015); Foo and Mahadimenakbar (2017)
4	<i>Avicennia alba</i> Blume	<ul style="list-style-type: none"> Kerteh River, Terengganu 	Jusoh et al. (2011)
5	<i>Avicennia marina</i>	<ul style="list-style-type: none"> Sibuti River, Miri, Sarawak Raan River, Miri, Sarawak 	Abdullah et al. (2021)
6	<i>Avicennia rumphiana</i>	<ul style="list-style-type: none"> Niah River, Miri, Sarawak 	Abdullah et al. (2021)
7	<i>Barringtonia</i> sp.	<ul style="list-style-type: none"> Chukai River Kemaman, Terengganu 	Mahmod et al. (2018)
8	<i>Barringtonia racemosa</i> (L.) Spreng.	<ul style="list-style-type: none"> Kerteh River, Terengganu 	Jusoh et al. (2011)
9	<i>Brownlowia argentata</i> Kurtz	<ul style="list-style-type: none"> Kerteh River, Terengganu 	Jusoh et al. (2011)
10	<i>Bruguiera gymnorrhiza</i> (L.) Lam.	<ul style="list-style-type: none"> Kerteh River, Terengganu 	Jusoh et al. (2011)
11	<i>Bruguiera parvifolia</i>	<ul style="list-style-type: none"> Raan River, Miri, Sarawak Niah River, Miri, Sarawak Garama River, Sabah 	Abdullah et al. (2021); Mahadimenakbar et al. (2007)
12	<i>Ceriops decandra</i> (Griff.) Ding Hou	<ul style="list-style-type: none"> Kerteh River, Terengganu 	Jusoh et al. (2011)
13	<i>Clerodendrum inerme</i> (Verbenaceae)	<ul style="list-style-type: none"> Garama River, Klias 	Chey (2010)
14	<i>Derris</i> sp.	<ul style="list-style-type: none"> Raan River, Miri, Sarawak 	Abdullah et al. (2021)
15	<i>Derris trifoliata</i> Lour	<ul style="list-style-type: none"> Kerteh River, Terengganu 	Jusoh et al. (2011)
16	<i>Excoecaria agallocha</i> L.	<ul style="list-style-type: none"> Teratak River Kerteh River, Terengganu 	Foo and Mahadimenakbar (2017); Jusoh et al. (2011)
17	<i>Excoecaria indica</i> L.	<ul style="list-style-type: none"> Garama River, Sabah 	Foo and Mahadimenakbar (2017)

Table 3 (continue)

No.	Scientific Name	Location	References
18	<i>Excoecaria indica</i> (Willd.) Muell. Arg. (Euphorbiaceae)	<ul style="list-style-type: none"> Garama River, Sabah Klias River, Sabah 	Chey (2004); Mahadimenakbar et al. (2007)
19	<i>Ficus binjamina</i>	<ul style="list-style-type: none"> Garama River, Sabah 	Mahadimenakbar et al. (2007)
20	<i>Ficus microcarpa</i> (Moraceae)	<ul style="list-style-type: none"> Garama River, Sabah Klias River, Sabah 	Chey (2010)
21	<i>Ficus</i> sp.	<ul style="list-style-type: none"> Selangor River, Kampung Kuantan 	Juliana et al. (2012); Shahara et al. (2017)
22	<i>Glochidion littorale</i> (Euphorbiaceae)	<ul style="list-style-type: none"> Sungai Bernam, Selangor Klias River, Sabah 	Chey (2010)
23	<i>Gluta velutina</i> Blume	<ul style="list-style-type: none"> Kerteh River, Terengganu 	Jusoh et al. (2011)
24	<i>Guilandina bonduc</i> L.	<ul style="list-style-type: none"> Chukai River Kemaman, Terengganu 	Mahmod et al. (2018)
25	<i>Heritiera littoralis</i> Dry. ex W. Ait. (Sterculiaceae)	<ul style="list-style-type: none"> Klias River, Sabah 	Chey (2004)
26	<i>Hibiscus tiliaceus</i>	<ul style="list-style-type: none"> Raan River, Miri, Sarawak Garama River, Sabah 	Abdullah et al. (2021); Cheng et al. (2017); Foo and Mahadimenakbar (2017); Juliana et al. (2012); Mahadimenakbar et al. (2007)
27	<i>Hibiscus tiliaceus</i> L.	<ul style="list-style-type: none"> Kerteh River, Terengganu Chukai River Kemaman, Terengganu 	Jusoh et al. (2011); Mahmod et al. (2018)
28	<i>Lumnitzera littorea</i> (Combretaceae)	<ul style="list-style-type: none"> Kawang River, Sabah 	Chey (2008); Chey (2009); Foo and Mahadimenakbar (2016)
29	<i>Nypa fruticans</i>	<ul style="list-style-type: none"> Garama River, Sabah Sungai Selangor, Kampung Kuantan 	Foo and Mahadimenakbar (2015); Foo and Mahadimenakbar (2017); Jusoh et al. (2010b); Juliana et al. (2012); Mahadimenakbar et al. (2007)
30	<i>Nypa fruticans</i> Wurm	<ul style="list-style-type: none"> Kerteh River, Terengganu Chukai River Kemaman, Terengganu 	Jusoh et al. (2011); Mahmod et al. (2018)
31	<i>Pandanus</i> sp.	<ul style="list-style-type: none"> Sibuti River, Miri, Sarawak 	Abdullah et al. (2021)
32	<i>Rhizophora apiculata</i> (Rhizophoraceae)	<ul style="list-style-type: none"> Raan River, Miri, Sarawak Sibuti River, Miri, Sarawak Niah River, Miri, Sarawak Garama River, Sabah Klias, River Teratak River, Sabah Paitan River, Sabah Mangrove of Sepilok Forest Reserve, Sandakan Sakar Island off coast of Lahad Datu Sabah 	Abdullah et al. (2021); Chey (2004); Chey (2006); Chey (2008); Chey (2010); Chey (2011); Foo and Mahadimenakbar (2015); Foo and Mahadimenakbar (2017); Mahadimenakbar et al. (2007)

Table 3 (continue)

No.	Scientific Name	Location	References
33	<i>Rhizophora apiculata</i> Blume	• Kerteh River, Terengganu	Jusoh et al. (2011)
34	<i>Rhizophora mucronata</i> (Rhizophoraceae)	• Mangrove of Sepilok Forest Reserve, Sandakan • Sakar Island off coast of Lahad Datu Sabah • Kawang River, Sabah	Chey (2008); Chey (2011); Foo and Mahadimenakbar (2016)
35	<i>Rhizophora</i> sp.	• Sepetang Estuary	Jusoh et al. (2010b)
36	<i>Rhizophora stylosa</i>	• Sakar Island off coast of Lahad Datu Sabah	Chey (2011)
37	<i>Scyphiphora hydrophyllacea</i> (Rubiaceae)	• Sakar Island off coast of Lahad Datu Sabah • Paitan River, Sabah • Mangrove of Sepilok Forest Reserve, Sandakan • Trayong, Tuaran	Chey (2006); Chey (2008); Chey (2009); Chey (2011)
38	<i>Sonneratia alba</i> J. Smith	• Weston River, Sabah	Foo and Mahadimenakbar (2017)
39	<i>Sonneratia caseolaris</i>	• Sepetang River, Kampung Dew • Sungai Selangor, Kampung Kuantan • Sepetang Estuary • Bernam River, Selangor	Cheng et al. (2017); Hazmi and Sagaff (2018); Juliana et al. (2012); Jusoh et al. (2010b); Shahara et al. (2017)
40	<i>Sonneratia caseolaris</i> (L.) Engl.	• Kerteh River, Terengganu • Chukai River Kemaman, Terengganu	Cheng et al. (2017); Jusoh et al. (2011); Mahmud et al. (2018)
41	<i>Thespesia populnea</i>	• Raan River, Miri, Sarawak	Abdullah et al. (2021)
42	<i>Xylocarpus granatum</i>	• Sibuti River, Miri, Sarawak	Abdullah et al. (2021); Chey (2006)
43	<i>Xylocarpus granatum</i> J. König	• Kerteh River, Terengganu	Jusoh et al. (2011)

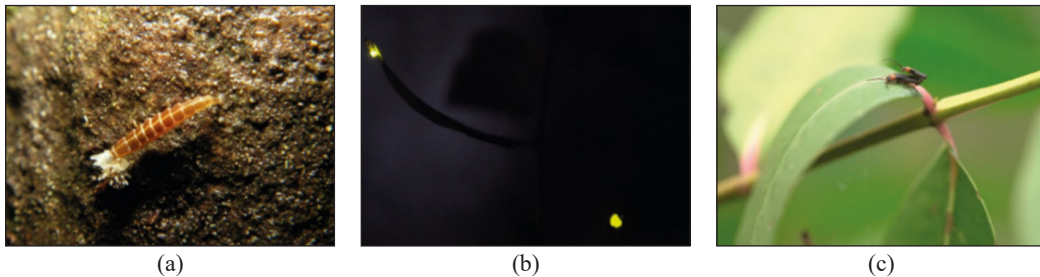


Figure 3. (a) *Pteroptyx tener* larvae feed on *Plectostoma fraternum* in Sukau, Kinabatangan, Sabah; (b) A pair of *Pteroptyx tener* flashes synchronously on a mangrove tree (Malaysia); (c) *Pteroptyx tener* mating in *Sonneratia caseolaris* (Berembang tree) during the day (Malaysia) (Cheng et al., 2021)

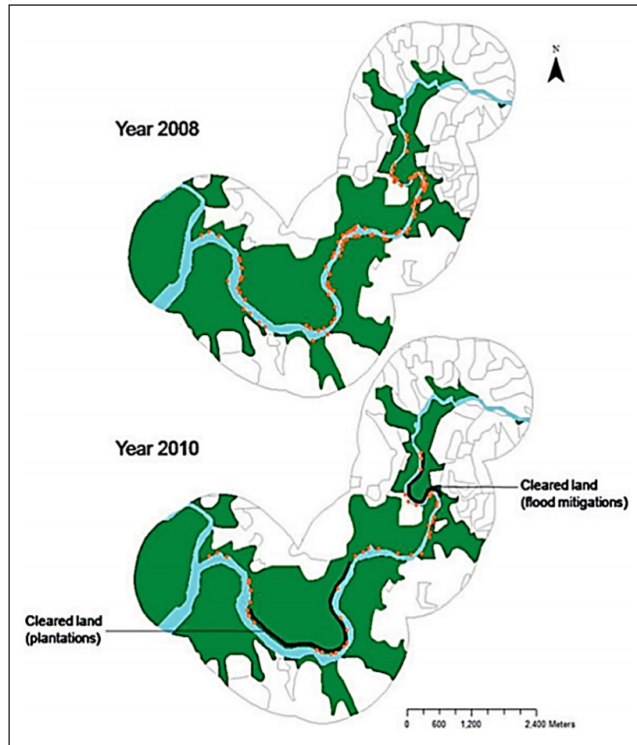


Figure 4. Changes in the number of firefly display trees (orange dots) along the banks of the Rembau-Linggi estuary (2008-2010) (Jusoh and Hashim, 2012)

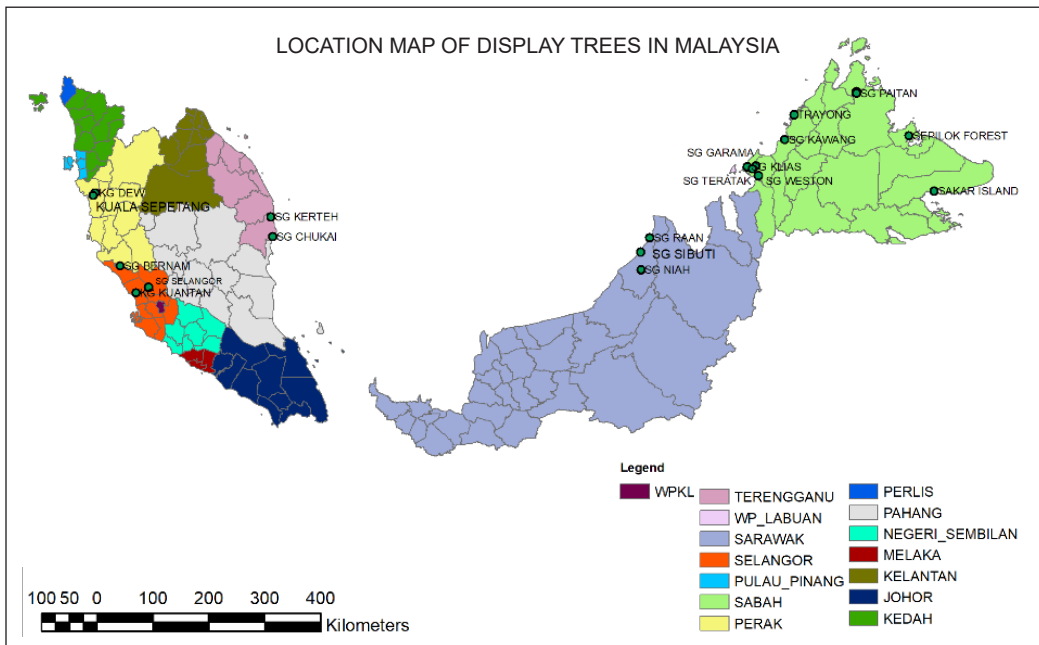


Figure 5. Distribution of firefly's display trees throughout Malaysia

CONCLUSION

Fireflies undergo a complete metamorphosis with four phases in their life cycle: egg, larva, pupa, and adult, all highly dependent on mangrove plants. Although they have been shown to rely on mangrove plants, particularly *Sonneratia caseolaris*, there are trees of other species that also host or display trees for fireflies. Therefore, there is a need to conserve all plant species near their habitat, including the host/display trees utilised by fireflies at different phases of their lifespan. The host/display trees are essential as they depend on different plant species for protection and feed (mangrove snails are a source for their diet). At the same time, the conservation of these plant species would aid in the protection of the diminishing firefly species, particularly in ecotourism hotspots such as Sabah (Likas), Rembau River (Negeri Sembilan), and Kuala Selangor (Selangor). Lastly, the richness and evenness of firefly species in Malaysia are infinite diverse with $D = 0.2255$ according to the Simpson's Diversity Index.

ACKNOWLEDGEMENTS

The Ministry of Higher Education Malaysia financed this research under the Fundamental Research Grant Scheme with project code: FRGS/1/2020/SS0/USM/02/6.

REFERENCES

- Abdullah, N. A., Asri, L. N., Radzi, S. N. F., Musbah, M., Hazmi, I. R., & Sulaiman, N. (2021). Abiotic factors influencing diversity and abundance of congregating fireflies (Coleoptera: Lampyridae) in Miri, Sarawak, Malaysia. *Oriental Insects*, 55(2), 149-164. <https://doi.org/10.1080/00305316.2020.1757529>
- Abdullah, N. A., Radzi, S. N. F., Asri, L. N., Idris, N. S., Husin, S., Sulaiman, A., Khamis, S., Sulaiman, N., & Hazmi, I. R. (2019). Insect community in riparian zones of Sungai Sepetang, Rembau River and Chukai River of Peninsular Malaysia. *Biodiversity Data Journal*, 7, 33-46. <https://doi.org/10.3897/bdj.7.e35679>
- Asri, L. N., Abdullah, N. A., Sulaiman, A., Asri, M. H. M., Sulaiman, N., Satiman, E. M. F. E. N., Husin, S. M., Shukor, A. M., & Darbis, N. D. A. (2020). Abundance and species composition of synchronous flashing firefly at Sungai Rembau, Negeri Sembilan, Malaysia. *International Journal of Tropical Insect Science*, 41, 1095-1106. <https://doi.org/10.1007/s42690-020-00295-5>
- Ballantyne, L. A., & Lambkin, C. (2001). A new firefly, *Luciola (Pygoluciola) kinabalua*, new species (Coleoptera: Lampyridae), from Malaysia, with observations on a possible copulation clamp. *Raffles Bulletin of Zoology*, 49(2), 363-377.
- Ballantyne, L. A., & Lambkin, C. (2006). A phylogenetic reassessment of the rare SE Asian firefly genus *Pygoluciola Wittmer* (Coleoptera: Lampyridae: Luciolinae). *Raffles Bulletin of Zoology*, 54(1), 21-48.
- Ballantyne, L. A., & McLean, M. R. (1970). Revisional studies on the firefly genus *Pteroptyx Olivier* (Coleoptera: Lampyridae: Luciolinae: Luciolini). *Transactions of the American Entomological Society (1890-)*, 96(2), 223-305. <https://www.jstor.org/stable/25077994>

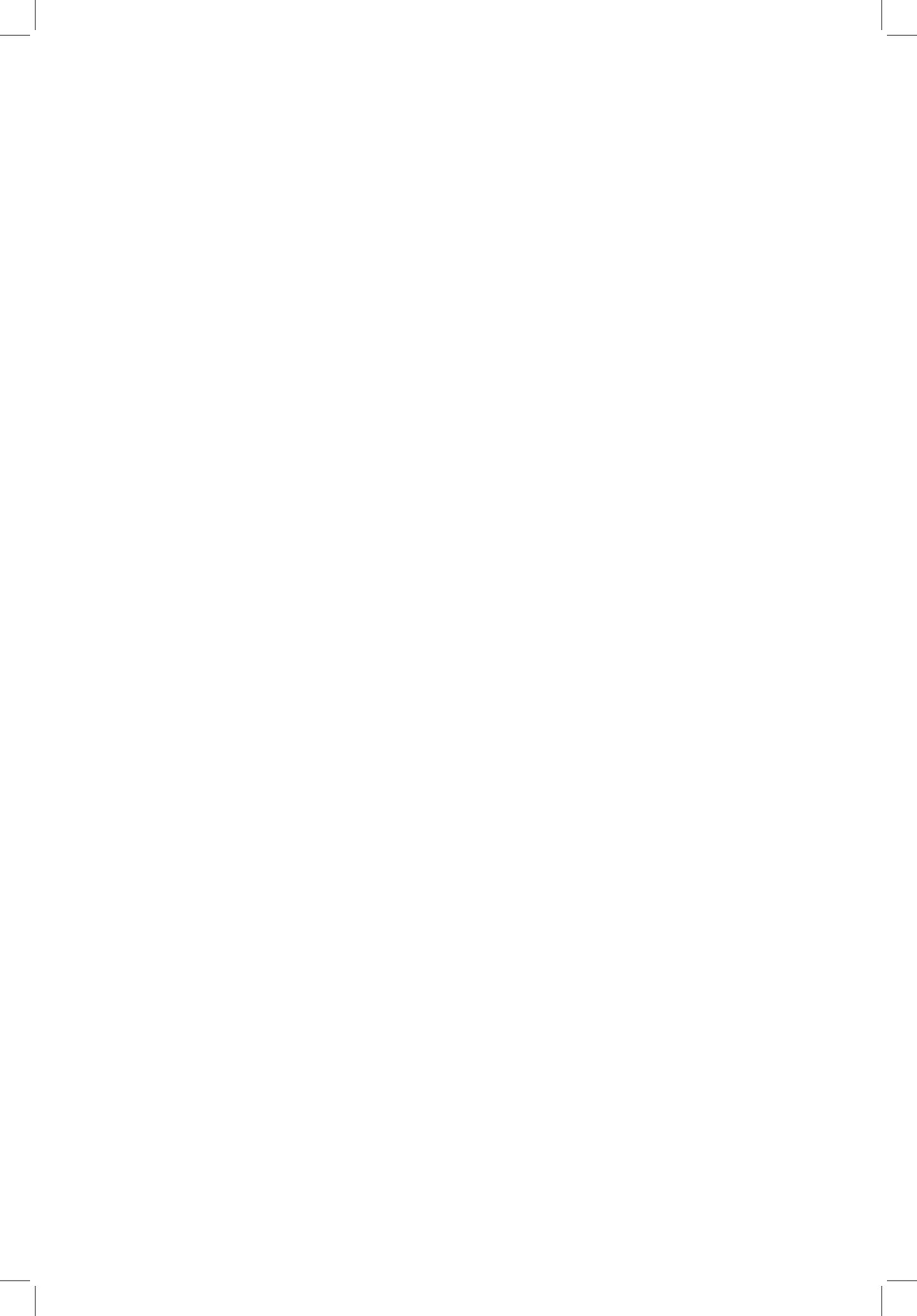
- Ballantyne, L. A., Lambkin, C. L., Ho, J. Z., Jusoh, W. F. A., Nada, B., Nak-Eiam, S., Thancharoen, A., Wattanachaiyingcharoen, W., & Yiu, V. (2019). The Luciolinae of S.E. Asia and the Australopacific region: A revisionary checklist (Coleoptera: Lampyridae) including description of three new genera and 13 new species. *Zootaxa*, 4687(1), 1-174. <https://doi.org/10.11646/zootaxa.4687.1.1>
- Ballantyne, L. A., Lambkin, C. L., Luan, X., Boontop, Y., Nak-Eiam, S., Pimpasalee, S., Silalom, S., & Thancharoen, A. (2016). Further studies on south eastern Asian Luciolinae: 1. *Sclerotia Ballantyne*, a new genus of fireflies with back swimming larvae 2. *Triangulara Pimpasalee*, a new genus from Thailand (Coleoptera: Lampyridae). *Zootaxa*, 4170(2), 201-249. <https://doi.org/10.11646/zootaxa.4170.2.1>
- Ballantyne, L., Lambkin, C. L., Boontop, Y., & Jusoh, W. F. A. (2015). Revisional studies on the Luciolinae fireflies of Asia (Coleoptera: Lampyridae): 1. The genus *Pyrophanes Olivier* with two new species. 2. Four new species of *Pteroptyx Olivier* and 3. A new genus *Inflata* Boontop, with redescription of *Luciola indica* (Motsch.) as *Inflata indica* comb. nov. *Zootaxa*, 3959(1), 1-84. <http://dx.doi.org/10.11646/zootaxa.3959.1.1>
- Bassot, J. M., & Polunin, I. (1967). Synchronous flashing fireflies in the Malay Peninsula. *Science Reports of the Yokosuka City Museum*, 13, 18-23.
- Bocakova, M., & Janisova, K. (2010). A new genus and species of ototretine firefly from Borneo (Coleoptera: Lampyridae). *Zootaxa*, 2347(1), 59-63. <https://doi.org/10.11646/zootaxa.2347.1.3>
- Buck, J., & Buck, E. (1966). Biology of synchronous flashing of fireflies. *Nature*, 211, 562-564. <https://doi.org/10.1038/211562a0>
- Buck, J., & Buck, E. (1968). Mechanism of rhythmic synchronous flashing of fireflies: Fireflies of Southeast Asia may use anticipatory time-measuring in synchronising their flashing. *Science*, 159(3821), 1319-1327. <https://doi.org/10.1126/science.159.3821.1319>
- Cheng, S., Chan, K. M., Ishak, S. F., Khoo, V., & Chew, M. Y. (2017). Elucidating food plants of the aggregative, synchronously flashing Southeast Asian firefly, *Pteroptyx tener* Olivier (Coleoptera, Lampyridae). *BioRisk*, 12, 25-39. <https://doi.org/10.3897/biorisk.12.14061>
- Cheng, S., Faidi, M. A., Tan, S. A., Vijayanathan, J., Malek, M. A., Bahashim, B., & Isa, M. N. M. (2021). Fireflies in Southeast Asia: Knowledge gaps, entomotourism and conservation. *Biodiversity and Conservation*, 30, 925-944. <https://doi.org/10.1007/s10531-021-02129-3>
- Cheng, S., Munian, K., Sek-Aun, T., Faidi, M. A., & Ishak, S. F. (2020). Mitochondrial DNA diversity and gene flow in Southeast Asian populations of the synchronously flashing firefly, *Pteroptyx tener* Olivier (Coleoptera: Lampyridae). *Oriental Insects*, 54(2), 175-196. <https://doi.org/10.1080/00305316.2019.1600594>
- Chey, V. K. (2004). Fireflies of Klias River and their display trees. *Sepilok Bulletin*, 1, 67-69.
- Chey, V. K. (2006). Fireflies of Sungai Paitan. *Sepilok Bulletin*, 5, 1-6.
- Chey, V. K. (2008). Fireflies of Sepilok. *Sepilok Bulletin*, 9, 3-11.
- Chey, V. K. (2009). Fireflies of Tuaran. *Sepilok Bulletin*, 10, 25-33.
- Chey, V. K. (2010). Fireflies of Beaufort with special reference to Sungai Garama and Sungai Klias. *Sepilok Bulletin*, 12, 13-19.

- Chey, V. K. (2011). Fireflies of Sakar Island. *Sepilok Bulletin*, 13&14, 27-32.
- Chung, A. Y. C. (2007). An overview of research on beetle diversity & taxonomy in Malaysia. In L. S. L. Chua, L. G. Kirton, & L. G. Saw (Eds.), *Status of biological diversity in Malaysia and threat assessment of plant species in Malaysia* (pp. 137-148). Forest Research Institute Malaysia (FRIM).
- Chung, A. Y., & Binti, M. (2008, October 20-24). Insect diversity in enhancing nature tourism, with reference to Tabin Wildlife Reserve in Sabah. In *15th Malaysian Forestry Conference* (pp. 1-5). Sarawak, Malaysia.
- Faudzi, R., Abas, A., Othman, N. W., & Mazlan, S. M. (2021). Effect of water quality on the abundance of firefly populations at Cherating River, Pahang, Malaysia. *Environment Asia*, 14(1), 69-79. <https://doi.org/10.14456/ea.2021.8>
- Foo, K., & Mahadimenakbar, M. D. (2015). Diversity of fireflies (Coleoptera: Lampyridae) of Sungai Teratak, Sabah, Malaysia. *Journal of Tropical Biology & Conservation*, 12, 1-11.
- Foo, K., & Mahadimenakbar, M. D. (2016). Short notes on fireflies of Kawang River, Sabah. *Journal of Tropical Biology & Conservation*, 13, 125-128.
- Foo, K., & Mahadimenakbar, M. D. (2017). Diversity of *Pteroptyx* fireflies (Coleoptera: Lampyridae) and their display trees at Klias Peninsula, Sabah, Malaysia. *Journal of Tropical Biology & Conservation*, 14, 95-103.
- Foo, K., Seelan, J. S. S., & Mahadimenakbar, M. D. (2017). Microfungi associated with *Pteroptyx* bearni (Coleoptera: Lampyridae) eggs and larvae from Kawang River, Sabah (Northern Borneo). *Insects*, 8(3), Article 66. <https://doi.org/10.3390/insects8030066>
- Hazmi, I. R., & Sagaff, S. A. S. (2018). Fireflies population and the aquaculture industry (Coleoptera: Lampyridae) of the Sungai Sepetang, Kampung Dew, Perak, Malaysia. *Serangga*, 22(2), 217-237.
- Jaafar, M., Ahmad, A., & Sakawi, Z. (2010). Kemandirian industri eko-pelancongan: Kes tarikan pelancong kelip-kelip Kg. Kuantan [The survival of an eco-tourism industry: Evidence from the Kg. Kuantan's firefly tourist attraction]. *Geografia Online Malaysian Journal of Society and Space*, 6(3), 89-97.
- Janisova, K., & Bocakova, M. (2013). Revision of the subfamily Otoretinae (Coleoptera: Lampyridae). *Zoologischer Anzeiger-A Journal of Comparative Zoology*, 252(1), 1-19. <https://doi.org/10.1016/j.jcz.2012.01.001>
- Juliana, W. W., Shahril, M. M., Rahman, N. N. A., Nurhanim, M. N., Abdullah, M., & Sulaiman, N. (2012). Vegetation profile of firefly habitat along the riparian zones of Sungai Selangor at Kampung Kuantan, Kuala Selangor. *Malaysian Applied Biology*, 41(1), 55-58.
- Jusoh, W. F. A. W., & Hashim, N. R. (2012). The effect of habitat modification on firefly populations at the Rembau-Linggi estuary, Peninsular Malaysia. *Lampyrid*, 2, 149-155.
- Jusoh, W. F. A. W., Hashim, N. R., & Ibrahim, Z. Z. (2010a). Distribution and abundance of *Pteroptyx* fireflies in Rembau-Linggi estuary, Peninsular Malaysia. *Environment Asia*, 3(special issue), 56-60.
- Jusoh, W. F. A. W., Hashim, N. R., & Ibrahim, Z. Z. (2010b). Firefly distribution and abundance on mangrove vegetation assemblages in Sepetang estuary, Peninsular Malaysia. *Wetlands Ecology and Management*, 18, 367-373. <https://doi.org/10.1007/s11273-009-9172-4>

- Jusoh, W. F. A. W., Wong, C. H., & Hashim, N. R. (2011). Zonation of firefly species and their display trees along Kerteh River, Terengganu. *Serangga*, 16(2), 59-66.
- Jusoh, W. F. A., Hashim, N. R., & Adam, N. A. (2013). Distribution of the synchronous flashing beetle, *Pteroptyx tener* Olivier (Coleoptera: Lampyridae), in Malaysia. *The Coleopterists Bulletin*, 67(4), 604-605. <http://dx.doi.org/10.1649/0010-065X-67.4.604>
- Jusoh, W. F., Ballantyne, L., & Chan, K. O. (2020). DNA-based species delimitation reveals cryptic and incipient species in synchronous flashing fireflies (Coleoptera: Lampyridae) of Southeast Asia. *Biological Journal of the Linnean Society*, 130(3), 520-532. <https://doi.org/10.1093/biolinnean/blaa072>
- Jusoh, W. F., Ballantyne, L., Lambkin, C. L., Hashim, N. R., & Wahlberg, N. (2018). The firefly genus *Pteroptyx* Olivier revisited (Coleoptera: Lampyridae: Luciolinae). *Zootaxa*, 4456(1), 1-71. <https://doi.org/10.11646/zootaxa.4456.1.1>
- Khoo, V., Nada, B., Kirton, L. G., & Phon, C. K. (2012). Monitoring the population of the firefly *Pteroptyx tener* along the Selangor River, Malaysia for conservation and sustainable ecotourism. *Lampyrid*, 2, 162-173.
- Kirton, L. G., Nada, B., Tan, S. A., Ang, L. H., Tang, L. K., Hui, T. F., & Ho, W. M. (2006). The Kampung Kuantan firefly project: A preliminary assessment of the habitat requirements of *Pteroptyx tener* (Coleoptera: Lampyridae). In Y. F. Ho & K. A. Sharifah (Eds.), *Highlights of FRIM's non-IRPA Projects* (pp. 1-4). Forest Research Institute Malaysia.
- Lewis, S. M., Wong, C. H., Owens, A., Fallon, C., Jepsen, S., Thancharoen, A., Wu, C., De Cock, R., Novak, M., Lopez-Palafox, T., Khoo, V., & Reed, J. M. (2020). A global perspective on firefly extinction threats. *BioScience*, 70(2), 157-167. <https://doi.org/10.1093/biosci/biz157>
- Mahadimenakbar, M. D., & Saikim, F. H. (2016). Studies on congregating fireflies (Coleoptera; Lampyridae; *Pteroptyx* sp.) in Sabah, Malaysia: A Review. *Journal of Tropical Biology & Conservation*, 13, 13-25.
- Mahadimenakbar, M. D., Hairul, H. M., & Mazidi, A. G., (2007). The distribution and phenology of *Pteroptyx* fireflies (Coleoptera; Lampyridae) along Garama River, Sabah, Malaysia. *Journal of Tropical Biology & Conservation*, 3, 1-9.
- Mahadimenakbar, M. D., Jeperi, S. R., Saikim, F. H., & Bagul, A. H. B. P. (2018). Notes on congregating fireflies (Coleoptera, Lampyridae) of Binsulok River, Sabah. *Journal of Tropical Biology & Conservation*, 15, 155-162.
- Mahmod, A. M., Sulaiman, A., Asri, L. N., Abdullah, N. A., Husin, S. M., Shukor, A., Darbis, N. D. A., Satiman, Faris, E. M., & Sulaiman, N. (2018). Kelimpahan kelip kelip bersinkron di Chukai River, Kemaman, Terengganu [Abundance of synchronize firefly at Chukai River, Kemaman, Terengganu]. *Undergraduate Research Journal for Integrative Biology*, 2, 117-123.
- Martin, G. J., Stanger-Hall, K. F., Branham, M. A., Da Silveira, L. F., Lower, S. E., Hall, D. W., Li, X. Y., Lemmon, A. R., Lemmon, E. M., & Bybee, S. M. (2019). Higher-level phylogeny and reclassification of Lampyridae (Coleoptera: Elateroidea). *Insect Systematics and Diversity*, 3(6), Article 11. <https://doi.org/10.1093/isd/ixz024>
- Mobilim, V., & Mahadimenakbar, M. D. (2020). Solitary fireflies of Kangkawat Research Station, Imbak Canyon, Sabah. *Journal of Tropical Biology & Conservation*, 17, 131-147.

- Mohd, F. A., Maulud, K. N. A., Karim, O. A., Begum, R. A., Awang, N. A., Ahmad, A., Azhary, W. A. H. W. M., Kamarudin, M. K. A., Jaafar, M., & Mohtar, W. H. M. W. (2019). Comprehensive coastal vulnerability assessment and adaptation for Cherating-Pekan coast, Pahang, Malaysia. *Ocean & Coastal Management*, 182, Article 104948. <https://doi.org/10.1016/j.ocecoaman.2019.104948>
- Muslim, N., Khen, C. V., Ansis, R. L., & Wahid, N. (2010). A preliminary checklist of beetles from Ginseng Camp, Maliau Basin, Sabah, Malaysia, as assessed through light-trapping. *Journal of Tropical Biology & Conservation*, 6, 85-88.
- Nada, B., & Ballantyne, L. A. (2018). A new species of *Pygoluciola* Wittmer with unusual abdominal configuration, from lowland dipterocarp forest in Peninsular Malaysia (Coleoptera: Lampyridae: Luciolinae). *Zootaxa*, 4455(2), 343-362. <https://doi.org/10.11646/zootaxa.4455.2.5>
- Nada, B., & Kirton, L. G. (2004). The secret life of fireflies. *IRBM Newsletter*, 3, 2-4.
- Nada, B., Kirton, L. G., & Norma-Rashid, Y. (2009). The fireflies of Kuala Selangor: Conservation of Berembang alone won't save them. *Conservation Malaysia*, 10, 4-5.
- Nallakumar, K. (2003). The synchronously flashing aggregative fireflies of Peninsular Malaysia. *Biodiversity*, 4(2), 11-16. <https://doi.org/10.1080/14888386.2003.9712684>
- Norela, S., Loo, M. C., & Abdullah, M. (2017). Association between the firefly population and some biotic and abiotic factors along the Sungai Sepetang river banks at Kampung Dew, Taiping, Perak, Malaysia. *Malayan Nature Journal*, 69(3), 110-118.
- Norela, S., Shahril, M. H., Noh, A. M., Abdullah, M., & Khairunisa, S. (2016). Abundance of Lampyridae in relation to the vegetation and abiotic conditions along the Sungai Johor, Johor, Malaysia. *Malayan Nature Journal*, 67(4), 395-402.
- Oba, Y., Branham, M. A., & Fukatsu, T. (2011). The terrestrial bioluminescent animals of Japan. *Zoological Science*, 28(11), 771-789. <https://doi.org/10.2108/zsj.28.771>
- Ohba, N., & Wong, C. H. (2004). External morphology and ecological study of the firefly, *Pteroptyx tener* at Kampong Kuantan, Selangor, Malaysia. *Science Report of Yokosuka City Museum*, 51, 1-33.
- Ollerton, J. (2017). Pollinator diversity: Distribution, ecological function, and conservation. *Annual Review of Ecology, Evolution, and Systematics*, 48, 353-376. <https://doi.org/10.1146/annurev-ecolsys-110316-022919>
- Othman, N. W., Sulaiman, N., Abdullah, N. H., & Ramli, R. (2018). Mouthpart and digestive tract morphology of the synchronised firefly, *Pteroptyx tener* (Coleoptera: Lampyridae). *Serangga*, 23(2), 170-182
- Paudel, B. R., Shrestha, M., Dyer, A. G., Zhu, X. F., Abdusalam, A., & Li, Q. J. (2015). Out of Africa: Evidence of the obligate mutualism between long corolla tubed plant and long tongued fly in the Himalayas. *Ecology and Evolution*, 5(22), 5240-5251. <https://doi.org/10.1002/ece3.1784>
- Razak, F. A., & Sulaiman, N. (2016). Synchronisation of Malaysian fireflies: The case of *Pteroptyx tener* at Kampong Kuantan, Selangor, Malaysia. *Malayan Nature Journal*, 68(part 1 & 2), 223-228.
- Roslan, N., & Sulaiman, N. (2015). Assessment of environmental factors that affect the fireflies for ecotourism in UNESCO Tasik Chini biosphere reserve. In *AIP Conference Proceedings* (Vol. 1678, Issue 1, Article 020025). AIP Publishing LLC. <https://doi.org/10.1063/1.4931210>

- Salleh, N. K. B., Othman, N. W. B., Sulaiman, N., & Sahid, I. (2019). Ultrastructure on the light organ of tropical synchronize firefly, *Pteroptyx tener*. *Sains Malaysiana*, 48(4), 727-733. <https://doi.org/10.17576/jsm-2019-4804-04>
- Shahara, A., Nura, A. M. R., Maimon, A., & Norela, S. (2017). Assessment of firefly abundance at a new ecotourism site of Sungai Bernam, Selangor, Malaysia. *Malayan Nature Journal*, 69(2), 67-74.
- Sulaiman, N., Ismail, B. S., Aiman, M. A., & Talip, N., (2020). Leaf ultrastructure of firefly display trees. *Malayan Nature Journal*, 72(1), 93-102.
- Takeda, M., Amano, T., Katoh, K., & Higuchi, H. (2006). The habitat requirement of the Genji firefly *Luciola cruciata* (Coleoptera: Lampyridae), a representative endemic species of Japanese rural landscapes. *Biodiversity and Conservation*, 15, 191-203. <https://doi.org/10.1007/s10531-004-6903-y>
- Wong, C. H., & Yeap, C. A. (2012). Conservation of congregating firefly zones (CFZs) in Peninsular Malaysia. *Lampyrid*, 2, 174-187.



Review Article

Trends of Filtration and Adsorption Technology Using Biomaterials from Agricultural Wastes: A Bibliometric Analysis

Awang Nasrizal Awang Ali^{1,2}, Jason Lowell Jitolis¹, Juferi Idris³, Ismail Saad¹ and Nurmin Bolong^{1*}

¹Faculty of Engineering, Universiti Malaysia Sabah (UMS), 88400, Kota Kinabalu, Sabah, Malaysia

²Faculty of Civil Engineering, Universiti Teknologi MARA (UiTM), 94300, Kota Samarahan, Sarawak, Malaysia

³Faculty of Chemical Engineering, College of Engineering, Universiti Teknologi MARA (UiTM), Sarawak Branch, Samarahan Campus, 94300, Kota Samarahan, Sarawak, Malaysia

ABSTRACT

This study aims to bibliometrically review the trends of literature related to agricultural wastes in the filtration and adsorption technology, published from 2016 to 2020 while providing future research directions. It includes removing suspended solids, chemical contaminants, and toxic gases from water, wastewater, and other industrial applications. A total of 206 published documents from the Scopus database, authored by 160 scholars across 63 countries, have been analyzed using Harzing's POP (for analyzing the citations) and VOSviewer (for constructing and visualizing bibliometric networks) program. The findings show that countries from Asia, mainly China, India, and Malaysia, dominate the publication in this field, with the Desalination and Water Treatment topping the journal list, followed by the Journal of Environmental Chemical Engineering and Science of the Total Environment. In terms of co-occurrence, the top author keywords are "agricultural wastes," "water and wastewater treatment," and "adsorption." In addition, five research streams were identified, namely "biomass characterization and optimization," "adsorbent for water and wastewater quality improvement," "filtration by activated carbon," "heat treatment for biochar," and "bio-adsorbents kinetics, isotherms and thermodynamic." Finally, the authors suggest potential research directions on filtration modeling for optimization, utilizing agricultural-based media for water and wastewater treatment.

ARTICLE INFO

Article history:

Received: 16 November 2021

Accepted: 24 February 2022

Published: 20 April 2022

DOI: <https://doi.org/10.47836/pjst.30.3.12>

E-mail addresses:

awang295@uitm.edu.my (Awang Nasrizal Awang Ali)

jason_lowell_jitolis_mk20@iluv.ums.edu.my (Jason Lowell Jitolis)

juferi@uitm.edu.my (Juferi Idris)

ismail_s@ums.edu.my (Ismail Saad)

nurmin@ums.edu.my (Nurmin Bolong)

* Corresponding author

Keywords: Agricultural wastes, bibliometric analysis, biomaterials, purification, trends

INTRODUCTION

Agricultural activity is one of the critical sectors with a multi-level impact on the socio-economic and environmental ecosystems. Moreover, this sector increased considerably in the past decades due to the rise in population, which affects demand and consumption habits. Therefore, it is to be expected that the agricultural sector will have continuous growth, remarkably, when the demand for food and raw material production increases, thus strengthening trade relations between countries (Grace et al., 2016).

The massive by-products from the agricultural sector may lead to global consequences when not appropriately managed and become a nuisance to the surroundings. However, with the current advancement in research and design (R&D), it has been demonstrated that agricultural wastes are potential renewable sources, inexpensive, readily available, environmental-friendly, and have become one of the income sources for the agricultural sector (Yahya et al., 2018). Nonetheless, it would be a wastage should these biomaterials not be fully utilized. Furthermore, they consist of characteristics that may be useful in various applications, such as water and wastewater treatment (Bolong et al., 2016), bioenergy production (Suzuki et al., 2017), biopolymer reinforcement (Alsubari et al., 2018), and food technology (Bhardwaj et al., 2019). Since then, the study related to agricultural wastes has been receiving greater attention.

Bibliometric analysis is a scientific study that can determine the recorded discourse quantitatively. It also can effectively describe the features and trends for a specific discipline. Table 1 shows the previous articles on bibliometric analysis in a similar field. The number

Table 1
Previous bibliometric analysis article on agricultural wastes

Domain	TDE	Source	BAE	By
agricultural waste, straw, livestock and poultry manure, energy, biogas, and fuel	4,062	CNKI (China National Knowledge Infrastructure)	<ul style="list-style-type: none"> • Literature quantity • Top institutions, journals, authors, & keywords • Research streams • Document & authorship • Co-citation of documents & authors • Co-occurrence of keywords & terms 	J. Wei et al. (2020)
agricultur*waste, agricultur*residue, crop*residue*	3,148	Scopus	<ul style="list-style-type: none"> • Impact factor of journals • Networking maps of main authors, institutions & countries • Publication trends • Subject areas 	Duque-Acevedo et al. (2020)
pineapple*, waste*, residue*, bagasse*, skin*, crown*, peel* core*	364	Scopus	<ul style="list-style-type: none"> • Top journals, countries & collaborations, authors, institutions & keywords with mapping • Research themes • Citation analysis 	Lima et al. (2018)

Notes. TDE=total documents examined; BAE=bibliometric attributes examined.

of documents extracted from the database will largely depend on the used domain, and the scope area desired to be studied. Thus, it is essential to have a searching strategy for bibliometric analysis.

The bibliometrics of this scope of the study has not been systematically analyzed. Hence, this study aims to determine and analyze bibliometrically the agricultural literature, which focuses on removing suspended solids, chemical contaminants, and toxic gases from water, wastewater, and other industrial applications for filtration purposes. The goal is to: 1) Identify the literature characteristics, including the number of articles, research subject, and journals; 2) Determine the top powerhouse of this research area, such as countries and authors; 3) Classify the significant research streams and trends over time; and 4) Point out potential opportunities for future research. The analysis includes the current publication trends between 2016–2020, including the popular themes, top authors, and influential articles among scholars. Also, to show the development and future research directions related to the utilization of agricultural wastes in water purification.

MATERIALS AND METHODOLOGY

The methodology in this study was divided into three sub-sections: searching strategy from database resources, search strings, screening, and data abstraction analysis, with the primary focus on applying agricultural wastes in the filtration and adsorption technology. The research questions (RQs) were:

RQ1: What are the document, source type, and research subject area?

RQ2: What are the citation patterns of publication on agricultural wastes and purification technology?

RQ3: What are the significant research streams and trends over time?

RQ4: What are the potential opportunities for future research?

Searching Strategy from Database Resources

A systematic search strategy from the Preferred Reporting Items for Systematic Reviews and Meta-Analyses (PRISMA), modified from Ali et al. (2021), was used to assess the collected data to produce quality and significant analysis. Published PRISMA guidelines allow the authors to use appropriate search strings with objective screening before examining the abstracted literature data. It is worth mentioning that there are no perfect databases available at present as they may have classification schemes and full coverage limitations (Pranikutè, 2021). Using more than a single database may offer better data collection, but due to constraints, this study used only one primary database, namely Scopus, which covers varying environment fields. Nonetheless, systematic reporting from recognized sources such as Scopus, or others, would benefit scholars as they contain massive databases of quality research literature. Furthermore, Scopus enables the export

of the list of articles in both CSV and RIS format, which aids in sorting data, albeit there is a limit of 2,000 documents per transfer for exporting the documents.

Search Strings and Screening

The topic and research questions (RQs) need to be narrowed before developing the search strings. Once done, relevant keywords for the search strings were identified based on the selected research area. The preliminary searching efforts include five keywords of “agriculture wastes,” “filtration,” “adsorption,” “purification,” and “treatment.” Table 2 shows the search strings with the Boolean and Truncation Operator used. A total of 493 documents were retrieved on 6th August 2021.

Table 2
The search strings with Boolean and Truncation Operator

Database Source	Scopus
Search Strings	TITLE (agr*-waste* AND filt* OR adsor* OR purif* OR treat*)

Usually, should the methodology involve more than one database, duplicate articles between the databases need to be removed. Surprisingly, one duplicate was found from the same database when data was imported, sharing a similar author name with a different ID but with different/additional publications. Thus, it was combined instead of excluded (later using Harzing’s POP for analysis). Then another 284 documents were removed (total n=285), according to the inclusion and exclusion criteria. The first criteria is the period year where only published literature between 2016 to 2020 was selected. Next is the publication stage, where only those documents in the final form were considered. In contrast, documents known as Articles in Press, accepted to be published but unassigned to any publication’s volume/issue, were excluded. Usually, these documents are in the stage of pre-proofs, uncorrected proofs, corrected proofs, and withdrawal of articles. As for the type of source, all were included. These comprise the review paper, conference proceedings, book, book series, trade journal, and others. Lastly, English was selected, excluding other languages from the selected articles. Table 3 summarizes the criteria used in this study.

After that, the exported data of the remaining documents were screened thoroughly to ensure that the selected articles were reliable as primary data. Two non-related documents

Table 3
The inclusion and exclusion criteria

Criteria	Inclusion	Exclusion
Period Year	2016-2020	<2016; 2021
Publication Stage	Final	Article in Press
Source Type	All	None
Language	English	Others

were excluded due to erratum (n=2). Hence, a final of 206 documents remains to be analyzed in the next stage. Figure 1 shows the overall systematic searching processes in this study.

Data Abstraction Analysis

Identifying major research streams was done by compiling and scrutinizing information where authors analyzed all the 206 documents to abstract data that fulfill the RQs' needs. First, the citations analysis was done using Harzing's POP, and the VOSviewer was used to map the bibliometric networks. Then, the directive groups were created according to the data connections and presented as tables and figures.

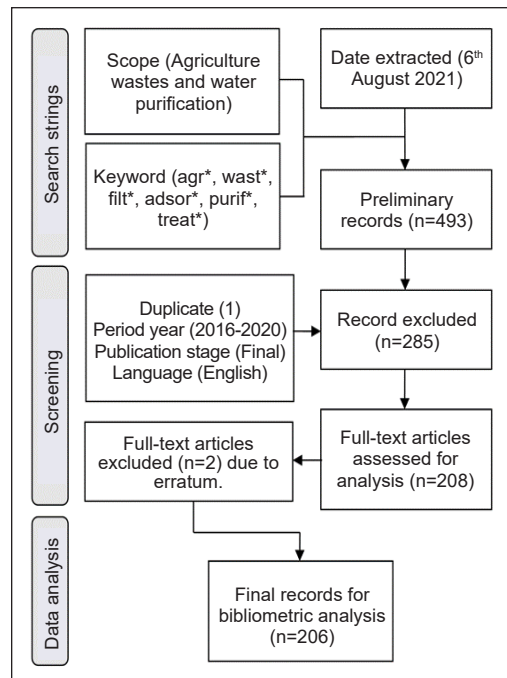


Figure 1. Overall systematic searching processes

RESULTS AND DISCUSSION

This section elaborates the literature characteristics, top contributors, research streams, and future directions. These aspects were analyzed: document types, source types, subject area, citation metrics, yearly publication by country and institution, source title, top articles, and productive authors. Findings are presented as frequency and percentage, and some are extended to the number of cited publications (NCP), total citations (TC), average citations per publication (C/P), average citations per cited publication (C/CP), h-index, and g-index.

Literature Characteristics

RQ1: What are the document, source type, and research subject area?

Document and Source Type. The current state of the publication related to agricultural wastes and purification technology is presented. Table 4 summarizes the four documents obtained from the Scopus database on 6th August 2021. They are articles, conference papers, reviews, and book chapters. Most of the publications are in the form of an article (80.58%), followed by a conference paper (11.65%), a review (6.31%), and a book chapter (1.46%). Book chapters may have a high acceptance rate for publication but are less prestigious and less rigorous in review (Woodrow, 2014). Vice versa, review papers usually include quantitative, narrative, and qualitative components. Commonly the review papers are

disproportionate to other research articles as it takes a considerable effort to prepare them (Suter, 2013), albeit these reviews tend to be highly cited (Palmatier et al., 2018). The ratio of citations per paper (C/P) can be seen from Table 4.

Table 4
Document type from Scopus database

Document Type	TP	(%)	TC	C/P
Article	166	80.58%	2064	12.43
Conference Paper	24	11.65%	48	2
Review	13	6.31%	380	29.23
Book Chapter	3	1.46%	10	3.33
Total	206	100.00		

Notes. TP=total publications; TC=total citations; and C/P=citations per paper

The source type refers to the documents based on the category of source title. For instance, a review paper document can be published in conferences and journals. Table 5 shows the summary of four source types obtained. As expected, the journals are the highest source type (87.86%), followed by conference proceedings (9.71%). Book and book series contribute with 1.46% and 0.97%, respectively. These results suggest that most authors prefer preparing article forms for publications in selected journals when reporting their scholarly works. Factors such as comprehensiveness, citations, publication speed (González-Albo & Bordons, 2011), publication frequency, citation impact, and subject fields (Zhang & Glänzel, 2012) may have a role.

Table 5
Source type during 2016-2020

Source Type	TP	Percentage (%)
Journal	181	87.86%
Conference Proceeding	20	9.71%
Book	3	1.46%
Book Series	2	0.97%
Total	206	100.00

Notes. TP=total publications

Subject Areas. The subject areas for most of the publications are currently under environmental science (24.9%), followed by chemical engineering (13.2%), engineering (11.1%), and chemistry (10.2%). This evidence shows how popular this subject is in those fields. The increase in studies related to agricultural wastes and purification technology would involve experimental methods and theories, which explains their dominance in science and engineering subject research. The summary of the subject areas is shown in Table 6. As for others, studies such as cost analysis and economic feasibility (Sharma & Ayub, 2019) is included, all of which are less than 1.6%. Thus, it indicates a multidisciplinary interest in the water applications subject of concern.

Table 6
Subject area in agricultural wastes and purification technology

Subject Area	TP	Percentage (%)
Environmental Science	110	24.9%
Chemical Engineering	58	13.2%
Engineering	49	11.1%
Chemistry	45	10.2%
Materials Science	27	6.1%
Agricultural and Biological Sciences	26	5.9%
Biochemistry, Genetics, and Molecular Biology	25	5.7%
Energy	24	5.4%
Physics and Astronomy	22	5.0%
Earth and Planetary Sciences	12	2.7%
Others	43	9.8% ($\leq 1.6\%$)

Notes. TP=total publications

Top Contributors

RQ2: What are the citation patterns of publication on agricultural wastes and purification technology?

Citation Metrics. The citation metrics are presented in Table 7. For the retrieved 206 documents, there is an average of 498.4 citations per year from 2,492 citations reported within the recent five-year period. However, out of the 206 documents, only 172 were cited when this data was analyzed. Whereas the remaining 34 have yet to be cited. With an average of 12.1 citations per paper, this would be a benchmark indicator, particularly for new researchers interested in majoring in this study field. Other bibliometric studies in a similar field of wastewater and activated sludge have reported average citations per paper in the range of 9.13-35.81 (Zyoud et al., 2016; Durán-Sánchez et al., 2020; Ahnert & Krebs, 2021).

Table 7
Citation metrics from Harzing's POP

Metrics	Data
Papers	206
Citations	2,492
Years	5
Cites/Year (C/Y)	498.4
Cites/Paper (C/P)	12.1

Yearly Publications. Table 8 shows the extended analysis for yearly publication. There has been a steady trend in publications from 2016 to 2019 (28 to 38 documents). However, a remarkable publication contribution can be identified in 2020 (67 documents), almost double the figure from the previous year (increase by 44.8%). The year 2020 also has the highest number of cited publications (32.52%), with total citations of 48, even though they are considered new publications. These results suggest that research productivity in this

subject area has increased and attracted more interest from researchers and is aligned with the needs and nature of scientific publishing (Niles et al., 2020).

Table 8

Yearly publication for agricultural wastes with filtration and adsorption technology

Year	TP	NCP	TC
2020	67	32.52%	48
2019	37	17.96%	33
2018	38	18.45%	31
2017	28	13.59%	26
2016	36	17.48%	33

Notes. TP=total publications; NCP=number of cited publications; and TC=total citations

Top Contributing Countries and Institutions. Overall, 160 authors are affiliated with various institutions from 63 countries recorded in the publications, and the top ten of the most productive countries are listed in Table 9. It is no surprise that the first three are from the Asia continent, namely China (TP=34), India (TP=32), and Malaysia (TP=17). Asia is well known for its biodiversity and agricultural activity, leading to massive agricultural waste (Neh, 2020). This observation can also be related to Table 10, by which two of the top three most active institutions are depicted to be from the same countries (Ministry of Education China and Universiti Kebangsaan Malaysia). In contrast, Aligarh Muslim University (India) is seventh from the top eight list. Hence, it can be inferred that these countries have considerable awareness and effort from their government supported by their respective educational advancement. When institutions are ranked according to the h-index, the Ministry of Education China and the University of Santa Maria are the top institutions with leading publications. The visualization map on the geographical distribution of these publications worldwide is shown in Figure 2.

Table 9

Top contributing countries in publications

Country	TP	NCP	TC	C/P	C/CP	h	g
China	34	16.50%	30	673	19.79	22.43	15
India	32	15.53%	28	398	12.44	14.21	12
Malaysia	17	8.25%	15	145	8.53	9.67	6
Egypt	12	5.83%	11	116	9.67	10.55	5
Iran	11	5.34%	10	137	12.45	13.70	7
U.S.	11	5.34%	8	98	8.91	12.25	5
Brazil	8	3.88%	8	133	16.63	16.63	6
Nigeria	7	3.40%	4	44	6.29	11.00	3
Thailand	6	2.91%	5	25	4.17	5.00	3
Turkey	6	2.91%	3	125	20.83	41.67	2

Notes. TP=total publications; NCP=number of cited publications; TC=total citations; C/P=citations per paper; C/CP=average citations per cited publication; h=h-index; and g=g-index

Table 10
Top contributing institutions with a minimum of three publications

Affiliation	TP	NCP	TC	C/P	C/CP	h	g
Ministry of Education China (China)	6	6	130	21.67	21.67	6	6
Universiti Kebangsaan Malaysia (Malaysia)	4	4	45	11.25	11.25	3	4
National Research Centre (Egypt)	4	4	21	5.25	5.25	3	4
University of Santa Maria (Brazil)	4	4	100	25.00	25.00	4	4
Silpakorn University (Thailand)	3	2	14	4.67	7.00	1	3
Czech Academy of Sciences (Czech Republic)	3	2	8	2.67	4.00	2	2
Aligarh Muslim University (India)	3	3	30	10.00	10.00	2	3
Qatar University (Qatar)	3	3	55	18.33	18.33	3	3

Notes. TP=total publications; NCP=number of cited publications; TC=total citations; C/P=citations per paper; C/CP=average citations per cited publication; h=h-index; and g=g-index

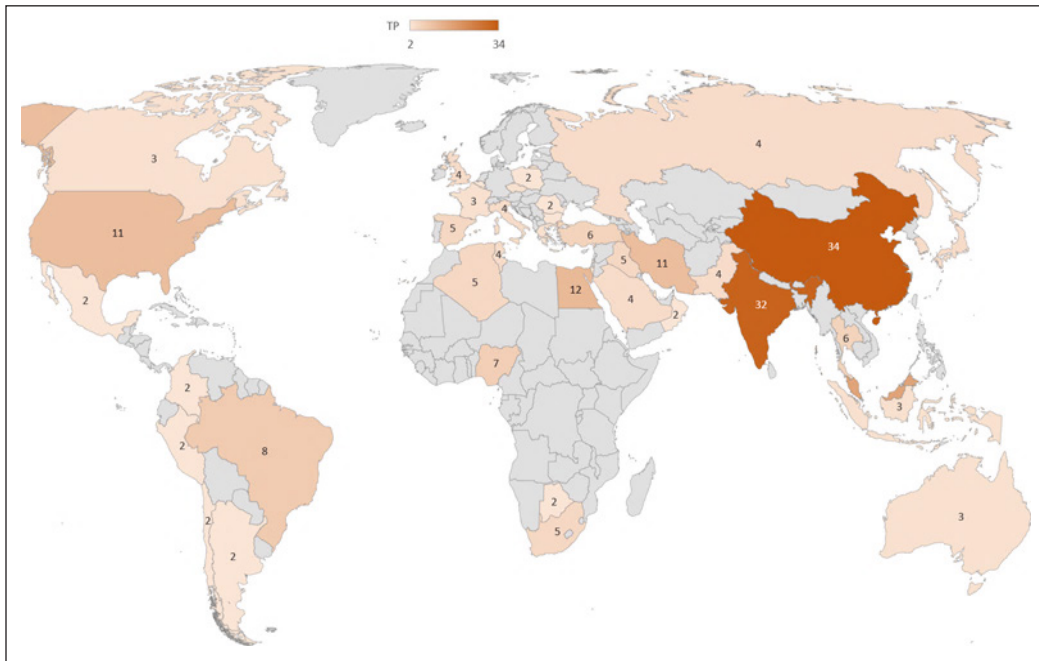


Figure 2. Geographical distribution of publications

Most Active Source and Top Cited Publications. Table 11 shows that the most active source title within the past five years is Desalination and Water Treatment, with 18 publications compared to others. It is followed by the Journal of Environmental Chemical Engineering (TP=7) and Science of the Total Environment (TP=6). It can also be seen that Elsevier dominated as a publisher, with 5 out of 8 in the list being journals published by them. The Cite Score, SCImago Journal Rank (SJR) 2020, and Source Normalized Impact per Paper (SNIP) 2020 are also shown. SJR measures weighted citations received by the

source title, while SNIP measures actual citations received relative to citations expected for the source title's subject field. Nonetheless, the factors in selecting a journal, such as reliability of reviewing, the usefulness of reviewers' feedback, the journal's reputation, and confidence that their article is in scope for the journal, may contribute to these results (Rowley et al., 2020).

Next, Table 12 shows the top ten highly cited documents with average citations per year. The document entitled "Utilizations of agricultural waste as adsorbent for the removal of contaminants: A review" by Dai et al. (2018) has the highest total of citations (141 citations or an average of 47 citations per year). Another interesting finding is that half of the top articles are published in the most active source, as mentioned previously. Hence, it would play a role in increasing the high citations.

Table 11
Most active source title in publications

Source Title (Publisher)	TP	TC	Cite Score	SJR 2020	SNIP 2020
Desalination and Water Treatment (Desalination Publications)	18	8.74%	1.6	0.251	0.351
Journal of Environmental Chemical Engineering (Elsevier)	7	3.40%	7.5	0.965	1.354
Science of the Total Environment (Elsevier)	6	2.91%	10.5	1.795	2.015
Journal of Molecular Liquids (Elsevier)	5	2.43%	8.4	0.929	1.420
Bioresource Technology (Elsevier)	4	1.94%	14.8	2.489	2.073
Chemosphere (Elsevier)	4	1.94%	10.1	1.632	1.708
IOP Conference Series Materials Science and Engineering (Conference Proceeding)	4	1.94%	0.7	0.198	0.484
Water Switzerland (Multidisciplinary Digital Publishing Institute)	4	1.94%	3.7	0.718	1.179

Notes. TP=total publications; and TC=total citations

Table 12
Top 10 highly cited documents (Retrieves as of 6th August 2021)

Title	Cites	Cites/Year	By
Utilizations of agricultural waste as adsorbent for the removal of contaminants: A review (Chemosphere)	141	47	Dai et al. (2018)
Tetracycline adsorption onto rice husk ash, an agricultural waste: Its kinetic and thermodynamic studies (Journal of Molecular Liquids)	92	18.4	Chen et al. (2016)
Valorization of agricultural waste with an adsorption/nanofiltration hybrid process: From materials to sustainable process design (Green Chemistry)	89	22.25	Didaskalou et al. (2017)
Adsorptive potential of agricultural wastes for removal of dyes from aqueous solutions (Journal of Environmental Chemical Engineering)	81	20.25	Singh et al. (2017)

Table 12 (continue)

Title	Cites	Cites/Year	By
Insight into the adsorption mechanism of cationic dye onto biosorbents derived from agricultural wastes (Chemical Engineering Communications)	60	15	Tran et al. (2017)
Management of agricultural waste for removal of heavy metals from aqueous solution: adsorption behaviors, adsorption mechanisms, environmental protection, and techno-economic analysis (Environmental Science and Pollution Research International)	57	14.25	Elhafez et al. (2017)
Biochar-based functional materials in the purification of agricultural wastewater: Fabrication, application and future research needs (Chemosphere)	54	18	Wei et al. (2018)
Exploring the adsorption mechanisms of cationic and anionic dyes onto agricultural waste peels of banana, cucumber, and potato: Adsorption kinetics and equilibrium isotherms as a tool (Journal of Environmental Chemical Engineering)	50	16.67	Stavrinou et al. (2018)
Adsorption of methylene blue on agro-industrial wastes: Experimental investigation and phenomenological modeling (Progress in Biophysics and Molecular Biology)	44	22	Meili et al. (2019)
Adsorptive behavior of methylene blue onto sawdust of sour lemon, date palm, and eucalyptus as agricultural wastes (Journal of Dispersion Science and Technology)	43	21.5	Esmacili & Foroutan (2019)

Productive Authors. No distinctive authors were identified as most active since most authors have similar publications (TP=2) except for the two (TP=3) shown in Table 13. Between their six authored and co-authored publications, wrapped a total of 147 citations. They are part of the contributors in top contributing institutions too.

Table 13

Most productive authors

Author (Affiliation)	TP	NCP	TC	C/P	C/CP	h	g
Almomani, F. (Qatar University, Qatar)	3	3	55	18.33	18.33	3	3
Dotto, G.L. (University of Santa Maria, Brazil)	3	3	92	30.67	30.67	3	3

Notes. TP=total publications; NCP=number of cited publications; TC=total citations; C/P=citations per paper; C/CP=average citations per cited publication; h=h-index; and g=g-index

Research Streams

RQ3: What are the significant research streams and trends over time?

Top Keywords. The authors' keywords are vital to review trends while assessing research areas (Babaii & Taase, 2013). Therefore, the authors' top keywords and co-occurrence are analyzed to determine the research streams and trends over time. Since the keywords

contain duplicated terms in singular, plural, or synonyms, they were merged manually using Microsoft Excel. Table 14 summarizes the top keywords found from the Scopus. The top favorite keyword is “agricultural wastes” (11.5%), followed by “water and wastewater treatment” (8.7%) and “adsorption” (7.8%). Thus, it can be concluded that these are the expected trends that have become a frequent target of current research.

Table 14
Top keywords

Author Keywords	Total Publications (TP)	Percentage (%)
Agricultural Wastes	159	11.5%
Water and Wastewater Treatment	121	8.7%
Adsorption	108	7.8%
Kinetics	76	5.5%
Agriculture	63	4.6%
Metals Removal	62	4.5%
Water Quality	50	3.6%
Article	48	3.5%
Water and Wastewater Management	48	3.5%
Isotherms	42	3.0%
Dye Removal	34	2.5%
pH	32	2.3%
Activated Carbon	30	2.2%
Waste Treatment	28	2.0%
Characterization	27	2.0%
Biochar	26	1.9%
Agricultural Robots	23	1.7%
Aqueous Solution	19	1.4%
Scanning Electron Microscopy	19	1.4%
Others	369	26.7% ($\leq 1.3\%$)

Co-Occurrence Analysis. Having more than one keyword in a single document shows a relationship between the concepts, known as co-occurrence (Baker et al., 2020). In this study, the minimum of co-occurrences of each keyword is set at six. Based on this threshold, 28 keywords emerged for selection in the VOSviewer program Figure 3 shows the network overlay visualization map generated based on keywords by authors. The color, font, and circle size indicate the keywords' relationship strength.

Five major clusters or research streams were formed based on the color grouping from the map. The first and second cluster consists of 8 items, themed as biomass characterization and optimization, and adsorbent for water and wastewater quality improvement. Then the remaining clusters, all consisting of 4 items, are themed as filtration by activated carbon, heat treatment for biochar, and bio-adsorbents kinetics, isotherms, and thermodynamic. Hence, based on the analysis, these themes are suggested as the primary research streams.

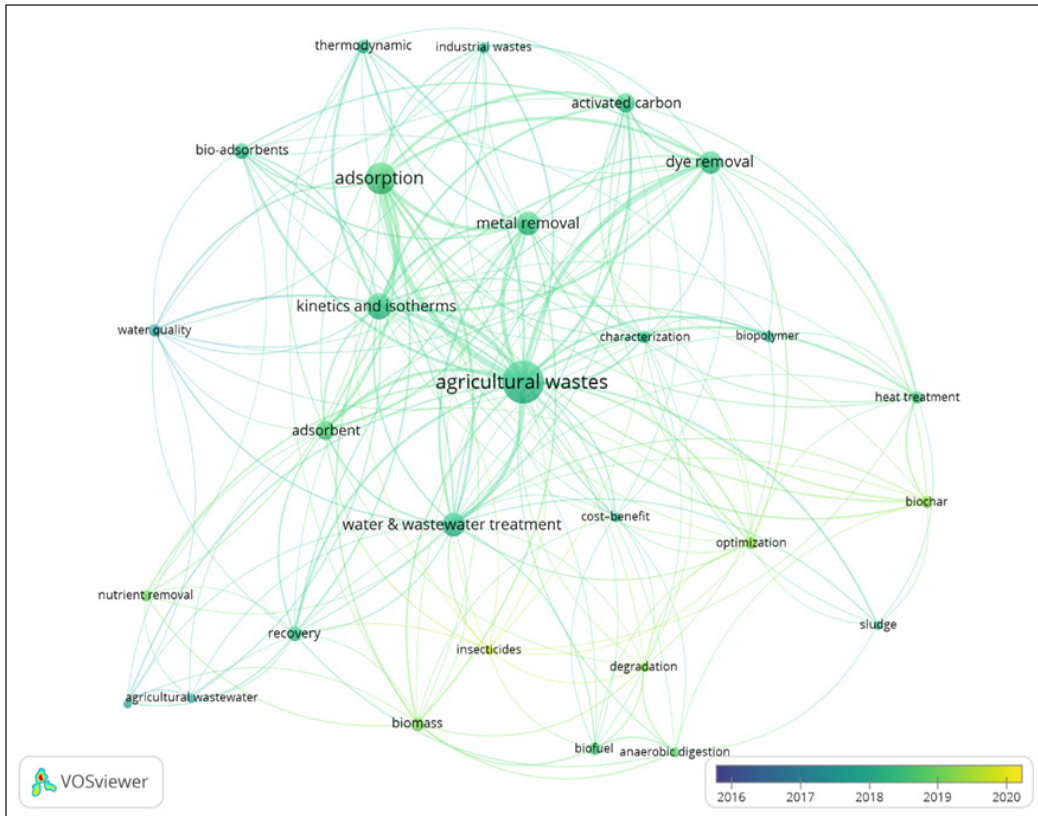


Figure 3. Network overlay visualization map of the author keywords

Future Directions

RQ4: What are the potential opportunities for future research?

Based on Figure 3, specific keywords labeled in yellow/light green can be observed leaning towards the year 2020. These keywords are “insecticides,” “biochar,” “biomass,” and “optimization.” It should be noted that these are not new terms or keywords used in this research field. Instead, they may be applied differently from the conventional way. Thus, the keyword trend will mostly rely on the authors’ research interests (Lu et al., 2021). The authors suggest that future research emphasizes filtration modeling for optimization, utilizing agricultural-based media for water and wastewater treatment.

Previous works of literature have demonstrated that agricultural-based media can be utilized for water and wastewater treatment (Kristianto et al., 2017; Farjana et al., 2018). They can be used either as raw or carbonized, with and without activation. In addition, some other studies successfully modified biochar from these wastes and improved adsorption capacity (Seixas et al., 2017; Bispo et al., 2018; Shakya & Agarwal, 2019). Nonetheless, more works are needed to study this alternative material (Hoslett et al., 2018).

Laboratory experiments are usually performed to analyze one factor, but it is time-consuming, costly, and tedious as it involves replications. Thus, computer modeling would offer flexibility to simulate and optimize the filter design. It can even determine the response prediction and show the relationship or interactions between several independent factors or variables (Dashti et al., 2018). It complements the conventional method, which requires changing variables one at a time while the others remain constant (Bashir et al., 2015).

CONCLUSION

Agricultural wastes as filtration media have attracted global interest due to their abundance and potential to be transformed from waste to wealth. This study has bibliometrically analyzed the agricultural waste literature related to their filtration and adsorption technology application. Here are some of the conclusions drawn based on the findings:

- There is noticeable growth (increase 44.8% in 2020) of interest in this field based on publications from 2016–2020 (as of 6th August 2021).
- Most authors prefer article form (80.58%) in journal publications (87.86%) for sharing their scientific findings.
- The agricultural waste and purification technology studies dominate science and engineering subject research.
- The top publication contributors for institutions and countries mainly come from Asia (China, India, and Malaysia).
- Half of the top-cited articles (50%) are published in the most active source title.
- The top keywords identified are “agricultural wastes” (11.5%), “water and wastewater treatment” (8.7%), and “adsorption” (7.8%).
- Five themes developed from co-occurrence analysis are 1) biomass characterization and optimization; 2) adsorbent for water and wastewater quality improvement; 3) filtration by activated carbon; 4) heat treatment for biochar; and 5. bio-adsorbents kinetics, isotherms, and thermodynamic.

On the bibliometric analysis, combining more than one database can be suggested. However, the duplicates need to be removed, and the database must be fully accessible for thorough data analysis. In terms of using Scopus export, the data downloaded needs to be checked to ensure no error in the file, such as non-related documents (proceeding/journal content information). Also, the study experienced the author’s name with split IDs. At the moment, Scopus users can only combine, run, edit, change the name, set up an alert for, and delete a saved search. Since the documents from the search result are based on the search criteria, they cannot be manually removed or combined from the results list. So, the study used Harzing’s POP to combine the author’s information (ID and publications record) to remove duplicates as the data is not added up.

ACKNOWLEDGMENT

The authors want to acknowledge the financial support from the Ministry of Higher Education (FRGS/1/2020/TK0/UMS/02/3) and Universiti Malaysia Sabah (GUG0441-1/2020). The authors also appreciate the reviewer's contribution and feedback.

REFERENCES

- Ahnert, M., & Krebs, P. (2021). Growth of science in activated sludge modelling - A critical bibliometric review. *Water Science and Technology*, 83(12), 2841-2862. <https://doi.org/10.2166/wst.2021.191>
- Ali, A. N. A., Bolong, N., & Taha, N. A. (2021). A review on the application of granular filter media and the utilization of agro-industrial wastes for stormwater quality improvement. *Jurnal Teknologi*, 83(4), 75-90. <https://doi.org/https://doi.org/10.11113/jurnalteknologi.v83.15159>
- Alsubari, B., Shafiqh, P., Ibrahim, Z., & Jumaat, M. Z. (2018). Heat-treated palm oil fuel ash as an effective supplementary cementitious material originating from agriculture waste. *Construction and Building Materials*, 167, 44-54. <https://doi.org/10.1016/j.conbuildmat.2018.01.134>
- Babaii, E., & Taase, Y. (2013). Author-assigned keywords in research articles: Where do they come from? *Iranian Journal of Applied Linguistics (IJAL)*, 16(2), 1-19.
- Baker, H. K., Pandey, N., Kumar, S., & Haldar, A. (2020). A bibliometric analysis of board diversity: Current status, development, and future research directions. *Journal of Business Research*, 108, 232-246. <https://doi.org/10.1016/j.jbusres.2019.11.025>
- Bashir, M. J. K., Amr, S. S. A., Aziz, S. Q., Aun, N. C., & Sethupathi, S. (2015). Wastewater treatment processes optimization using response surface methodology (RSM) compared with conventional methods : Review and comparative study. *Middle-East Journal of Scientific Research*, 23(2), 244-252.
- Bhardwaj, N., Kumar, B., Agarwal, K., Chaturvedi, V., & Verma, P. (2019). Purification and characterization of a thermo-acid/alkali stable xylanases from *Aspergillus oryzae* LC1 and its application in Xylo-oligosaccharides production from lignocellulosic agricultural wastes. *International Journal of Biological Macromolecules*, 122, 1191-1202. <https://doi.org/10.1016/j.ijbiomac.2018.09.070>
- Bispo, M. D., Schneider, J. K., Da Silva Oliveira, D., Tomasini, D., Da Silva Maciel, G. P., Schena, T., Onorevoli, B., Bjerck, T. R., Jacques, R. A., Krause, L. C., & Caramão, E. B. (2018). Production of activated biochar from coconut fiber for the removal of organic compounds from phenolic. *Journal of Environmental Chemical Engineering*, 6(2), 2743-2750. <https://doi.org/10.1016/j.jece.2018.04.029>
- Bolong, N., Saad, I., Makinda, J., Yaser, A. Z., Abdullah, M. H., & Ismail, A. F. (2016). Influence of oil palm empty fruit bunch (OPEFB) agro-waste properties as filtration medium to improve urban stormwater. *Jurnal Teknologi*, 78(8), 39-46. <https://doi.org/10.11113/jt.v78.5357>
- Chen, Y., Wang, F., Duan, L., Yang, H., & Gao, J. (2016). Tetracycline adsorption onto rice husk ash, an agricultural waste: Its kinetic and thermodynamic studies. *Journal of Molecular Liquids*, 222, 487-494. <https://doi.org/10.1016/j.molliq.2016.07.090>
- Dai, Y., Sun, Q., Wang, W., Lu, L., Liu, M., Li, J., Yang, S., Sun, Y., Zhang, K., Xu, J., Zheng, W., Hu, Z., Yang, Y., Gao, Y., Chen, Y., Zhang, X., Gao, F., & Zhang, Y. (2018). Utilizations of agricultural waste

- as adsorbent for the removal of contaminants: A review. *Chemosphere*, 211, 235-253. <https://doi.org/10.1016/j.chemosphere.2018.06.179>
- Dashti, A., Adlan, N., Hamidi, A., Aziz, A., Huddin, I., Adlan, M. N., Abdul Aziz, H., & Ibrahim, A. H. (2018). Application of response surface methodology (RSM) for optimization of ammoniacal nitrogen removal from palm oil mill wastewater using limestone roughing filter. *Journal of Applied Research in Water and Wastewater*, 9, 411-416. <https://doi.org/10.22126/ARWW.2018.892>
- Didaskalou, C., Buyuktiryaki, S., Kecili, R., Fonte, C. P., & Szekely, G. (2017). Valorisation of agricultural waste with an adsorption/nanofiltration hybrid process: From materials to sustainable process design. *Green Chemistry*, 19, 3116-3125. <https://doi.org/10.1039/C7GC00912G>
- Duque-Acevedo, M., Belmonte-Ureña, L. J., Cortés-García, F. J., & Camacho-Ferre, F. (2020). Agricultural waste: Review of the evolution, approaches and perspectives on alternative uses. *Global Ecology and Conservation*, 22, Article e00902. <https://doi.org/10.1016/j.gecco.2020.e00902>
- Durán-Sánchez, A., Álvarez-García, J., González-Vázquez, E., & Del Río-Rama, M. de la C. (2020). Wastewater management: Bibliometric analysis of scientific literature. *Water*, 12(11), Article 2963. <https://doi.org/10.3390/w12112963>
- Elhafez, S. E. A., Hamad, H. A., Zaatout, A. A., & Malash, G. F. (2017). Management of agricultural waste for removal of heavy metals from aqueous solution: Adsorption behaviors, adsorption mechanisms, environmental protection, and techno-economic analysis. *Environmental Science and Pollution Research*, 24(2), 1397-1415. <https://doi.org/10.1007/s11356-016-7891-7>
- Esmaceli, H., & Foroutan, R. (2019). Adsorptive behavior of methylene blue onto sawdust of sour lemon, date palm, and eucalyptus as agricultural wastes. *Journal of Dispersion Science and Technology*, 40(7), 990-999. <https://doi.org/10.1080/01932691.2018.1489828>
- Farjana, N., Kallesh, D. C., Manjunath, B. L., Priyesh, B. J., & Poornima, K. B. (2018). Rapid sand filter using coconut shell. *International Research Journal of Engineering and Technology (IRJET)*, 5(4), 5040-5043.
- González-Albo, B., & Bordons, M. (2011). Articles vs. proceedings papers: Do they differ in research relevance and impact? A case study in the Library and Information Science field. *Journal of Informetrics*, 5(3), 369-381. <https://doi.org/10.1016/j.joi.2011.01.011>
- Grace, M. A., Clifford, E., & Healy, M. G. (2016). The potential for the use of waste products from a variety of sectors in water treatment processes. *Journal of Cleaner Production*, 137, 788-802. <https://doi.org/10.1016/j.jclepro.2016.07.113>
- Hoslett, J., Massara, T. M., Malamis, S., Ahmad, D., van den Boogaert, I., Katsou, E., Ahmad, B., Ghazal, H., Simons, S., Wrobel, L., & Jouhara, H. (2018). Surface water filtration using granular media and membranes: A review. *Science of the Total Environment*, 639, 1268-1282. <https://doi.org/10.1016/j.scitotenv.2018.05.247>
- Kristianto, H., Katherine, K., & Soetedjo, J. N. M. (2017). Penyediaan air bersih masyarakat sekitar Masjid Al-Iklas Desa Cukanggenteng Ciwidey dengan menggunakan penyaringan air sederhana [Provision of clean water for the community around the Al-Iklas Mosque, Cukanggenteng Village, Ciwidey by using simple water filtration]. *Jurnal Pengabdian Kepada Masyarakat*, 3(1), 39-49. <https://doi.org/10.22146/jpkm.28148>

- Lima, F. D. C., Simoes, A. J. A., Vieira, I. M. M., Silva, D. P., & Ruzene, D. S. (2018). An overview of applications in pineapple agroindustrial residues. *Acta Agriculturae Slovenica*, *111*(2), 445-462. <https://doi.org/10.14720/aas.2018.111.2.18>
- Lu, W., Huang, S., Yang, J., Bu, Y., Cheng, Q., & Huang, Y. (2021). Detecting research topic trends by author-defined keyword frequency. *Information Processing and Management*, *58*(4), Article 102594. <https://doi.org/10.1016/j.ipm.2021.102594>
- Meili, L., Lins, P. V. S., Costa, M. T., Almeida, R. L., Abud, A. K. S., Soletti, J. I., Dotto, G. L., Tanabe, E. H., Sellaoui, L., Carvalho, S. H. V., & Erto, A. (2019). Adsorption of methylene blue on agroindustrial wastes: Experimental investigation and phenomenological modelling. *Progress in Biophysics and Molecular Biology*, *141*, 60-71. <https://doi.org/10.1016/j.pbiomolbio.2018.07.011>
- Neh, A. (2020). Agricultural waste management system [AWMS] in Malaysian. *Open Access Journal of Waste Management & Xenobiotics*, *3*(2), 1-2.
- Niles, M. T., Schimanski, L. A., McKiernan, E. C., & Alperin, J. P. (2020). Why we publish where we do: Faculty publishing values and their relationship to review, promotion and tenure expectations. *PLoS ONE*, *15*(3), Article e0228914. <https://doi.org/10.1371/journal.pone.0228914>
- Palmatier, R. W., Houston, M. B., & Hulland, J. (2018). Review articles: Purpose, process, and structure. *Journal of the Academy of Marketing Science*, *46*(1), 1-5. <https://doi.org/10.1007/s11747-017-0563-4>
- Pranckutė, R. (2021). Web of Science (WoS) and Scopus: The titans of bibliographic information in today's academic world. *Publications*, *9*(1), Article 12. <https://doi.org/10.3390/publications9010012>
- Rowley, J., Sbaffi, L., Sugden, M., & Gilbert, A. (2020). Factors influencing researchers' journal selection decisions. *Journal of Information Science*, *2020*, 1-5. <https://doi.org/10.1177/0165551520958591>
- Seixas, F. L., Golçanves, E. V., Olsen, M. H. N., Gimenes, M. L., & Fernandes-Machado, N. R. C. (2017). Activated carbon from sugarcane bagasse prepared by activation with CO₂ and bio oil recuperation. *Chemical Engineering Transactions*, *57*, 139-144. <https://doi.org/10.3303/CET1757024>
- Shakya, A., & Agarwal, T. (2019). Removal of Cr(VI) from water using pineapple peel derived biochars: Adsorption potential and re-usability assessment. *Journal of Molecular Liquids*, *293*, Article 111497. <https://doi.org/10.1016/j.molliq.2019.111497>
- Sharma, P. K., & Ayub, S. (2019). The cost analysis and economic feasibility of agro wastes to adsorb chromium (VI) from wastewater. *International Journal of Civil Engineering and Technology*, *10*(2), 2387-2402.
- Singh, H., Chauhan, G., Jain, A. K., & Sharma, S. K. (2017). Adsorptive potential of agricultural wastes for removal of dyes from aqueous solutions. *Journal of Environmental Chemical Engineering*, *5*(1), 122-135. <https://doi.org/10.1016/j.jece.2016.11.030>
- Stavrinou, A., Aggelopoulos, C. A., & Tsakiroglou, C. D. (2018). Exploring the adsorption mechanisms of cationic and anionic dyes onto agricultural waste peels of banana, cucumber and potato: Adsorption kinetics and equilibrium isotherms as a tool. *Journal of Environmental Chemical Engineering*, *6*(6), 6958-6970. <https://doi.org/10.1016/j.jece.2018.10.063>
- Suter, G. W. (2013). Review papers are important and worth writing. *Environmental Toxicology and Chemistry*, *32*(9), 1929-1930. <https://doi.org/10.1002/etc.2316>

- Suzuki, K., Tsuji, N., Shirai, Y., Hassan, M. A., & Osaki, M. (2017). Evaluation of biomass energy potential towards achieving sustainability in biomass energy utilization in Sabah, Malaysia. *Biomass and Bioenergy*, 97, 149-154. <https://doi.org/10.1016/j.biombioe.2016.12.023>
- Tran, H. N., You, S. J., Nguyen, T. V., & Chao, H. P. (2017). Insight into the adsorption mechanism of cationic dye onto biosorbents derived from agricultural wastes. *Chemical Engineering Communications*, 204(9), 1020-1036. <https://doi.org/10.1080/00986445.2017.1336090>
- Wei, D., Li, B., Huang, H., Luo, L., Zhang, J., Yang, Y., Guo, J., Tang, L., Zeng, G., & Zhou, Y. (2018). Biochar-based functional materials in the purification of agricultural wastewater: Fabrication, application and future research needs. *Chemosphere*, 197, 165-180. <https://doi.org/10.1016/j.chemosphere.2017.12.193>
- Wei, J., Liang, G., Alex, J., Zhang, T., & Ma, C. (2020). Research progress of energy utilization of agricultural waste in China: Bibliometric analysis by Citespace. *Sustainability*, 12(3), Article 812. <https://doi.org/10.3390/su12030812>
- Woodrow, L. (2014). Publishing research: Book chapters and books. In *Writing about Quantitative Research in Applied Linguistics* (pp. 162-169). Palgrave Macmillan UK. https://doi.org/10.1057/9780230369955_14
- Yahya, M. A., Mansor, M. H., Zolkarnaini, W. A. A. W., Rusli, N. S., Aminuddin, A., Mohamad, K., Sabhan, F. A. M., Atik, A. A. A., & Ozair, L. N. (2018). A brief review on activated carbon derived from agriculture by-product. *AIP Conference Proceedings*, 1972(1), Article 030023. <https://doi.org/10.1063/1.5041244>
- Zhang, L., & Glänzel, W. (2012). Proceeding papers in journals versus the “regular” journal publications. *Journal of Informetrics*, 6(1), 88-96. <https://doi.org/10.1016/j.joi.2011.06.007>
- Zyoud, S. H., Zyoud, S. H., Al-Jabi, S. W., Sweileh, W. M., & Awang, R. (2016). Contribution of Arab countries to pharmaceutical wastewater literature: A bibliometric and comparative analysis of research output. *Annals of Occupational and Environmental Medicine*, 28(1), Article 28. <https://doi.org/10.1186/s40557-016-0117-0>

Validity and Reliability of Typhoid Risk Factors Questionnaire (TRFQ) in Gombe Metropolis, Gombe State, Nigeria

Umar Abdullahi Tawfiq^{1,2}, Shamarina Shohaimi^{1*}, Noor Hisham Mohd Nadzir¹, Syafinaz Amin Nordin³, Abdul Hafiz Ab Rahman⁴ and Nader Salari⁵

¹Department of Biology, Faculty of Science, Universiti Putra Malaysia, 43400 UPM, Serdang, Selangor, Malaysia

²Department of Microbiology, Gombe State University, 760214 Tudun Wada, Gombe, Nigeria

³Department of Medical Microbiology, Faculty of Medicine and Health Sciences, Universiti Putra Malaysia, 43400 UPM, Serdang, Selangor, Malaysia

⁴Faculty of Social Sciences and Humanities, Universiti Kebangsaan Malaysia, 43600 UKM, Bangi, Selangor, Malaysia

⁵Department of Biostatistics, School of Public Health, Kermanshah University of Medical Sciences, 6715847141, Kermanshah, Iran

ABSTRACT

Typhoid poses a significant threat to human health, particularly in Africa and Asia, where the disease continues to be endemic. Typhoid caused approximately 8.4 million disability-adjusted life-years worldwide in 2017, with 116,814 deaths. While vaccinations effectively eradicate the endemic infection, limited resources frequently constrained vaccination strategies. Thus, an understanding of the risks associated with typhoid would aid in implementing targeted interventions. In many states of Nigeria, including Gombe, data on typhoid risk factors are unavailable. This study aimed to develop and validate a questionnaire on typhoid risk factors in the Gombe Metropolis. The questionnaire items were based on previously published questionnaires on typhoid and localized typhoid risk factors. After obtaining ethical approval, the drafted instrument was pilot tested among a small

population and checked for readability. The questionnaire's content validity was checked using Fleiss' Multi-rater kappa, while internal consistency and test-retest reliability were checked using Cronbach's alpha and intraclass correlation coefficient (ICC), respectively. The questionnaire validation results revealed that the instruments' readability was easy, content validity with Fleiss' kappa value of 0.623 was good, internal consistency with Cronbach's alpha

ARTICLE INFO

Article history:

Received: 16 November 2021

Accepted: 25 January 2022

Published: 20 April 2022

DOI: <https://doi.org/10.47836/pjst.30.3.13>

E-mail addresses:

gs53842@student.upm.edu.my (Umar Abdullahi Tawfiq)

shamarina@upm.edu.my (Shamarina Shohaimi)

syafinaz@upm.edu.my (Syafinaz Amin Nordin)

mnhisham@upm.edu.my (Noor Hisham Mohd Nadzir Mohd)

abhafizrahman@gmail.com (Abdul Hafiz Ab Rahman)

n.salari@kums.ac.ir (Nader Salari)

* Corresponding author

value of 0.720 and McDonald's omega of 0.703, and test-retest reliability with an ICC estimate of 0.736 was good. The questionnaire was valid and reliable for collecting data on typhoid risk factors in Gombe State, Nigeria, to develop targeted health interventions and guide the Government's resource prioritization and allocation decisions for efficient disease control.

Keywords: Questionnaire, reliability, risk, typhoid, validity

INTRODUCTION

Typhoid fever has persisted as a considerable threat to health, especially across African and Asian countries, despite efforts targeting water hygiene improvements. The disease resulted from an infected individual with typhoidal bacteria known as *Salmonella typhi* by consuming either foods or drinkable items that have been contaminated with the bacteria. In 2017, there were reports that around 14,300,000 individuals had an enteric fever, which comprises typhoid and paratyphoid fevers, and approximately one out of every 100 of them had died. Approximations of the 2017 worldwide Disability-Adjusted Life Years (DALYs) resulting from *S. typhi* infections were placed at about 8.4 million with approximately 116,814 mortalities based on information provided by the Institute for Health Metrics and Evaluation (IHME) (Masinaei et al., 2020).

Providing enough healthy water and appropriate sanitation is recommended for *S. typhi* infection deterrence. Control efforts followed closely with safeguarding processing methods and systems of foods and other consumable items, employing fecal interaction safeguards, and efficiently managing disease occurrences. Immunizations have become invaluable as complementarily efficient tactics to curb an endemic infection or disrupt its spread amidst an outbreak. However, in nations with elevated burdens resulting from typhoid fever, communal widespread and scheduled typhoid immunization strategies are usually constrained (Khan et al., 2015).

Because there are many associated behavioral, demographic, socio-cultural, and environmental risk factors for typhoid infection, a comprehensive understanding of *S. typhi* risk factors has become critical. This understanding will guide the planning and implementation of vaccine-involved and non-vaccine prevention and control efforts against the disease. The World Health Organization (WHO) has advocated focusing vaccine-based typhoid control efforts on populations with high typhoid risk. As a result, typhoid conjugate vaccination strategies that target populations with high typhoid risks rather than traditional mass immunization schedules will benefit greatly. In addition, methods that produce isolated risks for distinct populations inside countries are invaluable to control efforts against this disease (Mogasale et al., 2014). Also, it is imperative that planning for efficient utilization of vaccination against typhoid must selectively target locations encompassing

populations with identified increased risks of typhoid fever since many nations especially developing countries of Africa and parts of Asia, have inadequate resources, which leads to them having to cope with control of *S. typhi* infection spread mainly in locations where it is endemic (Lee et al., 2016).

Many states in Nigeria, including Gombe, lack data on typhoid risk factors (Wong et al., 2016). Therefore, the goal of this study is to develop and validate a questionnaire tailored to the Gombe metropolis that can be used to collect behavioral, socio-cultural, and demographic data from laboratory-confirmed typhoid patients to develop a standard instrument for identifying typhoid risk factors in the area and provide data to aid targeted control and prevention efforts against the disease.

MATERIALS AND METHODS

Ethics

This study received ethical approval from the Gombe State Ministry of Health headquarters under the reference number MOH/ADM/S/658/VOL/II/122. In addition, informed consent, confidentiality, anonymous data collection/handling, and ethical research conduct were all adhered to.

Design

Items in the questionnaire were derived from and modified from previously published typhoid investigation questionnaires and forms, including the CRF: Case and control enrolment questionnaire (Jenkins, 2017), Enhanced typhoid and paratyphoid surveillance questionnaire (National Institute for Communicable Diseases, 2016). The questionnaire also included some locally observed variables associated with typhoid risk. The drafted questionnaire, which the Gombe State Ministry of Health had approved was then tested in a pilot study involving twenty typhoid patients at the Gombe State Specialist Hospital to identify vague or unclear questions, possible errors, or any issues with the comprehension of the questions and their options (Blázquez-Sánchez et al., 2020). In addition, the questionnaire's readability was evaluated to determine how simple it is to read and comprehend (Patalay et al., 2018).

Finally, the validation tests of the draft questionnaire were done using standard methods to investigate and analyze the instruments' construct validity (Vova-Chatzi et al., 2020), content validity, i.e., inter-rater agreement (O'Connor et al., 2020), internal consistency (Bäckström et al., 2020) and test-retest reliability (Mansukhani et al., 2019).

Study Population and Sample

The study population was laboratory-confirmed typhoid patients in Gombe State Specialist Hospital in the state's metropolitan area. They included only respondents that gave their

informed consent to participate, and there were no non-citizens involved in the study. This site was chosen among other state-owned and private health facilities based on the following criteria: frequently visited, easily accessible, proximity to more populated areas, and relative availability of diagnostic facilities. The sample size was determined to be 663 at a 95% confidence interval (CI) using CDC's EpiInfo software version 7.2.2.6 (CDC, 2020). The sampling was done using simple random sampling, and only questionnaires that were answered completely and properly were included in the study (n = 663). Sampling was done between 2nd July 2019 to 30th July 2019.

Questionnaire Draft

The questions in the questionnaire draft were closed-ended, and the instrument was self-administered (Namazi et al., 2020). The draft instrument was composed of 71 items which were derived by taking items from similar questionnaires available from literature, removing duplicate items, selecting items that could be related to the study area, and adding locally suspected typhoid risk factors, then placing the items under relevant headings, as described below.

Section A: Demographic information such as town area of residence, age, marital status, gender, and occupation, were derived from the "Suspected/confirmed typhoid fever case investigation form" of the National Institute for Communicable Diseases (National Institute for Communicable Diseases, 2016).

Section B: Socioeconomic status, which includes items such as "number of people in the house, having visitor within past two weeks, having house help, house help preparing food for the home, cockroaches inside the home, houseflies inside the home, typhoid case in the home within past two weeks, having typhoid carrier at home, been vaccinated against typhoid in past two years, type of toilet in residence, and do people defecate openly near your water source," was derived from the "CRF: Enrolment questionnaire for case and control" produced by Jenkins (2017). Only grammatical changes were made to the original items.

Section C: Behavior related items, for example, "Do you eat food from commercial sellers, do you consume iced/frozen drinks, do you eat fruits directly from the seller, do you wash your hands with soap before preparing food, do you wash your hands with soap before eating, do you wash your hands with soap after using the toilet, do you boil water before drinking, what type of animal do you have in your house, and how many times has a doctor treated you for typhoid fever before now," were also sourced from the "CRF: Enrolment questionnaire for case and control" produced by Jenkins (2017) and only grammatical changes were made to the sourced items.

Also included in the draft questionnaire under Section C (Behavior) is locally suspected typhoid risk factors which included drinking water from commercial sellers, eating zogale

(local salad) from commercial sellers, drinking nono (locally fermented milk) from commercial sellers, and drinking kunu (local beverage) from commercial sellers.

Readability Test

After making corrections observed from the pilot test, the readability of the questionnaire was investigated using the Flesch reading ease test and Flesch-Kincaid grade level test to determine how easy it is to read and understand the questionnaire and at what grade level of school a person ought to be able to do that, respectively. These were done using the proofing option in Microsoft Office Word 2016 (Patalay et al., 2018).

Statistical Analysis: Validation Studies

Content Validity. Content validity describes the magnitude to which the questionnaire elements represent the whole theoretical construct the questionnaire is conceived to evaluate. An expert panel comprising two epidemiologists, two public health professionals, two medical microbiologists, and two medical doctors assessed the content validity of each item in the questionnaire on a Likert scale ranging from “not relevant, somewhat relevant, quite relevant, to highly relevant.” These responses were then analyzed using Fleiss’ Multi-rater kappa to obtain the inter-rater agreement value at 95% CI (O’Connor et al., 2020). The value of kappa was inferred based on the following guide: values ≤ 0 indicate no agreement, 0.01–0.20 indicate none to a slight agreement, 0.21–0.40 as fair agreement, 0.41–0.60 as moderate agreement, 0.61–0.80 as substantial agreement, and 0.81–1.00 as almost perfect agreement (McHugh, 2012). This analysis was done using Statistical Product and Service Solutions (SPSS) version 26 (v26) for Windows.

Construct Validity and Internal Consistency. Construct validity is the magnitude to which the dimensions utilized assess the theory they evaluate (Ginty, 2013). It was investigated using Cronbach’s alpha value after an exploratory factor analysis (EFA) with varimax rotation and eigenvalue greater than one extraction criterion to reduce the data’s dimensionality. Prior to factor analysis, the Kaiser-Meyer-Olkin (KMO) test of sampling adequacy and Bartlett’s test of sphericity were done to ensure the sample was adequate and fit for factor analysis (Vova-Chatzi et al., 2020). The analyses were done using SPSS v26 for Windows.

The McDonald’s Omega (ω) coefficient was also calculated and used as another measure of construct validity due to the limitations of Cronbach’s alpha, including the assumptions of normality, tau-equivalence, and uncorrelated errors (Crutzen & Peters, 2017). The Omega coefficient was calculated using maximum likelihood (ML) factor analysis with an OMEGA macro for SPSS provided by Hayes and Coutts (2020).

Internal consistency signifies the level to which the questionnaire entries are coherent in measuring the identical construct (Tsang et al., 2017). This was investigated using Cronbach's alpha and McDonald's omega (ML) already described in the previous paragraph. The values of alpha and omega were interpreted using documented guidelines: > 0.9 = Excellent, > 0.8 = Good, > 0.7 = Acceptable, > 0.6 = Questionable, > 0.5 = Poor, < 0.5 = Unacceptable (Taber, 2018). This test was done using SPSS v26 for Windows.

Test-Retest Reliability. Test-retest reliability gauges the stability of the scores of a construct acquired from the same group of individuals on multiple instances (Vilagut, 2014). A group of thirty subjects filled the questionnaire twice with 14 days intervals between sessions. Their responses were analyzed using intraclass correlation coefficient (ICC) with a two-way mixed-effects model, absolute agreement definition, and 95% confidence level using SPSS v26 for Windows. The obtained ICC values were interpreted using published criteria (Abdullah et al., 2019).

RESULTS AND DISCUSSION

Demographic Characteristics of the Respondents

The demographic characteristics of the respondents (Table 1) revealed that they were diverse in terms of their age, gender, occupation, and marital status. The typhoid pathogen *Salmonella typhi* is possibly transmitted through the fecal-oral route by consuming contaminated food or water. Hence, all demographic groups are at risk depending on their

Table 1
Demographic characteristics of respondents (n= 663)

Variable	Category	Frequency	Percentage
Gender	Male	356	53.7
	Female	307	46.3
Age (years)	9 to 17	52	7.8
	18 to 35	418	63.0
	36 to 55	128	19.3
	56 to 65	56	8.5
	66 to 85	9	1.4
Occupation	Student	164	24.7
	Skilled Professional	116	17.5
	Semi-Skilled Professional	352	53.1
	Unskilled Professional	20	3.0
	Not working	11	1.7
Marital Status	Single	283	42.7
	Married	370	55.8
	Divorced	10	1.5

level of hygiene, sanitation, and access to safe food and clean water (Mogasale et al., 2014). These results agree with Lee et al. (2016), who had documented typhoid disease burden among different age groups in low and middle-income countries.

Readability

The readability test results revealed that the draft questionnaire had a Flesch reading ease test value of 79.6 and a Flesch-Kincaid grade level test of 4.5. In contrast, the final validated questionnaire had a Flesch reading ease test value of 70.8 and a Flesch-Kincaid grade level test of 6.0. The results of the questionnaire readability test showed that the questionnaire was “easy to read” based on published guidelines which stated that outcomes of the Flesch reading ease test with values from 60 to 100 are deemed easy to read. In contrast, the Flesch-Kincaid grade level test result implied that the questionnaire could be read and understood by a person between the 4th and 6th grade of school according to documented criteria (Stetson et al., 2011).

Content Validity

The Fleiss’ kappa test to evaluate the agreement between the responses of the eight raters regarding the relevance of each questionnaire item as a typhoid risk factor revealed that there was an overall good agreement between the raters, $\kappa = 0.623$, standard error (S.E.) = 0.017, $p < 0.05$, with 95% CI values of 0.622 to 0.624. The level of inter-rater agreement on the rated categories of the individual questionnaire items is shown in Table 2. In addition, the results of the content validity test revealed that the items in the questionnaire are, to a good extent, representative of the total theoretical construct the questionnaire was devised to evaluate, based on the description of content validity and interpretation of Fleiss’ Kappa (McHugh, 2012) which implied that a kappa value above 0.60 signifies good agreement amongst raters and confidence ought to be attributed to the outcomes of that study.

Table 2
Values of Fleiss’ kappa test for inter-rater agreement

Questionnaire item rating category	Fleiss' kappa value	Standard error (S.E.)	Significance	95% Confidence Interval	
				Lower bound	Upper bound
1	0.475	0.023	$p < 0.05$	0.474	0.477
2	0.330	0.023	$p < 0.05$	0.329	0.332
3	0.688	0.023	$p < 0.05$	0.687	0.690
4	0.687	0.023	$p < 0.05$	0.685	0.688

Construct Validity and Internal Consistency

These were achieved by carrying out exploratory factor analysis (EFA) followed by Cronbach’s alpha determination and subsequent determination of McDonald’s omega.

Exploratory Factor Analysis

The outcome value of the KMO test for sampling adequacy was 0.799, and that of Bartlett's test of sphericity was $p < 0.01$, after which the EFA outcome (Table 3) was used to assign items to factors that were retained in the draft questionnaire. The EFA model estimates for

Table 3
Items retained in the draft questionnaire after EFA

Items used in the EFA	Factor loadings	Factor solution	Factor s/n	Variance explained
Toilets near a water source	0.824	Toilets/feces near a water source	1	4.855
Animal farms near a water source	0.741			
Humans defecate openly near a water source	0.731			
Crop farms near a water source	0.595			
Open sewage in home	0.345			
Eat commercial salads/ <i>zogale</i>	0.729	Eat commercial foods/ drinks	2	9.195
Eat food from commercial sellers	0.718			
Drink commercial <i>kunu</i>	0.696			
Drink water from commercial sellers	0.660			
Drink commercial cow milk/ <i>nono</i>	0.609			
Eat fruits directly from the seller	0.366			
Wash hands with soap before eating	0.796	Wash hands with soap before handling food	3	13.009
Wash hands with soap before preparing food	0.719			
Wash hands with soap after using the toilet	0.707			
Wash hands with soap after changing the diaper	0.469			
Type of water used for bathing	0.935	Type of drinking water	4	16.339
Type of water used for brushing teeth	0.881			
Type of drinking water	0.681			
Others in-home vaccinated against typhoid in last two years	0.768	Vaccination against typhoid in your area within last two years	5	19.179
Vaccinated against typhoid in last two years	0.738			
Tiles on the toilet floor	0.777	Have tiles on the kitchen floor	6	21.783
Tiles on the kitchen floor	0.759			
Proximity of water body to the main road	0.648	Collect any food material from river or stream	7	24.373
Collect other food material from a water body	0.582			

Table 3 (continue)

Items used in the EFA	Factor loadings	Factor solution	Factor s/n	Variance explained
Fishing in a water body	0.475			
Age group	0.782	Occupation	8	26.928
Marital status	0.729			
Occupation	0.651			
Consume iced or frozen drinks	0.870	Consume iced or frozen products	9	29.139
Use ice blocks or ice cubes	0.635			
Consume imported products within last two weeks	0.357			
Have house help	0.793	Have houseboy or house girl	10	31.292
House help prepare food	0.745			
Work with hands-on a farm	0.793	Work with hands-on a farm	11	33.427
Apply manure/local fertilizer with hands-on farm	0.712			
Attend mass gathering within last two weeks	0.975	Attend any mass gathering in the past two weeks	12	35.468
Consume anything in a mass gathering in the last two weeks	0.573			
Flood in the entire town	0.711	Flood in your area	13	37.417
Flood near home	0.674			
Flood inside home	0.354			
Re-heat kept food before eating	0.597	Re-heat kept food before eating	14	39.346
Keep cooked food in the refrigerator	0.546			
Keep cooked food for later	0.418			
Cockroaches inside home	0.681	Cockroaches inside home	15	41.040
Flies inside home	0.602			
Sharing plate with others at the same time	0.565	Sharing eating utensils with others at the same time	16	44.260
Sharing spoon with others at the same time	0.368			
Eating with bare hands	0.355			
Type of animal in the house	0.419	Type of kitchen in home	17	45.744
Type of kitchen	0.384			
Method of collecting stored drinking water	0.301			
Local Government Area (LGA) you live in	0.559	Area you live in your LGA	18	46.892
Area you live in your LGA	0.475			

goodness of fit include $p < 0.01$, $df = 1254$, and $\chi^2 = 1747.026$. Other items not included in the EFA but thought to have clinical importance to typhoid risk were retained in the draft questionnaire. These included: boiling water before drinking, other treatment for drinking water, using public toilets, having other typhoid patients in the home within the past two weeks, having a typhoid carrier at home, level of education, and previous typhoid episodes. The draft questionnaire was reduced to a total of 25 items.

Cronbach's Alpha Determination

The Cronbach's alpha test outcome revealed that overall, the alpha value was 0.720 with a mean of 43.76, a variance of 47.573, and a standard deviation of 6.897. To obtain the above alpha value and hence a good construct validity, results of the item-total statistics in the SPSS reliability (validity) test were used to delete draft questionnaire items with higher "Cronbach's alpha value if item deleted" until the remaining items ($n = 21$) had an overall Cronbach's alpha of 0.720. The deleted items included: type of drinking water (EFA factor 4), occupation (EFA factor 8), flood in your area (EFA factor 13), and area you live in your local government area (EFA factor 18). Also, some questionnaire items with Cronbach's alpha if item deleted value greater than the overall alpha value were retained because removing them would still maintain the overall alpha value within the same interpretive range it was previously. The items subsequently retained in the questionnaire are shown in Table 4.

Table 4
Items retained in the questionnaire after Cronbach's alpha determination

Questionnaire items	Scale Mean if Item Deleted	Scale Variance if Item Deleted	Corrected Item-Total Correlation	Cronbach's alpha if item deleted
1) Do you have a houseboy or housegirl?	41.42	43.652	0.268	0.711
2) Do you re-heat kept food before eating?	42.32	46.745	0.034	0.728
3) Do you usually see cockroaches inside your house?	42.21	46.312	0.078	0.725
4) Has anyone had typhoid in your house within the last two weeks?	41.78	44.445	0.201	0.717
5) Has a doctor ever told anyone in your house that he/she is a typhoid carrier?	41.69	42.231	0.403	0.700
6) Has there been typhoid vaccination in the last two years in your area?	41.54	41.916	0.432	0.697
7) Are there any toilets/feces near your water source?	41.36	42.446	0.413	0.699
8) Do you work with your hands on a farm?	41.51	42.259	0.393	0.700
9) Do you collect any food material from any river or stream?	41.29	42.694	0.428	0.699

Table 4 (continue)

Questionnaire items	Scale Mean if Item Deleted	Scale Variance if Item Deleted	Corrected Item-Total Correlation	Cronbach's alpha if item deleted
10) What is your level of education?	40.98	42.324	0.340	0.705
11) Do you consume food/drinks from commercial sellers?	42.09	44.832	0.177	0.719
12) Do you consume iced/frozen items?	42.11	44.543	0.215	0.716
13) Do you share eating utensils at the same time with others?	42.11	44.957	0.197	0.717
14) Did you attend any mass gatherings within the past two weeks?	41.72	44.369	0.204	0.717
15) Do you wash your hands with soap before handling food?	41.95	43.493	0.292	0.709
16) Do you boil water before drinking?	41.35	41.461	0.548	0.689
17) Do you use public toilets?	41.86	44.674	0.225	0.715
18) Do you have tiles on your kitchen floor?	41.76	43.072	0.289	0.710
19) What type of kitchen do you have?	41.41	44.468	0.189	0.719
20) Do you treat drinking water in any of these other ways?	41.31	42.410	0.418	0.699
21) How many times has a doctor treated you for typhoid fever before now?	41.52	45.513	0.118	0.724

McDonald's Omega Determination

The McDonald's Omega (ω) coefficient value was 0.703. However, it was only obtained after deleting EFA factor 14 (Do you re-heat kept food before eating? α if item deleted = 0.728) and EFA factor 15 (Do you usually see cockroaches inside your house? α if item deleted = 0.725) from the alpha-validated questionnaire which initially produced ω = 0.697. The remaining items in the questionnaire ($n = 19$) were then subjected to test-retest reliability analysis (Table 5).

The questionnaire's construct validity and internal consistency are acceptable based on the Cronbach's alpha and McDonald's omega values obtained in this study after an EFA. A KMO test for sampling adequacy and Bartlett's test for sphericity revealed that the data obtained using the content validated questionnaire was adequate and fit for factor analysis based on the interpretive criteria previously documented (Vova-Chatzi et al., 2020), which implied that KMO values with 0.50 and above are deemed suitable for factor analysis and that Bartlett's test of sphericity ought to be significant for factor analysis to be suitable to the data. The EFA model with statistically significant goodness of fit reduced the questionnaire items from 70 to 18. It is in line with a published work by Liu et al. (2018), where EFA was used to reduce 65 questions in a questionnaire into nine extracted dimensions. After the EFA, the questionnaire items were summed up to 25 by adding some items not included

in the EFA but are thought to have clinical significance to determining typhoid risk factors in the study area. Some items with factor loadings less than 0.4 were still retained in the questionnaire because it has been shown that a supplementary moderate score limit of ≤ 0.40 may be utilized to enable differentiation between items of a questionnaire during the initial stages of design and validation (Ugulu, 2013). Subsequently, the Cronbach's alpha and McDonald's omega analyses produced values indicative of good construct validity and internal consistency based on previously documented interpretive criteria, which described alpha and hence omega values greater than 0.70 as acceptable for instrument construct validity internal consistency.

Table 5
Items retained in the questionnaire after McDonald's omega determination

Questionnaire item	Mean	SD	Error variance
1) Do you have a houseboy or housegirl?	1.554	0.710	0.503
2) Has anyone had typhoid in your house within the last two weeks?	1.986	0.880	0.729
3) Has a doctor ever told anyone in your house that he/she is a typhoid carrier?	2.078	0.874	0.629
4) Has there been typhoid vaccination in the last two years in your area?	2.341	0.885	0.710
5) Are there any toilets/feces near your water source?	2.401	0.826	0.526
6) Do you work with your hands on a farm?	2.259	0.886	0.641
7) Do you collect any food material from any river or stream?	1.810	0.866	0.636
8) What is your level of education?	2.781	0.973	0.785
9) Do you consume food/drinks from commercial sellers?	2.457	0.823	0.503
10) Do you consume iced/frozen items?	2.047	0.889	0.751
11) Do you share eating utensils at the same time with others?	1.658	0.767	0.564
12) Did you attend any mass gatherings within the past two weeks?	1.658	0.822	0.642
13) Do you wash your hands with soap before handling food?	2.478	0.767	0.416
14) Do you boil water before drinking?	2.413	0.780	0.331
15) Do you use public toilets?	1.902	0.768	0.560
16) Do you have tiles on your kitchen floor?	2.002	0.948	0.777
17) What type of kitchen do you have?	2.359	0.905	0.774
18) Do you treat drinking water in any of these other ways?	1.243	0.504	0.253
19) How many times has a doctor treated you for typhoid fever before now?	2.243	0.846	0.684

Test-Retest Reliability

The resulting overall ICC value was 0.736 with 95% CI values of 0.533 to 0.878, and $p < 0.01$. The test-retest reliability overall ICC estimate indicated that the questionnaire has good test-retest reliability. The 95% CI values of the ICC estimates indicate that the

reliability of the questionnaire is moderate at the worst-case scenario represented by the lower bound ICC value of 0.533 and very good at the best-case scenario represented by the upper bound ICC value of 0.878. These interpretations were based on documented guidelines which also suggested that confidence intervals of the ICC estimate and not just the overall ICC estimate should be utilized as the elements for evaluating levels of instrument reliability (Koo & Li, 2016).

CONCLUSION

To the best of the authors' knowledge, this questionnaire specific to the Gombe metropolis of Gombe State, Nigeria, is the first of its kind to be designed and validated using standard methods. At the end of the various validation tests, it was established that the questionnaire is easy to read and understand, has moderate reliability, and has good validity. Hence, the instrument can collect data to identify typhoid risk factors in the study area to create targeted health interventions and guide the Government's financial decisions on resource prioritization and efficient allocation to prevent and control the disease.

ACKNOWLEDGEMENT

The authors wish to acknowledge Alh Umar Bappah for the ethical clearance process.

REFERENCES

- Abdullah, M., Maulahela, H., Utari, A. P., Kusumo, P. D., Soebandrio, A., Achmad, I., William, A., & Makmun, D. (2019). Patient assessment of constipation quality of life questionnaire: validity and reliability for Indonesian population. *Medical Journal of Indonesia*, 28(4), 345-350. <https://doi.org/10.13181/mji.v28i4.3353>
- Bäckström, J., Fogelberg, J., Gabrielsson, G., Lindberg, M., Arving, C., & Hellström, K. (2020). Reliability and internal consistency of the Swedish version of the MAaStricht Nurses Activities INventory (MAINtAIN(S))—A pilot testing of the tool. *Geriatric Nursing*, 41(6), 790-803. <https://doi.org/10.1016/j.gerinurse.2020.04.012>
- Blázquez-Sánchez, N., Rivas-Ruiz, F., Bueno-Fernández, S., Arias-Santiago, S., Fernández-Morano, M. T., & deTroya-Martín, M. (2020). Validation of a questionnaire designed to study knowledge, attitudes, and habits related to sun exposure among young adults: The CHACES questionnaire. *Actas Dermo-Sifiliográficas (English Edition)*, 111(7), 579-589. <https://doi.org/10.1016/j.adengl.2020.08.006>
- CDC. (2020). *Epi Info™* | CDC. Centers for disease control and prevention. <https://www.cdc.gov/epiinfo/index.html>
- Crutzen, R., & Peters, G. J. Y. (2017). Scale quality: alpha is an inadequate estimate, and factor-analytic evidence is needed first of all. *Health Psychology Review*, 11(3), 242-247. <https://doi.org/10.1080/17437199.2015.1124240>

- Ginty, A. T. (2013). Construct validity. In M. D. Gellman & J. R. Turner (Eds.), *Encyclopedia of Behavioral Medicine* (pp. 487-487). Springer. https://doi.org/10.1007/978-1-4419-1005-9_861
- Hayes, A. F., & Coutts, J. J. (2020). Use omega rather than cronbach's alpha for estimating reliability. *But...* *Communication Methods and Measures*, *14*(1), 1-24. <https://doi.org/10.1080/19312458.2020.1718629>
- Jenkins, A. P. (2017). *A nested environmental approach to typhoid epidemiology in Central Division, Fiji* (Doctoral dissertation). Edith Cowan University, Australia. <https://ro.ecu.edu.au/cgi/viewcontent.cgi?article=2994&context=theses>
- Khan, M. I., Pach, A., Khan, G. M., Bajracharya, D., Sahastrabuddhe, S., Bhutta, W., Tahir, R., Soofi, S., Thapa, C. B., Joshi, N., Puri, M. K., Shrestha, P., Upreti, S. R., Clemens, J. D., Bhutta, Z., & Ochiai, R. L. (2015). Typhoid vaccine introduction: An evidence-based pilot implementation project in Nepal and Pakistan. *Vaccine*, *33*(S3), C62-C67. <https://doi.org/10.1016/j.vaccine.2015.03.087>
- Koo, T. K., & Li, M. Y. (2016). A guideline of selecting and reporting intraclass correlation coefficients for reliability research. *Journal of Chiropractic Medicine*, *15*(2), 155-163. <https://doi.org/10.1016/j.jcm.2016.02.012>
- Lee, J. S., Mogasale, V. V., Mogasale, V., & Lee, K. (2016). Geographical distribution of typhoid risk factors in low and middle-income countries. *BMC Infectious Diseases*, *16*(1), Article 732. <https://doi.org/10.1186/s12879-016-2074-1>
- Liu, W., Zhao, T., Zhou, W., & Tang, J. (2018). Safety risk factors of metro tunnel construction in China: An integrated study with EFA and SEM. *Safety Science*, *105*, 98-113. <https://doi.org/10.1016/j.ssci.2018.01.009>
- Mansukhani, S. A., Hatt, S. R., Leske, D. A., & Holmes, J. M. (2019). Test-retest reliability of the revised diplopia questionnaire. *Journal of AAPOS*, *23*(6), 319.e1-319.e5. <https://doi.org/10.1016/j.jaaapos.2019.08.277>
- Masinaei, M., Eshrati, B., & Yaseri, M. (2020). Spatial and spatiotemporal patterns of typhoid fever and investigation of their relationship with potential risk factors in Iran, 2012-2017. *International Journal of Hygiene and Environmental Health*, *224*, Article 113432. <https://doi.org/10.1016/j.ijheh.2019.113432>
- McHugh, M. L. (2012). Interrater reliability: the kappa statistic. *Biochemia Medica*, *22*(3), 276-282. <https://doi.org/10.11613/bm.2012.031>
- Mogasale, V., Maskery, B., Ochiai, R. L., Lee, J. S., Mogasale, V. V., Ramani, E., Kim, Y. E., Park, J. K., & Wierzbica, T. F. (2014). Burden of typhoid fever in low-income and middle-income countries: a systematic, literature-based update with risk-factor adjustment. *The Lancet Global Health*, *2*(10), e570-e580. [https://doi.org/10.1016/S2214-109X\(14\)70301-8](https://doi.org/10.1016/S2214-109X(14)70301-8)
- Namazi, M., Zareiyan, A., Jafarabadi, M., & Moghadam, Z. B. (2020). Endometriosis reproductive health questionnaire (ERHQ): A self-administered questionnaire to measure the reproductive health in women with endometriosis. *Journal of Gynecology Obstetrics and Human Reproduction*, *50*(3), Article 101860. <https://doi.org/10.1016/j.jogoh.2020.101860>
- National Institute for Communicable Diseases (2016). *Typhoid: NICD guidelines for diagnosis, management and public health response*. http://www.nicd.ac.za/assets/files/Guidelines_typhoid_20160125.pdf.
- O'Connor, L., Porter, L., Dugas, J., Robinson, C., Carrillo, E., Knowles, K., Nelson, K. P., Gigliotti, R., Tennyson, J., Weisberg, S., & Rebesco, M. (2020). Measuring agreement among prehospital providers

- and physicians in patient capacity determination. *Academic Emergency Medicine*, 27(7), 580-587. <https://doi.org/10.1111/acem.13941>
- Patalay, P., Hayes, D., & Wolpert, M. (2018). Assessing the readability of the self-reported strengths and difficulties questionnaire. *BJPsych Open*, 4(2), 55-57. <https://doi.org/10.1192/bjo.2017.13>
- Stetson, B., Schlundt, D., Rothschild, C., Floyd, J. E., Rogers, W., & Mokshagundam, S. P. (2011). Development and validation of the personal diabetes questionnaire (PDQ): A measure of diabetes self-care behaviors, perceptions and barriers. *Diabetes Research and Clinical Practice*, 91(3), 321-332. <https://doi.org/10.1016/j.diabres.2010.12.002>
- Taber, K. S. (2018). The use of cronbach's alpha when developing and reporting research instruments in science education. *Research in Science Education*, 48(6), 1273-1296. <https://doi.org/10.1007/s11165-016-9602-2>
- Tsang, S., Royse, C. F., & Terkawi, A. S. (2017). Guidelines for developing, translating, and validating a questionnaire in perioperative and pain medicine. *Saudi Journal of Anaesthesia*, 11(5), S80-S89. https://doi.org/10.4103/sja.SJA_203_17
- Ugulu, I. (2013). Confirmatory factor analysis for testing validity and reliability of traditional knowledge scale to measure university students' attitudes. *Educational Research and Reviews*, 8(16), Article E2DD31C7190.
- Vilagut, G. (2014). Test-retest reliability. In A. C. Michalos (Ed), *Encyclopedia of Quality of Life and Well-Being Research* (pp. 6622-6625). Springer. https://doi.org/10.1007/978-94-007-0753-5_3001
- Vova-Chatzi, C., Symvoulakis, E., Parpoula, C., Sbarouni, V., & Lionis, C. (2020). Robustness of the EUROPEP questionnaire as regards data quality, reliability, and construct validity: The Greek experience before and after the economic crisis. *Health Policy*, 124(8), 856-864. <https://doi.org/10.1016/j.healthpol.2020.05.021>
- Wong, V. K., Holt, K. E., Okoro, C., Baker, S., Pickard, D. J., Marks, F., Page, A. J., Olanipekun, G., Munir, H., Alter, R., Fey, P. D., Feasey, N. A., Weill, F.-X., Le Hello, S., Hart, P. J., Kariuki, S., Breiman, R. F., Gordon, M. A., Heyderman, R. S., ... & Obaro, S. (2016). Molecular surveillance identifies multiple transmissions of typhoid in West Africa. *International Typhoid Consortium*, 10(9), Article e0004781. <https://doi.org/10.1371/journal.pntd.0004781>



Leaching of Electric Arc Furnace Slag for Selective Recovery of Iron: Effect of Temperature, H₂SO₄/HCl Acid, and Oxidant Concentration

Faizatul Syazwani Zulkifili¹, Hawaiah Imam Maarof^{1,2}, Norhaslinda Nasuha^{1,2} and Siti Wahidah Puasa^{1,3*}

¹School of Chemical Engineering, College of Engineering, Universiti Teknologi MARA, 40450 UiTM, Shah Alam, Selangor, Malaysia

²Hybrid Nanomaterials, Interfaces & Simulation (HYMFAST), School of Chemical Engineering, College of Engineering, Universiti Teknologi MARA, Cawangan Pulau Pinang, 13500 UiTM, Permatang Pauh, Pulau Pinang, Malaysia

³Integration Separation Technology Research Group (i-STRonG), College of Engineering, Universiti Teknologi MARA, 40450 UiTM, Shah Alam, Selangor, Malaysia

ABSTRACT

A significant amount of electric arc furnace slag (EAFS) is generated as a by-product from the steelmaking industry. Acid leaching was carried out with both the presence and absence of oxidants to intensify the iron recovery from EAFS in the final product. Oxidative leaching refers to the process whereby the oxidant helps in removing one or more electrons in a chemical reaction. In contrast, non-oxidative leaching means there is no transfer of electrons during the process. In this study, hydrogen peroxide and potassium permanganate were used as the oxidants in the leaching process. The influences of the leaching factors, such as the concentration of leaching reagent (0.5–8 M), leaching temperature (323–363 K), EAFS particle size (50–300 µm) and concentration of the oxidants (0.5–2 M), were also studied. The findings revealed that the particle size, acid dosage and type of oxidants significantly

influenced iron recovery. Smaller particle sizes greatly improved the recovery of iron. In the non-oxidative leaching environment, sulphuric acid exhibited a higher iron recovery than hydrochloric acid. The recovery efficiency was 21.47% higher. For oxidative leaching, the leaching efficiency of iron was more favourable at lower concentrations of hydrogen peroxide in both sulphuric and hydrochloric acid, and the

ARTICLE INFO

Article history:

Received: 07 December 2021

Accepted: 17 February 2022

Published: 20 April 2022

DOI: <https://doi.org/10.47836/pjst.30.3.14>

E-mail addresses:

faizatulsyazwani@gmail.com (Faizatul Syazwani Zulkifili)

hawaiah162@uitm.edu.my (Hawaiah Imam Maarof)

norhaslinda.nasuha@uitm.edu.my (Norhaslinda Nasuha)

sitiwahida@uitm.edu.my (Siti Wahidah Puasa)

* Corresponding author

opposite was the case for potassium permanganate. An overdose of hydrogen peroxide can cause radical quenching, which will reduce oxidant utilisation. Oxidative leaching resulted in better iron recovery at optimum leaching conditions with a temperature of 50°C, 5 M H₂SO₄, 1 M hydrogen peroxide, a leaching time of 60 minutes, a solid to liquid ratio of 1:20 and a stirring rate of 300 rpm.

Keywords: Acid leaching, EAF slag, hydrogen peroxide, iron, oxidant, sulphuric acid

INTRODUCTION

Steel makes a major contribution to the development of the modern world across the globe due to its many applications in appliances, construction, and transportation (Keymanesh et al., 2021; Kim & Azimi, 2020; Zhang et al., 2019). Thus, steelmaking production is expected to be tremendous to meet the high steel demand. As reported by the World Steel Association, the production of crude steel up to March 2021 was 169.5 million tonnes with an increment of 23.3% compared to April 2020 and with China being the largest steel producer. Monosi et al. (2016) reported that the discharged product from crude steel production is around 11–20 kg per ton of steel. Iron slag can be categorised into several categories corresponding to their processes: blast furnace slag (BFS) and electric arc furnace slag (EAFS).

EAFS is one of the by-products of the steelmaking industry, resulting from the melting and preliminary acid refining of the liquid steel. It is typically dark in colour, angular shaped fractions and has a hard and rough texture (Hafez et al., 2021; Martinho et al., 2018; Roy et al., 2020). Teo et al. (2019), Fisher and Barron (2019), and Roy et al. (2019) previously reported that the major components of EAFS consist of iron, calcium, silica and traces of manganese and lead. Most metallurgical companies generate large amounts of hazardous wastes containing dissolved toxic metals. Landfilling or incineration are the traditional techniques for disposing of this solid waste, although neither approach appears to be effective (Kremser et al., 2021; Plaza et al., 2021). Meanwhile, the constant opening of landfills is always linked to environmental risks as this not only disrupts flora and fauna but also takes up more space. Halli et al. (2020) reported that landfilling with this metal-containing waste should not be promoted due to the toxic and carcinogenic nature of EAFS. Furthermore, dumping can also reduce the porosity and permeability of the soil (Roy et al., 2018). Currently, waste reduction takes precedence over other methods, and landfilling waste should be the final option to be considered (Yang et al., 2017).

Recycling and promoting the utilisation of EAFS has been identified as the best sustainable alternative when handling the vast amount of solid waste generated by the steelmaking sector. Brooks et al. (2019) reported that recycling helps by diverting waste from landfills, allowing it to be recovered into usable secondary products, hence conserving

energy and resources. However, preliminary research on the recycling of ferrous metals from EAFS means its application has been limited. Prior research on leaching from electric arc furnace slag has been identified. However, those findings have focused on non-ferrous metals such as zinc, phosphate and manganese recovery with no iron in the final product. Several studies have been conducted on the recycling of iron for secondary applications. Previously, Nasuha et al. (2017) discovered the usage of activated EAFS as an effective Fenton catalyst in photodegrading methylene blue and acid blue. Additionally, Nasuha et al. (2016) explored how EAFS may be used and recycled as a wastewater treatment catalyst. It was found that through a heterogeneous Fenton-like reaction, the thermally treated EAFS was capable of eliminating organic dyes. However, the work to selectively recover and maximise the amount of iron in the final product (the catalyst) has not been adequately addressed due to the complex composition of iron itself.

In the previous work, the leaching of iron from EAFS was done (Nasuha et al., 2019); however, the leaching was done at a high temperature and longer reaction time. In addition, the total dissolution of iron from EAFS using nitric acid also has not been highlighted. Given these issues, the goal of this study was to evaluate an existing leaching technique for increasing the amount of selectively iron in the final product to be used as a catalyst in a shorter period and at a lower leaching temperature. Since iron is the element that makes up approximately half of the slag composition, this was seen as an excellent way to recover iron at its maximum capacity and a lower cost. By utilising this method, raw iron utilisation can be reduced, and earth sustainability can be achieved.

METHODOLOGY

Material

The EAFS was obtained from a local steel company in Penang. Sulphuric acid (H_2SO_4 , 98%), hydrogen peroxide (H_2O_2 , 30%), potassium permanganate (KMnO_4), nitric acid (HNO_3 , 70%) were purchased from Sigma-Aldrich while hydrochloric acid (HCl , 37%) was obtained from Merck. The particle size, temperature and concentration of the studied oxidant were 50-300 μm , 50–90°C and 0.5–8 M, respectively.

Method

The EAFS was crushed in a ball mill and sieved to a size range of 50–300 μm . The raw sample was sent for X-ray fluorescence (XRF) (PANanalytical, Epsilon 3-XL) to determine the minerals' composition. In determining the initial iron concentration, 0.5 g crushed EAFS was diluted in 100 mL nitric acid with a solid to liquid ratio of 1 to 200 for 120 minutes. The leachate was then sent for atomic absorption spectroscopy, AAS (Hitachi, Z-2000) for further analysis. For non-oxidative leaching, the powdered EAFS (5 g) was added into 100

mL of an acid solution of predetermined concentrations between 0.5-8 M at a solid to liquid ratio of 1:20. The mixture was heated at 50°C for 60 minutes and filtered. The filtrate was then sent for analysis using a spectrophotometer (Hach, DR6000). FerroVer iron reagent powder pillows (Hach, range: 0.02 to 3.00 mg/L) were used with the spectrophotometer (510 nm) to analyse the amount of iron in the leachate, and it was allowed to react for three minutes. Next, hydrogen peroxide was added as the oxidising agent to the leaching medium and stirred at 300 rpm for the oxidative leaching environment. Meanwhile, the hydrogen peroxide was replaced by potassium permanganate. The leaching experiments were conducted three times to achieve the average value.

RESULTS AND DISCUSSION

XRF Analysis

XRF analysis was performed to determine the chemical composition of EAFS and was tabulated in Table 1. It can be seen that Fe, Ca, Si, Al, Mg and Mn were all present in significant concentrations. Iron, calcium, and silicon oxides made up roughly around 75% of the chemical compositions with minor traces of magnesium and manganese oxides.

Size of Particles

Various particle sizes in the range of 50 to 300 µm was prepared. Nitric acid was chosen as the lixiviant in determining the initial concentration of iron in the raw EAFS as it acts as a strong oxidising agent, which renders it a competent leaching agent for EAFS (Rao et al., 2021). Furthermore, it can dissolve most metals to form metal nitrates (Mohammadzadeh et al., 2020). A solid to liquid of 1 to 200 was selected because it improved the solution’s viscosity and promoted better leaching. The initial iron concentration was exactly 5000 mg/L, and the characterisation in size variation on the recovery of iron is shown in Table 2. From the Table 2, it can be seen that 75 µm resulted in the highest iron recovery with 48% recovery efficiency. Particles below 50 and 125 µm were considered fine and coarse materials, respectively. Zhang and Liu (2017) reported that the tendency for finer materials to remain near the top and coarse materials to roll down towards the base of the container might result in spatial heterogeneity in particle size. Thus,

Table 1
Chemical composition of EAFS

<i>Oxides</i>	<i>%</i>
Fe ₂ O ₃	26.79
CaO	35.61
SiO ₂	15.04
Al ₂ O ₃	5.15
MgO	3.59
MnO	4.36

Table 2
Recovery of Fe in nitric acid solution

<i>Size (µm)</i>	<i>Amount of Iron Being Leached Out (mg/L)*</i>
50	1600
75	2400
125	1300
200	2000
300	1000

*Amount of iron being leached out: ± 1%

this occurrence leads to fluctuations in the recovery of iron from particles of different sizes. The highest iron recovery from the various sizes resulted from 75 μm because this size was gradually exposed to the leaching solution, enabling more dissolution (Ji et al., 2021; Yin & Chen, 2021). Therefore, 75 μm was selected as the size in the subsequent experiments.

Effect of Temperature

Temperature plays an important role in hydrometallurgy as it relates to the kinetics of the reaction (Hazaveh et al., 2020). The amounts of iron recovered from different leaching lixiviants are shown in Figure 1. It can be reported that leaching in sulphuric acid is higher than hydrochloric acid. Therefore, the optimum temperature was 50°C (at 5 M H_2SO_4) when 5966.7 mg/L of iron was leached out. Kukurugya et al. (2015) proclaimed that the highest iron reaction was 95°C with 1M H_2SO_4 . However, it was contradictory to this study as the leaching agent concentration made a major difference. It was because, at low sulphuric acid concentration, the amount of sulphuric acid remained low and unable to supply sufficient SO_4^{2-} . As a result, it could not form the $\text{Fe}_2(\text{SO}_4)_3$ complex. Also, the heat generated by 5 M H_2SO_4 was higher than that of 1 M H_2SO_4 , and it can react at a lower leaching temperature. The drastic drop in iron concentration between 50 and 60°C in the HCl environment was because most iron has been leached out at 50°C and the remaining hard iron in the core of EAFs was still accessible to the lixiviant albeit difficult. Also, the diffusion of the lixiviant to contact the surface of this metals fraction was the rate-limiting step. Therefore, 50°C was selected as the optimum temperature for iron dissolution.

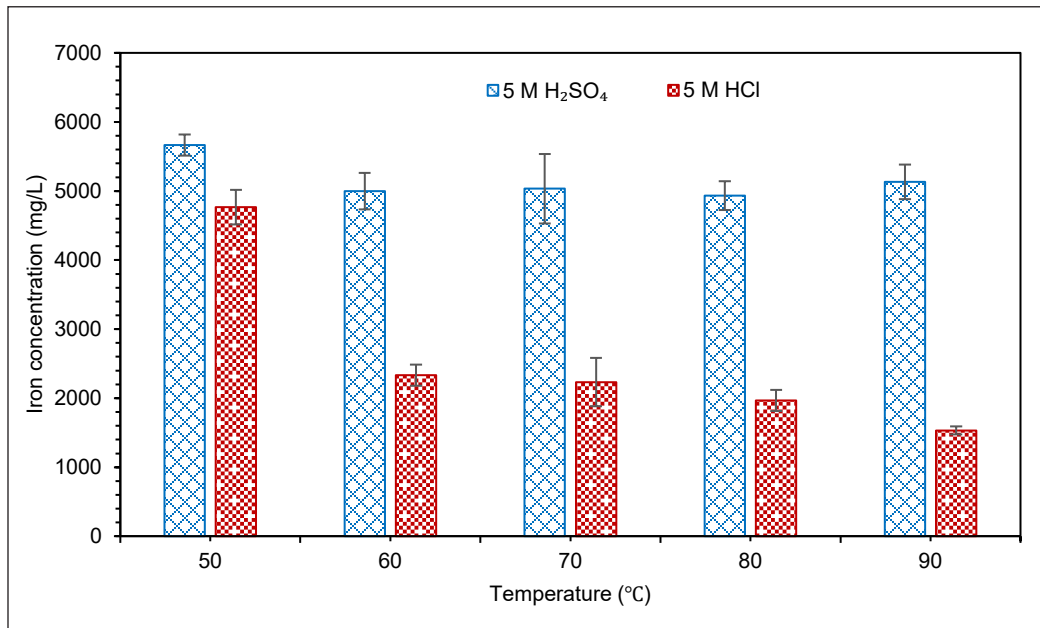


Figure 1. Effect of temperature on iron concentration in leachate

Effect of Oxidant Concentration

The oxidant concentration varied between 0.5–2 M, and the result is depicted in Figures 2a and 2b. It can be seen that the difference in H_2O_2 oxidant concentration between 0.5 and 1 M increased the iron recovery. Li et al. (2021) reported that an increase in the amount of hydrogen peroxide could provide more O^{2-} but the leaching efficiency would slowly decrease when the concentration of H_2O_2 is increased to a certain extent. However, an overdose supply of H_2O_2 may cause radical quenching, which reduces oxidant utilisation efficiency, limiting iron dissolution (Wang et al., 2021). It can also be seen that the recovery of iron in HCl with H_2O_2 as the oxidant all took place at approximately 8000 mg/L, which indicates that the effect of H_2O_2 concentration was not significant. KMnO_4 , on the other side, is capable of recovering more iron in HCl compared to H_2SO_4 . The recovery of iron decreases after 1 M in H_2SO_4 and HCl because the iron was saturated at 8000 mg/L in the leaching solution (Linsong et al., 2020). Lie et al. (2021) reported that the equilibrium state happened since all acidity was consumed; hence, no more iron could be leached out. The oxidation potential of H_2O_2 was 1.8 V. Meanwhile, KMnO_4 was 1.7 V. It was indicated that H_2O_2 is better than KMnO_4 even though the oxidation potential difference between each oxidant was not quite notable. H_2O_2 was known as a very reactive and the most powerful oxidiser. Thus, the optimum oxidant concentration was 1M H_2O_2 in H_2SO_4 .

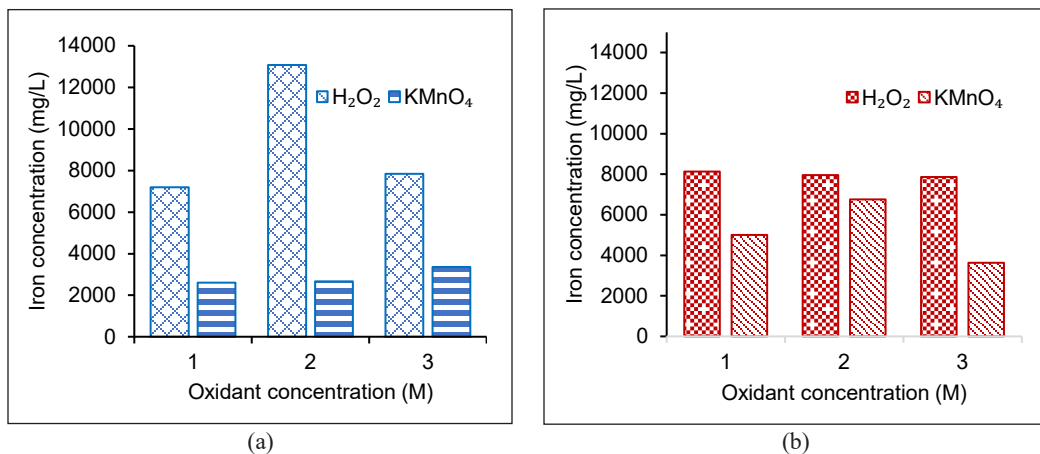


Figure 2. Amount of iron recovered at different H_2O_2 concentration and KMnO_4 concentrations in different leaching agents: (a) H_2SO_4 ; and (b) HCl

The function of H_2SO_4 and HCl were to serve as the oxidant that can help in increasing leaching efficiency

Effect of Acid Concentration

The effects of the concentration between 0.5–8 M were studied and are depicted in Figure 3. It can be seen that iron dissolution started between 0.5 M sulphuric acid and drastically increased at 1 M. The explanation for this is that the activity of the H^+ (protons) was

related to the reaction of the iron with the acid medium when the concentration of acid was increased (Hazaveh et al., 2020). However, the concentration of 8 M H_2SO_4 decreased iron leaching efficiency because of the formation of passive films that hindered further dissolution of the metal (Ichlas et al., 2020). The passive film appeared primarily composed of calcium oxide, resistant to sulphuric acid at high concentrations. Besides, the leaching was not solely controlled by the total metal content but was also significantly affected by other factors such as pH (Sun & Yi, 2021). The non-existing bar in 0.5 M H_2SO_4 denoted that no iron was leached out into the solution. When the HCl concentration was changed to between 1 and 3 M, the leaching efficiency of iron became more obvious with the increase of HCl concentration. Due to the volatilisation of HCl at high concentration, the leaching reaction has completed and remained steady as the concentrations were further raised to 8 M, with an average iron concentration of 7933 mg/L (Li et al., 2021). The metal ions tend to hydrolyse HCl ions quicker and inhibit HCl from being utilised effectively. In conclusion, 5 M was the most excellent acid concentration for recovering the most iron from EAFS.

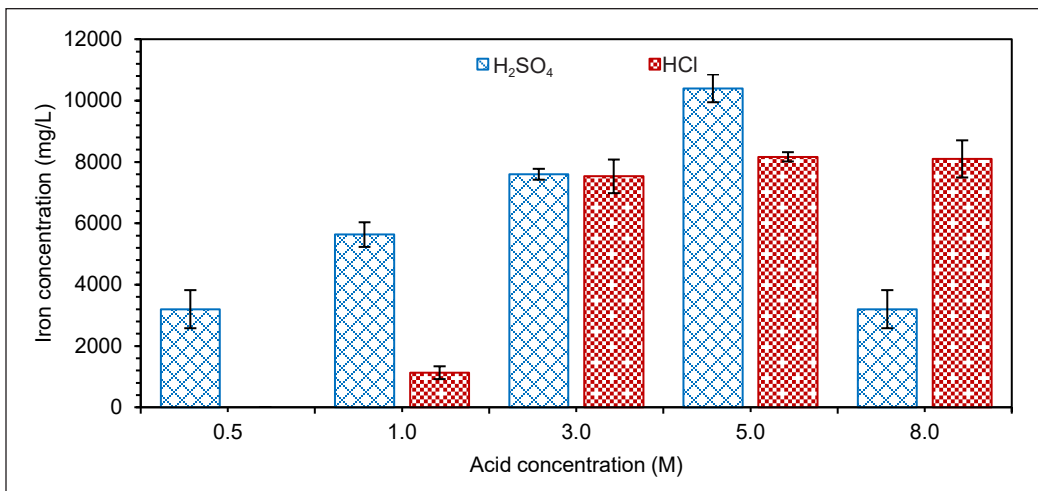


Figure 3. Effect of acid concentration on iron concentration after leaching

CONCLUSION

This study has focused on the leaching of electric arc furnace slag (EAFS) in the oxidative and non-oxidative leaching environment for the selective recovery of iron. In conclusion, the leaching performance was far better in a sulphuric acid environment than in hydrochloric acid. It can be concluded that the leaching efficiency of iron from EAFS can be further maximised in the appropriate conditions. Further study is necessary to analyse the iron-rich leached solution's kinetics and electrochemical activity.

ACKNOWLEDGMENT

The authors want to acknowledge the financial support from the Ministry of Higher Education (MOHE) and Universiti Teknologi MARA (UiTM) for Fundamental Research Grant (FRGS) (FRGS/1/2019/TK02/UITM/02/5). The authors also acknowledge the College of Engineering, UiTM Shah Alam, for providing the research facilities.

REFERENCES

- Brooks, L., Gaustad, G., Gesing, A., Mortvedt, T., & Freire, F. (2019). Ferrous and non-ferrous recycling: Challenges and potential technology solutions. *Waste Manag*, 85, 519-528. <https://doi.org/10.1016/j.wasman.2018.12.043>
- Fisher, L. V., & Barron, A. R. (2019). The recycling and reuse of steelmaking slags - A review. *Resources, Conservation and Recycling*, 146, 244-255. <https://doi.org/10.1016/j.resconrec.2019.03.010>
- Hafez, H., Kassim, D., Kurda, R., Silva, R. V., & de Brito, J. (2021). Assessing the sustainability potential of alkali-activated concrete from electric arc furnace slag using the ECO₂ framework. *Construction and Building Materials*, 281, Article 122559. <https://doi.org/10.1016/j.conbuildmat.2021.122559>
- Halli, P., Agarwal, V., Partinen, J., & Lundström, M. (2020). Recovery of Pb and Zn from a citrate leach liquor of a roasted EAF dust using precipitation and solvent extraction. *Separation and Purification Technology*, 236, Article 116264. <https://doi.org/10.1016/j.seppur.2019.116264>
- Hazaveh, P., Karimi, S., Rashchi, F., & Sheibani, S. (2020). Purification of the leaching solution of recycling zinc from the hazardous electric arc furnace dust through an as-bearing jarosite. *Ecotoxicology and Environmental Safety*, 202, Article 110893. <https://doi.org/10.1016/j.ecoenv.2020.110893>
- Ichlas, Z. T., Rustandi, R. A., & Mubarak, M. Z. (2020). Selective nitric acid leaching for recycling of lead-bearing solder dross. *Journal of Cleaner Production*, 264, Article 121675. <https://doi.org/10.1016/j.jclepro.2020.121675>
- Ji, H., Mi, X., Tian, Q., Liu, C., Yao, J., Ma, S., & Zeng, G. (2021). Recycling of mullite from high-alumina coal fly ash by a mechanochemical activation method: Effect of particle size and mechanism research. *Science of The Total Environment*, 784, Article 147100. <https://doi.org/10.1016/j.scitotenv.2021.147100>
- Keymanesh, M. R., Ziari, H., Zalnezhad, H., & Zalnezhad, M. (2021). Mix design and performance evaluation of microsurfacing containing electric arc furnace (EAF) steel slag filler. *Construction and Building Materials*, 269, Article 121336. <https://doi.org/10.1016/j.conbuildmat.2020.121336>
- Kim, J., & Azimi, G. (2020). Technospheric mining of niobium and titanium from electric arc furnace slag. *Hydrometallurgy*, 191, Article 105203. <https://doi.org/10.1016/j.hydromet.2019.105203>
- Kremser, K., Thallner, S., Strbik, D., Spiess, S., Kucera, J., Vaculovic, T., Vsiansky, D., Haberbauer, M., Mandl, M., & Guebitz, G. M. (2021). Leachability of metals from waste incineration residues by iron- and sulfur-oxidizing bacteria. *Journal of Environmental Management*, 280, Article 111734. <https://doi.org/10.1016/j.jenvman.2020.111734>

- Kukurugya, F., Vindt, T., & Havlík, T. (2015). Behavior of zinc, iron and calcium from electric arc furnace (EAF) dust in hydrometallurgical processing in sulfuric acid solutions: Thermodynamic and kinetic aspects. *Hydrometallurgy*, 154, 20-32. <https://doi.org/10.1016/j.hydromet.2015.03.008>
- Li, P., Luo, S. H., Wang, Y., Yan, S., Teng, F., Feng, J., Wang, Q., Zhang, Y., Mu, Wenning., Zhai, X., & Liu, X. (2021). Cleaner and effective recovery of metals and synthetic lithium-ion batteries from extracted vanadium residue through selective leaching. *Journal of Power Sources*, 482, Article 228970. <https://doi.org/10.1016/j.jpowsour.2020.228970>
- Lie, J., Lin, Y. C., & Liu, J. C. (2021). Process intensification for valuable metals leaching from spent NiMH batteries. *Chemical Engineering and Processing - Process Intensification*, 167, Article 108507. <https://doi.org/10.1016/j.cep.2021.108507>
- Linsong, W., Peng, Z., Yu, F., Sujun, L., Yue, Y., Li, W., & Wei, S. (2020). Recovery of metals from jarosite of hydrometallurgical nickel production by thermal treatment and leaching. *Hydrometallurgy*, 198, Article 105493. <https://doi.org/10.1016/j.hydromet.2020.105493>
- Martinho, F. C. G., Picado-Santos, L. G., & Capitão, S. D. (2018). Influence of recycled concrete and steel slag aggregates on warm-mix asphalt properties. *Construction and Building Materials*, 185, 684-696. <https://doi.org/10.1016/j.conbuildmat.2018.07.041>
- Mohammadzadeh, M., Bagheri, H., & Ghader, S. (2020). Study on extraction and separation of Ni and Zn using [bmim][PF6] IL as selective extractant from nitric acid solution obtained from zinc plant residue leaching. *Arabian Journal of Chemistry*, 13(6), 5821-5831. <https://doi.org/10.1016/j.arabjc.2020.04.019>
- Monosi, S., Ruello, M. L., & Sani, D. (2016). Electric arc furnace slag as natural aggregate replacement in concrete production. *Cement and Concrete Composites*, 66, 66-72. <https://doi.org/10.1016/j.cemconcomp.2015.10.004>
- Nasuha, N., Ismail, S., & Hameed, B. H. (2016). Activated electric arc furnace slag as an efficient and reusable heterogeneous Fenton-like catalyst for the degradation of Reactive Black 5. *Journal of the Taiwan Institute of Chemical Engineers*, 67, 235-243. <https://doi.org/10.1016/j.jtice.2016.07.023>
- Nasuha, N., Ismail, S., & Hameed, B. H. (2017). Activated electric arc furnace slag as an effective and reusable Fenton-like catalyst for the photodegradation of methylene blue and acid blue 29. *Journal of Environmental Management*, 196, 323-329. <https://doi.org/10.1016/j.jenvman.2017.02.070>
- Nasuha N, Shaziela N, et al. (2019) Recovery of iron from electric arc furnace slag: effect of heating temperature and time. *IOP Conference Series: Materials Science and Engineering* 551. <https://doi.org/10.1088/1757-899x/551/1/012119>
- Plaza, L., Castellote, M., Nevshupa, R., & Jimenez-Relinque, E. (2021). High-capacity adsorbents from stainless steel slag for the control of dye pollutants in water. *Environmental Science and Pollution Research*, 28, 23896-23910. <https://doi.org/10.1007/s11356-020-12174-0>
- Rao, M., Shahin, C., & Jha, R. (2021). Optimization of leaching of copper to enhance the recovery of gold from liberated metallic layers of WPCBs. *Materials Today: Proceedings*, 46(3), 1515-1518. <https://doi.org/10.1016/j.matpr.2021.01.052>

- Roy, S., Miura, T., Nakamura, H., & Yamamoto, Y. (2018). Investigation on applicability of spherical shaped EAF slag fine aggregate in pavement concrete - Fundamental and durability properties. *Construction and Building Materials*, 192, 555-568. <https://doi.org/10.1016/j.conbuildmat.2018.10.157>
- Roy, S., Miura, T., Nakamura, H., & Yamamoto, Y. (2019). Investigation on material stability of spherical shaped EAF slag fine aggregate concrete for pavement during thermal change. *Construction and Building Materials*, 215, 862-874. <https://doi.org/10.1016/j.conbuildmat.2019.04.228>
- Roy, S., Miura, T., Nakamura, H., & Yamamoto, Y. (2020). High temperature influence on concrete produced by spherical shaped EAF slag fine aggregate - Physical and mechanical properties. *Construction and Building Materials*, 231, Article 117153. <https://doi.org/10.1016/j.conbuildmat.2019.117153>
- Sun, X., & Yi, Y. (2021). Acid washing of incineration bottom ash of municipal solid waste: Effects of pH on removal and leaching of heavy metals. *Waste Management*, 120, 183-192. <https://doi.org/10.1016/j.wasman.2020.11.030>
- Teo, P. T., Anasyida, A. S., Kho, C. M., & Nurulakmal, M. S. (2019). Recycling of Malaysia's EAF steel slag waste as novel fluxing agent in green ceramic tile production: Sintering mechanism and leaching assessment. *Journal of Cleaner Production*, 241, Article 118144. <https://doi.org/10.1016/j.jclepro.2019.118144>
- Wang, F., Gu, Z., Hu, Y., & Li, Q. (2021). Split dosing of H₂O₂ for enhancing recalcitrant organics removal from landfill leachate in the Fe₀/H₂O₂ process: Degradation efficiency and mechanism. *Separation and Purification Technology*, 278, Article 119564. <https://doi.org/10.1016/j.seppur.2021.119564>
- Yang, G. C. C., Chuang, T. N., & Huang, C. W. (2017). Achieving zero waste of municipal incinerator fly ash by melting in electric arc furnaces while steelmaking. *Waste Management*, 62, 160-168. <https://doi.org/10.1016/j.wasman.2017.02.021>
- Yin, W., & Chen, K. (2021). Effect of the particle size and microstructure characteristics of the sample from HPGR on column bioleaching of agglomerated copper ore. *Hydrometallurgy*, 200, Article 105563. <https://doi.org/10.1016/j.hydromet.2021.105563>
- Zhang, N., Wu, L., Liu, X., & Zhang, Y. (2019). Structural characteristics and cementitious behavior of basic oxygen furnace slag mud and electric arc furnace slag. *Construction and Building Materials*, 219, 11-18. <https://doi.org/10.1016/j.conbuildmat.2019.05.156>
- Zhang, S., & Liu, W. (2017). Application of aerial image analysis for assessing particle size segregation in dump leaching. *Hydrometallurgy*, 171, 99-105. <https://doi.org/10.1016/j.hydromet.2017.05.001>

A Hybrid Technique for Analysis of Low-Frequency Oscillation in Power System

Abhinav Pathak^{1,2*} and Ratnesh Gupta¹

¹School of Instrumentation, Devi Ahilya Vishwavidyalaya Indore 452001 M.P., India

²Electrical Engineering, Medi-Caps University Indore 453331 M.P., India

ABSTRACT

Estimating the low-frequency oscillation in an interconnected power system is the most important requirement to keep the power system in a stable operating condition. This research work deals with a hybrid robust and accurate approach using a combination of Estimation of signal parameters via rotational invariant techniques (ESPRIT) and Prony algorithm to extract the low-frequency oscillatory modes present in the power system. The observation inspires the hybrid method that the true modes of the signal are present in any signal processing technique (for example, Prony algorithm) along with other fictitious modes regardless of the order of the power system. Moreover, this research obtained true modes by calculating Euclidean distance and applying the threshold value concept. The proposed technique is tested with different noise conditions and varying sampling rates of Phasor Measurement Unit (PMU) to check the proposed hybrid technique's robustness compared to Prony and the multiple ESPRIT method. Finally, the proposed method is applied to the real signal obtained from the Western Electricity Coordinating Council (WECC) network, and it estimates accurate and precise parameters compared to other methods. The accuracy for estimation of frequency and attenuation factor is calculated for the three-mode synthetic signal at a noise level of 10dB by the hybrid algorithm, multiple ESPRIT,

and Prony algorithm, which shows that hybrid algorithm has minimum percentage error. Thus the proposed hybrid algorithm accurately estimates the parameters of low-frequency oscillation as compared to other existing methods without involving any fictitious modes.

ARTICLE INFO

Article history:

Received: 8 December 2021

Accepted: 7 February 2022

Published: 20 April 2022

DOI: <https://doi.org/10.47836/pjst.30.3.15>

E-mail addresses:

abhinavgsits7@gmail.com (Abhinav Pathak)

ratneshg@hotmail.com (Ratnesh Gupta)

*Corresponding author

Keywords: Attenuation factor, damping ratio, Prony algorithm, stability, synthetic signal

INTRODUCTION

Modern power systems are highly interconnected and often share useful information regarding the operation and control of the power system in a reliable manner. However, these interconnected power systems have a major challenge to maintain stability, such as small-signal stability, which contains low-frequency oscillations (Kundur, 1994). Small signal stability results in the system due to small disturbances due to a rise in rotor angle or rotor oscillation of continuously rising amplitude. Due to the non-linear behavior of the power system and during transient operation, it leads to ring-down oscillation, which needs to stabilize. Therefore, identifying critical modes is crucial, which helps design a controller that mitigates the poorly damped oscillations. In this direction, traditional techniques use Eigen values-based analysis using a linear time-invariant model in which a non-linear system is linearized at the operating point to identify low-frequency oscillatory modes of the power systems (Wang & Semlyen, 1990). Unfortunately, the oscillation properties change significantly due to variation in operating conditions of the system, which makes offline methods (Eigenvalue analysis) insufficient and meaningless for system operators. Recently, rapid development in the synchrophasor-based Wide Area Monitoring System (WAMS) and Phasor Measurement Units (PMU) facilitated the collection of the time-tagged data at the Phasor Data Concentrator (PDC), which enable the use of the online tool to estimate oscillatory modes present in the signal (Xie et al., 2005; Zhang et al., 2008).

Some common techniques which use the measurement-based estimation approach are Fast Fourier transform (FFT) (Girgis & Ham, 1980; Glickman et al., 2007), Kalman filter (Korba et al., 2003), Prony analysis (Amono et al., 1999; Hauer, 1991; Qi et al., 2007; Rai et al., 2016; Trentini et al., 2019; Trudnowski, 1994; Trudnowski et al., 1999; Wadduwage et al., 2015), ARMA (Wies et al., 2003), Continuous Wavelet Transform (CWT) (Kang & Ledwich, 1999; Rueda et al., 2011; Avdakovic et al., 2012), Hilbert-Huang transform (Laila et al., 2009), Matix-Pencil (Grant & Crow, 2011; Hua & Sarkar, 1990) and ESPRIT (Rai et al., 2014; Tripathy et al., 2011; Wang et al., 2014).

Among these methods, FFT is a fast method and has the robustness to noise which is easy to implement (Girgis & Ham, 1980; Glickman et al., 2007). However, this method does not work with low-resolution data and does not estimate the attenuation factor. Another method based on the recursion technique, the Kalman filter, has instability problems that make it difficult to use in the real application (Korba et al., 2003). Wavelet-based methods like CWT (Kang & Ledwich, 1999; Rueda et al., 2011) and Discrete Wavelet Transform (DWT) (Avdakovic et al., 2012) use multi-resolution analysis using the variable length of wavelet, which estimates modal information effectively on the stationary signal. The above techniques are easy to implement, but their accuracy depends on the shape of the mother wavelet and decomposition level. In HHT, Empirical mode decomposition (EMD) is used to make them work on non-stationary and non-linear data along with Hilbert spectral

analysis (Laila et al., 2009). Unfortunately, estimation of frequency and damping ratio is accurate using this method if the modes obtained by EMD are mono-frequency components.

Moreover, EMD works only on the narrowband signal, which means the signal has adjacent frequency components or has a component that is not adjacent but has a large difference of energy intensity (Browne et al., 2008). Additionally, usage of EMD makes HHT based method slow and unable to fit in online mode estimation. On the other side, ARMA, which optimizes its parameter to estimate the model parameters more precisely, cannot estimate closely spaced modes (Wies et al., 2003). In Pierre et al. (1997), ambient noise is examined using Wiener-Hopf linear prediction. This method can estimate accurate details of frequencies but fails to predict precise information of damping. In literature, Zhou et al. (2008), regularized robust recursive least square (RLS) algorithm is used to estimate modal information. However, conceptually, it may diverge because regularized RLS have numerical instability problems.

Apart from these methods, Prony is a conventional method for modal analysis based on the frequency domain approach, estimating all required information like frequency, attenuation factor, phase, and amplitude (Qi et al., 2007). However, the usage of the Prony approach is limited because of its sensitivity to noise. Moreover, it cannot estimate true modes; the Prony algorithm obtains many fictitious modes. However, some efforts are made to improve the Prony method by separating signal and noise, but many fail due to improper model order estimation.

The ESPRIT method uses the shift-invariance property present in the signal to represent the auto-correlation matrix. Such a method is less sensitive to noise present in the signal but requires accurate information of modes to be extracted, otherwise leading to an incorrect finding of the true modes.

Normally, a simple order estimation technique is used with the ESPRIT algorithm to find true mode estimation. However, simple model order estimation often fails to accurately calculate the total number of modes in the power signal. To demonstrate the failure case of model order estimation, consider the following signal (Equation 1):

$$\begin{aligned}
 x_1 = & e^{-0.0909t} \cos(2\pi * 0.4t) + 0.9e^{-0.35t} \cos(2\pi * 0.5t) \\
 & + 0.7e^{-0.2001t} \cos\left(2\pi * 0.6t + \left(\frac{\pi}{6}\right)\right) \\
 & + 0.4e^{-0.666t} \cos\left(2\pi * 1.1t + \left(\frac{\pi}{4}\right)\right)
 \end{aligned}
 \tag{1}$$

The signal is sampled at 50Hz and corrupted with white Gaussian noise at 40dB. After applying Singular value decomposition (SVD) on the autocorrelation system, separating index $K(i)$ can be calculated using Equation 2.

$$K(i) = \frac{\delta_1 + \delta_2 + \dots + \delta_i}{\delta_1 + \delta_2 + \dots + \delta_i}
 \tag{2}$$

where l is the total number of singular values, and δ_i is the i^{th} singular value of the autocorrelation matrix. The order is estimated by selecting index i , at which $K(i)$ is closest to value 1. The plot of $K(i)$ vs. index i is shown in Figure 1, which shows that the value of $K(i)$ is closest to 1 at an index value of 5. However, the signal consists of only 4 frequency components. This incorrect result of order estimation fails ESPRIT to analyze the signal correctly.

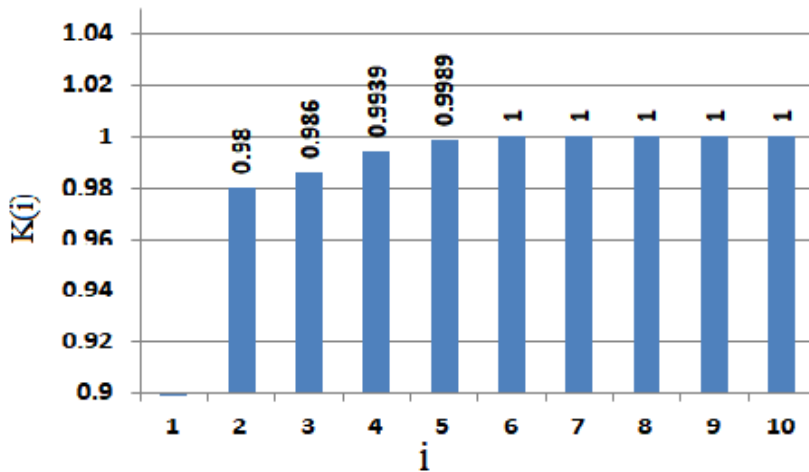


Figure 1. Plot of $K(i)$ vs. i to estimate the order of the system

Several efforts have been attempted to improve the ESPRIT algorithm, but it lacks performance under high noise conditions. This research proposed a hybrid system based on ESPRIT and Prony algorithm to combine both methods' advantages, making it more robust to noise and estimating directly true modes from the signal without using any model order estimation technique. The proposed hybrid method is described in section 2, followed by simulation and the result analysis on various synthetic signals and real signals in section 3. At the end of section 4 conclusion of the research paper is discussed.

PROPOSED HYBRID ALGORITHM

This section discussed the hybrid method using Prony and ESPRIT algorithms. As discussed, Prony and ESPRIT algorithm needs the information of exact (true) modes present in the signal to extract parameters of true modes. Moreover, the literature shows that improper mode estimation yields a failure case of the ESPRIT method. This research combined both methods and observed that true modes are present in both techniques with other fictitious modes to deal with the problem. Both the methods produced different fictitious modes, which can be removed easily by computing the Euclidean distance

between them. It motivates us to combine two different methods. A detailed discussion of the Prony and ESPRIT methods can be obtained in the literature, respectively (Qi et al., 2007 & Tripathy et al., 2011). This section only shows the mathematical problem statement of mode estimation in the power system followed by only the main steps of both methods (i.e., Prony and ESPRIT). Later in this section, the true mode identification method using Euclidean distance will be shown.

In the power system to represent the signal, the linear combination of a damped sinusoid with white Gaussian noise is taken for analysis.

$$y(n) = s(n) + \omega(n) = \sum_{k=1}^K a_k e^{b_k n} (\cos(n\omega_k + \varphi_k) + \omega(n)) \quad [3]$$

where $s(n)$ and $\omega(n)$ are the signal component and zero-mean Gaussian noise, respectively. Moreover, amplitude, damping factor, damping frequency, initial phase, and the number of sinusoids are represented by a_k , b_k , ω_k , φ_k , and k , respectively. So the task of modal analysis is to find the best estimation of the parameters of Equation 3 so that the modes of oscillation in the power system are identified.

Equation 3 represents the time domain signal for the Prony algorithm (Hauer et al., 1990; Zhou et al., 2010). Theoretical derivations are well mentioned in the literature. As a summary, it follows the following steps.

1. The model that best fits the given signal is constructed by discrete linear prediction (LP).
2. Eigenvalues, roots of the characteristic polynomial are determined from the above prediction model.
3. Determine the least square solution of the equation to find the amplitude and phase angle of the modes.

It is noted that the Prony algorithm performance depends on the solution of M number of unknowns using $(N-M)$ number of equations in above step-2, where M is the order of algorithm and N is the number of samples over the data windows, respectively. Hence, it is common to use the order M of the Prony should be taken as $M \leq (N/3)$ as given in Wadduwage et al. (2015) so that effect of noise is suppressed. So the order of ESPRIT and Prony algorithm in the proposed hybrid method is taken as M . However, the true modes are identified using Euclidean distance between the modes as given in next section of the paper irrespective of the order of the algorithm.

The main steps of the ESPRIT algorithm for estimating frequency can be summarised as given by Equations 4 to 11:

1. First construct Hankel matrix of order M from given signal to be analyzed which has a length of sample N . Mathematically, it is described as follows

$$X = \begin{bmatrix} X(0) & X(1) \dots & X(M-1) \\ X(1) & X(2) \dots & X(M) \\ \dots & \dots & \dots \\ X(N-M) & X(N-M+1) \dots & X(N-1) \end{bmatrix} \quad [4]$$

2. From constructed Hankel matrix, derive autocorrelation matrix R_x using given formula

$$R_x = \frac{1}{N-M} (X^H X) \quad [5]$$

3. Decompose the autocorrelation matrix using eigenvalue decomposition (via singular value decomposition) in the form of $R_x = UEV^*$ where E is a diagonal matrix that holds the Eigenvalues of R_x in decreasing order.

4. Separate orthonormal eigenvectors from U based on the order of the model (M), which can be expressed as,

$$S = U(:, 1:M) \quad [6]$$

5. Apply separation on matrix S to generate shifted submatrix as,

$$S_1 = [I_{M-1} \ 0]S \quad [7]$$

$$S_2 = [0 \ I_{M-1}]S \quad [8]$$

where I_{M-1} is the identity matrix of order M-1.

6. These shifted submatrices are connected to matrix Φ by using shift-invariance condition expressed as $S_2 = S_1 \Phi$. Solve the below equation using least square estimation to obtain matrix Φ .

$$\Phi = (S_1^H S_1)^{-1} (S_1^H S_2) \quad [9]$$

7. The frequency and damping factor of a signal can be estimated from eigenvalue λ_i of the matrix Φ as,

$$f_i = f_s * \left(\frac{\text{imag}(\log \lambda_i)}{2\pi} \right) \quad [10]$$

$$\delta_i = f_s * \text{real}(\log \lambda_i) \quad [11]$$

Consider a synthetically generated signal Y with three different modes, as shown in Table 1 with the sampling frequency of 60 Hz. Next, consider two different length signals from windows at 1–20 sec and 2–18 sec, respectively. Next, apply the ESPRIT algorithm on 20-sec window length and the Prony algorithm on 16-sec window length. In this case, the model order of ten for both algorithms, which estimate five modes with the positive frequency, is shown in Table 2.

Table 1

Details of three-mode synthetic signal

Mode	Frequency	Attenuation Factor	Amplitude	Damping Ratio %
1	0.25	-0.1102	1	7.0169
2	0.39	-0.1596	1	6.5143
3	0.7	-0.2199	0.5	5.0007

Table 2

Mode Estimation Result of Synthetic Signal from Table1 using ESPRIT and Prony method

Mode	ESPRIT			Prony		
	Frequency (Hz)	Attenuation Factor	Damping Ratio (%)	Frequency (Hz)	Attenuation Factor	Damping Ratio (%)
1	0.7000	-0.2199	5.0007	0.7003	-0.2198	4.9950
2	0.2500	-0.1102	7.0169	0.2500	-0.1102	7.0179
3	0.3900	-0.1596	6.5143	0.3902	-0.1596	6.5103
4	30.0152	-21.0835	11.1816	25.4421	-28.1292	17.5997
5	11.1988	-14.2470	20.2514	17.9317	-26.9529	23.9269

The core logic behind the proposed hybrid method is the observation that true modes appear consistently in both methods, whatever be the model order. However, due to the dynamic behavior of power systems and noise, other fictitious modes are also inherently present, not estimated the same in different methods. So it can easily be removed by applying a threshold on the closest distance with modes estimated by other methods.

This paper used Euclidean distance to find the distance between each mode estimated from ESPRIT and Prony methods. Assume that p_1 and p_2 modes are identified using ESPRIT and Prony methods. The modes can be identified as fictitious and rejected if the condition given in Equation 12 does not satisfy them. If,

$$\sqrt{(f_i - f_j)^2 + (\sigma_i - \sigma_j)^2} \leq \tau \quad i = 1,2,3,\dots,p_1 \ \& \ j = 1,2,3,\dots,p_2 \quad [12]$$

Here τ is the threshold value to pick out true modes, taken as 0.02. Finally, the average estimated value is taken to reduce calculation error in the solution using Equations 13 and 14. Here σ indicates the real part of the eigenvalue.

$$f = \frac{f_1 + f_2}{2} \quad [13]$$

$$\sigma = \frac{\sigma_1 + \sigma_2}{2} \quad [14]$$

The block diagram of the proposed algorithm to estimate the exact true modes in the signal is represented as in Figure 2. It has to be noted that complex eigenvalues occur in conjugate pairs, and each pair denotes the single mode of oscillation. Furthermore, this paper is concerned with low-frequency oscillation analysis, which means the higher frequencies from the solution can be omitted. Hence, it is only required to check Equation 12 for positive and frequencies lower than 5 Hz.

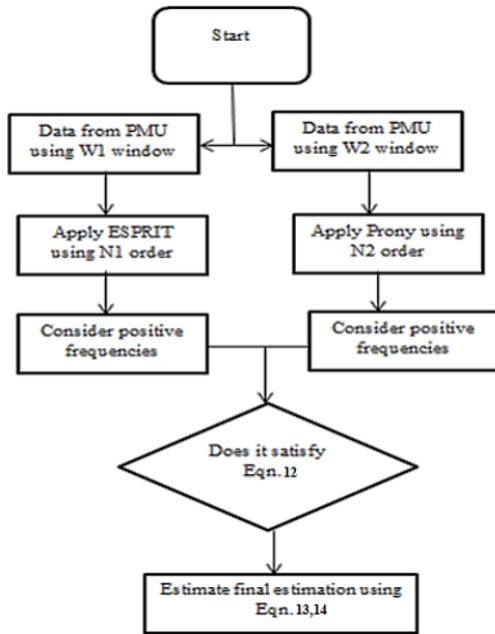


Figure 2. Block diagram representation of the proposed algorithm

RESULTS AND DISCUSSION

This research analyzes the hybrid method’s simulation result and other current state-of-the-art methods for different scenarios. The complete simulation has been done on MATLAB software under the Windows environment.

In the first case, this research analyzed synthetic signals with the same damping ratio and large separation in frequency components. The details of the synthetically generated signal are given in Table 3. The sampling frequency is 60 Hz in this case.

Here, to check the performance of the proposed algorithm under different noise levels, additive white Gaussian noise (AWGN) is added, and the robustness of the different methods is checked. As mentioned previously, both Prony and ESPRIT methods

are used to identify the hybrid approach’s true modes. Moreover, the performance of multiple ESPRIT and Prony methods is presented in Table 6, which justifies that the hybrid algorithm is more accurate as compared to Prony and ESPRIT methods under high noise conditions when there is a large separation in frequency components and closed damping ratio.

Table 3

Parameters of the synthetic signal with the same damping ratio

Mode No.	Freq (Hz)	Attenuation Factor	Amplitude	Damping Ratio %
1	0.2	-0.1	1	7.9592
2	0.8	-0.4	1	7.9592

Table 6 shows that the hybrid method is more robust than the Prony and multi ESPRIT methods in the varying condition of noise. In high noise conditions (i.e., 10dB noise level) hybrid method predicts accurate results compared to other methods. It is noted that the Prony method estimates all modes, including fictitious modes, which is further needed to be removed. However, this result only considers true mode estimation from the Prony method ignoring fictitious modes obtained from the analysis.

Apart from tabular measurement, visual estimated signals and the original noisy signal are analyzed in Figure 3. It is clear from the analysis that the hybrid method under the high level of noise condition can also estimate the exact information regarding the low-frequency oscillation parameters.

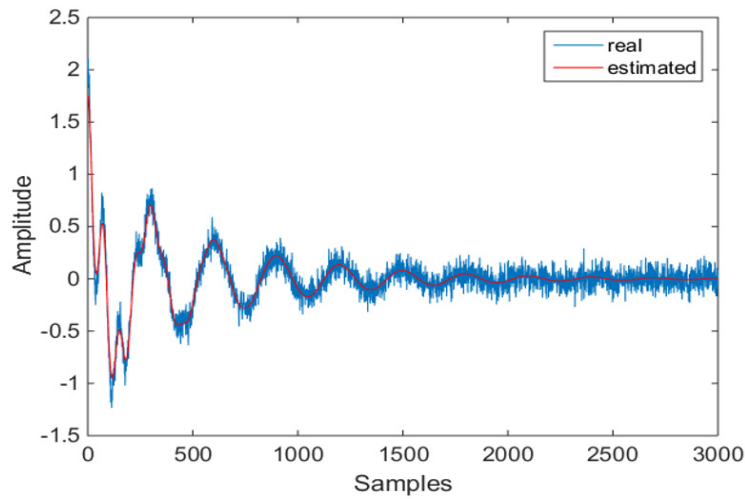


Figure 3. Estimated signal using the proposed hybrid method given in Table 3 with noise level 10dB

In the second case, this research generates a signal having two modes with closed frequency components and a twice damping ratio. Table 4 shows the detail of the synthetically generated signal. In this case, the sampling frequency is 60 Hz, and the estimated values are given in Table 7.

Table 4

Parameters of the synthetic signal with closed frequency components

Mode No.	Freq (Hz)	Attenuation Factor	Amplitude	Damping Ratio %
1	0.5	-0.25	1	7.9592
2	0.6	-0.15	1	3.9796

From Table 7 also, it is observed that the proposed hybrid method shows robust performance under varying noise conditions and is even capable of estimating the parameters of the low-frequency oscillation signal, which consists of almost the same frequency components. For example, Figure 4 shows how closely the proposed algorithm can estimate the true signal from the synthetic signal having a noise level of 10dB using the proposed hybrid algorithm.

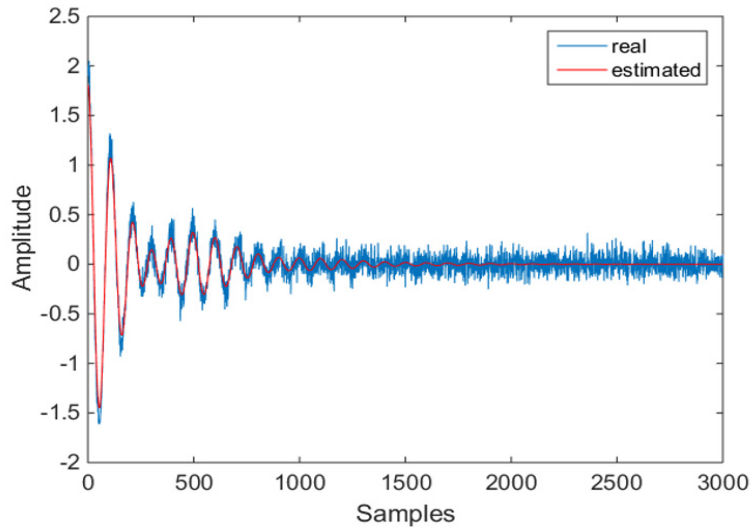


Figure 4. Estimated signal using the proposed hybrid method given in Table 4 with noise level 10dB

Preceding all results are taken under 60 Hz of sampling frequency. In practice, the reporting rate of PMU varies from 10 Hz to 100 Hz. Literature shows that some techniques have limitations to work under a certain sampling frequency range. Fortunately, the proposed method can work under even varying sampling rates also. In order to check its performance under such conditions, this research conducted the experiment in which it considered the same synthetic signal from Table 4 and tried to estimate true modes using the proposed hybrid method on different sampling frequencies ranging from 30 Hz to 60 Hz. Table 5 shows the result of the hybrid method under different sampling frequencies (PMU reporting rate) under 30 dB noise level. The proposed hybrid method provides accurate results for a range of PMU reporting rates, facilitating its application with any system with different PMU reporting rates.

In the next case, this research considers synthetic signal with parameters is shown in Table 1 with 60 Hz sampling frequency. This synthetic signal has three modes, with three frequency components and a damping ratio. In order to check the robustness of the proposed hybrid method, the signal is corrupted with distinct levels of additive white Gaussian noise (AWGN) varying from 50 dB to 10 dB. The result analysis is shown in Table 8, which

Table 5

Mode estimation by proposed hybrid method with varying PMU reporting rate

PMU Reporting Rate	Freq (Hz)	Attenuation Factor	Amplitude	Damping Ratio%
60Hz	0.5	-0.249	0.99	7.9274
	0.6	-0.149	1	3.9531
40 Hz	0.49	-0.247	0.99	8.0242
	0.59	-0.147	0.99	3.9661
30 Hz	0.48	-0.245	1.01	8.1251
	0.58	-0.145	0.99	3.9796

indicates how the proposed hybrid method accurately estimates low-frequency oscillatory modes of the synthetic signal having three frequency components even in the presence of noise and has better performance as compared to multiple ESPRIT and Porny algorithms.

The previous section shows the performance of the proposed hybrid method, multiple ESPRIT, and Porny algorithm in Tables 6, 7, and 8, respectively, for a different set of synthetic signals with varying noise levels. However, those results are one-time measurements that may vary every time due to the randomness of noise. Therefore, it is required to estimate accurate modes all the time despite the randomness of noise. It means estimation should have low variation in the output result all the time. This research performs a Monte Carlo simulation with 1000 samples and 300 samples for the proposed hybrid and ESPRIT methods, respectively, to test the performance of the proposed method. Figure 5 shows the histogram of estimated frequency versus the number of counts for multiple ESPRIT methods. From the histogram, it is observed that the multiple ESPRIT method estimate values with high variance. Hence, the research based on multiple ESPRIT needs to estimate several times and average it to estimate final results. Unfortunately, an improper control action may occur if the true modes are not identified in the real scenario. Figure 6 shows the histogram of estimated frequency versus the number of counts for the proposed hybrid method, which shows the very little variance in the result, making it suitable for real-time application.

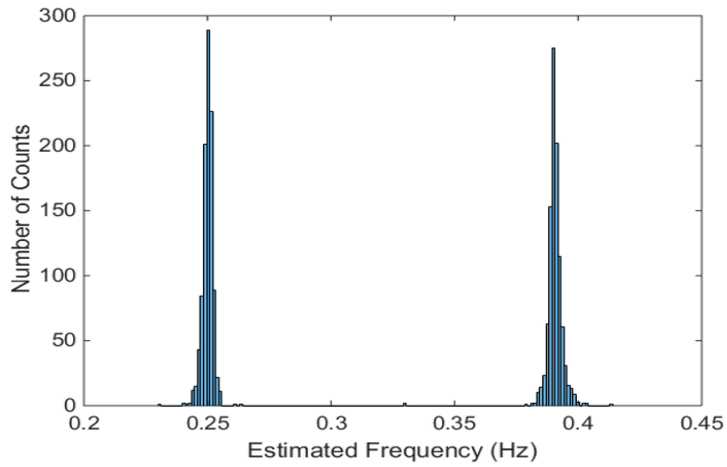


Figure 5. Histogram of estimated frequency by multiple ESPRIT method

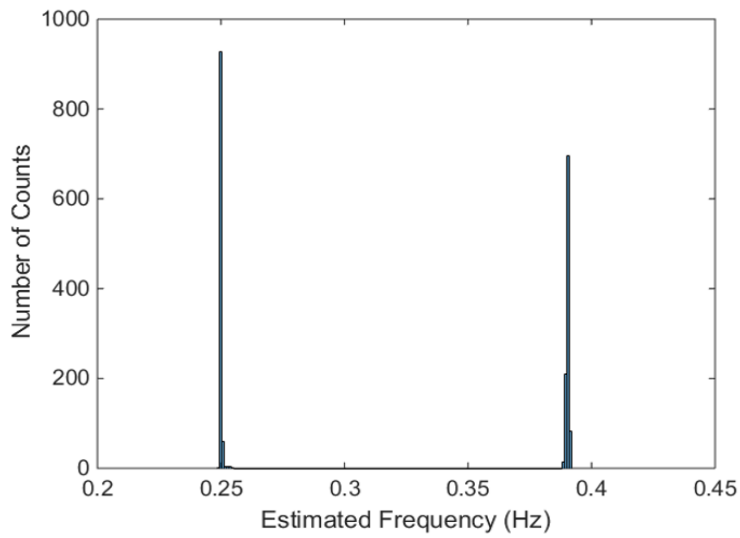


Figure 6. Histogram of estimated frequency by the proposed hybrid method

Table 6
 Mode Estimation on Synthetic Signal having same damping ratio

Method	No noise	50dB	30dB	20dB	10dB	
Hybrid	Freq (Hz)	0.200	0.199	0.197	0.195	0.797
	Attenuation Factor	-0.100	-0.099	-0.097	-0.097	-0.396
	Amplitude	1.000	1.000	0.990	0.970	1.030
	Damping Ratio %	7.9592	7.9193	7.9493	7.8380	7.9184
Multiple ESPRIT	Freq (Hz)	0.199	0.199	0.197	0.179	0.781
	Attenuation Factor	-0.100	-0.098	-0.098	-0.08	-0.349
	Amplitude	0.990	1.001	1.010	1.030	1.030
	Damping Ratio %	7.9992	7.8393	7.9188	7.1144	6.7677
Prony	Freq (Hz)	0.199	0.198	0.196	0.169	0.688
	Attenuation Factor	-0.099	-0.398	-0.097	-0.075	-0.319
	Amplitude	1.001	0.990	1.020	1.050	1.050
	Damping Ratio %	7.9193	7.8789	7.8780	7.0644	5.7066
						8.1103
						0.585
						-0.250
						0.750
						6.8028

Table 7
Mode Estimation on Synthetic Signal having closed frequency components

Method	No noise		50dB		30dB		20dB		10dB		
Hybrid	Freq (Hz)	0.499	0.600	0.500	0.599	0.499	0.599	0.497	0.596	0.495	0.594
	Attenuation Factor	-0.249	-0.150	-0.250	-0.150	-0.250	-0.149	-0.248	-0.147	-0.246	-0.145
	Amplitude	0.990	1.000	0.990	0.990	1.010	0.990	1.010	0.990	1.020	0.970
	Damping Ratio %	7.9433	3.9796	7.9592	3.9863	7.9752	3.9597	7.9432	3.9262	7.9110	3.8858
Multiple ESPRIT	Freq (Hz)	0.500	0.599	0.499	0.599	0.495	0.593	0.471	0.587	0.455	0.577
	Attenuation Factor	-0.249	-0.149	-0.251	-0.149	-0.248	-0.149	-0.229	-0.139	-0.221	-0.135
	Amplitude	1.010	1.010	0.990	0.990	0.990	1.010	1.020	0.970	1.040	0.910
	Damping Ratio %	7.9274	3.9597	8.0071	3.9597	7.9753	3.9998	7.7396	3.7695	7.7318	3.7244
Prony	Freq (Hz)	0.499	0.599	0.498	0.599	0.491	0.592	0.451	0.567	0.431	0.359
	Attenuation Factor	-0.249	-0.15	-0.248	-0.148	-0.246	-0.145	-0.211	-0.121	-0.157	-0.115
	Amplitude	0.990	0.990	0.990	0.990	0.980	1.020	1.020	0.970	1.090	0.850
	Damping Ratio %	7.9433	3.9863	7.9273	3.9331	7.9755	3.8990	7.4475	3.3971	5.7986	5.0992

Table 8
 Mode Estimation on Synthetic Signal having three modes

Method	Hybrid				Multiple ESPRIT				Prony			
	Freq (Hz)	Attenuation Factor	Amplitude	Damping Ratio%	Freq (Hz)	Attenuation Factor	Amplitude	Damping Ratio%	Freq (Hz)	Attenuation Factor	Amplitude	Damping Ratio%
No noise	0.7000	-0.2199	0.4990	5.0007	0.7002	-0.2198	0.4990	4.9978	0.7003	-0.2198	0.4980	4.9950
	0.3900	-0.1596	1.0000	6.5143	0.3901	-0.1596	1.0000	6.5118	0.3902	-0.1596	0.9970	6.5103
	0.2500	-0.1102	0.9970	7.0169	0.2500	-0.1101	0.9970	7.0108	0.2500	-0.1100	1.0001	7.0052
50dB	0.7000	-0.2170	0.4990	4.9347	0.7000	-0.2150	0.5000	4.8893	0.7001	-0.2195	0.4970	4.9896
	0.3900	-0.1601	1.0000	6.5343	0.3890	-0.1601	1.0000	6.5511	0.3900	-0.1594	0.9975	6.5054
	0.2500	-0.1098	0.9970	6.9912	0.2500	-0.1098	0.9980	6.9912	0.2500	-0.1100	1.0120	7.0052
30dB	0.6974	-0.2194	0.4975	5.0068	0.6898	-0.2224	0.4970	5.1331	0.6998	-0.2324	0.4980	5.2873
	0.3954	-0.1588	1.0173	6.3951	0.3900	-0.1594	0.9989	6.5054	0.3984	-0.1618	1.0083	6.4668
	0.2500	-0.1100	1.0012	7.0052	0.2514	-0.1141	1.0162	7.2212	0.2504	-0.1132	1.0262	7.1928
20dB	0.7011	-0.2252	0.4960	5.1130	0.6961	-0.2142	0.4950	4.8982	0.6971	-0.2092	0.4970	4.7770
	0.3904	-0.1614	1.0137	6.5818	0.3874	-0.1624	1.1107	6.6739	0.3874	-0.1624	1.1105	6.6739
	0.2505	-0.1147	1.0216	7.2863	0.2495	-0.1067	0.9716	6.8051	0.2345	-0.1056	0.9516	7.1657
10dB	0.6980	-0.2238	0.4910	5.1048	0.6880	-0.2038	0.4890	4.7162	0.7058	-0.2015	0.4890	4.5456
	0.3896	-0.1582	0.9083	6.4623	0.4011	-0.1703	1.1057	6.7573	0.4011	-0.1733	1.1057	6.8763
	0.2495	-0.1134	1.0380	7.2368	0.2525	-0.1048	0.9576	6.6032	0.4011	-0.1668	0.9476	6.6184

The accuracy of the proposed hybrid algorithm is checked for the synthetic signal having three modes at 10dB noise level. From the analysis given in Table 8 of the synthetic signal having three modes with frequency and attenuation factor as 0.25Hz and -0.1102, 0.39 Hz and -0.1596, 0.7 Hz and -0.2199, respectively, the percentage error for estimating frequency component of 0.39 Hz at 10dB noise level by hybrid algorithm, multiple ESPRIT, and Prony algorithm is 0.1%, 2.8%, and 2.8% whereas the percentage error for estimating the attenuation factor of -0.1596 at 10dB noise level by hybrid algorithm, multiple ESPRIT, and Prony algorithm is 0.87%, 6.7% and 8.5% which indicates that the proposed algorithm is having higher accuracy as compared to other methods even at 10dB noise level for three-mode signal.

In the subsequent section, this research tested the proposed hybrid method on the WECC system from probe test data obtained on 14th September 2005. Since this research is interested in transient analysis, it considers two windows, as shown in Figure 7. Analysis windows correspond to data obtained after two sequential probing of ±125 MW, as shown in Figure 7. Both analysis window is also corrupted by adding 30 dB AWGN white noise.

The estimation of frequency and damping ratio (ζ) is carried out on these two windows using the proposed hybrid method along with HTLS (Philip & Jain, 2018b), EMO-ESPRIT (Philip & Jain, 2018a), and TLS-ESPRIT (Tripathy et al., 2011) methods to compare the performance. The estimation result is shown in Table 9, including the estimated value as suggested by Philip and Jain (2018a) and Rai et al. (2014). Therefore, it can be inferred that the hybrid model accurately estimates frequency and damping ratio values on WECC probe data which is very close as given in Philip and Jain (2018a) and Rai et al. (2014). In the next part, parameters estimation on WECC data is obtained under the varying noise level ranging from 50 dB to 10 dB, and the result is tabulated in Table 10. The developed hybrid method is robust and reliable with various noise conditions, as discussed and tested earlier. The observation can be inferred from Table 10, where the hybrid method estimates damping ratio and frequency accurately from two different windows despite the presence of noise.

Table 9
Mode estimation of frequency and damping ratio of WECC Probe data

Window	Suggested value is given in Philip and Jain (2018a) and Rai et al. (2014)		Proposed Hybrid Method		HTLS (Philip & Jain, 2018b)		TLS-ESPRIT (Tripathy et al., 2011)		EMO-ESPRIT (Philip & Jain, 2018a)	
	Freq (Hz)	ζ	Freq (Hz)	ζ	Freq (Hz)	ζ	Freq (Hz)	ζ	Freq (Hz)	ζ
Window-1	0.318	8.30	0.3186	8.33	0.3183	8.39	0.3259	6.86	0.3207	8.30
Window-2	0.318	8.30	0.3141	8.11	0.316	8.11	0.3151	7.78	0.3149	7.88

Table 10

Estimation of damping ratio and frequency of WECC probe data under various noise levels by a hybrid method

Window	50 dB		35 dB		10 dB	
	Freq (Hz)	ζ	Freq (Hz)	ζ	Freq (Hz)	ζ
Window-1	0.3186	8.31	0.3176	8.23	0.3157	8.23
Window-2	0.3171	8.21	0.3161	8.11	0.3138	8.09

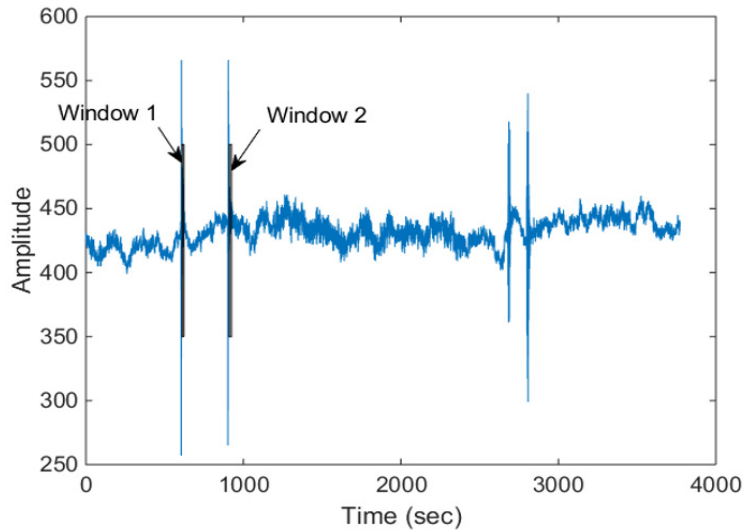


Figure 7. Test probe data of WECC system on 14th September 2005 with consideration of two windows to be analyzed.

CONCLUSION

In order to estimate true modes in the power system due to low-frequency oscillation, exact model order estimation is required for signal processing techniques like Prony or ESPRIT, which has been overcome in this research paper. This research work proposed a hybrid method based on the Prony and ESPRIT algorithm to find true modes from the low-frequency oscillatory signal based on the Euclidean distance concept irrespective of the model order of the algorithm. The proposed method is motivated by observing that true modes are present in both methods and other fictitious modes. However, it is encouraged to use different methods to remove fictitious modes accurately. This research has shown the robustness of the hybrid method with different noise levels and varying reporting rates of PMU. It is also shown that the discussed method is more reliable compared to multiple ESPRIT methods and estimate accurate modes in single and multiple trials. Moreover, the proposed method on WECC probe data was tested with the various noise levels and the current state-of-the-art methods, which show the outstanding performance of the proposed

method. Hence, the proposed method is more robust and reliable to use in practice under any conditions in terms of varying PMU sampling rates and different noise levels.

ACKNOWLEDGEMENT

The authors wish to pay gratitude to Devi Ahilya Vishwavidyalaya Indore Madhya Pradesh India for providing a conducive research environment.

REFERENCES

- Amono, M., Watanabe, M., & Banjo, M. (1999). Self-testing and self-tuning of power system stabilizers using Prony analysis. In *IEEE Power Engineering Society. Winter Meeting (Cat. No.99 CH36233)* (Vol 1, pp. 655-660). IEEE Publishing. <https://doi.org/10.1109/PESW.1999.747533>
- Avdakovic, S., Nuhanovic, A., Kusljagic, M., & Music, M. (2012). Wavelet transform applications in power system dynamics. *Electric Power Systems Research*, 83, 237-245. <https://doi.org/https://doi.org/10.1016/j.epr.2010.11.031>
- Browne, T. J., Vittal, V., Heydt, G. T., & Messina, A. R. (2008). A comparative assessment of two techniques for modal identification from power system measurements. In *IEEE Transactions on Power Systems*, (Vol. 23, pp. 1408-1415). IEEE Publishing. <https://doi.org/10.1109/TPWRS.2008.926720>
- Girgis, A. A., & Ham, F. M. (1980). A quantitative study of pitfalls in the FFT. In *IEEE Transactions on Aerospace and Electronic Systems*, (Vol. 4, pp. 434-439). IEEE Publishing. <https://doi.org/10.1109/TAES.1980.308971>
- Glickman, M., O'Shea, P., & Ledwich, G. (2007). Estimation of modal damping in power networks. In *IEEE Transactions on Power Systems*, (Vol. 22, pp. 1340-350). IEEE Publishing. <https://doi.org/10.1109/TPWRS.2007.901122>
- Grant, L. L., & Crow, M. L. (2011). Comparison of matrix pencil and prony methods for power system modal analysis of noisy signals. In *2011 North American Power Symposium* (pp.1-7). IEEE Publishing. <https://doi.org/10.1109/NAPS.2011.6024892>
- Hauer, J. F. (1991). Application of Prony analysis to the determination of modal content and equivalent models for measured power system response. In *IEEE Transactions on Power Systems*, (Vol. 6, pp.1062-1068). IEEE Publishing. <https://doi.org/10.1109/59.119247>
- Hauer, J. F., Demeure, C. J., & Scharf, L. L. (1990). Initial results in Prony analysis of power system response signals. In *IEEE Transactions on Power Systems*, (Vol. 5, pp. 80-89). IEEE Publishing. <https://doi.org/10.1109/59.49090>
- Hua, Y., & Sarkar, T. K. (1990). Matrix pencil method for estimating parameters of exponentially damped/undamped sinusoids in noise. In *IEEE Transactions on Acoustics, Speech, and Signal Processing*, (Vol. 38, pp. 814-824). IEEE Publishing. <https://doi.org/10.1109/29.56027>
- Kang, P., & Ledwich, G. (1999). Estimating power system modal parameters using wavelets. *ISSPA '99. Proceedings of the Fifth International Symposium on Signal Processing and Its Applications (IEEE Cat. No.99EX359)* (Vol. 2, pp. 563-566). IEEE Publishing. <https://doi.org/10.1109/ISSPA.1999.815735>

- Korba, P., Larsson, M., & Rehtanz, C. (2003). Detection of oscillations in power systems using Kalman filtering techniques. In *Proceedings of 2003 IEEE Conference on Control Applications, 2003. CCA 2003* (Vol. 1, pp. 183-188). IEEE Publishing. <https://doi.org/10.1109/CCA.2003.1223290>
- Kundur, P. (1994). *Power system stability and control*. Tata Mc-Graw Hill Co.
- Laila, D. S., Messina, A. R., & Pal, B. C. (2009). A refined Hilbert-Huang transform with applications to inter-area oscillation monitoring. In *IEEE Transactions on Power Systems*, (pp. 610-620). IEEE Publishing. <https://doi.org/10.1109/PES.2009.5275975>
- Philip, J. G., & Jain, T. (2018a). Analysis of low frequency oscillations in power system using EMO ESPRIT. *International Journal of Electrical Power & Energy Systems*, 95, 499-506. <https://doi.org/10.1016/j.ijepes.2017.08.037>
- Philip, J. G., & Jain, T. (2018b). Estimation of modal parameters of low frequency oscillations in power system using Hankels total least square method. In *2018 IEEE Innovative Smart Grid Technologies-Asia (ISGT Asia)*, (pp. 764-769). IEEE Publishing. <https://doi.org/10.1109/ISGT-Asia.2018.8467979>
- Pierre, J. W., Trudnowski, D. J., & Donnelly, M. K. (1997). Initial results in electromechanical mode identification from ambient data. In *IEEE Transactions on Power Systems* (Vol. 12, pp. 1245-1251). IEEE Publishing. <https://doi.org/10.1109/59.630467>
- Qi, L., Qian, L., Woodruff, S., & Cartes, D. (2007). Prony analysis for power system transient harmonics. *EURASIP Journal on Advances in Signal Processing*, 2007, Article 48406. <https://doi.org/10.1155/2007/48406>
- Rai, S., Tripathy, P., & Nayak, S. K. (2014). A robust TLS-ESPIRIT method using covariance approach for identification of low-frequency oscillatory mode in power systems. In *2014 Eighteenth National Power Systems Conference (NPSC)* (pp. 1-6). IEEE Publishing. <https://doi.org/10.1109/NPSC.2014.7103887>
- Rai, S., Lalani, D., Nayak, S. K. K., Jacob, T., & Tripathy, P. (2016). Estimation of low-frequency modes in power system using robust modified Prony. *IET Generation, Transmission & Distribution*, 10(6), 1401-1409.
- Rueda, J. L., Juarez, C. A., & Erlich, I. (2011). Wavelet-based analysis of power system low-frequency electromechanical oscillations. In *IEEE Transactions on Power Systems* (Vol. 26, pp. 1733-1743). IEEE Publishing. <https://doi.org/10.1109/TPWRS.2010.2104164>
- Trentini, R., Kutzner, R., Hofmann, L., Oliveira, J. de, & Nied, A. (2019). On the electromechanical energy approach: a novel modeling method for power systems stability studies. In *IEEE Transactions on Power Systems* (Vol. 34, pp. 1771-1779). IEEE Publishing. <https://doi.org/10.1109/TPWRS.2018.2887001>
- Tripathy, P., Srivastava, S. C., & Singh, S. N. (2011). A modified TLS-ESPRIT-based method for low-frequency mode identification in power systems utilizing synchrophasor measurements. In *IEEE Transactions on Power Systems* (Vol. 26, pp. 719-727). IEEE Publishing. <https://doi.org/10.1109/TPWRS.2010.2055901>
- Trudnowski, D. I. (1994). Order reduction of large-scale linear oscillatory system models. In *IEEE Transactions on Power Systems* (Vol. 9, pp. 451-458). IEEE Publishing. <https://doi.org/10.1109/59.317578>
- Trudnowski, D. J., Johnson, J. M., & Hauer, J. F. (1999). Making Prony analysis more accurate using multiple signals. In *IEEE Transactions on Power Systems* (Vol. 14, pp. 226-231). IEEE Publishing. <https://doi.org/10.1109/59.744537>

- Wadduwage, D. P., Annakkage, U. D., & Narendra, K. (2015). Identification of dominant low-frequency modes in ring-down oscillations using multiple Prony models. *IET Generation, Transmission & Distribution*, 9(15), 2206-2214.
- Wang, L., & Semlyen, A. (1990). Application of sparse eigenvalue techniques to the small signal stability analysis of large power systems. *IEEE Transactions on Power Systems* (Vol. 5, pp. 635-642). IEEE Publishing. <https://doi.org/10.1109/59.54575>
- Wang, X., Tang, F., Wang, X., & Zhang, P. (2014). Estimation of electromechanical modes under ambient condition via random decrement technique and TLS-ESPRIT algorithm. In *2014 International Conference on Power System Technology* (pp. 588-593). IEEE Publishing. <https://doi.org/10.1109/POWERCON.2014.6993775>
- Wies, R. W., Pierre, J. W., & Trudnowski, D. J. (2003). Use of ARMA block processing for estimating stationary low-frequency electromechanical modes of power systems. *IEEE Transactions on Power Systems* (Vol. 18, pp. 167-173). IEEE Publishing. <https://doi.org/10.1109/TPWRS.2002.807116>
- Xie, X., Zhang, S., Xiao, J., Wu, J., & Pu, Y. (2005). Small signal stability assessment with online eigenvalue identification based on wide-area measurement system. *2005 IEEE/PES Transmission Distribution Conference Exposition: Asia and Pacific*, (pp 1-5). IEEE Publishing. <https://doi.org/10.1109/TDC.2005.1546826>
- Zhang, S., Xie, X., & Wu, J. (2008). WAMS-based detection and early-warning of low-frequency oscillations in large-scale power systems. *Electric Power Systems Research*, 78(5), 897-906. <https://doi.org/10.1016/J.EPSR.2007.06.008>
- Zhou, N., Huang, Z., Tuffner, F., Pierre, J., & Jin, S. (2010). Automatic implementation of Prony analysis for electromechanical mode identification from phasor measurements. *IEEE PES General Meeting* (pp. 1-8). IEEE Publishing. <https://doi.org/10.1109/PES.2010.5590169>
- Zhou, N., Trudnowski, D. J., Pierre, J. W., & Mittelstadt, W. A. (2008). Electromechanical mode online estimation using regularized robust RLS methods. In *IEEE Transactions on Power Systems* (Vol. 23, pp. 1670-1680). IEEE Publishing. <https://doi.org/10.1109/TPWRS.2008.2002173>

Review Article

Mechanical Properties of Natural Fibre Reinforced Geopolymer Composites: A Review

Noor Abbas Al-Ghazali¹, Farah Nora Aznieta Abdul Aziz^{1*}, Khalina Abdan² and Noor Azline Mohd Nasir¹

¹Housing Research Centre (HRC), Department of Civil Engineering, Faculty of Engineering, Universiti Putra Malaysia, 43400 UPM, Serdang, Selangor, Malaysia

²Institute of Tropical Forestry and Forest Product (INTROP), Universiti Putra Malaysia, 43400 UPM, Serdang, Selangor, Malaysia

ABSTRACT

The cement production consumes many natural resources and energy, pollutes the environment, and cannot meet the current building materials' green and sustainable development requirements. Therefore, geopolymers have gained popularity as cement replacements in recent years. Geopolymers have promising characteristics such as low energy consumption and carbon footprint, valuable compressive strength, fire resistance, flame resistance and good durability. However, these materials suffer from low tensile and flexural strength. Hence, fibres are added to overcome these issues and enhance their toughness index. Natural fibres are biodegradable, low-cost, renewable materials and widely available in many countries. This article reviewed previous Natural Fibre Reinforced Geopolymer Composites (NFRGC) studies, focusing on compressive strength, tensile and flexural strengths, and toughness. In addition, the available literature on the effect of the treatment methods of natural fibres on the mechanical properties of NFRGC

has been addressed. The findings indicate that adding the appropriate type and content of natural fibres to geopolymer composites can enhance their mechanical properties. However, more attention should be paid to the effects of the pre-treatment of natural fibres on the performance of NFRGC.

Keywords: Fibres, geopolymer composites, mechanical properties, natural fibres

ARTICLE INFO

Article history:

Received: 15 December 2021

Accepted: 29 March 2022

Published: 20 April 2022

DOI: <https://doi.org/10.47836/pjst.30.3.16>

E-mail addresses:

na706050@gmail.com (Noor Abbas Al-Ghazali)

farah@upm.edu.my (Farah Nora Aznieta Abdul Aziz)

khalina@upm.edu.my (Khalina Abdan)

nazline@upm.edu.my (Noor Azline Mohd Nasir)

*Corresponding author

INTRODUCTION

Davidovits introduced the concept of geopolymers in 1978. These inorganic polymers are produced by the chemical reaction between an aluminosilicate source with an alkaline activator through the geopolymerisation process that results in polymeric chains and cross-linked networks consisting of Si-O-Al-O bonds of comparable or greater strength than that of Ordinary Portland Cement-based composites (OPCC) (Ganesh & Muthukannan, 2021; Farhan et al., 2018). A literature review showed that Geopolymer Composites (GPC) have excellent mechanical strength and durability. These outstanding attributes include low porosity (Fang et al., 2018), high early strength (Jawahar et al., 2016), and high performance in sulphate and acid environment (Gopalakrishnan & Chinnaraju, 2019), and elevated temperature resistance (Yasaswini & Rao, 2020). These features make GPC a potential candidate for various industrial applications (Zhang et al., 2020). However, both the OPCC and GPC are brittle materials with low tensile strength. Reinforcing these materials with different kinds of fibres, such as synthetic, steel, or natural fibres, is one of the most common methods to overcome these weaknesses. Besides, many researchers claimed that geopolymer composites had greater material greenness than traditional cement and that fibre reinforcing can improve their ductility and durability (Bellum, 2021).

The use of natural fibres as a replacement for conventional fibre reinforcements in composites has gained popularity in recent years. The production of economically viable, ecologically sustainable, and healthful products based on natural sources is gaining popularity. Using natural fibres as reinforcements in geopolymer composites is an attractive alternative for the building industry. Several studies on the strength and behaviour of geopolymer composites reinforced with natural fibres have been published in recent years. Since natural fibres are abundant in many developing countries, more in-depth studies should be conducted on the various issues related to their utilisation.

The Natural Fibre-Reinforced Geopolymer Composites (NFRGC) contain two main parts, as shown in Figure 1. The first part is the geopolymer matrix, which comprises two main components (the binder and the alkaline activator). For the binder, different aluminosilicates sources have been used by researchers to produce geopolymer binders. These sources are derived either from a natural source such as kaolinite, albite, clays or from industrial by-products like Ground Granulated Blast Slag (GGBS) (Gupta, 2021; Fang et al., 2018), Fly Ash (FA) (Abdulmuttaleb et al., 2022; Chen et al., 2022; Chindaprasirt et al., 2021), Palm Oil Fuel Ash (POFA) (Ayub et al., 2021), Rice Husk Ash (RHA) (Abbass & Singh, 2021) and Silica Fume (SF) (Liang et al., 2021). The other primary component of geopolymer is the alkaline activator, which is essential to creating Al and Si crystals. The most popular alkali activator is sodium silicate or potassium silicate combined with sodium hydroxide or potassium hydroxide. However, a single alkali activator can also be utilised in geopolymer composites.

On the other hand, the second part of NFRGC is the Natural Fibres (NF), which can be derived from three different sources (plant, animal, and mineral source). Compared to animal and mineral fibres, plant fibres are more favourable due to the difficulties of collecting the fibres from animals. In addition, these fibres contain a high amount of protein in their structure. While for the mineral fibres, fibres should undergo several processes before being included in the geopolymer. The plant fibres can be derived from different parts of the plant, such as the bast, stalk, leaf, seeds, grass, and fruit. This article reviews previous studies on the mechanical properties of NFRGC with a focus on compressive, tensile, and flexural strengths and toughness.

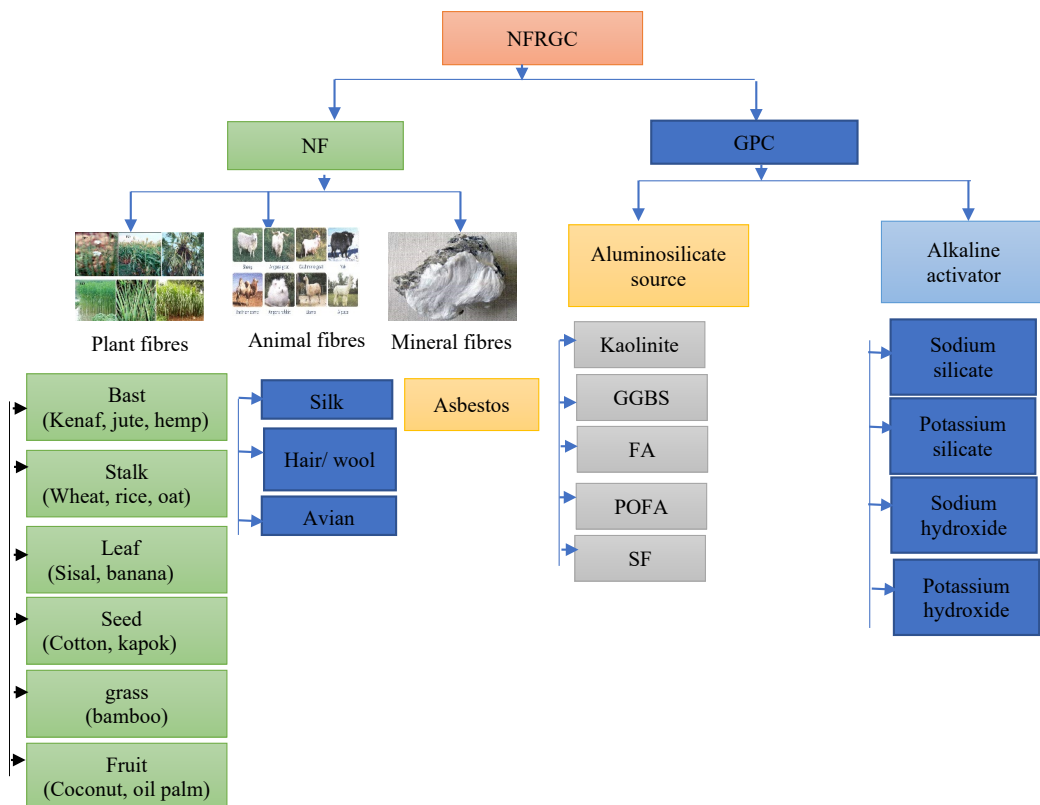


Figure 1. NFRGC components

MECHANICAL PROPERTIES OF NFRGC

Compressive Strength

The inclusion of NF can highly affect the compressive strength of geopolymers, and this effect is dependent on both the matrix and fibre type, properties, content and length.

Korniejenko et al. (2016) examined the performance of the NFRGC prepared with different types of NF and how adding 1% by weight of the composite fibres will affect the strength properties of geopolymer. The results showed that NFRGC containing coconut fibres, sisal, or cotton fibres achieved higher compressive strength than the neat geopolymer. Only the NFRGC prepared with raffia fibres showed lower strength than the latter unreinforced composite due to the weak interfacial bonding between raffia fibres and the geopolymer matrix. According to Yanou et al. (2021), the increase in the sugarcane bagasse fibres (SBF) content resulted in a reduction in the compressive strength of NFRGC. The findings revealed that the inclusion of SBF in percentages of 1.5%, 3%, 4.5%, 6% and 7.5% caused reductions of 18.3%, 31.8%, 43.1%, 65.9% and 71.8% in comparison with the neat geopolymer, respectively. The authors attributed the strength reduction to the high void content in the NFRGC mixtures, which created weaker zones within the geopolymer matrix.

On the contrary, Silva et al. (2020) reported that the compressive strength of NFRGC containing jute or sisal fibres was 64% and 76% higher, respectively, compared to the neat geopolymer. Besides, the test data showed that the strength of NFRGC tends to increase with the fibres content, up to a limit where a reduction was observed, and the type of fibre determines the optimum content and strength. Similarly, Alomayri and Low (2013) reported that increasing the cotton fibre percentage from 0.3% to 0.5% by weight in the NFRGC increased the compressive strength by 65%, while further adding cotton fibre (beyond 0.5%) caused a strength reduction. The improved compressive strength for the NFRGC containing the appropriate content of fibres is because a great amount of stress has transferred from the matrix to the fibres, which causes a higher load carried by the fibres. Besides, the good distribution of NF in the matrix enhanced the interfacial bonding between the fibre and the matrix.

On the other hand, the strength reduction with higher fibres could be attributed to the increased porosity due to the agglomeration of the fibres. In a different study, Alomayri et al. (2014) studied the performance of NFRGC prepared with cotton fibre in the fabric form with various contents and orientations. The findings revealed that NFRGC prepared with horizontally oriented fabric exhibited higher compressive strength than composites prepared with vertically oriented fabric. The horizontally oriented fabrics can absorb and transfer applied loads uniformly over the cross-section. Also, the horizontally oriented fabric-matrix interface is not subjected to shear loadings, which decreases the risk of fabrics detachment or delamination at high loads. Besides, increasing the fabric layers for both types increased the strength of NFRGC. Likewise, Assaedi et al. (2015) observed that the inclusion of the flax fabric significantly increased the strength properties of geopolymer, and increasing the fibre dosage caused a higher strength improvement. The compressive strength of plain geopolymer increased from 19 MPa to 91 MPa for NFRGC containing 4.1% by weight flax fibres. This improvement could be attributed to the ability of the fibres to absorb and transfer the stress from the matrix.

Zulfiati and Idris (2019) examined the influence of the length and content of NF and the alkalinity of the geopolymer on the performance of NFRGC. The authors incorporated three different lengths of pineapple leaf fibre (10 mm, 20 mm, and 30 mm) with a content of 0.25 and 0.5% to FA-based GPC activated by sodium silicate and sodium hydroxide of two different concentrations (14 M and 16 M). The findings indicated that the length of the fibre showed a very significant impact on the strength of the composite, and for both fibre percentages, NFRGC containing pineapple fibres of 30 mm length achieved better strength than the composites reinforced by fibres of 10 mm and 20 mm lengths, as shown in Figure 2. NFRGC containing 0.5% fibres of 30 mm length and activated with sodium hydroxide of 16 M achieved the highest compressive strength of 41.4 MPa. It could be attributed to the fact that fibres of 30 mm in length were more effective in withstanding and transferring the applied stress to other composite portions (Islam & Ju, 2018). Furthermore, the NFRGC activated by higher sodium hydroxide concentration has good performance because the matrix binding process is faster by increasing the concentration. Therefore, it causes the polymerisation process to be more maximal with increasing time, resulting in a stronger bond between the fibre. Hence, the matrix, and the composite's performance is highly dependent on interfacial bonding.

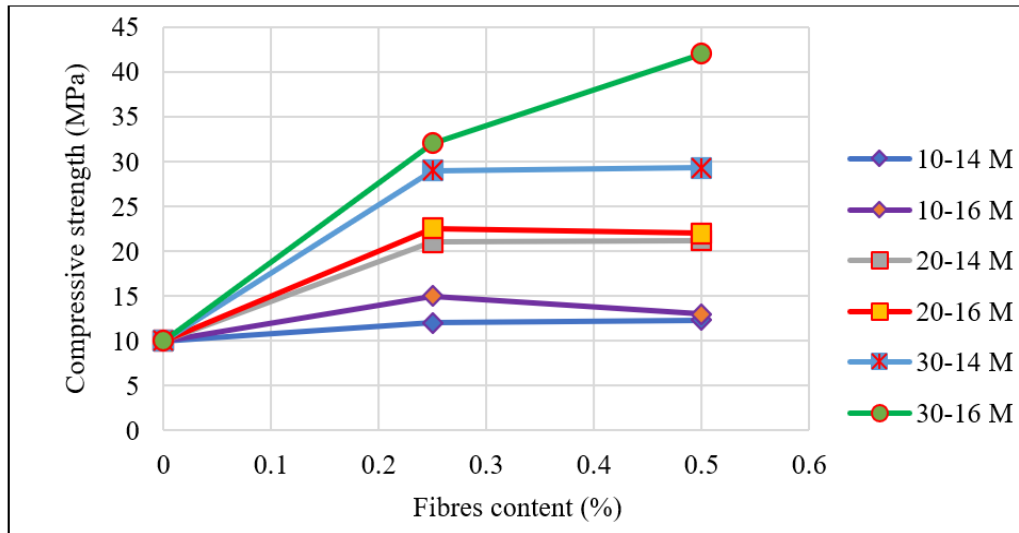


Figure 2. Impact of the length and content of NF on the compressive strength of NFRGC (Zulfiati & Idris, 2019)

In summary, NFRGC achieved a compressive strength of about 20% to almost 55% higher than the plain geopolymer mixes, as shown in Figure 3. Besides, in all the works related to NFRGC, there was an optimum content for fibre inclusion depending on the

matrix and fibre type and properties. Therefore, a preliminary study should be conducted before applying a large scale. Another note is that NFRGC containing the NF in the fabric form exhibited higher strength improvement than short fibres due to the better distribution of the continuous fibres in the geopolymer composites. Besides, their alignment in the direction of tension effectively bridges the cracks, resulting in higher stress transfer at the fibre-matrix interface.

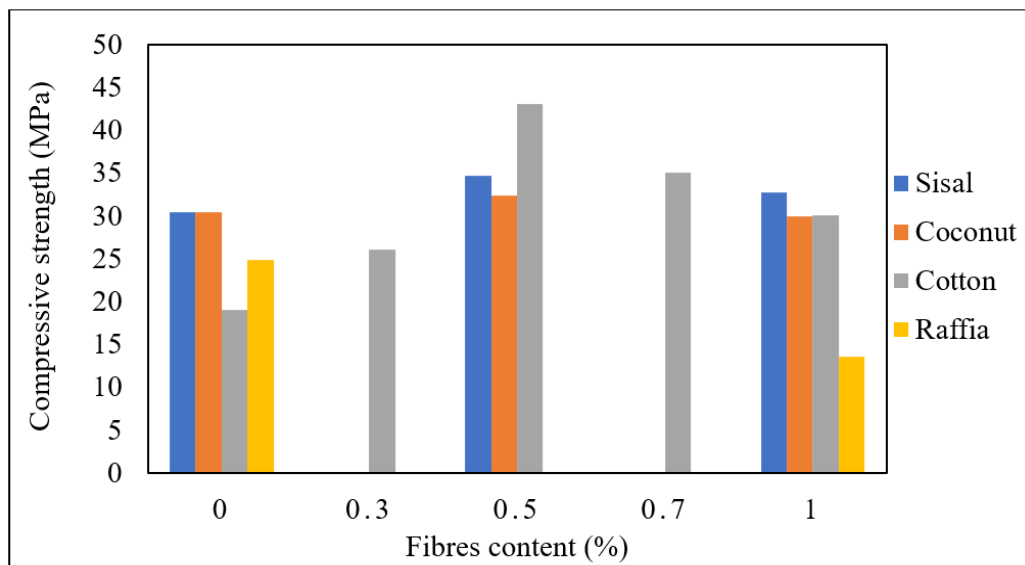


Figure 3. Variation of compressive strength of NFRGC prepared with different types of NF (Alomayri & Low, 2013; Korniejenko et al., 2016; Wongs a et al., 2020)

Flexural and Splitting Tensile Strengths

Wongs a et al. (2020) compared the performance of NFRGC prepared with two different types of NF and geopolymer composites prepared with synthetic fibres. The NFRGC was prepared with 0.5%–1% sisal fibre or coconut fibre, while the other composite was prepared with 0.5%–1% glass fibre. The results showed that the NFRGC and the composites prepared with the glass fibres achieved higher flexural and tensile strengths than the plain geopolymer. Besides, the tensile and flexural strengths of the fibrous composites tended to increase with increasing the content of the fibre. For example, NFRGC achieved a flexural strength of about 5.3–6.6 MPa, which was higher than the flexural strength of normal GPC (3.1 MPa), while GPC containing glass fibres achieved a flexural strength of about 3.1–3.7 MPa. The strength improvement could be attributed to the fibre’s high tensile strength and elasticity modulus. That stress in the matrix could be transferred to the fibre via the matrix-fibre interface.

Silva et al. (2020) examined the performance of NFRGC containing sisal fibres with an aspect ratio of 73 and content of 0.5%–3%, or jute fibres with an aspect ratio of 189 and content of 0.5%–2%. The results revealed that NFRGC showed higher tensile and flexural strength than the plain geopolymer without fibres. Besides, increasing fibre dosage until an optimum value increased the strength of the composites, as presented in Figure 4. The highest tensile strength was achieved by the NFRGC prepared with 1.5% of jute fibres (1.6 MPa) or 2.5% sisal fibres (2.3 MPa). At the same time, the highest flexural strength was achieved by the NFRGC prepared with the highest fibre percentage. For NFRGC containing jute fibres, the maximum flexural strength of 3.3 MPa was achieved with 2% fibre content. While for NFRGC prepared with sisal fibres, the highest flexural strength was obtained with the addition of 3% fibre content. Similarly, Alshaaer (2021) reported that the flexural strength of NFRGC containing jute fibres was four times higher than the strength of the geopolymer matrix without fibres. The ultimate flexural stress of the plain geopolymer was 3 MPa. However, NFRGC prepared with 15% by weight jute fibres achieved ultimate flexural stress of about 12 MPa.

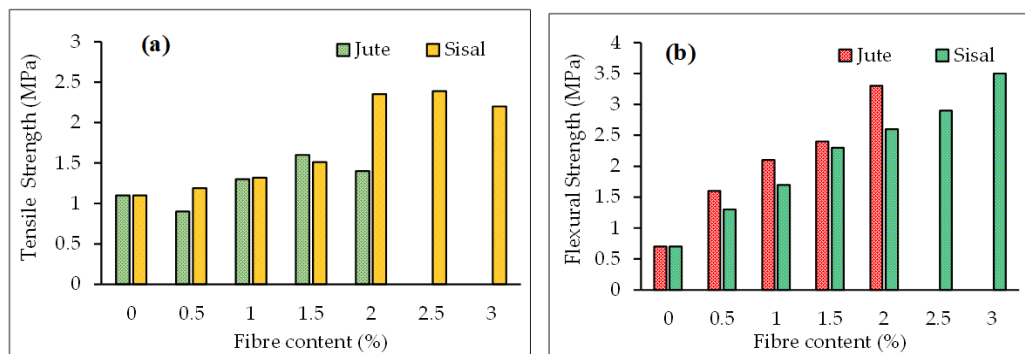


Figure 4. Strength performance of NFRGC containing jute or sisal fibres: (a) splitting tensile strength; (b) flexural strength (Silva et al., 2020)

Kavipriya et al. (2021) incorporated 0.25%–1% of sisal fibres to FA-based GPC activated by sodium silicate and sodium hydroxide solution. To reduce the self-weight of geopolymer concrete, the authors replaced the coarse aggregates with bamboo sticks at different proportions. The findings showed that the inclusion of sisal fibres was an effective solution to overcome the strength reduction due to the incorporation of bamboo sticks. Besides, increasing the dosage of the fibre from 0.25% to 0.75% increased the flexural strength of NFRGC. However, beyond 1% fibre content, a reduction in flexural strength was observed because incorporating more fibres negatively affects the geopolymerisation process, thus decreasing the strength. In another study, Abbass et al. (2021) observed that

the splitting tensile strength of NFRGC containing coconut fibres tends to increase first with the fibre content and then decrease. The gain in strength could be attributed to the ductile nature of the fibres; however, the reduction is owing to the increased porosity and low density of the fibres. The NF also can enhance the toughness of the composites and alter the failure mode from the brittle form to the ductile, as illustrated in Figure 5.

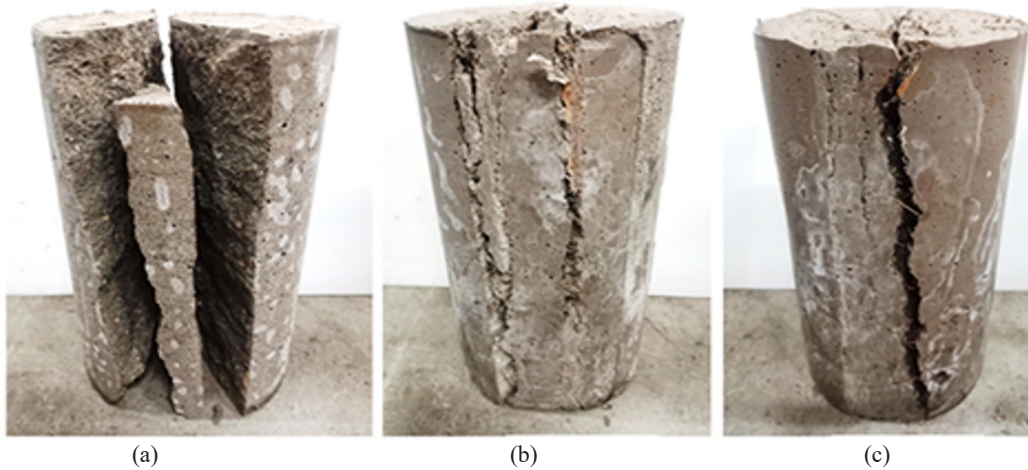


Figure 5. The failure mode of geopolymer composites; (a) plain GPC, (b) NFRGC containing 1% sisal fibre, (c) NFRGC containing 1% coconut fibre (Wongsa et al., 2020)

Assaedi et al. (2016) examined the impact of different nanoclay platelets contents on the mechanical properties of NFRGC containing flax fibres. The content of nanoclay platelets ranged from 1% to 3% by weight, while the content of flax fibre was 4.1% by weight. The results showed that NFRGC containing 2% by weight nanoclay achieved the highest flexural strength and toughness. The improvement in NFRGC strength with the inclusion of nanoclay could be related to the reduction of porosity and increased density of the composites. However, adverse mechanical properties were observed when the nanoclay content exceeded 2% by weight. In another study, Assaedi et al. (2019) observed that incorporating nano-silica particles was also effective in increasing the flexural strength of NFRGC prepared with flax fibre. After four weeks, the flexural strength of NFRGC containing nano-silica particles increased by 32.4% compared to NFRGC without nano-silica. This enhancement could be ascribed to reducing the unreacted fly ash particles, voids, and porosity, which led to a stronger bond between the geopolymer paste and the NF. However, after the ageing period of 32 weeks, all NFRGC exhibited a reduction in strength. This reduction was due to the weakening of the hemicellulose and lignin in the alkaline environment, which caused fibres brittleness (Filho et al., 2013). However, this

reduction was highly reduced for NFRGC containing nano-silica particles because nano-silica particles consumed some alkaline solutions, thus lowering the matrix's alkalinity. At the same time, the extra silica accelerated the geopolymerisation, thus increasing the amount of geopolymer gel in the composites. Consequently, the matrix's density increased, and the matrix-fibres bonding enhanced. The Scanning Electron Microscope (SEM) images of the fracture surface of the composites after 32 weeks indicated that the NF present in the NFRGC without nanoparticles had shown degradation signs and separation of the small fibrils, as obvious in Figures 6(a) and 6(b). On the other hand, NF embedded in the NFRGC containing nanoparticles did not show any notable degradation signs [Figures 6(c) & 6(d)].

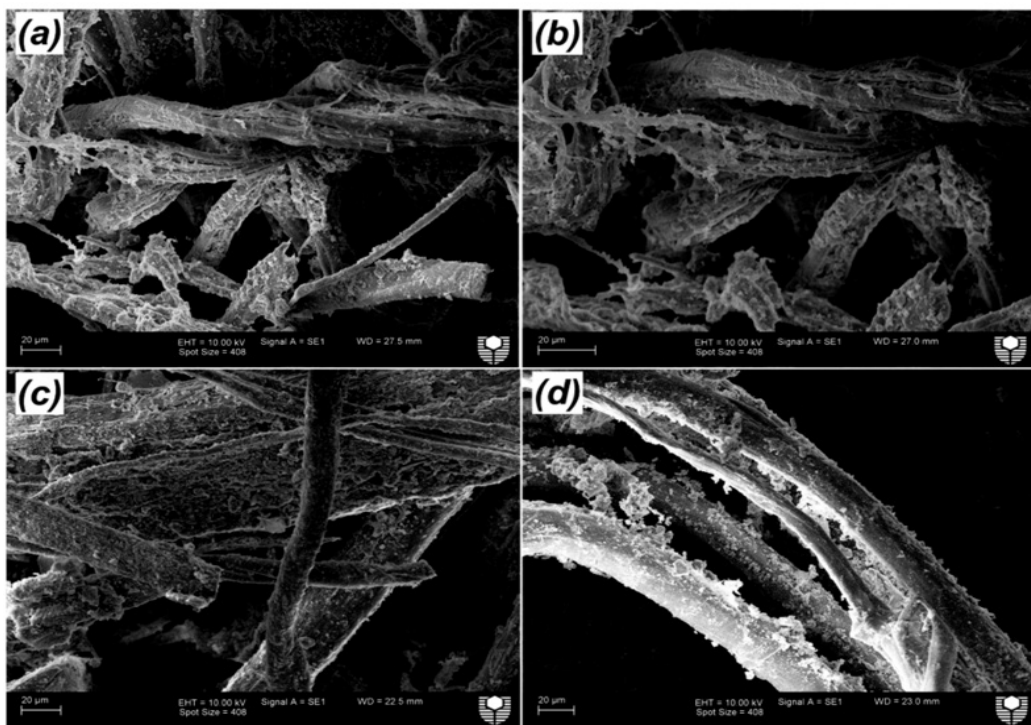


Figure 6. SEM images of flax fibre after 32 weeks in; (a) and (b) NFRGC without nano-silica particles, (c) and (d) NFRGC with nano-silica particles (Assaedi et al., 2019)

Natural Fibre Treatment and its Impact on the Mechanical Properties of NFRGC

Although NF has numerous advantages as reinforcing materials, such as low cost, lightweight, biodegradability, recyclability, and good mechanical properties, some obstacles like moisture absorption, biodegradation, and organic impurities should be addressed before the inclusion of these fibres in the geopolymer composites. The treatment or modification is usually done on natural fibres before embedment in composites. Waxes, oil, and other

undesirable components will be eliminated during the treatment process, allowing for better adhesion between natural fibres and the matrix. Many studies have revealed that suitable treatment can strengthen the interfacial bonding between the geopolymer and NF. The impact of NF pre-treatment on the mechanical characteristics of NFRGC is discussed in further depth in the following sections. The discussion will focus more on alkali-treated fibres, as this is one of the oldest and most well-known ways of modifying NF. Only a few studies have been conducted on the effects of other modifications methods.

The Impact of Treatment on the Compressive Strength

Maichin et al. (2020) studied the performance of NFRGC containing untreated or treated hemp fibres. The fibres were treated by soaking the hemp fibre in a 5 M sodium hydroxide (NaOH) solution for 48 hours before adding it to the FA-based GPC. The authors found that NFRGC achieved lower compressive strength than the plain geopolymer without fibres. There was no significant difference between the compressive strength values of NFRGC prepared with treated or untreated fibres. However, the highest deflection of about 0.64 mm was achieved by the NFRGC prepared with treated fibres compared to 0.41 mm and 0.51 mm deflection values of plain geopolymer and NFRGC prepared with untreated fibres. The low deflection of NFRGC prepared with untreated fibres could be attributed to impurities and waxes on the fibre's surface, which decreased the bonding strength between the fibre and the matrix.

Similarly, Chen et al. (2014) treated sweet sorghum fibre with a 2 M NaOH solution for 12 hours to reinforce FA-based GPC. The findings revealed that incorporating treated fibres into geopolymer slightly decreased the unconfined compressive strength. However, the post-peak toughness of the geopolymer matrix improved considerably with the addition of sweet sorghum fibres up to 2%, then declined slightly but remained much greater than that of the plain geopolymer matrix. Likewise, Pauline and Angelo (2018) treated abaca fibre with a 6% by weight NaOH solution to reinforce foamed geopolymer composite. The authors found that the compressive strength of NFRGC prepared with treated abaca fibres increased from 19.6 to 36.8 MPa. The alkali treatment improved not only the strength but also the fibre-matrix adhesion.

Zhang et al. (2021) studied the performance of NFRGC prepared with three different types of kenaf fibres: untreated kenaf fibres (KF), alkali-treated fibres (TKF) and CaCl_2 -treated kenaf fibre (TKF- CaCl_2). The fibres were incorporated at three different contents (5%, 10% and 15% by weight). The results showed that the compressive strength of NFRGC is affected by the content of the fibre, as shown in Figure 7(a). Increasing the fibre content from 5% to 15% by weight caused a reduction of about 10.7%, 6.1%, and 10.6% for NFRGC prepared with untreated, alkali-treated, and CaCl_2 -treated kenaf fibre, respectively. It is owing to the reduction in the proportion of geopolymer in the NFRGC containing higher

fibre content and increased porosity (Abbas et al., 2022). After compressive strength testing, images of destroyed specimens revealed a sudden fracture of the neat geopolymer [Figure 7(b)]. However, the NFRGC samples prepared with high TKF-CaCl₂ content retained their original shapes after the maximum load [Figures 7(c)–7(e)] due to the ability of the treated fibres to control the cracks propagation in the geopolymer composites.

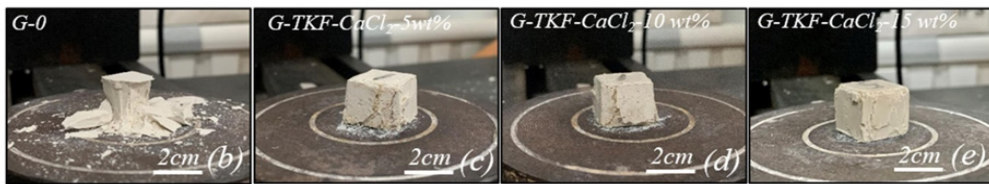
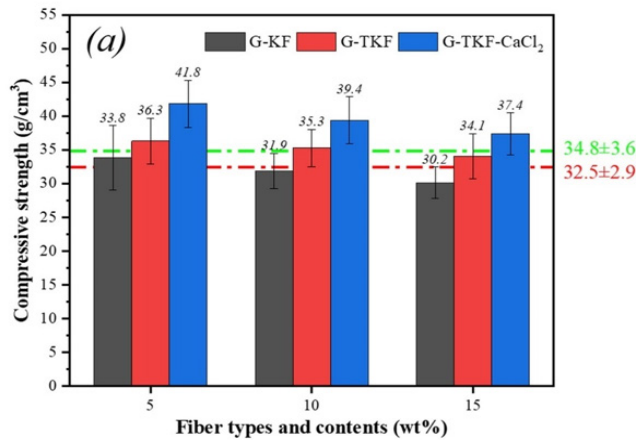


Figure 7. Compressive strength of (a) the NFRGC prepared with different types and contents of kenaf fibre; (b) failure mode of the plain geopolymer without fibres, (c) NFRGC prepared with 5% by weight TKF-CaCl₂; (d) NFRGC prepared with 10% by weight TKF-CaCl₂; and (e) NFRGC prepared with 15% by weight TKF-CaCl₂ (Zhang et al., 2021)

The Impact of Treatment on the Flexural and Splitting Tensile Strengths

Malenab et al. (2017) pre-treated abaca fibre using different types of chemical treatments: (i) alkali treatment by soaking the fibres in 6% by weight NaOH solution for 48 hours and (ii) aluminium sulphate treatment by soaking the fibres in 10% by weight of Al₂(SO₄)₃ solution. The findings revealed that treating the fibre with aluminium sulphate was efficient in forming AlOH₃ deposits on the surface of the NF, which increased the surface roughness for a better fibre-matrix interface. Then, they synthesized NFRGC by using untreated and pre-treated abaca fibre. The results showed that NFRGC prepared with treated fibres

exhibited lower compressive than that prepared with untreated fibre. However, the flexural strength was increased by 33% compared to the NFRGC with untreated fibres.

Furthermore, the SEM images indicated that NFRGC reinforced with untreated fibres displayed visible gaps between the fibre and matrix, indicating poor interfacial bonding [Figures 8(a) & 8(c)]. On the other hand, the NFRGC containing pre-treated fibres displayed narrower gaps, and the presence of the geopolymer products (zeolite particles) on the treated fibre surface referred to the strong interaction between the fibre, and the geopolymer paste [Figures 8(b) & 8(d)]. In another study, Chen et al. (2014) reported that NFRGC containing 2% alkali-treated sweet sorghum fibres exhibited higher tensile and flexural strength with about 36% to 39%, respectively, compared to the plain geopolymer.

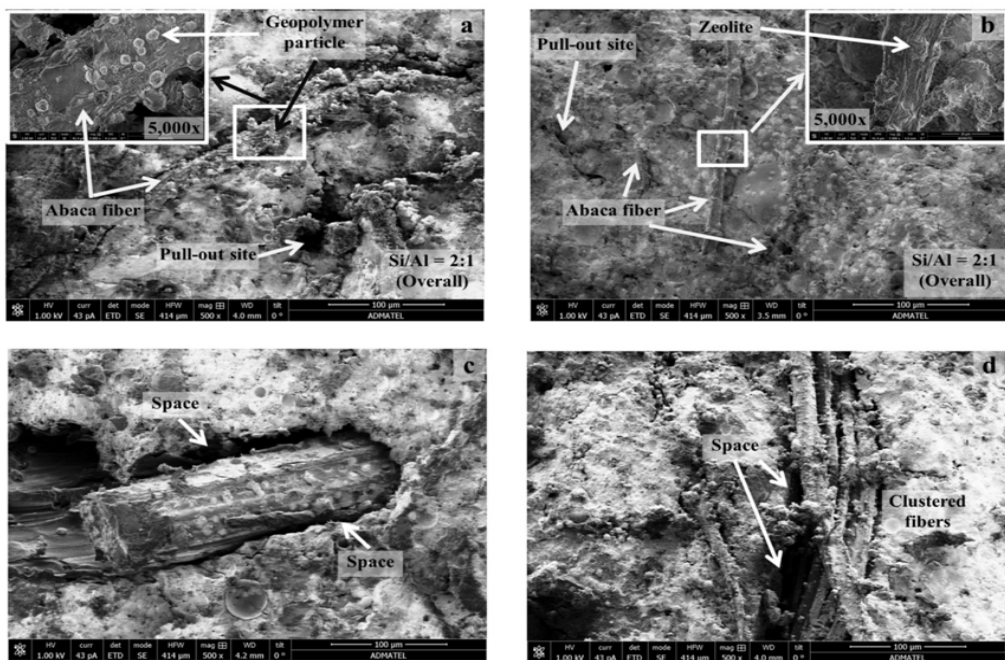


Figure 8. SEM images of NFRGC fractured surfaces: (a) NFRGC prepared with untreated abaca fibre; (b) NFRGC prepared with pre-treated fibres; (c) interface between geopolymer paste and untreated fibres and (d) interface between geopolymer paste and pre-treated abaca fibres (Malenab et al., 2017)

Researchers also investigated other modification methods. Findings by Alzeer and MacKenzie (2012) showed that the chemical modification of the wool fibre surface was very effective in reducing the lipids and fatty acids, and the treatment with formaldehyde enhanced the tensile strength and alkali resistance of the wool fibre. The flexural strength of the NFRGC containing formaldehyde-treated wool fibres was increased by 40% compared to the plain geopolymer composite. In another study, Suwan et al. (2022) reported that the

alkalinity of the GPC medium could act as an alkaline treatment reagent for the reinforced NF. The authors examined the impact of the alkaline environment in the geopolymer system on the modification process of the embedded fibres and the relationship between these factors and the properties of NFRGC containing hemp fibres. The untreated (UT) and pre-treated fibres (T) were examined in parallel to evaluate the effect of surface treatment of NF after being incorporated into the GPC mixes. The fibres were added at a content of 0.5% to FA-based GPC activated by sodium silicate and sodium hydroxide solution with different concentrations (5 M, 8 M, and 10 M). The findings indicated that the flexural strength of the NFRGC containing untreated fibres (5MUT, 8MUT, and 10MUT) appeared to be higher than that of treated fibres (5MT, 8MT and 10MT), as shown in Figure 9. It could be attributed to the unexpected decomposition of hemp fibre in the high alkalinity of the geopolymer system due to the double alkalisations processes of (a) pre-treatment process and (b) self-treatment process, respectively (Maichin et al., 2020).

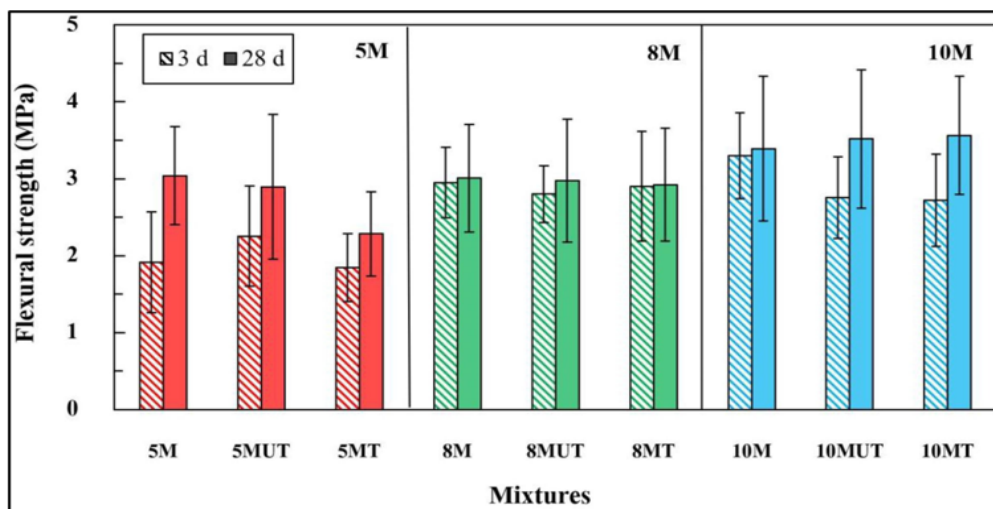


Figure 9. Flexural strength of NFRGC containing untreated (UT) and alkali-treated hemp fibres (T) in various NaOH concentrations (Suwan et al., 2022)

CONCLUSION

This paper presented a review of the published articles on the mechanical properties of NFRGC; the compressive strength, flexural and splitting tensile strengths of these composites were discussed. The following conclusions are drawn:

- NF are low-cost and ecologically sustainable alternatives to conventional fibres for improving the mechanical characteristics of geopolymer composites.

- Among NF, sisal, hemp, abaca, jute, cotton, flax, and coconut fibres are the most common fibres used for fibre-reinforced geopolymer materials due to their high specific strength and modulus.
- Literature showed that the mechanical characteristics of NFRGC are strongly influenced by the geopolymer matrix, NF type, content, and length of the fibres. However, the NFRGC containing the NF in the fabric form showed better strength improvement than the short fibres due to the better distribution of the continuous fibres in the geopolymer composites. Besides, their alignment in the direction of tension can effectively bridge the cracks, resulting in higher stress transfer at the fibre-matrix interface.
- The incorporation of nanoparticles can enhance the mechanical strength of NFRGC due to their ability to lower the geopolymer matrix's alkalinity by consuming some of the alkaline solutions, which can be used as a valuable technique to address the NF durability issues.
- The moisture absorption capability of NF, which harms the mechanical and durability characteristics of reinforced geopolymer composites, is an obstacle to their usage. However, as highlighted in this review, there are viable scenarios such as the pre-treatment or using the alkalinity of GPC medium as an alkaline treatment reagent for the reinforced NF, which can be used to minimise the water-absorbing chemical components of NF, thus improving their performance.
- In general, future studies are required to understand the processes of NF and NFRGC degradation. Furthermore, suitable and novel surface modification methods for NF should be developed to enhance their composites' moisture resistance, mechanical characteristics, and durability.

ACKNOWLEDGEMENT

The authors express gratitude for the financial support for this research by the Ministry of Education, Malaysia, under the Fundamental Research Grant Scheme (FRGS/1/2020/TKO/UPM/02/32) with Vot no: 5540372 for research work entitled 'An investigation of characterisation and parametric effect of kenaf bast fibre in the properties of geopolymer kenaf reinforced concrete.'

REFERENCES

- Abbas, A. N., Nora, F., Abdul, A., Abdan, K., Azline, N., Nasir, M., & Norizan, M. N. (2022). Kenaf fibre reinforced cementitious composites. *Fibers*, *10*, 1-24.
- Abbass, M., Singh, D., & Singh, G. (2021). Properties of hybrid geopolymer concrete prepared using rice husk ash, fly ash and GGBS with coconut fiber. *Materials Today: Proceedings*, *45*, 4964-4970. <https://doi.org/10.1016/j.matpr.2021.01.390>

- Abbass, M., & Singh, G. (2021). Impact strength of rice husk ash and basalt fibre based sustainable geopolymer concrete in rigid pavements. *Materials Today: Proceedings*, 1-8. <https://doi.org/10.1016/j.matpr.2021.09.053>
- Abdulmuttaleb, M., Yaltay, N., & Türkmeno, M. (2022). Properties of pumice-fly ash based geopolymer paste. *Construction and Building Materials*, 316, 1-10. <https://doi.org/10.1016/j.conbuildmat.2021.125665>
- Alomayri, T., & Low, I. M. (2013). Synthesis and characterization of mechanical properties in cotton fiber-reinforced geopolymer composites. *Journal of Asian Ceramic Societies*, 1(1), 30-34. <https://doi.org/10.1016/j.jascer.2013.01.002>
- Alomayri, T., Shaikh, F. U. A., & Low, I. M. (2014). Effect of fabric orientation on mechanical properties of cotton fabric reinforced geopolymer composites. *Materials and Design*, 57, 360-365. <https://doi.org/10.1016/j.matdes.2014.01.036>
- Alshaaer, M. (2021). Synthesis, characterization, and recyclability of a functional jute-based geopolymer composite. *Frontiers in Built Environment*, 7(March), 1-13. <https://doi.org/10.3389/fbuil.2021.631307>
- Alzeer, M., & MacKenzie, K. J. D. (2012). Synthesis and mechanical properties of new fibre-reinforced composites of inorganic polymers with natural wool fibres. *Journal of Materials Science*, 47(19), 6958-6965. <https://doi.org/10.1007/s10853-012-6644-3>
- Assaedi, H., Shaikh, F. U. A., & Low, I. M. (2016). Characterizations of flax fabric reinforced nanoclay-geopolymer composites. *Composites Part B*, 95, 412-422. <https://doi.org/10.1016/j.compositesb.2016.04.007>
- Assaedi, H., Alomayri, T., Shaikh, F., & Low, I. M. (2019). Influence of nano silica particles on durability of flax fabric reinforced geopolymer composites. *Materials*, 12(9), 1-14. <https://doi.org/10.3390/ma12091459>
- Assaedi, H., Alomayri, T., Shaikh, F. U. A., & Low, I. (2015). Characterisation of mechanical and thermal properties in flax fabric reinforced geopolymer composites. *Journal of Advanced Ceramics*, 4(4), 272-281. <https://doi.org/10.1007/s40145-015-0161-1>
- Ayub, M., Othman, M. H. D., Khan, I. U., Hubadillah, S. K., Kurniawan, T. A., Ismail, A. F., Rahman, M. A., & Jaafar, J. (2021). Promoting sustainable cleaner production paradigms in palm oil fuel ash as an eco-friendly cementitious material: A critical analysis. *Journal of Cleaner Production*, 295, Article 126296. <https://doi.org/10.1016/j.jclepro.2021.126296>
- Bellum, R. R. (2021). Influence of steel and PP fibers on mechanical and microstructural properties of fly ash-GGBFS based geopolymer composites. *Ceramics International*, 48(5), 6808-6818. <https://doi.org/10.1016/j.ceramint.2021.11.232>
- Chen, R., Ahmari, S., & Zhang, L. (2014). Utilization of sweet sorghum fiber to reinforce fly ash-based geopolymer. *Journal of Materials Science*, 49(6), 2548-2558. <https://doi.org/10.1007/s10853-013-7950-0>
- Chen, X., Zhang, J., Lu, M., Chen, B., Gao, S., Bai, J., Zhang, H., & Yang, Y. (2022). Study on the effect of calcium and sulfur content on the properties of fly ash based geopolymer. *Construction and Building Materials*, 314(PB), Article 125650. <https://doi.org/10.1016/j.conbuildmat.2021.125650>
- Chindaprasirt, P., Jitsangiam, P., Chalee, W., & Rattanasak, U. (2021). Case study of the application of pervious fly ash geopolymer concrete for neutralization of acidic wastewater. *Case Studies in Construction Materials*, 15, Article e00770. <https://doi.org/10.1016/j.cscm.2021.e00770>

- Fang, G., Ho, W. K., Tu, W., & Zhang, M. (2018). Workability and mechanical properties of alkali-activated fly ash-slag concrete cured at ambient temperature. *Construction and Building Materials*, 172, 476-487. <https://doi.org/10.1016/j.conbuildmat.2018.04.008>
- Farhan, N. A., Sheikh, M. N., & Hadi, M. N. S. (2018). Behaviour of ambient cured steel fibre reinforced geopolymer concrete columns under axial and flexural loads. *Structures*, 15, 184-195. <https://doi.org/10.1016/j.istruc.2018.07.001>
- Filho, J. D. A. M., Silva, F. D. A., & Filho, R. D. T. (2013). Degradation kinetics and aging mechanisms on sisal fiber cement composite systems. *Cement and Concrete Composites*, 40, 30-39. <https://doi.org/10.1016/j.cemconcomp.2013.04.003>
- Ganesh, A. C., & Muthukannan, M. (2021). Development of high performance sustainable optimized fiber reinforced geopolymer concrete and prediction of compressive strength. *Journal of Cleaner Production*, 282, Article 124543. <https://doi.org/10.1016/j.jclepro.2020.124543>
- Gopalakrishnan, R., & Chinnaraju, K. (2019). Durability of ambient cured alumina silicate concrete based on slag / fly ash blends against sulfate environment. *Construction and Building Materials*, 204, 70-83. <https://doi.org/10.1016/j.conbuildmat.2019.01.153>
- Gupta, A. (2021). Investigation of the strength of ground granulated blast furnace slag based geopolymer composite with silica fume. *Materials Today: Proceedings*, 44, 23-28. <https://doi.org/10.1016/j.matpr.2020.06.010>
- Islam, M. S., & Ju, S. (2018). Influence of jute fiber on concrete properties. *Construction and Building Materials*, 189, 768-776. <https://doi.org/10.1016/j.conbuildmat.2018.09.048>
- Jawahar, J. G., Lavanya, D., & Sashidhar, C. (2016). Performance of fly ash and GGBS based geopolymer concrete in acid environment. *International Journal of Research and Scientific Innovation*, 3(8), 101-104.
- Kavipriya, S., Deepanraj, C. G., Dinesh, S., Prakash, N., Lingeshwaran, N., & Ramkumar, S. (2021). Flexural strength of Lightweight geopolymer concrete using sisal fibres. *Materials Today: Proceedings*, 47, 5503-5507. <https://doi.org/10.1016/j.matpr.2021.08.135>
- Korniejenko, K., Fr, E., Pytlak, E., & Adamski, M. (2016). Mechanical properties of geopolymer composites reinforced with natural fibers. *Procedia Engineering*, 151, 388-393. <https://doi.org/10.1016/j.proeng.2016.07.395>
- Liang, G., Zhu, H., Li, H., Liu, T., & Guo, H. (2021). Comparative study on the effects of rice husk ash and silica fume on the freezing resistance of metakaolin-based geopolymer. *Construction and Building Materials*, 293, Article 123486. <https://doi.org/10.1016/j.conbuildmat.2021.123486>
- Maichin, P., Suwan, T., Jitsangiam, P., & Chindapasirt, P. (2020). Hemp fiber reinforced geopolymer composites: Effects of NaOH concentration on fiber pre-treatment process. *Key Engineering Materials*, 841, 166-170. <https://doi.org/10.4028/www.scientific.net/KEM.841.166>
- Malenab, R. A. J., Ngo, J. P. S., & Promentilla, M. A. B. (2017). Chemical treatment of waste abaca for natural fiber-Reinforced geopolymer composite. *Materials*, 10(6), Article 579. <https://doi.org/10.3390/ma10060579>

- Pauline, J. N. S. J., & Angelo, P. B. M. (2018). Development of abaca fiber-reinforced foamed fly ash geopolymer. *MATEC Web of Conferences*, 156, 1-8. <https://doi.org/10.1051/mateconf/201815605018>
- Silva, G., Kim, S., Bertolotti, B., Nakamatsu, J., & Aguilar, R. (2020). Optimization of a reinforced geopolymer composite using natural fibers and construction wastes. *Construction and Building Materials*, 258, Article 119697. <https://doi.org/10.1016/j.conbuildmat.2020.119697>
- Suwan, T., Maichin, P., Fan, M., Jitsangiam, P., Tangchirapat, W., & Chindaprasirt, P. (2022). Influence of alkalinity on self-treatment process of natural fiber and properties of its geopolymeric composites. *Construction and Building Materials*, 316, Article 125817. <https://doi.org/10.1016/j.conbuildmat.2021.125817>
- Wongsa, A., Kunthawatwong, R., Naenudon, S., & Sata, V. (2020). Natural fiber reinforced high calcium fly ash geopolymer mortar. *Construction and Building Materials*, 241, Article 118143. <https://doi.org/10.1016/j.conbuildmat.2020.118143>
- Yanou, R. N., Kaze, R. C., Adesina, A., Nemaleu, J. G. D., Jiofack, S. B. K., & Djobo, J. N. Y. (2021). Performance of laterite-based geopolymers reinforced with sugarcane bagasse fibers. *Case Studies in Construction Materials*, 15, Article e00762. <https://doi.org/10.1016/j.cscm.2021.e00762>
- Yasaswini, K., & Rao, A. V. (2020). Behaviour of geopolymer concrete at elevated temperature. *Materials Today: Proceedings*, 33(1), 239-244. <https://doi.org/10.1016/j.matpr.2020.03.833>
- Zhang, N., Ye, H., Pan, D., & Zhang, Y. (2021). Effects of alkali-treated kenaf fiber on environmentally friendly geopolymer-kenaf composites: Black liquid as the regenerated activator of the geopolymer. *Construction and Building Materials*, 297, Article 123787. <https://doi.org/10.1016/j.conbuildmat.2021.123787>
- Zhang, P., Wang, K., Li, Q., Wang, J., & Ling, Y. (2020). Fabrication and engineering properties of concretes based on geopolymers/alkali-activated binders - A review. *Journal of Cleaner Production*, 258, Article 120896. <https://doi.org/10.1016/j.jclepro.2020.120896>
- Zulfiati, R., & Idris, Y. (2019). Mechanical properties of fly ash-based geopolymer with natural fiber mechanical properties of fly ash-based geopolymer with natural fiber. *Journal of Physics: Conference Series*, 1198(8), Article 082021. <https://doi.org/10.1088/1742-6596/1198/8/082021>
- Zulfiati, R., Saloma, & Idris, Y. (2020). The nature of coconut fibre fly ash-based mechanical geopolymer. *IOP Conference Series: Materials Science and Engineering*, 807, Article 012041. <https://doi.org/10.1088/1757-899X/807/1/012041>



Case Study

An Unusual Cause of Tenosynovitis by Group B *Streptococcus* in the Immunocompromised Patient: A Case Report

AbdulRahman Muthanna¹, Nur Afiza Aziz², Mohd Nasir Mohd Desa¹, Nurul Diana Dzaraly¹, Nurul Hana Zainal Baharin¹, Mohammad Noor Amal Azmai³ and Syafinaz Amin-Nordin^{4*}

¹Department of Biomedical Sciences, Faculty of Medicine and Health Sciences, Universiti Putra Malaysia, 43400 UPM, Serdang, Selangor, Malaysia

²Department of Pathology, Sultanah Aminah Hospital, 80000 Johor Bahru, Johor, Malaysia

³Department of Biology, Faculty of Science, Universiti Putra Malaysia, 43400 UPM, Serdang, Selangor, Malaysia

⁴Department of Medical Microbiology, Faculty of Medicine and Health Sciences, Universiti Putra Malaysia, 43400 UPM, Serdang, Selangor, Malaysia

ABSTRACT

This case report describes a 49-year-old immunocompromised woman with tenosynovitis of the left middle finger caused by Group B *Streptococcus* (GBS). She claimed that a fishbone picked over her left middle finger. An orthopaedic surgeon operated for incision and drainage of pus discharge, wound debridement of the left middle finger and A1 and A2 pulley release. Treatment was initiated with parenteral cefepime three times per day given the growth of mixed *Enterobacter* species on the culture media and continued with oral cefuroxime twice daily upon discharge for one week. Unfortunately, during the orthopaedic clinic

follow-up, the wound was unclean with a slough and skin necrotic patch. Therefore, Ray's amputation of the left middle finger proceeded. This case contributes to further investigation of the GBS tenosynovitis due to the rise in GBS invasive infections and shows the importance of early diagnosing and initiating treatment with antibiotics that are effective against this pathogen.

Keywords: Group B *Streptococcus*, human, immunocompromised, tenosynovitis

ARTICLE INFO

Article history:

Received: 29 December 2021

Accepted: 2 March 2022

Published: 20 April 2022

DOI: <https://doi.org/10.47836/pjst.30.3.17>

E-mail addresses:

dr.abm1990@gmail.com (AbdulRahman Muthanna)

nurafiza45@gmail.com (Nur Afiza Aziz)

mnasir@upm.edu.my (Mohd Nasir Mohd Desa)

diana.dzaraly@gmail.com (Nurul Diana Dzaraly)

misshanazainal@gmail.com (Nurul Hana Zainal Baharin)

mnamal@upm.edu.my (Mohammad Noor Amal Azmai)

syafinaz@upm.edu.my (Syafinaz Amin-Nordin)

*Corresponding author

INTRODUCTION

Tenosynovitis is most often an infection caused by gram-positive bacterial infections. Most cases of tenosynovitis are caused by *Staphylococcus aureus*, which accounts for 80% of all cases (Stewart & Ward, 2020). However, group B streptococcal soft tissue infections, which often lead to septicaemia and amputation in immunocompromised patients such as inflammatory arthritis, diabetes, cancer, and others, have been on the rise, which ranged from 13.9% to 38% (Pang et al., 2007; Karunakaran et al., 2009). Most cases of suspected tenosynovitis should be treated surgically immediately; however, healthy patients can be treated with antibiotics alone for the first day and then reassessed to determine whether surgery is necessary (Franko & Abrams, 2013). According to a study, around 54% (302 out of 561) of cases were successfully treated with antibiotics and surgery, compared to 9.6% (17 out of 177) of cases successfully treated by surgery without antibiotics (Hyatt & Bagg, 2017). With the paucity of literature, this case reported GBS tenosynovitis in an immunocompromised patient. This report describes the diagnosis and treatment of tenosynovitis caused by GBS. Several disciplines played an important role in treating the patient, including primary care, orthopaedic surgery, radiology, and infectious disease. Orthopaedic surgeons diagnosed the patient and performed Ray's amputation of the left middle finger; radiologists took x-rays, while the clinical microbiologists identified the isolates and tested the antimicrobial susceptibility. The hospital ethics committee approved the publication of this case report based on an approval letter from the Medical Research and Ethics Committee of the Malaysian Ministry of Health.

CASE REPORT

On May 27, 2020, a 49-year-old Malaysian female with underlying diabetes mellitus (defaulted on follow up for five years) was admitted to the Hospital Sultanah Aminah, Johor Bahru, complaining of left middle finger pain and oedema. She reported that a fishbone punctured her finger three days prior to admission. She poked the swollen finger with a needle and observed minimal pus discharge and bleeding.

At the presentation time, the patient's vital signs were as follows: her blood pressure was 125/74 mmHg, her heart rate was 100 beats/minute, her body temperature was 36.9°C, and her oxygenation level was 98%. On examining her left hand, a blackish discolouration at the finger pulp with fusiform swelling up to the mid-hand was observed. Subsequent swelling occurred over the pulp of the left middle finger, and the swelling further extended to the metacarpal joints of the left middle finger. There was tenderness up to the distal 1/3 of the middle finger and erythematous surrounding the skin on palpation. A diagnosis of flexor tenosynovitis with pulp necrosis was made for the left middle finger. No other significant physical findings were noted. An X-ray of the left hand demonstrated a gas shadow over the top of the left middle finger (Figure 1).

Laboratory tests indicated that the leukocyte count was $5.2 \times 10^9/L$ (53.1% neutrophils, 33.9% lymphocytes, 7.6% monocytes, 5% eosinophils, and 0.4% basophils), with a haemoglobin level of 115 g/L and a C-reactive protein level of 8 mg/L (normal range: <5 mg/L). The sodium, potassium, chloride, urea, creatinine, and eGFR CKD-EPI levels were normal, while the Haemoglobin A1c level (7.3%) was high.



Figure 1. An X-ray of the left hand with a gas shadow over the top of the left middle finger indicates an anaerobic bacterial infection

The Gram-staining of pus aspirate revealed numerous pus cells with Gram-positive cocci (GPC), while the tissue revealed a few pus cells with Gram-negative bacilli (GNB). After overnight cultivation of the pus aspirate and tissue samples on blood agar, this report observed the growth of grey-whitish colonies surrounded by a β -haemolysis zone. The isolates were confirmed as GBS by a negative catalase test, a positive CAMP test, and a latex agglutination test (Oxoid™ Streptococcal Grouping Kit). Furthermore, the GBS isolates were positive for the *cfb* gene in a PCR analysis (Eskandarian et al., 2015). An antimicrobial susceptibility test was conducted on all isolates using disk diffusion and E-test methods. GBS isolates were sensitive to penicillin, clindamycin, erythromycin, ceftriaxone, and vancomycin (CLSI, 2020). The serotype was Ia based on a multiplex PCR assay using the protocol and specific primers that Imperi et al. (2010) developed. They were identified as sequence type (ST) 23 based on the Multilocus Sequence Typing (MLST) (Jones et al., 2003). *Enterobacter cloacae* which are sensitive to cefepime were also found in the tissue sample.

The patient was started empirically on cloxacillin 1 g QID and clindamycin 600 mg BD, administered intravenously for two days. She had undergone an operation for incision and the drainage of pus discharge, a wound debridement of the left middle finger, and an A1 and A2 pulley release. Intraoperative findings showed extensive sloughy subcutaneous tissue with a pus discharge of 5 mL and a friable pulley, digital nerve, and blood vessel. She was recommended for Ray's amputation of the left middle finger, but she refused. The antibiotic was changed to cefepime 2 g TDS for two days on the third day, given the bacterial cultivation results. After showing remarkable improvement on the following day, she was discharged from the hospital. She was advised to undergo daily wound dressing

The Gram-staining of pus aspirate revealed numerous pus cells with Gram-positive cocci (GPC), while the tissue revealed a few pus cells with Gram-negative bacilli (GNB). After overnight cultivation of the pus aspirate and tissue samples on blood agar, this report observed the growth of grey-whitish colonies surrounded by a β -haemolysis zone. The isolates were confirmed as GBS by a negative catalase test, a positive CAMP test, and a latex agglutination test (Oxoid™ Streptococcal Grouping Kit). Furthermore, the GBS isolates were positive for the *cfb* gene in a PCR analysis (Eskandarian et al., 2015). An antimicrobial susceptibility test was conducted on all isolates using disk diffusion and E-test methods. GBS isolates were sensitive to penicillin, clindamycin,

at a primary health clinic and continue taking antibiotics (cefuroxime tablets 250 mg BD) for one week, followed by appointment at an orthopaedic clinic.

On the orthopaedic clinic review day, skin necrosis was noted until the left middle phalanx, and the flexor tendon was exposed with slough. Given the poor progression of the wound, she was counselled by the orthopaedic surgeon to have Ray's amputation of the left middle finger. Ray's amputation of the left middle finger was done on 1/7/2020. Two weeks later, the wound was checked. It was clean, with no breakdown, and the sutures were intact. The sutures were then removed. One month after Ray's amputation, the orthopaedic surgeon again checked the wound. It had healed well with minimal scarring. All the other fingers were able to flex and extend. The patient recovered without any sequelae and did not have difficulty using the left hand in daily activities.

DISCUSSION

GBS infections among non-pregnant adults have increased over the years. Bacteremia (22%), osteoarticular infection (21.4%), skin and soft tissue infections (18.4%) and abscesses (13.9%) were the most common manifestation (Graux et al., 2021). A recent study indicated that autoimmune disease, immunosuppressive therapy, and diabetes disorders or comorbidities were important predisposing factors for GBS invasive infections among non-pregnant adults. In several cases, soft tissue infections, including muscles, tendons, and ligaments, have been reported, leading to septicaemia and amputation (Vuillemin et al., 2021). Tenosynovitis is a surgical emergency caused by penetrating trauma to a digit. In 1933, Kanavel developed four cardinal signs to diagnose tenosynovitis, including symmetrical swelling of the whole finger, profound tenderness along the finger's length, semi flexed finger and extreme pain with passive extension of the affected finger. *Staphylococcus aureus* is the most common cause of tenosynovitis (Stewart & Ward, 2020). However, the incidence of tenosynovitis by GBS is unknown in the local setting. GBS patients suffer from more severe infections marked by high inflammation markers and the most frequent wound complications (Pattnaik et al., 2020). In this case, the serotype and the ST of the GBS were found to be serotype Ib and ST23 using the multiplex PCR and MLST. ST23 has been identified as a dominant strain commonly associated with invasive GBS infections (Chang et al., 2014; Ezhumalai et al., 2020). Another study found that human ST23 GBS can be pathogenic to fish, possibly due to phage recombination (Wang et al., 2017). In conclusion, detailed history and clinical suspicion are the critical factors to diagnose GBS infections in tenosynovitis. An increasing number of invasive GBS cases among non-pregnant adults requires identifying clinical characteristics and risk factors such as immunodeficiency and environmental hazard exposure. GBS responds well to antibiotic therapy. Therefore, treatment options for GBS may consist of penicillin, erythromycin, clindamycin, ceftriaxone, cefuroxime, and vancomycin, depending on cultural sensitivities.

ETHICAL APPROVAL

The Medical Research and Ethics Committee of the Malaysian Ministry of Health, National Medical Research Register approved the study (approval no. NMRR 19-876-46665) and subsequently by the Clinical Research Centre of Hospital Sultanah Aminah, Johor Bahru.

ACKNOWLEDGEMENTS

This research was funded by the Research University Grant from Universiti Putra Malaysia, reference number [UPM/800-3/3/1/GPB/2020/9683800]. The authors would like to thank all staff of the orthopaedic and pathology departments at Hospital Sultanah Aminah, Johor Bharu, Johor, for their kind help in preparing this report.

REFERENCES

- Chang, B., Wada, A., Hosoya, M., Oishi, T., Ishiwada, N., Oda, M., Sato, T., Terauchi, Y., Okada, K., Nishi, J., Akeda, H., Kamiya, H., Ohnishi, M., Ihara, T., & Japanese Invasive Disease Study Group. (2014). Characteristics of group B *Streptococcus* isolated from infants with invasive infections: A population-based study in Japan. *Japanese Journal of Infectious Diseases*, 67(5), 356-360. <http://dx.doi.org/10.7883/yoken.67.356>
- CLSI. (2020). *Performance standards for antimicrobial susceptibility testing* (30th Ed.). Clinical and Laboratory Standards Institute.
- Eskandarian, N., Ismail, Z., Neela, V., Van Belkum, A., Desa, M. N. M., & Nordin, S. A. (2015). Antimicrobial susceptibility profiles, serotype distribution and virulence determinants among invasive, non-invasive and colonizing *Streptococcus agalactiae* (group B streptococcus) from Malaysian patients. *European Journal of Clinical Microbiology & Infectious Diseases*, 34(3), 579-584. <https://doi.org/10.1007/s10096-014-2265-x>
- Ezhumalai, M., Muthanna, A., Suhaili, Z., Dzaraly, N. D., Amin-Nordin, S., Amal, M. N. A., & Desa, M. N. M. (2020). Multilocus sequence typing analysis of invasive and non-invasive Group B *Streptococcus* of hospital origin in Malaysia. *The Malaysian Journal of Medical Sciences: MJMS*, 27(1), 134-138. <https://doi.org/10.21315/mjms2020.27.1.14>
- Franko, O. I., & Abrams, R. A. (2013). Hand infections. *Orthopedic Clinics*, 44(4), 625-634.
- Graux, E., Hites, M., Martiny, D., Maillart, E., Delforge, M., Melin, P., & Dauby, N. (2021). Invasive group B *Streptococcus* among non-pregnant adults in Brussels-Capital Region, 2005–2019. *European Journal of Clinical Microbiology & Infectious Diseases*, 40(3), 515-523. <https://doi.org/10.1007/s10096-020-04041-0>
- Hyatt, B. T., & Bagg, M. R. (2017). Flexor tenosynovitis. *Orthopedic Clinics*, 48(2), 217-227. <http://dx.doi.org/10.1016/j.jocl.2016.12.010>
- Imperi, M., Pataracchia, M., Alfarone, G., Baldassarri, L., Orefici, G., & Creti, R. (2010). A multiplex PCR assay for the direct identification of the capsular type (Ia to IX) of *Streptococcus agalactiae*. *Journal of Microbiological Methods*, 80(2), 212-214. <https://doi.org/10.1016/j.mimet.2009.11.010>

- Jones, N., Bohnsack, J. F., Takahashi, S., Oliver, K. A., Chan, M. S., Kunst, F., Glaser, P., Rusniok, C., Crook, D. W. M., Harding, R. M., Bisharat, N., & Spratt, B. G. (2003). Multilocus sequence typing system for group B *streptococcus*. *Journal of Clinical Microbiology*, 41(6), 2530-2536. <https://doi.org/10.1128/JCM.41.6.2530-2536.2003>
- Kanavel, A. B. (1933). *The symptoms, signs, and diagnosis of tenosynovitis and major fascial-space abscesses. Infections of the Hand* (6th Ed.). Lea and Febiger Publisher.
- Karunakaran, R., Raja, N. S., Hafeez, A., & Puthuchery, S. D. (2009). Group B *streptococcus* infection: Epidemiology, serotypes, and antimicrobial susceptibility of selected isolates in the population beyond infancy (excluding females with genital tract-and pregnancy-related isolates) at the University Malaya Medical Centre, Kuala Lumpur. *Japanese Journal of Infectious Diseases*, 62(3), 192-194.
- Pang, H. N., Teoh, L. C., Yam, A. K., Lee, J. Y. L., Puhaindran, M. E., & Tan, A. B. H. (2007). Factors affecting the prognosis of pyogenic flexor tenosynovitis. *The Journal of Bone & Joint Surgery*, 89(8), 1742-1748. <http://dx.doi.org/10.2106/JBJS.F.01356>
- Pattnaik, S., Syed, A., & Siddhardha, B. (2020). Pathogenesis, virulence factors, and antibiotic resistance of group B *streptococcus*. In *Model Organisms for Microbial Pathogenesis, Biofilm Formation and Antimicrobial Drug Discovery* (pp. 117-130). Springer. <https://doi.org/10.1007/978-981-15-1695-5>
- Stewart, C. N., & Ward, C. M. (2020). Infectious flexor tenosynovitis following trigger finger release: Incidence and risk factors. *Hand*, 2020. <https://doi.org/10.1177/1558944720930298>
- Vuillemin, X., Hays, C., Plainvert, C., Dmytruk, N., Louis, M., Touak, G., Saint-Pierre, B., Adoux, L., Letourneur, F., Frigo, A., Poyart, C., & Tazi, A. (2021). Invasive group B *streptococcus* infections in non-pregnant adults: A retrospective study, France, 2007–2019. *Clinical Microbiology and Infection*, 27(1), 129-e1-129-e4. <https://doi.org/10.1016/j.cmi.2020.09.037>
- Wang, R., Li, L., Huang, Y., Huang, T., Tang, J., Xie, T., Lei, A., Luo, F., Li, J., Huang, Y., Shi, Y., Wang, D., Chen, M., Mi, Q., & Huang, W. (2017). Pathogenicity of human ST23 *Streptococcus agalactiae* to fish and genomic comparison of pathogenic and non-pathogenic isolates. *Frontiers in Microbiology*, 8, Article 1933. <https://doi.org/10.3389/fmicb.2017.01933>

Thermal Performances of Hybrid Pin Fin with Connector Heat Sink Under Natural Convection

Rosnadiyah Bahsan^{1*}, Muhammad Aniq Asyraf Mohd Zamri¹, Alhassan Salami Tijani¹, Jeeventh Kubenthiran¹, Sajith Thottathil Abdulrahman² and Ibrahim Kolawole Muritala³

¹*School of Mechanical Engineering, College of Engineering, Universiti Teknologi MARA, 40450 UiTM, Shah Alam, Selangor, Malaysia*

²*Department of Mechanical Engineering, KMEA Engineering College, Kuzhivelippady, Edathala P.O., Cochin, Kerala, India*

³*Institute of Low-Carbon Industrial Processes, Department of Low Carbon Reducing Agents, Deutsches Zentrum für Luft- und Raumfahrt (DLR) / German Aerospace Centre, HSZG-Campus Haus Z VII, Schwenninger Weg 1, 02763 Zittau, Germany*

ABSTRACT

Heat transfer in engineering applications has shown progress, especially in electronic devices that raise the need for better heat sink designs. In addition, the generation of heat in devices and electronic circuits has also augmented, leading to the problem of heat dissipation. This study investigates the thermal and fluid flow characteristics of different geometrical configurations of pin fin heat sink under natural convection. The heat sink models studied are Hybrid Pin Fin with Connector Heat Sink (HPFWC HS) and Pin Fin with Connector Heat Sink (PFWC HS). All heat sinks models were simulated using CFD Ansys to analyse each heat sink's thermal performances and flow fields. The results show that adding wings to the HPFWC HS significantly increased heat dissipation. In terms of heat transfer characteristics, the HPFWC HS has about a 5.78% increase in Nusselt number compared with PFWC HS. The reason is that the heat sink HPFWC HS has wings around

it, and these wings help to promote vortex formation around the fins, which leads to a higher heat transfer coefficient. A fin spacing of 15mm is the best spacing for the heat sink compared to other fin spacing.

ARTICLE INFO

Article history:

Received: 18 June 2021

Accepted: 15 December 2021

Published: 25 May 2022

DOI: <https://doi.org/10.47836/pjst.30.3.18>

E-mail addresses:

aniqqasyraf@gmail.com (Muhammad Aniq Asyraf Mohd Zamri)

rosnadiyah@uitm.edu.my (Rosnadiyah Bahsan)

alhassan@uitm.edu.my (Alhassan Salami Tijani)

sar.me@kmeacollege.ac.in (Sajith Thottathil Abdulrahman)

jeeventh@hotmail.com (Jeeventh Kubenthiran)

ibrahim.muritala@dlr.de (Ibrahim Kolawole Muritala)

* Corresponding author

Keywords: Connector heat sink, electronic devices, fin spacing, heat transfer, hybrid fin pin, natural convection

INTRODUCTION

The development of machines and the widespread use of electronic devices have kept growing since the industrial era. The growth and evolution of the industrial revolution evolved exponentially to fulfil the needs and demands of the global industry (Immerman, 2017). Almost all machines are now focusing on automation, including the evolution of small electronic devices. Recent advances in electronic devices such as inverters, computers, transformers, and mobile phones have led to inadequate heat dissipation in these devices; hence the life span is reduced. During the operation of these electronic devices, heat is generated and must be dissipated as much as possible to avoid any malfunction of the systems (Schelling et al., 2005). Failure to dissipate the heat from the components and devices can affect their reliability and performance (Humphries, 2014).

Conduction and convection heat transfers are the most widely used heat transfer or heat dissipation through a medium in thermal management. Convection can be classified into two parts, namely, forced and natural convection. Forced convection, also known as active cooling, is the forced flow of fluid over a solid surface, while natural convection is also known as passive cooling; it depends on the difference in fluid buoyancy effect for heat dissipation from a solid surface (Vijay, 2019). Although forced convection is more efficient to transfer heat than natural convection, it is less reliable due to external devices such as fans or pumps (Joo & Kim, 2015). In addition, devices with frictional components have less reliability because these components deteriorate over time. Therefore, it gives an advantage to natural convection that has high reliability (Meng et al., 2018). Nada and Said (2019) studied the effects of fins geometries, arrangements, dimensions and number of fins on heat transfer due to natural convection and found that as the number of the fins increases, the effective thermal conductivity also increases.

The heat sink is a device used to remove or dissipate unwanted heat from electronic components to the surroundings. Heat sinks can keep the temperature of electronic devices at an optimum level and are used in many applications such as electronic devices, refrigeration, and heat engines (Kumar et al., 2016). Several heat sinks have different geometry, material, or even thermal characteristics. For example, fins are usually used in electronic devices and engineering applications to enhance the convective heat transfer with a large total surface area in a limited space (Jassem, 2013).

A considerable amount of literature has been published on investigating different geometrical configurations of the heat sink. Arefin (2016) stated that a pin fin heat sink with one-degree expansion performs better than the conventional zero-degree expansion in terms of heat transfer. At the same time, Haghighi et al. (2018) studied both plate and pin fin heat sinks and found out that increasing the number of fins causes better heat transfer, but the pressure drop penalty increases; there is, therefore, the need for optimisation of the geometrical configuration of the heat sink. Some authors also add perforations to the heat

sink to increase the heat sink’s convective heat transfer rate (Zaidshah & Yadav, 2019). Ibrahim et al. (2018) stated that the heat transfer coefficient for a fin with perforations is higher compared to a non-perforated fin. The best perforation shape, better than any other shape, is a triangular perforated shape. Adding some features to the pin fin or plate fin could increase the heat transfer rate of a heat sink. Choudhary et al. (2019) have studied the presence of wings on pin fin and found that pin fin with wings has better heat transfer results with a moderate rise in frictional losses, and increasing the wings size resulted in a decrease in Nusselt number with increment in frictional losses.

This research investigates the thermal performances of a new design heat sink: Hybrid Pin Fin with Connector Heat Sink (HPFWC HS) and Pin Fin with Connector Heat Sink (PFWC HS). All heat sinks models were simulated using CFD Ansys to observe each heat sink’s thermal performances and flow fields. Furthermore, thermal characteristics of the heat sinks such as Nusselt number, Rayleigh number, Prandlt number and heat transfer coefficient were also investigated.

METHODOLOGY

Hybrid Pin Fin with Connector Heat Sink

Two heat sinks have been investigated: Hybrid Pin Fin with Connector Heat Sink (HPFWC HS) and Pin Fin with Connector Heat Sink (PFWC HS). The Hybrid Pin Fin indicates the hybridisation of the conventional pin fin with structured plate fins or wings around the pin fins. Figures 1 and 2 show the HPFWC HS dimensions and PFWC HS, respectively.

The arrangement of pin fins on both heat sinks was in staggered form. The cross-sectional area of the base of the PFWC HS is 75mm × 75mm, the thickness of 5mm and the diameter pin fin is 6mm. The HPFWC HS also has a base plate area of 75mm × 75mm and a thickness of 5mm. The length of the connector depends on the fin spacing. Higher fin spacing means higher connector length. For example, the length of the connector for 15mm fin spacing is approximately 9mm. Table 1 shows the detailed specifications of both

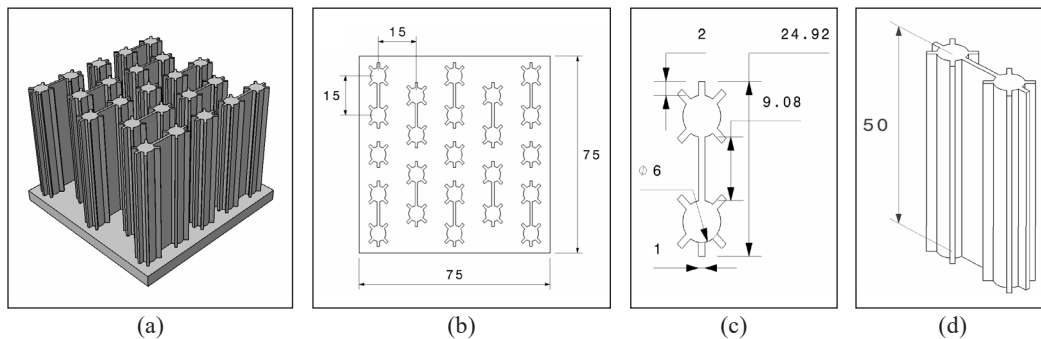


Figure 1. (a) Isometric view of HPFWC HS (b) Top view of HPFWC (c) Top view and dimensions of HPFWC (d) Isometric view and height of HPFWC

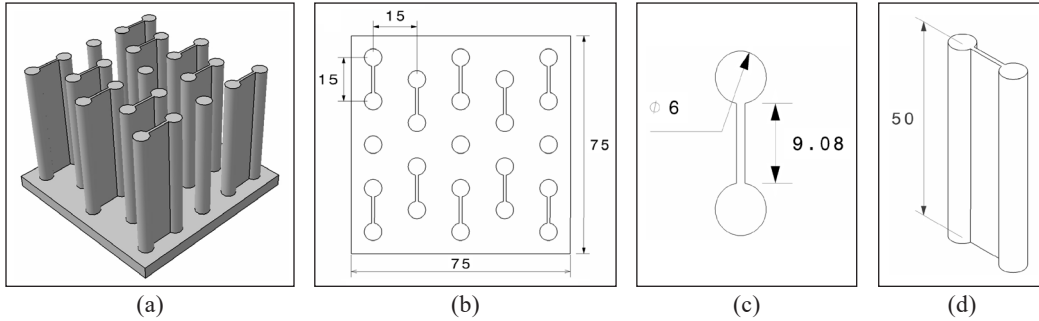


Figure 2. (a) Isometric view of PFWC HS (b) Top view and dimension of PFWC (c) Top view and dimension of PFWC (d) Isometric view and height of PFWC

heat sinks with different configurations. In this study, each design configuration was further modified into Type 1, Type 2 and Type 3. Details of the different types of geometries can be found in Table 1.

Table 1
Heat sinks configurations

Heat sink	H (mm)	W (mm)	S (mm)	D (mm)	N_{pf}	N_c
PFWC Type 1	50	-	15	6	23	10
PFWC Type 2	50	-	20	6	11	6
PFWC Type 3	50	-	25	6	7	2
HPFWC Type 1	50	10	15	6	23	10
HPFWC Type 2	50	10	20	6	11	6
HPFWC Type 3	50	10	25	6	7	2

Aluminium was selected as the material for the heat sink due to its high thermal conductivity (Zagala, 2016) and cost-effectiveness in most applications (Perry, 2017).

Modelling and Simulation

The geometric modelling of the design of all heat sinks is done by using CATIA V5R20 software. Then, the models are imported into Ansys 16 software to undergo Computational Fluid Dynamics (CFD) simulation under Fluent. CFD simulation's main purpose is to numerically determine the fluid behaviours around the heat sinks and investigate the thermal performances of heat sinks under natural convection.

Figure 3 shows the heat sink inside the fluid domain. The size of the domain that was used is $(200 \times 200 \times 300)$ mm (Effendi et al., 2018). The boundary conditions are set on the domain and the heat sink. The domain has one inlet, one outlet, one heated area, and other surfaces set as walls. A mesh model for the heat sinks was created to reduce the degree of freedom from infinite to finite (Jensen, 2018). Figure 4 shows the meshing models of both HPFWC HS and PFWC HS, respectively.

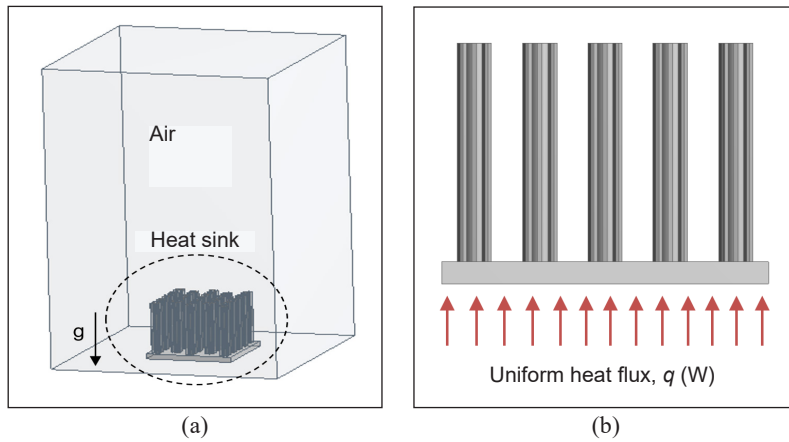


Figure 3. (a) Heat sink in the domain (b) Zoomed heat sink with uniform heat flux

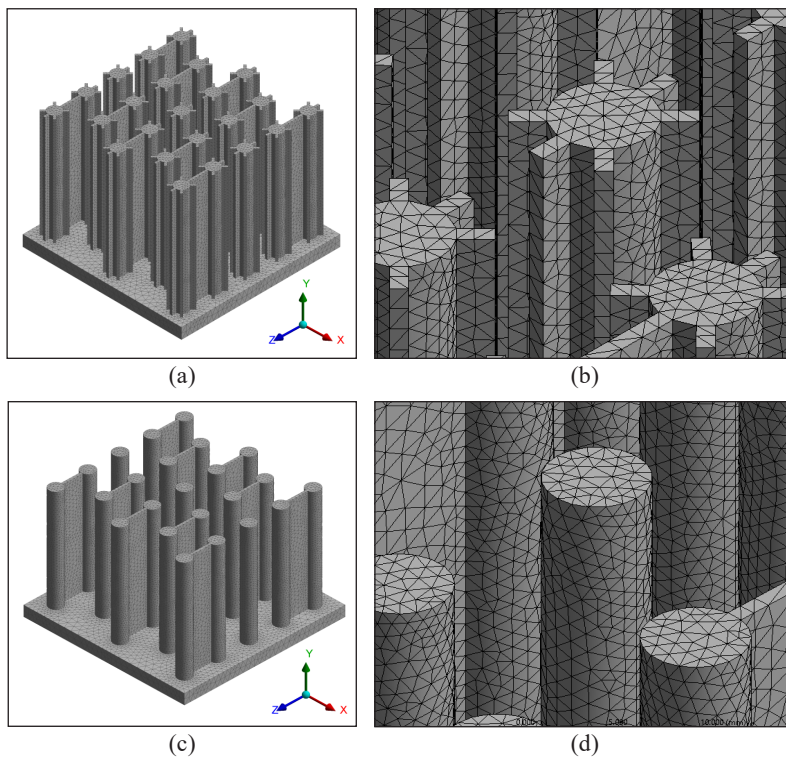


Figure 4. Meshing model of (a) HPFWC HS, (b) the zoomed part of HPFWC, (c) PFWC HS and (d) the zoomed part of PFWC

The fluid used for the heat exchange medium is steady and incompressible air. The ambient temperature is 25°C with inlet and outlet pressure at 1 atm. The base of the heat sink is heated from 5W to 30W. Meshing elements are around 1–2M for all designs with tetrahedra-type elements. The pressure-based solver type and SIMPLE pressure-velocity

coupling, and constant density model were set in the solution models. The pressure discretisation was done based on weighted body force, and gradient discretisation was based on the least square cell-based. In contrast, momentum and energy equations discretisation were carried out based on second-order upwind. Table 2 shows the numerical and boundary conditions used during the calculation (Effendi et al., 2018).

Convergence of numerical equations. The average relative error was computed for every iterative step using Equation 1.

$$R_c = \frac{1}{n.m} \sum_{i=1}^m \sum_{j=1}^n \left| \frac{(F_{i,j}^{S+1} - F_{i,j}^S)}{F_{i,j}^{S+1}} \right| \quad [1]$$

Where F = Unknown parameter such as Temperature (T)
 s = number of iterations
 (i,j)= the grid coordinate

It ensures a convergence solution for the operating variables such as temperature. The solution of the integrated model equations is terminated whenever the relative error between two subsequent solutions is equal to the convergent criteria. In the present study, convergence criteria are attained if Rc is below 10^{-5} for both Continuity equations and temperature, and convergence criteria are reached if Rc is below 10^{-5} for the energy equation.

Grid Independence Test

A grid independence test is carried out to determine the most suitable number and size of the elements to carry out the simulation. During the meshing process, the size of each element was varied and adjusted to increase the accuracy of the simulation. Smaller elemental size means an increment in the number of elements. A higher number of elements tend to result in high accuracy, but the simulation running time is dragged. The grid size and computational domain were carefully chosen such that there is a minimal variation of the physical parameter of interest, such as temperature. Table 3 summarises all elemental sizes, ranging from 18mm to 6mm. The test was carried out on PFWC HS Type 1 with a heat

Table 2
 Summary of numerical and boundary conditions

<i>Physical conditions</i>	
Fluid	Steady and incompressible air
Fluid volume (L × W × H)	200 × 200 × 300 (mm)
Heat sink material	Aluminium
<i>Boundary and thermal conditions</i>	
Air temperature	25°C
Ambient pressure	1 atm
Heat flux	888.89~5333.33 W/m ²
<i>Computational elements</i>	
Number of elements	1-2M elements
Elements type	Tetra
<i>Solution models</i>	
Viscous model	Laminar
Solver type	Pressure based
Pressure-velocity coupling	SIMPLE
Density model	Constant
<i>Spatial discretisation</i>	
Pressure	Body force weighted
Momentum	Second-order upwind
Gradient	Least square cell-based
Energy	Second-order upwind

flux of 5W. Five different element sizes were tested. Table 3 shows that the temperature started to be constant at an element size of 9mm at the number of elements of 1377670. The element size of 6mm gives the highest number of elements, 2514225. The difference in temperature between these two sizes of elements is the lowest compared to other sizes. Since the difference is not very significant, the element size chosen to run the calculations is 9mm.

Table 3
Summary of grid independence test

Element size (mm)	Number of elements	Nodes	Base Temperature (K)
18	1155656	227043	299.86548
15	1174251	230811	299.92877
12	1225566	240647	299.78117
9	1377670	270093	299.83811
6	2514225	483138	299.83290

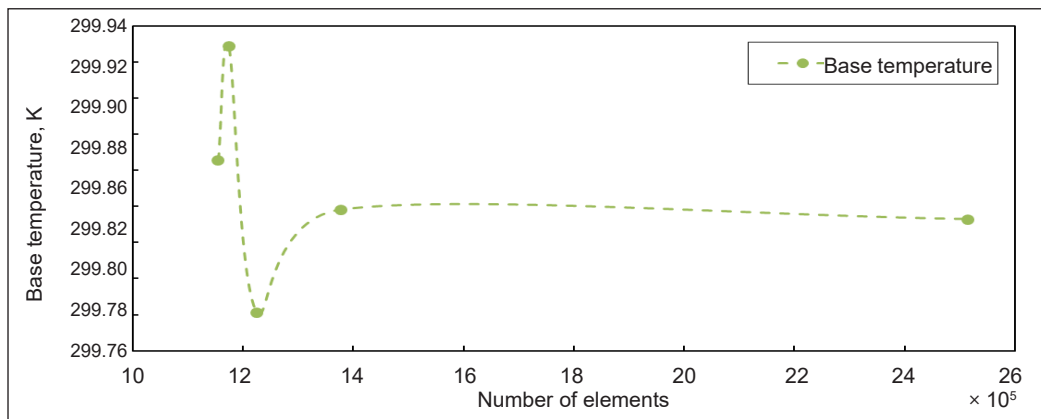


Figure 5. Mesh sensitivity analysis of grid independence test

Governing Equations

Natural convection flows have been simulated under the assumption of laminar, steady and incompressible flow conditions and the Boussinesq approximation. The governing equations related to this study are shown in Equations 2–7 (Effendi et al., 2018; Hoffmann & Chiang, 2000).

Based on the mass conservation principle, the following continuity Equation 2 can be expressed below:

$$\frac{\partial u}{\partial x} + \frac{\partial v}{\partial y} + \frac{\partial w}{\partial z} = 0 \tag{2}$$

Under heating conditions, the natural convection flow is driven by the air density change and gravity force. Therefore, for natural convection flow, the momentum Equations 3–5 can be written can be expressed as below:

$$u \frac{\partial u}{\partial x} + v \frac{\partial u}{\partial y} + w \frac{\partial u}{\partial z} = -\frac{1}{\rho} \frac{\partial P}{\partial x} + \nu \left(\frac{\partial^2 u}{\partial x^2} + \frac{\partial^2 u}{\partial y^2} + \frac{\partial^2 u}{\partial z^2} \right) \quad [3]$$

$$u \frac{\partial v}{\partial x} + v \frac{\partial v}{\partial y} + w \frac{\partial v}{\partial z} = -\frac{1}{\rho} \frac{\partial P}{\partial y} + \nu \left(\frac{\partial^2 v}{\partial x^2} + \frac{\partial^2 v}{\partial y^2} + \frac{\partial^2 v}{\partial z^2} \right) \quad [4]$$

$$u \frac{\partial w}{\partial x} + v \frac{\partial w}{\partial y} + w \frac{\partial w}{\partial z} = -\frac{1}{\rho} \frac{\partial P}{\partial z} + \nu \left(\frac{\partial^2 w}{\partial x^2} + \frac{\partial^2 w}{\partial y^2} + \frac{\partial^2 w}{\partial z^2} \right) + g\beta(T - T_\infty) \quad [5]$$

The energy equation is obtained based on energy balance characteristics. For example, the energy Equation 6 for the fluid region is expressed as below:

$$u \frac{\partial T}{\partial x} + v \frac{\partial T}{\partial y} + w \frac{\partial T}{\partial z} = \alpha \left(\frac{\partial^2 T}{\partial x^2} + \frac{\partial^2 T}{\partial y^2} + \frac{\partial^2 T}{\partial z^2} \right) \quad [6]$$

The energy equation for the solid region is expressed as Equation 7:

$$\left(\frac{\partial^2 T}{\partial x^2} + \frac{\partial^2 T}{\partial y^2} + \frac{\partial^2 T}{\partial z^2} \right) = 0 \quad [7]$$

Where u, v and w are the velocities in the direction of x, y and z , respectively. While P is pressure, ρ is density, g is the gravitational acceleration constant, β is volumetric expansivity, ν is kinematic viscosity, T is temperature, T_∞ is free stream temperature, and α is thermal diffusivity.

RESULTS AND DISCUSSION

Validation of Simulation with Experimental data from Literature

In order to justify the accuracy of the simulation of this research, the validation was done by quoting the experimental results from literature (Effendi & Kim, 2015). Therefore, this study did run a simulation base on operating parameters from literature (Effendi & Kim, 2015). The simulation was then compared with the experimental results from the literature (Effendi & Kim, 2015). The validation of the results in this study with the previous study is related to the effect of fins spacing on thermal resistance. Thermal resistance is one of the most important parameters for determining heat sinks' heat transfer characteristics and designing an electronic cooling device. In this study, the same geometrical configuration

of the experimental models was adopted for the simulation models for validation. The same fins spacing was adopted for the simulation and tested with a heat source of 5W and 30W. The comparison of results for validation was considered for both Solid Hybrid Fin heat sink (SHF HS) and Pin Fins heat sink (PF HS) since only that designs correlate with the designs in this study. It is to ensure the results are comparable and can be validated. Thermal resistance was the main parameter for testing the validity of the simulation with experimental work. Thermal resistance, R_{th} can be expressed as Equation 8:

$$R_{th} = \frac{T_b - T_a}{q} \tag{8}$$

Where T_b is the temperature of the base of heat sink, T_a is ambient air temperature and q is rate of heat transfer (Effendi & Kim, 2018). Table 4 shows the results for thermal resistance against different fins spacing.

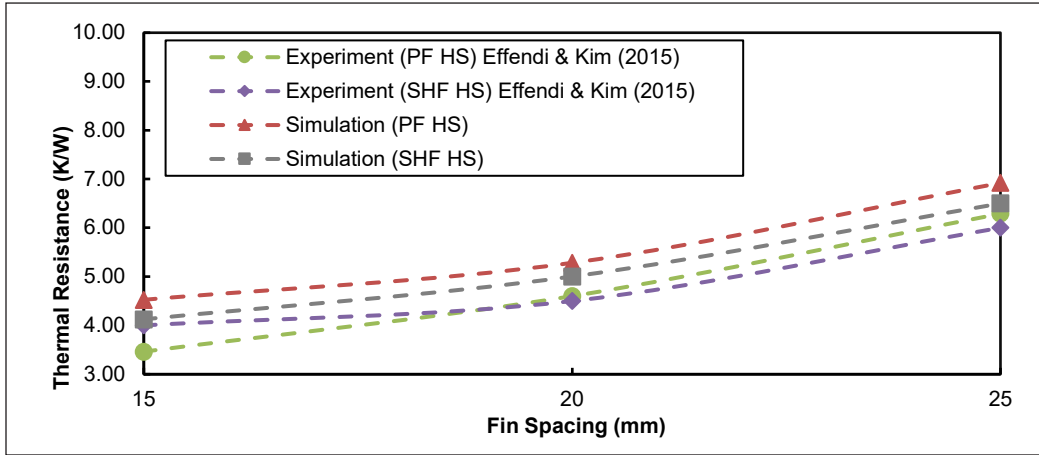
Table 4
Results of thermal resistance for both simulation and experimental from Effendi & Kim (2015)

Power (W)	Fin spacing (mm)	Thermal resistance (K/W) (Experimental)		Thermal resistance (K/W) (Simulation)	
		Solid Hybrid Fins Heat Sink	Pin Fins Heat Sink	Solid Hybrid Fins Heat Sink	Pin Fins Heat Sink
5	15	4.00	3.46	4.12	4.52
	20	4.50	4.60	5.00	5.28
	25	6.00	6.29	6.50	6.92
30	15	2.27	2.67	2.99	3.00
	20	3.00	3.49	4.30	4.00
	25	4.00	4.57	5.30	5.00

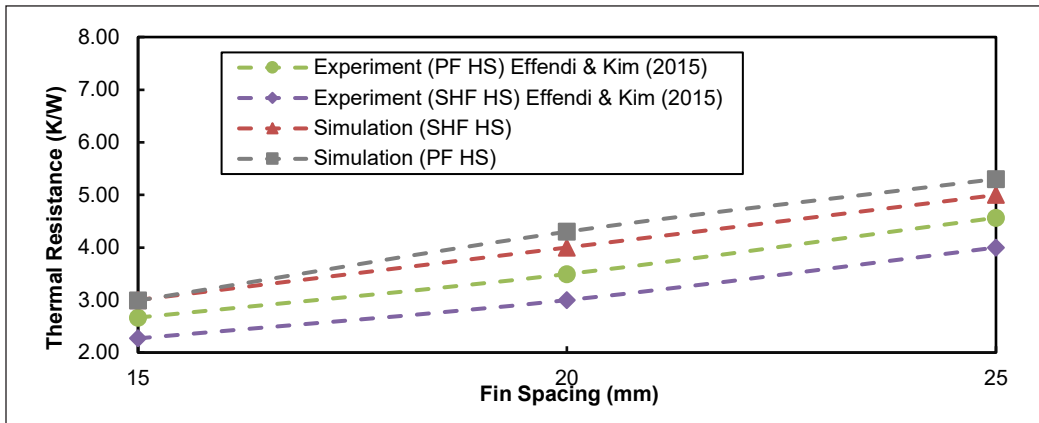
Table 5
MAPE Error percentages between simulation and experimental results

Power (W)	Average of MAPE Error percentage (%) (SHF HS)	Average of MAPE Error percentage (%) (PF HS)
5	11.40	10.11
30	10.34	10.56

Figure 6 is quite revealing in several ways. First, as indicated in Figures 6(a) and 6(b), the predicted thermal resistance is slightly higher than the experimental results. The reason is that, whereas the pins are in perfect contact with the upper bottom plate in the simulation, it is not so in the experiment. The limiting factor of the viscous laminar model could also contribute to the difference, as reported in (Lu & Jiang, 2006). The relationship between thermal resistance and fin spacing is directly proportional, and the results from



(a)



(b)

Figure 6. Validation of results of Thermal Resistance of HPFWC HS and PFWC HS against Fin Spacing on heat at (a) 5W and (b) 30W

simulations produce a similar result to the previous study by Effendi and Kim (2015). The second reason for the disparity between the simulation and experiment is that the aluminium used for the experiment is Aluminium 6063, which has slightly different properties than standard aluminium used in simulations. To further prove the validity of the simulation, the error between the simulations results and the previous study was calculated using the Mean Absolute Percentage Error (MAPE) formula. The formulation of MAPE can be expressed as Equation 9:

$$MAPE = \frac{100}{N} \times \sum_{i=1}^N \left| \frac{x_i - \hat{x}_i}{x_i} \right| \quad [9]$$

N , x_i and \hat{x}_i is the representatives of the number of values, simulation and experimental values, respectively. From the analysis using Equation 9, all validation errors are about 10%,

which can be referred to in Table 5. Based on these percentage errors that are relatively less than 12%, it can be concluded that the present model is significantly accurate to predict the thermal resistance of the heat sink.

Thermal and Flow Fields

Figures 7 and 8 show airflow’s temperature distributions and velocity profile around each heat sink. Figure 7 shows the temperature distributions between the two designs. It can be observed that the edges of PFWC HS are at a lower temperature than the central region. In comparison, the temperature distributions in HPFWC HS show an irregular pattern, with some of the pin fins at lower temperatures than others. The central region does not show any significant difference from the edges.

Table 6 shows the result of the base temperature for each heat sink. At the same heat flux, the base temperature of HPFWC HS Type 1 is higher compared to PFWC HS Type 1. The reason is that the surface area of HPFWC HS is higher than that of PFWC HS, and the wings around the HPFWC HS promote swirl flows and fluid mixing; this situation interrupts the thermal boundary layer through the HPFWC HS. It leads to a higher heat transfer coefficient, higher heat dissipation and higher baseplate temperature. This result is consistent with the result found in Acharya and Dash (2018).

Figures 8(a) to 8(d) show the velocity profile of the airflow around each heat sink. Although the flow pattern of air around each heat sink shows a non-uniform flow, it can be observed that some regions of high-velocity profile result in high vortex formation. For example, a comparison of airflow profile between HPFWC HS and PFWC HS shows a high-velocity profile of air around HPFWC HS than PFWC HS, resulting in high vortex formation around HPFWC HS than PFWC HS. The reason is that the wings around the HPFWC HS cause an irregular flow pattern of the air which eventually induces high vortex formation.

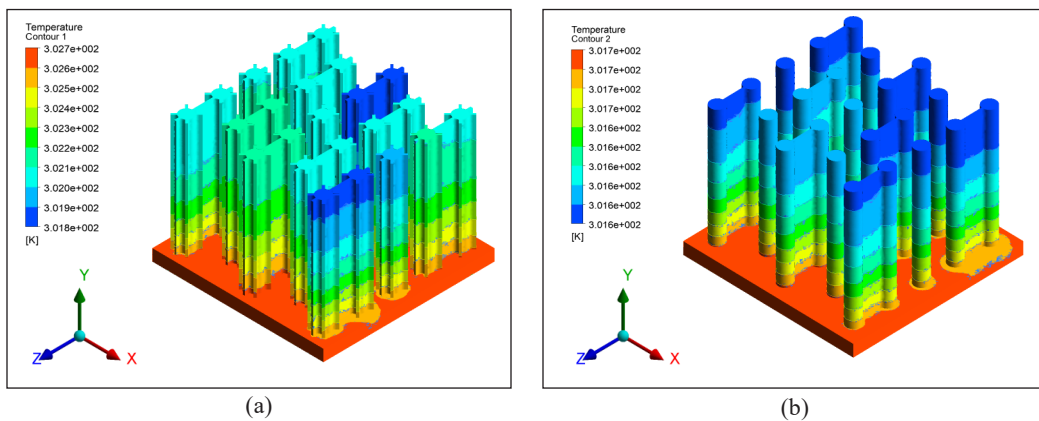


Figure 7. Temperature distributions (a) HPFWC HS (b) PFWC HS

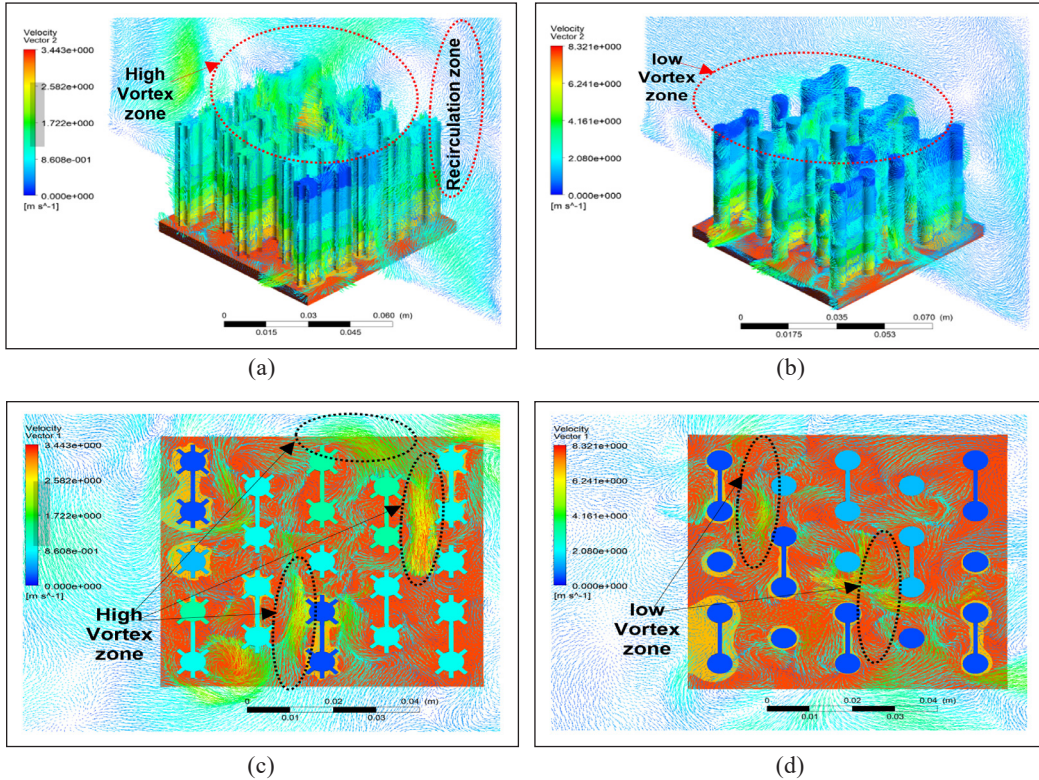


Figure 8. Airflow velocity profile around (a) Isometric view of HPFWC HS (b) Isometric view of PFWC HS (c) Top view of HPFWC HS (d) Top view of PFWC HS

Thermal Performances

Generally, the performance of a heat sink is a measure of the temperature difference between the bottom plate and atmospheric air ΔT . The ΔT is, however, a function of the rate of heat applied Q . Temperature differences can be expressed as Equation 10

$$\Delta T = T_b - T_a \quad [10]$$

Where T_b is the temperature of base of heat sink and T_a is ambient air temperature.

Figure 9 shows a linear variation in ΔT with respect to the heat applied to the base plate. Interestingly, both designs' heat sink type 3 shows a higher temperature difference. The reason is that heat sink type 3 has lower fin spacing. Thus, the heat dissipation rate from local hot spots on the plate to the fins is much higher, promoting higher fluid interaction with the solid surface and enhancing convective heat transfer. On the other hand, heat sink type 1 has a lower temperature difference because the higher fin spacing associated with heat sink type 1 does not enhance heat dissipation from hot spots on the base plate. Hence, heat sinks type 1 has a lower base temperature.

From the results in Figure 9, other parameters can also be calculated. As mentioned earlier, the following parameters for HPFWC HS Type 1 and PFWC HS Type 1 can be found in Table 6. All calculations are done by using Ansys FLUENT. The parameters that have been calculated are thermal conductivity, k , Prandlt number, Pr , Grashof number, Gr and Rayleigh number, Ra .

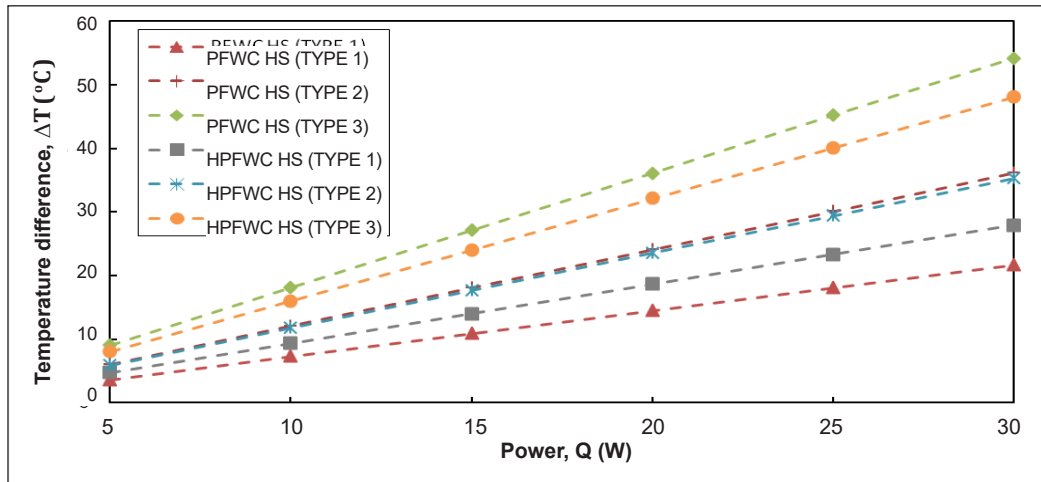


Figure 9. Graph of temperature differences, ΔT against the power input, Q tested for all configurations of heat sinks.

Table 6
Thermal parameters of HPFWC HS Type 1 and PFWC HS Type 1

Heat Sink	Power (W)	Base Temperature (°C)	T_{film} (°C)	k (W/m.K)	Pr	Gr	Ra
PFWC Type 1	5	28.6	26.8	0.02564	0.7291	4.725×10^2	3.445×10^2
	10	32.3	28.7	0.02578	0.7286	9.320×10^2	6.791×10^2
	15	35.9	30.5	0.02592	0.7281	1.354×10^3	9.861×10^2
	20	39.5	32.3	0.02605	0.7276	1.754×10^3	1.276×10^3
	25	43.1	34.1	0.02618	0.7271	2.132×10^3	1.550×10^3
	30	46.7	35.9	0.02632	0.7266	2.492×10^3	1.811×10^3
HPFWC Type 1	5	29.7	27.4	0.02569	0.7289	6.118×10^2	4.460×10^2
	10	34.3	29.7	0.02586	0.7283	1.170×10^3	8.523×10^2
	15	39.0	32.0	0.02603	0.7276	1.701×10^3	1.238×10^3
	20	43.6	34.3	0.02620	0.7270	2.186×10^3	1.589×10^3
	25	48.3	36.7	0.02638	0.7264	2.644×10^3	1.920×10^3
	30	52.9	39.0	0.02655	0.7258	3.061×10^3	2.222×10^3

The relationship between base temperature, T_b and other parameters has been observed. The first parameter observed is a relation between base temperature, T_b and thermal conductivity, k . The thermal conductivity data was a result of simulation from

CFD Ansys. It can be observed from Figure 10 that there is a linear correlation between thermal conductivity and base temperature. Interestingly both HPFWC HS and PFWC HS showed similar characteristics in responding to changes in thermal conductivity. This phenomenon is because, as expected, any increase in the thermal conductivity is always accompanied by an increase in heat transfer characteristics of that material.

Prandtl number, Pr has also been calculated to observe its relationship with base temperature, T_b . Then, the Prandtl number, Pr , can be expressed as Equation 11:

$$Pr = \frac{\nu}{\alpha} \quad [11]$$

Where ν is the momentum diffusivity and α is the thermal diffusivity. Figure 11 shown that as T_b increases, Pr is decreases for both heat sinks. HPFWC HS has lower Pr than PFWC HS which is 8.72% lower. Since the heat transfer rate is better in lower Pr , HPFWC HS has performed better efficiently dissipating heat into the ambient.

Table 7 shows the tabulated data of thermal performances of HPFWC HS Type 1 and PFWC HS Type 1.

Table 7
Thermal performances of HPFWC HS Type 1 and PFWC HS Type 1

Heat Sink	Base Temperature (°C)	Nu	h (W/m ² .K)
PFWC Type 1	28.6	2.96	5.062
	32.3	3.50	6.023
	35.9	3.85	6.645
	39.5	4.10	7.121
	43.1	4.30	7.512
	46.7	4.47	7.851
HPFWC Type 1	29.7	3.16	5.407
	34.3	3.71	6.393
	39.0	4.07	7.061
	43.6	4.33	7.565
	48.3	4.54	7.984
	52.9	4.71	8.333

$$h = \frac{Q}{A_s \Delta T} \quad [12]$$

The heat transfer coefficient, h , can be expressed as Equation 12 (Meng et al., 2018): Where Q is the input power, A_s is heat sink surface area, and ΔT is the temperature difference. While Nu that been used in this study is expressed by Shen et al. (2016) as Equation 13:

$$Nu = \frac{1}{0.25(((\pi(D + H)/N) - t)Ra^{0.13}/L)^{-1.7} + 1} \times \left(0.68 + \frac{0.670Ra^{1/4}}{\left(1 + (0.492/Pr)^{9/16}\right)^{4/9}} \right) \quad [13]$$

Which is also equivalent to Equation 14:

$$Nu = \frac{hL_c}{k} \quad [14]$$

Where h is convective heat transfer coefficient, L_c is characteristics length, and k is thermal conductivity. The hydraulic length for the heat sink is the fin spacing, S which depends on the respective spacing (Effendi et al., 2018). Rayleigh Number, Ra is a product of Grashof Number, Gr and Prandlt Number, Pr , which can be expressed as Equation 15:

$$Ra = Gr.Pr \quad [15]$$

Which Gr can be expressed as Equation 16

$$Gr = \frac{g\beta(T_b - T_\infty)L_c^3}{\nu^2} \quad [16]$$

Where g is gravity, β is thermal coefficient expansion, T_b is base temperature, T_∞ is free stream temperature, L_c characteristics length and ν is kinematic viscosity.

Figure 12 shows that as Ra increases, Nu also increases. HPFWC HS has the highest Nu while PFWC HS has the lowest Nu . The difference between the highest Nu of HPFWC HS and PFWC HS is 5.78%. From Figure 13, both heat sinks show some similarity, but the highest h results from HPFWC HS. It is proven again that HPFWC HS has better performance in heat transfer than PFWC HS.

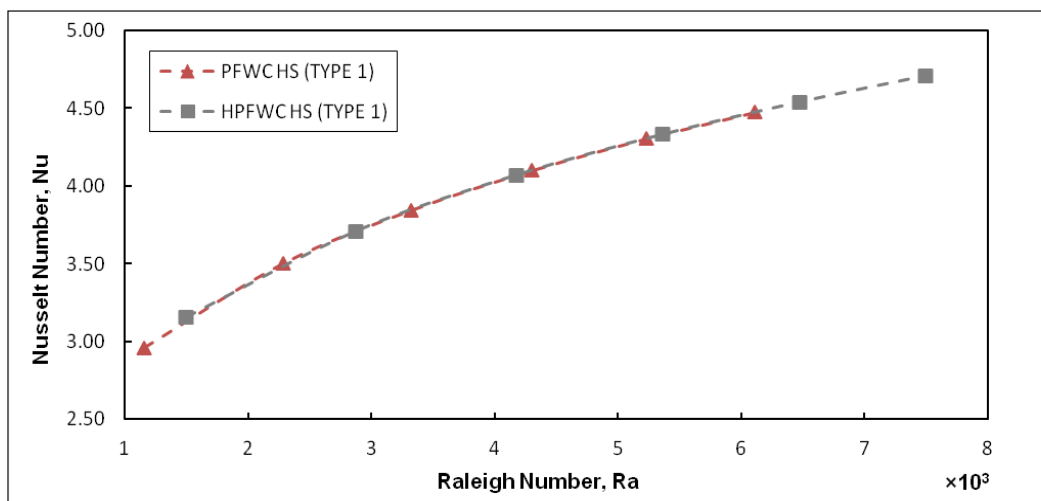


Figure 12. The relation of Nusselt number, Nu and Rayleigh number, Ra

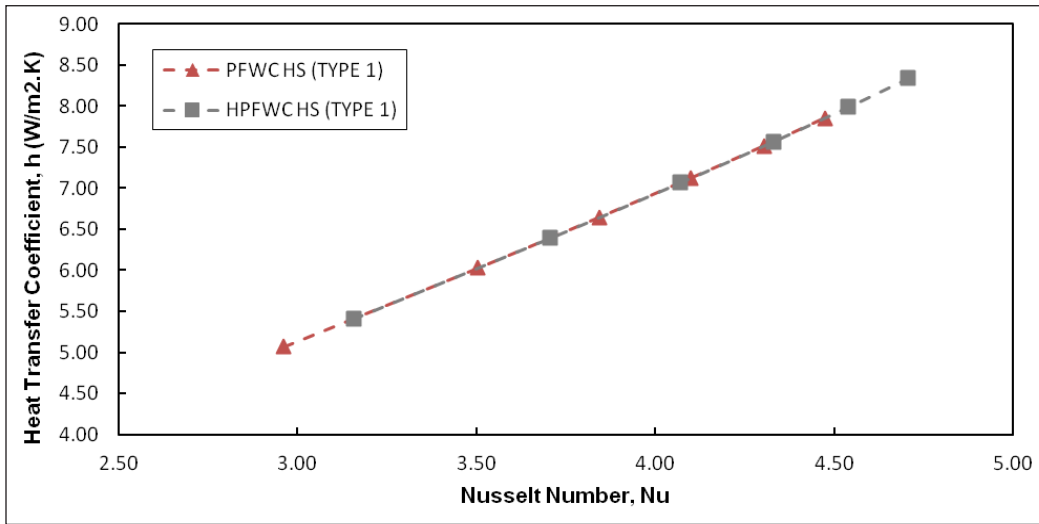


Figure 13. The relation of heat transfer coefficient, h and Nusselt number, Nu

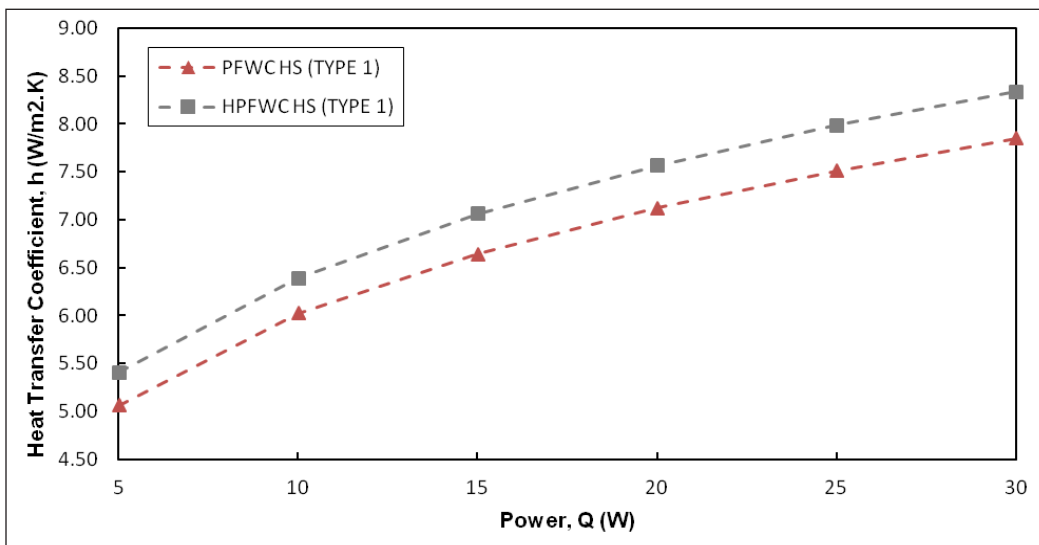


Figure 14. The relation of heat transfer coefficient, h and input power, Q

This study obtained the heat transfer coefficient, h , using Equation 14 with the Nu equation in Equation 13. The relationship between h and Nu is illustrated in Figure 13, and the effect of power input Q at the base of the heat sink is shown in Figure 14. The variation of input power, Q , has also been observed to increase slowly for h . Interestingly, HPFWC HS Type 1 shows a higher value of h for any variation of Q . The reason is that the wings attached to the pin fins of HPFWC HS Type 1 generate swirl flow which enhances the mixing of the fluid and interrupts the thermal boundary layer; this effect contributes to

an increase in h . This finding is consistent with Hosseinirad et al. (2019). Furthermore, the average difference between h of HPFWC HS and PFWC HS is 5.94%. Therefore, HPFWC HS Type 1 dissipates heat at 5.94% more than PFWC HS.

Fin Spacing Effect

Figure 15 shows the effect of fin spacing on the heat transfer coefficient of the heat sink under consideration. As can be observed, there is a linear increase in heat transfer coefficient with an increase in fin spacing. A possible explanation for these results may be that increasing pin fin spacing promotes more influx of fluid, enhances the interaction between the fluid flow across the solid surface. There was a significant difference between the two heat sinks. For example, at a fin spacing of 20mm, the heat transfer coefficient for HPFWC HS Type 1 is higher than that of PFWC HS type 1 by about 5%. The reason is that the heat sink HPFWC HS Type 1 has wings around it, and these wings help to promote vortex formation around the fins, and it is this vortex formation that enhances the heat transfer characteristics. This finding is similar to that of Haghghi et al. (2018).

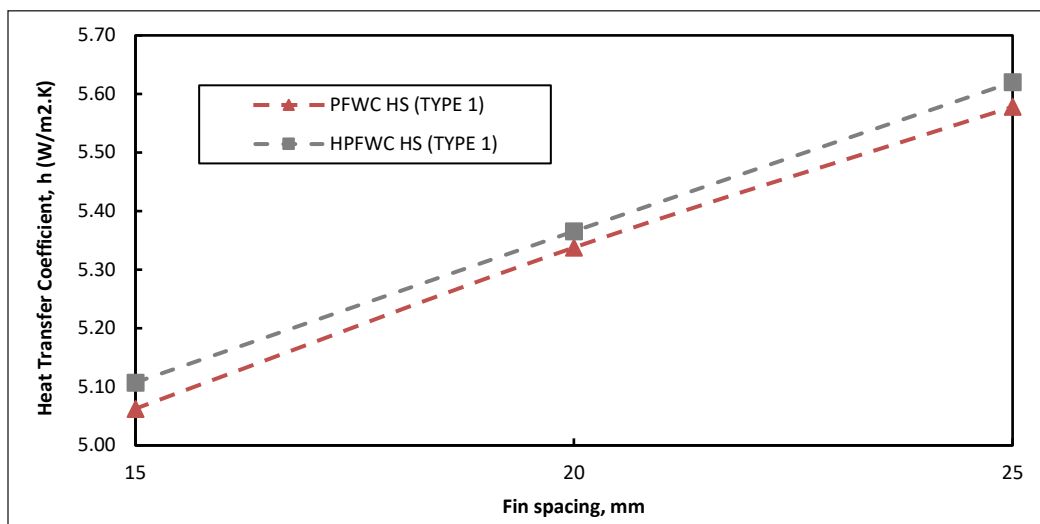


Figure 15. Fin spacing, S effect on heat transfer coefficient, h

CONCLUSION AND RECOMMENDATIONS

This study has numerically determined the thermal performances of Hybrid Pin Fin with Connector (HPFWC HS) and Pin Fin Heat Sink (PFWC HS). Three configurations were analysed based on the different spacing of the fins. The simulation was done to numerically determine the thermal parameters of the heat sinks under natural convection conditions and thermal performances. The simulation was validated with previous studies to observe

the correlation and the performances between designs of heat sinks. In this study, the results for validating the Ansys CFD simulation with experiment show about 12% error. It indicates how close was the simulation result with the experiment. Interestingly both HPFWC HS and PFWC HS showed similar characteristics in responding to changes in thermal conductivity. The reason for this output is that increasing thermal conductivity is always accompanied by increasing heat transfer characteristics. Also, increasing pin fin spacing promotes more influx of fluid, enhancing interaction between the fluid flow across the solid surface. However, there was a significant difference between the two heat sinks. For example, at a fin spacing of 20mm, the heat transfer coefficient for HPFWC HS Type 1 is higher than that of PFWC HS type 1 by about 5%. In conclusion, increasing the number of fins increases the total area and increases the heat transfer rate.

ACKNOWLEDGEMENT

The authors want to express their appreciation to the Universiti Teknologi MARA (UiTM) through the Geran Penyelidikan Khas UiTM (Grant No. 600-RMC/GPK 5/3 (133/2020)) for funding this research.

REFERENCES

- Acharya, S., & Dash, S. K. (2018). Natural convection heat transfer from a horizontal hollow cylinder with internal longitudinal fins. *International Journal of Thermal Sciences*, 134, 40-53. <https://doi.org/10.1016/j.ijthermalsci.2018.07.039>
- Arefin, A. M. E. (2016). Thermal analysis of modified pin fin heat sink for natural convection. In *2016 5th International Conference on Informatics, Electronics and Vision, ICIEV 2016* (pp. 1-5). IEEE Publishing. <https://doi.org/10.1109/ICIEV.2016.7759986>
- Choudhary, V., Kumar, M., & Patil, A. K. (2019). Experimental investigation of enhanced performance of pin fin heat sink with wings. *Applied Thermal Engineering*, 155, 546-562. <https://doi.org/10.1016/j.applthermaleng.2019.03.139>
- Effendi, N. S., & Kim, K. J. (2015). Thermal behaviours of passively-cooled hybrid fin heat sinks for lightweight and high performance thermal management. In *Proceedings of the ASME 2015 International Technical Conference and Exhibition on Packaging and Integration of Electronic and Photonic Microsystems InterPACK2015* (pp. 1-7). American Society of Mechanical Engineers.
- Effendi, N. S., & Kim, K. J. (2018). Natural convective hybrid fin heat sinks for lightweight and high performance thermal management. *Journal of Mechanical Science and Technology*, 32(10), 5005-5013. <https://doi.org/10.1007/s12206-018-0948-4>
- Effendi, N. S., Putra, S. S. G. R., & Kim, K. J. (2018). Prediction methods for natural convection around hollow hybrid fin heat sinks. *International Journal of Thermal Sciences*, 126, 272-280. <https://doi.org/10.1016/j.ijthermalsci.2018.01.002>

- Haghighi, S. S., Goshayeshi, H. R., & Safaei, M. R. (2018). Natural convection heat transfer enhancement in new designs of plate-fin based heat sinks. *International Journal of Heat and Mass Transfer*, 125, 640-647. <https://doi.org/10.1016/j.ijheatmasstransfer.2018.04.122>
- Hoffmann, K. A., & Chiang, S. T. (2000). *Computational fluid dynamics* (Vol. 1). Engineering Education System.
- Hosseini-rad, E., Khoshvaght-Aliabadi, M., & Hormozi, F. (2019). Effects of splitter shape on thermal-hydraulic characteristics of plate-pin-fin heat sink (PPFHS). *International Journal of Heat and Mass Transfer*, 143, Article 118586. <https://doi.org/10.1016/j.ijheatmasstransfer.2019.118586>
- Humphries, J. (2014). *Thermal management of electronics devices - The role it plays*. Electrolube. https://electrolube.com/knowledge_base/thermal-management-of-electronics-devices/
- Ibrahim, T. K., Mohammed, M. N., Mohammed, M. K., Najafi, G., Sidik, N. A. C., Basrawi, F., Abdalla, A. N., & Hoseini, S. S. (2018). Experimental study on the effect of perforations shapes on vertical heated fins performance under forced convection heat transfer. *International Journal of Heat and Mass Transfer*, 118, 832-846. <https://doi.org/10.1016/j.ijheatmasstransfer.2017.11.047>
- Immerman, G. (2017). *Why industry 4.0 is important and why manufacturers should care*. Machinemetrics. <https://www.machinemetrics.com/blog/why-industry-4-0-is-important>
- Jassem, R. R. (2013). Effect the form of perforation on the heat transfer in the perforated fins. *Academic Research International*, 4(3), 198-207. <https://doi.org/10.13140/RG.2.1.2437.0326>
- Jensen, M. (2018). *The importance of proper meshing in finite element analysis*. Steen Solutions. <http://steensolutions.com/2017/01/importance-proper-meshing-finite-element-analysis/>
- Joo, Y., & Kim, S. J. (2015). Comparison of thermal performance between plate-fin and pin-fin heat sinks in natural convection. *International Journal of Heat and Mass Transfer*, 83, 345-356. <https://doi.org/10.1016/j.ijheatmasstransfer.2014.12.023>
- Kumar, V. M., Farooq, S., & Rao, B. N. (2016). A detailed review on pin fin heat sink. *International Journal of Energy and Power Engineering*, 10(5), 1006-1015.
- Lu, B., & Jiang, P. X. (2006). Experimental and numerical investigation of convection heat transfer in a rectangular channel with angled ribs. *Experimental Thermal and Fluid Science*, 30(6), 513-521. <https://doi.org/10.1016/j.exptthermflusci.2005.09.007>
- Meng, X., Zhu, J., Wei, X., & Yan, Y. (2018). Natural convection heat transfer of a straight-fin heat sink. *International Journal of Heat and Mass Transfer*, 123, 561-568. <https://doi.org/10.1016/j.ijheatmasstransfer.2018.03.002>
- Nada, S. A., & Said, M. A. (2019). Effects of fins geometries, arrangements, dimensions and numbers on natural convection heat transfer characteristics in finned-horizontal annulus. *International Journal of Thermal Sciences*, 137, 121-137. <https://doi.org/10.1016/j.ijthermalsci.2018.11.026>
- Perry, J. (2017). *Thermal comparison of copper and aluminum heat sinks*. Advanced Thermal Solutions Inc. <https://www.qats.com/cms/2017/03/28/case-study-thermal-comparison-copper-aluminum-heat-sinks/>
- Schelling, P. K., Shi, L., & Goodson, K. E. (2005). Managing heat for electronics. *Materials Today*, 8(6), 30-35. [https://doi.org/10.1016/S1369-7021\(05\)70935-4](https://doi.org/10.1016/S1369-7021(05)70935-4)

- Shen, Q., Sun, D., Xu, Y., Jin, T., Zhao, X., Zhang, N., Wu, K., & Huang, Z. (2016). Natural convection heat transfer along vertical cylinder heat sinks with longitudinal fins. *International Journal of Thermal Sciences*, 100, 457-464. <https://doi.org/10.1016/j.ijthermalsci.2015.09.007>
- Vijay, V. (2019). *Free and forced convection study notes for mechanical engineering*. Gradeup. <https://gradeup.co/free-and-forced-convection-i-9d6951ec-c265-11e5-9f7c-7aa8072720c6>
- Zagala, E. J. (2016). Heat conductivity. In B. Bhushan (Ed.), *Encyclopedia of Nanotechnology* (pp. 1453-1453). Springer. https://doi.org/10.1007/978-94-017-9780-1_100385
- Zaidshah, S., & Yadav, V. (2019). Heat transfer from different types of fins with notches with varying materials to enhance rate of heat transfer: A review. *International Journal of Applied Engineering Research*, 14(9), 174-179.

Evaluation of Factors Affecting Microbial Growth Inhibition and Optimization Using Pineapple Leaves Juice

Norazwina Zainol^{1*}, Amirah Ya'acob¹, Putri Nurul Yasmin Mohd Ridza¹, Siti Hatijah Mortan¹ and Kamaliah Abdul Samad²

¹College of Engineering, Universiti Malaysia Pahang, Lebuhraya Tun Razak, 26300 UMP, Gambang, Kuantan, Pahang, Malaysia

²Faculty of Chemical and Process Engineering Technology, Universiti Malaysia Pahang, Lebuhraya Tun Razak, 26300 UMP, Gambang, Kuantan, Pahang, Malaysia

ABSTRACT

This study optimized microbial growth inhibition conditions using pineapple leaf juice (PLJ). The sugarcane press machine was used to press the PLJ. The study considered four factors to be analyzed by Two-level factorial design (TLFD), which are microbial inhibition time (0.5–5 h), the concentration of total phenolic content (TPC) (0.2563–0.5127 mg GAE/mL), temperature (26–37 °C), and the ratio of PLJ to microbe (PLJ/M) (v/v) (1:1 and 1:3). Colony-forming unit (CFU) method was employed to measure microbial growth inhibition. The microbial growth inhibition was expressed as a percent in terms of CFU/mL. A central composite design (CCD) experimental design created using response surface methodology (RSM) determined the optimum temperature (35–39 °C) and microbial inhibition time (10–50 min) of microbial growth inhibition. The best conditions were 0.5 h of microbial inhibition time, 0.5127 mg GAE/mL of TPC, 1:1 PLJ/M, and a temperature of 37 °C.

The analysis of variance (ANOVA) showed that temperature (Factor C) has the greatest contribution (1.56%) to inhibiting microbial growth, accompanied by TPC concentration in PLJ (Factor B) with 1.27%, microbial inhibition time (Factor A) with 1.07% and PLJ/M (Factor D) 0.29%. Optimization studies show that at an optimum temperature of 37 °C and an inhibition time of 34.25 min, maximum microbial growth inhibition of 94.73% with a minimum value of 9.12×10^4 CFU/mL was achieved. This research

ARTICLE INFO

Article history:

Received: 23 June 2021

Accepted: 17 January 2022

Published: 25 May 2022

DOI: <https://doi.org/10.47836/pjst.30.3.19>

E-mail addresses:

amymira96@gmail.com (Amirah Ya'acob)

azwina@ump.edu.my (Norazwina Zainol)

2506yasmin@gmail.com (Putri Nurul Yasmin Mohd Ridza)

hatijah@ump.edu.my (Siti Hatijah Mortan)

kamaliahabdulsamad@ymail.com (Kamaliah Abdul Samad)

* Corresponding author

suggests that PLJ can be utilized as a value-added natural product for application in the agricultural sector.

Keywords: Central composite design (CCD), microbial growth inhibition, phenolic compounds, pineapple leaf juice (PLJ), two-level factorial design (TLFD)

INTRODUCTION

Most synthetic microbial growth inhibitor (MGI) agents can cause severe toxicity. Using synthetic MGI to combat disease and infection is impactful, especially for humans and the environment. Therefore, finding a new alternative MGI agent from natural plant sources will be favorable. Nowadays, natural MGI from different sources has been used to inhibit microbial growth and pathogenic microorganisms. More than 30,000 antimicrobial components and 1,350 plants with antimicrobial activities have been extracted (Arshad & Batool, 2017). Pineapple (*Ananas comosus*) is a commercial fruit with MGI properties due to its high phenolic compounds (Domínguez et al., 2018). Pineapple leaves contain seven significant phenolic compounds, including Methyl-5-O-caffeoyl-quinic acid, octahydrocurcumin, meliadanoside A, stilbostemin D, feralolide, agrimol C and kukoamine A (Ya'acob et al., 2021). Phenolic compounds are important to provide a defensive mechanism against infection. Therefore, using pineapple leaf juice (PLJ) as a natural product will benefit the communities since they are abundantly available waste materials in Malaysia. However, at the current time, it has not been studied yet as it is required (Asim et al., 2015).

Because these factors can influence the process, analyzing the microbial growth inhibition process can consume much energy, money, and time. Therefore, it is decided to use a two-level factorial design (TLFD), a screening experiment to analyze the factors affecting the microbial growth inhibition process by using PLJ. It explains the correlations among various responses resulting from one or more factors (Shane, 2017). Screening designs offer an efficient approach for assessing many factors in a minimal number of experimental runs for further investigation. Thus, the use of TLFD is vital in analyzing the influence of several factors that contributed to the application of PLJ as MGI by evaluating all the interactions involved.

In order to utilize the PLJ as an effective MGI, it is needed to evaluate the optimum condition of inhibition of microbial growth through response surface methodology (RSM). The RSM method can also determine the interaction between the independent variables by decreasing the number of trials (Aydar, 2018). According to Noormohamadi et al. (2018), central composite design (CCD) is advantageous for second-order (quadratic) polynomial fitting, which is beneficial for the study of the optimization process. Ammer et al. (2016) employed RSM under CCD to investigate the antimicrobial potential of

Eucalyptus tereticornis leaf extracts against *Escherichia coli*. On the other hand, the research on microbial inhibition through factorial analysis and optimization with PLJ, on the other hand, has never been published. Thus, factorial analysis and optimization in determining microbial growth inhibition were beneficial in this study. This study aimed to analyze the factor affecting microbial growth inhibition and optimize the conditioning process using PLJ.

MATERIAL AND METHODS

Materials

Potato dextrose agar (PDA) powder (99%), gallic acid (99%), Folin-Ciocalteu reagent (99%), sodium carbonate (Na_2CO_3 , 99%), and methanol (99.8%).

Pineapple Leaf Juice (PLJ) Preparation

The pineapple leaf and tested microbe, which are mixed culture, were provided by a pineapple plantation in Pekan Pina, Pahang. An electrical press machine prepared the pineapple leaf juice (PLJ) extract and autoclaved it for 15 min at 121 °C.

Total Phenolic Content (TPC) Analysis

Total phenolic content (TPC) was determined using a Folin-Ciocalteu assay with Gallic acid as a standard. First, 10 mL of PLJ was centrifuged at 5000 rpm for 15 min. Next, 2.5 mL of 10-fold diluted Folin-Ciocalteu and 0.5 mL of its supernatant were combined. The mixture was kept at room temperature for 5 min. After that, 2 mL of Na_2CO_3 (7.5%) was added to the mixture and kept for 1 h. Then, the mixture was measured using a UV-Vis spectrophotometer at 450 nm. Gallic acid was prepared in an 80% methanol solution with a 0.1–1.0 mg/mL concentration as a standard curve. The solution was also subjected to a similar treatment, which included the addition of Folin-Ciocalteu reagent and 7.5% Na_2CO_3 . Mg of gallic acid equivalent per gram of PLJ extract (mg GAE/mL) was presented (Siddiqui et al., 2017).

Culture Medium

Thirty-nine grams of Potato dextrose agar (PDA) were completely dissolved in 1000 mL of distilled water before autoclaving for 15 min at 121 °C. Approximately 10 mL of the solution was poured into Petri plates.

The Cultivation of Microbe

In this study, a pineapple leaf infected with microbes obtained from a pineapple plantation was used as a microbe for testing. The agar was streaked with the microbe on its plate

from quadrant one to four before incubating at 37 °C for 24 h using a sterile loop (Zainol & Rahim, 2017). The microbe used in this study was mixed culture.

Microbial Growth Inhibition Experiment Set-up

The experiment began with re-culturing the microbe. Next, microbe broth (MB) was prepared by scraping and mixing the re-cultured microbes into the nutrient broth. Approximately one PDA plate of microbe was scraped and mixed with nutrient broth. In an incubator shaker, the MB was agitated at 100 rpm of 37 °C for 1 h. Then, the MB and PLJ was mixed at selected ratio (1:1 and 1:3) and agitated in the incubator shaker at 100 rpm at selected inhibition times (0.5–5h) for factorial design and (10–50 min) for optimization and temperature (26–37 °C) for factorial design and (35–39 °C) for optimization. The experiment was conducted according to factorial and optimization design tables. The colony-forming unit (CFU) count was then performed on all samples.

Analysis of Colony Forming Units (CFU)

One hundred microlitres (100 µL) of microbe and PLJ mixture from section 2.6 was evenly spread on a PDA plate with a triangular cell spreader and incubated for 24 h at 37 °C (Jayaratne & Dayarathna, 2015). After 24 h, the colony count was determined. Microbes were counted at a constant range between 30 and 300 colonies on the Petri plate (O'Toole, 2016). The total CFU/mL obtained was used to calculate the microbial growth inhibition (%) using Equations 1 and 2.

$$\text{CFU/mL} = \frac{\text{No. of colonies} \times \text{dilution factor}}{\text{Volume of culture in plate}} \quad (1)$$

$$\text{Microbial growth inhibition (\%)} = \frac{\left(\frac{\text{CFU}}{\text{mL}} \text{ of control} - \frac{\text{CFU}}{\text{mL}} \text{ of mixture}\right)}{\frac{\text{CFU}}{\text{mL}} \text{ of control}} \times 100 \quad (2)$$

Factorial Analysis Study on Microbial Growth Inhibition

The experimental design of two-level factorial design (TLFD) with some factors at different levels was constructed as shown in Table 1. The factorial design table was designed using Design-Expert software (v7) (Table 2). There are four selected factors for factorial analysis: microbial inhibition time (0.5–5 h), the concentration of TPC (0.2563–0.5127 mg GAE/mL), the ratio of PLJ to microbe (PLJ/M) (1:1 and 1:3) and temperature (26–37 °C). For 1:1 PLJ/M, the ratio was 20 mL PLJ: 20 mL MB, while for 1:3 PLJ/M, the ratio was 10 mL PLJ: 30 mL MB. The experiment began with re-culturing the microbe. Then, the experimental setup for microbial growth inhibition and CFU analysis was carried

out. Finally, the experiment for microbial growth inhibition was conducted based on the factorial design table (Table 2).

Table 1
Factors at different levels

Factors	Level	
	Low	High
Microbial inhibition time (h)	0.5	5
TPC concentration in PLJ (mg GAE/mL)	0.2563	0.5127
Temperature (°C)	26	37
Ratio of PLJ to microbe (PLJ/M) (v/v)	1:1	1:3

Table 2
Table of factorial analysis experimental design

Runs	Factor			
	A: Microbial inhibition time (h)	B: TPC concentration (mg GAE/mL)	C: Temperature (°C)	D: Ratio of PLJ to microbe (PLJ/M) (v/v)
1	0.5	0.2563	26	1:1
2	5	0.2563	26	1:1
3	0.5	0.5127	26	1:1
4	5	0.5127	26	1:1
5	0.5	0.2563	37	1:1
6	5	0.2563	37	1:1
7	0.5	0.5127	37	1:1
8	5	0.5127	37	1:1
9	0.5	0.2563	26	1:3
10	5	0.2563	26	1:3
11	0.5	0.5127	26	1:3
12	5	0.5127	26	1:3
13	0.5	0.2563	37	1:3
14	5	0.2563	37	1:3
15	0.5	0.5127	37	1:3
16	5	0.5127	37	1:3

Optimization Study

Microbial inhibition time and temperature factors were chosen to investigate their inhibition of microbial growth effect. The optimization studies were conducted through response surface methodology (RSM) under central composite design (CCD). The selected factors and their level are shown in Table 3, and the experimental design comprised 13 runs. The experiment was carried out based on the experimental design table (Table 4).

Table 3
Factors and level of CCD

Factors	-α	-1 level	0	+1 level	+α
A: Microbial inhibition time (min)	10	20	30	40	50
B: Temperature (°C)	35	36	37	38	39

Table 4
Experimental design table of CCD

Runs	Factor A: Microbial inhibition time (min)	Factor B: Temperature (°C)
1	20	36
2	40	36
3	20	38
4	40	38
5	10	37
6	50	37
7	30	35
8	30	39
9	30	37
10	30	37
11	30	37
12	30	37
13	30	37

Data Analysis

Design-Expert software analyzed the best condition and optimum conditions for inhibition of microbial growth.

Validation Studies

The optimum points suggested by Design-Expert software were further validated to verify the model. Finally, the errors between the experimental values and predicted values were calculated. Equation 3 was used to calculate the error.

$$\text{Error (\%)} = \frac{\text{Experimental} - \text{Predicted}}{\text{Predicted}} \times 100 \tag{3}$$

RESULTS AND DISCUSSIONS

Screening and Analysis by Two-Level Factorial Design (TLFD)

The screening of the four factors was analyzed using TLFD, and 16 experimental runs were carried out, as seen in Table 5. Analysis of variance (ANOVA) Table 6 reveals that temperature (Factor C) has the greatest contribution (1.56%) to inhibiting microbial growth,

accompanied by a concentration of TPC (Factor B) with 1.27%, microbial inhibition time (Factor A) with 1.07% and PLJ/M (Factor D) 0.29%. The highest value of 3.58×10^5 CFU/mL, which indicates the minimum inhibition of microbial growth, was achieved at 1:3 of PLJ/M, 0.5127 mg GAE/mL at 26 °C, and 0.5 h. On the other hand, the lowest value of 1.69×10^5 CFU/mL indicates the maximum inhibition of microbial growth was achieved at 1:1 of PLJ/M, 0.5127 mg GAE/mL at 37 °C, and 0.5 h. Design-Expert software's interpretation of the data analysis indicated that PLJ could only inhibit microbial growth without killing them. It might be explained by the variation of phenolic compounds found in PLJ, which have a certain efficiency in inhibiting microbial growth (Maqsood et al., 2014).

Table 5

Experimental data of factorial study

Std	Factor				Response 1
	A: Microbial inhibition time (h)	B: TPC concentration in PLJ (mg GAE/mL)	C: Temperature (°C)	D: Ratio of PLJ to microbe (PLJ/M) (v/v)	CFU/mL
1	0.5	0.2563	26	1:1	3.57×10^5
2	5	0.2563	26	1:1	2.12×10^5
3	0.5	0.5127	26	1:1	1.94×10^5
4	5	0.5127	26	1:1	3.58×10^5
5	0.5	0.2563	37	1:1	3.47×10^5
6	5	0.2563	37	1:1	2.58×10^5
7	0.5	0.5127	37	1:1	1.69×10^5
8	5	0.5127	37	1:1	2.89×10^5
9	0.5	0.2563	26	1:3	2.30×10^5
10	5	0.2563	26	1:3	2.91×10^5
11	0.5	0.5127	26	1:3	3.58×10^5
12	5	0.5127	26	1:3	2.19×10^5
13	0.5	0.2563	37	1:3	2.50×10^5
14	5	0.2563	37	1:3	2.68×10^5
15	0.5	0.5127	37	1:3	3.03×10^5
16	5	0.5127	37	1:3	2.14×10^5

Factorial Study Analysis of Variance (ANOVA)

The effects of various factors on microbial growth were studied by analysis of variance (ANOVA) (Table 6). The statistical test revealed that the significant factors of A, B, C, D, AB, AD, BC, BD, ABD, BCD, and ABCD are based on their $\text{prob} > F$ (less than 0.05). The model was accepted as the statistical test. The model was accepted as the linear regression coefficient R^2 of 0.9995. The adjusted R^2 of 0.9980 shows a good data fit (Saunders et al., 2012). The relationship of CFU/mL with the factors was shown through the codified linear regression shown in Equation 4.

$$Y = 2.703E + 005 - 6228.21A - 6789.28B - 7507.49C - 3243.17D + 13320.50AB - 12400.30AD - 116314.76B + 13657.16BD - 51475.21ABD + 4612.22BCD + 12018.73ABCD \tag{4}$$

Y was the predicted response (CFU/mL), A was the microbial inhibition time (h), B was the TPC concentration in PLJ (mg GAE/mL), C was the temperature (°C), and D was the PLJ/M (v/v).

Table 6
ANOVA of factorial study

	Sum of Square	df	Mean Square	F-Value	P-Value Prob > F	(%) Contribution	
Models	5.792E+010	11	5.265E+009	692.20	< 0.0001		significant
A: Microbial inhibition time	6.206E+008	1	6.206E+008	81.60	0.0008	1.07	
B: TPC concentration	7.375E+008	1	7.375E+008	96.96	0.0006	1.27	
C: Temperature	9.018E+008	1	9.018E+008	118.56	0.0004	1.56	
D: Ratio	1.683E+008	1	1.683E+008	22.12	0.0093	0.29	
AB	2.839E+009	1	2.839E+009	373.23	< 0.0001	4.90	
AD	2.83E+009	1	2.83E+009	323.45	< 0.0001	4.25	
BC	2.158E+009	1	2.158E+009	283.77	< 0.0001	3.72	
BD	2.984E+009	1	2.984E+009	392.34	< 0.0001	5.15	
ABD	4.240E+010	1	4.240E+010	5573.58	< 0.0001	73.16	
BCD	3.404E+008	1	3.404E+008	44.75	0.0026	0.59	
ABCD	2.311E+009	1	2.311E+009	303.85	< 0.0001	3.99	
Residual	3.043E+007	4	7.606E+006				
Cor. Total	5.795E+010	15					
R ²	0.9995						
Adjusted R ²	0.9980						

Factors Influencing Microbial Growth Inhibition

Table 7 shows the suggested best conditions obtained for microbial growth inhibition. The suggested best conditions, PLJ/M of 1:1, 0.5127 mg GAE/mL of concentration of TPC, and temperature of 37 °C for 0.5 h of microbial inhibition time, achieved 21.25% of microbial inhibition time with 2.81×10^5 CFU/mL. The main and interaction effects between factors on microbial growth inhibition were illustrated in the Pareto chart shown in Figure 1. The factors with the blue color represent the negative effect, while the orange color represents the positive effect. The negative effect of increasing the factor value lowered the microbial growth factor CFU/mL response value. From Figure 1, the factors A, B, and

C together affect the interaction between the PLJ/M and temperature and reduce the CFU/mL value. It contributes to the greater inhibition of microbial growth. The factors AD (microbial inhibition time and PLJ/M) and BC (concentration of TPC and temperature) interact negatively. When both interaction factors were increased, the CFU/mL value decreased. Figure 2 illustrates the effect of the two most significant factors.

Table 7
Suggested best conditions

Factors	Conditions
A: Microbial inhibition time	0.5 h
B: TPC concentration	0.5127 mg GAE/ mL
C: Temperature	37 °C
D: Ratio	1:1
CFU/mL	3.49×10^5 CFU/mL
Microbial growth inhibition	21.25%

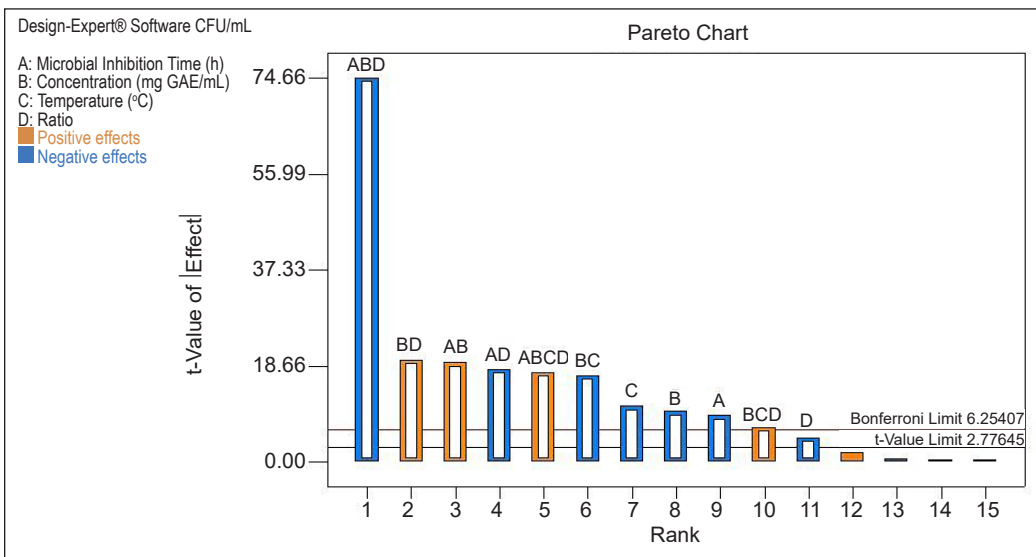


Figure 1. The factorial study's Pareto chart

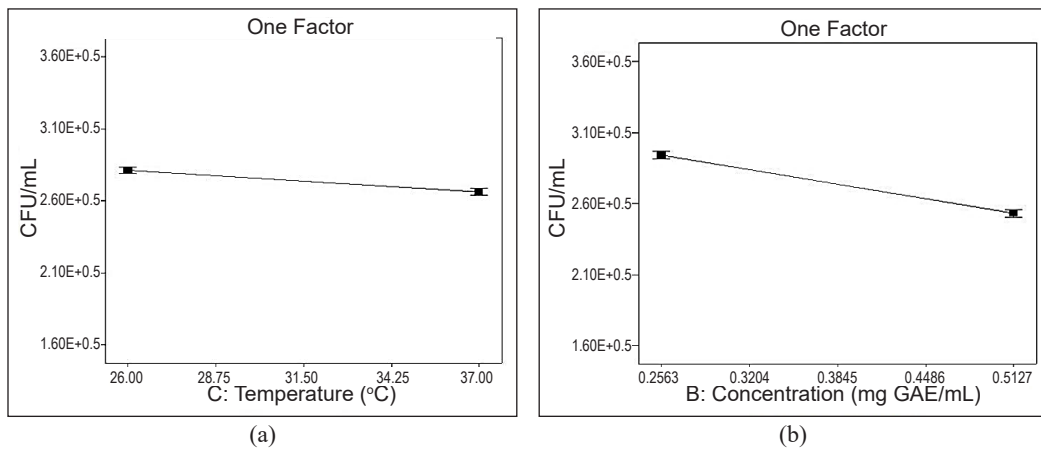


Figure 2. Factors on CFU/mL (a) C (temperature) and (b) B (TPC concentration)

From Figure 2(a), CFU/mL was slightly decreased with the increasing temperature from 26 to 37 °C. Higher temperatures cause the biofilm's thickness and no longer protect the microbe (Reichhardt et al., 2014). Figure 2(b) shows that CFU/mL decreased when the concentration of TPC increased from 0.256 to 0.513 mg GAE/mL. A higher concentration of TPC could increase the number of antioxidants, resulting in a higher inhibitory effect (Lobo et al., 2010).

Figure 3 illustrates the most significant interaction effect between microbial inhibition time and PLJ/M (v/v) (Factor AD) and also the concentration of TPC and temperature (Factor BC). As can be seen in Figure 3(a), the interaction effect of Factor AD indicates that the CFU/mL value was lower for 1:3 (PLJ/M) (v/v) when microbial inhibition time was 5 h and lower for 1:1 (PLJ/M) (v/v) when microbial inhibition time was 0.5 h. As for the interaction effect between Factor BC [Figure 3(b)], the temperature of 37 °C contributed to reducing CFU/mL when the concentration of TPC was 0.5127 mg GAE/mL. However, a temperature of 26 °C does not affect the CFU/mL at low and high TPC concentrations in PLJ. This claim was supported by Hajdu et al. (2010), in which an increase in the temperature of antimicrobial agents in certain plant-related infection treatments led to a higher decrease in microbe growth. It could be due to a decrease in the thickness of the microbe biofilm caused by the high temperature that triggers the release of the cells from the biofilm. The biofilm appears as a host defense for the microbes and acts as a protective barrier against antimicrobial agents (Reichhardt et al., 2014).

Additional research needs to be done to understand better how PLJ can act as an effective MGI agent and thus enhance maximum microbial growth inhibition. In order to construct substantially improved models, the CCD enables further assistance in optimizing the conditions of the variables identified in a factorial study. It also reduces the number of experimental runs required while giving the most powerful effect on the inhibition of microbial growth.

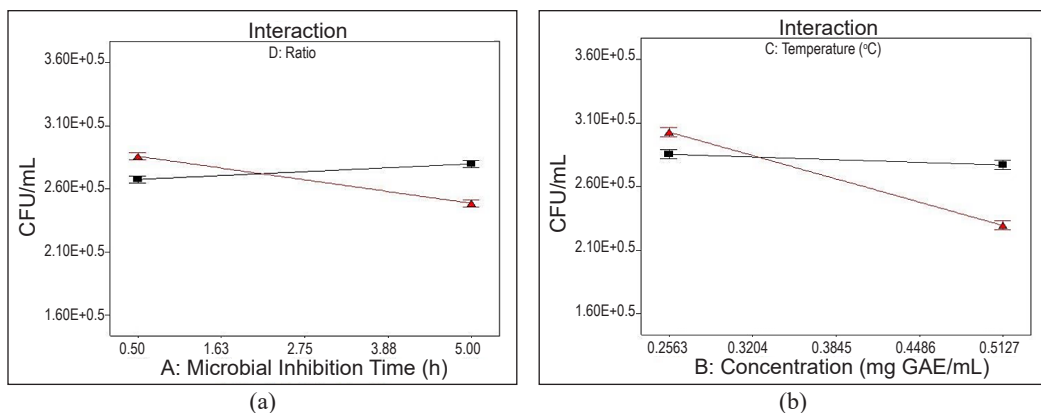


Figure 3. Interaction effects on CFU/mL (a) Factor AD (microbial inhibition time–ratio) and (b) Factor BC (concentration–temperature)

Optimization Study

The RSM method optimized the process parameters of the best conditions obtained from TLFD screening. The best conditions obtained were 0.5 h of microbial inhibition time, 0.5127 mg GAE/mL of concentration of TPC in PLJ, the temperature of 37 °C, and a 1:1 ratio of PLJ to microbe (PLJ/M) (v/v). For factorial analysis, the range and values used were higher than optimization, which used a smaller range and values. In order to assess the optimum conditions, the range and values chosen for optimization were smaller with temperature (35–39 °C) and microbial inhibition time (10–50 min). Temperature and microbial inhibition time are two major factors governing microbial growth inhibition. These factors can be systematically optimized with CCD. Thirteen experimental runs using the design shown in Table 8 with varying temperatures and microbial inhibition times were carried out. A model was developed to describe the microbial growth inhibition caused by independent variable levels (coded) and actual levels, as shown in Equations 5 and 6. X_1 was the temperature (°C), and x_2 was the microbial inhibition time (h).

$$\begin{aligned} \text{CFU (coded)} = & 64761.63 - 80544.01x_1 - 25333.17x_2 - 5071.98x_1x_2 \\ & + 94855.91x_1^2 + 55041.41x_2^2 \end{aligned} \quad (5)$$

$$\begin{aligned} \text{CFU (actual)} = & 7.69\text{E}+007 - 46201.62x_1 - 4.083\text{E}+006x_2 - 507.20x_1x_2 \\ & + 948.56x_1^2 + 55041.41x_2^2 \end{aligned} \quad (6)$$

From the analysis of variance (ANOVA) in Table 9, the regression analysis revealed a good fit of the experimental results to the polynomial model with a regression coefficient

Table 8
Experimental data of optimization study

Run	Factor A: Microbial inhibition time (min)	Factor B: Temperature (°C)	Response 1: CFU (CFU/mL)	Response 2: Microbial growth inhibition (%)
1	20.00	36.00	2.38×10^5	58.26
2	40.00	36.00	2.07×10^5	63.70
3	20.00	38.00	1.89×10^5	66.88
4	40.00	38.00	1.37×10^5	75.87
5	10.00	37.00	6.76×10^5	18.43
6	50.00	37.00	2.33×10^5	59.01
7	30.00	35.00	3.42×10^5	40.08
8	30.00	39.00	2.49×10^5	56.31
9	30.00	37.00	3.37×10^4	94.09
10	30.00	37.00	3.39×10^4	94.05
11	30.00	37.00	8.70×10^4	84.74
12	30.00	37.00	8.78×10^4	84.62
13	30.00	37.00	1.24×10^5	78.20

Table 9
ANOVA of optimization study

	Sum of Squares	df	Mean Square	F-Values	P-Values	Prob > F
Model	3.115E+011	5	6.230E+010	14.30	0.0015	significant
A: Microbial Inhibition Time	7.785E+010	1	7.785E+010	17.87	0.0039	
B: Temperature	7.701E+009	1	7.701E+009	1.77	0.2254	
AB	1.029E+008	1	1.029E+008	0.024	0.8822	
A ²	2.062E+011	1	2.062E+011	47.31	0.0002	
B ²	6.942E+010	1	6.942E+010	15.93	0.0052	
Residual	3.050E+010	7	4.358E+009			
Lack of Fit	2.438E+010	3	8.125E+009	5.30	0.0704	not significant
Pure Error	6.128E+009	4	1.532E+009			
Cor. Total	3.420E+010	12				
R ²	0.9108					
Adjusted R ²	0.8471					

(R²) value of 0.9108 and model F-value of 14.30. At the same time, the adjusted R² was 0.8471. Lee and Lemieux (2010) suggested that R² should be at least 0.80 to get a good fit. The ANOVA model significantly affects microbial inhibition with a p-value of 0.0015 (< 0.05) and a confidence level greater than 90%. With p-values of 0.2254 and 0.8822, respectively, the interactions between temperature and microbial growth inhibition in CFU/mL were insignificant. The p-value of 0.0039 shows that the microbial inhibition time was a significant factor in the microbial growth inhibition.

The association between the actual values of CFU/mL and predicted values of CFU/mL as microbial inhibition response was illustrated in Figure 4. Figure 5 shows the influence of two main factors on CFU/mL. These plots illustrate the influence of temperature and microbial inhibition time on CFU/mL. By increasing the timing of microbial inhibition from 20–30 min, CFU/mL was also decreased [Figure 5(a)]. This result shows that the increase influenced the CFU/mL value at microbial inhibition. Pineapple leaves contain seven significant phenolic compounds, including methyl-5-O-caffeoyl-quinic acid, octahydrocurcumin, meliadanoside A, stilbostemin D, feralolide, agrimol C and kukoamine A (Ya'acob et al., 2021). According to Hoskeri et al. (2012), phenolic compounds have potency as an agent against some microbes after 10 min.

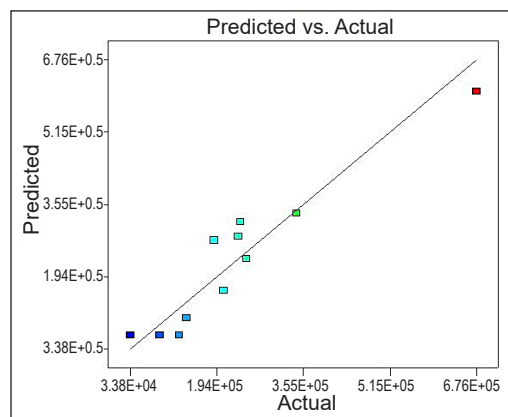


Figure 4. Actual and predicted values

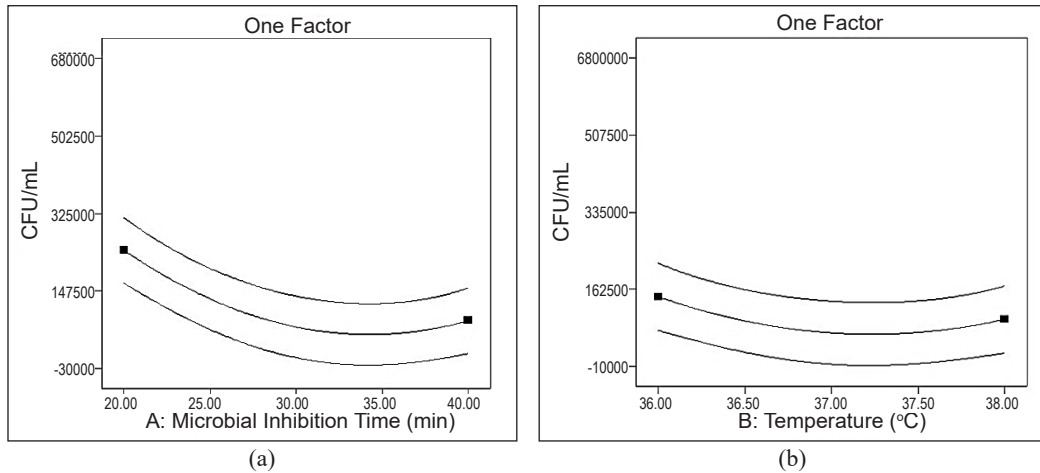


Figure 5. Effect of one factor on CFU/mL (a) microbial inhibition time and (b) temperature

It may be the shortest amount of time these seven phenolic compounds need to inhibit the microbe effectively. However, from 35 to 40 min, CFU/mL was increased, probably due to the loss of some phenolic compounds, thus making it ineffective to inhibit. A study by Zhang et al. (2021) stated that change could be explained by the different degradation rates and/or synthesis of each phenolic. Different phenolic have different chemical structures and present different structures in different fractions, such as free and bound phenolic fractions. Structural difference plays an important role in individual reducing capacity. The phenolic compound was sensitive to the presence of oxygen at ambient temperature. The yield of phenolic compounds increased during storage time due to the release of free acids from their bonds (Klimczak et al., 2007). The oxidation reaction is one of the processes that can cause modification of extracted pineapple leaves juice during storage (Zafrilla et al., 2003). In Figure 5(b), 37 °C was found optimum for temperature. The temperature did not significantly affect the CFU/mL value, as there was only a slight difference between the CFU/mL values from 35–39 °C. The result was validated by a 0.2254 *p*-value obtained from ANOVA. Thus, 37 °C was adequate to inhibit the process of microbial growth. At this temperature, plant microbes can be killed (Eddleman, 1998).

The contour and three-dimensional response surface plots of microbial growth inhibition in CFU/mL are shown in Figure 6. The surface plots [Figure 6(a)] show that the variables interacted significantly. The contour plot [Figure 6(b)] showing the interaction between the factors helps in the selection of variable ranges to accomplish the goal of targeted optimization (Zhang et al., 2012). Decreasing CFU/mL shows a higher inhibition of microbial growth. The data obtained show the optimum conditions of 37 °C and microbial inhibition time of 34.25 min resulted in maximum microbial growth inhibition of 94.73% and 9.12×10^4 CFU/mL. López-García et al. (2012) studied that bromelain extract from pineapple stems could inhibit 90% of *F. verticillioides* growth. The experimental response

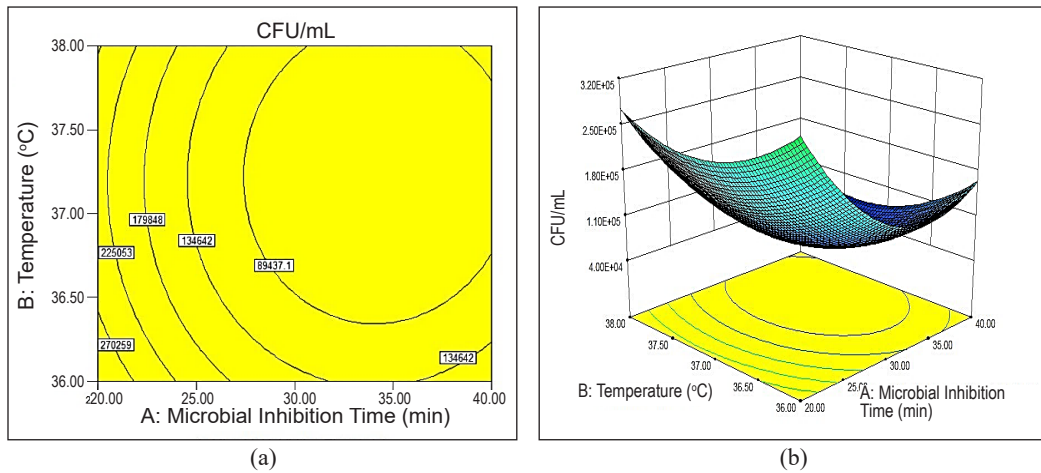


Figure 6. Contour and 3D surface plot (a) Contour plot and (b) 3D response surface plot

obtained (94.73%) based on the modeled optimum conditions was reasonably close to the predicted response.

Optimum Conditions

Table 10 presents the optimum conditions suggested by the Design Expert. Microbial growth inhibition by up to 91.65% was obtained at temperature and inhibition time of 37 °C and 34.25 min, respectively. Table 11 indicates the predicted and experimental values of microbial growth inhibition. The optimum conditions were experimentally verified with 94.73% of microbial growth inhibition, corresponding to a percentage error of 1.73% to 8.03%. The error was acceptable as the error percentage was less than 10%. The microbial growth inhibition obtained from the best conditions of factorial analysis was 21.74%. Compared to optimum conditions obtained by optimization, the percentage of microbial inhibition was increased to 94.73%. These results show a better increment of microbial inhibition than the optimization process could achieve.

Table 10
Suggested optimum condition

Factors and responses	Values
A: Microbial Inhibition Time	34.25 min
B: Temperature	37 °C
CFU/mL	4.77×10^4 CFU/mL
Microbial growth inhibition (%)	91.65%

Table 11
Predicted and experimental microbial growth inhibition (%)

Runs	Microbial growth inhibition (%)		Error (%)
	Predicted	Experimental	
Run 1	91.65	90.06	1.73
Run 2	91.65	94.73	3.36
Run 3	91.65	84.29	8.03

CONCLUSION

This study focuses on understanding the effects of several factors involved in microbial inhibition growth by applying the microbial growth inhibitor (MGI). Based on the Full Factorial Design Analysis (FFD), microbial inhibition time, the concentration of TPC, and temperature were found to significantly contribute to the microbial growth inhibition process with contribution percentages of 1.07%, 1.27%, and 1.56%, respectively. The best condition for microbial inhibition of 21.74% was achieved at PLJ/M of 1:1, 0.5127 mg GAE/mL of TPC concentration, and at 37 °C for 0.5 h of microbial inhibition time. The major factors contributing to the inhibition of microbial growth were further optimized through a central composite design (CCD). The quadratic model involving temperature and microbial inhibition time was best fitted to predict the microbial growth inhibition process. The maximum microbial growth inhibition was 94.73%. The microbe was most effectively inhibited at an optimum temperature and inhibition time of 37 °C and 34.25 min. It can be concluded that the maximum microbial growth inhibition was increased from 21.74% to 94.73% using the optimization process. This study shows that PLJ can be an alternative natural MGI from plant sources with microbial growth inhibition properties.

ACKNOWLEDGEMENTS

The authors thank the Universiti Malaysia Pahang for financial assistance through a research grant with RDU1903131.

REFERENCES

- Ammer, M. R., Zaman, S., Khalid, M., Bilal, M., Erum, S., Huang, D., & Che, S. (2016). Optimization of antibacterial activity of *Eucalyptus tereticornis* leaf extracts against *Escherichia coli* through response surface methodology. *Journal of Radiation Research and Applied Sciences*, 9(4), 376-385. <https://doi.org/10.1016/j.jrras.2016.05.001>
- Arshad, M. S., & Batool, S. A. (2017). Natural antimicrobials, their sources and food safety. In D. N. Karunaratne & G. Pamunuwa (Eds.), *Food Additives* (pp. 87-104). InTech. <https://doi.org/10.5772/intechopen.70197>
- Asim, M., Abdan, K., Jawaid, M., Nasir, M., Dashtizadeh, Z., Ishak, M. R., & Hoque, M. E. (2015). A review on pineapple leaves fibre and its composites. *International Journal of Polymer Science*, 2015, Article 950567. <https://doi.org/10.1155/2015/950567>
- Aydar, A. Y. (2018). Utilization of response surface methodology in optimization of extraction of plant materials. In V. Silva (Ed.), *Statistical Approaches with Emphasis on Design of Experiments Applied to Chemical Processes* (pp. 157-169). IntechOpen. <https://doi.org/10.5772/intechopen.73690>
- Domínguez, C. R., Avila, J. A. D., Pareek, S., Ochoa, M. A. V., Zavala, J. F. A., Yahia, E., & González-Aguilar, G. A. (2018). Content of bioactive compounds and their contribution to antioxidant capacity during ripening of pineapple (*Ananas comosus* L.) cv. Esmeralda. *Journal of Applied Botany and Food Quality*, 91, 61-68. <https://doi.org/10.5073/JABFQ.2018.091.009>

- Eddleman, H. (1998). *Optimum temperature for growth of bacteria*. Indiana Biolab Palmyra IN.
- Hajdu, S., Holinka, J., Reichmann, S., Hirschl, A. M., Graninger, W., & Presterl, E. (2010). Increased temperature enhances the antimicrobial effects of daptomycin, vancomycin, tigecycline, fosfomicin, and cefamandole on staphylococcal biofilms. *Antimicrobial Agents and Chemotherapy*, *54*(10), 4078-4084. <https://doi.org/10.1128/AAC.00275-10>
- Hoskeri, J., Krishna, H., Jignesh, V., Roshan, S., & Vijay, S. (2012). In-silico drug designing using β -sitosterol isolated from *Flaveria trinervia* against peptide deformylase protein to hypothesize bactericidal effect. *International Journal of Pharmacy and Pharmaceutical Sciences*, *4*, 192-196.
- Jayarathne, D. L., & Dayarathna, M. T. A. (2015). Phenotypic variability of ceratocystis paradoxa isolated from North Western and Western Provinces of Sri Lanka and its bio control by potential bio-control agent; *Trichoderma viride*. *Coconut Research & Development Journal*, *31*(2), 10-10. <https://doi.org/10.37833/cord.v31i2.61>
- Klimczak, I., Małecka, M., Szlachta, M., & Gliszczyńska-Świątło, A. (2007). Effect of storage on the content of polyphenols, vitamin C and the antioxidant activity of orange juices. *Journal of Food Composition and Analysis*, *20*(3-4), 313-322.
- Lee, D. S., & Lemieux, T. (2010). Regression discontinuity designs in economics. *Journal of Economic Literature*, *48*(2), 281-355. <https://doi.org/10.1257/jel.48.2.281>
- Lobo, V., Patil, A., Phatak, A., & Chandra, N. (2010). Free radicals, antioxidants and functional foods: Impact on human health. *Pharmacognosy Reviews*, *4*(8), 118-126. <https://doi.org/10.4103/0973-7847.70902>
- López-García, B., Hernández, M., & Segundo, B. S. (2012). Bromelain, a cysteine protease from pineapple (*Ananas comosus*) stem, is an inhibitor of fungal plant pathogens. *Letters in Applied Microbiology*, *55*(1), 62-67. <https://doi.org/10.1111/j.1472-765X.2012.03258.x>
- Maqsood, S., Benjakul, S., Abushelaibi, A., & Alam, A. (2014). Phenolic compounds and plant phenolic extracts as natural antioxidants in prevention of lipid oxidation in seafood: A detailed review. *Comprehensive Reviews in Food Science and Food Safety*, *13*(6), 1125-1140. <https://doi.org/10.1111/1541-4337.12106>
- Noormohamadi, H. R., Fat'hi, M. R., Ghaedi, M., Azizzadeh, S., & Nobakht, V. (2018). Mechanochemically synthesized Ag (I) coordination polymer as a new adsorbent and its application to ultrasound assisted wastewater treatment via the central composite design: Isotherm and kinetic studies. *Journal of Molecular Liquids*, *262*, 71-77. <https://doi.org/10.1016/j.molliq.2018.04.042>
- O'Toole, G. A. (2016). Classic spotlight: Plate counting you can count on. *Journal Bacteriol*, *198*(23), 3127-3127. <https://doi.org/10.1128/JB.00711-16>.
- Reichhardt, C., Lim, J. Y., Rice, D., Fong, J. N., & Cegelski, L. (2014). Structure and function of bacterial biofilms by solid-state NMR. *Biophysical Journal*, *106*(2), Article 192a.
- Saunders, L. J., Russell, R. A., & Crabb, D. P. (2012). The coefficient of determination: What determines a useful R2 statistic? *Investigative Ophthalmology & Visual Science*, *53*(11), 6830-6832. <https://doi.org/10.1167/iovs.12-10598>
- Shane, H. (2017). *What is the Purpose of Factor Analysis?* Sciencing. <https://sciencing.com/what-is-the-purpose-of-factor-analysis-12225143.html>

- Siddiqui, N., Rauf, A., Latif, A., & Mahmood, Z. (2017). Spectrophotometric determination of the total phenolic content, spectral and fluorescence study of the herbal Unani drug Gul-e-Zoofa (*Nepeta bracteata* Benth). *Journal of Taibah University Medical Sciences*, 12(4), 360-363. <https://doi.org/10.1016/j.jtumed.2016.11.006>
- Ya'acob, A., Zainol, N., Ridza, P. N. Y. M., Mortan, S. H., & Samad, K. A. (2021). Pineapple leaf juice characterization and evaluation of factors affecting microbial growth inhibition. *Biocatalysis and Agricultural Biotechnology*, 37, Article 102158. <https://doi.org/10.1016/j.bcab.2021.102158>
- Zafrilla, P., Morillas, J., Mulero, J., Cayuela, J. M., Martínez-Cachá, A., Pardo, F., & López Nicolás, J. M. (2003). Changes during storage in conventional and ecological wine: Phenolic content and antioxidant activity. *Journal of Agricultural and Food Chemistry*, 51(16), 4694-4700.
- Zainol, N., & Rahim, S. R. (2017). Factorial analysis on *Bacillus* Sp. removal using garlic solution. *Journal of Chemical Engineering and Industrial Biotechnology*, 1(1), 18-28. <https://doi.org/10.1088/1757-899X/342/1/012037>
- Zhang, Q. Y., Zhou, W. W., Zhou, Y., Wang, X. F., & Xu, J. F. (2012). Response surface methodology to design a selective co-enrichment broth of *Escherichia coli*, *Salmonella* spp. and *Staphylococcus aureus* for simultaneous detection by multiplex PCR. *Microbiological Research*, 167(7), 405-412. <https://doi.org/10.1016/j.micres.2012.02.003>
- Zhang, Y., Truzzi, F., D'Amen, E., & Dinelli, G. (2021). Effect of storage conditions and time on the polyphenol content of wheat flours. *Processes*, 9(2), Article 248. <https://doi.org/10.3390/pr9020248>



Short Communication

***Canarium odontophyllum* Miq. (Dabai) Leaf Phytoextracts and Their Medicinal Properties**

Muhammad Wahizul Haswan Abdul Aziz^{1,2}, Siti Fathiah Masre¹, Dayang Fredalina Basri³ and Ahmad Rohi Ghazali^{1*}

¹Centre for Toxicology and Health Risk Studies (CORE), Faculty of Health Sciences, Universiti Kebangsaan Malaysia, 50300 UKM, Kuala Lumpur, Malaysia

²Department of Para-clinical Sciences, Faculty of Medicine and Health Sciences, Universiti Malaysia Sarawak, 94300 UNIMAS, Kota Samarahan, Sarawak, Malaysia

³Centre for Diagnostic, Therapeutic & Investigative Studies (CODTIS), Faculty of Health Sciences, Universiti Kebangsaan Malaysia, 50300 UKM Kuala Lumpur, Malaysia

ABSTRACT

Canarium odontophyllum Miq., renowned locally as “dabai,” is an endemic plant in Sarawak, Malaysia. Most people, especially in rural areas, consume this plant to maintain their health. A few medicinal studies have investigated *C. odontophyllum* Miq.’s biological properties to substantiate its use as nutraceuticals and health supplements. Crude extracts from *C. odontophyllum* Miq. demonstrated various medicinal properties, including antibacterial, antimalarial, antioxidant, anticancer, antidiabetic, and antihypertensive. In addition, numerous phytoextracts studies have revealed the existence of a variety of beneficial compounds, including flavonoids, tannins, and terpenoids. However, despite various biological activities of *C. odontophyllum* Miq., there is currently no analysis summarizing the medicinal properties of its leaf. Thus, this short communication attempts to narrate the medicinal properties of *C. odontophyllum* Miq. leaf and their phytoextracts

responsible. In conclusion, we summarized *C. odontophyllum* Miq. leaf promising therapeutic effects with their phytoextracts and a step closer to developing it as potential nutraceuticals and health supplements to fulfill social interest.

ARTICLE INFO

Article history:

Received: 24 June 2021

Accepted: 01 November 2021

Published: 25 May 2022

DOI: <https://doi.org/10.47836/pjst.30.3.20>

E-mail addresses:

amwhaswan@unimas.my (Muhammad Wahizul Haswan Abdul Aziz)

sitifathiah@ukm.edu.my (Siti Fathiah Masre)

dayang@ukm.edu.my (Dayang Fredalina Basri)

rohi@ukm.edu.my (Ahmad Rohi Ghazali)

* Corresponding author

Keywords: *Canarium odontophyllum* Miq., dabai, flavonoids, medicinal properties, phytoextracts, terpenoids

INTRODUCTION

Borneo, Asia's largest island, is split politically between three countries: Malaysia, Brunei, and Indonesia to the north and south. The East Malaysian states of Sabah and Sarawak make up about 26% of the island in the north. Borneo is home to one of the world's oldest rainforests, rich in biodiversity and providing a plentiful supply of fruits and vegetables, especially in rural areas. Over the centuries, older generations have used wild plants for medicinal purposes, especially in traditional medicine. It is because they are rich sources of biologically active compounds. However, wild plants have been neglected over time, and the full potential use of the plants is not well explored. Plants are the main source for drug development, according to Craig (1999), and about 80% of the world's population uses plant extracts as conventional medicine for their immediate health care needs. *Canarium odontophyllum* Miq. or renowned locally as "dabai," is an endemic plant in Sarawak, Malaysia, and devoured as a snack food by the natives to maintain health and well-being (Latiff et al., 2000). However, *C. odontophyllum* Miq. is classified as an underutilized fruit and has not been fully explored due to lack of promotion. Our literature survey showed that only several scientific studies had been conducted to date to investigate the medicinal properties of *C. odontophyllum* Miq. leaf (Figure 1).

Hence, the present short communication attempts to narrate the medicinal properties of *C. odontophyllum* Miq. leaf and their phytoextracts to establish a scientific foundation for the medicinal use of *C. odontophyllum* Miq. leaf as nutraceuticals.



Figure 1. *Canarium odontophyllum* Miq. leaf

METHODOLOGY

This study was created by collecting and consulting recent articles on *C. odontophyllum* Miq. Leaf's medicinal uses and scientific evidence. Journals and electronic databases from PubMed, Elsevier, Google Web, Google Scholar, Web of Science, and Springer were used to gather all the knowledge about the leaf of this plant. Only texts written in English from January 2014 to December 2020 were considered for this study. Search on *C. odontophyllum* Miq. was done using combinations of keywords, including: '*Canarium odontophyllum* Miq.,' '*C. odontophyllum* leaf,' 'biological activity,' 'phytoconstituents,' 'phytochemical,' and 'phytoextract.' The plant's scientific name was validated using The Plant List (www.theplantlist.org). The structural formulae were drawn and checked from Chemspider (<https://www.chemspider.com>) and PubChem (<https://pubchem.ncbi.nlm.nih.gov/>) based on the reported chemical constituents from *C. odontophyllum* Miq.

MEDICINAL PROPERTIES OF *C. odontophyllum* Miq. LEAF

As outlined in Table 1, results from various studies indicated that *C. odontophyllum* Miq. leaf possessed many potentials, including antibacterial, antimalarial, antioxidant, anticancer, hypoglycemic, and vasorelaxant properties.

Antioxidant Capacity

The initial study to investigate the antioxidant efficacy of *C. odontophyllum* Miq. leaf was performed by Basri et al. (2014). The ferric reducing/antioxidant power (FRAP) assay screened the *C. odontophyllum* Miq. leaf aqueous, methanol, and acetone extracts antioxidant capacity. All *C. odontophyllum* Miq. leaf extracts were found to exhibit dose-dependent antioxidant potential. Acetone extract exhibited the uppermost antioxidant capacity of 355.26 $\mu\text{M FeSO}_4 \cdot 7\text{H}_2\text{O}$ at 50 $\mu\text{g/ml}$. In contrast, methanol extract exhibited moderate antioxidant activity (281.15 $\mu\text{M FeSO}_4 \cdot 7\text{H}_2\text{O}$ at 50 $\mu\text{g/ml}$) (no significant difference from that acetone extract), followed by aqueous extract with 140.29 $\mu\text{M FeSO}_4 \cdot 7\text{H}_2\text{O}$ at 50 $\mu\text{g/ml}$. Preliminarily, their findings showed that *C. odontophyllum* Miq. leaf extracts could provide a natural source of antioxidant constituents for medical use and health benefits. Furthermore, Budin et al. (2018) demonstrated that the *C. odontophyllum* Miq. leaf aqueous extract possesses the capability to decrease oxidative stress markers [malondialdehyde (MDA) reduced by 15.38%, protein carbonyl reduced by 35.26%, glutathione (GSH) increased by 12.5%, superoxide dismutase (SOD) increased by 20.29% and glutathione peroxidase (GPx) increased by 10.53%] in streptozotocin-induced diabetic rat's liver. This antioxidant capacity opened a wide possibility of more medicinal properties of the leaf.

Antibacterial Effects

Antibacterial derived from plants has immense medicinal potential, as they could fulfill the role with fewer adverse effects that are frequently related to synthetic antimicrobials. Today, continuous further discovery and production of antibacterial plant-derived products are needed. Basri and Nor (2014) performed *in vitro* antibacterial activity of *C. odontophyllum* Miq. and found methanol and acetone leaf extracts effective (MIC value 0.195 mg/ml) against *Staphylococcus aureus* ATCC 25923. Several studies on acetone and methanol extracts showed that methicillin-resistant *Staphylococcus aureus* (MRSA) was sensitive to the extracts (Basri & Sandra, 2016; Basri et al., 2016; Shamsuddin et al., 2018). However, more research is needed to identify and isolate the antibacterial compounds from the *C. odontophyllum* Miq. leaf. Thus, the leaf extract could open more possibilities to discover new, clinically useful antibacterial compounds.

Table 1
Reported medicinal properties of *Canarium odontophyllum* Miq. leaf

Medicinal properties	Solvent of extract(s)	Experimental model	Result	Conclusion	Researchers (Year)
Antioxidant	Aqueous Methanol Acetone	FRAP assay was done on aqueous, methanol, and acetone extracts to screen theirs in vitro antioxidant capacity.	All leaf extracts exhibited dose-dependent antioxidant potential with acetone extract (highest), methanol extract (moderate), and aqueous extract (lowest antioxidant power).	Preliminarily shown that <i>C. odontophyllum</i> leaf extracts contain antioxidant constituents.	Basri et al. (2014)
	Aqueous	The diabetic induced rats were treated with the extract (300 mg/kg/day for 28 days) in comparison to the control group. In addition, for diabetic induction, 65 mg/kg of streptozotocin (STZ) was given intravenously.	Oxidative stress testing indicated lower protein carbonyl and MDA levels, significantly ($p < 0.05$) elevated activity of GSH, GPx, and SOD than the untreated diabetic group.	<i>C. odontophyllum</i> leaf aqueous extract protects against liver damage in diabetic rats.	Budin et al. (2018)
Antibacterial	Methanol Acetone	For growth inhibition, the extracts were tested against <i>Bacillus cereus</i> , <i>Staphylococcus aureus</i> , <i>Escherichia coli</i> , and <i>Pseudomonas aeruginosa</i> .	Methanol and acetone extract inhibited <i>S. aureus</i> growth.	Both extracts contain potentially therapeutic compounds against <i>S. aureus</i> .	Basri and Nor (2014)
	Methanol Acetone	The broth microdilution method was used to test the antibacterial properties of extracts against MRSA.	Minimum inhibitory concentrations (MIC) values obtained were 312.5 µg/mL (methanol) and 156.25 µg/mL (acetone). Minimum bactericidal concentrations (MBC) were 625 µg/mL (methanol) and 312.5 µg/mL (acetone).	Both extracts showed the anti-MRSA effect that is comparable to vancomycin.	Basri and Sandra (2016)

Table 1 (continue)

Medicinal properties	Solvent of extract(s)	Experimental model	Result	Conclusion	Researchers (Year)
	Acetone	Post-antibiotic effect (PAE) was done for extract against MRSA ATCC 33591. In addition, MIC and MBC values were determined.	With an identical MIC and MBC value of 1250 g/ml, <i>C. odontophyllum</i> leaf acetone extract was bactericidal against MRSA ATCC 33591. In addition, the extract demonstrated extended PAE time (0.85 ± 1.74 hours) compared to oxacillin (0.18 ± 2.43 hours) against MRSA.	Extract exhibited bacteriostatic activity as well as a long-lasting antibacterial effect.	Basri et al. (2016)
	Acetone	MIC, MBC, and TKA analyses against MRSA (ATCC 33591 and Mu50).	MIC/MBC ratio showed the bacteriostatic effect of extract against both MRSA strains. The extract inhibited MRSA growth at low concentrations.	The extract inhibited the growth of MRSA and might be explored as an anti-MRSA agent.	Shamsuddin et al. (2018)
Antimalarial	Methanol	Ex-vivo antimalarial activity of extracts (methanol, acetone, and aqueous) was evaluated on <i>Plasmodium berghei</i> NK65 infected erythrocytes. In addition, Plasmodium lactate dehydrogenase (pLDH) and SYBR green I fluorescence assay were done.	Methanol extract showed the lowest IC ₅₀ values (0.0004 µg/ml) from pLDH Assay and SYBR green I fluorescence assay (0.002 µg/ml) compared to positive control chloroquine 0.0011 µg/ml (pLDH assay) and 0.029 µg/ml (SYBR green I fluorescence assay).	<i>C. odontophyllum</i> leaf methanol extract showed promising antimalarial activity and could be developed into a schizonticidal agent.	Ishak et al. (2020)
Cytotoxic/ Anticancer	Methanol Acetone Aqueous	Cytotoxicity (MTT assay) of extracts against human colorectal carcinoma cells HCT 116 was carried out.	After a 24-hour treatment with extracts, IC ₅₀ values were obtained (methanol 0.10 ± 0.011 mg/mL, acetone 0.08 ± 0.003 mg/mL, aqueous 0.40 ± 0.162 mg/mL).	According to this preliminary finding, <i>C. odontophyllum</i> leaf extracts have promising anticancer properties.	Basri et al. (2015)

Table 1 (continue)

Medicinal properties	Solvent of extract(s)	Experimental model	Result	Conclusion	Researchers (Year)
	Acetone	The Ames test was used to determine the extract mutagenicity and antimutagenicity.	No mutagenesis activity was detected from the extract. However, the presence of the metabolic activator S9 system resulted in the highest antimutagenic action with inhibition of 62.38% (TA98) and 58.24% (TA100).	<i>The extract had strong inhibitory effects on mutagenicity; and it also showed antimutagenic activity and, therefore, could be developed as an anticancer agent.</i>	Ghazali et al. (2017)
Antidiabetic	Aqueous	Diabetic-induced rats were treated with extract orally 300 mg/kg/day for 28 days compared to diabetic control. In addition, 65 mg/kg of STZ was given intraperitoneally to induce diabetes.	The extract-treated diabetic group had lower ($p<0.05$) fasting blood glucose levels than the diabetic control.	The aqueous extract can reduce blood glucose levels.	Saari et al. (2017)
Vasorelaxation/ Antihypertension	Aqueous	Isolated thoracic aortic rings were positioned between two tungsten wires coupled to an isometric force transducer after being suspended in a tissue bath. A data capture system was used to record the changes in tension.	The extract elicited relaxation in endothelium-intact and endothelium-denuded aortic rings.	The extract has a vasorelaxant effect mediated by the inhibition of calcium channels.	Basri et al. (2018)

Antimalarial

We cannot afford to ignore the hunt for antimalarial drugs derived from plant sources. Furthermore, essential antimalarial medications today, such as artemisinin and quinine, have been isolated from plants (Bhatnagar & Das, 2007). Similarly, the *C. odontophyllum* Miq. methanol leaves extract showed the lowest plasmodium lactate dehydrogenase (pLDH) assay half-maximal inhibitory concentration (IC₅₀) values. It was the most potent against the schizont stage of *Plasmodium berghei* NK65. The methanol extract also exhibits promising antimalarial activity and the potential to be a schizonticidal agent (Ishak et al., 2020).

Anticancer Agents

Many attempts have also been made to find the correlation between the phytoextracts' antioxidant properties and their potential for anticancer. While no conclusive evidence of such correlation has been found, it has been suggested that phytoextracts antioxidant activity is also an indicator of its anticancer potential. The dabai fruit has excellent potential to be exploited as a nutraceutical due to its nutrient-rich and antioxidant capabilities. Thus, the initial study to investigate the antioxidant efficacy in leaf extracts of *C. odontophyllum* Miq. was done by Basri et al. (2014). In another preliminary study, all three extracts showed cytotoxic activity after 24 hrs treatment with acetone extract at an IC₅₀ value of 0.08 ± 0.003 mg/mL against human colorectal cancer cells (HCT 116) compared to methanol and aqueous extracts with IC₅₀ values of 0.10 ± 0.011 mg/mL and 0.40 ± 0.162 mg/mL, respectively (Basri et al., 2015). These studies could provide an insight into its promising anticancer activity. Furthermore, the extract may also be developed as a chemopreventive agent based on its significant antimutagenic activity demonstrated, where *C. odontophyllum* Miq. leaf acetone extract in the presence of the metabolic activator S9 system with inhibition percentage greater than 50% in both bacteria *Salmonella typhimurium* strains TA98 and TA100 (Ghazali et al., 2017).

Antidiabetic

The aqueous extract of *C. odontophyllum* Miq. leaf (300 mg/kg for 28 days) induced a significant reduction in glucose level. The fasting blood glucose of the diabetic group treated with *C. odontophyllum* Miq. was significantly lower than the diabetic group ($p < 0.05$). The original manuscript stated no exact values, but according to their bar chart, the values were roughly 34 mmol/L and 21 mmol/L for the diabetic and treated groups, respectively. The discovery implied that the *C. odontophyllum* Miq. leaf aqueous extract could lower blood glucose levels in diabetic rats (Saari et al., 2017). *C. odontophyllum* Miq. leaf could also be exploited as a new prospective with many medicinal properties in nutraceutical products.

Vasorelaxation and Antihypertensive

With the elevated incidence of hypertension, researchers aim for alternative therapies from plant origins for their phytoextract compounds with vasorelaxant and hypotensive properties. The aqueous extract of *C. odontophyllum* Miq. leaf was studied on isolated thoracic aortic rings suspended in a tissue bath. The extract had an EC₅₀ of 5.89 mg/ml in the endothelium-denuded aorta ring and 8.36 mg/ml in the endothelium-intact aortic ring. The extract (3–15 mg/ml) induced relaxation in endothelium-intact and endothelium-denuded aortic rings precontracted with phenylephrine. Therefore, the study suggested that the vasorelaxant effect of the extract was endothelium-independent and could be developed as a hypotensive agent (Basri et al., 2018).

MAJOR PHYTOEXTRACTS IN *C. odontophyllum* Miq. LEAF

Phytoextracts are naturally present in almost all plants. With fibers and nutrients, phytoextracts in plants serve as a protection mechanism against disease. Table 2 shows the phytoextracts in *C. odontophyllum* Miq. leaf. The major constituents of the extracts are flavonoids, tannins, and terpenoids. Flavonoids are compounds that possess many biological features that benefit human health. In diets, flavonoids supply an abundance of natural antioxidants to humans. In the best of situations, flavonoids neutralize free radicals' adverse effects and thereby tend to resist certain disorders. In addition, they interact with various cellular targets such as antioxidants and free-radical scavenger activities, providing anti-inflammatory, antiviral, antibacterial, anti-aging, and notably anticancer properties (Karak, 2019). Tannins are a type of polyphenolic compound with complex plant structures. Its molecular weights are typically greater than 500 Da. Several natural tannins and related compounds have been reported to have various medicinal activities, including antioxidant, antitumor, antidiabetic, and antibacterial (Zou et al., 2014; Pajari et al., 2016; Singh et al., 2018).

Terpenoids are secondary metabolites with carbon backbone-containing molecular structures of isoprene (2-methylbuta-1,3-diene) units. In growth and development, thousands of terpenoids produced by plants have no discernible role, thus classifying them as 'secondary' metabolites. Important medicinal activities are shown by the terpenoids group, such as antiviral, antibacterial, antimalarial, anti-inflammatory, cholesterol synthesis inhibition, and anticancer (Mahato & Sen, 1997). According to Basri and Nor (2014), saponin and phenolic compounds were only detected in methanol and aqueous extracts. None of the extracts contained alkaloids. However, there have yet been no single bioactive compounds extracted from *C. odontophyllum* Miq. leaf from all previous studies.

Table 2
Phytoextracts in Canarium odontophyllum Miq. leaf

Phytoextracts	Acetone	Methanol	Aqueous
Alkaloids	-	-	-
Flavonoids	+	+	+
Tannins	+	+	+
Terpenoids	+	+	+
Saponin	-	+	+
Phenolic compound	-	+	+

- = not detected, + = detected

HEALTH BENEFITS OF *C. odontophyllum* Miq. LEAF

Further laboratory research and clinical studies should be carried out to assess relevant biochemical markers and specific phytoextracts to understand the mechanism of medicinal actions. As for its anticancer properties, other investigatory activities must be carried out in several different animal tumor systems for more conclusive findings and further scientific validation. It is also essential to understand that *C. odontophyllum* Miq. can be effective in isolation and could have a potential effect when given in combination with other herbs or medicines. However, the review findings are very favorable for using *C. odontophyllum* Miq. leaf as a multi-purpose therapeutic agent. There are currently some limitations in the existing literature, and further clinical trials should be carried out to promote its use of remedial use, thus fulfilling social interest.

CONCLUSION

C. odontophyllum Miq. leaf possesses many medicinal properties. Their role is played by the phytoextracts found in the leaf itself. Therefore, *C. odontophyllum* Miq. leaf would offer promising therapeutic effects and, in the future, be developed as potential nutraceuticals and health supplements.

ACKNOWLEDGMENTS

Muhammad Wahizul Haswan Abdul Aziz and Ahmad Rohi Ghazali shared the conceptualization and analyzed the data. Dayang Fredalina Basri provided valuable input to the discussion. Muhammad Wahizul Haswan Abdul Aziz, Siti Fathiah Masre, and Ahmad Rohi Ghazali wrote and edited the manuscript. All authors critically revised the manuscript and approved the final manuscript.

REFERENCES

- Basri, D. F., & Nor, N. H. M. (2014). Phytoconstituent screening and antibacterial activity of the leaf extracts from *Canarium odontophyllum* Miq. *American Journal of Plant Sciences*, 5, 2878-2888. <https://dx.doi.org/10.4236/ajps.2014.519303>
- Basri, D. F., & Sandra, V. (2016). Synergistic interaction of methanol extract from *Canarium odontophyllum* Miq. leaf in combination with oxacillin against methicillin-resistant *Staphylococcus aureus* (MRSA) ATCC 33591. *International Journal of Microbiology*, 7, Article 5249534. <https://doi.org/10.1155/2016/5249534>
- Basri, D. F., Heng, K. Y., Meng, C. K., & Ghazali, A. R. (2014). Screening of antioxidant phytoextracts of *Canarium odontophyllum* Miq. leaves *in vitro*. *IOSR Journal of Pharmacy*, 4(12), 1-6. <http://iosrphr.org/papers/v4i12/Version-3/A041230106.pdf>
- Basri, D. F., Rahman, N. S., Ali, S. S., & Zainalabidin, S. (2018). The vasorelaxant effect of *Canarium odontophyllum* Miq. (dabai) extract in rat thoracic aorta. *Egyptian Journal of Basic and Applied Sciences*, 5, 75-79. <https://doi.org/10.1016/j.ejbas.2017.11.004>
- Basri, D. F., Shabry, A. S. M., & Meng, C. K. (2015). Leaves extract from *Canarium Odontophyllum* Miq. (dabai) exhibits cytotoxic activity against human colorectal cancer cell HCT 116. *Natural Products Chemistry & Research*, 3, 1-4. <https://doi.org/10.4172/2329-6836.1000166>
- Basri, D. F., Shamsuddin, N. A. M., & Ishak, S. F. (2016). Time-kill assay and post-antibiotic effect of acetone extract of *Canarium odontophyllum* leaves against methicillin-resistant *Staphylococcus aureus* (MRSA). *International Journal of Current Medical and Pharmaceutical Research*, 2(9), 630-635.
- Bhatnagar, S., & Das, P. (2007). Antimalarial activity in tropical plants: A review. *Journal of Herbs, Spices & Medicinal Plants*, 13(1), 103-132. https://doi.org/10.1300/J044v13n01_09
- Budin, S. B., Kumar, S., Warif, N. M. A., Saari, S. M., & Basri, D. F. (2018). Protective effect of aqueous extracts from *Canarium odontophyllum* Miq. leaf on liver in streptozotocin-induced diabetic rats. *Life Sciences, Medicine and Biomedicine*, 2(1), 1-5. <https://doi.org/10.28916/lsm.2.1.2018.5>
- Craig, W. J. (1999). Health-promoting properties of common herbs. *The American Journal of Clinical Nutrition*, 70(3), 491s-499s. <https://doi.org/10.1093/ajcn/70.3.491s>
- Ghazali, A. R., Khairuddin, F. M., Nagapan, T. S., & Basri, D. F. (2017). The mutagenicity and antimutagenicity of *Canarium odontophyllum* (dabai) acetone leaves extracts. *Journal of Agricultural Science*, 9, 62-72. <https://doi.org/10.5539/jas.v9n13p62>
- Ishak, S. A., Azmi, F. F., Zahari, A., & Basri, D. F. (2020). Antimalarial activity of *Canarium odontophyllum* leaf extracts against erythrocytes infected with *Plasmodium berghei* NK65 using Plasmodium Lactate Dehydrogenase (pLDH) and SYBR Green 1 fluorescence assay. *SSRN Electronic Journal*, 1-23. <http://dx.doi.org/10.2139/ssrn.3747151>
- Karak, P. (2019). Biological activities of flavonoids: An overview. *International Journal of Pharmaceutical Sciences and Research*, 10(4), 1567-1574.
- Latiff, A., Faridah, H. I., & Zakri, A. H. (2000). The importance of biodiversity conservation research and collaboration in the ASEAN: A view from Asean scientists. In *Proceedings of the First Scientific Planning*

Conference & Report of the Second Scientific Experts Meeting (SEC) Meeting of ARCBC (Vol. 24). Kuala Lumpur, Malaysia.

- Mahato, S. B., & Sen, S. (1997). Advances in triterpenoid research, 1990-1994. *Phytochemistry*, 44(7), 1185-1236. [https://doi.org/10.1016/S0031-9422\(96\)00639-5](https://doi.org/10.1016/S0031-9422(96)00639-5)
- Pajari, A. M., Päivärinta, E., Paavolainen L., Vaara, E., Koivumäki, T., Garg, R., Heiman-Lindh, A., Mutanen, M., Marjomäki, V., & Ridley, A. J. (2016). Ellagitannin-rich cloudberry inhibits hepatocyte growth factor induced cell migration and phosphatidylinositol 3-kinase/AKT activation in colon carcinoma cells and tumors in Minmice. *Oncotarget*, 7(28), 43907-43923. <https://doi.org/10.18632/oncotarget.9724>
- Saari, S. M., Basri, D. F., Budin, S. B., & Warif, N. M. A. (2017). Effects of *Canarium odontophyllum* leaves on plasma glucose and T lymphocyte population in streptozotocin- induced diabetic rats. *Saudi Journal of Biological Sciences*, 24(2), 320-323. <https://doi.org/10.1016/j.sjbs.2015.09.032>
- Shamsuddin, N. A. M., Zin, N. M., & Basri, D. F. (2018). An assessment of the acetone extract from the leaves of *Canarium odontophyllum* (Miq.) for antibacterial activity against methicillin-resistant *Staphylococcus aureus* (MRSA). *Malaysian Journal of Microbiology*, 14(6), 601-605. <https://dx.doi.org/10.21161/mjm.1461821>.
- Singh, B., Singh, J. P., Kaur, A., & Singh N. (2018). Phenolic compounds as beneficial phytochemicals in pomegranate (*Punica granatum* L.) peel: A review. *Food Chemistry*, 261, 75-86. <https://doi.org/10.1016/j.foodchem.2018.04.039>
- Zou, B., Ge, Z. Z., Zhang, Y., Du, J., Xu, Z., & Li, C. M. (2014). Persimmon tannin accounts for hypolipidemic effects of persimmon through activating of AMPK and suppressing NF-kappaB activation and inflammatory responses in high-fat diet rats. *Food and Function*, 5(7), 1536-1546. <https://doi.org/10.1039/c3fo60635j>



Synthesis, Characterisation, and Electrochemical Impedance Spectroscopy Study of Green and Sustainable Polyurethane Acrylate from Jatropha Oil Using a Three Step Process

Kai Ling Chai¹, Min Min Aung^{1,2,3*}, Hong Ngee Lim², Ikhwan Syafiq Mohd Noor⁴, Luqman Chuah Abdullah⁵ and Hiroshi Uyama⁶

¹Higher Education Centre of Excellence (HiCoE), Institute of Tropical Forestry and Forest Products, Universiti Putra Malaysia, 43400 UPM, Serdang, Selangor, Malaysia

²Department of Chemistry, Faculty of Science, Universiti Putra Malaysia, 43400 UPM, Serdang, Selangor, Malaysia

³Unit Chemistry, Centre of Foundation Studies for Agricultural Science, Universiti Putra Malaysia, 43400 UPM, Serdang, Selangor, Malaysia

⁴Physics Division, Centre of Foundation Studies for Agricultural Science, Universiti Putra Malaysia, 43400 UPM, Serdang, Selangor, Malaysia

⁵Department of Chemical and Environmental Engineering, Faculty of Engineering, Universiti Putra Malaysia, 3400 UPM, Serdang, Selangor, Malaysia

⁶Department of Applied Chemistry, Graduate School of Engineering, Osaka University, Suita, Osaka 565-0871, Japan

ABSTRACT

Bio-based polymer is a promising candidate to substitute conventional petroleum-derived polymer as it is sustainably produced from renewable resources, which helps reduce the production process' carbon footprint. It also helps reduce humankind's dependability on fossil fuel-based feedstock. In this work, a sustainable jatropha oil-based polyurethane acrylate (PUA) was successfully prepared and synthesised using a 3-steps process; epoxidation (formation of an epoxy group), hydroxylation (addition of -OH group to

opened ring), and acrylation (addition of acrylate group into polyol). The yellowish PUA prepared has a gel consistency, which is sticky and slightly runny. The PUA was characterised by using wet chemical tests such as oxirane oxygen content (OOC), acid value (AV), hydroxyl number (OHV) and iodine value. OOC value for the PUA synthesised was 4.23 % at the 5 hr reaction time. At the same time, the Epoxidised

ARTICLE INFO

Article history:

Received: 07 August 2021

Accepted: 02 November 2021

Published: 25 May 2022

DOI: <https://doi.org/10.47836/pjst.30.3.21>

E-mail addresses:

kailingchai345@gmail.com (Kai Ling Chai)

minmin_aung@upm.edu.my (Min Min Aung)

imnoor@upm.edu.my (Ikhwan Syafiq Mohd Noor)

hongnglee@upm.edu.my (Hong Ngee Lim)

chuah@upm.edu.my (Luqman Chuah Abdullah)

uyama@chem.eng.osaka-u.ac.jp (Hiroshi Uyama)

* Corresponding author

jatropha oil (EJO) used to prepare polyol records a hydroxyl number of hydroxyl 185.81 mg KOH/g and an acid value of 1.06. The polyol prepared was mixed with 2, 4-toluene-diisocyanate (TDI) and Hydroethylmethacrylate (HEMA) to produce PUA. The PUA was characterised by thermogravimetry analysis (TGA) and electrochemical impedance spectroscopy (EIS). TGA analysis shows that the polymer is stable up to 373 K, whereas the EIS analysis records an ionic conductivity of $(5.60 \pm 0.03) \times 10^{-6} \text{ S cm}^{-1}$. This polymer's great thermal stability properties make it suitable for outdoor application where high temperature due to sun exposure is common. Furthermore, PUA prepared gel-like properties to make it a suitable candidate for preparing a gel polymer electrolyte.

Keywords: Jatropha oil, polyurethane acrylate

INTRODUCTION

Polymer is a material that consists of a large molecule made up of many repeating subunits. Because of this, polymers can be chemically engineered with desired properties to meet the basic needs of society (Ahvazi et al., 2016).

In this study, the polymer should have excellent chemical, electrochemical, mechanical, photochemical, and thermal properties to be suitable for being used as an electrolyte host polymer. Ideally, the polymer should contain electron donor groups such as O, NH, CN, & F. This is important as the metal cation can form coordinate bonds with electron donor groups, allowing the polymer to dissolve iodide salts readily.

The polymer can be classified into two types: petroleum-based polymer and bio-based polymer. Petroleum-based polymers are currently being used extensively in our daily life. However, due to its environmental and sustainability issue paired with unstable oil prices, the bio-based polymer was introduced as a promising candidate to replace petroleum-based polymer (Mangaraj et al., 2019; Mohanty et al., 2005; Nagalakshmaiah et al., 2018; Siracusa et al., 2008). Bio-based polymers are derived mainly from plants. It makes biopolymers sustainable to produce, environmentally friendly and great availability (Mohiuddin et al., 2017; Sharmin et al., 2015). Examples of bio-based polymers are cellulose (Chua et al., 2020; Du et al., 2019), chitosan (Ogino et al., 2020; Zulkifli et al., 2020), and starch (Lobregas & Camacho, 2019; Tiwari et al., 2019).

Vegetable oils such as palm oil (Adam et al., 2020; Daud et al., 2015), soybean (Huo et al., 2019; Nan et al., 2020), castor (Ibrahim et al., 2015; Ibrahim et al., 2018), neem oil (Desappan et al., 2019) and jatropha oil (Ling et al., 2019; Sammaiah et al., 2014) are suitable to be used in preparing a green and sustainable bio-based polymer. In this work, jatropha oil was selected as starting material. Jatropha oil has unique properties, making it suitable to be used as a feedstock in making a bio-based polymer. Jatropha oil contains a toxic phorbol ester group, making it a non-edible oil (Hazmi et al., 2013). As the oil is

non-edible, a future increase in demand for jatropha oil will not affect the prices of food items. *Jatropha Curcas*, the plant that produces jatropha oil, is also easily cultivated in harsh environments which are not suitable for food cultivation.

Jatropha oil was used to prepare polyol ($R'-(OH)_n$), which will then be used in producing polyurethane acrylate (PUA). PUA is considered a unique polymer consisting of soft and hard segments arranged in an alternating repeating pattern within the same macromolecular chain (Unal et al., 2005). The soft segment of the PUA polymer can act as a solvent to dissolve iodide salts more readily to produce an electrolyte. In contrast, the hard segments help to maintain the electrochemical stability of the gel polymer electrolyte in electrochemical devices. Therefore, PUA polymer is a suitable candidate for an electrolyte system as a host polymer (Su'Ait et al., 2014).

MATERIALS AND METHODS

Material

Jatropha oil (JO) was procured from a local supplier named Bionas Biofuel Sdn Bhd, Malaysia. Formic acid (99 % purity), sulfuric acid (H_2SO_4), N, N-dimethylformamide (DMF), potassium hydrogen phthalate, potassium hydrogen and phenolphthalein were obtained from R&M Chemical, Malaysia. Methanol (CH_3OH) was purchased from HmbG[®] Chemical, Malaysia. Aqueous hydrogen peroxide (purity 30 %) was sourced from Merck, Germany. Technical grade 2-Hydroethylmethacrylate (HEMA) with 80 % purity, chlorobenzene, crystal violet, toluene, phthalic anhydride, pyridine, and sodium thiosulphate was procured from Sigma Aldrich, Germany. In addition, 2,4-toluene-diisocyanate (TDI) with 80 % technical grade, hydrogen bromide and glacial acetic acid were purchased from Acros Organics, New Jersey. Sodium hydroxide, starch solution and cyclohexane were supplied from Pubchem.

Preparation of Polyurethane Acrylate (PUA)

There are three steps in the synthesis process of PUA: the epoxidation, hydroxylation and introduction of the acrylate group in the urethanation process (Chai et al., 2020; Ling et al., 2019). For the epoxidation process, a mixture of 200 g of Jatropha oil and 23.32 g of formic acid was stirred using an overhead stirrer with a temperature of 40 °C for 10 min. Then, 146.52 g of 30 % hydrogen peroxide was added dropwise into the mixture via a dropping funnel. The mixture was stirred at 60 °C for 6 h after adding hydrogen peroxide. Every 1 h interval, a small amount of mixture was taken out and analysed for oxirane oxygen content (OOC) following the methodology described by ASTM D1652-97 Method A standard. 6 h later, the mixture obtained was then transferred into a separating funnel. It was left to cool to room temperature naturally. The settled aqueous layer was discarded, and the remaining acid was rinsed away with slightly warm distilled water several times

until a clear yellowish Epoxidised Jatropa Oil (EJO) was produced. From there, 0.6 g of EJO was used to test for Iodine Value (IV) according to the method described by Ainie et al. (2004).

For the hydroxylation process, 133 g methanol, 0.93 g sulphuric acid and 15 g of distilled water were pre-mixed into a three-neck round bottom flask at 50 °C for 15 min. Next, 150 g of EJO was added slowly to the three-neck round bottom flask. The mixture was then heated gradually to a temperature of 65 °C and stirred continuously for an additional 30 min. Finally, the mixture was transferred to a separating funnel and was left to cool naturally back to room temperature. The aqueous layer was removed, and the residue was then rinsed with slightly warm distilled water several times until it was clear. The excess distilled water and methanol were removed using a rotary evaporator, and polyol with a clear golden colour was successfully synthesised. The polyol sample was tested for Hydroxyl Value (OHV) and Acid Value (AV) using ASTM D 4274-99 in Method C and ASTM D4662-03 Method A, respectively.

In order to prepare PUA, the polyol was synthesised earlier, and DMF solvent was stirred using an overhead stirrer at 60 °C at 500 rpm. Then, TDI was added dropwise into the mixture and was stirred for 2 h at 80°C. After that, the mixture's temperature was then cooled to 40 °C, and HEMA was added slowly into the mixture. After adding HEMA, the mixture was heated up to 70 °C for another 1 h. A 25 mL of DMF was gradually added to produce PUA during the process. It was being done to lower the overall viscosity of the PUA polymer. The PUA synthesised were then stored in the desiccator properly to be used in the future (Figure 1).

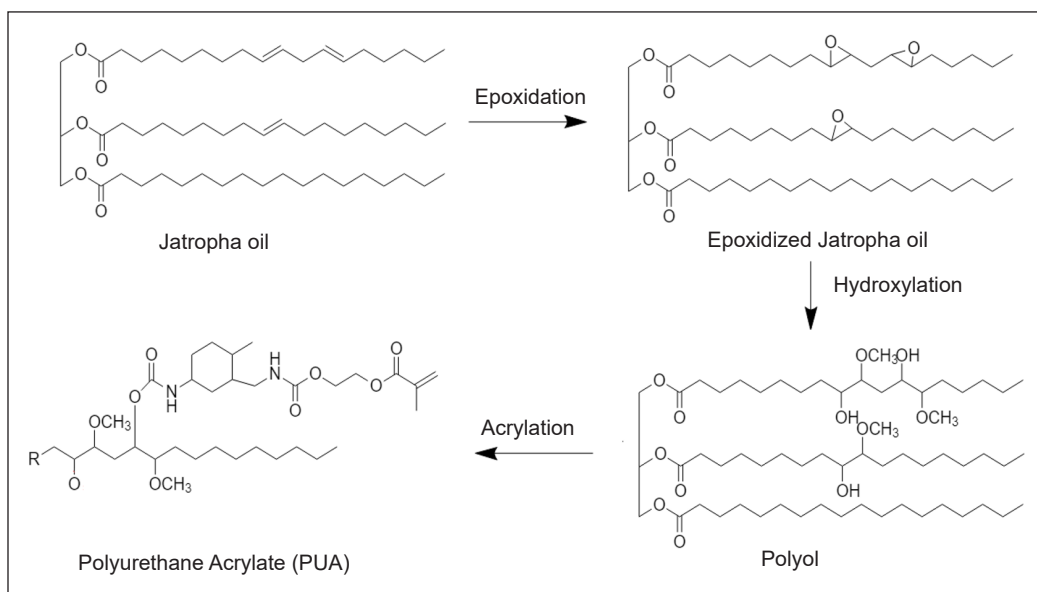


Figure 1. Reaction diagram

Thermal Gravimetric Analysis (TGA)

The PUA gel polymer electrolyte's thermal stability was analysed using TG Analyzer, Perkin Elmer TGA7. TGA was used to measure the PUA weight change as a function of temperature. The PUA gel polymer electrolyte was heated from 298 K to 873 K with a constant heating rate of 283 K/min under a nitrogen atmosphere.

Electrochemical Impedance Spectroscopy (EIS)

HIOKI IM3570 Impedance Analyser obtained the PUA gel polymer electrolyte impedance. The measurement was conducted in the frequency range between 50 Hz to 1 MHz at room temperature (298 K). The PUA was filled in a coin cell with both electrodes being stainless steel. From the Nyquist plot obtained, the value of ionic conductivity can be calculated using Equation 1:

$$\sigma = \frac{t}{A \times R} \quad (1)$$

Here, t is the sample thickness (0.26 cm), A is the electrode/electrolyte contact area (2.01 cm²), and R is electrolyte bulk resistance.

RESULTS AND DISCUSSION

Chemical Properties

Oxirane Oxygen Content Values (OOC) and Iodine Value. OOC is used to determine the double bond conversion value in the vegetable oils into epoxy rings or three-membered rings () (Hernández-Cruz et al., 2021; Saurabh et al., 2011). During the epoxidation process, formic acid and hydrogen peroxide were used because formic acid plays an oxygen carrier role, while hydrogen peroxide is an oxygen donor. Therefore, formic acid is responsible for facilitating the transfer of oxygen from hydrogen peroxide to react with a double bond in the unsaturated fatty acid of the Jatropha oil in the formation of epoxy rings.

The EJO sample was tested hourly to monitor the OOC level during the epoxidation process. Figure 2 and Table 1 show that the OOC level increased from (3.85±0.030) % mol⁻¹ at 1 h until it reached the maximum level, (4.23±0.015) % mol⁻¹ at 5 h. Beyond 5 h, the OOC level decreased to (3.92±0.035) % mol⁻¹. Furthermore, Hazmi et al. (2013) reported that the produced EJO had an OOC value of 3.67 % to 3.89 %. Another example of epoxidation reaction was mentioned by Meyer et al. (2008). The OOC value achieved was 4.75 %, and the time taken was about 10 h. Although it had a higher OOC value, the time taken was prolonged. The OOC value recorded in this work is on par with previous research as it was able to achieve an OOC value of 4.23 % with a shorter time of up to 5 h (Hazmi et al., 2013; Meyer et al., 2008).

Based on the OOC value observed, the relative conversion to oxirane can be calculated as below (Goud et al., 2010):

$$\text{Relative Conversion to Oxirane} = \frac{OOC_{exp}}{OOC_{theo}} \times 100\% \quad (2)$$

OOC_{exp} is the experimental OOC value, and OOC_{theo} is the theoretical OOC value (6.15 %).

Based on Equation 2, the relative conversion to oxirane calculated increases from 62.60 % to 68.70 % at the 5th hour. It is desirable as higher relative conversion to oxirane will allow the OH group to form more sites. In addition, it is due to the oxirane ring being a favourable site for nucleophilic attack by the hydroxyl group via ring-opening reaction. The hydroxyl group can then be attached to an aliphatic fatty acid chain to form polyol during hydroxylation (Mohamed et al., 2020).

Furthermore, the iodine value method evaluated the sample's degree of unsaturation (C=C). Jatropha oil had an iodine value of 101.25 mg I₂ /g. It was because jatropha oil has a high content of unsaturated fatty acids such as palmitic acid, C16:0 (16 %), stearic acid, C18:0 (6 %–7 %), oleic acid, C18:1 (42 %–43.5 %), linoleic acid, C18:2 (33 %–34.5 %) and linoleic acid, C18:3 (0.8%) (Akbar et al., 2009; Amri et al., 2021).

After completing the epoxidation process, EJO presents 5.60 mg I₂ /g for iodine value. The epoxidation process caused this decrease in iodine value.

Hydroxyl Value (OH Value) and Acid Value (AV). In this work, the OH value was carried out to determine the free content of the hydroxyl group that is present in the polyol by using phthalic anhydride pyridine (PAP) at a temperature of 115 °C for 1 h. For the hydroxylation process, the hydrogen atom from the acid alcohol will react with the oxygen atom from the symmetric ether (C-O-C) to form a hydroxyl group, producing polyol. The OH value calculated was 185.81 mg KOH / g. Saalah et al. (2015 & 2021) listed that the

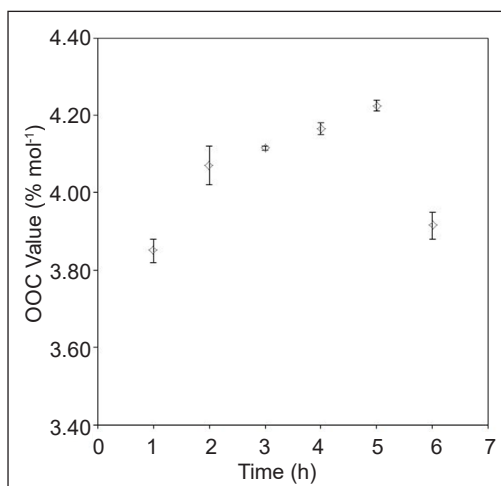


Figure 2. OOC value (%) for 6 h

Table 1
Parameters of OOC value and relative conversion to oxirane for 6 h

Time (h)	OOC value (%)	Relative Conversion to Oxirane (%)
1	3.85	62.60
2	4.07	66.18
3	4.12	66.91
4	4.17	67.72
5	4.23	68.70
6	3.92	63.66

Jatropha oil-based polyol had recorded an OH number of 138 mg KOH / g, while Hazmi et al. (2013) proved that the hydroxyl number achieved by jatropha oil-based polyol was in the range of 171 to 179 mg KOH / g with functionality 5.1 until 5.3. Another example of epoxidation reaction was mentioned by Mudri et al. (2020). They reported that OHV for their Jatropha oil-based polyol (JOL) was 149.44 mg KOH / g. Based on the results cited above, the OH value obtained in this work is higher.

A higher OH value indicated the increase of bond strength as a high crosslinking structure was formed (Park et al., 2020; Somani et al., 2003). Polyol with a high OH value will have good mechanical properties (Wang et al., 2009; Zhang et al., 2017).

Other than that, the acid value was tested on the polyol sample. First, the acid value was calculated to determine the free fatty acid, such as the acidic residue groups in the polyol. The polyol sample recorded (1.06±0.11) mg KOH/g acid value. This low acid value will be able to prevent the corrosion of electrodes in dye-sensitised solar cell applications.

Thermal Gravimetric Analysis (TGA)

TGA was used to measure the changes in weight as the sample was gradually heated. The polymer electrolyte must be heat resistant and must be able to resist a temperature of more than 373 K to achieve the stability of the electrochemical devices. This polymer electrolyte will be applied in the DSSC application, which was agreed upon by Holdt and Kraan (2011). Figure 3 shows the TGA thermogram and DTG curves of pure PUA in the temperature range of 300 K to 873 K. As the temperature increases, it will liberate some moisture and DMF solvent (Fu et al., 2020). It can be observed in the temperature range of 303 K and 500 K. It was deduced that the boiling point of DMF solvent was 425 K–427 K (Adachi & Sakka, 1988; Wannatong et al., 2004). Therefore, DMF was added during the synthesis process of PUA. Furthermore, it showed degradation of the hard segment block of urethane linkage at the temperature of 500 K and 620 K (Adam et al., 2020; Mendes-Felipe et al., 2020; Saalah et al., 2015; Wei et al., 2018). Based on Figure 3, it can be seen that a maximum peak of thermal degradation happened at 620 K to 780 K with 33 % of weight loss. It was caused by the degradation of a soft polyester segment (Adam et al., 2020; Su'Ait et al., 2014; Wei et al., 2018). Thus, Figure 3 proves that this PUA sample is suitable for DSSC application as it can endure at temperatures exceeding 423 K (Fu et al., 2020).

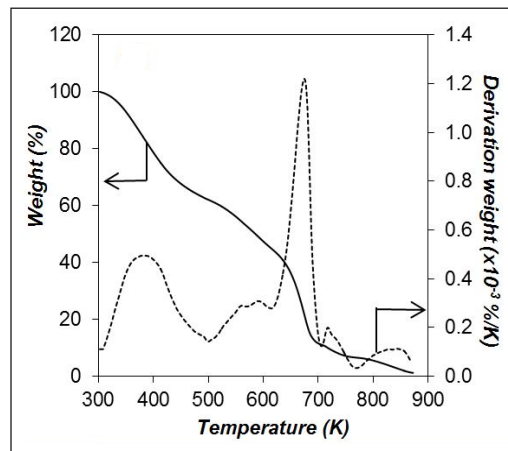


Figure 3. TGA analysis of PUA

Electrochemical Impedance Spectroscopy (EIS)

In this work, PUA is used as a medium for charge transport. In order to determine its properties, ionic conductivity becomes a main concern in the polymer electrolyte. Figure 4 shows the Nyquist plot of pure polyurethane acrylate at room temperature. Based on the Nyquist plot in Figure 4, it presented only a semicircle due to the bulk property of the material. Besides that, the R-value of the pure PUA determined from the Nyquist plot was 29400 Ω . With the R-value obtained, the ionic conductivity of the pure PUA can be calculated. The pure PUA recorded an ionic conductivity of $(5.60 \pm 0.03) \times 10^{-6} \text{ S cm}^{-1}$. This observation shows the ionic conductivity of the polymer to be better than previous work done by Rayung et al. (2019 & 2020). Rayung et al. (2019 & 2020) reported that their samples only managed to obtain an ionic conductivity value of $1.09 \times 10^{-8} \text{ S cm}^{-1}$. The ionic conductivity in this work is two orders of magnitude higher than in previous studies (Rayung et al., 2019; Rayung et al., 2020).

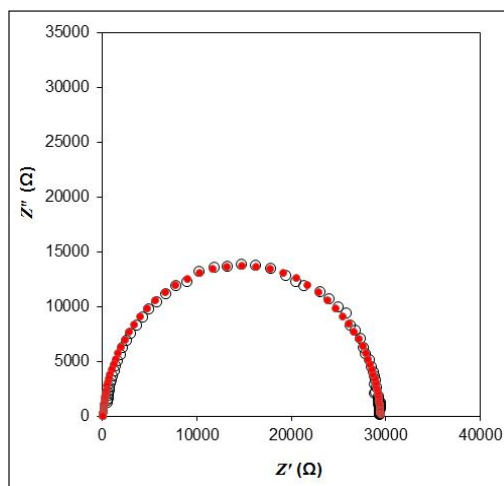


Figure 4. Nyquist plots of pure PUA at ambient temperature (o corresponds to experimental points and • corresponds to fitted points)

CONCLUSION

Jatropha oil is a suitable candidate for preparing a sustainable biopolymer polyurethane acrylate electrolyte. TGA analysis shows the high thermal stability of the polymer, which makes it a great candidate to be used as a host polymer in outdoor dye sensitised solar cells applications. Furthermore, EIS analysis of the polymer prepared shows a relatively good ionic conductivity value which indicates that it is a good starting material to be used in electrochemical applications.

ACKNOWLEDGMENTS

The authors acknowledge with gratitude the Universiti Putra Malaysia for IPS Grant (GP-IPS/2019/9682100).

REFERENCE

- Adachi, T., & Sakka, S. (1988). The role of N,N-dimethylformamide, a DCCA, in the formation of silica gel monoliths by sol-gel method. *Journal of Non-Crystalline Solids*, 99(1), 118-128. [https://doi.org/10.1016/0022-3093\(88\)90464-4](https://doi.org/10.1016/0022-3093(88)90464-4)

- Adam, N. I., Hanibah, H., Subban, R. H. Y., Kassim, M., Mobarak, N. N., Ahmad, A., Badri, K. H., & Su'ait, M. S. (2020). Palm-based cationic polyurethane membranes for solid polymer electrolytes application: A physico-chemical characteristics studies of chain-extended cationic polyurethane. *Industrial Crops and Products*, 155, Article 112757. <https://doi.org/10.1016/j.indcrop.2020.112757>
- Ahvazi, B., Cloutier, É., Wojciechowicz, O., & Ngo, T. D. (2016). Lignin profiling: A guide for selecting appropriate lignins as precursors in biomaterials development. *ACS Sustainable Chemistry and Engineering*, 4(10), 5090-5105. <https://doi.org/10.1021/acssuschemeng.6b00873>
- Akbar, E., Yaakob, Z., Kamarudin, S. K., Ismail, M., & Salimon, J. (2009). Characteristic and composition of *Jatropha curcas* oil seed from Malaysia and its potential as biodiesel feedstock feedstock. *European Journal of Scientific Research*, 29(3), 396-403.
- Amri, M. R., Al-Edrus, S. S. O., Guan, C. T., Yasin, F. M., & Hua, L. S. (2021). Jatropha Oil as a substituent for palm oil in biobased polyurethane. *International Journal of Polymer Science*, 2021, Article 6655936. <https://doi.org/10.1155/2021/6655936>
- Ainie, K., Siew, W. L., & Tan, Y. A. (2004). *Test methods - A compendium of test on palm oil products, palm kernel products, fatty acids, food related products and others*. Malaysian Palm Oil Board.
- Chai, K. L., Noor, I. M., Aung, M. M., Abdullah, L. C., & Kufian, M. Z. (2020). Non-edible oil based polyurethane acrylate with tetrabutylammonium iodide gel polymer electrolytes for dye-sensitized solar cells. *Solar Energy*, 208, 457-468. <https://doi.org/10.1016/j.solener.2020.08.020>
- Chua, K. Y., Azzahari, A. D., Abouloula, C. N., Sonsudin, F., Shahabudin, N., & Yahya, R. (2020). Cellulose-based polymer electrolyte derived from waste coconut husk: Residual lignin as a natural plasticizer. *Journal of Polymer Research*, 27(5), 1-14. <https://doi.org/10.1007/s10965-020-02110-8>
- Daud, F. N., Ahmad, A., & Badri, K. H. (2015). Characterisations of palm-based polyurethane solid polymer electrolyte. In *Advanced Materials Research* (Vol. 1107, pp. 163-167). Trans Tech Publications Ltd. <https://doi.org/10.4028/www.scientific.net/amr.1107.163>
- Desappan, V., Priyadarshini, M., Preethi, K. K., Kumar, K. T., Vediappan, K., Chandrabose, R. S., & Viswanathan, J. (2019). Thermal and electrochemical investigation of neem oil based novel polyurethane/polyvinylpyrrolidone solid polymer electrolytes. *Analytical and Bioanalytical Electrochemistry*, 11(7), 851-876.
- Du, Z., Su, Y., Qu, Y., Zhao, L., Jia, X., Mo, Y., Yu, F., Du, J., & Chen, Y. (2019). A mechanically robust, biodegradable and high performance cellulose gel membrane as gel polymer electrolyte of lithium-ion battery. *Electrochimica Acta*, 299, 19-26. <https://doi.org/10.1016/j.electacta.2018.12.173>
- Fu, J., Yu, H., Wang, L., Lin, L., & Khan, R. U. (2020). Preparation and properties of UV-curable hyperbranched polyurethane acrylate hard coatings. *Progress in Organic Coatings*, 144, Article 105635. <https://doi.org/10.1016/j.porgcoat.2020.105635>
- Goud, V. V., Dinda, S., Patwardhan, A. V., & Pradhan, N. C. (2010). Epoxidation of Jatropha (*Jatropha curcas*) oil by peroxyacids. *Asia-Pacific Journal of Chemical Engineering*, 5(2), 346-354. <https://doi.org/10.1002/apj.285>

- Hazmi, A. S. A., Aung, M. M., Abdullah, L. C., Salleh, M. Z., & Mahmood, M. H. (2013). Producing jatropha oil-based polyol via epoxidation and ring opening. *Industrial Crops and Products*, *50*, 563-567. <https://doi.org/10.1016/j.indcrop.2013.08.003>
- Hernández-Cruz, M. C., Meza-Gordillo, R., Domínguez, Z., Rosales-Quintero, A., Abud-Archila, M., Ayora-Talavera, T., & Villalobos-Maldonado, J. J. (2021). Optimization and characterization of in situ epoxidation of chicken fat with peracetic acid. *Fuel*, *285*, Article 119127. <https://doi.org/10.1016/j.fuel.2020.119127>
- Holdt, S. L., & Kraan, S. (2011). Bioactive compounds in seaweed: Functional food applications and legislation. *Journal of Applied Phycology*, *23*(3), 543-597. <https://doi.org/10.1007/s10811-010-9632-5>
- Huo, P., Ni, S., Hou, P., Xun, Z., Liu, Y., & Gu, J. (2019). A crosslinked soybean protein isolate gel polymer electrolyte based on neutral aqueous electrolyte for a high-energy-density supercapacitor. *Polymers*, *11*(5), Article 863. <https://doi.org/10.3390/polym11050863>
- Ibrahim, S., Ahmad, A., & Mohamed, N. S. (2015). Synthesis and characterization of castor oil-based polyurethane for potential application as host in polymer electrolytes. *Bulletin of Materials Science*, *38*(5), 1155-1161. <https://doi.org/10.1007/s12034-015-0995-8>
- Ibrahim, S., Ahmad, A., & Mohamed, N. S. (2018). Comprehensive studies on polymer electrolyte and dye-sensitized solar cell developed using castor oil-based polyurethane. *Journal of Solid State Electrochemistry*, *22*(2), 461-470. <https://doi.org/10.1007/s10008-017-3775-0>
- Ling, C. K., Aung, M. M., Rayung, M., Abdullah, L. C., Lim, H. N., & Noor, I. S. M. (2019). Performance of ionic transport properties in vegetable oil-based polyurethane acrylate gel polymer electrolyte. *ACS Omega*, *4*(2), 2554-2564. <https://doi.org/10.1021/acsomega.8b02100>
- Lobregas, M. O. S., & Camacho, D. H. (2019). Gel polymer electrolyte system based on starch grafted with ionic liquid: Synthesis, characterization and its application in dye-sensitized solar cell. *Electrochimica Acta*, *298*, 219-228. <https://doi.org/10.1016/j.electacta.2018.12.090>
- Mangaraj, S., Yadav, A., Bal, L. M., Dash, S. K., & Mahanti, N. K. (2019). Application of biodegradable polymers in food packaging industry: A comprehensive review. *Journal of Packaging Technology and Research*, *3*(1), 77-96. <https://doi.org/10.1007/s41783-018-0049-y>
- Mendes-Felipe, C., Barbosa, J. C., Gonçalves, S., Pereira, N., Costa, C. M., Vilas-Vilela, J. L., & Lanceros-Mendez, S. (2020). High dielectric constant UV curable polyurethane acrylate/indium tin oxide composites for capacitive sensing. *Composites Science and Technology*, *199*, Article 108363. <https://doi.org/10.1016/j.compscitech.2020.108363>
- Meyer, P., Techaphattana, N., Manundawee, S., Sangkeaw, S., Junlakan, W., & Tongurai, C. (2008). Epoxidation of soybean oil and Jatropha oil. *Thammasat International Journal of Science and Technology*, *13*, 1-5.
- Mohamed, M., Assem, Y., & Ramadan, A. (2020). Soybean oil-based polyol as a modified natural binder for polyurethane turf-adhesive. *Egyptian Journal of Chemistry*, *64*(2), 4-6. <https://doi.org/10.21608/ejchem.2020.31470.2670>
- Mohanty, A. K., Misra, M., & Drzal, L. T. (2005). *Natural fibers, biopolymers, and biocomposites*. CRC press. <https://doi.org/10.1201/9780203508206.ch1>

- Mohiuddin, M., Kumar, B., & Haque, S. (2017). Biopolymer composites in photovoltaics and photodetectors. In K. K. Sadasivuni, D. Ponnamma, J. Kim, J. J. Cabibihan & M. A. AlMaadeed (Eds.), *Biopolymer composites in electronics* (pp. 459-486). Elsevier. <https://doi.org/10.1016/B978-0-12-809261-3.00017-6>
- Mudri, N. H., Abdullah, L. C., Aung, M. M., Salleh, M. Z., Biak, D. R. A., & Rayung, M. (2020). Comparative study of aromatic and cycloaliphatic isocyanate effects on physico-chemical properties of bio-based polyurethane acrylate coatings. *Polymers*, *12*(7), Article 1494. <https://doi.org/10.3390/polym12071494>
- Nagalakshmaiah, M., Afrin, S., Malladi, R. P., Elkoun, S., Robert, M., Ansari, M. A., Svedberg, A., & Karim, Z. (2018). Biocomposites: Present trends and challenges for the future. In *Green composites for automotive applications* (pp. 197-215). Woodhead Publishing. <https://doi.org/10.1016/B978-0-08-102177-4.00009-4>
- Nan, J., Zhang, G., Wang, L., Wang, H., Chu, F., & Wang, C. (2020). Preparation of ionic liquid-based gel electrolytes and application in supercapacitors. *Chemistry and Industry of Forest Products*, *40*(4), 17-23. <https://doi.org/10.3969/j.issn.0253-2417.2020.04.003>
- Ogino, M., Kotatha, D., Torii, Y., Shinomiya, K., Uchida, S., Furuike, T., Tamura, H., & Ishikawa, M. (2020). Preparation and electrochemical performance of chitosan-based gel polymer electrolyte containing ionic liquid for non-aqueous electric double layer capacitor. *Electrochemistry*, *88*(3), 132-138. <https://doi.org/10.5796/electrochemistry.20-63009>
- Park, C. K., Lee, J. H., Kim, I. S., & Kim, S. H. (2020). Castor oil-based polyols with gradually increasing functionalities for biopolyurethane synthesis. *Journal of Applied Polymer Science*, *137*(4), Article 48304. <https://doi.org/10.1002/app.48304>
- Rayung, M., Aung, M. M., Ahmad, A., Su'ait, M. S., Abdullah, L. C., & Jamil, S. N. A. M. (2019). Characteristics of ionically conducting jatropha oil-based polyurethane acrylate gel electrolyte doped with potassium iodide. *Materials Chemistry and Physics*, *222*, 110-117. <https://doi.org/10.1016/j.matchemphys.2018.10.009>
- Rayung, M., Aung, M. M., Su'Ait, M. S., Abdullah, L. C., Ahmad, A., & Lim, H. N. (2020). Performance analysis of jatropha oil-based polyurethane acrylate gel polymer electrolyte for dye-sensitized solar cells. *ACS Omega*, *5*(24), 14267-14274. <https://doi.org/10.1021/acsomega.9b04348>
- Saalah, S., Abdullah, L. C., Aung, M. M., Salleh, M. Z., Biak, D. R. A., Basri, M., & Jusoh, E. R. (2015). Waterborne polyurethane dispersions synthesized from jatropha oil. *Industrial Crops and Products*, *64*, 194-200. <https://doi.org/10.1016/j.indcrop.2014.10.046>
- Saalah, S., Abdullah, L. C., Aung, M. M., Salleh, M. Z., Biak, D. R. A., Basri, M., Jusoh, E. R., Mamat, S., & Al Edrus, S. S. O. (2021). Chemical and thermo-mechanical properties of waterborne polyurethane dispersion derived from jatropha oil. *Polymers*, *13*(5), Article 795. <https://doi.org/10.3390/polym13050795>
- Sammaiah, A., Padmaja, K. V., & Prasad, R. B. N. (2014). Synthesis of epoxy jatropha oil and its evaluation for lubricant properties. *Journal of Oleo Science*, *63*(6), 637-643. <https://doi.org/10.5650/jos.ess13172>
- Saurabh, T., Patnaik, M., Bhagst, S. L., & Renge, V. (2011). Epoxidation of vegetable oils: A review. *International Journal of Advanced Engineering Technology E*, *2*(4), 491-501.
- Sharmin, E., Zafar, F., Akram, D., Alam, M., & Ahmad, S. (2015). Recent advances in vegetable oils based environment friendly coatings: A review. *Industrial Crops and Products*, *76*, 215-229. <https://doi.org/10.1016/j.indcrop.2015.06.022>

- Siracusa, V., Rocculi, P., Romani, S., & Rosa, M. D. (2008). Biodegradable polymers for food packaging: A review. *Trends in Food Science and Technology*, *19*(12), 634-643. <https://doi.org/10.1016/j.tifs.2008.07.003>
- Somani, K. P., Kansara, S. S., Patel, N. K., & Rakshit, A. K. (2003). Castor oil based polyurethane adhesives for wood-to-wood bonding. *International Journal of Adhesion and Adhesives*, *23*(4), 269-275. [https://doi.org/10.1016/S0143-7496\(03\)00044-7](https://doi.org/10.1016/S0143-7496(03)00044-7)
- Su'Ait, M. S., Ahmad, A., Badri, K. H., Mohamed, N. S., Rahman, M. Y. A., Ricardo, C. L. A., & Scardi, P. (2014). The potential of polyurethane bio-based solid polymer electrolyte for photoelectrochemical cell application. *International Journal of Hydrogen Energy*, *39*(6), 3005-3017. <https://doi.org/10.1016/j.ijhydene.2013.08.117>
- Tiwari, T., Kumar, M., Yadav, M., & Srivastava, N. (2019). Study of arrowroot starch-based polymer electrolytes and its application in MFC. *Starch-Stärke*, *71*(7-8), Article 1800313. <https://doi.org/10.1002/star.201800313>
- Unal, S., Oguz, C., Yilgor, E., Gallivan, M., Long, T. E., & Yilgor, I. (2005). Understanding the structure development in hyperbranched polymers prepared by oligomeric A₂+B₃ approach: Comparison of experimental results and simulations. *Polymer*, *46*(13), 4533-4543. <https://doi.org/10.1016/j.polymer.2005.03.073>
- Wang, C. S., Yang, L. T., Ni, B. L., & Shi, G. (2009). Polyurethane networks from different soy-based polyols by the ring opening of epoxidized soybean oil with methanol, glycol, and 1,2-propanediol. *Journal of Applied Polymer Science*, *114*(1), 125-131. <https://doi.org/10.1002/app.30493>
- Wannatong, L., Sirivat, A., & Supaphol, P. (2004). Effects of solvents on electrospun polymeric fibers: Preliminary study on polystyrene. *Polymer International*, *53*(11), 1851-1859. <https://doi.org/10.1002/pi.1599>
- Wei, D., Liao, B., Yong, Q., Li, T., Wang, H., Huang, J., & Pang, H. (2018). Castor oil based hyperbranched urethane acrylates and their performance as UV-curable coatings. *Journal of Macromolecular Science, Part A: Pure and Applied Chemistry*, *55*(5), 422-432. <https://doi.org/10.1080/10601325.2018.1453263>
- Zhang, C., Garrison, T. F., Madbouly, S. A., & Kessler, M. R. (2017). Recent advances in vegetable oil-based polymers and their composites. *Progress in Polymer Science*, *71*, 91-143. <https://doi.org/10.1016/j.progpolymsci.2016.12.009>
- Zulkifli, A. M., Said, N. I. A. M., Aziz, S. B., Dannoun, E. M. A., Hisham, S., Shah, S., Bakar, A. A., Zainal, Z. H., Tajuddin, H. A., Hadi, J. M., Brza, M. A., Saeed, S. R., & Amin, P. O. (2020). Characteristics of dye-sensitized solar cell assembled from modified chitosan-based gel polymer electrolytes incorporated with potassium iodide. *Molecules*, *25*(18), Article 4115. <https://doi.org/10.3390/molecules25184115>

Review Article

A Review on Soil Erodibility Studies in Malaysia

Adnan Derahman¹, Mohd Fairuz Bachok^{2*}, Muhamad Fuad Shukor², Farah Wahida Mohd Latib³ and Rohaya Alias³

¹*School of Civil Engineering, College of Engineering, Universiti Teknologi MARA, 40450 UiTM, Shah Alam, Selangor, Malaysia*

²*School of Civil Engineering, College of Engineering, Universiti Teknologi MARA Cawangan Johor, 85000 UiTM, Segamat, Johor, Malaysia*

³*School of Civil Engineering, College of Engineering, Universiti Teknologi MARA Cawangan Pahang, 26400 UiTM, Pahang, Malaysia*

ABSTRACT

Studies on soil erodibility in Malaysia were critically reviewed. Soil erodibility is the only factor of Universal Soil Loss Equation (USLE), which requires laboratory work and analysis complexity to estimate soil loss. Therefore, the main objective is to review soil erodibility studies to enhance understanding of Malaysia's soil erosion impacts. These studies were summarized in their application, purpose, value, utilization method/approach, and study location. On the other hand, a summarization of what, why, where, and how the soil erodibility was used was analyzed. Therefore, the importance of soil erodibility as input for environmental management and conservation practices can be addressed. For a large-scale area, the soil erodibility factor will be analyzed as one of the USLE variables in estimating the erosion rate. As for a small-scale area, this factor is an adaption of the ROM Scale, which use to identify the slopes or riverbanks prone to landslides induced by erosion. However, the determination of this factor requires extensive artistry, time, and cost. These would be an obstacle to the holistic assessment of soil erosion impacts since only a little

soil sampling will be analyzed. Therefore, the simplified version for the determination of soil erodibility without any requirement of laboratory works will be an extra mile, especially for an area that does not have any information on soil series.

Keywords: ROM scale, RUSLE, soil erodibility, soil erosion, soil loss, USLE

ARTICLE INFO

Article history:

Received: 19 August 2021

Accepted: 03 February 2022

Published: 25 May 2022

DOI: <https://doi.org/10.47836/pjst.30.3.22>

E-mail addresses:

dradnan@uitm.edu.my (Adnan Derahman)

mohdfairuz@uitm.edu.my (Mohd Fairuz Bachok)

fuad9845@uitm.edu.my (Muhamad Fuad Shukor)

farahwahidaml@uitm.edu.my (Farah Wahida Mohd Latib)

rohayaalias@uitm.edu.my (Rohaya Alias)

* Corresponding author

INTRODUCTION

Soil contains a mixture of an organism, minerals, gases, liquids, and organic matter, while erosion is a kind of soil degradation of the displacement of the upper layer of soil. Erosion is a natural process contributed by many erosion agents such as water, ice, snow, air, plants, animals, and humans. As a developing country, Malaysia faces rapid physical developments, which cause it to be unavoidable from having problems related to soil erosion and sedimentation (Ministry of Natural Resources and Environment Malaysia, 2010). It has a huge impact on daily life and the environment, where it will lead to pollution and sedimentation of water streams and bodies as well as reduce soil productivity (Rickson, 2014). Yusof et al. (2011) mentioned that erosion from mountains and agricultural land is the major source of sediment transport by the stream and results in deposits in the reservoir. On the other hand, both studies agreed that soil erosion can resulting sedimentation through the stream.

In the mountainous area, erosion would slowly diminish the sides of a mountain through flowing water. If a stream constantly went through a mountain, it would pull soil particles and dirt from the ground and carry them down to where the river ends. In agricultural activities, when land is worked through agricultural processes, it reduces the overall structure of the soil and levels of organic matter and results in soil on land surfaces exposed directly to the rains. This unprotected soil could be easily removed from the land surfaces by the combined action of rain and the resulting flow. Besides, soil erosion reduces soil fertility which causes a detrimental impact on agricultural output. These findings also prove that soil properties contribute to soil erosion and sedimentation.

While Zhou et al. (2016), Hou et al. (2016), and Wang et al. (2016) mentioned that soil erosion could cause and be driven by severe vegetation loss. Consequently, the soil surface will be exposed to erosive agents. Since rainfall concentrates more on surface runoff rather than seepage infiltration into the earth, it will weaken the bonding between soil particles at the soil surface and later lead to the soil disintegration process. Soil-laden transport by water downstream cause thick layers of sediment, obstructing the flow of streams and finally leading to flooding.

Erodibility is the vulnerability of the ground surface to erosion and is usually characterized by coarse grain soils with little or no resistance to erosion (Kaffas & Hrisanthou, 2019). It has been thoroughly used in both theoretical and practical approaches to determining soil erosion, but many parameters need to address in measuring soil erosion, including soil properties (Wang et al., 2016), terrain (Mwaniki et al., 2015; Parajuli et al., 2015), climate (Hussein, 2013), vegetation (Sepúlveda Lozada et al., 2009), and land use (Tang et al., 2016).

Many approaches have been developed to clarify and calculate soil erodibility, such as physical and chemical soil properties, instrumental measurements, mathematical models,

and graphical methods (Wei et al., 2017). Extremely from the previous researchers, the in-situ or direct measurement of soil erosion on-site under natural rainfall over long periods had been implemented, and this method represents the most accurate estimates of soil erodibility results, but on the other side, this method is time-consuming and expensive (Vaezi et al., 2016). There are five empirical models using soil erodibility as a variable for estimation of soil erosion and sediment yield, which are Universal Soil Loss Equation (USLE), Revised Universal Soil Loss Equation (RUSLE), Modified Universal Soil Loss Equation (MUSLE), Erodibility Index (EI) and Sediment Delivery Ratio (SDR). However, Malaysia's widely used soil erodibility studies were USLE, RUSLE, and EI.

Universal Soil Loss Equation (USLE)

The Universal Soil Loss Equation (USLE) has been used to investigate whether climate affects the susceptibility of soils to water erosion (Algayer et al., 2014). This equation is an empirical-based and derived by using a large mass of field data, primarily involving erosion plots and rainfall simulator experiments, and computes sheet and rill erosion as follows (Equation 1):

$$A = RKLSCP \quad [1]$$

where A is computed soil loss, R is the rainfall-runoff erosivity factor, K is a soil erodibility factor, L is the slope length factor, S is the slope steepness factor, C is a cover management factor, and P is a supporting practice factor.

Asmamaw and Mohammed (2019), and El Jazouli et al. (2019) referred to the soil erodibility factor, K, as the ability of soil to be displaced by the rainfall forces, while Yusof et al. (2011) refer to K as a rate of soil loss per erosivity index unit. It is based on a standard plot 22.1 m long and has a 9 % slope continuously in a clean-tilled fallow condition, with tillage performed upslope and downslope.

Revised Universal Soil Loss Equation (RUSLE)

The second method uses the Revised Universal Soil Loss Equation (RUSLE). This method upgrades USLE, whereby land use is an independent factor. It can be utilized on cropland, aggravated forestland, rangeland, development locales, mined arrive, recovered arrive, military preparing grounds, landfills, squander transfer locales, and other lands. The precipitation and its associated overland stream can cause soil disintegration. RUSLE was, to begin with, presented within the USDA Soil and Water Conservation Service in 1993. RUSLE keeps up the same observationally-based condition as USLE to compute sheet and rill disintegration.

Soil erodibility factor (K) within the RUSLE accounts for the influence of soil properties on soil loss throughout storm events in upland areas. K value can be assessed in the event

if the organic content, structure, grain size distribution, and permeability of the soil are known (Hashim & Abdullah, 2005). Table 1 shows Malaysia’s soil loss tolerance rates (Mir et al., 2015) using USLE and RUSLE methods.

Table 1
Soil loss tolerance rates

Soil erosion	Potential soil loss (ton.ha ⁻¹ .yr ⁻¹)
Very low	< 10
Low	10–50
Moderate high	50–100
High	100–150
Very high	> 150

Erodibility Index

Numerous endeavors have been made to create a record of erodibility. Those endeavors crossed from the properties of soils to the reaction of the soil to rainfalls. Bouyoucos (1962) proposed that erodibility corresponds between sand, silt, and clay. This erodibility was extended by Abidin and Mukri (2002) with the thought of erodibility in Malaysia by creating the ROM scale. The purpose is to utilize the introduction of coherent prescient calculation to show the degree of soil disintegration tragedies. The establishment of the ROM Scale was based, as it were, on soil grading characteristics. The scale is made to review the degree of erosion for soil erodibility in Malaysia. The ROM Scale condition is given as Equation 2:

$$EI_{ROM} = \frac{(\% \text{ sand} + \% \text{ silt})}{2(\% \text{ clay})} \quad [2]$$

If the soil textural composition of sand, silt, and clay are known, at that point, the erodibility scale can as it was being decided. If the clay substance is exceptionally low, the ROM Scale will be in real esteem and vice versa. The digit two at the denominator is utilized after considering the degree of values to be categorized almost other measures of overall values such as the Richter scale for seismic intensity. The scale range of ROM and the degree of soil erosion risk has appeared in Table 2.

Table 2
ROM scale and soil erodibility category

EI _{ROM}	ROM Scale
Low	< 1.5
Moderate	1.5 – 4.0
High	4.0 – 8.0
Very high	8.0 – 12.0
Critical	> 12.0

SOIL ERODIBILITY STUDIES IN MALAYSIA

This section lists the studies related to soil erodibility conducted in Malaysia. It summarized why and how this soil erosion factor is being used. In addition, the value of soil erodibility factor and where this study is conducted. Summarizing these studies is shown in Table 3 and elaboration on each of the studies.

Table 3
Soil erodibility studies in Malaysia

Year	Application of soil erodibility factor	Purpose	Location	Method/ Approach	Value of K factor (Mg ha h ha-1 MJ-1 mm-1)	Result	Finding	Resource
2005	Classification and prediction of areas susceptible to landslides.	Determine the soil erodibility index (EI) value.	Fraser Hill, Pahang and Genting Highlands, Pahang	Based on the value of soil erodibility obtained using the ROM Scale method.	-	<ul style="list-style-type: none"> The EIROM value for the ROM scale is classified as 'High' with a value of 4.55 for the entire Fraser hill area. The EI value for the ROM scale is classified as being 'Moderate' with a value of 2.91 for the entire Genting Highlands area. 	<ul style="list-style-type: none"> Fraser Hill area is susceptible to erosion-induced landslides. Genting Highland area less susceptible to erosion induced landslide. 	Roslan and Zulkifli (2005)
2011	Determine landslide levels at 12 problematic slopes.	Determine the soil erodibility index (EI) value.	Universiti Kebangsaan Malaysia, Selangor	ROM Scale	-	<ul style="list-style-type: none"> Four slopes are categorized as critical, three slopes high, three slopes moderate, and two slopes low. 	<ul style="list-style-type: none"> Problematic slopes prone to erosion induced landslide. 	Mokhtar et al., 2011
2012	Assess the potential for soil loss and detect areas at risk of erosion.	Adopt a managed environment and plan land use. Maintain the authenticity of the aquatic and terrestrial biodiversity of the lake.	Tasik Chini, Pahang	Combination of RUSLE and Geographic Information System (GIS).	0.03 - 0.3	<ul style="list-style-type: none"> There are 71.54 % of Tasik Chini areas categorized as very low erosion risk, 2.94 % categorized as low erosion risk, 3.38 % classified as the moderate risk of erosion, 1.45 % categorized as high risk of erosion, and 13.25 % categorized as very high erosion risk. 	<ul style="list-style-type: none"> The area of Tasik Chini, which is near a high risk and a very high-risk area, was found much shallower in-depth due to massive accumulations of sediment at the beds of lakes in the areas. 	Sujaul et al., 2012

Table 3 (continue)

Year	Application of soil erodibility factor	Purpose	Location	Method/ Approach	Value of K factor (Mg ha h ha-1 MJ-1 mm-1)	Result	Finding	Resource
2017	Assess riverbanks at risk of failure along the river.	<ul style="list-style-type: none"> Plan, design, and carry out remedial actions. 	Sungai Langat, Selangor	<ul style="list-style-type: none"> ROM Scale 	-	<ul style="list-style-type: none"> 73% of the riverbanks along Hulu Langat River were categorized as a critical erosion risk level. 	<ul style="list-style-type: none"> The middle reach of the Hulu Langat River is susceptible to severe erosion due to the low percentage of clay. Most of the riverbanks along Hulu Langat River need remedial erosion actions. 	Abidin et al., 2017
2017	Analyze the status of the 20 slopes stability.	<ul style="list-style-type: none"> Identify the soil erodibility degree. 	Sultan Idris Education University campus	<ul style="list-style-type: none"> ROM Scale 	-	<ul style="list-style-type: none"> Sixteen slopes with critical status to be experienced erosion-induced landslides. 	<ul style="list-style-type: none"> Sultan Idris Education University campus areas are susceptible to erosion-induced landslides. 	Mohmadisa et al., 2017
2018	Estimating soil loss.	<ul style="list-style-type: none"> Improvement of agricultural productivity. Managing the natural resources effectively. 	Seremban district, Negeri Sembilan	<ul style="list-style-type: none"> RUSLE with remote sensing and GIS technique. Production of distribution maps to estimate the average value of annual soil loss. 	0.002 - 0.005	<ul style="list-style-type: none"> No soil loss was recorded in the forest area of Lenggeng, Panti, Ampangan, and Seremban. Soil loss in the open area of Labu, Renggam, and Lenggeng was recorded as > 100 tons hectare per year. Estimated soil loss is 883 tons/hectare/year, covering 198 tons of agricultural areas, 39 tons of forest areas, 20.45 tons of rural areas, 610 tons of open areas, 12 tons of urban areas, and 1.4 tons of inland waters. 	<ul style="list-style-type: none"> The districts of Lenggeng, Panti, Setui, and Ampangan recorded less soil erosion, while Seremban and Rasah recorded moderate soil erosion, and Pantai and Rentau had the highest levels of soil loss in that region. 	Ahmed et al., 2018

Table 3 (continue)

Year	Application of soil erodibility factor	Purpose	Location	Method/ Approach	Value of K factor (Mg ha h ha-1 MJ-1 mm-1)	Result	Finding	Resource
2018	Determine the soil erodibility of the slopes.	<ul style="list-style-type: none"> Classify the slopes erosion risk. 	Universiti Pertahanan Nasional Malaysia, Selangor	<ul style="list-style-type: none"> ROM Scale 		<ul style="list-style-type: none"> No area in the study area has a low risk of soil erosion. Mess cadet area is a critical area to experience erosion, block Lestari was classified as high risk, and MTD hill was ranked as a moderate risk of soil erosion. 	<ul style="list-style-type: none"> Some parts of Universiti Pertahanan Nasional Malaysia need a quick erosion mitigation measure. Landslides that occurred in the study area are due to the high sand content in the soil. 	Zuliziana et al., 2018
2018	Development of soil erosion risk map.	<ul style="list-style-type: none"> Plan conservation actions for areas that are highly prone to erosion. Implement a managed environment and plan land use. 	State of Perak	<ul style="list-style-type: none"> Utilized USLE to determine the annual soil loss through integration between maps overlay for each parameter, pixel by pixel. Production of erosion risk map into categories according to an annual loss Arc GIS software is a tool for map production. Soil erodibility factor is based on properties and structure classes of soil series acquired from the Department of Agriculture Malaysia through the Malaysian Soil Report. 	0.03 - 0.50	<ul style="list-style-type: none"> The study area, which is covered with mangroves, paddy fields, roads and utilities, forests, and waters, are areas with a low to moderate risk of soil erosion. Areas with steep slopes, open land, deforested areas, grasslands or rubber tree areas, oil palm tree areas, and areas with mixed crops were found to have a high to very high risk of soil erosion. 	<ul style="list-style-type: none"> The area protected from direct impacts of a raindrop on the soil surface (covered by vegetation and impervious area) and effectively intercepting rainfall-runoff (forest) will reduce the soil loss due to water erosion. 	Omar et al., 2018

Table 3 (continue)

Year	Application of soil erodibility factor	Purpose	Location	Method/ Approach	Value of K factor (Mg ha h ha-1 MJ-1 mm-1)	Result	Finding	Resource
2012	Produce predictions for soil erosion rates and make the spatial mapping.	<ul style="list-style-type: none"> Estimate the erosion rate. 	Pansoon sub-basin at Htulu Selangor, Selangor	<ul style="list-style-type: none"> RUSLE is used to predict the rate of soil erosion, and Geographical Information System (GIS) is a tool to develop spatial maps. 	0.042 - 0.052	<ul style="list-style-type: none"> 66% of the Pansoon sub-basin was classified as the very low-risk potential of soil erosion, the low-risk areas were 22 % and 5 % moderate, and the high and very high-risk areas were 5 % and 2 %, respectively. Pansoon sub-basin experiences a lot of soil erosion in the southwest, and among the causes of soil erosion are the long and steep slopes. 	<ul style="list-style-type: none"> The area of the Pansoon sub-basin is less susceptible to erosion risk except in the area with long and steep slopes. 	Yusof et al., 2012
2019	Produce a map of soil erosion risk.	<ul style="list-style-type: none"> Identify areas prone to soil erosion. 	Temengor Reservoir Basin, Perak	<ul style="list-style-type: none"> Utilize USLE to determine annual soil loss Geographic Information System (GIS) to develop a soil erosion risk map. 	0.06	<ul style="list-style-type: none"> The soil loss in a year is 8 tons/hectare/year. 28.8 % of the total area recorded high erosion, particularly in the high elevations zone. The location of logging activity in the southeastern Temengor Reservoir Basin was categorized as an area of extreme erosion, which is 4 %. 	<ul style="list-style-type: none"> Logging activities zone, especially in the hilly area, need to be monitored and take necessary erosion mitigation measures. 	Basri et al., 2019

According to Roslan and Zulkifli (2005), based on the soil erodibility assessment using the ROM Scale method, the Fraser Hill area is more susceptible to erosion-induced landslides compared to the Genting Highland area. The soil at Fraser's Hill was looser and more sensitive than Genting Highland, making it more susceptible to erosion-induced landslides. In addition, it has low strength and is easily compressible. Besides, with the high rainfall, soils in steep terrain are subjected to surface erosion when exposed or landslides if the rainwater percolates into the soil profile. Therefore, additional landslide mitigation and prevention measures in the Fraser hill area should be taken to stabilize the slopes.

Mokhtar et al. (2011) studied landslide levels at problematic slopes in Universiti Kebangsaan Malaysia (UKM), Selangor campus using the ROM Scale. It was found that most problematic slopes in the UKM are prone to failure or landslide in the future, as the terrain in the UKM area is hilly, and the area receives a high intensity of annual rain. High amounts of rainfall will worsen the situation as the rainwater infiltrates into the soil and undermines the soil structure. In addition, heavy rainfalls can have adverse effects on soil particles because it heightens the ability of raindrops to detach particles. Problematic slopes lead to slope failure caused by artificial factors, mainly design and construction errors with non-maintenance slopes.

Besides the ROM Scale as the indicator in determining the degree of soil erodibility for slope, it has also been used to accelerate the erosion risk identification at a stretch of the riverbanks. Riverbank erosion would cause the riverbed to degrade and dump particles and sediments into receiving water bodies. The bedform particles, along with riverbank particles, would be detached from their interlocking due to the action of water flow. The transportable particles would then start to move and deposit at the downstream part of a river section. This process would cause severe engineering and environmental problems if monitoring programs are not well-managed and practiced. The impact of the flow of eroded material into river basins will increase the cost of managing the river basin. Abidin et al. (2017) found that the middle reach of the Hulu Langat River is susceptible to severe erosion due to the low percentage of clay. The percentage of clay decreased, and the susceptibility index became higher and approached a critical level. A reasonable explanation for this consequence is that clays are pastier and stickier and hence can provide an adhesive pattern to interlocking particles. The least resistant particles are silts and sands; thus, soils with high silt and sand content are more erodible than soils with clay content.

Mohmadisa et al. (2017) also found that the high risk of slope failure and soil erosion in the Sultan Idris Education University campus area is closely related to the soil texture, which lacks clay content. Clay plays an important role in strengthening and stabilizing the slope, compared to sand and silt. It is because clay can hold greater water content, has a high level of resistance toward the actions of raindrops and surface runoff, and is capable of binding soil particles. Therefore, additional protective measures should be taken to

increase the level of soil moisture and improve the bond between soil compositions with the implementation of slope protection measures by engineering and bioengineering techniques.

Furthermore, Zuliziana et al. (2018) noticed that landslides in the Universiti Pertahanan Nasional Malaysia area were due to the high sand content in the soil. It is due to clay as a binder between the sand, rock, and silt particles. The slope will be more intact and stable when clay particles indirectly bind the sand, rock, and silt particles. The physical characteristics of the sandy soil also affect the slope's stability. Sandy soil structure will improve soil porosity and increase the infiltration rate during heavy rainfall, thus contributing to slope failure. Therefore, some Universiti Pertahanan Nasional Malaysia parts need quick erosion mitigation measures.

Omar et al. (2018) conducted a study estimating the annual soil loss in Perak by using USLE. It found that areas protected from direct impacts of rainfall on the soil surface (covered by vegetation and impervious area) and effective intercepting rainfall-runoff (forest) will reduce the soil loss due to water erosion. Cover crops have various functions in stabilizing slopes. Cover crops can prevent and reduce direct water drops from eroding the ground surface. The growth of plant roots will encourage significant changes in the physical and chemical properties of the soil and will indirectly strengthen the soil structure. A thick vegetative cover reduces the erosion hazards of the soil. Plants with large roots improve the structure and aeration of the soil, for soils under such a condition tend to develop crumb structures.

According to Basri et al. (2019), the logging activities zone, especially in the hilly Temengor Reservoir Basin, Perak, needed to be monitored with necessary erosion mitigation measures. Land use activities around Temengor Reservoir Basin have changed from primary forest to logging areas for timber production or agricultural purposes. These logging activities substantially influence soil erosion and affect the reservoir system's ecological, biological, and hydrological functions. When logging activities are carried out, the topsoil is exposed and is often blown away by wind or washed away by rain compared to forests filled with vegetation.

Sujaul et al. (2012) conducted a study using RUSLE to assess the potential of soil loss in Tasik Chini, Pahang. The result revealed that areas of Tasik Chini, which are near high-risk and very high-risk areas, were found much shallower in-depth due to massive accumulations of sediment at the beds of lakes from the areas. This situation proves that the developmental activities and uncontrolled deforestation in the Tasik Chini area have significantly affected and caused soil erosion problems. Soil erosion affects the soil productivity of upland fields and the water quality of the streams in the catchment areas. These conditions have been created by the runoff phenomenon in the bare and half bare sloped surfaces to the streams and finally to the lake, and they will undoubtedly decrease the lake depth in the long term.

Ahmed et al. (2018) also using RUSLE in estimating of soil loss in Seremban district, Negeri Sembilan. The districts of Lenggeng, Pantai, Setul, and Ampangan recorded less soil erosion. In contrast, Seremban and Rasah recorded moderate soil erosion, and Pantai and Rentau had the highest levels of soil loss in that region. The finding shows that land use is one of the main factors contributing to soil loss due to the erosion in the Seremban district. The increment rate of deforestation and random land clearing that the region of Seremban has witnessed the urban expansion and infrastructural severe soil erosion is the aftermath of development. As such, relevant management practices and land-use planning activities should be adopted in areas of high to very high erosion risk to reduce soil loss.

Yusof et al. (2019) noticed that the area of the Pansoon sub-basin at Hulu Selangor is less susceptible to erosion risk, except in areas with long and steep slopes. The predicted soil erosion rate was performed using RUSLE. The slope gradient plays an important role in affecting the rate of erosion and slope stability. Slopes with higher gradients are at a higher risk of experiencing erosion. The high gradient will produce high water velocity and increase the erosion rate. When the surface runoff has high velocity, the water flow will carry sediments easily and rapidly via the erosion and transportation processes.

DISCUSSION

The main purpose of the soil erosion factor is to assess the degree of erosion and the risk of erosion-induced landslides. The approach and limitation to achieve both evaluation objectives are shown in Figure 1.

Erosion degree assessment identifies areas prone to soil loss due to water erosion. Appropriate mitigation measures to minimize erosion can be taken in areas that experience high soil loss. Mitigation measures aim to preserve the surrounding environment from the adverse effects of erosion, especially in water bodies' areas. The assessment of the erosion degree for a large-scale area is by adapting the USLE or RUSLE method and need to use a supporting tool such as remote sensing and Arc GIS software. The soil erodibility factor is based on the soil series published in the Malaysia Soil Report. On the other hand, assessing the erosion degree at a large-scale area, acquiring all the soil series in the particular area, needs to be known beforehand.

It will be different if the assessment of the water erosion impacts is to assess the risk of erosion-induced landslides. This assessment does not need to identify the soil series in the area. The method of determining soil erodibility factor is by taking a soil sample on the surface slope or riverbank, and then the soil sample is tested in the laboratory. The risk is classified according to the ROM Scale. Slopes or riverbanks classified as critical or high need to be taken erosion mitigation measures (remedial actions) so that the impacts of erosion can be minimized the impacts the landslide occurrence furthermore. The assessment is only appropriate for a small-scale area.

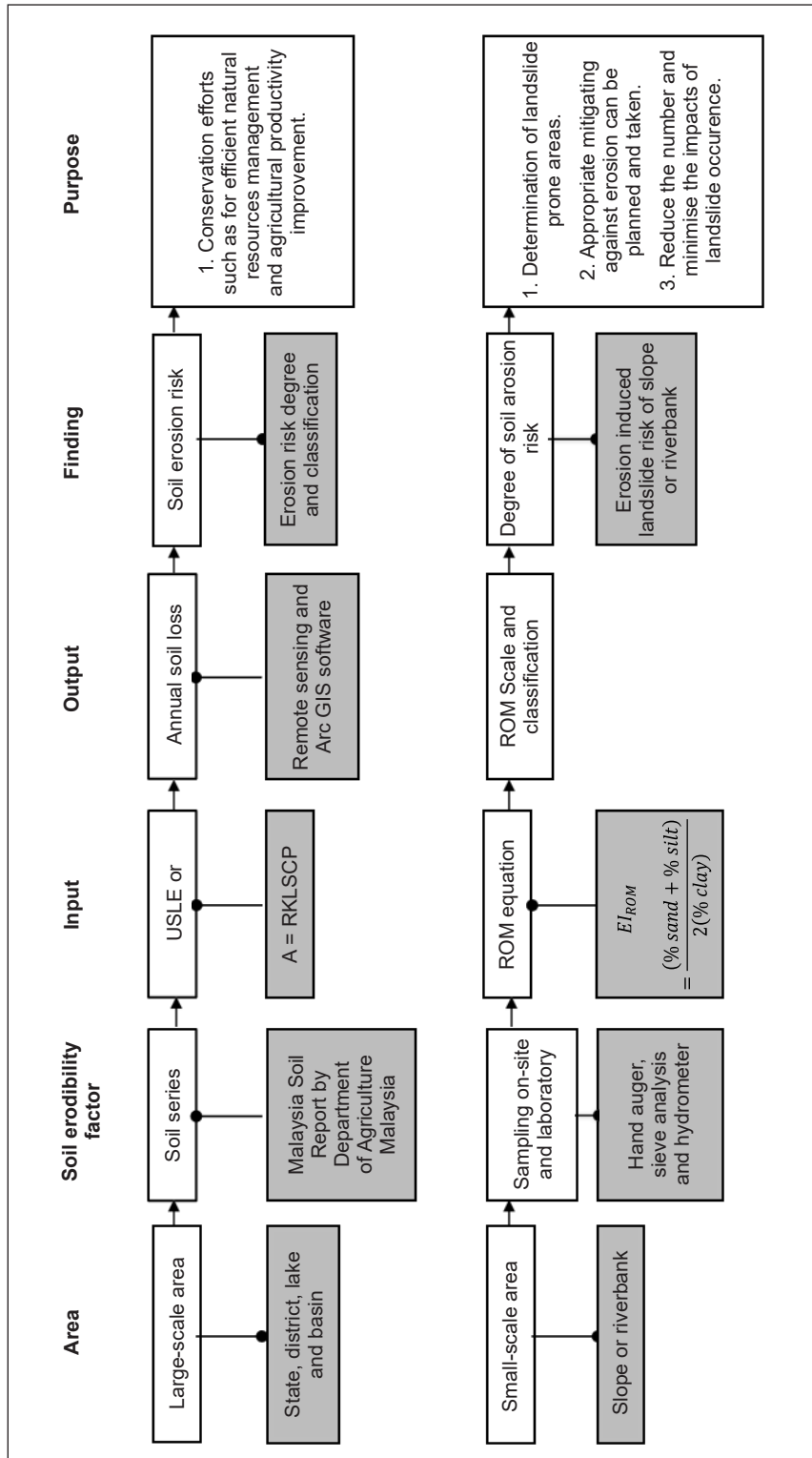


Figure 1. The flow of soil erodibility factor determination and application

Both assessment approaches lead to the same aim, which is to identify the water erosion impacts on an area. Provide the same output and identify erosion-prone areas that need mitigation measures to minimize the erosion impacts. Without mitigation measures, the erosion pollution such as sedimentation in streams and rivers in these areas will accelerate to be experienced. Severe erosion at slopes, especially at the toe, will induce landslide. The impacts of a landslide can be extensive such as destruction to properties, including loss of life, and damage to land, including loss of natural resources.

The fact is that assessing water erosion impacts based on the soil erodibility factor gives an advantage in conserving the environment. The more soil erodibility factors of soil series, slopes, and riverbanks can be determined in an area will better the understanding of erosion degree and risk. However, compared to the other parameters in the USLE equation, the soil erodibility factor is the only parameter acquired in laboratory testing, which involves more artistry, time, and cost. Besides the complexity of the analysis. For that reason, there are studies in Malaysia that simplified the analysis to determine this soil erodibility factor. Yusof et al. (2012) utilized Artificial Neural Network (ANN) to determine soil erodibility of soil series, whereby the approach simplified the determination by relying on four parameters instead of three index parameters. The approach simplified the determination of soil erodibility factor and overcame the complexity analysis and uncertainty associated with the determination. Even though the study had overcome the complexity in analysis, the input data are still acquired from soil sampling and laboratory testing. On the other hand, some of the difficulties in determining this factor had been solved but not all the difficulties. However, the study proves that the adaptation of machine learning tools can simplify the analysis to determine the soil erodibility factor and has the potential without the need to do the conversational practice in the future.

Modeling the internal factors (slope and erosion features) together with external factors (erosive agent) using machine learning tools could be a potential approach to determining the soil erodibility. Slope features such as slope length, slope steepness, slope aspect, land use, cropping management, an artificial construction, and erosion features such as erosion type, erosion channel width, erosion channel depth, and erosion channel direction are the variables that can be determined or measured by on-site works and observation. Slope features are the variables in USLE, while erosion features are the variables that could indicate general grain size distribution and erodibility tendency. For example, Nebeokike et al. (2020) found that soil samples from 15 gully sites contained a high percentage of sands, low silts and gravels, and insignificant clays. Besides, the samples have similar s-shapes of grain size distribution. These indicate soil surface with gully feature content predominantly sands and high erodibility. External factors also need to be considered since soil erodibility expresses the susceptibility of soil to erode by erosive agents. Erosive agent data such as rainfall can be collected from the government agency. Identifying significant

internal or external factors simulated by a machine learning model will produce a soil erodibility algorithm.

Moreover, the wide range of soil erodibility factors from 0.002 to 0.5 Mg ha h ha⁻¹ MJ⁻¹ mm⁻¹ with an increment of 0.001 Mg ha h ha⁻¹ MJ⁻¹ mm⁻¹ as shown in Table 3, is among the factors the determination of this soil erodibility factor needs to be simplified. A wide range with a small increment indicates that much sampling needs to be done so that the reading value is more accurate due to the high possibility of determination error.

CONCLUSION

Currently, in Malaysia, there are two widely used soil erodibility approaches, mainly to assess the impacts of soil erosion on washed and transported sediments in water bodies and landslide occurrence in slope areas. The methods are USLE and ROM scale. Both methods had advantages and disadvantages depending on the site's data availability application. Determination of soil erodibility will lead to soil erosion assessment, whereby this input significantly is one of the key factors in local authorities' decision-making in determining the safety, impact, and mitigation of any physical development in an area. However, the conventional method of determining soil erodibility involves complicated laboratory work, and analysis would be an obstacle to the holistic assessment of soil erosion, especially for erosion-induced landslide risk. Thus, new approaches are needed which practicality in terms of less artistry, time and cost, and simplicity in analysis so that more soil erodibility for soil samples could be determined. This matter is essential since rapid physical development in Malaysia also acquires the development at the sensitive area, besides limitation area with soil series information.

ACKNOWLEDGEMENT

Thanks to the Research Management Centre (RMC), Universiti Teknologi MARA (UiTM) for the financial support through Special Research Grant/Geran Penyelidikan Khas UiTM 2020 RMI file number: 600-RMC/GPK 5/3 (215/2020).

REFERENCES

- Abidin, R. Z., & Mukri, M. (2002, July 22-25). Establishment of soil erosion scale with regards to soil grading characteristic. In *2nd World Engineering Congress* (pp. 235-239). Sarawak, Malaysia.
- Abidin, R. Z., Sulaiman, M. S., & Yusoff, N. (2017). Erosion risk assessment: A case study of the Langat Riverbank in Malaysia. *International Soil and Water Conservation Research*, 5(1), 26-35. <https://doi.org/10.1016/j.iswcr.2017.01.002>
- Ahmed, G. B., Shariff, A. R. M., Balasundram, S. K., & Abdullah, A. F. B. (2018). Estimation of soil loss in Seremban, Malaysia using GIS and remote sensing technique. In *IOP Conference Series: Earth and*

- Environmental Science* (Vol. 169, No. 1, p. 012062). IOP Publishing. <https://doi.org/10.1088/1755-1315/169/1/012062>
- Algayer, B., Wang, B., Bourennane, H., Zheng, F., Duval, O., Li, G., Le Bissonnais, Y., & Darboux, F. (2014). Aggregate stability of a crusted soil: differences between crust and sub- crust material, and consequence for interrill erodibility assessment. An example from the Loess Plateau of China. *European Journal of Soil Science*, 65(3), 325-335. <https://doi.org/10.1111/ejss.12134>
- Asmamaw, L. B., & Mohammed, A. A. (2019). Identification of soil erosion hotspot areas for sustainable land management in the Gerado catchment, North-eastern Ethiopia. *Remote Sensing Applications: Society and Environment*, 13, 306-317. <https://doi.org/10.1016/j.rsase.2018.11.010>
- Basri, E. M., Adam, O. M., Teh, S. Y., & Maznah, W. W. (2019). Identification of critical erosion prone areas in Temengor Reservoir Basin using Universal Soil Loss Equation (USLE) and Geographic Information System (GIS). In *IOP Conference Series: Earth and Environmental Science* (Vol. 380, No. 1, p. 012011). IOP Publishing. <https://doi.org/10.1088/1755-1315/380/1/012011>
- Bouyoucos, G. J. (1962). Hydrometer method improved for making particle size analysis of soil. *Agricultural Journal*, 54(5), 464-465. <https://doi.org/10.2134/agronj1962.00021962005400050028x>
- El Jazouli, A., Barakat, A., Khellouk, R., Rais, J., & El Baghdadi, M. (2019). Remote sensing and GIS techniques for prediction of land use land cover change effects on soil erosion in the high basin of the Oum Er Rbia River (Morocco). *Remote Sensing Applications: Society and Environment*, 13, 361-374. <https://doi.org/10.1016/j.rsase.2018.12.004>
- Hashim, G. M., & Abdullah, W. Y. (2005). Prediction of soil and nutrient losses in a highland catchment. *Water, Air, & Soil Pollution: Focus*, 5(1), 103-113. <https://doi.org/10.1007/s11267-005-7406-x>
- Hou, J., Wang, H., Fu, B., Zhu, L., Wang, Y., & Li, Z. (2016). Effects of plant diversity on soil erosion for different vegetation patterns. *Catena*, 147, 632-637. <https://doi.org/10.1016/j.catena.2016.08.019>
- Hussein, M. H. (2013). A sheet erodibility parameter for water erosion modeling in regions with low intensity rain. *Hydrology Research*, 44(6), 1013-1021. <https://doi.org/10.2166/nh.2013.029>
- Kaffas, K., & Hrissanthou, V. (2019). Introductory chapter: Soil erosion at a glance. In *Soil Erosion-Rainfall Erosivity and Risk Assessment* (pp. 3-14). IntechOpen. <https://doi.org/10.5772/intechopen.89773>
- Ministry of Natural Resources and Environment Malaysia. (2010). *Guideline for erosion and sediment control in Malaysia*. Department of Irrigation and Drainage Malaysia. <https://www.water.gov.my/jps/resources/auto%20download%20images/5844dff6dadd8.pdf>
- Mir, S. I., Sahid, I., Gasim, M. B., Abd Rahim, S., & Toriman, M. E. (2015). Prediction of soil and nutrient losses from the lake Chini watershed, Pahang, Malaysia. *Journal of Physical Science*, 26(1), 53-70.
- Mohmadisa, H., Farhan, N. D. N. M., Zahid, M. S., Nasir, N., Zainudin, O., Yazid, S., Kadaruddin, A., & Hanifah, M. (2017). An analysis of the collapse potential of slope using the ROM scale: A case study of Sultan Azlan Shah campus, Sultan Idris Education University, Malaysia. *International Journal of Academic Research in Business and Social Sciences*, 7(6), 821-835. <http://dx.doi.org/10.6007/IJARBS/v7-i6/3041>
- Mokhtar, J., Halim, Y. A., & Asiah, Y. (2011). Analisis tahap kebolehruntuhan tanah dengan menggunakan skala ROM: Kajian di kampus Universiti Kebangsaan Malaysia, Bangi [Soil erosion level analysis using

- ROM scale: A study on the campus of Universiti Kebangsaan Malaysia, Bangi]. *Geografia - Malaysian Journal of Society and Space*, 7(3), 45–55.
- Mwaniki, M. W., Agutu, N. O., Mbaka, J. G., Ngigi, T. G., & Waithaka, E. H. (2015). Landslide scar/soil erodibility mapping using Landsat TM/ETM+ bands 7 and 3 normalised difference index: A case study of central region of Kenya. *Applied Geography*, 64, 108-120. <https://doi.org/10.1016/j.apgeog.2015.09.009>
- Nebeokike, U. C., Igwe, O., Egbueri, J. C., & Ifediegwu, S. I. (2020). Erodibility characteristics and slope stability analysis of geological units prone to erosion in Udi area, southeast Nigeria. *Modeling Earth Systems and Environment*, 6(2), 1061-1074. <https://doi.org/10.1007/s40808-020-00741-w>
- Omar, M. N., Rahaman, Z. A., & Hashim, M. (2018). The development of a soil erosion risk map for Perak, Malaysia. *International of Academic Research in Business and Social Sciences*, 8(4), 1109-1123. <https://doi.org/10.6007/IJARBS/v8-i4/4149>
- Parajuli, S. P., Yang, Z. L., & Kocurek, G. (2015). Mapping erodibility in dust source regions based on geomorphology, meteorology, and remote sensing. *Journal of Geophysical Research: Earth Surface*, 119(9), 1977-1994. <https://doi.org/10.1002/2014JF003095>
- Rickson, R. J. (2014). Can control of soil erosion mitigate water pollution by sediments? *Science of The Total Environment*, 468, 1187-1197. <https://doi.org/10.1016/j.scitotenv.2013.05.057>
- Roslan, Z. A. & Zulkifli, A. H. (2005). 'ROM' scale for forecasting erosion induced landslide risk on hilly terrain. In K. Sassa, H. Fukuoka, F. Wang & G. Wang (Eds.), *Landslides* (pp. 197-202). Springer. <https://doi.org/10.1007/3-540-28680-224>
- Sepúlveda-Lozada, A., Geissen, V., Ochoa-Gaona, S., Jarquin-Sanchez, A., de la Cruz, S. H., Capetillo, E., & Zamora-Cornelio, L. F. (2009). Influence of three types of riparian vegetation on fluvial erosion control in Pantanos de Centla, Mexico. *Revista de Biología Tropical*, 57(4), 1153-1163. <https://doi.org/10.15517/rbt.v57i4.5453>
- Sujaul, I. M., Muhammad, B. G., Ismail, B. S., Sahibin, A. R., & Mohd, E. T. (2012). Estimation of the rate of soil erosion in the Tasik Chini catchment, Malaysia using the RUSLE model integrated with the GIS. *Australian Journal of Basic and Applied Sciences*, 6(12), 286-296.
- Tang, F. K., Cui, M., Lu, Q., Liu, Y. G., Guo, H. Y., & Zhou, J. X. (2016). Effects of vegetation restoration on the aggregate stability and distribution of aggregate-associated organic carbon in a typical karst gorge region. *Solid Earth*, 7(1), 141-151. <https://doi.org/10.5194/se-7-141-2016>
- Vaezi, A. R., Hasanzadeh, H., & Cerda, A. (2016). Developing an erodibility triangle for soil textures in semi-arid regions, NW Iran. *Catena*, 142, 221-232. <https://doi.org/10.1016/j.catena.2016.03.015>
- Wang, Z. J., Jiao, J. Y., Rayburg, S., Wang, Q. L., & Su, Y. (2016). Soil erosion resistance of “Grain for Green” vegetation types under extreme rainfall conditions on the Loess Plateau, China. *Catena*, 141, 109-116. <https://doi.org/10.1016/j.catena.2016.02.025>
- Wei, H., Zhao, W. W., & Wang, J. (2017). Research process on soil erodibility. *Chinese Journal of Applied Ecology*, 28, 2749-2759.
- Yusof, M. F., Abdullah, R. O. Z. I., Azamathulla, H. M., Zakaria, N. A., & Ghani, A. A. B. (2011, December 6-9). Modified soil erodibility factor, K for Peninsular Malaysia soil series. In *3rd International Conference*

on Managing Rivers in the 21st Century. Sustainable Solutions for Global Crisis of Flooding, Pollution and Water Scarcity (pp. 799-808). Penang, Malaysia.

- Yusof, M. F., Azamathulla, H. M., & Abdullah, R. (2014). Prediction of soil erodibility factor for Peninsular Malaysia soil series using ANN. *Neural Computing and Applications*, 24(2), 383-389. <https://doi.org/10.1007/s00521-012-1236-3>
- Yusof, N. F., Lihan, T., Idris, W. M. R., & Rahman, Z. A. (2019). Prediction of soil erosion in Pansoon Sub-basin, Malaysia using RUSLE integrated in Geographical Information System. *Sains Malaysiana*, 48(11), 2565-2574. <http://dx.doi.org/10.17576/jsm-2019-4811-26>
- Zhou, J., Fu, B., Gao, G., Lü, Y., Liu, Y., Lü, N., & Wang, S. (2016). Effects of precipitation and restoration vegetation on soil erosion in a semi-arid environment in the Loess Plateau, China. *Catena*, 137, 1-11. <https://doi.org/10.1016/j.catena.2015.08.015>
- Zuliziana, S., Anis, A. R. M. A., & Nordila, A. (2018). Predicting of soil erosion with regarding to rainfall erosivity and soil erodibility. In *AIP Conference Proceedings* (Vol. 1930, p. 020054-1). AIP Publishing. <https://doi.org/10.1063/1.5022948>



Review Article

Classification of Fault Prediction: A Mapping Study

Sasha Farhana Shamsul Anwar¹, Marshima Mohd Rosli^{1,2*} and Nur Atiqah Sia Abdullah¹

¹Faculty of Computer and Mathematical Sciences, Universiti Teknologi MARA, 40450 UiTM, Shah Alam, Selangor, Malaysia

²Institute for Pathology, Laboratory and Forensic Medicine (I-PPerForM), University Teknologi MARA, 47000 UiTM, Sungai Buloh, Selangor, Malaysia

ABSTRACT

Software fault prediction is an important activity in the testing phase of the software development life cycle and involves various statistical and machine learning techniques. These techniques are useful for making accurate predictions to improve software quality. Researchers have used different techniques on different datasets to build fault prediction in software projects, but these techniques vary and are not generalised. As a result, it creates challenges that make it difficult to choose a suitable technique for software fault prediction in a particular context or project. This mapping study focuses on research published from 1997 to 2020 involving fault prediction techniques, intending to determine a classification of fault prediction techniques based on problem types that researchers need to solve. This study conducted a systematic mapping study to structure and categorise the research evidence that has been published in fault prediction. A total of 82 papers are mapped to a classification scheme. This study identified research gaps and specific issues for practitioners, including the need to classify fault prediction techniques according to problem types and to provide a systematic way to identify suitable techniques for fault prediction models.

Keywords: Fault prediction techniques, fault prediction, software metrics, systematic mapping

ARTICLE INFO

Article history:

Received: 20 August 2021

Accepted: 16 December 2021

Published: 25 May 2022

DOI: <https://doi.org/10.47836/pjst.30.3.23>

E-mail addresses:

sashafarhana95@gmail.com (Sasha Farhana Shamsul Anuar)

marshima@uitm.edu.my (Marshima Mohd Rosli)

atiqah684@uitm.edu.my (Nur Atiqah Sia Abdullah)

* Corresponding author

INTRODUCTION

Software development projects in any organisation worldwide include software quality management strategies and processes to determine the stability of software before

the deployment phase (Kassie & Singh, 2020). However, software development projects are mainly a human-driven process, requiring intensive efforts from software engineers to manage requirements, design, source codes, defect data and documentation, and this human-driven process may introduce defects or faults throughout the software development life cycle, which may affect the project management process, particularly concerning project schedules and budget (Illes-Seifert & Paech, 2010; Kim et al., 2008; Rosli et al., 2011).

Software fault prediction is a process of estimating and predicting faults or defects in software modules during a defined period of development and operation. Research in the field of software fault prediction mainly focuses on various methods and tools, such as artificial intelligence and data mining, to detect faults in the software modules (Dejaeger et al., 2013; Geng et al., 2018; Khoshgoftaar et al., 2006; Al Qasem et al., 2020). In general, efforts are concentrated on the number of fault predictions, and system reliability estimation focuses on time failure and understanding the significance of the design and testing process on the defect count (Kastro & Bener, 2008). There are three components commonly involved in software fault prediction: data mining techniques and machine learning algorithms, software characteristics, and fault data.

Software fault prediction reduces cost and improves data quality performance with a characteristics identifier to differentiate and filter the available software modules to continue the next process testing phase (Al Qasem et al., 2020). However, most of the existing prediction models use binary classification that explains whether a source code module or method level is categorised as faulty or non-faulty. Software project managers may, therefore, not differentiate the results of the prediction information regarding the nature and type of fault-prone modules. Thus, it is better to devise a prediction model with actionable results for managers (Caglayan et al., 2015).

Prior review studies reporting on software prediction (Catal, 2011; Catal & Diri, 2009; Murillo-Morera et al., 2015) explored a particular area of fault prediction activities. Recently, Rathore et al. reported a similar review study that examined the main activities in fault prediction, including fault prediction techniques, software metrics, performance measurements and data quality issues (Rathore & Kumar, 2017). They presented a taxonomy of fault prediction techniques based on machine learning and the statistics environment. They found that most studies used object-oriented metrics and process metrics in the fault prediction model.

This research, therefore, presents the outcome of a systematic mapping study of recent research on activities of the software fault prediction process, particularly to obtain information about which techniques are suitable for which form of prediction and what software metrics are used. The mapping study addresses the following research questions: (1) What problem types are contended with in fault prediction models addressed in the literature? (2) What forms of prediction are used in fault prediction models addressed in

the literature? (3) What software metrics are used in fault prediction models addressed in the literature?

Researchers propose a variation of robust techniques for different reasons. Some propose techniques concerning how the technique affects the fault prediction results. Others propose a technique to deal with the fault prediction capabilities and a different set of software metrics for improving fault prediction. Both groups are important, but the earlier group that captures the fault prediction model may perform best when the right technique is selected for the appropriate domain of the dataset. This study classifies the papers regarding how researchers use the techniques in software fault prediction.

This study also aims to highlight important research gaps in fault prediction techniques. A total of 82 studies were selected for this mapping study. This study presents the synthesis of evidence for fault prediction techniques based on six classification subcategories: (1) classification, (2) prediction, (3) clustering, (4) optimisation, (5) anomaly detection and (6) rendering. This study also discusses the form of prediction and software metrics used in the studies.

RELATED WORK

Over the past decade, many studies have been published in fault prediction research, but only a few have reported explicitly on the fault prediction techniques. This absence of fault prediction techniques reporting is confirmed by four studies that conducted reviews of fault prediction in software engineering (Catal, 2011; Catal & Diri, 2009; Murillo-Morera et al., 2015; Rathore & Kumar, 2017).

In 2009, Catal and Diri performed a systematic review of fault prediction studies (Catal & Diri, 2009). They identified 74 studies published from 1997 to 2007 that addressed fault prediction activities in the literature. They classified the papers into four categories: (1) types of metrics, (2) types of methods, (3) evaluation criteria and (4) publication types. They mostly assessed the usage of machine learning algorithms, public datasets, and software metrics in fault prediction research. They reported that most of the papers used machine learning algorithms as the preferred method for fault prediction.

In 2011, Catal performed an updated systematic review on fault prediction techniques (Catal, 2011). He found 90 papers published from 1990 to 2009 and classified the papers according to the publication year. He evaluated the performance of fault prediction techniques to predict software fault modules. He reported that most papers applied method-level metrics and machine learning techniques.

In 2015, Murillo-Morera et al. performed a systematic mapping study to categorise fault prediction techniques, metrics and performance metrics to determine patterns and schemes to predict software faults (Murillo-Morera et al., 2015). They found 70 studies published from 2002 to 2014. They classified the papers into three main categories: software metrics,

techniques, and models. They proposed six categories of techniques: (1) machine learning, (2) machine learning and classification, (3) machine learning and clustering, (4) machine learning and statistical analysis, (5) clustering and (6) statistical analysis.

In 2017, Rathore et al. conducted a comprehensive review study on software fault prediction activities that included fault prediction techniques, software metrics and performance evaluation (Rathore & Kumar, 2017). They found 78 papers published from 1993 to 2016. They classified the papers into four categories: software metrics, forms of prediction, fault prediction techniques and performance measurements. They proposed four categories of prediction techniques: (1) statistical techniques, (2) supervised learning algorithms, (3) semi-supervised learning algorithms and (4) unsupervised learning algorithms. They reported that several research studies used faulty and non-faulty techniques as the performance measure of fault prediction. However, many studies paid scant attention to performance-based predicting faults and the severity of faults issues.

These review studies focused on a specific dimension or area in fault prediction activities; however, none specifically examined which fault prediction techniques are suitable for a given problem. Such review studies mainly help us recognise the fault prediction techniques discussed in the literature. However, these studies tend to focus on how researchers use fault prediction techniques rather than how they affect their fault prediction model for a given problem. This study conducts a systematic mapping study to determine which fault prediction techniques might affect the prediction model for a specific problem. Although the general goal of the mapping study appears to be similar to past review studies (Catal, 2011; Murillo-Morera et al., 2015; Rathore & Kumar, 2017), this study aims to identify studies that are concerned with how the fault prediction techniques influence the fault prediction model for a particular problem.

METHOD

A systematic mapping study involves a well-defined methodology to identify and review relevant research evidence. Therefore, it provides a clear explanation for specific research questions. Further, these specific research questions must have been used before exploring the topic under investigation. Therefore, the mapping study adopted the guidelines suggested by Peterson et al. (2008), Kitchenham et al. (2011), and Budgen et al. (2008).

This study aimed to categorise and structure empirical evidence in papers that discussed fault prediction techniques. This study will help researchers and practitioners gather, classify, and aggregate results in related studies to identify research gaps and challenges for improvement in the body of knowledge. The systematic mapping process consists of five steps: (1) defining the research questions, (2) searching, (3) selection of papers, (4) abstract keywording, and (5) data extraction and mapping of publications.

Definition of Research Questions

This research formulated the research questions according to the PICOC model by Kitchenham et al. (2011). The research questions are detailed below:

- RQ1: What problem types of fault prediction techniques are dealt with in fault prediction models addressed in the literature?
- RQ2: What forms of prediction are used in fault prediction models addressed in the literature?
- RQ3: What software metrics are used in fault prediction models addressed in the literature?

Conducting Search

A thorough search is required to identify relevant literature. For this reason, a search strategy is necessary, which entails identifying the right search string with the relevant terms and keywords. It will ensure wide coverage and increase the chance of identifying the right publication. Therefore, in this mapping study, the steps used to construct the search string were as follows:

- identify keywords in relevant papers
- search synonyms for identified keywords
- formulate search strings using Boolean OR to include alternative spellings and synonyms and Boolean AND to combine major terms.

The search string was as follows:

("software fault prediction" OR "software defect prediction") AND ("fault prediction techniques" OR "defect prediction techniques" OR "software fault prediction techniques") AND ("software fault datasets" OR "software defect datasets") AND ("systematic mapping") AND ("software metrics") AND ("empirical studies")

Papers from important conferences and journals in the research field, such as *IEEE Transaction of Software Engineering*, *IET Software* and *Journal of Software Engineering*, were included in this process. This study is limited to the fields of computer science and software engineering.

This study examined papers written in the last 23 years, from 1997 to 2020. This decision was based on an earlier study (Rathore & Kumar, 2017) conducted in a systematic study published in 2017. The search method was divided into two parts: primary and secondary searches.

This study used the search string in the primary search on Scopus, ScienceDirect, SpringerLink, ACM Digital and IEEE Xplore online databases. According to the requirements, the above search string was customised for each online database. Table 1 summarises the results of the primary search.

This study used a snowball method in the secondary search to find related papers by reviewing references for the papers chosen in the first part. Then, from the earlier systematic review (Rathore & Kumar, 2017), related papers were selected that were released between 1997 and 2020. With that analysis, a similar search string was used. Table 2 summarises the search results used for a secondary search.

Selection of Papers

This study defined inclusion and exclusion criteria for this mapping study to avoid a biased selection of papers. The inclusion criteria were (1) peer-review papers that discuss the fault prediction techniques in fault prediction models and (2) peer-review papers that discuss the forms of prediction and software metrics in fault prediction models. The exclusion criterion was peer-review papers that describe fault prediction techniques but not the software metrics.

After performing the automatic search, a set of 366 papers was obtained. The screening process was done by inspecting the title and abstract of each paper to exclude unrelated and identical documents. As a result, it reduced the number of papers in the primary search from 366 to 22 relevant papers. For the secondary search results, basic and detailed inclusion and exclusion criteria were applied for the 82 selected papers, reducing the relevant papers to 60. At this point, the total screening results were reduced to only 82 relevant papers¹.

Developing Classification Schemes

This study developed classification schemes by identifying the keywords and concepts in the abstract of each paper. Next, the keywords and concepts were combined to produce the outline of the terms used in the research. Then, suitable keywords were selected to structure the schemes or categories. Finally, three categories were determined: problem type of prediction (RQ1), a form of prediction (RQ2) and software metrics (RQ3).

Data Extraction And Mapping of Studies

Excel spreadsheet was used for data logging and output production. All the data and

¹ The list of papers included in this study is available from: <https://tinyurl.com/SMFaultdata>

Table 1
Results of primary search

Online database	Search results	Relevant papers
Scopus	191	6
SpringerLink	100	7
ScienceDirect	31	3
ACM Digital Library	23	2
IEEE Xplore	21	4
Total	366	22

Table 2
Results of secondary search

Method	Search results	Relevant papers
Snowball	4	2
Papers from the previous study	78	58
Total	82	60

identified papers were mapped into three categories. Results were tabulated into tables, and publication frequencies were calculated in each category.

RESULTS

Problem Type of Prediction (RQ1)

A classification scheme of fault prediction techniques was constructed into groups of problem types based on the issues that researchers need to solve. The problem types are shown in Table 3.

Table 3
Problem type of fault prediction

Problem type	Fault prediction techniques
Classification	Naive Bayes, decision tree, K-nearest neighbour
Prediction	Linear regression, logistic regression
Clustering	Random forest, bagging boosting
Optimisation	Gradient algorithm, batch gradient descent, mini-batch gradient descent, stochastic gradient descent
Anomaly detection	Support vector machine, least squares—support vector machine, kernel
Rendering	Rank boost

The 82 papers were grouped into six categories of problem type for fault prediction techniques: (1) classification, (2) prediction, (3) clustering, (4) optimisation, (5) anomaly detection and (6) rendering. As shown in Table 4, the distribution of papers was not consistent throughout the years 1997–2020. However, there are high numbers of publications in 2012 to solve problems related to classification (seven papers) and clustering (four papers). Classification techniques such as Naive Bayes performed better than more complex predictors and produced good precision among the other statistical techniques. However, Naive Bayes had the lowest recall of the predictor models, and its lack of cross-project prediction is well documented (Hosseini et al., 2016; Peters et al., 2013).

Twelve papers were published in 2016 that solved problems related to clustering and prediction. The clustering techniques included k-means algorithms, X-mean clustering (Seo & Bae, 2013), fuzzy and expectation maximisation (EM) clustering, and density-based spatial clustering (Garcia et al., 2016). In addition, a reasonable number of papers have been published to solve problems with anomaly detection, rendering and prediction. However, the trend of publications decreased for optimisation using gradient algorithms, with five papers throughout the years.

Table 4
Distribution of papers on problem type of fault prediction technique

Year	Classification	Prediction	Clustering	Optimisation	Anomaly detection	Rendering	Total
1997	0	1	0	0	0	0	1
2000	0	1	0	0	0	0	1
2004	4	0	0	0	0	0	4
2005	1	1	0	0	1	0	3
2006	1	0	1	0	0	0	2
2007	5	0	1	0	1	2	9
2008	1	0	0	0	0	1	2
2009	1	0	0	0	0	2	3
2010	0	0	0	1	0	0	1
2011	1	0	1	2	0	1	5
2012	7	1	4	0	5	1	18
2013	2	0	1	1	1	1	6
2014	0	0	2	0	2	1	5
2015	1	0	0	0	1	0	2
2016	1	5	5	0	0	1	12
2020	3	0	2	1	2	0	8
Total	28	9	17	5	13	10	

Form of Prediction (RQ2)

As shown in Figure 1, three types of fault prediction addressed in the literature, and two papers that applied more than one type of fault prediction in their research were found, so the counts sum up to more than 82. In addition, the category (‘Did not say’) was added

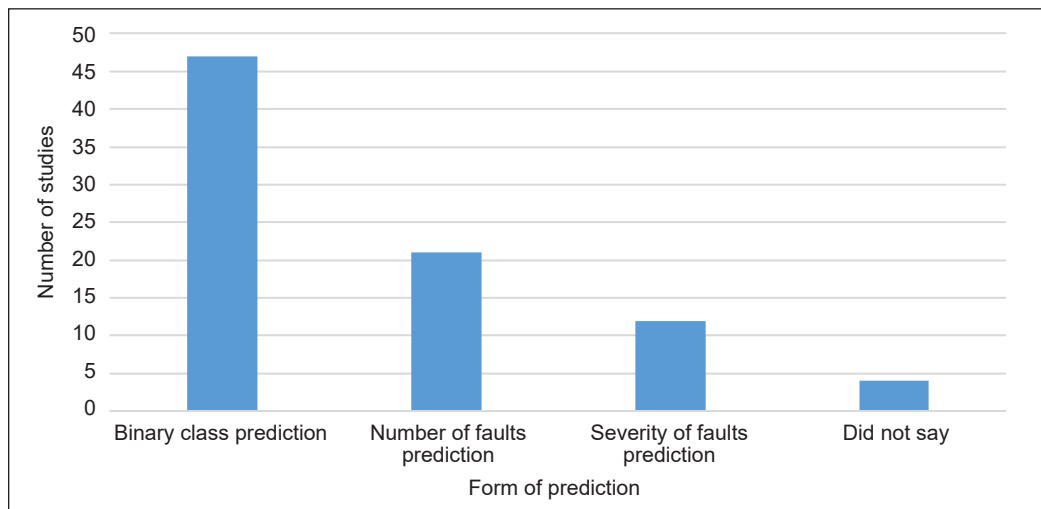


Figure 1. Form of prediction

to group papers that described fault prediction techniques but did not identify the form of prediction.

In this study, most of the published papers (47) used binary class prediction in the fault prediction model, and most of these divided the category into faulty or non-faulty classes. In addition, these studies identified the faulty class as a module that captures more than one fault and the non-faulty class as a module that captures zero faults (Gokhale & Lyu, 1997; Mendes-Moreira et al., 2012; Vandecruys et al., 2008).

As shown in Figure 1, 21 papers used the number of faults prediction, and 12 papers used the severity of faults prediction. Past studies rarely used severity of faults prediction because the available datasets categorised fault severity according to various classifications. However, few studies built fault prediction based on the severity of faults using object-oriented metrics and reported that object-oriented metrics improve fault severity prediction in software projects (Ardil & Sandhu, 2010; Zhou & Leung, 2006).

Software Metrics (RQ3)

This study aimed to identify the software metrics used in fault prediction models. Figure 2 shows the frequency of software metrics used in the selected papers. The software metrics were classified into five categories: traditional metrics, object-oriented metrics, dynamic metrics, process metrics, and did not say.

Traditional metrics (34 papers) were used most frequently in fault prediction models in the literature. In addition, the traditional metrics are used during the beginning of software engineering evolution. This study found four kinds of traditional metrics: size-based (e.g., source lines of code (SLOC), function points (FP), and kilo-SLOC), quality-based (e.g.,

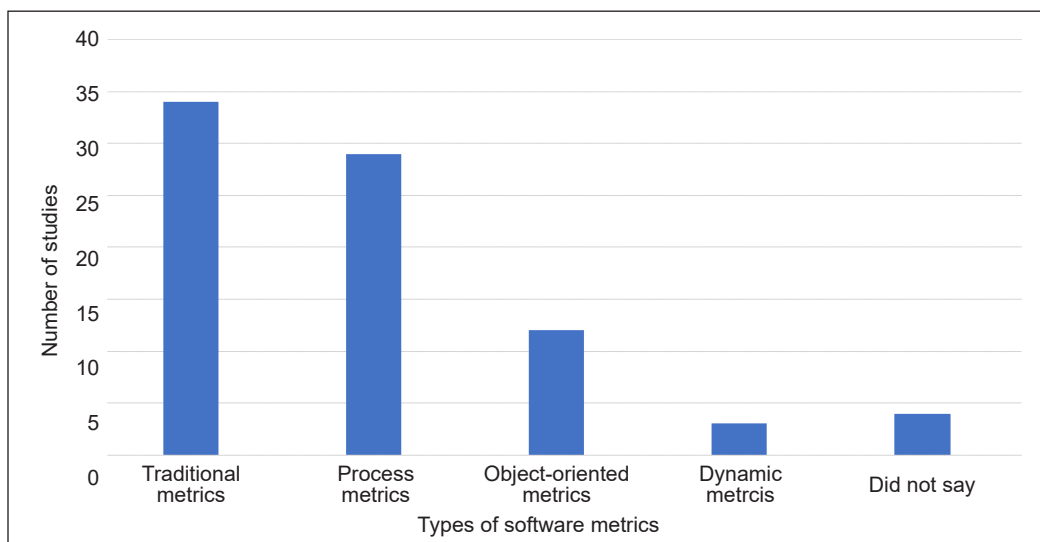


Figure 2. Types of software metrics

defects per function points and defects per source lines of code after delivery), system-complexity (e.g., cyclomatic complexity and McCabe complexity) and Halstead metrics (e.g., a total of distinct operands and a total of distinct operators).

Process metrics are measures of characteristics of the software development process collected across the software development life cycle. These metrics are used to improve software development and maintenance. This study found 29 papers that used process metrics, including code delta, code churn (Shin et al., 2011), change, developer-based and requirement metrics (Yadav & Yadav, 2015). Code delta is the delta of LOC and delta of changes. Code churn mainly involves total LOC, churned LOC, deleted LOC, file count, churn count and files churned. Finally, change metrics are LOC related to revisions, refactoring, bug fixes and authors.

Object-oriented metrics are commonly used in modern software development for fault prediction models. However, this study found only 12 papers that used object-oriented metrics, indicating low usage of object-oriented metrics reported from 1997 to 2020, inconsistent with results from the past study (Murillo-Morera et al., 2015). It may be due to differences in the search string for systematic mapping applied in that study.

Three studies used dynamic metrics in building fault prediction for their software projects. Some of the dynamic metrics are metrics suite (e.g., export object coupling and import object coupling) (Hall et al., 2012), Arisholm metrics suite (e.g. IC_OD and IC_OM) (Shin et al., 2009), and Mitchell metrics suite (e.g. coupling between objects and dynamic coupling between two classes) (Weyuker et al., 2007).

Mapping

Figure 3 presents a distribution map of papers over a defined classification scheme: problem type of prediction, a form of prediction and software metrics. Problem type of prediction is shown on the *y*-axis, a form of prediction - on the left *x*-axis, and software metrics on the right *x*-axis. The size and number of each bubble represent the number of publications in the corresponding category pair. Papers were assembled in more than one classification scheme for each category because they could make several contributions. Therefore, the total paper count does not equal the final total of 82.

The mapping results imply that most of the research effort involved solving problems related to classification using traditional metrics and LOC metrics and applied binary class prediction in the fault prediction model. Furthermore, it indicates that techniques such as naive Bayes, decision tree and K-nearest neighbour might have outperformed other techniques in terms of performance.

Another technique that the researchers widely used is anomaly detection in binary class prediction. This technique was applied mostly with LOC metrics to improve intrusion detection and security attacks (Hosseinzadeh et al., 2021; Khan et al., 2007; Mohammed &

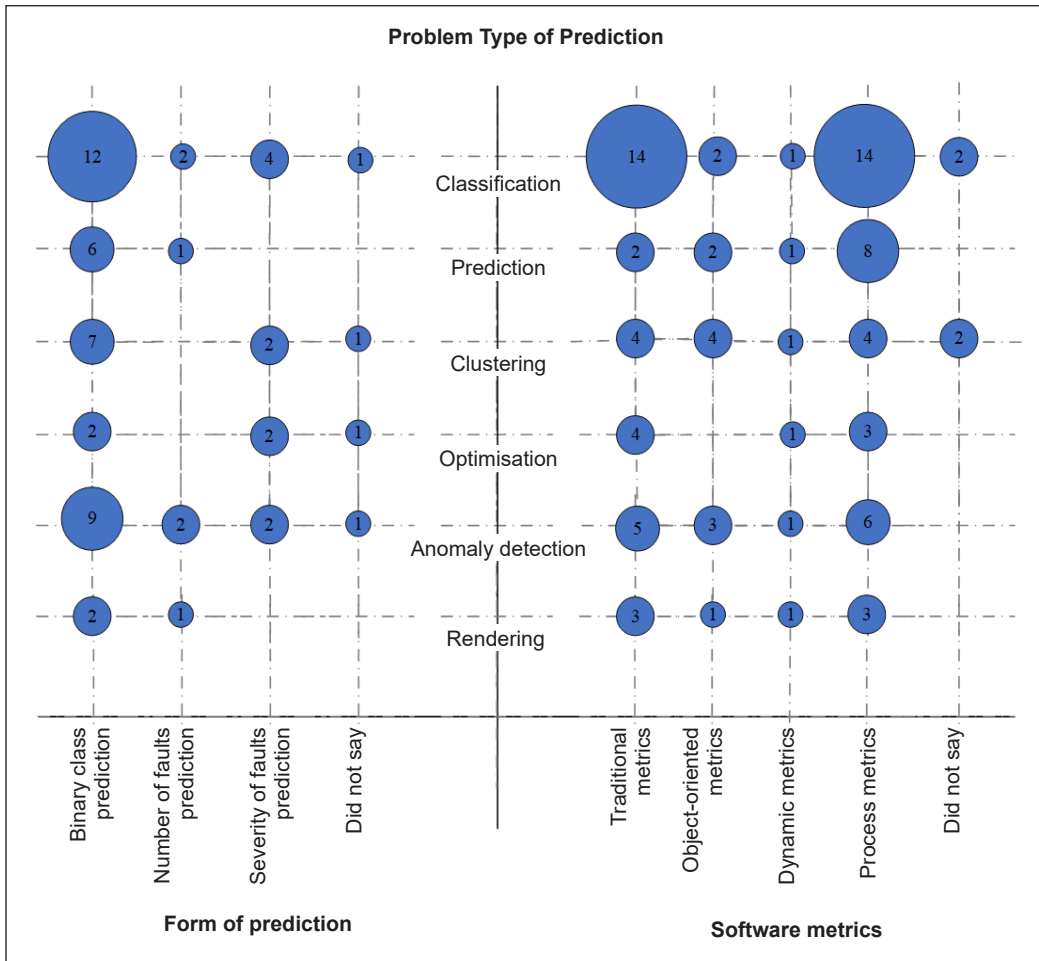


Figure 3. Distribution of research by problem type of prediction, a form of prediction and software metrics

Sulaiman, 2012). The researchers have widely used clustering techniques in binary class prediction with traditional, object-oriented, and LOC metrics. The problem types that received the least attention among researchers were rendering and optimisation.

DISCUSSIONS

The mapping study was designed to investigate current research on the software fault prediction process activities, such as fault types, forms of prediction and software metrics used in fault prediction. This study found 82 papers from a total of 366 potential papers. These papers were classified into three categories: problem type of prediction, a form of prediction and software metrics.

Many papers on fault prediction techniques to solve various problems have been published (Catal & Diri, 2009; Murillo-Morera et al., 2015; Rathore & Kumar, 2017).

However, some fault prediction techniques effectively solve specific problems, and no categories that classify the fault prediction techniques exist. As mentioned earlier, this study constructed a classification scheme for fault prediction techniques based on the issues or problems that needed to be solved. The classification scheme consists of six groups: classification, prediction, clustering, optimisation, anomaly detection and rendering.

These groups are based on the issues or problems that researchers need to solve. Eighty-two relevant papers were classified into these categories and found that these groups are common and useful in choosing a suitable fault prediction technique to solve a particular problem.

The results highlight that binary class prediction is the most popular prediction form used by researchers with various classification prediction techniques. This finding shows that most researchers preferred to perform binary class prediction as it is a less complex and straightforward prediction for a given dataset. These findings are consistent with past studies (Rathore & Kumar, 2017), showing that most publications applied binary class prediction in fault prediction models.

Traditional metrics and LOC have been widely discussed in the literature concerning the many types of software metrics. However, this study found that the number of papers based on object-oriented and dynamic metrics is relatively low. This finding shows that various factors may influence researchers to select suitable software metrics for fault prediction techniques.

The validity threat in this mapping study is the inappropriate selection of publications due to inadequate search terms in the search string. This study has refined the search string and performed search testing before executing the search strategy process to mitigate the threat. In addition, the search string was verified by another researcher to locate any missing terms in the search string.

CONCLUSION

This mapping study aimed to determine a classification scheme for fault types, forms of prediction and software metrics applied in fault prediction models. The results of this mapping study have revealed that some fault prediction techniques are effective in solving specific kinds of problems. Hence, there is a need to construct categories of fault prediction techniques and have taken the first step by proposing a classification scheme for fault prediction techniques based on the issues or problems needed to be solved.

The authors are currently constructing a model for building software fault prediction by applying the classification scheme of fault prediction techniques. In future, the authors plan to develop a recommender system to recommend the most suitable fault prediction technique to solve a fault prediction problem.

ACKNOWLEDGEMENT

The authors want to thank the Universiti Teknologi MARA and the Ministry of Education Malaysia for their financial support of this project under FRGS Grant No. 600-IRMI/FRGS 5/3 (212/2019).

REFERENCES

- Al Qasem, O., Akour, M., & Alenezi, M. (2020). The influence of deep learning algorithms factors in software fault prediction. *IEEE Access*, 8, 63945-63960. <https://doi.org/10.1109/ACCESS.2020.2985290>
- Ardil, E., & Sandhu, P. S. (2010). A soft computing approach for modeling of severity of faults in software systems. *International Journal of Physical Sciences*, 5(2), 74-85. <https://doi.org/10.5897/IJPS.9000037>
- Budgen, D., Turner, M., Brereton, P., & Kitchenham, B. (2008, September 10-12). Using mapping studies in software engineering. In *Proceedings of Psychology of Programming Interest Group Workshop* (Vol. 8, pp. 195-204). Lancaster, UK.
- Caglayan, B., Misirli, A. T., Bener, A. B., & Miranskyy, A. (2015). Predicting defective modules in different test phases. *Software Quality Journal*, 23(2), 205-227. <https://doi.org/10.1007/s11219-014-9230-x>
- Catal, C. (2011). Software fault prediction: A literature review and current trends. *Expert Systems with Applications*, 38(4), 4626-4636. <https://doi.org/10.1016/j.eswa.2010.10.024>
- Catal, C., & Diri, B. (2009). A systematic review of software fault prediction studies. *Expert Systems with Applications*, 36(4), 7346-7354. <https://doi.org/10.1016/j.eswa.2008.10.027>
- Dejaeger, K., Verbraken, T., & Baesens, B. (2013). Toward comprehensible software fault prediction models using bayesian network classifiers. *IEEE Transactions on Software Engineering*, 39(2), 237-257. <https://doi.org/10.1109/TSE.2012.20>
- Garcia, L. P. F., de Carvalho, A. C. P. L. F., & Lorena, A. C. (2016). Noise detection in the meta-learning level. *Neurocomputing*, 176, 14-25. <https://doi.org/10.1016/j.neucom.2014.12.100>
- Geng, R., Wang, X., Ye, N., & Liu, J. (2018). A fault prediction algorithm based on rough sets and back propagation neural network for vehicular networks. *IEEE Access*, 6, 74984-74992. <https://doi.org/10.1109/ACCESS.2018.2881890>
- Gokhale, S. S., & Lyu, M. R. (1997). Regression tree modeling for the prediction of software quality. In *Proceedings of the Third ISSAT International Conference on Reliability and Quality in Design* (pp. 31-36). International Society of Science and Applied Technologies.
- Hall, T., Beecham, S., Bowes, D., Gray, D., & Counsell, S. (2012). A systematic literature review on fault prediction performance in software engineering. *IEEE Transactions on Software Engineering*, 38(6), 1276-1304. <https://doi.org/10.1109/TSE.2011.103>
- Hosseini, S., Turhan, B., & Mäntylä, M. (2016). Search based training data selection for cross project defect prediction. In *Proceedings of the The 12th International Conference on Predictive Models and Data Analytics in Software Engineering* (pp. 1-10). ACM Publishing. <https://doi.org/10.1145/2972958.2972964>

- Hosseinzadeh, M., Rahmani, A. M., Vo, B., Bidaki, M., Masdari, M., & Zangakani, M. (2021). Improving security using SVM-based anomaly detection: Issues and challenges. *Soft Computing*, 25(4), 3195-3223. <https://doi.org/10.1007/s00500-020-05373-x>
- Illes-Seifert, T., & Paech, B. (2010). Exploring the relationship of a file's history and its fault-proneness: An empirical method and its application to open source programs. *Information and Software Technology*, 52(5), 539-558. <https://doi.org/10.1016/j.infsof.2009.11.010>
- Kassie, N. B., & Singh, J. (2020). A study on software quality factors and metrics to enhance software quality assurance. *International Journal of Productivity and Quality Management*, 29(1), 24-44. <https://doi.org/10.1504/IJPQM.2020.104547>
- Kastro, Y., & Bener, A. B. (2008). A defect prediction method for software versioning. *Software Quality Journal*, 16(4), 543-562. <https://doi.org/10.1007/s11219-008-9053-8>
- Khan, L., Awad, M., & Thuraisingham, B. (2007). A new intrusion detection system using support vector machines and hierarchical clustering. *The VLDB Journal*, 16(4), 507-521. <https://doi.org/10.1007/s00778-006-0002-5>
- Khoshgoftaar, T. M., Seliya, N., & Sundaresh, N. (2006). An empirical study of predicting software faults with case-based reasoning. *Software Quality Journal*, 14(2), 85-111. <https://doi.org/10.1007/s11219-006-7597-z>
- Kim, S., Whitehead, E., & Zhang, Y. (2008). Classifying software changes: Clean or buggy? *IEEE Transactions on Software Engineering*, 34(2), 181-196. http://ieeexplore.ieee.org/xpls/abs_all.jsp?arnumber=4408585
- Kitchenham, B. A., Budgen, D., & Brereton, O. P. (2011). Using mapping studies as the basis for further research - A participant-observer case study. *Information and Software Technology*, 53(6), 638-651. <https://doi.org/10.1016/j.infsof.2010.12.011>
- Mendes-Moreira, J., Soares, C., Jorge, A. M., & de Sousa, J. F. (2012). Ensemble approaches for regression. *ACM Computing Surveys*, 45(1), 1-40. <https://doi.org/10.1145/2379776.2379786>
- Mohammed, M. N., & Sulaiman, N. (2012). Intrusion detection system based on SVM for WLAN. *Procedia Technology*, 1, 313-317. <https://doi.org/10.1016/j.protcy.2012.02.066>
- Murillo-Morera, J., Quesada-López, C., & Jenkins, M. (2015, April 22-24). Software fault prediction: A systematic mapping study. In *CIBSE 2015 - XVIII Ibero-American Conference on Software Engineering* (pp. 446-459). Lima, Peru.
- Peters, F., Menzies, T., & Marcus, A. (2013). Better cross company defect prediction. In *2013 10th Working Conference on Mining Software Repositories (MSR)* (pp. 409-418). IEEE Publishing. <https://doi.org/10.1109/MSR.2013.6624057>
- Petersen, K., Feldt, R., Mujtaba, S., & Mattsson, M. (2008, June 26-27). Systematic mapping studies in software engineering. In *12th International Conference on Evaluation and Assessment in Software Engineering, EASE 2008* (pp. 1-10). University of Bari, Italy. <https://doi.org/10.14236/ewic/EASE2008.8>
- Rathore, S. S., & Kumar, S. (2017). A study on software fault prediction techniques. *Artificial Intelligence Review*, 51(2), 255-327. <https://doi.org/10.1007/s10462-017-9563-5>

- Rosli, M. M., Teo, N. H. I., Yusop, N. S. M., & Mohammad, N. S. (2011). The design of a software fault prone application using evolutionary algorithm. In *2011 IEEE Conference on Open Systems* (pp. 338-343). IEEE Publishing. <https://doi.org/10.1109/ICOS.2011.6079246>
- Seo, Y. S., & Bae, D. H. (2013). On the value of outlier elimination on software effort estimation research. *Empirical Software Engineering*, *18*(4), 659-698. <https://doi.org/10.1007/s10664-012-9207-y>
- Shin, Y., Bell, R., Ostrand, T., & Weyuker, E. (2009). Does calling structure information improve the accuracy of fault prediction? In *2009 6th IEEE International Working Conference on Mining Software Repositories* (pp. 61-70). IEEE Publishing. <https://doi.org/10.1109/MSR.2009.5069481>
- Shin, Y., Meneely, A., Williams, L., & Osborne, J. A. (2011). Evaluating complexity, code churn, and developer activity metrics as indicators of software vulnerabilities. *IEEE Transactions on Software Engineering*, *37*(6), 772-787. <https://doi.org/10.1109/TSE.2010.81>
- Vandecruys, O., Martens, D., Baesens, B., Mues, C., De Backer, M., & Haesen, R. (2008). Mining software repositories for comprehensible software fault prediction models. *Journal of Systems and Software*, *81*(5), 823-839. <https://doi.org/10.1016/j.jss.2007.07.034>
- Weyuker, E. J., Ostrand, T. J., & Bell, R. M. (2007). Using developer information as a factor for fault prediction. In *Third International Workshop on Predictor Models in Software Engineering (PROMISE'07: ICSE Workshops 2007)* (pp. 8-8). IEEE Publishing. <https://doi.org/10.1109/PROMISE.2007.14>
- Yadav, H. B., & Yadav, D. K. (2015). A fuzzy logic based approach for phase-wise software defects prediction using software metrics. *Information and Software Technology*, *63*, 44-57. <https://doi.org/10.1016/j.infsof.2015.03.001>
- Zhou, Y., & Leung, H. (2006). Empirical analysis of object-oriented design metrics for predicting high and low severity faults. *IEEE Transactions on Software Engineering*, *32*(10), 771-789. <https://doi.org/10.1109/TSE.2006.102>



Effect of Khat Chewing on Gingival Health of Patients with Fixed Orthodontic Appliances: A Controlled-Clinical Trial

Ahmed Taher Al-Hajj^{1*}, Rami Ishaq¹, Anas Shamala¹, Mohammed Al-Wesabi¹, Khalid Aldhorae^{2,3}, Mohammed Sultan Alakhali⁴ and Mohammed Al-Labani¹

¹Department of Preventive and Biomedical Sciences, Faculty of Dentistry, University of Science and Technology, Sana'a 00000, Yemen

²Department of Orthodontics, College of Dentistry, Thamar University, Dhamar 87246, Yemen

³Department of Orthodontics, College of Dentistry, University of Ibn al-Nafis for Medical Sciences, Sana'a 00000, Yemen

⁴Department of Preventive Dental Sciences, College of Dentistry, Jazan University, Jazan 45142, Saudi Arabia

ABSTRACT

This clinical trial aimed to evaluate the effect of Khat chewing on the gingival health of patients with fixed orthodontic appliances (FOAs) by measuring some periodontal parameters before and during 6-time intervals of orthodontic therapy. It also aimed to evaluate this effect regarding gender. The study included 39 Yemeni orthodontic patients with a mean age of 25.7 ± 4.5 ; divided into two groups, a control (non-chewers) with a mean age of 25.81 ± 4.3 and an experimental (chewers) group with a mean age of 25.61 ± 4.8 . An examination sheet was used for data collection, including the patient's personal information, oral health status, and three periodontal parameters: plaque index (PI), gingival index (GI), and pocket depth (PD). These data measurements were analyzed using SPSS v.24. The study showed an increase in mean plaque, gingival, and pocket depth indices at all-time visits after the appliance insertion compared to all patients' pre-treatment status. It indicates that Khat chewing harms all periodontal parameters during the orthodontic treatment period. Mean PI, GI and

PD were lower in female patients than male patients after the appliance insertion. The khat chewing process mechanically removes the dental plaque, decreasing PI and GI, while PD was worse in Khat chewers than non-chewers. Finally, it is recommended that chewing Khat should be avoided during orthodontic therapy.

Keywords: Clinical trial, fixed orthodontic appliances, gingival health, Khat chewer patients, Yemen

ARTICLE INFO

Article history:

Received: 21 August 2021

Accepted: 10 January 2022

Published: 25 May 2022

DOI: <https://doi.org/10.47836/pjst.30.3.24>

E-mail addresses:

dr.alhajj11@hotmail.com (Ahmed Taher Al-Hajj)

ishaqramy@gmail.com (Rami Ishaq)

anasshamala@gmail.com (Anas Shamala)

malwossabi@gmail.com (Mohammed Al-Wesabi)

drdurai2008@gmail.com (Khalid Aldhorae)

sultanperiodontics@gmail.com (Mohammed Sultan Alakhali)

mabdullah100@yahoo.com (Mohammed Al-Labani)

* Corresponding author

INTRODUCTION

Treatment of malocclusion may be achieved by orthodontic appliances generally classified into removable and fixed types. On average, treatment with fixed orthodontic appliances (FOAs) lasts between 18 to 36 months (Rashkova, 2012; Tsihklaki et al., 2016). The orthodontic treatment outcome depends on the periodontal tissue condition, which ought to be optimal (Kitaura et al. 2014). Fixed orthodontic therapy represents a potential risk for the periodontal health due to the difficulty in maintaining the oral hygiene, thus increasing the accumulation of the plaque (Baseer et al., 2021; Türkkahraman et al., 2005), the oral biofilm and inflammation of the periodontal tissues (Lee et al. 2005).

Dental plaque is “a highly complex bacterial structure which causes periodontal diseases” (Rakhshan & Rakhshan, 2015, p. 87). It is commonly accumulated during orthodontic treatment leading to gingival hyperplasia, swelling, and bleeding (Guo et al., 2016). Besides, the short-term effect of the orthodontic band on gingival tissues occurs after the placement of the fixed appliances. The probing depth increase can result from the gingival enlargement throughout the orthodontic treatment (Alexander, 1991; Kumar et al., 2021). In addition, mechanical irritations resulting from the brackets, bands, cement, and trapped plaques may be implicated (Boyd et al., 1989). When such an iatrogenic irritation is inevitable, risks of attachment loss can be expected (Alexander, 1991; Kumar et al., 2021).

Patients with previous periodontal diseases have higher risks if plaque control is compromised (Al-Anezi & Harradine 2012; Karkhanechi et al. 2013). Periodontal diseases are caused by many factors, including plaque accumulation, immune factors, and Khat chewing habit.

Khat is “the name generally used for *Catha edulis*, a dicotyledonous evergreen shrub of the family Celastraceae” (Al-Hebshi & Skaug, 2005b, p. 299). It has various types because it is widely cultivated in many different areas in Yemen and East Africa, wherein chewing Khat is a commonly practiced habit (Al-Hebshi & Skaug, 2005b). Chewing Khat implies turning Khat leaves into the right or left side of the mouth in the lower distal mesiobuccal fold, chewing them, and keeping them in that vascular side of the mouth for a long time. This process is repeated until an observably large bolus is noticed. It is practiced for different time intervals ranging from 2 to 10 hours (Al-Hajj et al., 2020; Al-Hebshi & Skaug, 2005b). Additionally, the noticeably large bolus of chewed Khat in the mouth creates a relevant question about the effect of this habit on periodontal health (Al-Hajj et al., 2020).

The association of periodontal health with the orthodontic treatment has been an essential issue in previously published studies, which revealed a controversy regarding the long and short-term FOAs effect on the periodontium (Al-Moghrabi et al., 2016; Cerroni et al., 2018; Chhibber et al., 2018; Mazin et al., 2016).

Furthermore, studies that evaluated Khat chewing effects on the periodontium showed controversial results and reported that higher levels of periodontitis were found on Khat

chewing sides than on non-chewing sides (Al-Akhali, 2002; Al-Hajj et al., 2020; Ali, 2007; Al-Sharabi, 2003). For example, Al-Sharabi et al. (2013), Al-Hebshi, and Al-Ak'hali (2010) reported that Khat chewing per se cannot be considered a risk factor for periodontium because periodontal parameters' values of Khat-chewing sides were significantly lower than those of non-chewing sides. On the contrary, Al-Hajj et al. (2020) stated that Khat chewing leads to a higher rate of periodontitis. Similarly, Al-Sharabi (2003) reported that gingivitis, increased pocket depth (PD), gingival recession, tooth mobility, and mortality are due to Khat chewing.

However, none of the studies mentioned above have been performed to evaluate the effect of Khat chewing habit on the orthodontic patients' periodontal health. Therefore, this clinical trial aimed to evaluate the Khat chewing effect on the gingival health of patients with fixed orthodontic appliances (FOAs). Furthermore, it also aimed to evaluate this effect regarding gender. Therefore, a hypothesis (H) can be set which states, "There is a significant effect of Khat chewing on the gingival health of patients with FOAs," from which a sub-hypothesis was derived which states (Ha) "There is a significant effect of Khat chewing on the gingival health of patients with FOAs attributed to gender."

MATERIALS AND METHODS

Study Design

The study was designed as a controlled clinical trial.

Study Setting

The study was conducted at the clinics of the Faculty of Dentistry, University of Science and Technology, Sana'a, Yemen, between November 2018 and June 2019.

Participants

The study was conducted on male and female orthodontic patients who underwent fixed orthodontic treatment in the clinics of the Faculty of Dentistry at the USTY. The inclusion criteria comprised patients requiring FOAs on upper and lower arches aged 18–35. However, patients with smoking habits, cleft palatal or congenital malformation, history of systemic diseases, periodontal problems, or previous orthodontic or prosthetic therapy treatment were excluded.

Study Sample Size

The required sample size was calculated using the OpenEpi® statistics calculation software (Sullivan et al., 2009), considering a confidence level of 95 % and power of 80 % using the study of Lees and Rocks (2000) a reference. Therefore, the minimal sample size required

was 40 orthodontic patients wearing FOAs. The initial study sample was 62 male and female orthodontic patients. After applying the inclusion and exclusion criteria, the remaining participants were 42 orthodontic patients. Then three participants were withdrawn two months after bonding the appliance. Consequently, the study sample was 39 participants divided into 18 Khat chewer patients (Experimental group) and 21 non-chewer patients (control group). All participants in the experimental group are chronic Khat chewers as they have been chewing Khat for at least five years, 3 hours a day.

Variables

The study was conducted to evaluate the effect of Khat chewing on the gingival health of patients with fixed orthodontic appliances (FOAs) by measuring some periodontal parameters before and at 6-times intervals of orthodontic therapy. Therefore, the study variables included an independent variable (i.e., Khat chewing) and a dependent variable (i.e., gingival health). The latter has three parameters (i.e., dental plaque (PI), gingival index (GI), and pocket depth PD). Besides, the demographic variables include gender and age.

Interview Questions

Before the appliance insertion, an interviewed questionnaire was distributed to every participant to collect data consisting of his/her personal information, including gender, age, and Khat chewing status (Mahindra et al., 2017).

Clinical Examination

A clinical examination sheet was used by one examiner (A.T.A) to record the measurements of three clinical parameter indices: plaque index (PI) (Silness & Loe, 1964), GI (Loe & Silness, 1963), and PD (Newman et al., 2011) at seventh-time visits (T0–T6) before and after first, second, third, fourth, fifth and sixth months of the appliance insertion. These parameters were evaluated on mesiodistal vestibular, middle surfaces of 6 examined teeth which were designated for epidemiological studies of human periodontal diseases by Ramfjord (1959) and called Ramfjord teeth (RT), including upper right first molar, upper left central incisor, upper left first premolar, lower left first molar, lower right central incisor, and lower right first premolar (Rams et al., 1993).

A week before the FOAs insertion, patients were subjected to a protocol of oral hygiene motivation, including scaling, polishing, and instructions regarding brushing teeth three times a day as per the Bass modified technique with toothpaste consisting of fluoride concentration following the placement of the appliance (Peros et al. 2011). FOAs of the 0.022*0.028 slot MBT bracket system (SIA, Italy) were placed (Figure 1). Bands were placed on the first molars according to each patient's treatment needs. Adhesive

materials (Trans bond, 3M Unitek, USA) were used (Figure 2). All patients were supplied with adequate materials for cleaning aids and toothbrushes.

Appliances were inserted using additional instruments and materials, including dental mirrors No. 4, bracket holder, light cure, kidney dishes, masks, gloves, and cotton (for dryness). The insertion procedure of the fixed appliance is described in Figure 3.

Dental plaque was assessed using the modified PI of Silness and Løe (1964), classified into four grades (0, 1, 2, and 3), as explained in Table 1.

The gingival condition was assessed using the GI of Løe and Silness (1963), classified into four grades (0, 1, 2, and 3), as explained in Table 2.



Figure 1. SIA bracket system



Figure 2. 3M Unitek adhesive material

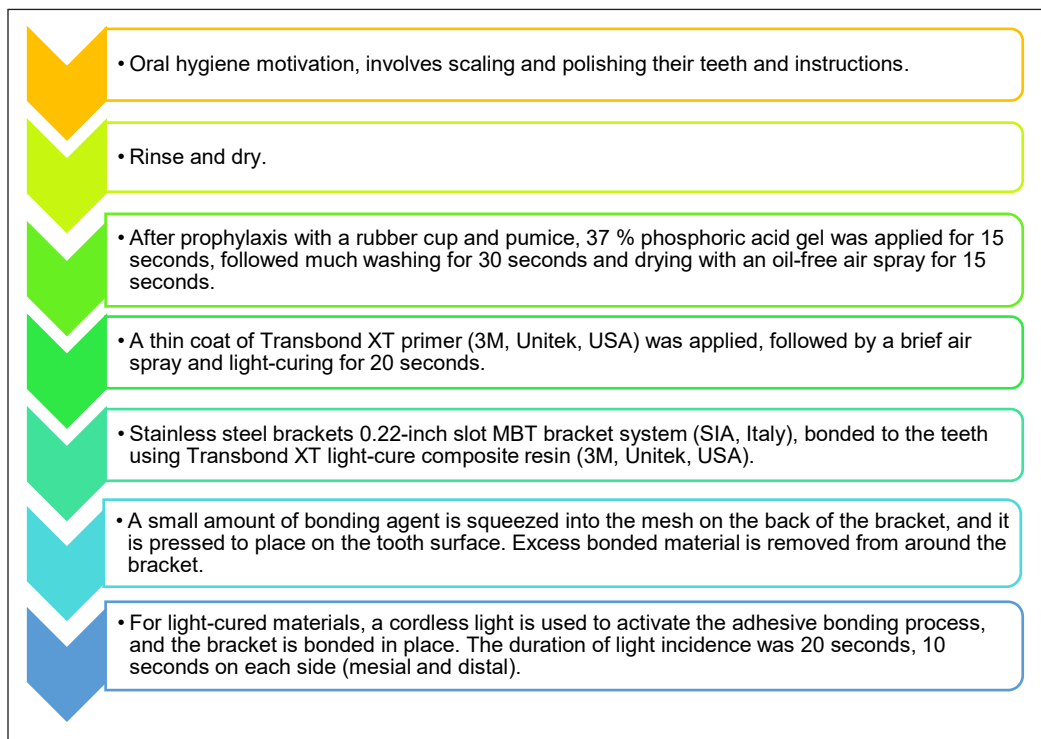


Figure 3. Insertion procedure of fixed appliance

Table 1
Modified PI of Silness and Løe (1964)

Score	Criteria
0	“No plaque.”
1	“A film of plaque adhering to the free gingival margin and adjacent area of the tooth. The plaque which cannot be seen with the naked eye may be seen in situ only after application of disclosing solution or by using the probe on the tooth surface.”
2	“Moderate accumulation of soft deposits within the gingival pocket, or the tooth and gingival margin which can be seen with the naked eye.”
3	“Abundance of soft matter within the gingival pocket and/or on the tooth and gingival margin.”

Table 2
Løe and Silness (1963) gingival index

Score	Criteria
0	“Absence of inflammation.”
1	“Mild inflammation—slight change in color and little change in texture.”
2	“Moderate inflammation—moderate glazing, redness, oedema, and hypertrophy. Bleeding on pressure.”
3	“Severe inflammation—marked redness and hypertrophy, ulceration. Tendency to spontaneous bleeding. Ulceration.”

PD was recorded by measuring the distance from the sulcus/ pocket base to the free gingival margin (Eckley et al., 2012) using a millimeter-calibrated periodontal probe (Michigan O probe with William’s markings) having markings at 3, 6, and 8 mm and William’s probe having circumferential lines at 1, 2, 3, 5, 7, 8, 9, and 10 mm. Graduated periodontal probes were used to explore and measure gingival pockets (Dannan et al., 2008; Newman et al., 2011). The probe was inserted with gentle pressure into the deepest part of the gingival sulcus (Dannan et al., 2008; Newman et al., 2011).

For the examination reliability of measurements, the investigator was trained by a periodontist to perform the measurements of dental parameter indices (i.e., PI, GI, and PD). Then he assessed five participants. After a week, both examined the same five participants to calibrate their examination methods. Finally, Cohen’s Kappa was used to compare the two measurement results, which showed a ‘substantial’ agreement.

Statistical Analysis

SPSS v.24 was used for data analysis using frequencies for the study sample distribution according to demographic characteristics and the Shapiro-Wilk test for the normality assessment. For comparing between two groups, the Mann-Whitney U test was used. In addition, Wilcoxon signed ranks test was used for assessing the difference between every two-time visit. Results were presented using the mean with standard deviation (SD), and the p-value < 0.05 was considered statistically significant.

Bioethical Considerations

Ethical approval was attained from the Ethics Committee of the Faculty of Medicine and Health Sciences at the University of Science and Technology, Yemen (USTY) (MECA No.: EAC/UST164). Furthermore, a consent form was received from all participants who had the right to accept or refuse their study participation.

RESULTS

Figure 4 shows a CONSORT format presenting how the study was designed and how the participants were allocated, excluded, or followed up.

Both genders showed equal distribution in the experimental group, whereas the control group included 42.9 % male and 57.1 % female patients. Regarding age, the experimental group included 27.8 %, 61.1 %, and 11.1 % of patients aged 18–23, 24–30, and 31–35 years, respectively, while the control group included 38.1 %, 42.9 %, and 19.0 % of patients aged 18–23, 24–30 and 31–35 years, respectively (Table 3).

Mann-Whitney U test was also used to evaluate the differences in PI, GI, and PD scores between Khat chewer and non-chewer patients (Tables 4 and 5). The differences in all parameters (i.e., PI, GI, and PD) scores at all visits (T1, T2, T3, T4, T5, and T6) showed a statistically significant increase ($p < 0.05$) in Khat chewer than non-chewer patients.

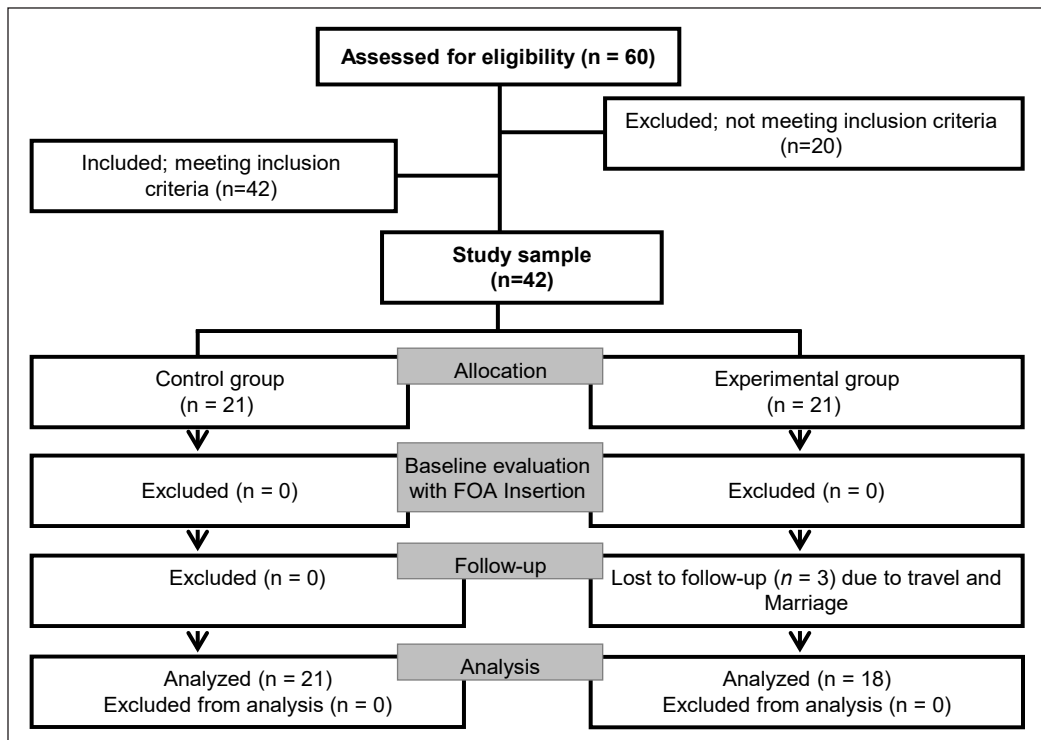


Figure 4. CONSORT format for presenting allocation, evaluation, or follow-up of a sample

Table 3
 Distribution of study sample in both groups

Variable	Experimental group (Chewers, n=18)		Control group (Non-chewers, n=21)		
	N	%	N	%	
Gender	Male	9	50	9	42.9
	Female	9	50	12	57.1
Age	18-23 years	8	38.1	5	27.8
	24-30 years	9	42.9	11	61.1
	31-35 years	4	19.0	2	11.1
Total	21	53.8	18	46.2	

Table 4
 Comparison of PI, GI, and PD scores between groups

Parameter	Time	Chewer (n=18)		Non-chewer (n=21)		P-value
		Mean	SD	Mean	SD	
PI	T1	0.85	0.36	1.27	0.26	0.001*
	T2	0.90	0.40	1.34	0.39	0.001*
	T3	1.20	0.35	1.47	0.32	0.017*
	T4	1.29	0.40	1.61	0.31	0.013*
	T5	1.37	0.43	1.66	0.29	0.034*
	T6	1.45	0.43	1.79	0.25	0.025*
GI	T1	0.22	0.24	0.46	0.35	0.021*
	T2	0.28	0.24	0.58	0.32	0.004*
	T3	0.39	0.30	0.72	0.30	0.002*
	T4	0.47	0.29	0.80	0.32	0.003*
	T5	0.57	0.24	0.87	0.39	0.008*
	T6	0.63	0.30	0.99	0.37	0.004*
PD	T1	3.16	0.15	3.02	0.04	0.003*
	T2	3.34	0.16	3.16	0.14	0.002*
	T3	3.52	0.19	3.28	0.15	0.000*
	T4	3.81	0.30	3.42	0.17	0.000*
	T5	4.30	0.29	3.54	0.23	0.000*
	T6	4.60	0.36	3.69	0.25	0.000*

* Significant at $p < 0.05$

Table 5
 Comparison of PI, GI, and PD scores at T1 and T6 between groups

Parameter	Chewer (n=18)		Non-chewer (n=21)		P-value
	Mean	SD	Mean	SD	
PI	1.15	0.38	1.53	0.20	0.001*
GI	0.43	0.24	0.73	0.33	0.008*
PD	3.88	0.23	3.36	0.13	0.000*

* Significant at $p \leq 0.05$

Moreover, statistically significant differences ($p < 0.05$) were shown in the PI, GI, and PD scores at T1 and T6 between Khat chewer and non-chewer patients. Scores of PI and GI were worse in non-chewer than chewer patients. However, those of PD were better in non-chewer than chewer patients. Therefore, the study hypothesis (H) was accepted.

Mann-Whitney U test assessed the differences in PI, GI, and PD scores between male and female patients, and within the control and experimental group.

Generally, it was revealed that the differences in PI, GI, and PD scores at all visits (T1, T2, T3, T4, T5, and T6) showed a statistically significant increase ($p < 0.05$) in males than female patients (Table 6).

Within groups, the differences in PI, GI, and PD scores within the experimental group at all visits showed a statistically significant increase ($p < 0.05$) in male than female chewer patients. However, the difference in PI scores within the control group at only T6 showed a statistically significant increase ($p < 0.05$) in male than female patients. However, the PI scores' differences in the control group during the remaining visits showed an insignificant increase ($p > 0.05$) in male than female patients, except for T4, at which the difference showed an insignificant decrease ($p > 0.05$) in male than female patients. Unlike the differences in T1, T2, and T3, T4, T5, and T6 GI scores within the control group showed a statistically significant increase ($p < 0.05$) in male than female patients. On the contrary, the differences in PD scores within the control group showed a statistically insignificant increase ($p > 0.05$) in male than female patients (Table 7).

The differences in PI and PD scores of T1 and T6 in general and within the experimental group (chewer patients) showed a statistically significant increase ($p < 0.05$) in male than female patients. In contrast, those within the control group (non-chewer patients) showed an insignificant increase ($p > 0.05$) in male than female patients. However, the differences in GI scores of T1 and T6 in general and within both groups showed a statistically significant increase ($p < 0.05$) in male than female patients (Table 8). Therefore, the study sub-hypothesis was accepted.

Table 6
Comparison of PI scores by gender

Time	Male (n=18)		Female (n=21)		P-value
	Mean	SD	Mean	SD	
T1	1.24	0.25	0.94	0.41	0.024*
T2	1.32	0.39	0.98	0.44	0.016*
T3	1.50	0.26	1.21	0.38	0.019*
T4	1.61	0.28	1.34	0.43	0.046*
T5	1.69	0.29	1.38	0.41	0.015*
T6	1.83	0.17	1.46	0.43	0.004*

* Significant at $p \leq 0.05$

Table 7
 Comparison of PI, GI, and PD scores within groups by gender

Parameter	Time	Experimental group (n=18)					Control group (n=21)				
		Male (n=9)		Female (n=9)		P-value	Male (n=9)		Female (n=12)		P-value
		Mean	SD	Mean	SD		Mean	SD	Mean	SD	
PI	T1	1.16	0.13	0.54	0.21	0.000*	1.32	0.31	1.23	0.21	0.564
	T2	1.24	0.13	0.56	0.25	0.000*	1.40	0.54	1.29	0.23	0.141
	T3	1.47	0.10	0.93	0.30	0.000*	1.53	0.36	1.43	0.30	0.465
	T4	1.62	0.19	0.97	0.25	0.000*	1.59	0.36	1.63	0.28	0.971
	T5	1.72	0.20	1.01	0.25	0.000*	1.67	0.36	1.66	0.24	0.797
	T6	1.76	0.13	1.14	0.41	0.004*	1.91	0.18	1.69	0.26	0.036*
GI	T1	0.39	0.21	0.06	0.13	0.001*	0.61	0.42	0.35	0.25	0.169
	T2	0.43	0.17	0.12	0.20	0.004*	0.71	0.38	0.48	0.24	0.095
	T3	0.57	0.22	0.22	0.27	0.011*	0.84	0.30	0.63	0.28	0.148
	T4	0.62	0.18	0.32	0.30	0.024*	0.99	0.24	0.65	0.30	0.015*
	T5	0.69	0.18	0.46	0.25	0.024*	1.17	0.17	0.65	0.36	0.000*
	T6	0.77	0.17	0.50	0.34	0.025*	1.31	0.15	0.75	0.29	0.000*
PD	T1	3.28	0.08	3.03	0.07	0.000*	3.01	0.03	3.03	0.05	0.422
	T2	3.46	0.10	3.22	0.11	0.001*	3.17	0.15	3.16	0.14	0.917
	T3	3.63	0.13	3.40	0.18	0.006*	3.31	0.16	3.26	0.14	0.554
	T4	4.01	0.25	3.60	0.19	0.000*	3.44	0.17	3.40	0.18	0.554
	T5	4.49	0.23	4.11	0.20	0.002*	3.62	0.28	3.48	0.17	0.219
	T6	4.83	0.35	4.37	0.19	0.001*	3.80	0.32	3.61	0.14	0.169

* Significant at $p < 0.05$

Table 8
 Differences between PI, GI, and PD scores of T1 and T6 by gender

Parameter	Group		Mean	SD	P-value
PI	Experimental group (Chewer patients)	Male	1.46	0.12	0.000*
		Female	0.84	0.29	
	Control group (Non-chewer patients)	Male	1.62	0.19	0.129
		Female	1.46	0.19	
	Total	Male	1.54	0.17	0.006*
		Female	1.20	0.39	
GI	Experimental group (Chewer patients)	Male	0.58	0.13	0.003*
		Female	0.28	0.23	
	Control group (Non-chewer patients)	Male	0.96	0.27	0.004*
		Female	0.55	0.24	
	Total	Male	0.77	0.29	0.001*
		Female	0.43	0.27	
PD	Experimental group (Chewer patients)	Male	4.06	0.16	0.000*
		Female	3.70	0.11	
	Control group (Non-chewer patients)	Male	3.41	0.16	0.193
		Female	3.32	0.09	
	Total	Male	3.73	0.37	0.035*
		Female	3.48	0.21	

* Significant at $p < 0.05$

DISCUSSION

This clinical trial aimed to evaluate the effect of Khat chewing on the gingival health of patients with fixed orthodontic appliances by measuring some periodontal parameters before and during 6-time intervals of orthodontic therapy. In addition, to evaluate this effect regarding gender. The study included 39 Yemeni orthodontic patients divided into two groups, a control (non-chewers) and an experimental (chewers) group. An examination sheet was used for data collection, including the patient's personal information, oral health status, and three periodontal parameters: plaque index (PI), gingival index (GI), and pocket depth (PD). The study findings showed a significant worsening of all the outcomes measured throughout the study compared to patients' pre-treatment status. This result is similar to the finding of Altaee et al. (2015), Bue et al. (2008), Cerroni et al. (2018), Chhibber et al. (2018), Karkhanechi et al. (2013), Kumar et al. (2021), Mazin et al. (2016), Peng et al. (2014), and Ren et al. (2014). The study findings also showed changes in PI, GI, and PD observed at the first visit (T1). This finding agrees with that of Faridha and Navaneethan (2018), Mazin et al. (2016), and Ristic et al. (2007), who showed an increase in PI, GI, and PD parameters after one month of appliance placement. It is due to the increase in plaque and the inability of the patient to perform adequate oral hygiene. Similarly, Karacaoğlu et al. (2016), Kaygisiz et al. (2015), and Nalçacı et al. (2014) reported that PI and GI showed changes after 4 and 6 weeks of the FOAs insertion. Besides, Zachrisson and Zachrisson (1971) indicated that mild to moderate gingivitis was shown within one and two months after the FOAs insertion.

The increase in PI and GI may also occur because the placement of the brackets influences the ecological environment through accumulating the biofilm at the retentive sites, leading to more inflammation and bleeding that deteriorate the periodontal condition (Kumar et al., 2021; Naranjo et al., 2006). PI and GI were increased because the plaque retentive properties of FOAs may lead to increased plaque accumulation and gingival inflammation (Abbate et al., 2015; Jiang et al., 2017; Ristic et al., 2007). Fixed orthodontic bands and brackets make tooth brushing difficult and reduce natural self-cleansing through the saliva and tongue (Ren et al., 2014; Türkkahraman et al., 2005). Since fixed orthodontic patients face difficulty maintaining good oral hygiene, gingivitis and enamel demineralization could be caused by the accumulated plaque (Bue et al., 2008; Kumar et al., 2021; Peng et al., 2014), leading to increased PI and GI. This result agrees with that of Moosa et al. (2015), who reported that the probing depth and plaque accumulation could be increased in patients with FOAs, leading to destructed periodontal tissue, which according to Almansob et al. (2021) and Jadhav et al. (2013), increases plaque accumulation leading to gingival hyperplasia and gingival pockets. The increase in PD scores could be attributed to the increase in the overall anaerobic bacterial species in the banded-bracketed sites (Karkhanechi et al., 2013)

or the pseudopocket or deeper-probe penetrations into the weakened connective tissue (Gastel et al., 2011). Although fixed appliances may adversely affect all periodontal parameters, which influence the periodontal condition in a short-time period starting instantly after the band and bracket placement, they do not have destructive effects due to their transient conditions (Ristic et al., 2007).

The current study showed that periodontal PI and GI parameters at all visits were better in chewer than non-chewer patients regarding Khat chewing habit. However, the PD parameter was worse among chewers than non-chewer patients. Besides, the PI, GI, and PD parameters increased more among male chewers than female chewer patients.

According to gender, the current study generally showed a significant worsening of all periodontal parameters (i.e., PI, GI, and PD) at all visits in male than female patients after six months of the appliance placement. This result is consistent with that of Almansob et al. (2021), Amran and Alhajj (2016), Karacaoğlu and Akkaya (2018), and Kumar and Shristi (2015) who reported that females showed better oral self-care, gingival health, knowledge about oral health, and more involved in dental behaviors than males.

However, studies that assessed associations of Khat chewing with periodontal health supported the results of the current study regarding this independent factor (i.e., Khat chewing). Some studies showed that repeated chewing of Khat modifies the subgingival biofilm microbial composition incompatibility with the periodontal health (Al-Hebshi & Skaug, 2005a; Al-Hebshi et al., 2010). Moreover, Khat chewing seems to mechanically cleanse dental plaque, decrease GI (Al-Hebshi & Al-Akhali, 2010; Al-Maweri & Al-Akhali, 2017), and increase PD (Al-Maweri & Al-Akhali, 2017; Amran & Alhajj, 2016; Dhaifullah et al., 2015). Additionally, repeatedly chewing Khat may cause chronic trauma and vertical impaction to the periodontium (Al-Sharabi et al., 2013) that most likely leading to increases in the PD (Al-Hajri et al., 2013; Al-Hebshi & Al-Akhali, 2010; Ali, 2007; Al-Kholani, 2010).

On the other side, some studies are inconsistent with the present study findings. They reported that Khat chewing harms oral hygiene and periodontal condition in the form of gingival inflammation and is associated with a higher prevalence of gingival bleeding (Al-Juboury, 2006; Amran & Alhajj, 2016; Dhaifullah et al., 2015). Moreover, Al-Kholani (2010) showed that PI and GI parameters were significantly higher in Khat chewers than in non-chewer patients. Al-Hebshi and Skaug (2005a) and Al-Maweri and Al-Akhali (2017) reported that Khat chewing affected the PD parameter positively.

Accordingly, the study findings showed significant changes in the patients' periodontal condition, which agrees with Kumar et al. (2021) and Naranjo et al. (2006), who reported that the FOA placement influences the ecological environment through accumulating the biofilm at the retentive sites.

CONCLUSION

The current study concluded that fixed appliances negatively affect all periodontal parameters during the treatment period, and periodontal PI, GI, and PD parameters at all visits after the appliance insertion were better in females than in males. Besides, Khat chewing was considered an independent factor with significant and remarked changes in the association of fixed appliances with periodontal tissues. It also seems to cleanse dental plaque, which decreases PI and GI mechanically. Frequent chewing of Khat may cause chronic trauma and vertical impaction to the periodontium, which most likely leads to increases in the PD. Therefore, further research is recommended to conduct a similar study among similar populations but with more independent variables, including smoking, tobacco, age, and/or gum chewing.

ACKNOWLEDGEMENT

The authors want to thank all faculty members of the Faculty of Dentistry, University of Science and Technology, Sana'a, Yemen, for facilitating the process of data collection, Assistant Lecturer Amr Mohammed Saleh Ali for statistical analysis, and Mr. Hudhaifa Hasan Al-Shameri for copyediting and proofreading.†

REFERENCES

- Abbate, G. M., Caria, M. P., Montanari, P., Mannu, C., Orrù, G., Caprioglio, A., & Levrini, L. (2015). Periodontal health in teenagers treated with removable aligners and fixed orthodontic appliances. *Journal of Orofacial Orthopedics*, 76, 240-250. <https://doi.org/10.1007/s00056-015-0285-5>
- Al-Akhali, M. S. (2002). *Periodontal health status of the khat chewers among Yemeni population* [Unpublished master dissertation]. Baghdad University, Iraq. <https://www.researchgate.net/publication/282507093>
- Al-Anezi, S. A., & Harradine, N. W. (2012). Quantifying plaque during orthodontic treatment: A systematic review. *The Angle Orthodontist*, 82(4), 748-753. <http://doi.org/10.2319/050111-312.1>
- Alexander, S. A. (1991). Effects of orthodontic attachments on the gingival health of permanent second molars. *American Journal of Orthodontics and Dentofacial Orthopedics*, 100(4), 337-340. [https://doi.org/10.1016/0889-5406\(91\)70071-4](https://doi.org/10.1016/0889-5406(91)70071-4)
- Al-Hajj, W., Hwaiti, H., Shamala, A., Al-Azazi, H., & Alwesabi, M. (2020). Association of Khat chewing, smoking, age and sex with periodontal status among Yemeni adults. *Brazilian Dental Science*, 23(1), 1-8. <https://doi.org/10.14295/bds.2020.v23i1.1861>
- Al-Hajri, M., El Refaey, M., Fathalla, G., & El-Firt, E. Y. (2013). Apoptosis due to Khat chewing analyzed by p53 expression in gingival tissue. *Egyptian Dental Journal*, 59, 1-9.
- Al-Hebshi, N. N., & Al-Akhali, M. S. (2010). Experimental gingivitis in male Khat (*Catha edulis*) chewers. *Journal of the International Academy of Periodontology*, 12(2), 56-62.

- Al-Hebshi, N. N., & Skaug, N. (2005a). Effect of Khat chewing on 14 selected periodontal bacteria in a sub-and supragingival plaque of a young male population. *Oral Microbiology and Immunology*, 20(3), 141-146. <https://doi.org/10.1111/j.1399-302X.2004.00195.x>
- Al-Hebshi, N. N., & Skaug, N. (2005b). Khat (*Catha edulis*) - An updated review. *Addiction Biology*, 10(4), 299-307. <https://doi.org/10.1080/13556210500353020>
- Al-Hebshi, N. N., Al-Sharabi, A. K., Shuga-Aldin, H. M., Al-Haroni, M., & Ghandour, I. (2010). Effect of Khat chewing on periodontal pathogens in the subgingival biofilm from chronic periodontitis patients. *Journal of Ethnopharmacology*, 132(3), 564-569. <https://doi.org/10.1016/j.jep.2010.08.051>
- Ali, A. A. (2007). Qat habit in Yemen society: A causative factor for oral periodontal diseases. *International Journal of Environmental Research and Public Health*, 4(3), 243-247. <https://doi.org/10.3390/ijerph2007030008>
- Al-Juboury, H. A. (2006). Oral health status among a group of dental students in Yemen. *Journal of Baghdad College of Dentistry*, 18(3), 60-62.
- Al-Kholani, A. I. (2010). Influence of Khat chewing on periodontal tissues and oral hygiene status among Yemenis. *Dental Research Journal*, 7(1), 1-6.
- Almansob, Y. A., Alhammedi, M. S., Luo, X. J., Alhajj, M. N., Zhou, L., Almansoub, H. A., & Mao, J. (2021). Comprehensive evaluation of factors that induce gingival enlargement during orthodontic treatment: A cross-sectional comparative study. *Nigerian Journal of Clinical Practice*, 24(11), 1649-1655. https://doi.org/10.4103/njcp.njcp_69_21
- Al-Maweri, S. A., & Al-Akhali, M. (2017). Oral hygiene and periodontal health status among Khat chewers. A case-control study. *Journal of Clinical and Experimental Dentistry*, 9(5), e629-e634. <https://doi.org/10.4317/jced.53520>
- Al-Moghrabi, D., Pandis, N., & Fleming, P. S. (2016). The effects of fixed and removable orthodontic retainers: A systematic review. *Progress in orthodontics*, 17(1), 1-22. <https://doi.org/10.1186/s40510-016-0137-x>
- Al-Sharabi, A. K. K. (2003). *Oral and para-oral lesions caused by Takhzeen Al-Qat* [Published Doctoral dissertation]. University of Khartoum, Sudan. <http://khartoumspace.uofk.edu/bitstream/handle/123456789/7671/ORAL%20AND%20PARA-ORAL.pdf?sequence=1>
- Al-Sharabi, A. K., Shuga-Aldin, H., Ghandour, I., & Al-Hebshi, N. N. (2013). Qat chewing as an independent risk factor for periodontitis: A cross-sectional study. *International Journal of Dentistry*, 2013, Article 317640. <https://doi.org/10.1155/2013/317640>
- Altaee, Z. H., Al Fatlawi, F. A., & Mohammed, W. (2015). Periodontal consideration for patients with a fixed orthodontic appliance in Ramadi city. *Tikrit Journal for Dental Sciences*, 3(1), 89-94.
- Amran, A. G., & Alhajj, M. N. (2016). Assessment of gingival health status among a group of preclinical and clinical dental students at Tamar University, Yemen. *IOSR Journal of Dental and Medical Sciences*, 15(2), 69-75. <https://doi.org/10.9790/0853-15256975>
- Baseer, M. A., Almayah, N. A., Alqahtani, K. M., Alshaye, M. I., & Aldahri, M. M. (2021). Oral impacts experienced by orthodontic patients undergoing fixed or removable appliances therapy in Saudi Arabia:

- A cross-sectional study. *Patient Preference and Adherence*, 15, 2683-2691. <https://doi.org/10.2147/PPA.S343084>
- Boyd, R. L., Leggott, P. J., Quinn, R. S., Eakle, W. S., & Chambers, D. (1989). Periodontal implications of orthodontic treatment in adults with reduced or normal periodontal tissues versus those of adolescents. *American Journal of Orthodontics and Dentofacial Orthopedics*, 96(3), 191-198. [https://doi.org/10.1016/0889-5406\(89\)90455-1](https://doi.org/10.1016/0889-5406(89)90455-1)
- Bue, A. M. L., Blandino, G., Milazzo, I., Cali, G., Rossetti, B., & Marco, R. D. (2008). Microbiological and clinical periodontal effects of fixed orthodontic appliances in pediatric patients. *Microbiologica-Quarterly Journal of Microbiological Sciences*, 31(2), 299-302.
- Cerroni, S., Pasquantonio, G., Condò, R., & Cerroni, L. (2018). Orthodontic fixed appliance and periodontal status: An updated systematic review. *The Open Dentistry Journal*, 12, 614-622. <https://doi.org/10.2174/1745017901814010614>
- Chhibber, A., Agarwal, S., Yadav, S., Kuo, C. L., & Upadhyay, M. (2018). Which orthodontic appliance is best for oral hygiene? A randomized clinical trial. *American Journal of Orthodontics and Dentofacial Orthopedics*, 153(2), 175-183. <https://doi.org/10.1016/j.ajodo.2017.10.009>
- Dannan, A., Darwish, M., & Sawan, M. (2008). How do the periodontal tissues react during the orthodontic alignment and leveling phase? *Virtual Journal of Orthodontics*, 8(1), 1-7.
- Dhaiyallah, E., Al-Maweri, S. A., Al-Motareb, F., Halboub, E., Elkhatat, E., Baroudi, K., & Tarakji, B. (2015). Periodontal health condition and associated factors among university students, Yemen. *Journal of Clinical and Diagnostic Research (JCDR)*, 9(12), ZC30-Z33. <https://doi.org/10.7860/JCDR/2015/16435.6964>
- Eckley, B., Thomas, J., Crout, C., & Ngan, P. (2012). Periodontal and microbiological status of patients undergoing orthodontic therapy. *Hong Kong Dental Journal*, 9(1), 11-20.
- Faridha, S., & Navaneethan, R. (2018). Periodontal status in different stages of orthodontic treatment: A cross-sectional study. *Drug Invention Today*, 10(3), 3282-3284.
- Gastel, J., Quirynen, M., Teughels, W., Coucke, W., & Carels, C. (2011). Longitudinal changes in microbiology and clinical periodontal parameters after the removal of fixed orthodontic appliances. *The European Journal of Orthodontics*, 33(1), 15-21. <https://doi.org/10.1093/ejo/cjq032>
- Guo, L., Feng, Y., Guo, H. G., Liu, B. W., & Zhang, Y. (2016). Consequences of orthodontic treatment in malocclusion patients: Clinical and microbial effects in adults and children. *BMC Oral Health*, 16(1), 1-7. <https://doi.org/10.1186/s12903-016-0308-7>
- Jadhav, T., Bhat, K. M., Bhat, G. S., & Varghese, J. M. (2013). Chronic inflammatory gingival enlargement associated with orthodontic therapy - A case report. *Journal of Dental Hygiene*, 87(1), 19-23.
- Jiang, F., Chen, J., Kula, K., Gu, H., Du, Y., & Eckert, G. (2017). Root resorptions associated with canine retraction treatment. *American Journal of Orthodontics and Dentofacial Orthopedics*, 152(3), 348-354. <https://doi.org/10.1016/j.ajodo.2017.01.023>
- Karacaoğlu, F., & Akkaya, M. (2018). Agresif periodontitis epidemiyolojisi [Epidemiology of aggressive periodontitis]. *Türkiye Klinikleri Periodontoloji-Özel Konular*, 4(1), 6-10.

- Karacaoğlu, F., Gazioglu, C., Akkaya, S., & Akkaya, M. (2016). Are the effects of fixed orthodontic treatment on gingival health similar in adolescents and young adults? *Journal of Biomedical Sciences*, 6, 1-13.
- Karkhanechi, M., Chow, D., Sipkin, J., Sherman, D., Boylan, R. J., Norman, R. G., Craig, R. G., & Cisneros, G. J. (2013). Periodontal status of adult patients treated with fixed buccal appliances and removable aligners over one year of active orthodontic therapy. *The Angle Orthodontist*, 83(1), 146-151. <https://doi.org/10.2319/031212-217.1>
- Kaygisiz, E., Uzuner, F. D., Yuksel, S., Taner, L., Çulhaoğlu, R., Sezgin, Y., & Ateş, C. (2015). Effects of self-ligating and conventional brackets on halitosis and periodontal conditions. *The Angle Orthodontist*, 85(3), 468-473. <https://doi.org/10.2319/041714-289.1>
- Kitaura, H., Kimura, K., Ishida, M., Sugisawa, H., Kohara, H., Yoshimatsu, M., & Takano-Yamamoto, T. (2014). Effect of cytokines on osteoclast formation and bone resorption during mechanical force loading of the periodontal membrane. *The Scientific World Journal*, 2014, Article 617032. <https://doi.org/10.1155/2014/617032>
- Kumar, R. P., & Shristi, N. (2015). Oral health knowledge, attitude, and practice of patients visiting a private hospital in Chennai. *Journal of Dental and Medical Sciences*, 14(6), 12-5. <https://doi.org/10.4103/1305-7456.126244>
- Kumar, S., Kumar, S., Hassan, N., Anjan, R., Shaikh, S., & Bhowmick, D. (2021). A comparative assessment of the effect of professional oral hygiene measures on the periodontal health of patients undergoing fixed orthodontic appliance therapy. *Journal of Pharmacy and Bioallied Sciences*, 13(6), 1324-1326. https://doi.org/10.4103/jpbs.jpbs_141_21
- Lee, S. M., Yoo, S. Y., Kim, H. S., Kim, K. W., Yoon, Y. J., Lim, S. H., Shin, H. Y., & Kook, J. K. (2005). Prevalence of putative periodontopathogens in subgingival dental plaques from gingivitis lesions in Korean orthodontic patients. *Journal of Microbiology*, 43(3), 260-265.
- Lees, A., & Rock, W. P. (2000). A comparison between written, verbal, and videotape oral hygiene instruction for patients with fixed appliances. *Journal of Orthodontics*, 27(4), 323-328. <https://doi.org/10.1093/ortho/27.4.323>
- Löe, H., & Silness, J. (1963). Periodontal disease in pregnancy I. Prevalence and severity. *Acta Odontologica Scandinavica*, 21(6), 533-551. <https://doi.org/10.3109/00016356309011240>
- Mahindra, R. K., Suryawanshi, G. R., & Doshi, U. H. (2017). Effects of fixed orthodontic treatment on gingival health: An observational study. *International Journal of Applied Dental Sciences*, 3(3), 156-161.
- Mazin, H., Ali, S., & Salah, R. (2016). The effect of fixed orthodontic appliances on gingival health. *IOSR Journal of Dental and Medical Sciences*, 15(11), 82-88. <https://doi.org/10.109790/0853-1517078288>
- Moosa, Y., Han, L. N., Safdar, J., Sheikh, O. A., & Pan, Y. P. (2015). Periodontal status of Pakistani orthodontic patients. *Brazilian Oral Research*, 29(1), 1-5. <https://doi.org/10.1590/1807-3107BOR-2015.vol29.0091>
- Nalçacı, R., Özat, Y., Çökakoğlu, S., Türkahraman, H., Önal, S., & Kaya, S. (2014). Effect of bracket type on halitosis, periodontal status, and microbial colonization. *The Angle Orthodontist*, 84(3), 479-485. <https://doi.org/10.2319/061913-461.1>

- Naranjo, A. A., Triviño, M. L., Jaramillo, A., Betancourth, M., & Botero, J. E. (2006). Changes in the subgingival microbiota and periodontal parameters before and 3 months after bracket placement. *American Journal of Orthodontics and Dentofacial Orthopedics*, *130*(3), 275.e17-275.e22. <https://doi.org/10.1016/j.ajodo.2005.10.022>
- Newman, M. G., Takei, H., Klokkevold, P. R., & Carranza, F. A. (2011). *Carranza's clinical periodontology*. Elsevier.
- Peng, Y., Wu, R., Qu, W., Wu, W., Chen, J., Fang, J., Chen, Y., Farella, M., & Mei, L. (2014). Effect of visual method vs plaque disclosure in enhancing oral hygiene in adolescents and young adults: A single-blind randomized controlled trial. *American Journal of Orthodontics and Dentofacial Orthopedics*, *145*(3), 280-286. <https://doi.org/10.1016/j.ajodo.2013.10.021>
- Peros, K., Mestrovic, S., Anic-Milosevic, S., & Slaj, M. (2011). Salivary microbial and nonmicrobial parameters in children with fixed orthodontic appliances. *The Angle Orthodontist*, *81*(5), 901-906. <https://doi.org/10.2319/012111-44.1>
- Rakhshan, H., & Rakhshan, V. (2015). Effects of the initial stage of active fixed orthodontic treatment and sex on dental plaque accumulation: A preliminary prospective cohort study. *The Saudi Journal for Dental Research*, *6*(2), 86-90. <https://doi.org/10.1016/j.sdentj.2014.11.002>
- Ramfjord, S. P. (1959). Indices for prevalence and incidence of periodontal disease. *The Journal of Periodontology*, *30*(1), 51-59. <https://doi.org/10.1902/jop.1959.30.1.51>
- Rams, T. E., Oler, J., Listgarten, M. A., & Slots, J. (1993). Utility of Ramfjord index teeth to assess periodontal disease progression in longitudinal studies. *Journal of Clinical Periodontology*, *20*(2), 147-150. <https://doi.org/10.1111/j.1600-051x.1993.tb00330.x>
- Rashkova, M. (2012). Influence of systemic diseases and removable orthodontic appliances on the quality of saliva in childhood. *Journal of IMAB - Annual Proceeding Scientific Papers*, *18*(2), 163-167. <https://doi.org/10.5272/jimab.2012182.163>
- Ren, Y., Jongsma, M. A., Mei, L., van der Mei, H. C., & Busscher, H. J. (2014). Orthodontic treatment with fixed appliances and biofilm formation - A potential public health threat? *Clinical Oral Investigations*, *18*(7), 1711-1718. <https://doi.org/10.1007/s00784-014-1240-3>
- Ristic, M., Svabic, M. V., Sasic, M., & Zelic, O. (2007). Clinical and microbiological effects of fixed orthodontic appliances on periodontal tissues in adolescents. *Orthodontics & Craniofacial Research*, *10*(4), 187-195. <https://doi.org/10.1111/j.1601-6343.2007.00396.x>
- Silness, J., & Løe, H. (1964). Periodontal disease in pregnancy II. Correlation between oral hygiene and periodontal condition. *Acta Odontologica Scandinavica*, *22*(1), 121-135. <https://doi.org/10.3109/00016356408993968>
- Sullivan, K. M., Dean, A., & Soe, M. M. (2009). On academics: OpenEpi: A web-based epidemiologic and statistical calculator for public health. *Public Health Reports*, *124*(3), 471-474. <https://doi.org/10.1177/003335490912400320>
- Tsichlaki, A., Chin, S. Y., Pandis, N., & Fleming, P. S. (2016). How long does treatment with fixed orthodontic appliances last? A systematic review. *American Journal of Orthodontics and Dentofacial Orthopedics*, *149*(3), 308-318. <https://doi.org/10.1016/j.ajodo.2015.09.020>

Ahmed Taher Al-Haj, Rami Ishaq, Anas Shamala, Mohammed Al-Wesabi, Khalid Aldhorae,
Mohammed Sultan Alakhali and Mohammed Al-Labani

- Türkkahraman, H., Sayın, M., Bozkurt, F. Y., Yetkin, Z., Kaya, S., & Önal, S. (2005). Archwire ligation techniques, microbial colonization, and periodontal status in orthodontically treated patients. *The Angle Orthodontist*, 75(2), 231-236. [https://doi.org/10.1043/0003-3219\(2005\)075<0227:ALTMCA>2.0.CO;2](https://doi.org/10.1043/0003-3219(2005)075<0227:ALTMCA>2.0.CO;2)
- Zachrisson, B. U., & Zachrisson, S. (1971). Caries incidence and oral hygiene during orthodontic treatment. *European Journal of Oral Sciences*, 79(4), 394-401. <https://doi.org/10.1111/j.1600-0722.1971.tb02028.x>

Statistical Analysis of Dry Grinding of Mica in Planetary Mill

Ku Esyra Hani Ku Ishak*, Shafinaz Saad, Syed Fuad Saiyid Hashim and Hashim Hussin

School of Materials and Mineral Resources Engineering, Engineering Campus, Universiti Sains Malaysia, 14300 USM, Nibong Tebal, Penang, Malaysia

ABSTRACT

A huge amount of energy can be used for fine particle breakage using the planetary mill resulting in high-cost consumption. Understanding how these operating parameters could affect the dry grinding mechanism in a planetary mill is still not sufficiently discussed. The effect of different operating parameters of planetary mills in the dry grinding of mica was investigated using statistical analysis. A laboratory scale of the planetary mill was used by varying the operating parameters such as grinding time (minutes), rotational speed (rpm), and percentage of grinding media (%). A full factorial design was used involving 48 experiments, and the grinding process' efficiency was evaluated using the cut size of particles (d_{50}) obtained from the particle size distribution analysis. The analysis was supported by morphological analysis by SEM image and structural distortion by XRD test. The statistical analysis showed a good correlation with the R^2 value of 0.874 with the standard deviation of 0.852. It was found that the optimum parameters for grinding time, grinding speed, and grinding media were 20 minutes, 400 rpm, and 30% media charged, respectively, with the d_{50} value of 7.44 μm . This study provides further insight into the mica breakage operating parameters in a planetary mill.

Keywords: Dry grinding, fine grinding, mica grinding, planetary mill, statistical analysis

ARTICLE INFO

Article history:

Received: 23 August 2021

Accepted: 09 February 2022

Published: 25 May 2022

DOI: <https://doi.org/10.47836/pjst.30.3.25>

E-mail addresses:

kuesyrahani@usm.my (Ku Esyra Hani Ku Ishak)

saad.shafinaz@gmail.com (Shafinaz Saad)

mrsyfuad@usm.my (Syed Fuad Saiyid Hashim)

srhashim@usm.my (Hashim Hussin)

* Corresponding author

INTRODUCTION

Mica is an important mineral widely utilized in applying fine particles in which the bulk of domestic output is being processed into small-size mica by a wet or dry grinding process (Andrić et al., 2013). Mica was usually used to improve strength and thermal properties (Abd, 2016). For example, Roshanaei et al. (2020) studied rubber

reinforcement in addition to silica and mica particles, and the results showed that the mica-containing composites have increased in strength. Another research investigated the relationship between rheology and the qualitative appearance of dried, mica-based paint coatings used in the aerospace industry (Anderson et al., 2020). The mica usually being used as paint filler for its natural glossy appearance.

Mica fine particles are produced by fine grinding, which is the main unit process in the mineral industry. The involved processes are impact or compression caused by pressures applied almost regularly to the particle surface, chipping caused by oblique forces, abrasion caused by forces operating parallel to the surfaces, and other mechanisms (Usman, 2015). Grinding procedures such as wet grinding (product range from 95 to 45 μm) and dry grinding (product in the range of 1.2mm to 150 μm) are being utilized in the industries (Pérez-Maqueda et al. 2004). However, the production of this fine grinding process requires a large amount of energy, has high overall cost consumption, and has low production rates. Furthermore, due to the following factors, it is difficult to fulfill the rigorous requirements for fineness, purity, shape, and crystallinity:

- (a) Because particle strength increases dramatically as particle size decreases, particle breakage intensity must be high.
- (b) Particles of brittle materials deform plastically below the tough brittle transition size, depending on the materials' types. Therefore, the breakage of these particles becomes difficult.
- (c) The adhesion force in the fine particles can cause agglomeration. The stringent demand from the industries according to the specific application has made the grinding industry able to move ahead to produce custom-made minerals that can suit the specific application for the industrial product.

The industries have been finding ways to decrease the amount of energy needed in the fine grinding process by using several approaches. Generally, the efficiency of the grinding operations can be increased by developing new technologies which require a lot of cost and time or by optimizing the currently available grinding process. Planetary mill, stirred mill, jet mill, vibration mill, and peripheral mill are considered high-intensity grinding mills that could exhibit mechanochemical effects due to high power bulk density compared to ball mill (Palaniandy & Jamil, 2009). In the industry, the planetary mill is one type of popular equipment that has been used in producing a finely ground product and for the mechanical activation process (Atanov et al., 2020; Ajaka & Akinbinu, 2011; Li & Hitch, 2017; Pribytkov et al., 2019; Guzzo et al., 2014). In the planetary mill, the product (powders) depends on the low or high energy impact and the number of energy impacts received throughout the process. The huge amount of energy can be used for fine particle breakage, and the excess energy will be used for crystal structural changes besides transformation to the energy. These are the few reasons why mills are chosen for

the fine grinding process. Other than that, the abrasion between the container and balls also impacts the product quality. The planetary mill has been used widely in industries and therefore has received lots of attention from researchers on its operation mechanism and performance (Atanov et al., 2020; Feng et al., 2004; Real & Gotor, 2019; El-Mofty et al., 2020; Burmeister et al., 2018; Ashrafizadeh & Ashrafizaadeh, 2012). The planetary mill has also been used to reduce the size of the mica for a variety of industrial uses, including insulators, pearlescent pigments, polymers, aeronautical devices, condensers, and plastic fillers (Barlow & Manning, 1999). In manufacturing these advanced materials, micronized mica can be utilized as fillers to enhance the product quality (Cheng et al., 1999).

A recent study investigated particle impact energy in a planetary mill by varying the size of particles and numbers (Hirosawa et al., 2021). The behavior of particles and the grinding medium were simulated using the discrete element method (DEM). The results indicate that the grinding medium, which was the grinding balls size, must be appropriately selected in response to particle size and number changes so that the particles can acquire a significant amount of impact energy during the grinding. The effect of planetary operating parameters such as grinding time, rotational speed, the ratio of media to powder, mill filling, and media size was investigated in talc grinding (El-Mofty et al., 2020). The study suggested that the ratio of media to powder and grinding time were the most significant parameters. An optimum ball size was selected as inappropriate size of balls could produce a larger particle size. Simultaneously, a reduction of the mill filling and an increase in the mill speed produce finer output. The effect of the operating parameters is important to develop more advanced technologies and computer simulations. For example, in recent research, the controlled grinding process of the planetary mill was investigated and developed with the function of automatic control in a closed-loop system using a linear-quadratic controller (Atanov et al., 2020). Another study involves the study of the optimum ratio of the gyration diameter to mill tube diameter (G/D ratio) of the planetary mill (Cho et al., 2006). Despite these developing technologies, the understanding of how these operating parameters could affect the dry grinding mechanism in a planetary mill is still not sufficiently discussed.

In this study, the effect of operating parameters of planetary mills such as grinding period, rotational speed grinding, and percentage of grinding media during the mica grinding was evaluated in size particles. In addition, the structure of the mica products was discussed, and optimum conditions for the mica grinding in the planetary mill were determined. It provides further insight into understanding a planetary mill's mica breakage operating parameters.

METHODOLOGY

The sample used for this experiment was mica powder obtained from a local kaolin company in Perak, Malaysia, with an average particle size of 13.8 μm . The sampling

process was done using the cone and quartering method for 10 kg of sample. The cone and quartering method reduces the bulk sample size without introducing systematic bias by forming a cone and dividing it into quarters. Two quarters will be discarded while the other two are combined and used as a sample. The feed of the sample was characterized in terms of the particle size distribution, X-ray Fluorescence (XRF), X-ray diffraction (XRD), and Field Emission Scanning Electron Microscope (FESEM) before the grinding process. This particle size analysis was performed using a particle size analyzer, Malvern model Mastersizer E Ver. 1.2, which can measure the size in the range of $0.1\mu\text{m}$ to $1000\mu\text{m}$ for 0.5 g – 3.0 g of a sample. X-ray Fluorescence (XRF) was used to determine the chemical composition present in the sample tested in terms of oxide minerals. 25 g sample of raw material was sent for Rigaku X-ray Spectrometer RIX 3000. The purpose of the XRD test for this study was to determine the structural distortion due to the grinding in the tested sample. The pattern of the XRD was obtained using the XRD Model D8 Advance. The DIFFRAC.EVA software was used to interpret the pattern from XRD data to determine the intensity of each high peak.

In this study, FESEM Model ZEISS SUPRA 35VP was used. Three or four photomicrographs for every sample were selected from a different location under a certain magnification. Delaminate layer and a thin film of sample, morphology, and structural shape were observed under magnification.

The grinding process was done using a 250 ml pot in a planetary mill with a fixed feed rate which was 50 g , as shown in Figure 1. The maximum feed size for the planetary mill was 10 mm , and the sample can be grounded up to $1\mu\text{m}$. The grinding pot was made up

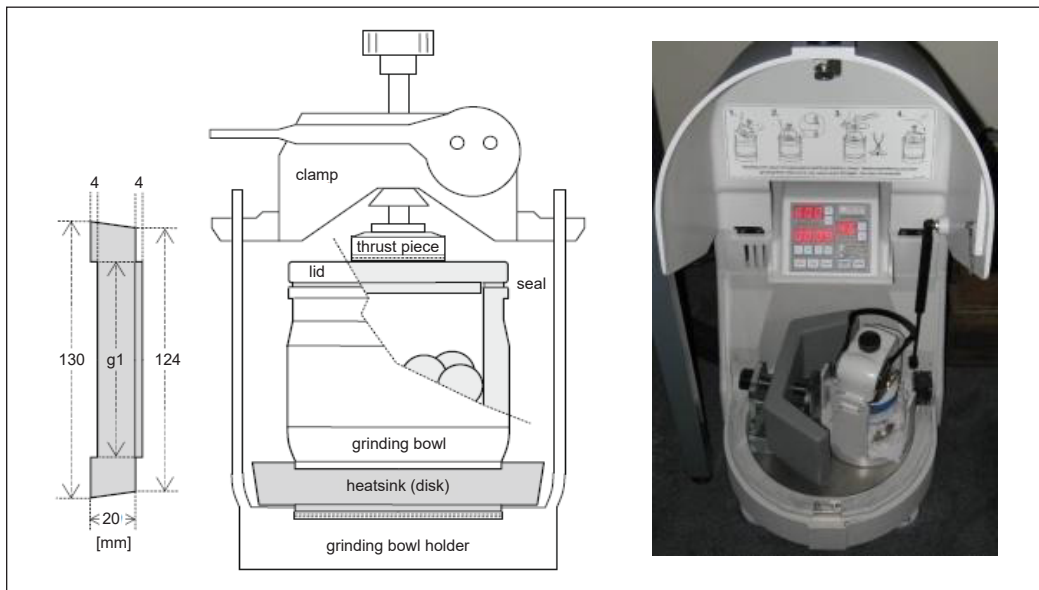


Figure 1. Planetary mill

of stainless steel and agate, which had been used as a grinding media type in this study. The rotational speed of the grinding bowl was in the range of 100 rpm to 500 rpm. A full randomized factorial design with 48 experiments with various combinations of the grinding time, rotational speed, and percentage media content was used, as shown in Table 1. The statistical software Minitab 16 was used for the statistical analysis. Experimental runs of general full factorial design (FFD) and the results of the factorial design were analyzed based on d_{50} , which was determined from the particle size distribution graph obtained from the particle size distribution testing. The standard deviation and R^2 for each response were observed.

Table 1
The operating parameters involved in this study

No	Grinding period (min)	Rotational speed (rpm)	Percentage of grinding media (%)	No	Grinding period (min)	Rotational speed (rpm)	Percentage of grinding media (%)
1	40	400	30	25	10	100	30
2	60	100	20	26	40	200	40
3	10	200	40	27	60	400	20
4	20	400	30	28	60	100	40
5	60	200	20	29	40	100	20
6	40	200	30	30	60	200	30
7	20	500	40	31	10	400	20
8	40	200	20	32	40	500	40
9	60	100	30	33	20	200	20
10	60	500	20	34	10	200	30
11	10	100	40	35	40	500	20
12	20	100	20	36	60	500	30
13	10	100	20	37	10	500	20
14	20	400	40	38	40	400	40
15	20	500	30	39	40	100	30
16	20	500	20	40	60	200	40
17	10	400	30	41	40	500	30
18	60	500	40	42	10	400	40
19	20	100	30	43	40	400	20
20	20	400	20	44	40	100	40
21	10	500	30	45	10	500	40
22	20	100	40	46	60	400	30
23	20	200	30	47	20	200	40
24	60	400	40	48	10	200	20

RESULTS AND DISCUSSIONS

Characterization of Sample

Table 2 shows the percentage of the chemical composition found in the raw sample of mica using XRF. The predominant constituents of the sample were SiO_2 and Al_2O_3 with

55% and 34%, respectively, while other elements were less than 1%. A high percentage of SiO₂ low percentage of Al₂O₃ and Fe₂O₃ contents had decreased the grind ability process (Paine, 2019).

Table 2
Percentage of chemical composition present in the mica

Composition	Weight (%)	Composition	Weight (%)
SiO ₂	54.86	CaO	0.035
Al ₂ O ₃	34.37	P ₂ O ₅	0.034
K ₂ O	7.23	ZrO ₂	0.033
Fe ₂ O ₃	1.15	NiO	0.021
MgO	1.15	ThO	0.011
TiO ₂	0.83	CuO	0.01
Rb ₂ O	0.059	ZnO	0.007
Cr ₂ O ₃	0.053	Nb ₂ O ₅	0.006
		VO ₂	Trace

Figure 2 shows the photomicrograph of mica with 1000 times and 10, 000 times magnification. It can be seen that the mica was in the form of layered structural and irregular shapes.

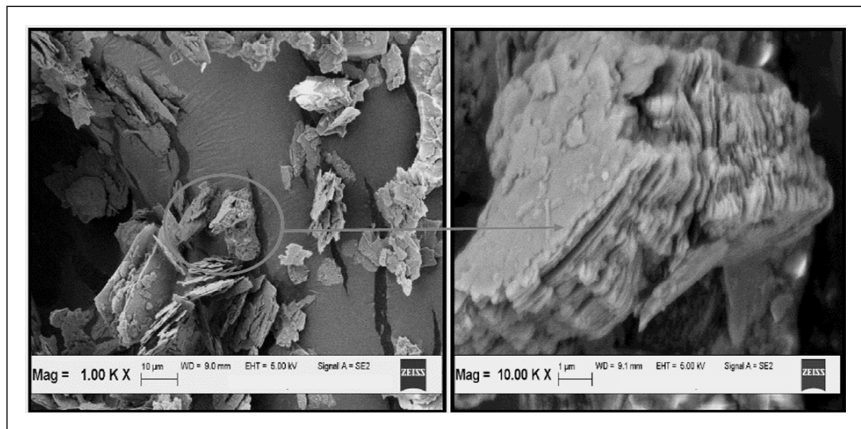


Figure 2. Photomicrograph of mica with 1000 times and 10, 000 times magnification

ANOVA STATISTICAL ANALYSIS

The statistical analysis (ANOVA) was presented in Table 3, and the final model equation in the genuine factor represented the d₅₀ value shown in Equation 1.

$$d_{50} = 13.9 - (0.0144 * \text{grinding time}) - (0.00723 * \text{speed}) \quad [1]$$

Table 3
ANOVA analysis to predict d_{50} of the product

Source	Seq SS	Adj SS	Adj MS	F	P	Significance	% Contribution
Grinding Time	8.6395	8.6395	2.8798	3.97	0.025	Significant	8.33
Speed	63.2325	63.2325	21.0775	29.05	0.000	Significant	60.99
Grinding Media	0.7116	0.7116	0.3558	0.49	0.620		0.69
Grinding Time * Speed	8.1197	0.81197	0.9022	1.24	0.330		7.83
Grinding time * Grinding media	3.0088	3.0088	0.5015	0.69	0.660		2.90
Speed * Grinding Media	6.9004	6.9004	1.1501	1.59	0.208		6.66
Error	13.0580	13.0580	0.7254				12.59
Total	103.6740						100

Based on the value presented in Table 3, it was found that the grinding time and speed were significant parameters in determining the d_{50} of the product for having a P-value less than 0.05. On the other hand, the grinding media percentage did not significantly affect having a P-value of more than 0.05. The coefficient of determination (R^2) was 0.8 with a standard deviation of 0.85. The average absolute percentage error (AAPE) was 6.09, while the average error was 0.21. The actual and predicted data of the d_{50} as shown in Figure 3. However, it was found that the contribution for the error

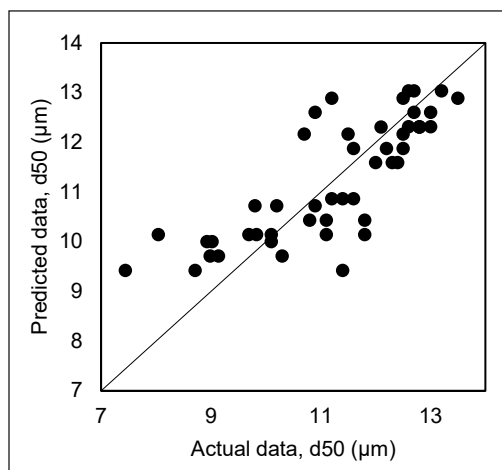


Figure 3. Actual and predicted data of d_{50}

term is 12.59, which is higher than the contribution of one factor. Therefore, this model does not cover as much of the surface roughness variance. The possible reason for this is the measurement error in the mill material discharge system, which could contribute to the cut size determined from the particle size distribution results. Further investigation of the discharge system should be conducted in the next study. However, in this study, the reliability of the trends was confirmed by SEM and the XRD analysis.

The Effect of Grinding Time

Figure 4 shows the plot of the grinding time to the cut size (d_{50}). The size of the particles was decreased with the increase of the grinding time from 10 to 20 minutes. Increasing time had allowed more impact on the particles. Figure 5 shows the breakage mechanism of the

ground mica in the planetary mill. The particles with irregular shapes had undergone the breakage mechanism and delaminated into a layered structure. It was due to the collision between the grinding media-feed-grinding media. Feed that stuck between the grinding media during a collision would undergo the deformation process and crack, determining the particle structure (Liu et al., 2016). With increasing grinding time, the coarse particles with angular morphology decreased, while the fine particles with granular morphology increased, resulting in an improvement of sphericity in the particle size distribution. The collision process depended on the feed's mechanical behavior, stable feed phase, and levels of emphasis during the grinding process.

However, increasing the time from 20 minutes to 60 minutes had increased the size of the particles due to the agglomeration. During the grinding process, the size of particles reached a critical point in which the milling equilibrium was reached. It is the stage where the cut size shows insignificant changes or remains constant. At this state, larger agglomerates were formed by stronger chemical bonds and van der Waals forces (Lee et al., 2020). Figures 6 and 7 show the morphological analysis of the grinding time effect

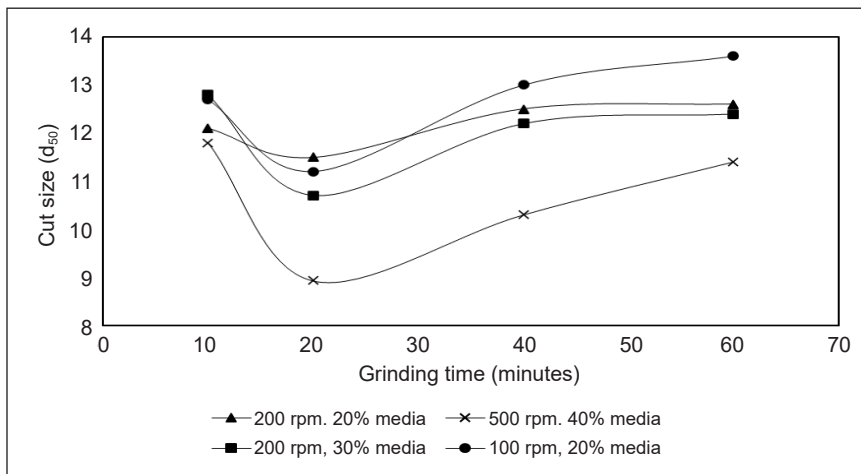


Figure 4. The effect of grinding time to cut size, d_{50} (μm)

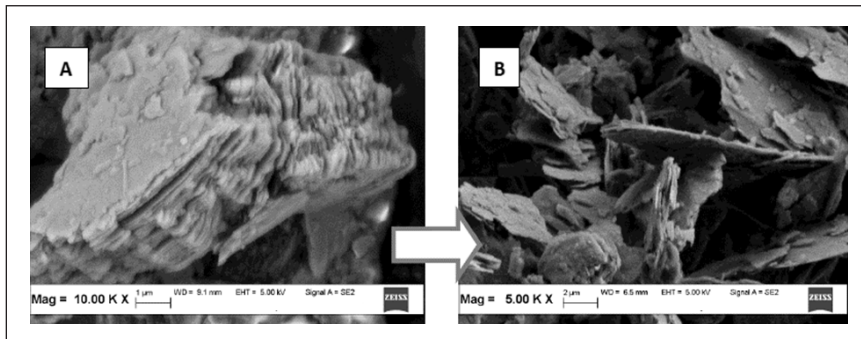


Figure 5. Breakage mechanism applied on mica (A) and delaminated into a layered structure (B)

on the agglomeration of the mica. A longer grinding period tended to cause an increase in amorphism (Zhao et al., 2021; Arbain et al., 2011). The agglomeration process started because of the high surface energy that increases the adhesion forces between the particles. Therefore, longer grinding time produced bigger particles size in this agglomeration phenomenon. Another possible reason for agglomeration is the solid residue produced during grinding, cemented by highly reactive amorphous material that serves as a coating. The accumulation of these small particles on the agglomerates' surface could reduce the milling efficiency as broken particles reassemble to form large particles. This condition should be avoided in the production of fineness particles, for example, in the filler industries, as it could not disperse well in the rubber matrix and would give a poor property.

Increasing the grinding time may also change the structure of the mica particle. It can be shown by a structural distortion test using XRD, as shown in Figure 8 and Table 4. In Figure 3, the XRD patterns had different grinding times ranging from 10 min to 60 min. Due to their significant distortion, two peaks were observed based on the XRD pattern. It can be observed clearly at the first peak, 2θ angles of 17.82° . Based on Table 4, the intensity peak before the grinding was 337.0727. Then, the peak increased until the value achieved 1385.071 for 10 and 20 minutes of the grinding period, but after 40 min of grinding, the intensity was reduced to 322.5305. A great intensity reduction was observed during 40 min of the grinding. After that, it continuously decreased until the period of grinding achieved 60 min. The grinding process transformed the crystallinity of all the ground mica from crystalline to partially amorphous. Another peak was also observed at 2θ angles of

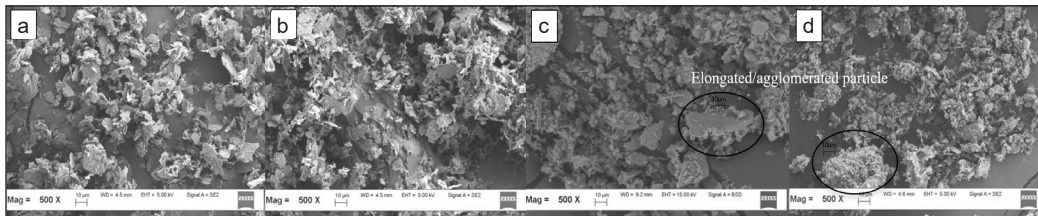


Figure 6. Photomicrographs of ground mica at a) 10 minutes, b) 20 minutes, c) 40 minutes, and d) 60 minutes

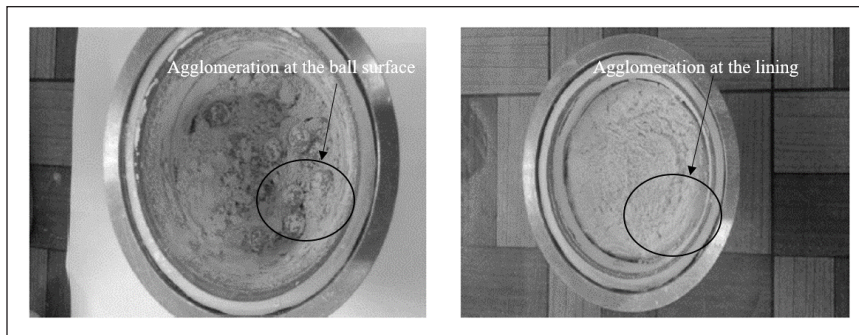


Figure 7. Agglomeration of mica powder at the lining and surface of the ball

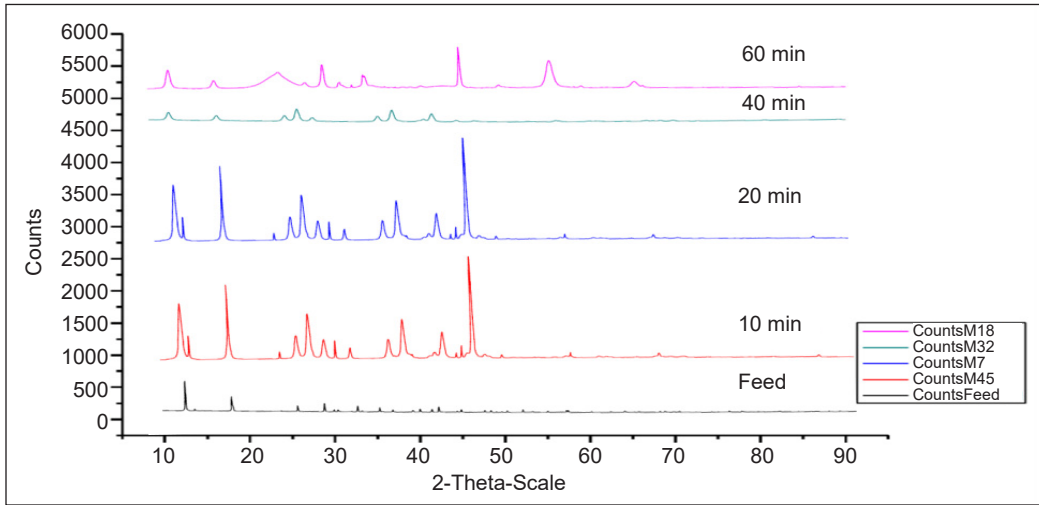


Figure 8. XRD pattern with the rotational speed of 500 rpm and 40% of percentage grinding media at the different grinding time

Table 4
Peak intensity and d_{50} value for the various grinding periods

Sample	Raw sample	45	7	32	18
Grinding time, minutes		10	20	40	60
Rotational speed, rpm		500	500	500	500
Grinding media, %		40	40	40	40
d_{50} , μm	13.8	11.8	9.02	10.3	11.4
2-Theta Scale	17.82	17.82	17.82	17.82	17.82
Intensity, calc	337.0727	1385.071	1385.071	322.5305	298.682
2-Theta Scale	45.53	45.53	45.53	45.53	45.53
Intensity, calc	157.332	1755.751	1755.751	162.8971	755.2411

45.53°. At this peak, intensity tended to increase with the grinding time. However, after 40 minutes, the intensity value reduced, and at 60 minutes of the grinding, the peak intensity increased again. Within 10 minutes of the grinding operation, a significant change in the crystal structure of mica was observed.

The Effect of Grinding Speed

Figure 9 shows the plot of the grinding speed to d_{50} . A significant size reduction was observed when the mill rotational speed increased from 400 rpm to 500 rpm. Micronized mica below 10 μm was obtained as the mill rotational speed was more than 200 rpm. This observable fact was due to the rate of impulses. As the mill speed increased, the rate of impulses and acceleration also increased. The size reduction per unit time also increased due to more repetitive stress. The increase in mill rotational speed would cause the frequency

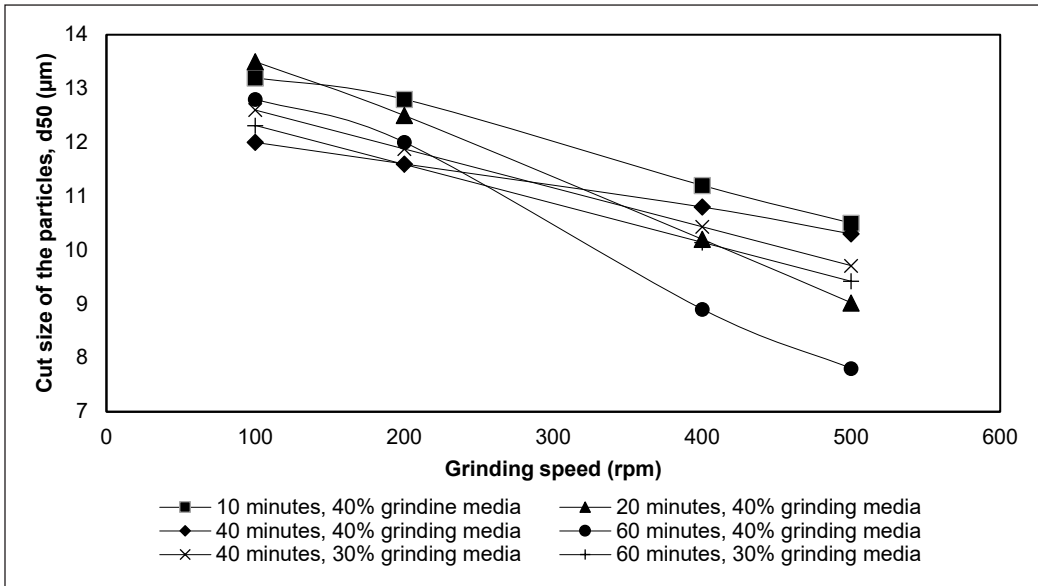


Figure 9. The effect of grinding speed on the cut size of the particles (d_{50})

of collision between the grinding media to increase. This phenomenon may contribute to the breakage of the particle at coarse size because the frequency of collision between the grinding media and the coarse particle was higher than the collision between the grinding media and fine particles. There are two probable reasons for this phenomenon. The first one is that it might be explained by the heat generated by the higher operational speed that might lead to the particles being in a brittle stage. The other reason is that the increasing speed might behave like an abrasive compound that breaks the particles (Real & Gato, 2019; Sato et al., 2010).

The optimization of the dry grinding of mica was predicted using the Minitab 16. In this case, it was found that the optimum parameters for grinding speed, grinding time, and grinding media were 20 minutes, 400 rpm, and 30% charged, respectively, with the d_{50} value of 7.44 μm .

CONCLUSION

Mica with predominant constituents of 55% SiO_2 and 34% Al_2O_3 was grounded in the planetary mill. The effect of dry grinding of mica on the d_{50} of the ground product in a planetary mill was investigated. Statistical analysis was done, and it was found that the grinding process of mica depended on the various operating variables such as grinding speed and grinding time while grinding media charge only gives a small contribution during mica grinding. During the extreme condition when the operating variables were at the maximum level, such as 60 min of the grinding period with 500 rpm rotational speed

of grinding and 40% of the grinding media, it was observed that the fine particles of mica tended to agglomerate, contributing to the inefficient of the grinding process. The coefficient of determination (R^2) was 0.874 with a standard deviation of 0.852, which indicated good agreement between the actual and predicted data of the d_{50} . It was suggested that an appropriate grinding aid for mica grinding was determined and used in a future study to avoid particle agglomeration issues and improve process efficiency.

ACKNOWLEDGEMENT

The authors want to thank the School of Materials and Mineral Resources Engineering, USM, and USM RUI Grant 8014148RUI.

REFERENCES

- Andrić, L., Terzić, A., Aćimović-Pavlović, Z., Trumić, M., Petrov, M., & Pavlović, L. (2013). A kinetic study of micronization grinding of dry mica in a planetary ball mill. *Advances in Materials Science and Engineering*, 2013, 1-6. <https://doi.org/10.1155/2013/543857>
- Abd, A. A. (2016). Study the effect of mica as filler in natural rubber properties. *Journal of University of Babylon*, 24(3), 773-781.
- Ajaka, E. O., & Akinbinu, V. A. (2011). Design, fabrication and performance analysis of a planetary roll mill for grinding effect. *ARPN Journal of Engineering and Applied Sciences*, 4(6), 75-90.
- Anderson, J., Shori, S., Jabbari, E., Ploehn, H. J., Gadala-Maria, F., & Priftis, D. (2020). Correlating coating quality of coverage with rheology for mica-based paints. *Applied Rheology*, 30(1), 119-129. <https://doi.org/10.1515/arh-2020-0110>
- Arbain, R., Othman, M., & Palaniandy, S. (2011). Preparation of iron oxide nanoparticles by mechanical milling. *Minerals Engineering*, 24(1), 1-9. <https://doi.org/10.1016/j.mineng.2010.08.025>
- Ashrafzadeh, H., & Ashrafzaadeh, M. (2012). Influence of processing parameters on grinding mechanism in planetary mill by employing discrete element method. *Advanced Powder Technology*, 23(6), 708-716. <https://doi.org/10.1016/j.appt.2011.09.002>
- Atanov, S. K., Bigalieva, A. F. Z., Apachidy, N. K., & Rusak, A. V. (2020). Process control issues of fine grinding in a planetary mill. *Applied Mathematics Computer Science Control Processes*, 16(3), 277-292. <https://doi.org/10.21638/11701/spbu10.2020.306>
- Barlow, S. G., & Manning, D. A. C. (1999). Influence of time and temperature on reactions and transformations of muscovite mica. *British Ceramic Transactions*, 98(3), 122-126. <https://doi.org/10.1179/096797899680327>
- Burmeister, C., Titscher, L., Breitung-Faes, S., & Kwade, A. (2018). Dry grinding in planetary ball mills: Evaluation of a stressing model. *Advanced Powder Technology*, 29(1), 191-201. <https://doi.org/10.1016/j.appt.2017.11.001>
- Cheng, K., Wan, J., & Liang, K. (1999). Enhanced mechanical properties of oriented mica glass-ceramics. *Materials Letters*, 39(6), 350-353. [https://doi.org/10.1016/S0167-577X\(99\)00033-6](https://doi.org/10.1016/S0167-577X(99)00033-6)

- Cho, H., Lee, H., & Lee, Y. (2006). Some breakage characteristics of ultra-fine wet grinding with a centrifugal mill. *International Journal of Mineral Processing*, 78(4), 250-261. <https://doi.org/10.1016/j.minpro.2005.11.005>
- El-Mofty, S. E., Abuhasel, K. A., Elbendari, A. M., & El-Midany, A. A. (2020). Ultrafine dry grinding of talc by planetary mill: Effects of operating conditions. *Obogashchenie Rud*, 6(4), 21-25. <https://doi.org/10.17580/or.2020.06.04>
- Feng, Y. T., Han, K., & Owen, D. R. J. (2004). Discrete element simulation of the dynamics of high energy planetary ball milling processes. *Materials Science and Engineering: A*, 375, 815-819. <https://doi.org/10.1016/j.msea.2003.10.162>
- Guzzo, P. L., Santos, J. B., & David, R. C. (2014). Particle size distribution and structural changes in limestone ground in planetary ball mill. *International Journal of Mineral Processing*, 126, 41-48. <https://doi.org/10.1016/j.minpro.2013.11.005>
- Hirosawa, F., Iwasaki, T., & Iwata, M. (2021). Particle impact energy variation with the size and number of particles in a planetary ball mill. In *MATEC Web of Conferences* (Vol. 333, pp. 1-6). EDP Sciences. <https://doi.org/10.1051/mateconf/202133302016>
- Lee, J. R., Lee, K. S., Park, Y. O., & Lee, K. Y. (2020). Fluidization characteristics of fine cohesive particles assisted by vertical vibration in a fluidized bed reactor. *Chemical Engineering Journal*, 380, Article 122454. <https://doi.org/10.1016/j.cej.2019.122454>
- Li, J., & Hitch, M. (2017). Ultra-fine grinding and mechanical activation of mine waste rock using a planetary mill for mineral carbonation. *International Journal of Mineral Processing*, 158, 18-26. <https://doi.org/10.1016/j.minpro.2016.11.016>
- Liu, S., Li, Q., Xie, G., Li, L., & Xiao, H. (2016). Effect of grinding time on the particle characteristics of glass powder. *Powder Technology*, 295, 133-141. <https://doi.org/10.1016/j.powtec.2016.03.030>
- Paine, K. A. (2019). Physicochemical and mechanical properties of portland cements. In P. C. Hewlett & M. Liska (Eds.), *Lea's Chemistry of Cement and Concrete* (pp. 285-339). Elsevier. <https://doi.org/10.1016/B978-0-08-100773-0.00007-1>
- Palaniandy, S., & Jamil, N. H. (2009). Influence of milling conditions on the mechanochemical synthesis of CaTiO₃ nanoparticles. *Journal of Alloys and Compounds*, 476(1-2), 894-902. <https://doi.org/10.1016/j.jallcom.2008.09.133>
- Pérez-Maqueda, L. A., Blanes, J. M., Pascual, J., & Pérez-Rodríguez, J. L. (2004). The influence of sonication on the thermal behavior of muscovite and biotite. *Journal of the European Ceramic Society*, 24(9), 2793-2801. <https://doi.org/10.1016/j.jeurceramsoc.2003.10.002>
- Pribytkov, G. A., Baranovskiy, A. V., Korosteleva, E. N., Krinitcyn, M. G., & Korzhova, V. V. (2019). A production of fine ferrotitanium powder by intensive planetary mill grinding. In *Materials Today: Proceedings* (pp. 461-463). Elsevier. <https://doi.org/10.1016/j.matpr.2019.12.177>
- Real, C., & Gotor, F. J. (2019). Effects of the speed ratio on the efficiency of planetary mills. *Heliyon*, 5(2), Article e01227. <https://doi.org/10.1016/j.heliyon.2019.e01227>

- Roshanaei, H., Khodkar, F., & Alimardani, M. (2020). Contribution of filler-filler interaction and filler aspect ratio in rubber reinforcement by silica and mica. *Iranian Polymer Journal*, 29(10), 901-909. <https://doi.org/10.1007/s13726-020-00850-4>
- Sato, A., Kano, J., & Saito, F. (2010). Analysis of abrasion mechanism of grinding media in a planetary mill with DEM simulation. *Advanced Powder Technology*, 21(2), 212-216. <https://doi.org/10.1016/j.apt.2010.01.005>
- Usman, H. (2015). *Measuring the efficiency of the tumbling mill as a function of lifter configurations and operating parameters* (Doctoral dissertation). Colorado University, USA. https://mountainscholar.org/bitstream/handle/11124/17125/Usman_mines_0052E_10720.pdf
- Zhao, S., Wang, G., Yang, H., Chen, G., & Qiu X. (2021). Agglomeration-aggregation and leaching properties of mechanically activated chalcopyrite. *Transactions of Nonferrous Metals Society of China*, 31(5), 1465-1474. [https://doi.org/10.1016/S1003-6326\(21\)65590-5](https://doi.org/10.1016/S1003-6326(21)65590-5)

Water Quality Assessment of Surface Water at the Urban Area of An Giang Province, Vietnam

Khanh Tran Thien Nguyen^{1,2*}, Chi Thi Dao Vo^{1,2}, An Thuy Ngo^{1,2}, Nghi Thanh Doan^{1,2}, Luyen Phuc Huynh³ and Dung Huynh Thuy Tran³

¹An Giang University - Vietnam National University Ho Chi Minh City, 18 Ung Van Khiem, Long Xuyen, An Giang, Vietnam

²Vietnam National University, Ho Chi Minh City, Vietnam

³An Giang Center for Environmental Monitoring and Techniques, Resources, 822 Tran Hung Dao, Long Xuyen, An Giang, Vietnam

ABSTRACT

The development of residential areas in the trend of urbanization and the development of industrial parks and clusters have caused risks to reduce the surface water quality of the Mekong River in An Giang province. This study was conducted by sampling surface water affected by urban areas and affected by industrial parks/clusters (seven sampling points) in June 2021 and analyzing the parameters of temperature, pH, DO, TSS, COD, BOD₅, N-NO₃⁻, N-NH₄⁺, P-PO₄³⁻, Coliform, As, Pb, Hg, Benzene hexachloride, Dieldrin. The analytical results of water samples were compared with the National Technical Regulation of Vietnam. The water quality index was calculated according to the technical guidelines of the Vietnam Environment Administration (VN_WQI). The results show that domestic and industrial wastewater has polluted the surface water of the Tien River and the Hau River, two

important rivers of the downstream Mekong River, flowing through An Giang province. The pollution shows in parameters of TSS, DO, BOD₅, COD, N-NH₄⁺, and Coliform that exceeds allowable limits. However, other parameters such as temperature, pH, N-NO₃⁻, P-PO₄³⁻ are mostly at the acceptable range and within allowable limits. Based on the WQI, most of the water quality at the sampling points is poor. Therefore, it is recommended that people not directly use the Tien River and Hau River water in

ARTICLE INFO

Article history:

Received: 5 September 2021

Accepted: 27 January 2022

Published: 25 May 2022

DOI: <https://doi.org/10.47836/pjst.30.3.26>

E-mail addresses:

nttkhanh@agu.edu.vn (Khanh Tran Thien Nguyen)

vtdchi@agu.edu.vn (Chi Thi Dao Vo)

ntan@agu.edu.vn (An Thuy Ngo)

dtngghi@agu.edu.vn (Nghi Thanh Doan)

pl.huynh.mt280594@gmail.com (Luyen Phuc Huynh)

thuy_dung1592002@yahoo.com (Dung Huynh Thuy Tran)

*Corresponding author

An Giang for drinking and domestic purposes. It is necessary to apply appropriate water treatment measures. In the coming time, authorities need to monitor and take appropriate measures to treat and manage wastewater from urban areas and industrial parks/clusters.

Keywords: Domestic wastewater, industrial wastewater, Mekong surface water, water quality

INTRODUCTION

An Giang is a province in southwest Vietnam located downstream of the Mekong River. The province is the first land area receiving water from the Mekong River at the northwest border, with Cambodia divided into two main courses (known as the Tien and Hau Rivers). An Giang occupies an important position in the Mekong Delta, with the terrain of hills and plains lying along the Hau River and the Tien River, branches of the Mekong River. An Giang has the potential to develop agriculture, commerce, services, and tourism. In the context of international integration and economic development, the environment of An Giang province is under increasing pressure, especially water pollution, which has affected the supply of freshwater for agricultural irrigation, domestic use, and industry (Shipin et al., 2005; Khanh et al., 2013; Khanh et al., 2015; An Giang Center for Environmental Monitoring and Techniques, Resources, 2019; Van et al., 2020). The development of residential areas in the trend of urbanization and the development of industrial parks and clusters have caused risks to reduce the surface water quality of the Mekong River in An Giang province. Therefore, it is necessary to assess the effects of domestic and industrial wastewater on the surface water quality of the Mekong River in An Giang province.

Water quality monitoring is critical to identifying problems and tackling pollution. The Mekong River is one of the world's largest rivers. The water quality of the Mekong River is the great interest to many researchers in the world (Wilbers et al., 2014; Chea et al., 2016). There are many studies conducted on Mekong River water quality in neighboring provinces of An Giang (Huong et al., 2006; Nhan & Nhan, 2014; Dieu et al., 2016; Tam et al., 2021). Some studies were conducted on surface water in An Giang (Lien et al., 2016; Nguyen et al., 2021; Phat et al., 2019). The previous studies conducted in An Giang did not focus on assessing the impact of residential areas and industrial zones/clusters on water resources, and the indicators used in these surveys were still limited. In this study, water samples were collected in June 2021 (dry season), analyzed physio-chemical parameters, and calculated Water Quality Index to obtain information on levels and characteristics of pollution. Thereby, the study provides an overview of the surface water quality of the Mekong River affected by domestic and industrial wastewater in An Giang province, which has great significance for the control of the province's water quality. This new research has most recent data and parameters than previous studies. The results are the foundation for making recommendations to the citizens and proposing environmental solutions in

the upcoming time. Data of the study are a useful source of information to help the local authority take positive actions of management, environmental protection, and response to climate change in the current situation. The research is meaningful in providing data, knowledge, and references in environmental assessment.

Previous studies have reported that water quality has widely fluctuated among the provinces. A previous study showed that the maximum pH of surface water pollution in Mekong Delta, Vietnam was 8.6 (Wilbers et al., 2014). The temperature and pH of the mainstream and tributaries of the Hau River were suitable for aquatic life in most of the sampling locations (Lien et al., 2016). DO of the mainstream and tributaries of the Hau River fluctuated at 1.76–7.96 mg/L, averaging 4.9 ± 1.4 mg/L (Lien et al., 2016). The DO of surface water affected by residential and industrial areas in Can Tho province was 4.4 mg/L and 4.8 mg/L, respectively (Tam et al., 2021). TSS of the Tien River surface water fluctuated at 9–475 mg/L (Dieu et al., 2016). TSS in the rainy season was higher than in the dry season (Lien et al., 2016). The TSS of surface water affected by residential and industrial areas in Can Tho province was 35.6 mg/L and 39.8 mg/L, respectively (Tam et al., 2021). The average COD value of the Tien River surface water was 14.3 ± 6.3 mg/L (Lien et al., 2016). COD and BOD of the mainstream and tributaries of the Hau River fluctuated at 2–13 mg/L and 2–16 mg/L, respectively (Dieu et al., 2016). In Can Tho province, BOD₅ and COD of surface water were affected by residential areas were 11.4 mg/L and 18.8 mg/L, BOD₅ and COD of surface water were affected by industrial areas were 8.7 mg/L and 14.1 mg/L, respectively (Tam et al., 2021).

The average N-NO₃⁻ value of surface water of the Tien River was 0.11 ± 0.07 mg/L (Lien et al., 2016). N-NH₄⁺ of the mainstream and tributaries of the Hau River fluctuated at 0.02–0.60 mg/L (Dieu et al., 2016). The value of NO₃⁻ of surface water affected by residential areas and industrial areas in Can Tho province was 0.47 mg/L and 0.61 mg/L, respectively, while the value of NH₄⁺ was 1.18 mg/L and 0.53 mg/L (Tam et al., 2021). The average value of P-PO₄³⁻ in the surface water of the Tien River is 0.1 ± 0.07 mg/L (Lien et al., 2016). P-PO₄³⁻ of the mainstream and tributaries of the Hau River fluctuates at 0.06–0.47 mg/L (Dieu et al., 2016). PO₄³⁻ of surface water affected by residential and industrial areas in Can Tho province were 1.17 mg/L and 2.12 mg/L, respectively (Tam et al., 2021). The previous study reported that total Coliforms in surface water pollution in Mekong Delta, Vietnam was 2,500,000 CFU/100 mL (Wilbers et al., 2014). The study by Wilbers et al. (2014) indicated that the value of arsenic and mercury in the surface water pollution in the Mekong delta was 44.1 µg/L and 45.5 µg/L, respectively. The study of Phat et al. (2019) showed that indicators of arsenic were not detected in the surface water of the Tien River flowing through the Tan Chau River in Tan Chau town, An Giang province. Dieu et al. (2016) showed that the concentration of toxic dissolved metals in surface water of the mainstream and tributaries of the Hau River was low.

Many previous studies in Vietnam used the national technical regulations on surface water quality (QCVN 08-MT:2015/BTNMT) to assess surface water quality. For example, previous studies have reported that the value of PO_4^{3-} , NH_4^+ , and NO_2^- of surface water quality of the Tien River flowing through the Tan Chau River in Tan Chau town, An Giang province exceeded the allowable limits (Phat et al., 2019). In addition, the concentrations of TSS, BOD, COD, N-NH_4^+ , N-NO_2^- , P-PO_4^{3-} , Coliform, and *E. coli* in surface water quality in Dong Thap province exceed the allowable limits (Giao et al., 2021). However, pH, temperature, DO, BOD and COD parameters of surface water quality in some canals connecting the Tien River and the Hau River in Vinh Long province, Dong Thap province, and Tien Giang province has within the allowable limits (Nam et al., 2009).

The research conducted by Nguyen et al. (2021) found that the surface water in An Giang was contaminated by organic matters, suspended solids, and Coliforms. On the other hand, the surface water of the Hau River was quite nutritious, especially in the areas affected by aquaculture and agricultural production (Lien et al., 2016). Surface water quality affected by the residential area was the worst compared to surface water affected by the industrial zone, fruit area, and rice field area in Can Tho province. The surface water quality in Can Tho province has decreased due to poor wastewater management by companies and industrial parks (Tam et al., 2021). Another study found that significant degradations were mainly associated with human disturbance and were particularly apparent in sites distributed along the artificial canals in the Vietnam delta, where intensive population growth and agricultural development (Chea et al., 2016). The increase in population density, the number of industrial establishments, the number of commercial and service establishments, and the number of livestock and poultry are the main reasons for the increase of organic matter content in the surrounding surface water. Meanwhile, the increase in rice area, rice production, aquaculture area, and aquaculture production are the main reasons for the increase of suspended solids, nitrogen and the decrease of pH in the surrounding surface water (Nhan & Nhan, 2014).

The water quality index (WQI) model is a popular tool for evaluating surface water quality. In Vietnam, the water quality index was calculated according to the technical guidelines for calculation and publication of the water quality index of the Vietnam Environment Administration (VN_WQI). The previous study showed that VN_WQI values of surface water in An Giang province ranged from 15 to 71, indicating surface water quality was very bad to medium, in which the water quality in larger and smaller rivers in the dry season was less polluted than that in the rainy season due to erosion and runoff water containing waste materials in the wet season (Nguyen & Huynh, 2020). On the other hand, the research conducted by Giao et al. (2021) showed that the water quality index of surface water in Dong Thap province is ranked at level IV (poor) using the VN_WQI method, which was suitable for irrigation and other equivalent purposes.

MATERIALS AND METHODS

Study Area

In 2020, the average population of An Giang province was 1,909,335 people, and the density was 540 people/km². There is a high concentration of population in urban areas and a low concentration in rural areas. The migration of the population from rural to urban areas has a significant impact on the environment. The environment in the urban area is becoming more and more polluted with the progress of urbanization. In the cities, untreated or inadequately treated domestic wastewater has been discharged into the environment, and domestic waste has not been collected and treated with suitable treatment solutions. In addition, there are still production facilities and factories located in residential areas. The total amount of domestic wastewater in the province is estimated at 176,000 m³/day.night in wastewater in the urban area is approximately 72,000 m³/day.night. The province includes 11 districts, towns, and cities but only two wastewater treatment systems. There is the Chau Doc wastewater treatment system with a capacity of 5,000 m³/day.night and the Long Xuyen wastewater treatment system with a capacity of 30,000 m³/day.night which is in trial operation (An Giang Department of Natural Resources and Environment, 2020).

According to the report on the environmental status of An Giang province in the period 2016–2020, An Giang province currently has two industrial Parks: Binh Long Industrial Park and Binh Hoa Industrial Park, and eight industrial clusters that are operating and new industrial zones and clusters will be constructed as planned. The centralized wastewater treatment system in Binh Hoa Industrial Park with a capacity of 2,000 m³/day.night is in operation, and the centralized wastewater treatment system in Binh Long Industrial Park with a capacity of 4,000 m³/day is still building. Up to now, the province has invested in infrastructure for eight industrial clusters and put them into operation. However, it has not yet been invested in building a centralized wastewater collection and treatment system. Investment projects in these industrial clusters must have separated wastewater treatment systems if the activities generate wastewater. The industry of An Giang province mainly focuses on processing industries of foodstuffs, agricultural products, aquatic products, garments, leather shoes, and construction materials (An Giang Department of Natural Resources and Environment, 2020).

Location of Water Sampling

Surface water samples were collected at five sampling points from affected urban areas and two surface water sampling points from industrial parks and clusters. The sample collection schedule was in June 2021 (dry season). Figure 1 shows the location map of surface water sampling. Table 1 shows the code, coordinates, and characteristics of the sampling location.

Table 1
Location of sampling

No.	Code	Coordinate	Location	Characteristics
Basin affected by urban area				
1	UB1	554.699 1.194.414	Long Thanh Ward, Tan Chau town	The total population of Long Thanh Ward is 13,979 people. The location is affected by wastewater from many production and business activities and residents in the area. It is the location affected by wastewater from the Tan Chau urban area on the Tien River.
2	UB2	571.273 1.166.986	Cho Moi commune, Cho Moi district	The total population of Cho Moi commune is 11,318 people. The location is affected by wastewater from many production and business activities and residents in the area. It is the location affected by wastewater from Cho Moi urban area on the Tien River.
3	UB3	581.029 1.162.307	My Luong commune, Cho Moi district	The total population of the My Luong commune is 13,540 people. The location is affected by wastewater from many production and business activities and residents in the area. It is the location affected by wastewater from the My Luong urban area on the Tien River.
4	UB4	576.273 1.147.845	My Long ward, Long Xuyen city	The total population of the My Long ward is 16,750 people. The location is affected by wastewater from many production and business activities and residents in the area. It is the location affected by wastewater from the Long Xuyen urban area on the Hau River.
5	UB5	553.659 1.168.368	Cai Dau commune, Chau Phu district	The total population of the Cai Dau commune is 16,958 people. The location is affected by wastewater from many production and business activities and residents in the area. It is the location affected by wastewater from Cai Dau urban area on the Hau River (Primary canal)

Table 1 (Continue)

No.	Code	Coordinate	Location	Characteristics
Basin affected by industrial parks and industrial clusters				
1	ID1	554.720 1.168.808	Binh Long Industrial Park, Binh Chanh Hamlet, Binh Long Commune, Chau Phu District	Binh Long is a mixed industrial park with many industries, mainly seafood processing, aquatic food processing, and fruit and vegetable processing. The location is affected by wastewater from Binh Long industrial area on the Hau River.
2	ID2	577.294 1.146.119	My Quy Industrial Cluster, Long Xuyen city	Seafood processing is the main industry in My Quy Industrial Cluster. The location is affected by industrial wastewater from My Quy Industrial Cluster on the Hau River.

Methods of Sampling, Preserving, Measuring, and Analyzing Water Samples

The parameters for assessment included: Temperature, pH, Dissolved Oxygen (DO), Total Suspended Solids (TSS), Chemical oxygen demand (COD), Biological oxygen demand (BOD₅), Nitrate (NO₃⁻ calculated by N), Phosphate (PO₄³⁻ calculated by P), Ammonium (NH₄⁺ calculated by N), Coliform, Arsenic (As), Lead (Pb), Mercury (Hg), Benzene hexachloride, Dieldrin.

The order and environmental monitoring methods are implemented under Circular 24/2017/TT-BTNMT on promulgating technical regulations on environmental monitoring and Vietnamese standards and regulations (Vietnam Ministry of Natural Resources and Environment, 2017). Furthermore, methods of sampling, preservation and analysis of samples are under the Vietnam National standard on water quality, as displayed in Tables 2, 3, and 4 (Vietnam Ministry of Science and Technology, 1995; Vietnam Ministry of Science and Technology, 1996; Vietnam Ministry of Science and Technology, 2008; Vietnam Ministry of Science and Technology, 2011a; Vietnam Ministry of Science and Technology, 2011b; Vietnam Ministry of Science and Technology, 2011c; Vietnam Ministry of Science and Technology, 2016).

Table 2

Method of measuring parameters at the location

No.	Parameter	Methods of measuring	Measuring range
1	Temperature	SMEWW 2550B:2012	4-50°C
2	pH	TCVN 6492:2011	2-12
3	DO	TCVN 7325:2016	0-20 mg/L

Table 3

Methods of sampling, preservation of samples

No.	Parameter	Methods of sampling	Methods of sample preservation
1	Surface water sample	TCVN 6663-1:2011 TCVN 5994:1995 TCVN 6663-6:2008	TCVN 6663-3:2016

Table 4

Method of analyzing water samples in a laboratory

No.	Parameter	Method of analyzing	Measuring range
1	Chemical oxygen demand (COD)	SMEWW 5220C:2012	3 mg/L
2	Biological oxygen demand (BOD ₅)	SMEWW 5210B:2012	1 mg/L
3	Total Suspended Solids (TSS)	SMEWW 2540D:2012	10 mg/L
4	Nitrate (NO ₃ ⁻ calculated by N)	SMEWW 4500-NO3-.E:2012	0.01 mg/L
5	Phosphate (PO ₄ ³⁻ calculated by P)	SMEWW 4500-P.E:2012	0.03 mg/L
6	Coliform	TCVN 6187-2:1996	3 MPN/100ml
7	Arsenic (As)	SMEWW 3114B:2012	0.0006 mg/L
8	Lead (Pb)	TCVN 6665:2011	0.004 mg/L
9	Mercury (Hg)	SMEWW 3112B:2012	0.0003 mg/L
10	Ammonium (NH ₄ ⁺ calculated by N)	SMEWW 4500 -NH3.B&F:2012	0.03 mg/L
11	Benzene hexachloride	US.EPA Method 3510C + US.EPA Method 3630C US.EPA Method 8081B	0.005 µg/L
12	Dieldrin	US.EPA Method 3510C + US.EPA Method 3630C US.EPA Method 8081B	0.005 µg/L

Machines and equipment used to analyze water samples include a meter to measure temperature, DO, pH - PCD 650/ pH 600 Eutech; Satellite navigation device - GPS map 76CSX Garmin; Incubator-LI20-Shellab; Digester block-Merck TR420; Microbiology cabinet cabin- AC2-4E1 Esco; Drying cabinet-ED105 Binder; UV-vis-2700 Labomed; Atomic absorption spectrophotometric-AAS 400 Perkin Elmer; Digital analytical balance-PA224S Satorius brand. These machines and equipment are calibrated once a year.

Water Quality Assessment

The analytical results of water samples are compared with surface water quality parameters according to QCVN 08-MT:2015/BTNMT-National technical regulation on surface water quality of Vietnam (Vietnam Ministry of Natural Resources and Environment, 2015).

The Water Quality Index (WQI) is calculated based on the Decision 1460/QD-TCMT on promulgating technical guidelines for calculation and Vietnam water quality index (VN_WQI) (Vietnam Environment Administration, 2019). Parameters used to calculate WQI in this study include temperature, pH, DO, BOD₅, COD, N-NO₃⁻, N-NH₄⁺, P-PO₄³⁻, and Coliform.

For parameters of BOD₅, COD, N-NO₃⁻, N-NH₄⁺, P-PO₄³⁻, Coliform, and WQI are calculated according to Equations 1 and 2:

$$WQI_{SI} = \frac{q_i - q_{i+1}}{BP_{i+1} - BP_i} (BP_{i+1} - C_p) + q_{i+1} \quad [1]$$

In particular:

BP_i: lower limit concentration of monitoring parameters corresponding to level i;

BP_{i+1}: upper limit concentration of monitoring parameters corresponding to level i+1;

q_i: WQI at level i given corresponds to BP_i;

q_{i+1}: WQI at level i+1 corresponds to BP_{i+1};

C_p: Monitoring parameters are taken into account.

Calculating WQI_{DO}:

$$WQI_{SI} = \frac{q_{i+1} - q_i}{BP_{i+1} - BP_i} (C_p - BP_i) + q_i \quad [2]$$

In particular:

C_p: Saturated DO%;

BP_i, BP_{i+1}, q_i, q_{i+1} are the values corresponding to the level i, i+1

Calculating WQI_{pH}:

If pH < 5.5 or pH > 9, WQI_{pH} = 10.

If 5.5 < pH < 6, using formula [2] to calculate WQI_{pH}

If 6 ≤ pH ≤ 8.5, WQI_{pH} = 100.

If 8.5 < pH < 9, using formula [1] to calculate WQI_{pH}

After calculating WQI for each of the above parameters, the WQI calculation is applied according to Equation 3:

$$WQI = \frac{WQI_I}{100} \left(\frac{\prod_{i=1}^n WQI_{II}}{100} \right)^{\frac{1}{n}} \left(\frac{\prod_{i=1}^m WQI_{III}}{100} \right)^{\frac{1}{m}} \left[\frac{1}{k} (\sum_{i=1}^k WQI_{IV})^2 \frac{1}{l} (\sum_{i=1}^l WQI_V) \right]^{\frac{1}{3}} \quad [3]$$

In particular:

WQ_I: Calculation results for pH

WQ_{II}: Calculation results for the group of pesticides parameters

WQ_{III}: Calculation results for the group of heavy metal parameters

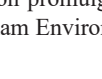
WQ_{IV}: Calculation results for the group of organic and nutritional parameters

WQ_V: Calculation results for microbiological parameters

Table 5 displays the water quality rating based on the water quality index range and recommendation of surface water usage.

Table 5

Water Quality Rating and recommendation of usage according to Vietnam Environment Administration

Water quality Index Range	Water Quality Rating	Color	Intended use
91-100	Excellent		Good for water supply
76-90	Good		For water supply but needs appropriate treatment measures
51-75	Medium		For irrigation and other similar purposes
26-50	Poor		For water transport and other similar purposes
10-25	Polluted		Water is heavily polluted, needs future treatment
<10	Serious polluted		Water is poisoned, needs treatment

Note. From “Decision 1460/QĐ-TCMT on promulgating technical guidelines for calculation and Vietnam water quality index (VN_WQI)” by Vietnam Environment Administration, 2019

RESULTS AND DISCUSSION

Table 6 displays the analytical results of surface water affected by urban areas. Table 7 displays the analytical results of surface water affected by industrial parks and industrial clusters. The water temperature at the sampling locations ranges from 29.5 to 32.1°C in the area affected by domestic wastewater and ranges from 31.7 to 32.3°C in the area affected by industrial wastewater. Since the study area is completely within the An Giang province and the air temperature in the area is relatively uniform, the water temperature between the sampling locations in the study areas does not have a significant difference. However, the temperature varies between 25°C to 35°C, where most metabolic activities within a living organism occur with maximum ease and efficiency (Asthana, 2006). Therefore, the water temperature in sampling locations generally does not affect the area’s aquatic life, consistent with Lien et al. (2016). While the average temperature in An Giang from 2016 to July 2020 is about 28°C (An Giang Department of Natural Resources and Environment, 2020), the water temperature in sampling locations is slightly higher than the area’s average temperature. Since the time of sampling is in the dry season, the water

temperature was higher than that in the rainy season. Higher temperature will increase the rate of degradation of organic materials (BOD) and decrease the solubility of oxygen in water resulting in a lower stream DO than would exist under the same condition but at a lower oxygen temperature (CH2M Hill, 1979).

The pH of surface water affected by urban areas ranges from 7.22 to 7.63, and the pH of surface water affected by industrial parks and clusters ranges from 7.12 to 7.26. According to the National Technical Regulation on Surface Water Quality of Vietnam, column A1 (6–8.5), these values are all within the allowable limits. This result is consistent with Wilbers et al. (2014) and Lien et al. (2016).

Dissolved oxygen (DO) at the sampling locations affected by urban areas ranges from 2.81 to 6.05 mg/L. According to the national technical regulation on surface water quality of Vietnam, only the DO in the locations of Tan Chau residential area, Tan Chau town (6.05 mg/L) is still within the allowable limit (≥ 6 mg/L); the remaining locations are lower than the allowable value from 1.07 to 2.81 times. DO at sampling locations affected by industrial zones and clusters ranges from 4.95 to 5.98 mg/L, lower than the allowable limit from 0.83 to 0.99 times. This result is consistent with Lien et al. (2016) and Tam et al. (2021) that the value of DO was low. The average value of DO in this study is higher than that in the study of Lien et al. (2016) but lower than that in the study of Tam et al. (2021).

Total Suspended Solids (TSS) of surface water at five locations affected by domestic wastewater range from 45.00 to 59.00 mg/L are 2.25 to 2.95 times higher than the allowable limits in National technical regulation on surface water quality of Vietnam (20 mg/L). TSS at two locations affected by industrial wastewater has values ranging from 47.67 to 52.00 mg/L, which are 2.38 to 2.60 times higher than the allowable limits. This result is consistent with the previous of Tam et al. (2021). However, the average value of TSS in this study is many times lower than that in the study of Dieu et al. (2016). In addition, this study was conducted for the dry season, making the result of TSS lower than results in the rainy season or the whole year.

The Chemical Oxygen Demand (COD) at five sampling locations in urban areas values from 18.67 to 91 mg/L; these values exceed 1.87 to 9.10 times compared to the limits in National Technical Regulations (10 mg/L). The COD at sampling locations in industrial parks and clusters ranges from 20 to 27 mg/L, exceeding the permissible limits from 2.00 to 2.70 times. The COD in this study is much higher than data in the previous studies by Lien et al. (2016) and Dieu et al. (2016). However, this result is consistent with Tam et al. (2021). This comparison shows that the organic pollution of the surface water of the Mekong River has increased over time due to socio-economic development.

Biological Oxygen Demand (BOD₅) of surface water affected by urban areas ranges from 12.67 to 63.00 mg/L, exceeding the allowable limit (4 mg/L) from 3.17 to 15.75 times, according to the National Technical Regulation on surface water quality of Vietnam.

On the other hand, BOD_5 of the surface water affected by the industrial parks has values ranging from 12.67 to 16.00 mg/L, exceeding the permissible limits from 3.17 to 4.00 times. These values are higher than the results in the study of Ut et al. (2016), Dieu et al. (2016), and Tam et al. (2021).

BOD and COD are the main parameters analyzed to indicate the degree of pollution in the river. BOD is the measurement of oxygen required to decompose organic matter biologically under aerobic conditions. In contrast, COD measures the total oxygen required to oxidize all biologically available and inert organic matter into carbon dioxide and water. BOD values thus are always smaller than COD values. Thus, BOD and COD are two widely used parameters for organic pollution measurements. BOD:COD ratio is a reliable and useful indicator of the river's organic matter content under tropical climate conditions (Aik & Hamid, 2015). Wastewater with high COD to BOD ratio indicates that a substantial part of organic matter will be difficult to degrade biologically (Von, 2015). Therefore, depending on the value of the COD/ BOD_5 ratio, conclusions can be drawn about the biodegradability of the wastewater and the treatment process to be employed (Mogens et al., 2008). In this study, the COD/ BOD_5 ratio obtained for the sampling locations affected by urban areas varies between 1.44 to 1.74. The sampling locations affected by industrial parks and clusters vary from 1.58 to 1.69. These ratios are considered low. That means the biodegradable fraction in the surface water is high, which is a good indication for biological treatment (Mogens et al., 2008; Von, 2015).

Nitrate (NO_3^-) at sampling locations ranges from 0.02 to 0.19 mg/L for areas affected by urban areas and 0.06 to 0.19 mg/L for industrial parks and clusters affected. According to the National Technical Regulation on surface water quality of Vietnam, these values are within the allowable limits (2 mg/L). These values are lower than the Tam et al. (2021) study results but consistent with the study of Dieu et al. (2016).

Ammonium (NH_4^+) at sampling locations affected by urban wastewater ranges from 0.90 to 2.78 mg/L. According to the National Technical Regulation on surface water quality of Vietnam, ammonium value at all locations exceeds permissible value (0.3 mg/L) from 3.00 to 9.27 times. Ammonium (NH_4^+ calculated by N) at sampling points affected by industrial parks and clusters ranges from 0.46 to 1.81 mg/L exceeding the allowable limits from 1.53 to 6.03 times. These values are higher than the Dieu et al. (2016) study results but consistent with the study of Tam et al. (2021).

Phosphate (PO_4^{3-}) at the sampling locations affected by urban areas ranges from 0.06 to 0.25 mg/L. Although the values of Phosphate at the sampling point of Tan Chau residential area, Tan Chau town, and Cai Dau residential area, Chau Phu district exceeds the permissible value (0.1 mg/L) according to the National Technical Regulation on surface water quality of Vietnam, the remaining sampling locations are still within the allowable limits. In the sampling points affected by industrial parks and industrial clusters, the

Phosphate ranges from 0.03 to 0.09 mg/L and is within the allowable limits. These values are lower than the results in the study of Dieu et al. (2016) and Tam et al. (2021) but are consistent with the result in the study of Lien et al. (2016).

Parameters of Coliform at sampling locations affected by domestic wastewater value from 2,967 to 215,333 MPN/100 mL that exceed the permissible limit from 1.19 to 86.13 times compared to the National Technical Regulations on surface water quality in Vietnam (2,500 MPN/100 mL). Parameters of Coliform at sampling points in industrial parks and clusters range from 4,800-3,667 MPN/100 mL, all values exceeding the allowable limits from 1.92 to 5.47 times. This result is higher than the value of Coliform in the study to assess the water quality of the Tien River and the Hau River in some residential areas conducted by Huong et al. (2006). The results show that Coliform in surface water affected by domestic wastewater is much higher than in surface water affected by industrial wastewater. Coliform organisms are frequently used as indicators of human pollution. In addition, total Coliform is often used as an indicator of waste effluent disinfection.

Analytical results of all surface water samples show that As, Pb, Hg, Benzene hexachloride, and Dieldrin are not detected in water samples. These results are similar to Phat et al. (2016), which do not detect As in the Tien River. However, these results are different from Dieu et al. (2016), in which concentrations of toxic dissolved metals including As, Pb, and Hg in surface water of the mainstream and tributaries of the Hau River were low.

Therefore, most of the water samples exceed the allowable limits of TSS, DO, BOD₅, COD, NH₄⁺, and Coliform according to the National Technical Regulation on the surface water quality of Vietnam. Temperature, pH, NO₃⁻, PO₄³⁻ are mostly at suitable levels and within allowable limits. As, Pb, Hg, Benzene hexachloride, and Dieldrin are not detected at all sampling points. This result shows that the surface water of the Mekong River in An Giang is contaminated by organic matters, suspended solids, and coliforms, which is consistent with the findings of Nguyen et al. (2021) and Lien et al. (2016).

For surface water sources affected by domestic wastewater, the main cause of water pollution is that most of the domestic wastewater discharged into the river is untreated. Many wastewater and solid waste from trading, production, and business activities in markets, residential areas, and densely populated urban centers along the Tien River and the Hau River are discharged into water sources. The surface water affected by the Cai Dau urban area is the most polluted location with the highest values of parameters. This location is the primary canal connected to the mainstream with a narrow surface, no strong flow, low dispersion capacity, and low self-cleaning. Therefore, a high concentration of pollutants dispersed into the environment causes local pollution. For surface water sources affected by industrial wastewater, the main reason for pollution is that the wastewater has not been thoroughly treated and has not met the standards for discharge into water

sources. The development of residential areas and industrial parks and clusters has caused a deterioration of the surface water quality of the Mekong River in An Giang province. The finding is consistent with the results of Nhan and Nhan (2014), Chea et al. (2016), and Tam et al. (2021).

Table 6
Analytical results of surface water affected by urban area

Parameters	Location									
	UB1		UB2		UB3		UB4		UB5	
	Mean	SD	Mean	SD	Mean	SD	Mean	SD	Mean	SD
Temperature (°C)	30.7		29.5		30.3		32.1		30.2	
pH	7.63		7.40		7.41		7.46		7.22	
DO (mg/L)	6.05	0.07	4.98	0.10	5.15	0.09	5.59	0.14	2.81	0.12
TSS (mg/L)	54.33	2.08	51.00	2.65	45.00	2.00	48.67	2.08	59.00	4.36
COD (mg/L)	29.67	4.04	23.67	2.52	25.00	1.00	18.67	2.08	91.00	3.00
BOD ₅ (mg/L)	19.00	2.65	13.67	2.08	14.33	1.16	12.67	1.53	63.00	2.65
Nitrate (mg/L)	0.10	0.01	0.13	0.00	0.19	0.01	0.07	0.00	0.02	0.01
Phosphate (mg/L)	0.17	0.02	0.06	0.01	0.06	0.01	0.07	0.01	0.25	0.02
Ammonium (mg/L)	1.09	0.06	0.90	0.05	0.90	0.05	0.95	0.04	2.78	0.10
Coliform MPN/100 mL	17,000	3,464	30,000	13,892	11,633	8,445	2,967	1,155	215,333	211,888
As (mg/L)	ND	ND	ND	ND	ND	ND	ND	ND	ND	ND
Pb (mg/L)	ND	ND	ND	ND	ND	ND	ND	ND	ND	ND
Hg (mg/L)	ND	ND	ND	ND	ND	ND	ND	ND	ND	ND
Benzene hexachloride (µg/L)	ND	ND	ND	ND	ND	ND	ND	ND	ND	ND
Dieldrin (µg/L))	ND	ND	ND	ND	ND	ND	ND	ND	ND	ND

Note. ND = Not detected

Table 7

Analytical results of surface water affected by industrial parks and industrial clusters

Parameters	Location				Column A1-Regulation
	ID1		ID2		
	Mean	SD	Mean	SD	
Temperature (°C)	31.7		32.3		
pH	7.12		7.26		6-8.5
DO (mg/L)	5.98	0.06	4.95	0.03	≥6
TSS (mg/L)	47.67	1.53	52.00	2.65	20
COD (mg/L)	27.00	1.00	20.00	1.73	10
BOD ₅ (mg/L)	16.00	1.73	12.67	0.58	4
Nitrate (mg/L)	0.19	0.00	0.06	0.00	2
Phosphate (mg/L)	0.09	0.01	0.03	0.00	0.1
Ammonium (mg/L)	1.81	0.09	0.46	0.04	0.3
Coliform (MPN/100 mL)	13,667	6,429	4,800	2,606	2,500
As (mg/L)	ND	ND	ND	ND	0.01
Pb (mg/L)	ND	ND	ND	ND	0.02
Hg (mg/L)	ND	ND	ND	ND	0.001
Benzene hexachloride (µg/L)	ND	ND	ND	ND	0.02
Dieldrin (µg/L)	ND	ND	ND	ND	0.1

Note. ND = Not detected

The level of water pollution due to the impact of urban areas, industrial parks, and industrial clusters calculated by the WQI index is shown in Figure 2.

WQI of location affected by urban areas and industrial parks, industrial clusters range from poor level (able to be used for water transport and other similar purposes) to good level - (able to use for water supply but needs appropriate treatment measures).

Long Xuyen city's urban area affects the two sampling points with the highest WQI, reaching a good water level (WQI = 79). The location affected by the My Quy industrial cluster in Long Xuyen city (WQI = 76) on the Hau River, water on this level can be used for domestic water supply purposes but needs appropriate treatment measures. Next, the locations affected by Tan Chau urban area, Tan Chau town (WQI = 35), Cho Moi urban area, Cho Moi district (WQI = 36), My Luong urban area, Cho Moi district (WQI = 36), on the Tien River and Binh Long industrial park, Chau Phu district on the Hau River (WQI = 36) are rated poor water level, water on this level can be used for water transport and other similar purposes. WQI is the lowest in the surface water area affected by Cai Dau

urban area, Chau Phu district on the Hau River (WQI = 26), which is poor. The causes of the poor water quality and low WQI ($26 \leq \text{WQI} \leq 50$) are the high value of Coliform in the water and the high value of other parameters participating in the calculation of WQI such as DO, COD, BOD₅, and Ammonium that exceeds the allowable limits. The values of WQI in the sampling locations are higher than the values in the study of Nguyen and Huynh (2020). Most sampling locations have the value of WQI ranked at a poor level, consistent with the study findings of Giao et al. (2021).

Based on the results of this study, it is recommended that people should not directly use water of the Tien River and Hau River in An Giang for drinking and domestic purposes to ensure their health in the long term. Appropriate water treatment measures are necessary if people want to use this water source for drinking and domestic purposes. In the coming time, authorities need to monitor and take measures to treat wastewater in markets, commercial centers, and urban areas to ensure the wastewater quality before discharging into the river based on regulations on discharge. In addition, authorities need to monitor the surface water quality affected by waste sources in industrial zones and clusters to take the most appropriate and strict management measures and promptly warn people about using water for domestic purposes.

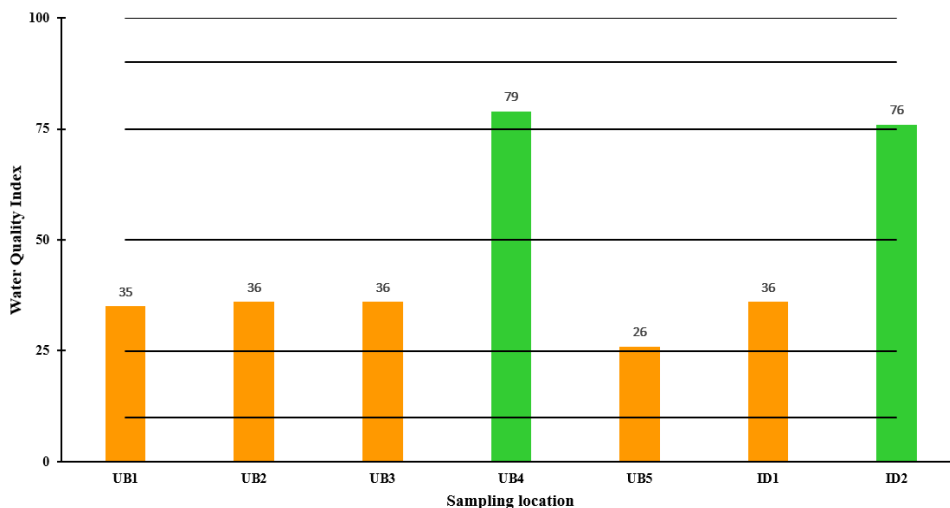


Figure 2. Water Quality Index of sampling location

CONCLUSION

Domestic and industrial wastewater have polluted the surface water of the Tien River and the Hau River, two important rivers of the lower Mekong flowing through An Giang province. The pollution shows in parameters of TSS, DO, BOD₅, COD, N-NH₄⁺, and Coliform that

exceeds allowable limits. Other parameters of temperature, pH, N-NO_3^- , PO_4^{3-} are mostly at suitable levels and within the allowable limits compared with the National Technical Regulation on surface water quality of Vietnam. As, Pb, Hg, Benzene hexachloride, and Dieldrin are not detected at all sampling points. In general, most sampling locations have the water quality index at a poor level, can be used for water transport, requires appropriate treatment before being used for domestic purposes, and have appropriate water quality management measures in place. Sampling location in the urban area of Long Xuyen city has the highest water quality (highest WQI) at a good level. Cai Dau urban area, Chau Phu district, has the lowest water quality (lowest WQI) at the poor level. In the coming time, authorities need to monitor and take appropriate measures to treat and manage wastewater from urban areas and industrial parks/clusters.

ACKNOWLEDGEMENT

This research is funded by Vietnam National University Ho Chi Minh City (VNU-HCM) under grant number “B2021-16-03.”

REFERENCES

- Aik, H. L., & Hamid, N. (2015). BOD:COD ratio as an indicator for river pollution. *International Proceedings of Chemical, Biological and Environmental Engineering*, 88(15), 89-94. <https://doi.org/10.7763/IPCBE.2015.V88.15>
- An Giang Center for Environmental Monitoring and Techniques, Resources. (2019). *Report on results of environmental monitoring in An Giang province November, 2019*. People’s Committee of An Giang province. https://media.angiang.gov.vn/pictures/2021/01/31/58_dinh%20kem_cong%20bo%20hien%20trang%20moi%20truong%20ag%202016-2020.pdf
- An Giang Department of Natural Resources and Environment. (2020). *Report on environmental status of An Giang province in the period 2016-2020*. People’s Committee of An Giang province. https://media.angiang.gov.vn/quan%20trac%20moi%20truong/2019/12/BC%20Ket%20qua%20quan%20trac%20dot%20T11_2019.pdf
- Asthana, D. K. (2006). *Text book of environmental studies* (pp. 158-159). S. Chand Publishing.
- CH2M Hill. (1979). *Rock creek watershed conservation study* (pp. 8-2). The Region.
- Chea, R., Grenouillet, G., & Lek, S. (2016). Evidence of water quality degradation in lower Mekong basin revealed by self-organizing map. *Plos One*, 11(1), Article e0145527. <https://doi.org/10.1371/journal.pone.0145527>
- Dieu, H. T. Q., Phong, N. H., & Hop, N. V. (2016). Study on the Tien River water quality assessment. *Vietnam Journal of Analytical Sciences Society*, 21(1), 38-48.
- Giao, N. T., Nhien, H. T. H., Anh, P. K., & Ni, D. V. (2021). Classification of water quality in low-lying area in Vietnamese Mekong delta using set pair analysis method and Vietnamese water quality index. *Environmental Monitoring and Assessment*, 193, Article 319. <https://doi.org/10.1007/s10661-021-09102-1>

- Huong, T. T., Ngoc, T. B., & Thanh, N. T. B. (2006). Assessment of water quality of the Tien River and the Hau River in some residential areas in Dong Thap, Vinh Long and Can Tho province in 2006. *Ho Chi Minh City Journal of Medicine*, 12(4), 185-191.
- Khanh, N., Kitaya, Y., Liya X., Endo, R., & Shibuya, T. (2015). Microalgae culture with digestate from methane fermentation - Effects of pH and concentrations of digestate on growth of *Euglena gracilis*. *Eco-Engineering*, 27(1), 7-11. <https://doi.org/10.11450/seitaikogaku.27.7>
- Khanh, N., Kitaya, Y., Xiao, L., Endo, R., & Shibuya, T. (2013). Selection of microalgae suitable for culturing with digestate from methane fermentation. *Environmental Technology*, 34(13-14), 2039-2045. <https://doi.org/10.1080/09593330.2013.828093>
- Lien, N. T. K., Ut, V. N., Phu, T. Q., Oanh, D. T. H., & Huy, L. Q. (2016). Water quality in mainstream and tributaries of the Hau River. *Can Tho University Journal of Science*, 43, 68-79. <https://doi.org/10.22144/ctu.jvn.2016.138>
- Mogens, H., Mark, C. M. V. L., Ekama, G. A., & Damir, B. (2008). *Biological wastewater treatment: Principles, modelling and design* (pp. 40-41). IWA Publishing. <https://doi.org/10.2166/9781780401867>
- Nam, C. P., Hiep, T. V., Vien, D. V., & Duong, V. H. T. (2009). Study on pollution assessment and eutrophication of surface water in some canals connecting the Tien River and the Hau River in Vinh Long, Dong Thap and Tien Giang province. *Vietnam Journal of Hydrometeorology*, 581, 29-35. <http://tapchikttv.vn/article/488>
- Nguyen, G. T., & Huynh, T. H. N. (2020). Evaluating water quality variation in the Vietnamese Mekong Delta area using cluster and discriminant analysis. *Applied Environmental Research*, 43(1), 14-27. <https://doi.org/10.35762/AER.2021.43.1.2>
- Nguyen, G. T., Huynh, T. H. N., & Truong, H. D. (2021). Characteristics of surface water quality and diversity of Zoo benthos in water bodies, An Giang Province, Vietnam. *Applied Environmental Research*, 43(2), 60-76. <https://doi.org/10.35762/AER.2021.43.2.5>
- Nhan, T. T., & Nhan, D. K. (2014). Correlation between surface water quality and socio-economic in Can Tho and Soc Trang. *Can Tho University Journal of Science*, 2014(3), 92-100.
- Phat, P. H., Nam, N. Đ. G., Toan, P. V., Tri, V. P. Đ., & Truc, D. T. (2019). Surface water quality of the Tien River flowing through Tan Chau area, An Giang province. *Can Tho University Journal of Science*, 55, 53-60. <https://doi.org/10.22144/ctu.jsi.2019.131>
- Shipin O., Koottatep T., Khanh, N. T. T., & Polprasert, C. (2005). Integrated natural systems for developing communities: Low-tech N-removal through fluctuating microbial pathways. *Water Science and Technology*, 51(12), 299-306. <https://doi.org/10.2166/wst.2005.0488>
- Tam, N. T., Bao, T. Q., Minh, H. V. T., Thanh, N. T., Lien, B. T. B., & Tuyet, N. D. (2021). Evaluating the surface water quality affected by activities in Can Tho City. *Vietnam Journal of Hydrometeorology*, 2022(733), 39-55. [http://doi.org/10.36335/VNJHM.2022\(733\).39-55](http://doi.org/10.36335/VNJHM.2022(733).39-55)
- Ut, V. N., Phu, T. Q., Lien, N. T. K., Oanh, D. T. H., & Huy, L. Q. (2016). Water quality in mainstream and tributaries of the Hau River. *Can Tho University Journal of Science*, 43, 68-79. <https://doi.org/10.22144/ctu.jvn.2016.138>
- Van, N. P., Khanh, N. T. T., Loc, T. T., Dong, N. T., Khuong, N. Q., Mai, V. T., & Hai, T. N. (2020). Dual-electronic nanomaterial (synthetic clay) for effective removal of toxic cationic and oxyanionic metal ions from water. *Journal of Nanomaterials*, 2020, Article 1783749. <https://doi.org/10.1155/2020/1783749>

- Vietnam Environment Administration. (2019). *Decision No.1460/QĐ-TCMT on promulgating technical guidelines for calculation and publication of Vietnam water quality index (VN_WQI)*. http://www.quantracmoitruong.gov.vn/storage/news_file_attach/QD%201460%20TCMT%20ngay%2012.11.2019%20WQI.pdf
- Vietnam Ministry of Natural Resources and Environment. (2015). *QCVN 08-MT:2015/BTNMT-National technical regulation on surface water quality of Vietnam*. <http://cem.gov.vn/storage/documents/5d6f3ecb26484qcvn-08-mt2015btnmt.pdf>
- Vietnam Ministry of Natural Resources and Environment. (2017). *Circular 24/2017/TT-BTNMT on promulgating technical regulations on environmental monitoring and Vietnamese standards and regulations*. http://vanban.chinhphu.vn/portal/page/portal/chinhphu/hethongvanban?class_id=1&mode=detail&document_id=191603&category_id=0
- Vietnam Ministry of Science and Technology. (1995). *TCVN 5994:1995-Vietnam National standard on water quality-sampling-guidance on sampling from natural lakes and man-made lakes*. <https://tieuchuan.vsqi.gov.vn/tieuchuan/view?sohieu=TCVN+5994%3A1995>
- Vietnam Ministry of Science and Technology. (1996). *TCVN 6187-2:1996 - Vietnam National standard on water quality-detection and enumeration of organisms thermotolerant coliform organisms and presumptive Escherichia coli. Part 2: Multiple tube (most probable number) method*. <https://tieuchuan.vsqi.gov.vn/tieuchuan/view?sohieu=TCVN%206187-2:2020>
- Vietnam Ministry of Science and Technology. (2008). *TCVN 6663-6:2008-Vietnam National standard on water quality-sampling-part 6: Guidance on sampling of rivers and streams*. <https://tieuchuan.vsqi.gov.vn/tieuchuan/view?sohieu=TCVN+6663-6%3A2008>
- Vietnam Ministry of Science and Technology. (2011a). *TCVN 6492:2011-Vietnam National standard on water quality-water quality-determination of pH*. <https://tieuchuan.vsqi.gov.vn/tieuchuan/view?sohieu=TCVN+6492%3A2011>
- Vietnam Ministry of Science and Technology. (2011b). *TCVN 6663-1:2011-Vietnam National standard on water quality-sampling-part 1: Guidance on the design of sampling programmes and sampling techniques*. <https://tieuchuan.vsqi.gov.vn/tieuchuan/view?sohieu=TCVN%206663-1:2011>
- Vietnam Ministry of Science and Technology. (2011c). *TCVN 6665:2011-Vietnam National standard on water quality-determination of selected elements by inductively coupled plasma optical emission spectrometry (ICP-OES)*. <https://tieuchuan.vsqi.gov.vn/tieuchuan/view?sohieu=TCVN+6665%3A2011>
- Vietnam Ministry of Science and Technology. (2016). *TCVN 7325:2016-Vietnam National standard on water quality-determination of dissolved oxygen-Electrochemical probe method*. <https://tieuchuan.vsqi.gov.vn/tieuchuan/view?sohieu=TCVN+7325%3A2016>
- Von, S. M. (2015). *Wastewater characteristics, treatment and disposal* (pp. 40-41). IWA Publishing. <https://doi.org/10.2166/9781780402086>
- Wilbers, G. J., Becker, M., Sebesvari, Z., & Renaud, F. G. (2014). Spatial and temporal variability of surface water pollution in the Mekong Delta, Vietnam. *Science of the Total Environment*, 485, 653-665. <https://doi.org/10.1016/j.scitotenv.2014.03.049>



The Effectiveness of Workplace Health Promotion Programme in Improving Sickness Absenteeism, Medical Cost Claims and Work Engagement Among Manufacturing Workers in Malaysia: A Randomised Control Trial

Ahmad Fairuz Mohamed^{1*}, Marzuki Isahak², Mohd Zaki Awg Isa³ and Rusli Nordin⁴

¹School of Graduate Studies, Management and Science University, 40100 MSU, Shah Alam, Selangor, Malaysia

²Department of Social and Preventive Medicine, Faculty of Medicine, University of Malaya, 50603 UM, Kuala Lumpur, Malaysia

³MSU Centre of Excellence for Vision and Eyecare (MSU-iCARE), Management and Science University, 40100 MSU, Shah Alam, Selangor, Malaysia

⁴Bioscience and Nursing, Faculty of Medicine, MAHSA University, 42610 Jenjarom, Selangor, Malaysia

ABSTRACT

Job-related stress at the workplace has a tremendous effect on employees' work performance. This study aims to evaluate the effectiveness of the Workplace Health Promotion (WHP) programme on employee sickness absenteeism, medical cost claims and work engagement among blue-collar manufacturing workers in Malaysia. The WHP intervention comprised organisational and individual stress management programmes delivered through the Occupational Stress Management Course and Employee Assistance Programme. Data on sickness absenteeism and medical cost claims were gathered from the records of the Human Resource Department. In addition, work engagement data were collected through the Malay Validated Utrecht Work Engagement Scale (UWES). Eighty-eight employees

participated in the study. Most employees worked 45 hours a week, with more than 80% working overtime and shifts. Pre-intervention sickness absenteeism among manufacturing workers varied from 0.98 to 2.57 days. At baseline, medical cost claims ranged from RM92 to RM196 for three months and RM127 to RM359 for six months. After six months of participation in the WHP programme, sickness absenteeism was significantly reduced ($d = 0.414$) and

ARTICLE INFO

Article history:

Received: 10 September 2021

Accepted: 25 January 2022

Published: 25 May 2022

DOI: <https://doi.org/10.47836/pjst.30.3.27>

E-mail addresses:

drfairuz.edu@gmail.com; fairuz@cyberjaya.edu.my

(Ahmad Fairuz Mohamed)

drmarzuki@ummc.edu.my (Marzuki Isahak)

m_zaki@msu.edu.my (Mohd Zaki Awg Isa)

rusli@mahsa.edu.my (Rusli Nordin)

*Corresponding author

work engagement was significantly enhanced ($d = 1.958$) in the intervention group. Medical cost claims, on the other hand, increased significantly post-intervention ($d = 0.039$). These findings are intended to help organisations and government bodies in recognising the potential of WHP to enhance employee work engagement and reduce sickness absenteeism to improve work organisation and personal development.

Keywords: Employee assistance programme, medical cost claims, sickness absenteeism, work engagement, workplace health promotion programme

INTRODUCTION

Work-related stress is the harmful physical and emotional reactions that arise when work requirements do not match workers' skills, resources and needs, affecting individual work performance and health outcomes (NIOSH, 1998). Today, work-related stress is increasing and has adversely impacted the organisation. The high level of stress among workers will result in low productivity, a higher incidence rate of occupational injuries, increased absenteeism, job insecurity, lower job satisfaction, lower productivity, and greater intention to leave. Moreover, work stress can lead to other problems such as alcoholism, drug abuse, domestic violence, hypertension, and cardiovascular diseases (Ajayi, 2018).

Malaysia is a newly industrialised country that relies on manufacturing as one of the main economic revenues. Industrial workplaces are associated with working conditions that have harmful effects, heavy lifting, and repetitive work that can be sources of stress for workers. The Department of Occupational Safety and Health (DOSH) recently published a report on Occupational Accident Statistics by States in Malaysia, revealing that 6933 work-related accidents occurred between January and December 2020, resulting in permanent and non-permanent disabilities at the construction sites (DOSH, 2020).

While the effects of stress on individuals are gaining much attention, the effects on employers and organisations are equally important. Therefore, in this study, it was interesting to investigate the consequences of occupational stress on the organisational level related to sickness absenteeism, medical cost claims and work engagement. Indeed, it has been estimated that stress-related illness results in the loss of at least 9.9 million working days in the United Kingdom between 2014 and 2015 (ILO, 2016). In Europe, the estimated cost of depression related to work stress for the year 2012 was 617 billion, which includes the cost of absenteeism and presenteeism (271 billion), loss of productivity (242 billion), and healthcare (63 billion) and social welfare (39 billion). While in Malaysia, Chee (2003) reported that 42.9% of employees took 1–7 days of sick leave in the past year. The common causes of employee absenteeism were related to the musculoskeletal system (31.4%), gastrointestinal system (25.8%), hypertension (24.4%), respiratory system (18.1%) and minor ailments (19.3%) (Manjunatha et al., 2011).

Meanwhile, the financial costs for employers may be equally significant as occupational stress leads to increased sick pay, increased healthcare costs and disability payments, higher compensation costs as well as costs of equipment damage (Vokić & Bogdanić, 2007). The United States spent almost 2.79 trillion dollars on healthcare costs in 2012. The employers reported nearly 4 million non-fatal workplace injuries and illnesses, and 55,000 deaths from work-related injuries and illnesses, annually (CDC, 2015). Malaysia's total health expenditures between 1997 and 2012 increased from RM 8,286 million to RM 42,256 million (Ministry of Health, 2014). De Beer et al. (2013) reported that employees in the high burnout group had significantly more GP visits, higher GP insured benefits expenditure, higher total insured benefits expenditure, and more medical claims than low burnout participants.

Furthermore, work engagement plays an important part in the organisation that contributes to job performance. It is an indicator of positive psychology characterised by vigour, dedication and absorption, influencing worker health (Schaufeli, 2012). Therefore, stress affecting one employee increases the work demands and workloads on colleagues, thereby affecting their morale and job satisfaction leading to poor internal communications, diminished cooperation, more internal conflicts, and a dysfunctional workplace climate, which in turn lead to productivity losses, poor services and damaging the corporate image and reputation (Beheshtifar & Nazarian, 2013).

In recent years, intervention studies for work-related stress have mainly focused on individual intervention and individual psychological outcomes (Edimansyah et al., 2008; Jesus et al., 2014; McConachie et al., 2014). However, there are limited RCTs that documented the effectiveness of the WHP programme on the organisational outcomes in the manufacturing industry in Malaysia. Therefore, this study aims to determine the effectiveness of the WHP intervention programme in reducing the rate of sickness absenteeism and medical cost claims and improving work engagement levels among blue-collar manufacturing workers in Malaysia. In this study, a comprehensive WHP programme was developed, consisting of both individual and organisational interventions. In addition, the effectiveness of the intervention programme was further evaluated between the intervention and control groups.

The study's findings can provide evidence of the effectiveness of the workplace stress management programme implementation, which will initiate further necessary measures by employers and policymakers to develop strategies that contribute to a healthy working environment and reduce the burden of medical cost claims.

METHODS

Population, Sample Size and Participants

The population studied consisted of blue-collar workers involved in the production line of a Food and Beverage (F&B) manufacturing company located in Kuala Lumpur, Malaysia. The factory chosen for this study is part of Malaysia's large international chain of food and beverage manufacturing facilities. This factory was chosen because workers were exposed to machines daily in their production lines, and the factory had never implemented an employee assistance programme prior to this study. The white-collar (office) workers were not included in this study due to their work nature, which is different from those involved in the production line. The sample size was estimated using an unpaired t-test via PS Software Version 3.1.2 with a 95% confidence interval, $\alpha = 0.05$. The total sample size for this study was 88 ($n = 44/\text{group}$).

This study included participants aged 18 and 65, Malaysian citizens, who worked in the factory for at least one year and completed the informed consent. The exclusion criteria included individuals diagnosed with a psychiatric disorder and currently monitored by a psychiatrist, who have chronic diseases with major complications such as heart diseases and chronic kidney diseases, a known case of cancer, participated in the stress management programme within the last two years and currently on medications for any psychiatric illnesses.

Study Design

A parallel, randomised-controlled trial study design was conducted using a 1:1 allocation ratio. Purposive sampling was performed to select the study area and target population. Convenient sampling was then applied to select participants who met the inclusion criteria in this study. The intervention programme was based on individual practice and a participatory intervention model.

Recruitment, Randomisation and Blinding

Permission to conduct this study was obtained from the factory's management prior to the recruitment process. The recruitment process took two months by advertising on the notice board and through the factory supervisors. In addition, informed consent was obtained from all selected study subjects.

A simple randomisation technique was applied in this study. First, the name list of the study subjects was arranged in alphabetical order to ensure allocation concealment. Then, a list of random numbers was generated from the computer software that produced a random allocation sequence to ensure each participant had equal chances of being assigned to the intervention or control group. Based on the sample size calculation, each group consisted of 44 subjects.

Single blinding was applied to the outcome assessors, data collectors and participants. The health promotion team assessed outcome measures. The health promotion programme provider and the participants were aware of group allocations.

The intention-to-treat analysis was applied in this study; thus, all participants were included in all analyses regardless of their attendance or response to the intervention programmes.

Research Instruments

Data collection on sickness absenteeism and medical cost claims were obtained from the Human Resource records. Pre-intervention data include 3-month and 6-month records from the beginning of the study (baseline). Post-intervention data include 3-month and 6-month follow-ups following intervention implementation.

Malay Validated Utrecht Work Engagement Scale (UWES)

Work engagement is an important part of the organisation that contributes to job performance. Work engagement is an indicator of positive psychology and works well-being. The UWES was widely used in international studies, with translations available in various languages, including Italian, Norwegian, Japanese, and Spanish (Shimazu et al., 2008; Balducci et al., 2010; Nerstad et al., 2010). The robustness and relevance of the construct of work engagement have been demonstrated in different cultures. Previous research has suggested acceptable psychometric properties for the UWES-17 in terms of internal consistency and constructs validity (Schaufeli & Bakker, 2004; Van Doornen et al., 2009). Schaufeli and Bakker (2003) reported that the UWES has reliability ranging from .80 to .90.

The UWES-17 is composed of 17 items consisting of three domains, which are vigour (six items), dedication (five items), and absorption (six items). A previous study showed that UWES should be treated as a unidimensional construct in which the individual scores be interpreted in a summative manner giving a single global score (De Bruin et al., 2013). Therefore, this questionnaire uses a seven-point Likert scale where '0' indicates "Never," and '6' indicates always.

A psychometric study of the Japanese version of UWES (UWES-J) was conducted to examine the suitability of UWES-J using a total of 2334 samples. The analysis results did not change the three subscales: vigour, dedication, and absorption. Furthermore, the internal consistency was high with $\alpha = .92$, and test-retest reliability within a two-month range was 0.66 (Shimazu et al., 2008).

In Malaysia, the validation study was conducted among 205 salespersons above 18 years old in Kuala Lumpur. Prior to the study, the samples were tested using Measures of Sampling Adequacy Kaiser-Meyer-Olkin (KMO) to determine whether they fulfilled

the measurement sampling adequacy and the results obtained showed the KMO value was 0.608 ($p < 0.01$), indicating an acceptable and significant value. In addition, three items (i.e., items 4, 14 and 16) with poor factor loadings were eliminated as the meanings were deemed unsuitable for Malaysian culture upon direct translation. The final result of factor analysis was between 0.321 and 0.795. The reliability test was performed using the internal consistency method with Cronbach's alpha value of 0.514 (Sulaiman & Zahoni, 2016). Furthermore, concurrent validation was also conducted in this study to assess job performance using the Contextual and Task Performance Scale (Goodman & Svyantek, 1999), job meaningfulness using the Meaningfulness Scale (May et al., 2004) and turnover intention using Turnover Intention Scale (Shore & Martin, 1989). The UWES and job performance showed a significant and positive relationship with $r = 0.541$, $p < 0.01$. In addition, a positive and significant relationship was observed between UWES and job meaningfulness with $r = 0.828$, $p < 0.01$. Meanwhile, a negative association was observed between UWES and turnover intention ($r = -0.657$, $p < 0.01$) (Sulaiman & Zahoni, 2016). These findings also contributed to the concurrent validity of the UWES questionnaire.

Therefore, this study adopted the Malay validated UWES by Sulaiman and Zahoni (2016). The mean difference of UWES between the pre-and post-intervention programmes was compared.

Intervention

The Workplace Health Promotion (WHP) intervention programme is comprised of a personalised and organisational stress management programme. The study period consisted of an intervention period of three months followed by a post-intervention period of three and six months. Four different modules were used in this study as part of the WHP programme since each module focused on a different aspect of job stress-related factors and interventions. The mental health promotion intervention programme was based on:

- i. Healthy Mental Health Module by the Ministry of Health, Malaysia (MOH, 2005) aims to provide awareness and knowledge on mental and early detection of mental health problems in society. In addition, this module allows users to conduct healthy mind screening, identify the signs of stress, depression, and anxiety, perform healthy mind interventions, and serve as referrals based on healthy mind screening scores.
- ii. Anxiety Management Technique Book (Wehrenberg, 2008) provides techniques to understand and manage the anxious brain, body, mind and behaviour.
- iii. Mindfulness for stress (Breathworks, 2017) provides a foundation in mindfulness, compassion, and meditation skills and teaches how to apply them in life.

- iv. Stress at work (NIOSH, 1998) provides knowledge to understand better the influence of 'work organisation' or 'psychosocial' factors on stress, illness and injury and identify ways to redesign jobs to create safer, healthier workplaces.

The following intervention components were offered in the intervention group (n = 44):

- i. Educational and behavioural group sessions (organisational-level intervention)
This part of the programme comprised the Occupational Stress Management Course (OSMC) consisted of five modules delivered in two sessions within two months. The course comprised of (a) psychological screening test, (b) discussion on occupational stress, (iii) personalised stress management therapy that included diaphragmatic breathing technique, mindfulness relaxation technique, anger control and healthy lifestyles, (iv) corporate occupational stress management that focused on organisational change and (v) corporate empowerment organisation that focused on SWOT analysis (strength, weakness, opportunity, and threats), problem-solving skills, interpersonal and communication skills.
- ii. Individual counselling session (individual-level intervention)
All participants in the intervention group received one counselling session via the Employee Assistance Programme (EAP) that discussed their physical and psychological health, management of stress at the workplace and daily application of personalised stress management therapy. There was also a daily practice on diaphragmatic breathing, progressive muscle relaxation, and the mindfulness technique.

The details of the OSMC course and modules are attached in Appendix. All programmes were delivered by the Occupational Safety and Health specialist (i.e., principal investigator) and supported by the health promotion team from the Ministry of Health Malaysia. Without further intervention, the control group participants received a general brochure on stress from the Promotion Unit, Ministry of Health. The response rate monitored the process evaluation during the assessment and intervention. This study followed the Consort flowchart for the randomised controlled trial study (Figure 1).

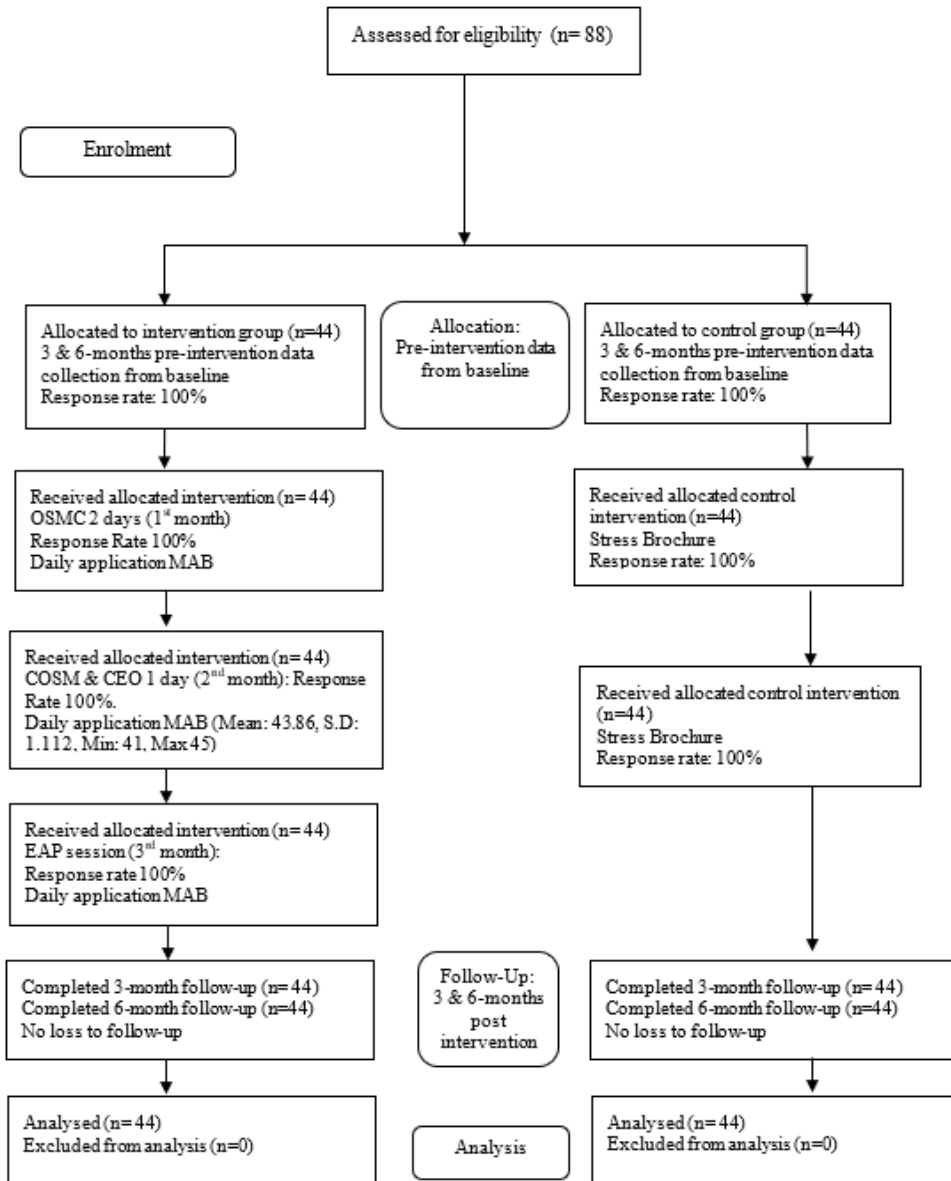


Figure 1. CONSORT Flow chart of the study

Note. OSMC: Occupational Stress Management Course; MAB: Managing Anxious Body; COSM: Corporate Occupational Stress Management; CEO: Corporate Empowerment Organisation; EAP: Employee Assistant Programme

Health Promotion Team

This study comprised a health promotion team led by the principal investigator, the Occupational Safety and Health specialist, and the health promotion team. The principal investigator trained the team. The team was responsible for the overall planning, implementation, follow-up, and study evaluation. This study received support from the Occupational Safety and Health team of the factory to monitor all planned activities.

Ethical Approval

The Medical Ethics Committee, University Malaya Medical Centre (MECID NO: 201512-1975) reviewed and approved this study protocol. This study was also registered with the National Medical Research Register (NMRR ID: 16-504-30274).

Statistical Analysis

Data analysis was carried out using SPSS Version 20.0. Data were presented in mean \pm SD, frequency, and percentage (%). The intention-to-treat analysis was applied. Differences between the intervention and control groups were analysed using the Chi-Square test and Independent *T*-Test. The results include the mean difference between within-group (time effect) and between-group (group effect), 95% confidence interval, *p*-value, and Cohen's *d* effect size.

RESULTS

Socio-Demographic Characteristics

A total of 88 Malaysian manufacturing workers were recruited for this study. There was no follow-up loss in this study from the beginning until the post-intervention stage. The intention-to-treat analysis was applied in this study; thus, all participants were included in all analyses regardless of their attendance or response to the intervention programmes making the response rate 100%. Most employees were male, 88.6% in the intervention group and 79.5% in the control group. The mean age of the intervention group participants was 35.98 ± 9.31 , and the control group participants were 36.05 ± 8.09 . More than two-thirds of the employees had secondary education (SPM and lower); 81.8% were intervention group participants, and 77.3% were control group participants. More than 90% of the employees were Malay and Muslim. Most of the employees were married (75% in the intervention group and 88.6% in the control group). There was no significant difference between the intervention and control groups regarding their demographic characteristics (Table 1).

Table 1
Socio-demographic characteristics of the employees

Variables	Intervention Group		Control Group		<i>P</i> -Value
	Frequency (%)	Mean (SD)	Frequency (%)	Mean (SD)	
Gender:					
Male	39 (88.6)		35 (79.5)		0.244
Female	5 (11.4)		9 (20.5)		
Age (Years)		35.98 (9.31)		36.05 (8.09)	0.971
Education:					
SPM and lower	36 (81.8)		34 (77.3)		0.597
STPM and above	8 (18.2)		10 (22.7)		
Marital Status:					
Single, Divorce	11 (25.0)		5 (11.4)		0.097
Married	33 (75.0)		39 (88.6)		
Race:					
Malay	43 (97.7)		41 (93.2)		0.306
Non-Malay	1 (2.3)		3 (6.8)		
Religion:					
Islam	44 (100)		41 (93.2)		0.078
Non-Muslim	0 (0)		3 (6.8)		
Employment:					
Permanent	44 (100)		44 (100)		a
Contract	0 (0)		0 (0)		
Job Position:					
Operator	37 (84.1)		31 (70.5)		0.127
Supervisor	7 (15.9)		13 (29.5)		
Unit:					
Production	38 (86.4)		33 (75.0)		0.177
Warehouse, R&D, Engineering	6 (13.6)		11 (25.0)		
Working Duration (Months)		131.73 (85.55)		113.34 (80.20)	
Working hours per day (hours)		8.0 (0.43)		8.11 (0.43)	0.219
Working hours per week (days)		5.64 (0.39)		5.53 (0.42)	0.220
Working shift:					
Yes	38 (86.4)		34 (77.3)		0.269
No	6 (13.6)		10 (22.7)		

Table 1 (Continue)

Variables	Intervention Group		Control Group		P-Value
	Frequency (%)	Mean (SD)	Frequency (%)	Mean (SD)	
Overtime:					
Yes	41 (93.2)		36 (81.8)		0.107
No	3 (6.8)		8 (18.2)		
Monthly income (RM)		2603.61 (1018.51)		2584.86 (967.28)	0.930
Smoking status:					
Non-smoker	18 (47.4)		20 (52.6)		0.667
Smoker	26 (52.0)		24 (48.0)		
Alcohol Intake:					
Yes	1 (2.3)		1 (2.3)		1.000
No	43 (97.7)		43 (97.7)		
Daily sleep time (hours)		6.63 (1.12)		6.40 (1.50)	0.401
Exercise:					
Moderate intensity (150 mins/week)	13 (40.6)		19 (59.4)		0.184
Non-active exercise (less than 150 mins/week) & Not exercise	31 (55.4)		25 (44.6)		

a: No statistic was computed because it is a constant

Workplace Characteristics

All participants were permanent employees (100%), and most of them were operators (>70.5%) working in the production unit (>75%). Most of the participants have worked in this company for more than nine years. Regarding hours spent at work, the employees worked eight hours per day, 5.6 days a week, making approximately 45 hours per week. Most of the employees worked in shifts (86.4% in the intervention group and 77.3% in the control group), and more than 80% worked overtime. The average salary of the employees was between RM 2500 to RM 2600 per month. There was no significant difference between the intervention and control groups regarding their workplace characteristics (Table 1).

Sickness Absenteeism Pre- and Post-Intervention Programme

The mean scores of sickness absenteeism among intervention and control group participants in the pre-and post-intervention programme are presented in Table 2. No significant improvement was recorded in 3-month sickness absenteeism among the intervention group participants pre-and post-intervention programme, with 0.98 ± 1.36 and 1.11 ± 1.63 , respectively ($p = 0.613$). Similarly, no significant changes were found in the sickness absence between the 3-month pre-and post-intervention scores among the control participants, with 1.20 ± 1.36 and 1.30 ± 1.17 ($p = 0.647$). In contrast, the means of 6-month sickness absenteeism were significantly reduced in the intervention group participants, from 2.48 ± 2.85 pre-intervention to 1.50 ± 2.13 post-intervention ($p = 0.017$). No significant changes were observed in the control group. Overall, the mean of sickness absenteeism increased between the pre-intervention periods of 3-months and 6-months in both groups. Moreover, control group participants showed a higher sickness absence at 3-months and 6-months pre-intervention periods than the intervention group participants. However, the results were not significant ($p > 0.05$). The Cohen effect showed that the intervention programme had a small effect size for sickness absence at 3-months ($d = 0.031$) and 6-months ($d = 0.414$) post-intervention programme.

Medical Cost Claim Pre- and Post-Intervention Programme

Table 3 shows the mean scores of medical cost claims at 3-months and 6-months among intervention and control group participants pre-and post-intervention. Results showed that claims for medical care increased between 3-months and 6-months pre-intervention study periods in both groups. In the intervention group, the 3-months period of medical cost claims increased from 92.42 ± 135.58 pre-intervention to 185.93 ± 432.62 post-intervention. However, the increment was not significant ($p = 0.170$). Meanwhile, 6-months medical cost claims were significantly increased among the intervention group participants, from 127.16 ± 185.77 pre-intervention to 393.11 ± 829.42 post-intervention ($p = 0.039$).

Regarding medical cost claims among the control group participants, no significant difference was observed between the 3-months and 6-months pre-and post-intervention scores ($p > 0.05$). The intergroup mean difference and Cohen d values for medical cost claims among study participants showed small effect sizes at 3-months and 6-months post-intervention programmes with $d = 0.214$ and $d = 0.332$, respectively.

Table 2
The mean scores of sickness absenteeism among intervention and control group participants pre- and post-intervention implementation

Variables	Pre-Score mean (SD)	Post-Score mean (SD)	Mean Score Diff (95% CI)	Mean Score	t-statistic	P-value	Inter-group mean differences (95% CI)	d
Sickness Absence (3 months)								
Intervention	0.98 (1.36)	1.11 (1.63)	0.14 (-0.40, 0.68)	1.77	0.510	0.613	0.049	0.031
Control	1.20 (1.36)	1.30 (1.17)	0.091 (-0.31, 0.49)	1.31	0.461	0.647	(-0.09, 0.19)	
Sickness Absence (6 months)								
Intervention	2.48 (2.85)	1.50 (2.13)	-0.98 (-1.77, -0.18)	2.62	-2.475	0.017*	-1.03	0.414
Control	2.57 (2.50)	2.61 (1.79)	0.05 (-0.66, 0.75)	2.33	0.129	0.898	(-1.11, -0.93)	

*Results were statistically significant with $p \leq 0.05$
Data were homogenous between the study groups.

Table 3
The mean scores of medical cost claim among intervention and control group participants, pre- and post-intervention implementation

Variables	Pre-Score mean (SD)	Post-Score mean (SD)	Mean Score Diff (95% CI)	t-statistic	P-value	Inter-group mean differences (95% CI)	d
Medical Cost Claim (3 months)							
Intervention	92.42 (135.58)	185.93 (432.62)	-93.51 (-228.71, 41.68)	-1.395	0.170	-82.63 (-159.60, -5.67)	0.214
Control	196.65 (160.30)	185.77 (133.89)	-10.88 (-69.11, 47.35)	-0.377	0.708		
Medical Cost Claim (6 months)							
Intervention	127.16 (185.77)	393.11 (829.42)	-265.95 (-518.33, -13.57)	-2.125	0.039*	-241.48 (-403.31, -52.50)	0.332
Control	359.15 (220.28)	383.62 (277.91)	-24.47 (-115.02, 66.07)	-0.545	0.589		

*Results were statistically significant with $p \leq 0.05$
Data were homogenous between the study groups.

Bonferroni Post-hoc Test

The Bonferroni post-hoc test results for sickness absenteeism and medical cost claim among the study participants between the 3-month and 6-month intervention programme are presented in Table 4. A statistically significant effect of time on sickness absence among the intervention group participants, $F(3,129) = 5.668$, ($p = 0.003$). The adjustment for multiple comparison Bonferroni revealed that trial 4 was statistically significant with trials 1, 2, and 3 with decrement of mean difference, -0.59 ($p = 0.032$), -1.11 ($p = 0.007$) and -0.73 ($p = 0.007$). There was no statistically significant time effect on sickness absence among the control group participants, $F(3,129) = 0.104$ ($p = 0.927$).

The 3-month and 6-month intervention programmes had no significant effects on medical cost claims among the intervention group participants, $F(3,129) = 3.394$ ($p = 0.066$). However, trials 3 and 4 were statistically significant with a mean difference of -57.677 ($p = 0.017$) after adjustment for multiple comparison Bonferroni. There was no significant effect of time on medical cost claims among the control group participants, $F(3,129) = 0.260$, ($p = 0.790$).

Work Engagement Pre- and Post-Intervention Programme

Table 5 shows the mean UWES scores for work engagement among the study participants pre-and post-intervention. At the beginning of the study, work engagement among manufacturing workers was 58.16 ± 10.43 in the intervention group and 61.11 ± 13.93 in the control group. Following the Workplace Health Promotion Intervention Programme's implementation, the intervention group participants observed a significant improvement in work engagement, with a mean score of 68.91 ± 5.00 ($p < 0.001$). However, no significant improvement was observed in the control group, 61.18 ± 11.97 ($p = 0.896$). The overall effect of work engagement was large, with $d = 1.958$.

Table 4

Bonferroni post-hoc test for sickness absenteeism and medical cost claim among intervention and control group participants between 3-month and 6-month intervention programmes

Variables	Groups	Trials	Mean (95% CI)	F Statistics (df)	P-value
Sickness Absenteeism	Intervention	1	0.977 (0.565, 1.39)	5.668 (3,129)	0.003*
		2	1.5 (0.82, 2.18)		
		3	1.11 (0.62, 1.61)		
		4	0.39 (0.16, 0.62)		
	Control	1	0.977 (0.565, 1.39)	0.104 (3,129)	0.927
		2	1.5 (0.82, 2.18)		
		3	1.11 (0.62, 1.61)		
		4	0.39 (0.16, 0.62)		

Table 4 (Continue)

Variables	Groups	Trials	Mean (95% CI)	F Statistics (df)	P-value
Medical Cost Claim	Intervention	1	185.93 (54.41, 317.46)	3.394 (3,129)	0.066
		2	243.63 (42.56, 444.71)		
		3	92.42 (51.20, 133.64)		
		4	34.74 (10.94, 58.54)		
	Control	1	196.65 (147.91, 245.38)	0.260 (3,129)	0.790
		2	167.87 (95.92, 239.81)		
		3	185.77 (145.06, 226.47)		
		4	173.38 (130.16, 216.61)		

Trials = Variables of different study intervals (i.e., pre-intervention at 3-month, pre-intervention at 6-month, post-intervention at 3-month, post-intervention at 6-month)

*Results were statistically significant with $p \leq 0.05$

Repeated measures ANOVA

Table 5

The mean UWES scores of work engagement among intervention and control group participants, pre- and post-intervention implementation

Variables	Pre-Score mean (SD)	Post-Score mean (SD)	Mean Score Diff (95% CI)	Mean Score Diff SD	t-statistic	P-value	Inter-group mean differences (95% CI)	d
Work Engagement								
Intervention	58.16 (10.44)	68.91 (5.00)	10.75 (8.65, 12.85)	6.90	10.337	<0.001*	10.68 (9.63,11.73)	1.958
Control	61.11 (13.93)	61.18 (11.97)	0.07 (-0.98, 1.12)	3.45	0.131	0.896		

*Results were statistically significant with $p \leq 0.001$

Data were homogenous between the study groups

DISCUSSION

This study demonstrates the importance of employees' sickness absence rate, medical cost claims and work engagement as determinants of the organisational outcomes of job stress at the workplace. In this study, the magnitude of sickness absenteeism among the manufacturing workers' pre-intervention programme between three to six months was between 0.98 to 2.57 days. This finding is comparable to studies by Tadesse et al. (2015) and Zare et al. (2017), which reported that employees' means of sickness absenteeism were 2.16 days and 1.73 days, respectively. A report by RAND Europe revealed that the overall health-related absenteeism in Malaysia was 8.2 days/67 working days per employee per year, while presenteeism was 58.8 days (Whitmore et al., 2018). It is estimated that the average annual costs of absenteeism and presenteeism exceed the medical costs associated with diseases. In the United States, absenteeism resulted in a total loss of \$118 billion (Prater & Smith, 2011) and £8.4 billion in the United Kingdom (Wang et al., 2016). While in Malaysia, the cost of absenteeism and presenteeism in 2015 amounted to 4.5% of GDP with an average annual cost of RM2.7 million (Rasmussen et al., 2016).

The causes of sickness absenteeism are not always health or illness. Personal factors may also affect absenteeism. In the United States, the most common causes of employee absenteeism are illness (34%), followed by family issues (22%) and personal needs (18%) (Chenoweth, 2011). In addition, absenteeism is significantly associated with role overload, sleep quality, role limitation, responsibility, job dissatisfaction and job stress (Tadesse et al., 2015; Zare et al., 2017). Increased absenteeism is associated with the severity of depression, and according to a cohort study in Sweden, sickness absence is one of the predictors of suicidal behaviour (Ishtiak-Ahmed et al., 2013; Johnston et al., 2019).

According to the U.S. Bureau of Labor Statistics (2020), the highest rate of absence per industry includes healthcare (3.5%), the public sector (3.4%), education (3.3%), hospitality & food services (3.0%) and manufacturing (2.5%). Previous studies have shown an association between absenteeism and health-related risk factors (Suzuki et al., 2015; Brborovic et al., 2016). Workers in the manufacturing industry have reported high levels of job stress. The prevalence of depression among manufacturing workers ranged from 2.6% to 23.4% (Roche et al., 2016). Work-related stress is higher among blue-collar workers in the manufacturing sector than workers in other sectors because they are exposed to frequent and diverse stressors such as extreme noise, less lighting, stuffy atmosphere, high temperatures and mechanical/physical hazards (Mazerall, 2002).

In terms of socio-demographic factors of the studied population, most of the employees in this study belonged to the lower-income group, young age, lower education level and married. Previous studies have indicated that these demographic characteristics are common determinants of higher risk factors for absenteeism and presenteeism (Hansen & Andersen, 2008; Johns, 2009). Low income is associated with a high prevalence of absenteeism,

reduced work productivity and mental illnesses (Callan et al., 2015). Employees with a higher education level exhibit less absenteeism and are healthier mentally and physically than those with less education. Married employees with young children may also show a high degree of absenteeism due to emotional exhaustion and the burden of juggling work-life responsibilities compared to single employees (Greaves et al., 2017).

In addition, the employees in this study worked approximately 45.12 hours per week, with 81.8% to 93.2% of the employees working overtime. On average, Malaysian employees worked 44 hours per week. Despite the high number of hours spent at work in the Asian culture, there is a higher productivity loss of 66 days annually to absenteeism and presenteeism than in western countries, which worked 35 hours a week but lost only 30 days annually (Jack, 2017). A previous study reported that employees who worked more than 48 hours per week and worked overtime were more likely to experience sickness absenteeism than those who did not (Viswanathan et al., 2012). In addition, working above regular working hours would cause mental tiredness and muscle fatigue, leading to an increased risk of accidents in the workplace.

Sickness absenteeism can harm various individuals and entities. At the individual level, high absenteeism results in loss of pay and discipline issues. It also increases the workload and conflicts between co-workers. In terms of organisation, absenteeism results in lower productivity, higher costs and a higher risk of accidents. Furthermore, the negative consequences for the family and society include lower incomes, lower work reputation and aggravated marriage and child problem. Therefore, sickness absenteeism implicates organisational financial loss and a lower quality of life among employees.

Most industrial jobs are associated with a certain degree of injury or illness. Musculoskeletal disorders, such as strains and sprains, are the leading cause (34%) of work disability in the industrial sector, with estimated costs for long-term disability between USD 13 and USD 20 billion annually (Baldwin, 2004). Therefore, medical cost claims were an important measure for the organisation. In this study, the average medical cost claims at baseline were between RM92 and RM196 for three months and RM127 and RM359 for six months. A report on the medical costs associated with musculoskeletal claims by industries between the years 1999 to 2004 indicated that most of the claims were from the manufacturing industry (25.1%). The average medical cost per claim among the manufacturing workers was USD 2,593, with the total cost for all claims amounting to USD 673 million (Dunning et al., 2009).

The average age group of participants in this study was 36 years. According to Muir et al. (2020), younger age groups between 35 and 44 made most medical claim requests. The most harmful condition in working adults is due to mood disorders. Approximately 15 to 20% of workers will receive short-term disability benefits each year.

The WHP programme has emerged as an attractive strategy for its health and cost benefits. Therefore, the study designed the WHP and EAP programmes to target both organisational and individual levels. The goal of the WHP programme is to improve employee lifestyles, which will improve health, work ability and work productivity (Rongen, 2013). Meanwhile, the EAP aims to rehabilitate the workers, reduce the absence rate and improve health. Previous studies and reviews have demonstrated the positive effects of the WHP programme on overall health and well-being (Groeneveld et al., 2010), mental health (Martin et al., 2008), as well as work-related outcomes such as sickness absence (Kuoppala et al., 2008) and work productivity (Cancelliere et al., 2011).

This study demonstrated a significant improvement in the primary organisational outcome measures, i.e., sickness absenteeism, following a 6-month WHP intervention programme. Hendriksen et al. (2016) reported similar results of significant improvements in employees' vitality, work performance, sickness absence and self-management among the white-collar workers of an insurance company after undergoing a 5-month workplace health promotion programme. Bertera (1990) reported that comprehensive WHP programmes among the blue-collar employees of a diversified industrial company reduced sickness absenteeism among the intervention participants up to 14% over two years compared to a 5.8% decline in control participants. This achievement has resulted in a good return on investment. Similarly, a cluster of randomised controlled trials in Sweden showed less sickness absenteeism among the intervention group participants 6 months post-intervention and managed to sustain after 12 months of follow-up compared to control group participants. In addition, the study found that the participatory intervention group had an early return to work and a significant improvement in their mental health status, such as depression, anxiety and exhaustion (Van De Poll et al., 2020).

The key elements of the WHP intervention include strong management support, effective communication, and involvement of employees at both individual and organisational levels. Moreover, the WHP programme targets improving self-management related to individual vitality, including goal setting, action planning and reflective counselling by well-trained coaches. By increasing employees' self-awareness and knowledge of health practices and stimulating the sense of responsibility, they are willing to improve their health behaviour resulting in improved health and vitality, increased work engagement and decreased absenteeism (Rongen et al., 2013).

No significant effect was found in sickness absenteeism during at 3-months intervention programme. It could be due to the short duration of intervention which is perhaps not adequate for changes in behaviour, and minimising the level of work stress might take longer. This outcome was supported by a randomised controlled trial study on work-related stress intervention via the Work Stress Questionnaire (WSQ), which conducted a brief consultation from the general practitioner (GP) that had two hours of training before the

conduct of the study and the results showed no significant difference in sick leave within 3, 6 and 12 months post-intervention programme (Holmgren et al., 2019). However, job stress is a complex issue that requires a multidisciplinary approach to treatment and a qualified trainer to handle the stress-management intervention programme. Therefore, brief intervention is inadequate to impact the individual and the organisation.

This study found that medical cost claims were not significantly reduced during the 3-months and 6-months post-intervention programme. Van De Poll et al. (2020) supported these findings, which found a higher cost for short-term sickness absence and production loss at work among the problem-solving intervention group from the employer's perspective. It is due to the intervention group being able to return early to work following a long-term sickness absence. Therefore, the long-term sickness absence turned into short-term sickness absenteeism, and the employer bore the cost compared to the long-term sickness absence, borne by the workers' social insurance benefit. Therefore, the costs of short-term and long-term sickness absenteeism incurred by the employer should be measured.

Measuring work engagement is important to an organisation because it mediates the relationship between high-performance work systems, perceived organisational support and affective commitment (Teo et al., 2020). The organisational intervention in this study emphasised organisational support. A study in Belgium found that perceived organisational support moderates the association between work engagement and job satisfaction (Côté et al., 2020). Besides that, the intervention also includes personality training like self-evaluation in mindfulness and effective training. It was supported by a study in Romania which showed that work engagement mediates personality characteristics (core self-evaluation, proactive personality and success-oriented) with job performance and mental health (Tisu et al., 2020). Moreover, high work engagement showed a reduced risk of cardiovascular diseases by lowering systolic blood pressure and heart rate (Black et al., 2017). Therefore, work engagement impacts mental health, job performance and affective commitment and has also reduced cardiovascular risk.

In this study, there was a significant improvement in work engagement among the participants in the intervention group compared to the control group post-intervention. This finding was supported by the stress intervention with a quasi-experimental and longitudinal study in Spain among 72 employees, showing a significant improvement in vigour and dedication in work engagement. On the other hand, the work engagement in the control group remained constant, which is consistent with this study (Cifre et al., 2011). Furthermore, this study trained the intervention group participants with venting, emotional support, and anger control. According to Chen et al. (2020), work engagement increased emotional exhaustion for less conscientious workers, while emotional exhaustion decreased for more conscientious workers that were emotionally stable. Besides that, the intervention programme also promoted a healthy lifestyle that includes exercise as one

of the components. This approach was supported by a study in Japan that indicated that workplace exercise is significantly related to work engagement (Jindo et al., 2020).

Work engagement cannot be achieved if we focus solely on individual intervention. Work engagement requires an organisational intervention in which the intervention must include managers and supervisors to ensure that the subordinates' opinions are heard. The intervention programme in this study included the supervisor and the management when workers highlighted some of their concerns, such as work schedule, claims, and attendance, among others. This approach was supported by a study by Gameda and Lee (2020), which indicated that the transformational leadership style had a significant positive relationship with workers' engagement, and it also mediated the work outcome. This finding is also consistent with a study in the United States that found that schedule control and work engagement were mediated by schedule satisfaction and perceived supervisor support (Swanberg et al., 2011).

The study's strength includes a 100 response rate and no follow-up loss among the participants. Rigorous participant-retention strategies were employed in the design phase, at the beginning and throughout the study period. All the programmes were scheduled earlier to avoid production interruptions. All activities were monitored by the Human Resources and their Occupational Safety and Health team. All programmes were conducted in their internal training centre to ensure a high attendance rate. Frequent phone calls, site visits, and reminders on upcoming visits may have improved the likelihood of a high response rate. It is important to have experienced research coordinators who can implement the procedures that minimise loss to follow-up. Additionally, this study keeps participants interested and motivated by providing non-monetary incentives such as the stress management kit and free products from the company's brand.

Several limitations were observed in this study. First, data confidentiality and the implications on the company's brand from mental health issues that might be exposed to researchers and other parties made it challenging to find a suitable industry willing to engage in this study. Second, due to the participatory intervention study, double-blinding was not possible because the investigator was required to perform an intervention on the intervention group participants. It was, therefore, impossible to blind the participants and the investigator. However, blinding was still applied to data collectors and outcome assessors. Third, there is a risk of contamination between the intervention and control group participants because of the same workplace. This situation can create diffusion between groups. However, this study can minimise this effect due to the intervention programme focused on group intervention and individual intervention. In addition, the health promotion material was distributed to them to reduce the potential of resentful demoralisation among the control group members. Additionally, there is a possibility of a Hawthorne effect. Finally, the intervention group demonstrated an improvement in outcome measurement due to using self-reported questionnaires rather than biological measurements.

CONCLUSION

This study highlights the importance of sickness absenteeism, medical cost claims and work engagement in determining organisational outcomes. This study also suggested that the WHP programme is a good strategy that can be implemented to address the problem of workplace stress absenteeism because it helps improve health indicators among blue-collar employees, resulting in a favourable return on investment. However, it is important to note that employee absenteeism and work engagement can be influenced by many factors, from individual and social to organisational levels. Thus, a more detailed study should be carried out using different samples and methods. Furthermore, future studies may consider other socio-economic and background factors of employees that may contribute to the absence behaviour. In addition, interventions to reduce sickness absenteeism and medical cost claims may cover periodic medical check-ups, monitor employees' working hours, improve job satisfaction, and reduce workplace stress.

ACKNOWLEDGEMENTS

The authors want to thank the participating manufacturing workers.

REFERENCES

- Ajayi, S. (2018). Effect of stress on employee performance and job satisfaction: A case study of Nigerian banking industry. *SSRN Electronic Journal*, 1-71. <https://doi.org/10.2139/ssrn.3160620>
- Balducci, C., Fraccaroli, F., & Schaufeli, W. B. (2010). Psychometric properties of the italian version of the Utrecht Work Engagement Scale (UWES-9). *European Journal of Psychological Assessment*, 26(2), 143-149. <https://doi.org/10.1027/1015-5759/a000020>
- Baldwin, M. L. (2004). Reducing the costs of work-related musculoskeletal disorders: Targeting strategies to chronic disability cases. *Journal of Electromyography and Kinesiology*, 14(1), 33-41. <https://doi.org/10.1016/j.jelekin.2003.09.013>
- Beheshtifar, M., & Nazarian, R. (2013). Role of occupational stress in organizations. *Interdisciplinary Journal of Contemporary Research in Business*, 4(9), 648-657.
- Bertera, R. L. (1990). The effects of workplace health promotion on absenteeism and employment costs in a large industrial population. *American Journal of Public Health*, 80(9), 1101-1105. <https://doi.org/10.2105/ajph.80.9.1101>
- Black, J. K., Balanos, G. M., & Whittaker, A. C. (2017). Resilience, work engagement and stress reactivity in a middle-aged manual worker population. *International Journal of Psychophysiology*, 116, 9-15. <https://doi.org/10.1016/j.ijpsycho.2017.02.013>
- Brborovic, H., Brborovic, O., & Mustajbegovic, J. (2016). Looking for the possible association between stress, presenteeism and absenteeism among Croatian nurses: A cross-sectional study. *Iranian Journal of Psychiatry and Behavioral Sciences*, 10(4), Article e4587. <https://doi.org/10.17795/ijpbs-4587>

- Breathworks. (2017). *Mindfulness for stress course*. Breathworks. <https://www.breathworks-mindfulness.org.uk/mindfulness-for-stress>
- Callan, M. J., Kim, H., & Matthews, W. J. (2015). Predicting self-rated mental and physical health: The contributions of subjective socioeconomic status and personal relative deprivation. *Frontiers in Psychology*, 6, Article 1415. <https://doi.org/10.3389/fpsyg.2015.01415>
- Cancelliere, C., Cassidy, J. D., Ammendolia, C., & Côté, P. (2011). Are workplace health promotion programs effective at improving presenteeism in workers? A systematic review and best evidence synthesis of the literature. *BMC Public Health*, 11(1), Article 395. <https://doi.org/10.1186/1471-2458-11-395>
- CDC. (2015). *CDC - TWH: Infographic - NIOSH workplace safety & health topics*. Centers for Disease Control and Prevention. https://www.cdc.gov/niosh/twh/topreasons/infographic_text.html
- Chee, H. L. (2003). Relation between sick leave and selected exposure variables among women semiconductor workers in Malaysia. *Occupational and Environmental Medicine*, 60(4), 262-270. <https://doi.org/10.1136/oem.60.4.262>
- Chen, H., Richard, O. C., Dorian Boncoeur, O., & Ford, D. L. (2020). Work engagement, emotional exhaustion, and counterproductive work behavior. *Journal of Business Research*, 114, 30-41. <https://doi.org/10.1016/j.jbusres.2020.03.025>
- Chenoweth, D. (2011). *Promoting employee well-being: Wellness strategies to improve health, performance and the bottom line* (Rep.). SHRM Foundation.
- Cifre, E., Salanova, M., & Rodríguez-Sánchez, A. M. (2011). Dancing between theory and practice: Enhancing work engagement through work stress intervention. *Human Factors and Ergonomics In Manufacturing*, 21(3), 269-286. <https://doi.org/10.1002/hfm.20232>
- Côté, K., Lauzier, M., & Stinglhamber, F. (2020). The relationship between presenteeism and job satisfaction: A mediated moderation model using work engagement and perceived organizational support. *European Management Journal*, 39(2), 270-278. <https://doi.org/10.1016/j.emj.2020.09.001>
- De Beer, L., Pienaar, J., & Rothmann Jr, S. (2013). Linking employee burnout to medical aid provider expenditure. *SAMJ: South African Medical Journal*, 103(2), 89-93.
- De Bruin, D. P., Hill, C., Henn, C. M., & Muller, K. P. (2013). Dimensionality of the UWES-17: An item response modelling analysis. *SA Journal of Industrial Psychology*, 39(2), Article a1148. <https://doi.org/10.4102/sajip.v39i2.1148>
- DOSH. (2020). *Occupational accidents statistics by state January to December 2020 (investigated)*. Department of Occupational Safety and Health Malaysia. <https://www.dosh.gov.my/index.php/statistic-v/occupational-accident-statistics/occupational-accident-statistic-2020/3877-occupational-accidents-statistics-by-state-january-to-december-2020-investigated/file>
- Dunning, K. K., Davis, K. G., Cook, C., Kotowski, S. E., Hamrick, C., Jewell, G., & Lockey, J. (2009). Costs by industry and diagnosis among musculoskeletal claims in a state workers compensation system: 1999 - 2004. *American Journal of Industrial Medicine*, 53, 276-284. <https://doi.org/10.1002/ajim.20774>
- Edimansyah, B. A., Rusli, B. N., Naing, L., Rusli, B. A. M., Winn, T., & Ariff, B. R. H. T. M. (2008). Self-perceived depression, anxiety, stress and their relationships with psychosocial job factors in

- male automotive assembly workers. *Industrial Health*, 46(1), 90-100. <https://www.ncbi.nlm.nih.gov/pubmed/18270454>
- Gemeda, H. K., & Lee, J. (2020). Leadership styles, work engagement and outcomes among information and communications technology professionals: A cross-national study. *Heliyon*, 6(4), Article e03699. <https://doi.org/10.1016/j.heliyon.2020.e03699>
- Goodman, S. A., & Svyantek, D. J. (1999). Person-organization fit and contextual performance: Do shared values matter. *Journal of Vocational Behavior*, 55(2), 254-275. <https://doi.org/10.1006/jvbe.1998.1682>
- Greaves, C. E., Parker, S. L., Zacher, H., & Jimmieson, N. L. (2017). Working mothers' emotional exhaustion from work and care: The role of core self-evaluations, mental health, and control. *Work & Stress*, 31(2), 164-181. <https://doi.org/10.1080/02678373.2017.1303760>
- Groeneveld, I. F., Proper, K. I., Van der Beek, A. J., Hildebrandt, V. H., & Van Mechelen, W. (2010). Lifestyle-focused interventions at the workplace to reduce the risk of cardiovascular disease - A systematic review. *Scandinavian Journal of Work, Environment & Health*, 36(3), 202-215. <https://doi.org/10.5271/sjweh.2891>
- Hansen, C. D., & Andersen, J. H. (2008). Going ill to work - What personal circumstances, attitudes and work-related factors are associated with sickness presenteeism? *Social Science & Medicine*, 67(6), 956-964. <https://doi.org/10.1016/j.socscimed.2008.05.022>
- Hendriksen, I. J., Snoijer, M., De Kok, B. P., Van Vilsteren, J., & Hofstetter, H. (2016). Effectiveness of a multilevel workplace health promotion program on vitality, health, and work-related outcomes. *Journal of Occupational & Environmental Medicine*, 58(6), 575-583. <https://doi.org/10.1097/jom.0000000000000747>
- Holmgren, K., Hensing, G., Bültmann, U., Hadzibajramovic, E., & Larsson, M. E. H. (2019). Does early identification of work-related stress, combined with feedback at GP-consultation, prevent sick leave in the following 12 months? A randomized controlled trial in primary health care. *BMC Public Health*, 19(1), 1-10. <https://doi.org/10.1186/s12889-019-7452-3>
- ILO. (2016). *Workplace stress, a collective challenge* (Vol. 1). International Labour Organization. <https://doi.org/10.1017/CBO9781107415324.004>
- Ishtiak-Ahmed, K., Perski, A., & Mittendorfer-Rutz, E. (2013). Predictors of suicidal behaviour in 36,304 individuals sickness absent due to stress-related mental disorders - A Swedish register linkage cohort study. *BMC Public Health*, 13, Article 492. <https://doi.org/10.1186/1471-2458-13-492>
- Jack, A. (2017, September 13). The price of success for Asia's workers. *The Financial Times*. <https://www.ft.com/content/3e27eae2-3fa9-11e7-82b6-896b95f30f58>
- Jesus, S. N. D., Miguel-Tobal, J. J., Rus, C. L., Viseu, J., & Gamboa, V. (2014). Evaluating the effectiveness of a stress management training on teachers and physicians' stress related outcomes. *Clinica y Salud*, 25(2), 111-115. <https://doi.org/10.1016/j.clysa.2014.06.004>
- Jindo, T., Kai, Y., Kitano, N., Tsunoda, K., Nagamatsu, T., & Arao, T. (2020). Relationship of workplace exercise with work engagement and psychological distress in employees: A cross-sectional study from the MYLS study. *Preventive Medicine Reports*, 17, Article 101030. <https://doi.org/10.1016/j.pmedr.2019.101030>
- Johns, G. (2009). Presenteeism in the workplace: A review and research agenda. *Journal of Organizational Behavior*, 31(4), 519-542. <https://doi.org/10.1002/job.630>

- Johnston, D. A., Harvey, S. B., Glozier, N., Calvo, R. A., Christensen, H., & Deady, M. (2019). The relationship between depression symptoms, absenteeism and presenteeism. *Journal of Affective Disorders*, *256*, 536-540. <https://doi.org/https://doi.org/10.1016/j.jad.2019.06.041>
- Kuoppala, J., Lamminpää, A., & Husman, P. (2008). Work health promotion, job well-being, and sickness absences - A systematic review and meta-analysis. *Journal of Occupational & Environmental Medicine*, *50*(11), 1216-1227. <https://doi.org/10.1097/jom.0b013e31818dbf92>
- Manjunatha, R., Kiran, D., & Thankappan, K. R. (2011). Sickness absenteeism, morbidity and workplace injuries among iron and steel workers - A cross sectional study from Karnataka, Southern India. *Australasian Medical Journal*, *4*(3), 143-147. <https://doi.org/10.4066/AMJ.2011.576>
- Martin, A., Sanderson, K., & Cocker, F. (2008). Meta-analysis of the effects of health promotion intervention in the workplace on depression and anxiety symptoms. *Scandinavian Journal of Work, Environment & Health*, *35*(1), 7-18. <https://doi.org/10.5271/sjweh.1295>
- May, D. R., Gilson, R. L., & Harter, L. M. (2004). The psychological conditions of meaningfulness, safety and availability and the engagement of the human spirit at work. *Journal of Occupational and Organizational Psychology*, *77*(1), 11-37. <https://doi.org/10.1348/096317904322915892>
- Mazerall, L. (2002). *Stress management within a manufacturing environment* (Unpublished Master's Thesis). National Library of Canada= Bibliothèque nationale du Canada, Ottawa.
- McConachie, D. A. J., McKenzie, K., Morris, P. G., & Walley, R. M. (2014). Acceptance and mindfulness-based stress management for support staff caring for individuals with intellectual disabilities. *Research in Developmental Disabilities*, *35*(6), 1216-1227. <https://doi.org/10.1016/j.ridd.2014.03.005>
- MOH. (2005). *Modul minda sihat* [Healthy Mind Module]. Ministry of Health Malaysia. <https://www.infosihat.gov.my>
- Ministry of Health. (2014). *Health expenditure report 1997 - 2012*. Ministry of Health Malaysia. <https://www.mma.org.my/Portals/0/PDF%202015/Health%20Expenditure%20Report%201997%20-%202012.pdf>
- Muir, C., Prang, K. H., Sheppard, D., & Newnam, S. (2020). Occupational injuries among police workers: Patterns and contributing factors in an Australian jurisdiction. *Safety Science*, *122*, Article 104525. <https://doi.org/10.1016/j.ssci.2019.104525>
- Nerstad, C. G., Richardsen, A. M., & Martinussen, M. (2010). Factorial validity of the Utrecht Work Engagement Scale (UWES) across occupational groups in Norway. *Scandinavian Journal of Psychology*, *51*(4), 326-333. <https://doi.org/10.1111/j.1467-9450.2009.00770.x>
- NIOSH. (1998). *Stress at work*. National Institute for Occupational Safety and Health USA. <https://www.cdc.gov/niosh>
- Prater, T., & Smith, K. (2011). Underlying factors contributing to presenteeism and absenteeism. *Journal of Business & Economics Research*, *9*(6), 1-14. <https://doi.org/10.19030/jber.v9i6.4374>
- Rasmussen, B., Sweeny, K., & Sheehan, P. (2016). *Health and economy: The impact of wellness on workforce productivity in global markets* [Report to the U.S. Chamber of Commerce's Global Initiative on Health and Economy, VISES]. Victoria University. https://www.uschamber.com/assets/archived/images/documents/files/global_initiative_on_health_and_the_economy_-_report.pdf

- Roche, A. M., Pidd, K., Fischer, J. A., Lee, N., Scarfe, A., & Kostadinov, V. (2016). Men, work, and mental health: A systematic review of depression in male-dominated industries and occupations. *Safety and Health at Work*, 7(4), 268-283. <https://doi.org/10.1016/J.SHAW.2016.04.005>
- Rongen, A., Robroek, S. J. W., Van Lenthe, F. J., & Burdorf, A. (2013). Workplace health promotion: A meta-analysis of effectiveness. *American Journal of Preventive Medicine*, 44(4), 406-415. <https://doi.org/10.1016/j.amepre.2012.12.007>
- Schaufeli, W. B. (2012). Work engagement. What do we know and where do we go? *Romanian Journal of Applied Psychology*, 14(1), 3-10.
- Schaufeli, W. B., & Bakker, A. B. (2003). *Test manual for the Utrecht Work Engagement Scale* [Unpublished manuscript]. Utrecht University, the Netherlands. <http://www.schaufeli.com>
- Schaufeli, W. B., & Bakker, A. B. (2004). Job demands, job resources, and their relationship with burnout and Engagement: A multi-sample study. *Journal of Organizational Behavior*, 25(3), 293-315. <https://doi.org/10.1002/job.248>
- Shimazu, A., Schaufeli, W. B., Kosugi, S., Suzuki, A., Nashiwa, H., Kato, A., Sakamoto, M., Irimajiri, H., Amano, S., Hirohata, K., Goto, R., & Kitaoka-Higashiguchi, K. (2008). Work engagement in Japan: Validation of the Japanese version of the Utrecht Work Engagement Scale. *Applied Psychology*, 57(3), 510-523. <https://doi.org/10.1111/j.1464-0597.2008.00333.x>
- Shore, L. M. F., & Martin, H. J. (1989). Job satisfaction and organizational commitment in relation to work performance and turnover intentions. *Human Relations*, 42(7), 625-638. <https://doi.org/10.1177/001872678904200705>
- Sulaiman, W., & Zahoni, N. (2016). Validation of the Utrecht Work Engagement Scale (UWES) in the Malaysian context. *International Journal of Social*, 6(9), 672-676.
- Suzuki, T., Miyaki, K., Song, Y., Tsutsumi, A., Kawakami, N., Shimazu, A., Takahashi, M., Inoue, A., & Kurioka, S. (2015). Relationship between Sickness presenteeism (WHO-HPQ) with depression and sickness absence due to mental disease in a cohort of Japanese workers. *Journal of Affective Disorders*, 180, 14-20. <https://doi.org/10.1016/j.jad.2015.03.034>
- Swanberg, J. E., McKechnie, S. P., Ojha, M. U., & James, J. B. (2011). Schedule control, supervisor support and work engagement: A winning combination for workers in hourly jobs? *Journal of Vocational Behavior*, 79(3), 613-624. <https://doi.org/10.1016/j.jvb.2011.04.012>
- Tadesse, S., Ebrahim, K., & Gizaw, Z. (2015). Sickness absenteeism and associated factors among horticulture employees in lume district, southeast Ethiopia. *Journal of Occupational Medicine and Toxicology*, 10(1), 1-6. <https://doi.org/10.1186/s12995-015-0074-5>
- Teo, S. T. T., Bentley, T., & Nguyen, D. (2020). Psychosocial work environment, work engagement, and employee commitment: A moderated, mediation model. *International Journal of Hospitality Management*, 88, Article 102415. <https://doi.org/10.1016/j.ijhm.2019.102415>
- Tisu, L., Lupşa, D., Virgă, D., & Rusu, A. (2020). Personality characteristics, job performance and mental health the mediating role of work engagement. *Personality and Individual Differences*, 153, Article 109644. <https://doi.org/10.1016/j.paid.2019.109644>

- U.S. Bureau of Labor Statistics. (2020). *Labor force statistics from the current population survey*. U.S. Bureau of Labor Statistics. <https://www.bls.gov/cps/>
- Van De Poll, M. K., Bergström, G., Jensen, I., Nybergh, L., Kwak, L., Lornudd, C., & Lohela-Karlsson, M. (2020). Cost-effectiveness of a problem-solving intervention aimed to prevent sickness absence among employees with common mental disorders or occupational stress. *International Journal of Environmental Research and Public Health*, 17(14), 1-15. <https://doi.org/10.3390/ijerph17145234>
- Van Doornen, L. J., Houtveen, J. H., Langelaan, S., Bakker, A. B., van Rhenen, W., & Schaufeli, W. B. (2009). Burnout versus work engagement in their effects on 24-hour ambulatory monitored cardiac autonomic function. *Stress and Health*, 25(4), 323-331. <https://doi.org/10.1002/smi.1279>
- Viswanathan, H., Sridharan, P., & Thiyagarajan, S. (2012). Absenteeism - A menace in Indian BPO industry. *SMART Journal of Business Management Studies*, 9, 43-50.
- Vokić, N. P., & Bogdanić, A. (2007). Individual differences and occupational stress perceived: A Croatian survey. *EFZG Working Paper Series*, 5, 1-15.
- Wang, H., Naghavi, M., Allen, C., Barber, R. M., Bhutta, Z. A., Carter, A., Casey, D. C., Charlson, F. J., Chen, A. Z., Coates, M. M., Coggeshall, M., Dandona, L., Dicker, D. J., Erskine, H. E., Ferrari, A. J., Fitzmaurice, C., Foreman, K., Forouzanfar, M. H., Fraser, M. S., ... & Murray, C. J. L. (2016). Global, regional, and national life expectancy, all-cause mortality, and cause-specific mortality for 249 causes of death, 1980-2015: A systematic analysis for the Global Burden of Disease Study 2015. *Lancet*, 388(10053), 1459-1544. [https://doi.org/10.1016/s0140-6736\(16\)31012-1](https://doi.org/10.1016/s0140-6736(16)31012-1)
- Wehrenberg, M. (2008). *The 10 best-ever anxiety management techniques* (1st Ed.). W.W. Norton & Company Inc.
- Whitmore, M., Stewart, K., Pollard, J., Belle, J. V., Yang, M., & Stolk, C. V. (2018). *Promising practices for health and wellbeing at work*. RAND Europe.
- Zare, R., Choobineh, A., & Keshavarzi, S. (2017). Association of amplitude and stability of circadian rhythm, sleep quality, and occupational stress with sickness absence among a gas company employees - A cross sectional study from Iran. *Safety and Health at Work*, 8(3), 276-281. <https://doi.org/10.1016/j.shaw.2016.09.007>

APPENDIX

The Intervention Module Programme

No	Programmes	Time/Duration
1	Occupational Stress Management Course (OSMC)	1 st Month (2-day course)
	Module 1: Psychological Screening Test <ul style="list-style-type: none"> • Personality Traits assessment 	
	Module 2: Occupational Stress <ul style="list-style-type: none"> • Definition of Occupational Stress • Magnitude of Occupational Stress Problems • Models of Occupational Stress • Know Your Stressors • Symptoms and Signs of Stress • Effect of Stress 	
	Module 3: Personalised Stress Management Therapy <ul style="list-style-type: none"> • Managing Anxious Body (MAB) <ul style="list-style-type: none"> ◊ Technique 1: Change your intake <ul style="list-style-type: none"> • Create Demand Delays • Lower Stimulation Intake ◊ Technique 2: Breathe (Diaphragmatic Breathing), Mindfulness breathing ◊ Technique 3: Mindfulness with shifting awareness ◊ Technique 4: Relax (Progressive Muscle Relaxation, Cued Relaxation) and Mindfulness Relaxation • Mindfulness for stress and anxiety • Anger control • Healthy Lifestyles (10 B, stress buster) 	
	Module 4: Corporate Occupational Stress Management (COSM) <ul style="list-style-type: none"> • Organisational Change (PIE Concept) 	2 nd Month (1-day course)
	Module 5: Corporate Empowerment Organisation (CEO) <ul style="list-style-type: none"> • SWOT Analysis • Problem Solving Skills • Interpersonal Communication Skills • Assertiveness • Root cause problems • Discussion on the application of the corporate module (COSM & CEO) 	
2	EAP Counselling <ul style="list-style-type: none"> • Discussion on physical and psychological health • Discussion on management of stress at workplace • Discussion on daily application of personalised stress management therapy 	3 rd Month (1 session per individual)
3	Application of Managing Anxious Body (MAB) Module <ul style="list-style-type: none"> • Diaphragmatic breathing • Progressive muscle relaxation • Mindfulness 	Daily practice (individual) for 3 months

Facies Mapping of the Holocene Carbonate Complexes in Kepulauan Seribu Java Basin, Indonesia Using Satellite-Derived Data Set

Shafiqah Amir^{1,2*}, Haylay Tsegab^{1,2}, Grisel Jimenez Soto² and Ali Imran Azman²

¹Department of Geosciences, Universiti Teknologi PETRONAS, 32610 UTP, Seri Iskandar, Perak, Malaysia

²South East Asia Carbonate Laboratory (SEACaRL), Universiti Teknologi PETRONAS, 32610 UTP, Seri Iskandar, Perak, Malaysia

ABSTRACT

The analog study is common in understanding buried reservoirs and the relationship between architectural complexity and heterogeneity of carbonate deposits. This study processed satellite and false-color images using single-band images and classified them using a supervised classification technique to generate an environmental facies map. Thus, the study's objectives are to map facies distribution in selected carbonate depositional environment and investigate oceanographic parameters that influence the development and evolution of modern carbonates in Holocene Kepulauan Seribu patch reef complexes, Java Basin. The main sub-environments are reef sand apron, subtidal reefal margin, and shallower subtidal lagoon. Annual wind patterns in the Java Basin have influenced the development of carbonate sediment in the Kepulauan Seribu archipelago, resulting in the formation of an isolated carbonate platform pattern with a single crest and asymmetrical dipping flanks. Meanwhile, the salinity of seawater influences the production of modern carbonate deposits as the Java basin is situated at the equator line, where the salinity of the seawater is moderately salty (35‰) and contributes to the favorable conditions for carbonate growth. The analysis of oceanographic elements with the integration of quantified environmental facies distribution is conducted to monitor the deposition of carbonate sediments which

gives insight into carbonate distribution on the studied platforms. Satellite-derived facies maps provide an accurate overview of depositional facies patterns at the field scale in the oil and gas industry, enabling geologists to assess the potential of an oil and gas reservoir.

Keywords: Facies map, Holocene carbonate, Landsat imagery, remote sensing, supervised classification

ARTICLE INFO

Article history:

Received: 12 September 2021

Accepted: 15 December 2021

Published: 25 May 2022

DOI: <https://doi.org/10.47836/pjst.30.3.28>

E-mail addresses:

shafiqah_19000176@utp.edu.my (Shafiqah Amir)

haylay.tsegab@utp.edu.my (Haylay Tsegab)

jimenezsotogrisel@gmail.com (Grisel Jimenez Soto)

imran.azman@utp.edu.my (Ali Imran Azman)

*Corresponding author

INTRODUCTION

Landsat satellite imagery is a remote sensing technology utilized to acquire satellite data of objects on Earth's surface. Landsat data is considered user-friendly compared to conventional mapping techniques or hand-drawn mapping (Kaczmarek et al., 2010). Compared to traditional mapping techniques, Landsat image satellites are suitable for producing facies maps, architecturally diverse and heterogeneous (Kaczmarek et al., 2010). Modern-day carbonate environment is often used as an analog for ancient counterpart carbonate settings strived at understanding the pattern of carbonate sediment distribution through dimensional data extraction processes (Harris, 1996; Harris, 2010), asserting that the deposition process for Holocene carbonate settings is similar to the ancient carbonate systems. Therefore, Holocene carbonate sediment distribution patterns are valuable as an analog to studying the heterogeneity of the ancient carbonate system.

This study utilizes Landsat data input from open access sources. It saves the cost of satellite data acquisition and time for data processing. The data generated from this carbonate facies mapping process can provide new insights into sediment distribution patterns, heterogeneity levels, and structure of selected carbonate platforms and potentially serve as a realistic and practical analog for the fossil carbonate oil field reservoirs.

The satellite system distinguishes and classifies objects or features found on the modern-day carbonate platform. The satellite data is collected through reflection and absorption of the electromagnetic spectrum on these features. This research focuses on the extraction of satellite image layers, data processing steps, and visual surveys of carbonate depositional patterns on the platform using spectral and multispectral sensors.

Remote sensing technologies were first used as a tool to monitor and study the development of coral reef populations, sediment composition, and diversity of the reefal system in the 1990s (Andrefouët & Riegl, 2004; Purkis, 2005; Purkis et al., 2007; Riegl et al., 2007). Researchers have used the technology because it possesses sensors capable of capturing clear surface images, providing high-resolution satellite data, and potentially being used to study shallow marine environments with high seawater clarity and a massive amount of carbonate components (Purkis, 2005).

Carbonates are formed primarily in warm, clear tropical to subtropical marine waters' photic zones (up to 200 m). They are mostly formed by organisms through algal photosynthesis or transported in-situ, organically precipitated tests and shells (Wilson, 1997). Light, water temperature, water salinity, depth, sedimentation, and surface exposure are all factors that limit carbonate growth (Ahr, 2011). The photic zone is the ideal environment for carbonate formation.

The study aims to map facies distribution in selected carbonate depositional environment and investigate oceanographic parameters that influence the development and evolution of modern carbonates in Holocene Kepulauan Seribu patch reef complexes, Java Basin. This study has utilized remote sensing methods to obtain aerial photographs and satellite data. Satellite images are needed to process the spectrum bands and generate a satellite-derived environmental facies distribution map.

STUDY AREA

The study area is located northwest of the Java Basin, which is 6° South on the equatorial line of West Java, Indonesia, or 50 km from the Northwest, Jakarta, between 106° 32′ 53.97″ and 106° 35′ 48.99″ East, 5° 34′ 17.38″ and 5° 37′ 33.67″ South (cite map). The study area comprises a portion of the Kepulauan Seribu patch reef complexes and two isolated carbonate platforms (Figure 1). The area is located about 59.2 km north of the City of North Jakarta and is surrounded by an ocean with a water depth of about 27.4 m. These isolated carbonate platforms are from the 192 chains of carbonate platforms that exhibit north-south chain patterns. Kepulauan Seribu patch reef complexes show different physiological patterns in the South and North of the islands. The carbonate platforms in the southern part show several large platforms, with lagoons less than 3 m in depth and larger reef sand apron and smaller sand cays with an estimated area of several square kilometers. On the other hand, the carbonate platform in the northern part of the archipelago is smaller and records less than 1 km² and no lagoon formation.

The study area, approximately 26.3 km², covers selected carbonate platform sand the recorded shallow ocean. The area of the respective carbonate platform is not much different. However, the present-day Putri Island carbonate platform is measured to have an area of 7.02 km² with a length of 7.9 km and a width of 7.05 km compared to Pulau Bira, measuring 5.84 km² with a length and width of the platform of 7.21 km and 5.31 km respectively. Most platforms have only one sand cay or small island. A small-sized lagoon at 1452 m² is observed in the western part of Putri Besar Island. However, the average present-day carbonate platforms in the area have no lagoon formation due to Kepulauan Seribu being tectonically a deep, shallow-water back-arc basin with a north-south faulting pattern.

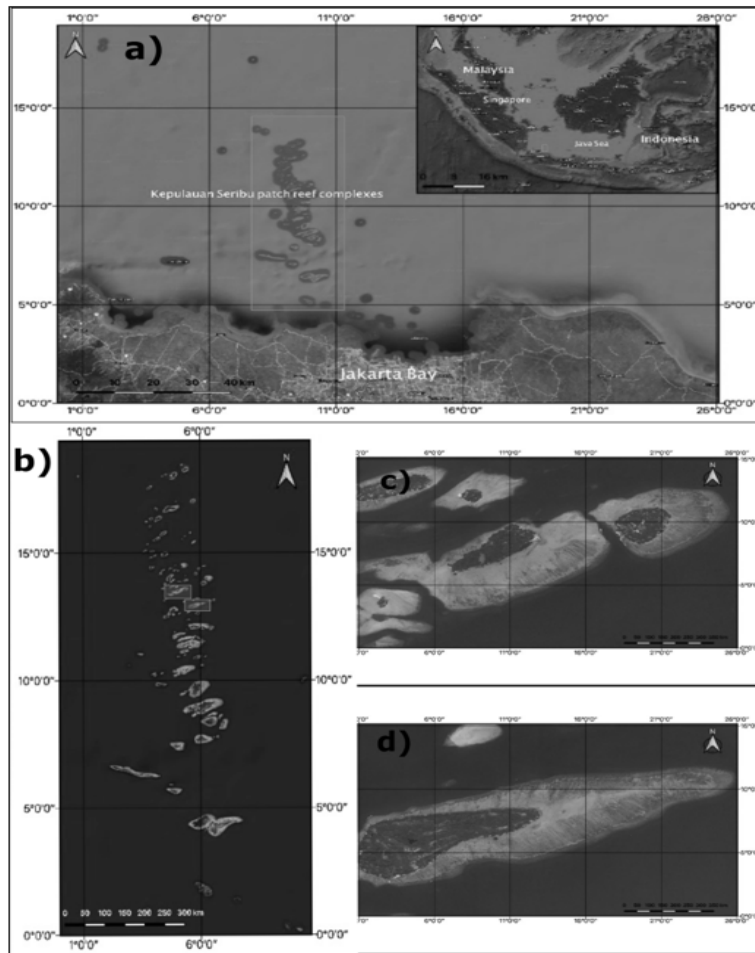


Figure 1. Study area as indicated in the red box (a) Holocene Kepulauan Seribu patch reef complexes, North-West Java Basin, Indonesia. (b) Location of selected present-day carbonate platforms; Pulau Putri and Pulau Bira. (c) and (d) Chosen Holocene carbonate platforms of Putri and Bira Islands in an aerial view from sources of Open Street Map and Bing Aerial

METHODOLOGY

Remote sensing is one of the most widely used geophysical methods for exploring oil and gas as well as minerals and natural resources (Hoover et al., 1995). Solar sources induce electromagnetic radiation, classified into seven spectrum regions: radio waves, microwaves, infrared (IR), visible light, ultraviolet (UV), X-rays, and gamma rays. Remote sensing technology works with the help of sensors to detect the electromagnetic spectrum, which is divided into visible light (0.4–0.7 μm), near-reflected infrared (0.77–0.90 μm), mid-reflected infrared (1.55–1.75 μm), thermal infrared (10.40–12.50 μm) and microwaves (1 mm–1 m) (Murai, 1993). Waves detected by sensors are recorded through digital data for

processing and producing an image for an area of interest (Hoover et al., 1995). According to Kaczmarek et al. (2010), remote sensing technology plays a role in measuring the electromagnetic radiation emitted by solar energy to the Earth's surface and is reflected in the satellite's sensors. The wavelength data obtained from the earth's surface are analyzed to determine the geomorphological features and functions of the surface area.

Data Acquisition

The satellite images used in this study are obtained from open access on Google Hybrid, Bing Aerial, Google Road, and Open Street maps. The acquired aerial images were within 15 m–15 cm for Google Hybrid, 30 m multispectral Landsat images, and 15 m Landsat panchromatic images for Google Road (Figure 1). Aerial photographs of the study area were captured in December 2015 [Figure 1(a)]. Meanwhile, aerial photographs taken via Aerial Bing open access do not reveal the date of the photo.

The satellite images in Figures 1(c) and 1(d) are accessed through a combination of hybrid data, Aerial Bing, and Open Street map to acquire a clearer Holocene carbonate platform image without the interruption of noises and cloud coverage. OpenStreet map uses high-resolution satellite images; Landsat 7 possesses an Enhanced Thematic Mapper Plus (ETM+) sensor, which enables the mapping of a wide range of areas as compared to the Thematic Mapper (TM) sensors used in Landsat 4 and 5 (Masek et al., 2001). Landsat satellite imagery could potentially be a tool for monitoring the development of modern-day carbonate platforms located in shallow marine. Kaczmarek et al. (2010) discuss that the potential for water penetration is closely associated with TM spectral band and visible wavelength, in which they assert that solar radiation affects the wavelength, potential penetration, and reflection of waves from the earth's surface to the sensors. Practically, a short wave has a high penetration potential. Kaczmarek et al. (2010) demonstrated that the TM 3 (red band) had a penetration potential of about 5 m (16 ft) as compared to the TM 1 (blue band), capable of penetrating the surface to about 20 m (66 ft) and the TM 2 (green band) reported a penetration potential of 10 m (33 ft). However, TM 4 to TM 7 bands were noted to have no penetration potential due to longer wave absorption by the water bodies. Hence, it is often found that water bodies with deeper depths are difficult to identify features found at the bottom of the ocean as satellite images suffer from a lack of data to categorize the features of water bodies. Geologists and explorationists attribute the uncertainty of data and derivative products to areas with deep water depths (Kaczmarek et al., 2010). Whereas Aerial Bing utilizes Bird's eye view approach that captures 45° ground-level images and applies a ground-level sample distance (GSD) of 10 cm per pixel, permitting more detailed present-day carbonate platform images and geomorphological features (Yu et al., 2017).

Qualitative Assessment of Geomorphic Patterns

Selected carbonate platforms are qualitatively analyzed to illustrate the environmental facies geometric patterns of selected carbonate platforms. Platform images are interpreted by creating satellite-derived facies maps using Quantum Geographical Information System (QGIS3.10) to characterize the spectrum of patterns on each platform.

RESULTS AND DISCUSSION

The visual survey technique used in this study attempts to interpret geological features in terms of shape, size, and distribution of surface brightness on the respective modern carbonate platforms. In addition, this technique helps to provide the geomorphological information found on the platforms by analyzing the individual image band used in the satellite image data for this research.

The mapping scheme generated three major sub-depositional environments; subtidal reef margin/sparse coral, shallower subtidal part lagoon/platform margin, and sand apron, to demonstrate the geomorphic characteristics of the build-ups (Rankey, 2016). The reef sand apron is classified into three classes; sand apron with sparse seagrass, sand apron without seagrass, and sand apron with dense seagrass as a supervised classification technique defined by Utami et al. (2018). Schlager and Purkis (2013) discuss that this method is useful and plausible even without ground-truthing. The visual observance was carried out by using satellite images of Bira Island and Putri Island. Based on this observation, there are discrepancies between the respective build-ups. Among the discrepancies discovered were abundant reefs, distribution of sand aprons, and appearances of the sand cay or small island. A semi-quantitative analysis is also carried out in the study area. This method is used to deduce seascape patterns based on geomorphic facies' spectral character, width, length, and orientation. By minimizing potential errors, correct facies can be mapped rigorously.

Visible and Near-Infrared Image Bands

Based on the visual survey method performed on the processed satellite images, various geological or geomorphological features and depths of water bodies can be observed. The brightness distribution of a feature on the surface of the present-day carbonate platform is also varied based on its reflection potential from the surface. Satellite imagery using the blue band presents geomorphological features with different brightness distributions of different features. It is evident when shallow-water features are seen to be brighter than vegetation due to the chlorophyll content in the plants effectively absorbing the blue band [Figures 2(a) & 2(b)]. The brightness of the blue band is brighter than the red band satellite image.

Figure 2 illustrates the feature of a shallow water body with a shallower depth of color than the deep ocean. However, color differences can be observed between vegetation features

of the blue band and green band, where satellite images with green bands exhibit brighter images as compared to the blue band [Figures 2(c) & 2(d)]. It makes it easy for researchers to study and analyze the differences in the features of the study area.

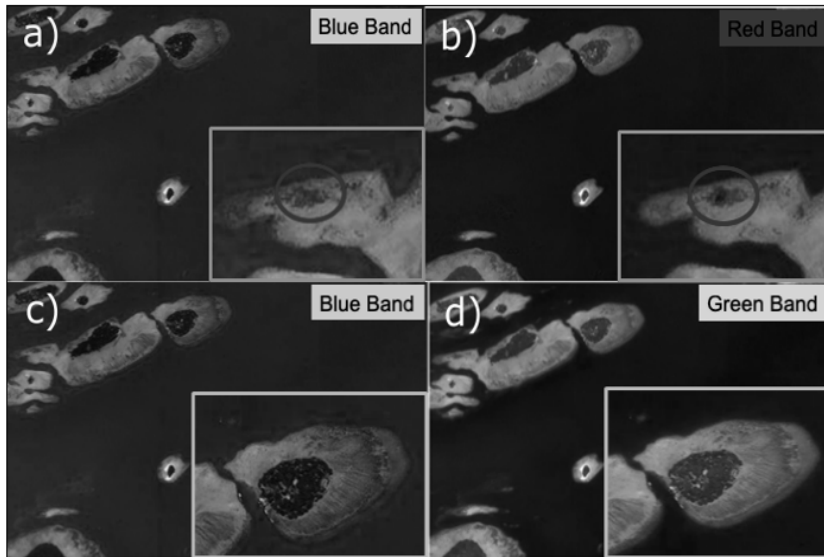


Figure 2. Satellite imagery with a) blue band, b) red band, and d) green band. Satellite imagery with a) blue band and b) red band, which represent shallow lagoon feature as highlighted in the red circle. Satellite imagery with c) blue band and d) green band which represent vegetated landmass feature as shown in the green box

In general, chlorophyll content contributes to the vegetation features on the Earth's surface that effectively absorb red and blue radiation (Vincent, 1997). Satellite images with the red band display dark color, which represents vegetation on the surface of the present-day carbonate platform, but the feature does not dominate the entire platform. The darkest color is recorded as a body of water due to the high absorption rate in the open sea or shallow lagoon [Figure 2(b)]. However, sediment shows the brightest light level due to higher wave reflectivity than the feature's absorption.

Pseudo-Color Images

Pseudo-color satellite images of the blue, green, and red bands were utilized in this study to further examine and decipher the geological features of the carbonate platform in greater detail by increasing the distance in the color space between successive grey levels. Based on the visual observations made on the satellite images in Figures 3 and 4, no uncommon features were detected on the surface of the present-day carbonate platforms. Satellite images with pseudo-color (blue band) still display all the features on the surface of the earth

with varying colors and brightness levels [Figure 3(a)]. However, slight differences can be observed in the pseudo-color satellite image (green band), where small islands exhibited faded blue color [Figure 3(b)] as compared to the pseudo-color image (blue band).

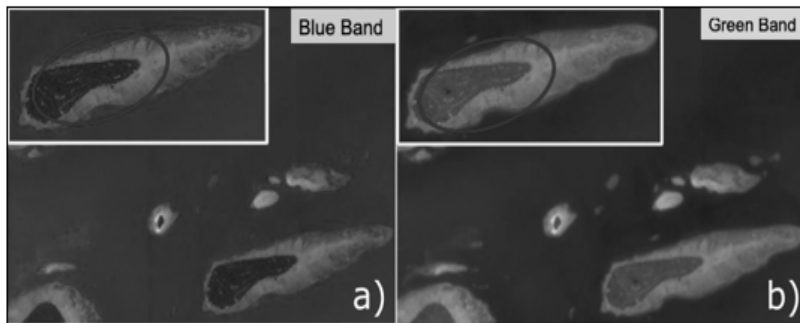


Figure 3. Satellite imagery with pseudo-color of a) blue band and b) green band which represent small island feature as highlighted in the red circle

Meanwhile, the pseudo-color image (red band) reveals minor reefal features than the pseudo-color satellite image of the blue and green bands (Figure 4). However, the sedimentary features are seen more clearly through the pseudo-color image (red band) than the pseudo-color image of the blue and green bands.

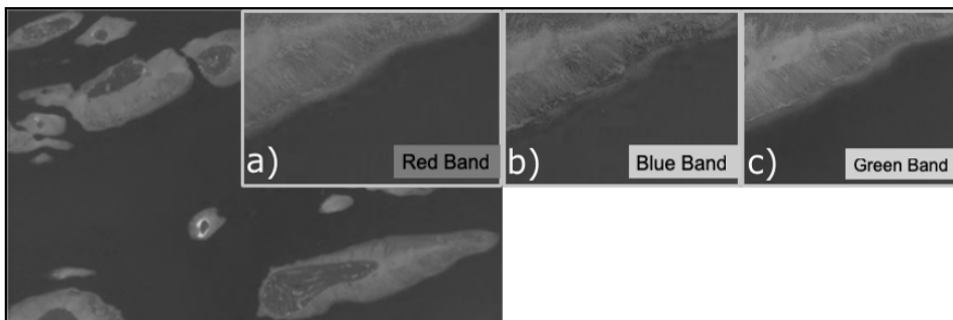


Figure 4. Satellite imagery with pseudo-color of a) red band, b) blue band, and c) green band which represents reefal feature as shown in the pink box

Color Combination of Visible Bands

Visual surveys of satellite images and interpretations of band images are very practical. However, the interpretation of geomorphological features on the present-day carbonate platform is based on the spectrum used and the brightness distribution of the features. In this study, multispectral images were added to enhance the discrimination of existing spectral images.

In general, the basic spectral bands commonly used in the satellite system consist of three main bands, blue, green, and red. The spectral bands help researchers to clarify geomorphological features of the Holocene carbonate platform that are viewed through satellite or aerial photographs, such as small islands, vegetation, water bodies, sediment, lagoons, and more.

Based on satellite images with bands 1, 2, and 4, the sedimentary features of the Holocene carbonate platform have the brightest distribution of brightness. Meanwhile, shallow water features such as lagoons are distinguished by light blue color [Figure 5(a)]. The open ocean displays the darkest levels of brightness. Small islands or landmass is distinguished by brownish.

Satellite images of bands 1, 3, and 4 [Figure 5(b)] exhibit small islands and reefal features in brackish color. At the same time, water bodies such as the open ocean are displayed in dark green, and sedimentary features remain as the brightest object on the platforms.

Bands 3, 4, and 2 are used in satellite images in Figure 5(c), where small islands, sand cays, and reefal are displayed in dark blue. The water body features are of the old mauve color, while the sediment features are exhibited in magenta color. As satellite images with bands 3, 4, and 2 do not utilize the blue band, researchers have a predicament distinguishing shallow water bodies from deep water as described about satellite images in Figures 5(a) and 5(b).

Kaczmarek et al. (2010) demonstrated that the usage of Landsat satellite data with a resolution of 28.5 m (93.5 ft) was eligible for accomplishing uniformity in the distribution of facies in conjunction with collected sediment data. High-resolution satellite images have the best absorption potential and enable researchers to review and interpret the carbonate features found in water bodies, especially in shallow marine areas. Multispectral satellite images with the blue band are most suitable for usage in facies mapping for Holocene carbonate platforms such as in Kepulauan Seribu modern reef complexes (Chalabi et al., 2012).

Satellite-Derived Facies Maps

Satellite imagery reveals varieties in geomorphic sizes, shapes, and patterns found on the present-day carbonate platforms. Based on visual inspection of the satellite image, various geomorphic elements can be seen and aligned as anticipated on the Holocene carbonate platform of the Kepulauan Seribu. Jordan Jr. (1998) reassures that the platform-margin reefs are inboard of deep open ocean and forereefs characterized by spurs and grooves. Platform-margin reefs are commonly seen as orangish or reddish on satellite imagery. Meanwhile, the sand aprons area looks white or bright blue in the image and is characterized by bare, shallow, gravelly, and sandy, albeit there are patch reefs and seagrass patches. The

reef sand apron that passes through the interior platform is interpreted to have deeper shades of blue, which the sea level is deeper than reef sand aprons and may include patch reefs.

Interpreted satellite images and satellite-derived facies maps of geomorphic elements from a representative suite of images (Figures 6 & 7) illustrate some of the characteristics of selected carbonate build-ups. Bira's present-day carbonate platform can be elongated [Figure 6(a)] and have a narrow reef (14%) and wide reef sand apron (59%) [Figure 6(b)]. Putri platform and Bira platform are characterized by vegetated landmass or small islands, approximately 31% and 27%, respectively (Figures 6 & 7). These different geomorphic elements on each platform have a range of abundances, sizes, configurations, and relations. Reefal at both platforms is not dominant and can be discontinuous. Meanwhile, reefal in the Bira platform is continuous around all or most platforms. A shallow reef sand apron is evident between the reefal and the landmass or small island.

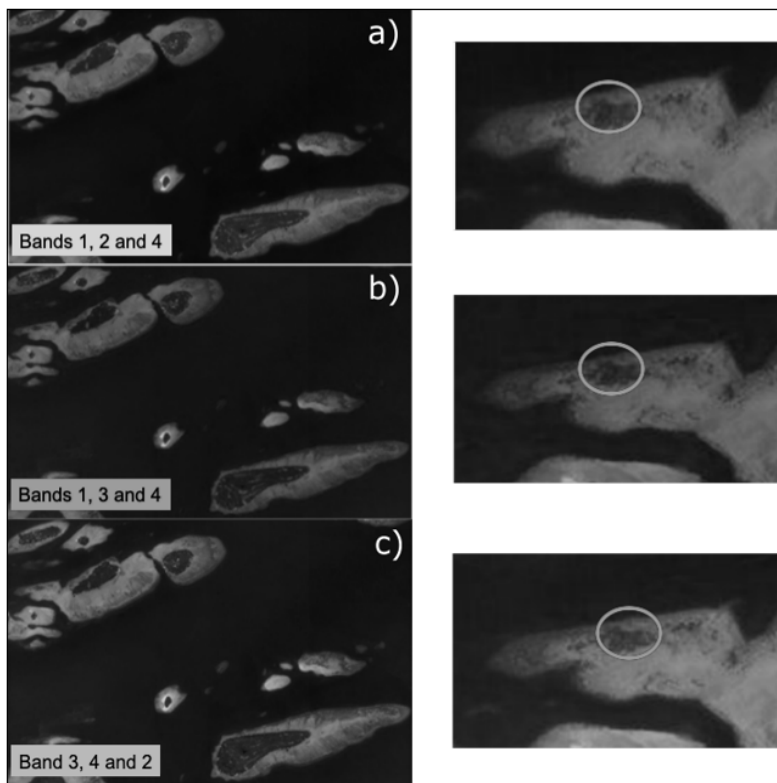


Figure 5. Satellite imagery with a combination of multispectral bands of a) 1, 2, and 4 bands, b) 1, 3, and 4 bands, and c) 3, 4, and 2 bands, which provide insight to differentiate geomorphological features in selected present-day carbonate platforms in Kepulauan Seribu.

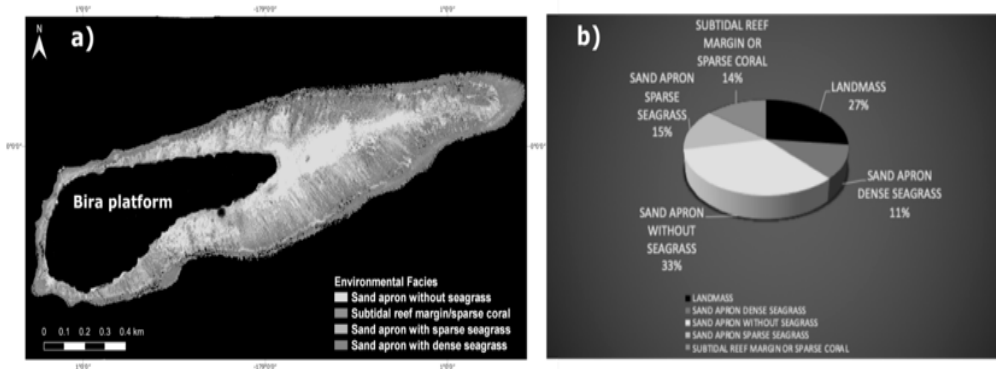


Figure 6. a) Satellite-derived facies map of Bira platform showing environmental facies with depositional environment overlays and b) Spatial facies percentages of Bira platform calculated from the Landsat-derived facies map

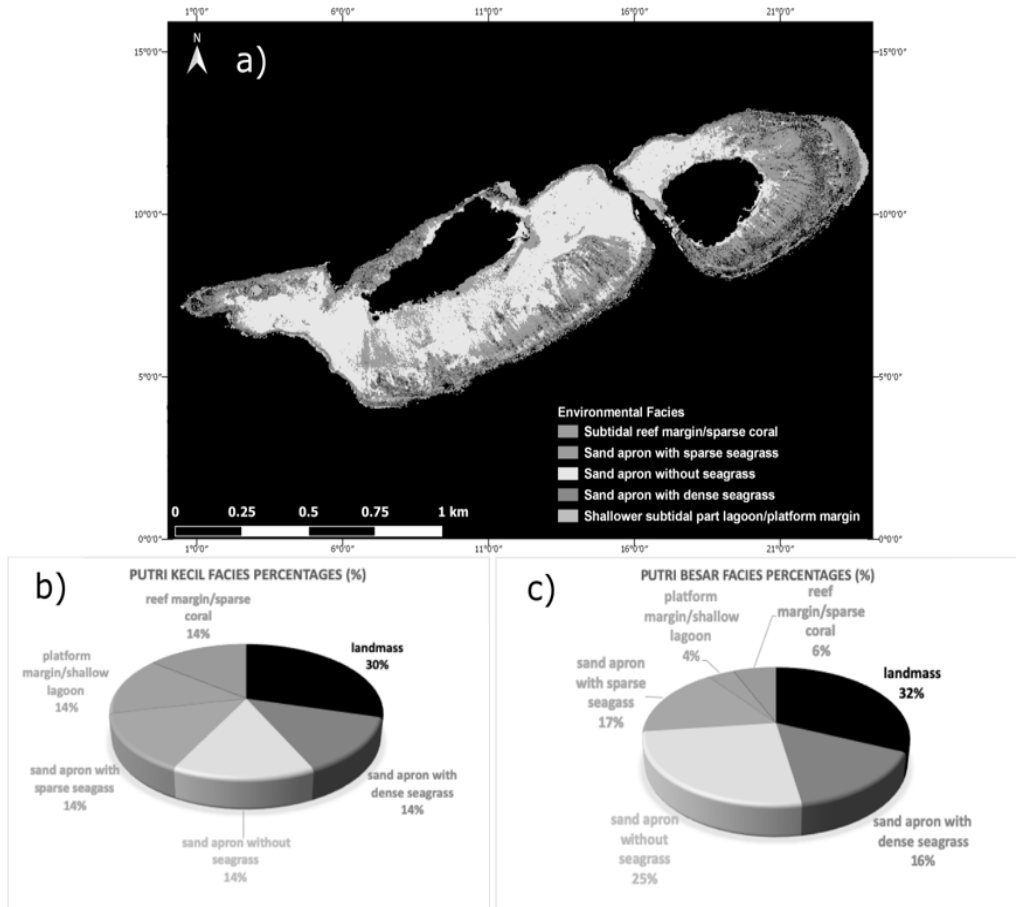


Figure 7. a) Satellite-derived facies map of Putri platform generated by utilizing supervise classification, b) Spatial facies percentages of Putri Kecil platform calculated from satellite-derived facies map, and c) Spatial facies percentages of Putri Besar platform calculated from satellite-derived facies map

Quantitative Facies Analysis

Quantitative physics analysis was performed on two selected carbonate platforms, namely the Bira and the Putri platforms. Satellite images from aerial photographs without sediment carbonate sample data show the total distribution of facies produced from the combined classification of TM bands and satellite image processing with a resolution of 15 m from the Holocene Kepulauan Seribu complexes. This quantitative analysis was performed to identify the potential of carbonate reservoirs based on the amount of uniformity (homogeneous/heterogeneous) distribution of facies from the two currently selected carbonate platforms located in the North-West Java Basin.

The total distribution of facies in the two selected carbonate platforms is summarized in Table 1. The table shows the differences in the distribution of facies and their uniformity on both platforms. The high number of facies distribution in a carbonate platform causes the level of a platform to be classified as a reservoir potentially accumulating hydrocarbon sources is predicted to be lower meanwhile carbonate reservoirs categorized as potential hydrocarbon reservoirs are characterized by a more uniform distribution of facies (Chalabi et al. 2012). For example, the Bira platform and Putri platform are characterized by 5 and 6 classes of carbonate facies where the uniformity distribution is homogeneous and is categorized as a present-day platform that has the potential to be a carbonate reservoir. However, the number of facies distributions recorded is still inaccurate due to sediment carbonate sampling. Furthermore, the accuracy analysis of the total carbonate facies in the research area has not been carried out due to several natural disaster factors and pandemic coronavirus in the Indonesia.

The total distribution of facies present in the carbonates of selected platforms is recorded in Table 1. The Bira platform records a perimeter of about 5.84 km. The larger the perimeter of a carbonate platform, the more complex the total distribution of facies on the platform is recorded (Harris & Vlaswinkel, 2008). Putri Kecil platform has a parameter of about 2.53 km, where the carbonate perimeter of this platform is recorded as the smallest compared to the Bira platform and Putri Besar platform. According to Harris and Vlaswinkel (2008), the small perimeter of the platform carbonate does not show such significant diversity of facies, and the total distribution of facies is also more uniform. The Putri Besar platform recorded a perimeter of about 4.49 km and is the second-largest carbonate platform after the Bira platform. These two carbonate platforms show the more homogeneous distribution of facies following the large perimeter of the platform. Chalabi et al. (2012) proved that the range of diversity of carbonate facies distribution in a platform is closely related to the number of facies distributed in the platform.

However, based on the results of quantitative analysis in the latest research shows the uniformity of the total distribution of facies in Bira, Putri Kecil, and Putri Besar carbonate platforms, where the range of facies diversity recorded is low (five facies classes for the

Bira platform and six facies classes for Putri Besar and Putri Kecil platform). Quantitative analysis of the total distribution of facies aims to investigate the relationship between the size of a carbonate platform and the heterogeneity facies distribution that has been successfully recorded. The authors found that the size of a carbonate platform did not affect the distribution of carbonate facies on the platform. This statement is in line with Harris and Vlaswinkel (2008), who argues that parameters such as platform size do not affect the distribution of facies in a carbonate build-up.

Table 1

Tabulation information of facies distribution on respective Holocene carbonate platforms

Percentage of each facies (%)			
	Bira platform	Putri Kecil platform	Putri Besar platform
Island/sand cay	27	30	32
Shallow lagoon/platform margin	none	14	4
Subtidal reef margin/sparse coral	14	14	6
Sand apron with dense seagrass	11	14	16
Sand apron without seagrass	33	14	25
Sand apron with sparse seagrass	15	14	17

Oceanographic Elements

This research was conducted in the Kepulauan Seribu patch reef complexes near Jakarta Bay in the Northwestern part of the Java Basin, Indonesia. The Kepulauan Seribu archipelago area is classified into three zones defined by Cleary and Hoeksema (2006): inshore, mid-shore, and offshore. Areas near Jakarta Bay (inshore zone) show high nutrient content levels (De Voogd & Cleary, 2008). The mid-shore zone is 22–40 km from Jakarta, and more than 60 km is categorized as an offshore zone. These three zones are characterized by varying levels of sea depth, where the inshore zone is classified as shallow with a depth of several meters up to a maximum depth of 30 m. Meanwhile, the mid-shore zone indicates a depth of more than 50 m and the offshore zone far from the coast has a seawater depth of more than 40 m (Figure 8).

According to Ali and Abolins (1999), carbonate build-ups are divided into two types: conical build-up and platform build-up based on geometric elements and morphology. The current research conducted in the Kepulauan Seribu archipelago is one of the Holocene-age build-up platforms in the Java Basin. Therefore, it has the potential to be utilized as a reference for the analog study. The Kepulauan Seribu build-up platform was growing on fault-bounded regional highs, an ideal region for the growth and development of carbonate

platform build-ups (Hamilton, 1979; Prior, 1986; Jordan Jr., 1998). The archipelago shows the position of modern carbonate build-ups experiencing uplifting due to a tectonic setting before the regional block that extends from the South to the North direction. In terms of geological and morphological elements, the archipelago forms a large-sized carbonate platform (Figure 8) with a West-East platform orientation caused by biological parameters; the bidirectional monsoon winds that blow across the Java Basin every year. From the top view of the aerial photograph, it can be observed that the present-day carbonate platform is characterized by a flatter top of the platform (Figure 8).

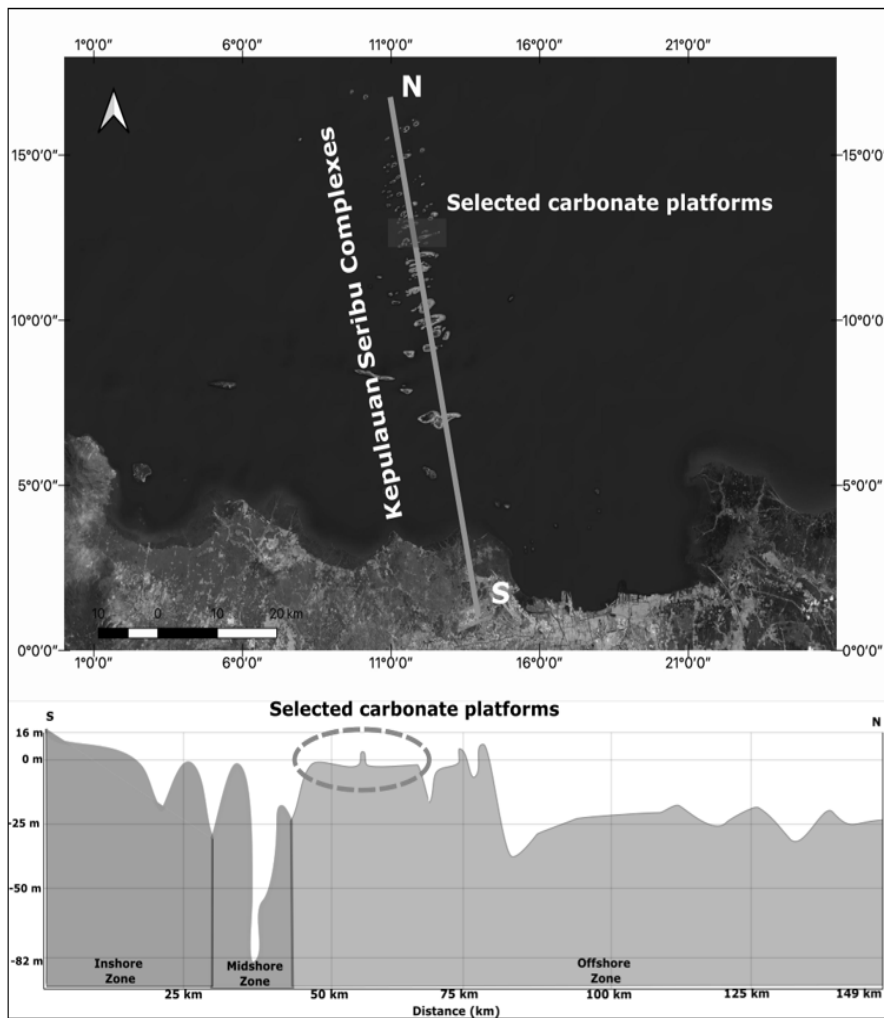


Figure 8. Cross-section from the onshore zone to the offshore zone

Indonesia's position is between two continents, Australia, and Asia's continental plate, separated by two oceans; the Pacific Ocean and the Indian Ocean, which eventually affect the monsoon winds that blow through the Kepulauan Seribu modern-day carbonate build-ups throughout the year. Further details on the orogenic effects and physical characteristics affecting monsoon winds in Indonesia are explained in detail in the paper by Tjasyono et al. (2008). Bidirectional monsoon winds are divided into western monsoon and eastern monsoon.

Jordan Jr (1998) described the Java Basin used to experience two seasons, namely the monsoon season and the dry season, due to the factors of monsoon wind exchange and followed by changes in the surface water flow of the Java Sea. Jordan Jr (1998), Naseer (2003), and Poerbandono (2016) agreed that the formation of carbonate build-ups strongly depends on seasonal wind and current ocean directions. The statement is supported by the data of a 20-year rainfall distribution study conducted by Tjasyono et al. (2008), which proves that the Java Sea experienced frequent rainfall from December to May and the least rain from June to November throughout the year.

Due to the annual wind pattern in the Java Basin, which highly impacted the formation and deposition of carbonate sediment in the Kepulauan Seribu archipelago, this phenomenon forms an individual carbonate platform pattern that comprises a single crest and asymmetrical dipping flanks. It is especially evident if observations are made on selected carbonate platforms (Bira and Putri platforms) which have two different sides: windward and leeward flanks. Both sides are also characterized by the accumulation of different skeletal carbonate sediments. However, the windward is characterized by a steeper flank than leeward due to the shape of the platform or a bidirectional monsoon pattern that contributes to the platform orientation pattern. The pattern can be viewed on most modern carbonate platforms.

In addition to the factor of bidirectional monsoon winds, another parameter contributing to the formation of modern carbonate build-ups is the salinity level of seawater. The salinity of the seawater influences the favorable condition for growing carbonate platforms. The salinity rate in the Java basin is uniform throughout the year. It, in turn, applies to ideal conditions for the formation and deposition of carbonates in the Java Sea (Figure 9). The salinity of the seawater in the Java Sea is recorded as moderately saline because of Java basin is located at the equator line, where the salinity of the seawater is 35 ‰. The high salinity value recorded at the equator is also due to the high evaporation process and the high rainfall rate in the Java basin (Prawiwardoyo, 1996).

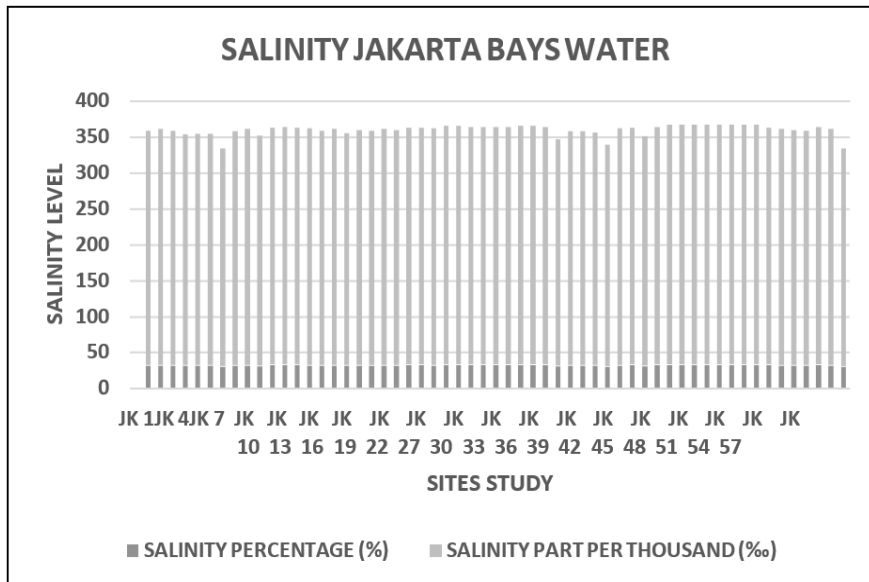


Figure 9. The salinity level of Jakarta Bay was modified by Williams et al. (2000)

CONCLUSION

This paper intends to describe and illustrate a satellite-based approach for mapping facies distribution. Landsat spectral data supervised classifications, and qualitative assessment of geomorphic patterns was utilized to demonstrate the facies distribution of selected Holocene carbonate platforms. In addition, satellite-derived facies maps were presented for the Putri and Bira platforms.

The supervised classification method applied for the mapping of environmental facies provides a holistic result by using quantitative and qualitative data, enabling the creation of sensible facies distribution maps. For example, the satellite-derived facies map provides insight into the diversity of carbonate facies and facies distribution on Indonesia's Kepulauan Seribu platform. Satellite-derived facies maps, meanwhile, offer a perfect description of depositional facies trends at the field scale in the oil and gas industry, thus allowing geologists or geophysicists to evaluate the quality and potential of an oil and gas reservoir.

Biological parameters such as monsoon winds and salinity rate control the patterns of carbonate formation in the shallow marine area of the Holocene, Kepulauan Seribu archipelago.

ACKNOWLEDGMENT

The authors are thankful to Southeast Asia Carbonate Laboratory (SEACaRL), Geoscience Department, Universiti Teknologi PETRONAS (UTP) for facilities and financial support.

REFERENCES

- Ahr, W. M. (2011). *Geology of carbonate reservoirs: The identification, description and characterization of hydrocarbon reservoirs in carbonate rocks*. John Wiley & Sons.
- Ali, M. Y., & Abolins, P. (1999). Central luconia province. *The Petroleum Geology and Resources of Malaysia, 1*, 369-392.
- Andrefouet, S., & Riegl, B. (2004). Remote sensing: A key tool for interdisciplinary assessment of coral reef processes. *Coral Reefs, 23*(1), 1-4. <https://doi.org/10.1007/s00338-003-0360-z>
- Chalabi, A., Pierson, B., & Ab Talib, J. (2012). Remote Sensing analysis of recent carbonate platforms, east of Sabah: Potential analogues for Miocene carbonate platforms of the South China Sea. *Indonesian Journal on Geoscience, 7*(3), 123-135.
- Cleary, D. F., & Hoeksema, B. W. (2006). Coral diversity across a disturbance gradient in the Pulau Seribu reef complex off Jakarta, Indonesia. In D. L. Hawksworth & A. T. Bull (Eds.), *Marine, Freshwater, and Wetlands Biodiversity Conservation* (pp. 285-306). Springer. https://doi.org/10.1007/978-1-4020-5734-2_19
- De Voogd, N. J., & Cleary, D. F. (2008). An analysis of sponge diversity and distribution at three taxonomic levels in the Thousand Islands/Jakarta Bay reef complex, West-Java, Indonesia. *Marine Ecology, 29*(2), 205-215. <https://doi.org/10.1111/j.1439-0485.2008.00238.x>
- Hamilton, W. B. (1979). *Tectonics of the Indonesian region*. USGS Publication.
- Harris, P. M. (1996). Reef styles of modern carbonate platforms. *Bulletin of Canadian Petroleum Geology, 44*(1), 72-81. <https://doi.org/10.35767/gscpgbull.44.1.072>
- Harris, P. M. (2010). Delineating and quantifying depositional facies patterns in carbonate reservoirs: Insight from modern analogs. *AAPG Bulletin, 94*(1), 61-86. <https://doi.org/10.1306/07060909014>
- Harris, P. M. M., & Vlaswinkel, B. (2008). Modern isolated carbonate platforms: Templates for quantifying facies attributes of hydrocarbon reservoirs. In J. Lukasik & J. A. Simo (Eds.), *Controls on Carbonate Platform and Reef Development* (Vol. 89, pp. 323-341). SEPM Special Publication. <https://doi.org/10.2110/pec.08.89.0323>
- Hoover, D. B., Klein, D. P., Campbell, D. C., & du Bray, E. (1995). Geophysical methods in exploration and mineral environmental investigations. *Preliminary compilation of descriptive geoenvironmental mineral deposit models: USGS Open-File Report, 95*(831), 19-27.
- Jordan Jr, C. F. (1998). *The sedimentology of Kepulauan Seribu: A modern patch reef complex in the west Java Sea, Indonesia*. Indonesian Petroleum Association.
- Kaczmarek, S. E., Hicks, M. K., Fullmer, S. M., Steffen, K. L., & Bachtel, S. L. (2010). Mapping facies distributions on modern carbonate platforms through integration of multispectral Landsat data, statistics-based unsupervised classifications, and surface sediment data. *AAPG Bulletin, 94*(10), 1581-1606. <https://doi.org/10.1306/04061009175>

- Masek, J. G., Honzak, M., Goward, S. N., Liu, P., & Pak, E. (2001). Landsat-7 ETM+ as an observatory for land cover: Initial radiometric and geometric comparisons with Landsat-5 Thematic Mapper. *Remote Sensing of Environment*, 78(1-2), 118-130. [https://doi.org/10.1016/S0034-4257\(01\)00254-1](https://doi.org/10.1016/S0034-4257(01)00254-1)
- Murai, S. (1993). *Remote sensing notes*. Japan Association of Remote Sensing.
- Naseer, A. (2003). *The integrated growth response of coral reefs to environmental forcing: Morphometric analysis of coral reefs of the Maldives* (Doctoral dissertation). Dalhousie University, Canada.
- Poerbandono. (2016). Wind characteristics and the associated risk of erosion in Seribu Islands patch reef complexes, Java Sea, Indonesia. In *AIP Conference Proceedings* (Vol. 1730, No. 1, p. 080001). AIP Publishing LLC. <https://doi.org/10.1063/1.4947416>
- Prawiwardoyo, S. (1996). *Meteorologi*. Penerbit ITB.
- Prior, S. W. (1986). *Bima Field, Indonesia, a sleeping giant*. Circum Pacific Council Publications.
- Purkis, S. J. (2005). A reef-up approach to classifying coral habitats from IKONOS imagery. *IEEE Transactions on Geoscience and Remote Sensing*, 43(6), 1375-1390. <https://doi.org/10.1109/TGRS.2005.845646>
- Purkis, S. J., Kohler, K. E., Riegl, B. M., & Rohmann, S. O. (2007). The statistics of natural shapes in modern coral reef landscapes. *The Journal of Geology*, 115(5), 493-508.
- Rankey, E. C. (2016). On facies belts and facies mosaics: Holocene isolated platforms, South China Sea. *Sedimentology*, 63(7), 2190-2216. <https://doi.org/10.1111/sed.12302>
- Riegl, B. M., Halfar, J., Purkis, S. J., & Godinez-Orta, L. (2007). Sedimentary facies of the eastern Pacific's northernmost reef-like setting (Cabo Pulmo, Mexico). *Marine Geology*, 236(1-2), 61-77. <https://doi.org/10.1016/j.margeo.2006.09.021>
- Schlager, W., & Purkis, S. J. (2013). Bucket structure in carbonate accumulations of the Maldives, Chagos and Laccadive archipelagos. *International Journal of Earth Sciences*, 102(8), 2225-2238. <https://doi.org/10.1007/s00531-013-0913-5>
- Tjasyono, H. K. B., Gernowo, R., Sri Woro, B. H., & Ina, J. (2008, September 16-18). The character of rainfall in the Indonesian monsoon. In *The International Symposium on Equatorial Monsoon System* (pp. 1-11). Yogyakarta, Indonesia.
- Utami, D. A., Reuning, L., & Cahyarini, S. Y. (2018). Satellite-and field-based facies mapping of isolated carbonate platforms from the Kepulauan Seribu Complex, Indonesia. *The Depositional Record*, 4(2), 255-273. <https://doi.org/10.1002/dep2.47>
- Vincent, R. K. (1997). *Fundamentals of geological and environmental remote sensing*. PrenticeHall.
- Williams, T. M., Rees, J. G., & Setiapermana, D. (2000). Metals and trace organic compounds in sediments and waters of Jakarta Bay and the Pulau Seribu Complex, Indonesia. *Marine Pollution Bulletin*, 40(3), 277-285.
- Wilson, J. L. (1997). Carbonate depositional environments and diagenesis. In I. Palaz & K. J. Marfurt (Eds.), *Carbonate Seismology* (pp. 9-28). Society of Exploration Geophysicists.
- Yu, S. L., Westfechtel, T., Hamada, R., Ohno, K., & Tadokoro, S. (2017). Vehicle detection and localization on bird's eye view elevation images using convolutional neural network. In *2017 IEEE International Symposium on Safety, Security and Rescue Robotics (SSRR)* (pp. 102-109). IEEE Publishing. <https://doi.org/10.1109/SSRR.2017.8088147>

Hybrid Lean Practices Integrated with IR 4.0 and Sustainability in Malaysia Food and Beverages Companies: Conceptual Framework and Hypothesis Development

Muslim Diekola Akanmu* and Norshahrizan Nordin

Faculty of Applied and Human Sciences, Universiti Malaysia Perlis, 01000 UniMAP, Kangar, Perlis, Malaysia

ABSTRACT

The growing competition within manufacturing practices has motivated organizations to upgrade their conventional production system to a smart, sophisticated systems. This study evaluates the impact of lean manufacturing practices (LMP) and industrial revolution 4.0 technologies on sustainability in the food and beverages industry. Past literature has revealed that lean practices significantly affect sustainable performance. However, the integrated effects of lean manufacturing practices and IR 4.0 technologies on sustainable performance have not been examined empirically. In order to fill the void of this gap, this study intends to have a preliminary investigation of the combined effects of LMP and IR 4.0 technologies on sustainable performance, specifically in the food and beverages industry. Furthermore, the study aims to confirm the future direction of the food industry that is recently employing new technologies in its manufacturing systems. This study is underpinned by the theories of contingency and practice-based view by highlighting the contributions of operations management practices to implement successful strategies in enhancing sustainability performance in food and beverages companies through performance variations. This study extends the current literature on IR 4.0 technologies and lean manufacturing practices

as enablers of economic, environmental, and social sustainability. Also, the study provides implications and future direction for industry consultants, practitioners, and academicians.

Keywords: Food and beverages, industrial revolution 4.0 technologies, lean manufacturing practices, sustainable performance

ARTICLE INFO

Article history:

Received: 15 September 2021

Accepted: 7 February 2022

Published: 25 May 2022

DOI: <https://doi.org/10.47836/pjst.30.3.29>

E-mail addresses:

diekola@unimap.edu.my (Muslim Diekola Akanmu)

norshahrizan@unimap.edu.my (Norshahrizan Nordin)

*Corresponding author

INTRODUCTION

Sustainable performance in the service and manufacturing sectors has gained attention in various business practitioners' research documents and projects. The practice and theory of sustainable performance have become a critical issue in the dynamic business market within manufacturing practices. There is urgency in discussion regarding sustainability in manufacturing industries. However, this discussion was mainly focused on the societal level—and sometimes on environmental issues; it is now obvious there is an increase in its relevance for manufacturing companies worldwide. Many organizations have taken these opportunities to implement sustainable practices in product quality, competitive positioning, customer relationship, environmental management and supply chains management, environmental costs, operational practices, strategic plan and action, material selection, and continuous growth and expansion. However, studies have revealed an insufficient number of research that elucidate the limitations of lean manufacturing practices. The emerging trend of industrial revolution 4.0 provides the necessary platforms for both academic and industrial sectors to grow further on this methodology in solving problems as lean practices have been adopted by different industries. However, barriers and constraints such as social, financial, capacity, and steering factors are created by sustainability for professional practices to successfully implement sustainable practices (Ali & Alkayed, 2019). Therefore, this study intends to systemically review past literature to identify the emerging trends followed by developing a conceptual framework, questionnaire development, and hypothesis development.

LITERATURE REVIEW

Food and Beverages Industry in Malaysia

Food production and consumption are major causes of global environmental degradation (Salim et al., 2018). The agro-based industries are major providers of income and employment worldwide. In recent decades, food and beverage companies (FBC) have significantly grown in which the agricultural development policies have changed from a production-oriented approach to a broader system that emphasizes agro-food chain coordination, value creation, and institutional strategies under which the chain operates (Konig et al., 2013). However, agro-allied industries face challenges to survival due to the unfriendly operating environment and global economic meltdown. The concern for sustainability can be traced back to the third Malaysia plan between 1976 and 1980 when the country built its economic foundation. Through environmental stewardship, the Worldwide Fund (WWF) revealed that in 2007, 57% of the population was reported to have good environmental behavior in Malaysia. In recent times, the food processing and the agro-allied industries are becoming prominent with the eradication of certain food grades and their importation as enjoined by the government policy, according to the Malaysia Competition Commission (MyCC, 2019).

According to Glover et al. (2014), sustainability practices in food and production are critical, precisely in productivity. Currently, the food industry must adapt alongside other industries to the new challenges of sustainable production (Glover et al., 2014). The production index of FBC has increased by 4.4% as a result of strong domestic demand within the sector with a significant increase in the record of productions of sugar confectionery, cocoa and chocolate (15.5%), sugar refineries (1.4%), biscuit (12.2%), and other processed food (8.8%), according to Saleh and Ndubisi (2006). With the yearly importation of more than 12 billion ringgit, Malaysia is still a net importer of food products despite the fact that the export performance of this sector has multiplied over the year (FMM, 2017). Few attempts, however, have been made to provide a holistic approach to the identification of the potential pathways, drivers, and barriers to overcome the challenges (Boiral et al., 2017).

Sustainable Performance

The main inductors of sustainability in any organization are the internal strategic practices and organizational factors that must be considered from the upper management to the lower management (Caiado et al., 2018). Sustainable performance is achieved in business when a firm or company builds continuous values for its shareholders and stakeholders while abiding by environmental regulations (Brent & Labuschagne, 2004). The sustainable performance value has a few essential parts: making the shareholders and customers happy and, more importantly, performing well for the environment and society (Hassan et al., 2018). In addition, sustainable performance comprises practices that socially facilitate the useful life of an organization, promoting the capacity to renew and maintain the viability of the ecosystem, provide for the living beings, and promote the ability of a society to sustain itself in solving the major crisis and maintain decent welfare, personal freedom and participation for human present and future generation (Dunphy, 2011). Furthermore, sustainable performance is a product of executing transactions, and business toward a sustainable enterprise creates a constructive and innovative corporate culture (Hassan et al., 2018).

The developed healthy culture can then create an enabling environment and high performance to maximize the use of available assets to lead to good outcomes within the economy and society (Dunphy, 2011). There are three categories of sustainable performance: social, environmental, and economic sustainable performance (Akanmu et al., 2017). As confirmed by the European Commission, sustainable development strategies emphasize the significance of economic growth, environmental protection, and social cohesion (Pei et al., 2010). Sustainable management is addressed by Guan et al. (2010) as a modern pattern of management focusing on the joint integration of the environment, economy, and society through processes such as procurements, production, packaging, storage, consumption, transportation, and end-life product disposal as enhanced by technologies with the final goals to achieve economic, societal and environmentally sustainable development.

Lean Manufacturing Practices

Lean manufacturing is a methodology designed to reduce the cost of production and waste minimization (Alhuraish et al., 2016). Similarly, lean manufacturing is a business method or strategy that facilitates process performance and increases customer satisfaction and triple-bottom-line results (Snee, 2010). Lean manufacturing started with the Toyota production system (TPS), where the system was integrated with practices such as Just-in-time to improve time delivery and quality. Nordin et al. (2014) affirmed that the TPS started the lean manufacturing concept, and it aimed to improve quality and reduce cost through non-value added and waste minimization. Lean manufacturing is formed from different practices (Yang et al., 2017). Similarly, the lean manufacturing practices cluster includes human resources management, productive maintenance, just-in-time, total quality management, total preventive maintenance employee involvement, and controlled processes. Recent studies have proven the importance of customer participation and downstream collaboration (Martinez-Jurado & Moyano-Fuentes, 2014). Lean practices are product design, customer relationship, supplier relationship, manufacturing planning and control, process and equipment, and human resources. These categories are suitable for all industries (Bergmiller, 2006). Therefore, forward coordination with the customers and backward coordination with the suppliers is important to implement lean manufacturing practices successfully. In that manner, the products are designed, produced, packaged, and specifically delivered to meet the operational and environmental objectives (Dües et al., 2013). These objectives seeking to achieve lean management performance include natural environment, sustainable and ecological performance dimensions.

Industrial Revolution 4.0 Technologies

In the last 30 years, the history of the industrial revolution has highlighted a shift in power from power sources to automated production, information technology, and connectivity. Notably, the industrial revolution revolves around three main categories: technologies, processes, and people, with one of these driving the change and initiating a circular pattern of mutual influence. According to Ahuett-Garza and Kurfess (2018), Industrial Revolution 4.0 is the digital manufacturing system provided by successfully incorporating information technologies, techniques, and production processes. The main objective of Industrial Revolution 4.0 (IR 4.0) is to improve the efficiency and responsiveness of the manufacturing systems. The IR 4.0 technologies operating on vertical and horizontal manufacturing system integration are influenced by real-time data interchange between many partners in a manufacturing value chain (Fatorachian & Kazemi, 2018). Additive manufacturing (AM), the internet of things (IoT), robotic systems (RS), big data analytics (BDA), augmented reality (AR), cloud computing (CC), and cyber-physical system (CPS) are identified as the significant Industrial revolution 4.0 technologies that promote process integration, leading to sustainable performance (Kamble et al., 2018a).

METHODOLOGY

It is imperative to carefully design the questionnaire items to reflect and measure the variables employed for the research framework. The items for the questionnaires are developed from past studies—adapted or adopted (Zikmund et al., 2010). Items measuring the lean manufacturing practices (i.e., continuous flow, employee involvement, supplier involvement, setup time reduction, customer involvement, just in time, supplier development, total productive maintenance, statistical process control and pull system), IR 4.0 technologies, and sustainable performance of the company are divided into three sections. The survey instrument is constructed using related literature as guidance. Meanwhile, supporting literature is cited adequately in places with newly developed items.

Sustainability Performance Dimensions

Sustainability performance is measured using social, economic, and environmental performance. A total of twenty items are adopted from the study of Brent and Labuschagne (2004) and Akanmu et al. (2021). The last three years are designated as the assessment period for the companies. Table 1 presents the items measuring sustainability performance and their respective coding.

Table 1

Sustainable performance coding

Economic Sustainability Performance Items	Code
<i>In the last three years, our company has achieved:</i>	
Reduced costs of production	EP01
Improved profits	EP02
Reduced product development costs	EP03
Decreased energy costs	EP04
Reduced inventory costs	EP05
Reduction in rework and rejection cost	EP06
Decrease in the purchase cost of raw material	EP07
Decrease in the cost of the waste treatment	EP08
Social Sustainability Performance	
Improved condition of work	SP1
Improved safety in the workplace	SP2
Improved health of the employees	SP3
Improved relations on labor	SP4
Improvement in morale	SP5
Decrease in work pressure	SP6

Table 1 (Continue)

Economic Sustainability Performance Items	Code
In the last three years, our company has achieved:	
Environmental Sustainability Performance	
Reduced solid wastes	EVP01
Reduced liquid wastes	EVP02
Reduced gas emission	EVP03
Reduction in energy wastes	EVP04
Decreased consumption of toxic/hazardous/harmful materials	EVP05
Improved environmental condition of the company	EVP06

Lean Manufacturing Practice Dimensions

The construct domain specification and item generation are developed using the first set of lean manufacturing practice constructs proposed by Shah and Ward (2007). These constructs are continuous flow, employee involvement, supplier involvement, set-up time reduction, customer involvement, just in time, supplier development, statistical process control, pull system, and total productive maintenance, as indicated in Table 2.

Table 2

Lean manufacturing practices coding

Item	Code
Supplier Involvement	
Our organization is in close connection always with the suppliers	SI1
Our company provides feedback to the suppliers on delivery and quality performance	SI2 SI3
Our company applies utmost efforts in creating a long-term relationship with the suppliers	
Just-in-time	
All our key suppliers involved in a new process of product development	JIT1
Our organization is delivered by our suppliers on a just-in-time basis	JIT2
Our organization has a supplier certification program in place	JIT3
Supplier Development	
Our company's supplier strives to achieve cost reduction annually	SD1
Our key supplier is situated in close vicinity to our organization	SD2
We have established a system to convey important issues to the suppliers	SD3
Our company makes an effort to have a lesser number of suppliers in every category	SD4
The inventories are managed by the key suppliers	SD5
Supplier evaluation is not done per unit price but on the total cost purchase	SD6

Table 2 (Continue)

Item	Code
Customer Involvement	
Our organization is in close relationship with the customers	CI1
Our company gets feedback on delivery and quality performance from the customers	CI2
Our firm involves customers in new and existing product development and improvement process	CI3
The customers/clients participate in the existing and new product development and improvement process	CI4
The customers share their future and present demands with our organization	CI5
Continuous Flow	
Our products are categorized into classes with the same processing criteria	CF1
Our products are categorized into classes with the same routing criteria	CF2
Our equipment is classified to provide continual flows of products	CF3
Our product determines the factory layout	CF4
Pull System	
Our productions are pulled by the shipments of the completed products	PS1
Our productions are at workstation are pulled by the present requirement of the next workstation	PS2
A production system of pull is adopted	PS3
Our company uses a container of signal or Kaban for production control	PS4
Total Productive Maintenance	
Our company is daily dedicated to planning activities related to equipment maintenance	TPM1
Our company carries out daily maintenance of all equipment	TPM2
Our company maintains excellent conditions for all equipment	TPM3
Our company posts records of equipment maintenance for active sharing with the employees	TPM4
Statistical Process Control (SPC)	
Our company covers most of the process/equipment under SPC	SPC1
Our company uses statistical techniques to control the process variance	SPC2
Our company uses charts as tools to show defect rates	SPC3
Our company uses fishbone illustration to identify causes of quality problem	SPC4
Our company conducts research on process capability before product launching	SPC5
Employee Involvement	
Our company believes that employee plays a significant role in solving problems	EI1
Our employees motivate the company through a suggestion program	EI2
Our employees do lead the process/product improvement efforts	EI3
Our company provides cross-functional training for the employees	EI4

Table 2 (Continue)

Item	Code
Setup Time Reduction	
Our company provides various practices on setup reduction techniques for our employees	STR1
Our company works continuously towards setup time reduction	STR2
Our company has a high setup time of equipment	STR3

Industrial Revolution 4.0 Technologies Dimensions

Most organizations are yet to explore the sophisticated features of IR 4.0 technologies; therefore, they are uncertain about what benefits of IR 4.0 Technologies would be in the future (Tortorella & Fettermann, 2018). Furthermore, Kamble et al. (2018b) posit that the adoption of IR 4.0 technologies in manufacturing industries is still at the infant stage but slowly gathering momentum. Therefore, the degree of implementation of IR 4.0 Technologies are aimed to be measured by items but not the successful level of its implementation. Table 3 presents the measuring items for IR 4.0 Technologies as adopted from the Kamble et al. (2020) study.

Table 3

Industrial revolution 4.0 technologies coding

Items	Code
Our company is planning to implement cloud computing	IR1
Our company is planning to implement big data analytics	IR2
Our company is planning to implement the internet of things	IR3
Our company is planning to implement additive manufacturing	IR4
Our company is planning to implement a robotic system	IR5
Our company is planning to implement augmented reality	IR6

Therefore, from the theoretical background of the trending issues, the framework of this study is developed, as illustrated in Figure 1.

The theories of practice-based view (PBV) and contingency are adopted from the theoretical background to develop the research hypotheses. According to Sousa and Voss (2008), the theory of contingency provides guidelines on the distinctive selection of sets of practices in operations management that are most suitable in a particular context of an organization. In other words, Bromiley and Rau (2016) posit that PBV is adopted as some organizations do not make use of all the existing practices that are beneficial; thus, performance variations are explained based on the use of a particular practice.

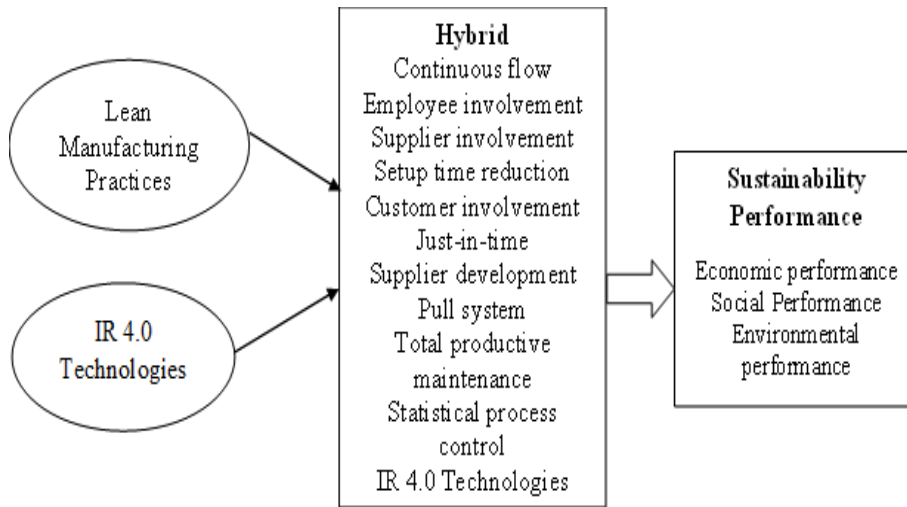


Figure 1. The development stage of the conceptual framework of the study

RESULTS AND DISCUSSION

From the past studies, the hypotheses formulation of this study is highlighted as follows:

Relationship Between Lean Manufacturing Practice and Sustainability Performance

Relationship Between Supplier Involvement and Sustainable Performance. Past literature (e.g., Vachon, 2007; Zhu et al., 2010) has shown that sustainability performance is significantly affected by supplier involvement in an organization. The collaboration with suppliers by an organization environmentally and economically improves sustainability performance (Vachon & Klassen, 2006). Vachon (2007) added that collaborative relationship with suppliers leads to effective adoption, development, and lean manufacturing towards social contribution. Companies can be disciplined by the stakeholders when they become aware of unacceptable sustainability-related conditions among suppliers arguing that buyers are capable of averting such wrongdoings through supplier selection and involvement (Hofmann et al., 2014; Busse et al., 2016).

Bussie (2016) reported that supplier involvement is related to economic and environmental goals (e.g., waste reduction or energy efficiency), and social-ethical goals are directly tied to sustainability-related conditions of the company. The importance of the relationship between supplier involvement and sustainability performance is also reported by Zhu et al. (2010). The study showed that the absence of supplier collaboration weakens the sustainability improvement performance among manufacturing companies. Following the past mentioned above studies, it is proposed that:

H1: supplier involvement has a positive and significant relationship with sustainable performance

Relationship between Just in Time and Sustainable Performance. According to Bicheno and Holweg (2009), JIT and automation are the two pillars required to support the Toyota Production System. Similarly, Zelbst et al. (2014) mentioned that JIT is a part of lean manufacturing practices that needs timely and accurate information sharing to be successfully implemented. In lean manufacturing, accurate inventory data are important as safety stocks, and large buffers are removed. Zelbst et al. (2014) reported that a digitized sustainable supply chain provides accurate and timely data about the locations and levels of inventories. In addition, JIT provides machine intelligence to distinguish between abnormal and normal operations. Thus, a machine will stop if a problem cannot be sustained to avoid producing defective products (Buer et al., 2018). The implementation of JIT provides machine intelligence for production, therefore facilitating automation. Thoben et al. (2014) categorically state that with JIT, the machines can report and analyze deviations and causes faster and automatically initiate measures.

Furthermore, JIT is also one of the tools of lean practice that offers organization assistance by providing strategies on waste reduction besides kaizen events, statistical process control, cellular manufacturing, supplier relationship, value stream mapping, visual management, and plant layout reconfiguration, analytic tools, and everyday work. Chiarini (2014) reported that JIT has effects on reducing manufacturing companies' social and environmental impact. Therefore, many organizations have adopted the tool to make more social and environmental progress (Cherrafi et al., 2016). With the above discussion, this study hypothesized that:

H2: Just in time has a positive and significant relationship with sustainable performance

Relationship between Supplier Development and Sustainable Performance. Supplier development is "any activity undertaken by a buying firm to improve either supplier performance, supplier capabilities, or both, and to meet the buying firm's short- and/or long-term supply needs" (Krause et al., 2000). Conventionally, supplier development focuses on economic sustainability and poses to grow the economic capabilities and performance of the suppliers as related to quality: cost and delivery. From the concept of the triple bottom line, supplier development comprises attaining environmental goals (e.g., waste reduction or energy efficiency), economic goals, and socio-ethical goals (e.g., abstinence from dysfunctional behavior or fairness of wages) (Busse et al., 2016). Similarly, supplier development in terms of social and environmental goals implies indirect "enlightened self-interest" of the buyer and is directly tied to the buyers' interests in terms of the economic goals (Busse, 2016).

According to Foerstl et al. (2015), supplier development has recently attracted scholarly studies in response to the organization's stakeholders' requests for practical, sustainable situations. Some past studies (e.g., Blome et al., 2014; Sancha et al., 2015) focused on green practices that enable suppliers to reduce the adverse effect of the natural environments on social practices. Based on the arguments presented by Haigh and Hoffmann (2014) that sustainability measures can influence stakeholder reactions and Busse (2016) stated that both are in the enlightened self-interest of the buyers, it is therefore hypothesized that:

H3: Supplier development has a positive and significant relationship with sustainable performance

Relationship between Customer Involvement and Sustainable Performance. According to Danarahmanto et al. (2020), a business model needs to support customer involvement or participation to achieve sustainable performance. A past study by Chen et al. (2012) showed that customers are ready to liaise to achieve environmental sustainability with the manufacturers and willing to patronize environmentally responsible companies. The study shows a significant relationship between customer involvement and sustainable performance where these technology-oriented customers access newly developed technological features of a product or service through purchase. Organizational sustainability performance is affected by economic, social, and environmental performance (Chen et al., 2012).

Also, Andic et al. (2012) reported that customer involvement determines an organization's economic performance and competitive advantage. Eltayeb et al. (2011) added a significant and positive relationship between customer involvement and sustainability performance. Customer involvement is always important when a new product is introduced, as the features of the products need to be presented and clearly defined by manufacturers (Chan et al., 2012).

In addition, Ellram et al. (2008) emphasize that the relationship between the customers and the manufacturers can lead to sustainable organizational performance. Simpson et al. (2007) added that the collaboration level of customers has a significant relationship with environmental and social sustainability performance. Similarly, researchers such as Chang and Taylor (2016) and Joo and Shin (2017) found a significant relationship between customer involvement and sustainable performance. This study, therefore, hypothesized that:

H4: Customer involvement has a positive and significant relationship with sustainable performance

Relationship between Continuous Flow and Sustainable Performance. According to Benavent et al. (2005), lean manufacturing practices increase customer satisfaction through the continuous process flow. In order to effectively integrate every aspect of the organizational process, such as the management styles and activities, every organization

should create continuous improvement practices. Baker (2003) posits that the expected final result is to achieve a high level of customer satisfaction. Sagandira et al. (2022) reported that continuous flow of advanced inline flow downstream processing, artificial intelligence, robotics, in-process monitoring by process analytical technology in flow and flow automation dramatically enhances quality, agility, flexibility, and efficiency for sustainable manufacturing.

Furthermore, Escrig-Tena (2004) states that although there are many factors such as the top management support and effective information system for enhancing and facilitating continuous improvement practices in an organization, quality-conscious customers and critical innovation are the drivers of continuous sustainable flow. Iranmanesh et al. (2019) added that continuous flow of waste reduction is a prerequisite factor for achieving the aim of lean manufacturing, which is the foundation of successful sustainable lean practices. Studies showed that continuous flow has a significant and positive effect on an organization's long-term competitive position, sustainable performance, and productivity (e.g., Fotopoulos & Psomas, 2010; Yusuf et al., 2007). However, the study of Burli et al. (2012) reported no significant effect between continuous flow and sustainable performance. Thus, this study hypothesized that:

H5: there is a significant relationship between continuous flow and sustainability performance

Relationship between Pull System and Sustainable Performance. Womack et al. (2007) argued that the introduction of the pull system is part of the five methodologies: value expectation from the customer perspective when the flow is not possible as part of the lean, identification of the value stream to each service or product to remove or reduce wastes, implement continuous flow, and finally achieve perfection. The pull system consists of squares, Kanban, and signal containers for production controls. Similarly, the pull system comprises those practices with the lowest adoption. Therefore, the low applicability of a pull system support in the food industry can lead to difficulty implementing the pull construct (Panwar et al., 2017).

Akkerman and van Donk (2007) reported that production is often continuous or in batch in the food industry. Abdulmalek et al. (2006) added that the beverages industry often embraced continuous production. The authors added that although tools such as the Kaban pull system in a continuous environment may not be realistic, the availability and reliability of the equipment are critical. Therefore, practices such as pull are very crucially useful for sustainability. Hallam and Contreras (2016) reported that lean is promulgated by a pull system to align production capabilities with customer rate of demands and pursue sustainability to remind that the process of transitioning to lean should never end. The adoption of pull practices is also affected by the equipment used in the process. There

is less need for equipment to be used in other products or services or fast changeover practices as the equipment becomes specialized more for a particular product or production (Abdulmalek et al., 2006).

H6: Pull system has a positive and significant relationship with sustainable performance

Relationship between Total Preventive Maintenance and Sustainable Performance. According to Shah and Ward (2002), lean manufacturing is a synergetic integration of different reinforcing practices classified into four complementary practices: human resources management, total preventive maintenance, total quality management, and JIT. Some lean tools in a manufacturing company are more applicable largely than others. The tools such as team-based problem solving, value stream mapping and work standardization, total productive maintenance, 5S, and quality management programs do not depend on the process characteristics. Nevertheless, companies that adopt total preventive maintenance and pursue social and environmental sustainability can align their practices to avoid contradictory impacts. Herrero et al. (2002) reported that total preventive maintenance is related to social practices concerning social sustainability. Thus, there should be a parallel between safety principles and quality.

According to Longoni and Cagliano (2015), the strategic alignment of the lean manufacturing bundles (such as HRM, TPM, TQM, and JIT) is affected by work involvement and cross-functional executive participation with social and environmental practices and goals. In particular, the effect of TPM on the practices of lean manufacturing aligns with social and environmental sustainability. Thus, the implementation of lean manufacturing as aligned with social and environmental sustainability is positively affected by preventive maintenance. Kovilage (2020) stated that preventative maintenance is the dominant lean practice that determines sustainable performance. In addition, Kovilage (2018) reported that total preventive maintenance lessens the likelihood of unexpected equipment breakdown when regularly performed.

Moreover, Herrero et al. (2002) stated that many industries had been explored TPM practices with the advanced manufacturing model to develop their organizational social, and environmental performance. For instance, operation executives design TPM to identify and address safety, environmental and health issues while monitoring social and environmental indicators. Thus, TPM is equally designed to reduce material waste and energy loss. This study therefore proposed:

H7: There is a positive and significant relationship between total preventive maintenance system and sustainable performance

Relationship between Statistical Process Control and Sustainable Performance. Kumar et al. (2006) found that lean practices play important roles in minimizing non-value-added activities and wastes across organizational levels by applying statistical techniques and

tools that can take organizations to improved performance or process. Laureani and Antony (2017) reported that lean practices require tools from statistical process control to derive the best outcome and increase accuracy and speed. Finally, Neuman and Cavanagh (2000) showed that lean manufacturing has developed into a flexible and comprehensive system of maximizing, achieving, and sustaining a successful business, uniquely driven by a mutual understanding of customer satisfaction, diligent attention to reinventing, managing, and improving business performance and discipline use of data, fact and statistical analysis.

According to Aziz (2015), the dimensions of statistical process control are among the least adopted practices by any sector. Financial capabilities are required by the practices to get the belt team trained. These practices are challenging in sectors with a low margin that is constantly looking for ways to minimize costs and rely on knowledge of statistical techniques and are relatively considered too advanced and complex for the sector. The sector less considers these practices in the first instance, but their adoption increases with the statistical process control, showing that they are suitable for the sector. After considering the literature above, it can be empirically proposed that:

H8: Statistical process control has a positive and significant effect on sustainable performance

Relationship between Employee Involvement and Sustainable Performance. Employee involvement is one of the lean manufacturing practices that comprise employee participation, employee empowerment, and employee training. Yusuf et al. (2007) posit that employees need the motivation to involve in the financial breakthrough, decision making, and problem-solving of an organization. Furthermore, it indicates that every employee can be involved in the corporate business and aware of the organization's economic performance's current and possible future situation (Diekola, 2016). Therefore, employees can be more closely involved in the core business and positively contribute to sustainable organizational performance.

Employees are motivated by being allowed to practice, thereby becoming closer to the objectives and the organizational goals. In lean manufacturing practices, employee involvement is a critical element. Therefore, a model of lean manufacturing practices that comprises employee involvement should be developed to support the employees and successfully achieve sustainable performance. Additionally, lean manufacturing practices are related positively to sustainable organizational performance with the support of employees (Akdere & Yilmaz, 2006). Employees can add value to the organization if they are given enough training, empowerment, and teamwork involvement, as they are considered the live asset of the organization (Akanmu et al., 2020). Therefore, employee involvement is one of the major drivers of any successful implementation of lean manufacturing practices in any organization. Arawati (2005) reported a significant relationship between employee involvement and sustainability performance in the same view. Therefore, it can be proposed that:

H9: Employee involvement has a positive and significant relationship with sustainability performance

Relationship between Set-up Time Reduction and Sustainable Performance. A well-organized environment in any industry requires a continuous implementation of lean manufacturing practice with setup time reduction (Dora et al., 2013). The adoption of lean manufacturing affects any sector's setup time reduction characteristics to a certain level. For example, the compulsory clean process, which must be performed properly, affects the setup time reduction in the food and beverages sector to ensure food safety and avoid contamination. The setup time reduction is adopted mostly by companies with a high percentage of specialized equipment, focusing on sustaining the equipment's availability and reliability criticality (Dora et al., 2013). However, the setup time reduction practice is rarely adopted despite the company's characteristics.

Green et al. (2012) reported that internal cooperation and collaboration among the firms lead to overall effective, sustainable performance through setup time reduction. Economic goals can be achieved through effective internal integration of setup time reduction by adopting lean manufacturing practices. Many organizations that incorporate setup time reduction into their practices have the chance of increased profitability and the ability to create competitive market shares (Chien & Shih, 2007). Zhu et al. (2010) added that the lack of internal practice like setup time reduction leads to economic failure. Jakhar et al. (2018) reported that set-up time reduction from the operations point of view is an important factor related to inventory optimization leading to improve performance concerning the environment. Dev et al. (2020) found that reducing resources and time consumption is part of the decision-making process for environmentally sustainable operations.

Furthermore, Eltayeb et al. (2011) reported a significant relationship between internally integrated set-up time reduction and environmentally sustainable performance. Therefore, the environmental management system affects the operations performed in production and time waste reduction. Zhu et al. (2012) also posit that profit, income, and employees' welfare are all improved through integrated sustainable design practices within the manufacturing industry. Similarly, Zhu et al. (2010) discovered that internal coordination mechanisms such as requiring employees to attend to environmental issues, reducing set-up time, and exposure to cross-functional cooperation have a significant impact on social sustainability performance (e.g., high involvement and participation, increased happiness, motivation, and social commitment, and safer working environment). Thus, this study proposes that:

H10: Set-up time reduction has a positive and significant relationship with sustainability performance.

Relationship Between Industrial Revolution 4.0 Technologies and Sustainable Performance

According to Kolberg and Zuhlke (2015), lean practices provide huge potential to implement innovative automotive technologies in a manufacturing system. Sanders et al. (2016) reported that IR 4.0 technologies enhance manufacturing companies to overcome the modern challenges of lean manufacturing. The real-time information facilitated by IR 4.0 technologies is useful for preparing accurate value stream maps that are considered the initial step in lean manufacturing practices and implementation (Meudt et al., 2017).

Technologies such as the value stream map are employed to set activities that take products and services to the customers from the initial stage. These technologies analyze the present problem and design the future state to reduce waste (Meudt et al., 2017). Furthermore, the IR 4.0 technologies positively affect sustainable performance (Tortorella & Fettermann, 2018). Thus, the following hypothesis is proposed:

H14: There is a positive and significant relationship between Industrial Revolution 4.0 technologies and sustainable performance

CONCLUSION

Modern organizations continuously seek new methods to perform their activities, remain competitive, and improve performance. Continuous improvement initiatives such as lean practices help organizations reach a high level of performance, remain competitive, and make quick or cohesive process changes by incorporating operations processes. These practices, coupled with IR 4.0 technologies, focus on creating more value for the customers by removing waste activities and adding products and services. In addition, these modern technologies are integrated into manufacturing practices to assess and get rid of mistakes and defects in business processing by concentrating on effective results to sustain the organization's social, environmental, and economic performance. Similarly, the hybrid lean practices with IR 4.0 technologies have synergized the strength of both distinctive practices to increase the performance of any organization through customer satisfaction while improving the triple bottom line result.

Moreover, researchers have shown that integrating IR 4.0 technologies into hybrid lean manufacturing practices are among the least adopted practices by organization as many manufacturing companies are still in the infant stage of smart system. Understandably, these practices require financial resources, which poses constraints, especially for low-margin companies that are constantly seek ways to minimize costs and rely on statistical knowledge. Therefore, this unique integrated system's relatively complex and advanced has called for further study in the manufacturing industry.

ACKNOWLEDGEMENT

The authors are grateful to Universiti Malaysia Perlis for the financial support through 9001-00677.

REFERENCE

- Abdulmalek, F. A., Rajgopal, J., & Needy, K. L. (2006). A classification scheme for the process industry to guide the implementation of lean. *Engineering Management Journal*, 18(2), 15-25. <https://doi.org/10.1080/10429247.2006.11431690>
- Ahuett-Garza, H., & Kurfess, T. (2018). A brief discussion on the trends of habilitating technologies for Industry 4.0 and smart manufacturing. *Manufacturing Letters*, 15, 60-63. <https://doi.org/10.1016/j.mfglet.2018.02.011>
- Akanmu, M. D., Bahaudin, A. Y. B., & Jamaludin, R. (2017). A partial least square structural equation modelling preliminary analysis on total quality management elements and environmental regulation and policy influencing organisational performance in the food and beverage companies of Malaysia. *International Journal of Productivity and Quality Management*, 22(1), 60-81. <https://doi.org/10.1504/ijpqm.2017.085847>
- Akanmu, M. D., Hassan, M. G., & Bahaudin, A. Y. B. (2020). A preliminary analysis modeling of the relationship between quality management practices and sustainable performance. *Quality Management Journal*, 27(1), 37-61. <https://doi.org/10.1080/10686967.2019.1689800>
- Akanmu, M. D., Hassan, M. G., Mohamad, B., & Nordin, N. (2021). Sustainability through TQM practices in the food and beverages industry. *International Journal of Quality & Reliability Management*, 1-30. <https://doi.org/10.1108/IJQRM-05-2021-0143>
- Akdere, M., & Yilmaz, T. (2006). Team performance based compensation plans: Implications for human resources and quality improvement from agency theory perspective. *International Journal of Human Resources Development and Management*, 6(1), 77-91. <https://doi.org/10.1504/ijhrdm.2006.009750>
- Akkerman, R., & van Donk, D. P. (2007). Product prioritization in a two-stage food production system with intermediate storage. *International Journal of Production Economics*, 108(1-2), 43-53. <https://doi.org/10.1016/j.ijpe.2006.12.018>
- Alhuraish, I., Robledo, C., & Kobi, A. (2016). Assessment of lean manufacturing and six sigma operation with decision making based on the analytic hierarchy process. *IFAC-PapersOnLine*, 49(12), 59-64. <https://doi.org/10.1016/j.ifacol.2016.07.550>
- Ali, H. H., & Alkayed, A. A. (2019). Constrains and barriers of implementing sustainability into architectural professional practice in Jordan. *Alexandria Engineering Journal*, 58(3), 1011-1023. <https://doi.org/10.1016/j.aej.2019.09.003>
- Andiç, E., Yurt, Ö., & Baltacıoğlu, T. (2012). Green supply chains: Efforts and potential applications for the Turkish market. *Resources, Conservation and Recycling*, 58, 50-68. <https://doi.org/10.1016/j.resconrec.2011.10.008>

- Arawati, A. (2005). The structural linkages between TQM, product quality performance, and business performance: Preliminary empirical study in electronics companies. *Singapore Management Review*, 27(1), 87-105.
- Azizi, A. (2015). Evaluation improvement of production productivity performance using statistical process control, overall equipment efficiency, and autonomous maintenance. *Procedia Manufacturing*, 2, 186-190. <https://doi.org/10.1016/j.promfg.2015.07.032>
- Baker, B. L. (2003). *TQM practice and theory: A meta-analysis of empirical studies*. Colorado Technical University.
- Benavent, F. B., Cruz Ros, S., & Moreno-Luzon, M. (2005). A model of quality management self-assessment: An exploratory research. *International Journal of Quality & Reliability Management*, 22(5), 432-451. <https://doi.org/10.1108/02656710510598366>
- Bergmiller, G. G. (2006). *Lean manufacturers transcendence to green manufacturing: Correlating the diffusion of lean and green manufacturing systems* (Doctoral dissertation). University of South Florida, USA. <https://digitalcommons.usf.edu/etd/2457/>
- Bicheno, J., & Holweg, M. (2009). *The lean toolbox: The essential guide to lean transformation*. PICSIE Book.
- Blome, C., Hollos, D., & Paulraj, A. (2014). Green procurement and green supplier development: Antecedents and effects on supplier performance. *International Journal of Production Research*, 52(1), 32-49. <https://doi.org/10.1080/00207543.2013.825748>
- Boiral, O., Guillaumie, L., Heras-Saizarbitoria, I., & Tene, C. V. T. (2017). Adoption and outcomes of ISO 14001: A systematic review. *International Journal of Management Reviews*, 20(2), 411-432. <https://doi.org/10.1111/ijmr.12139>.
- Brent, A. C., & Labuschagne, C. (2004). Sustainable life cycle management: Indicators to assess the sustainability of engineering projects and technologies. In *2004 IEEE International Engineering Management Conference (IEEE Cat. No. 04CH37574)* (Vol. 1, pp. 99-103). IEEE. <https://doi.org/10.1109/iemc.2004.1407084>
- Bromiley, P., & Rau, D. (2016). Operations management and the resource based view: Another view. *Journal of Operations Management*, 41(1), 95-106. <https://doi.org/10.1016/j.jom.2015.11.003>
- Buer, S. V., Strandhagen, J. O., & Chan, F. T. S. (2018). The link between Industry 4.0 and lean manufacturing: Mapping current research and establishing a research agenda. *International Journal of Production Research*, 56(8), 2924-2940. <https://doi.org/10.1080/00207543.2018.1442945>
- Burli, S., Bagodi, V., & Kotturshettar, B. (2012). TQM dimensions and their interrelationships in ISO certified engineering institutes of India. *Benchmarking: An International Journal*, 19(2), 177-192. <https://doi.org/10.1108/14635771211224527>
- Busse, C. (2016). Doing well by doing good? The self-interest of buying firms and sustainable supply chain management. *Journal of Supply Chain Management*, 52(2), 28-47. <https://doi.org/10.1111/jscm.12096>
- Busse, C., Schleper, M. C., Niu, M., & Wagner, S. M. (2016). Supplier development for sustainability: Contextual barriers in global supply chains. *International Journal of Physical Distribution & Logistics Management*, 46(5), 442-468. <https://doi.org/10.1108/ijpdlm-12-2015-0300>

- Caiado, R. G. G., Quelhas, O. L. G., Nascimento, D. L. M., Anholon, R., & Filho, W. L. (2018). Measurement of sustainability performance in Brazilian organizations. *International Journal of Sustainable Development and World Ecology*, 25(4), 312-326.
- Chan, H. K., He, H., & Wang, W. Y. C. (2012). Green marketing and its impact on supply chain management in industrial markets. *Industrial Marketing Management*, 41(4), 557-562. <https://doi.org/10.1016/j.indmarman.2012.04.002>
- Chang, W., & Taylor, S. (2016). The effectiveness of customer participation in new product development: A meta-analysis. *Journal of Marketing*, 80(1), 47-64. <https://doi.org/10.1509/jm.14.0057>
- Chen, C. C., Shih, H. S., Shyur, H. J., & Wu, K. S. (2012). A business strategy selection of green supply chain management via an analytic network process. *Computers & Mathematics with Applications*, 64(8), 2544-2557. <https://doi.org/10.1016/j.camwa.2012.06.013>
- Cherrafi, A., Elfezazi, S., Chiarini, A., Mokhlis, A., & Benhida, K. (2016). The integration of lean manufacturing, six sigma and sustainability: A literature review and future research directions for developing a specific model. *Journal of Cleaner Production*, 139, 828-846. <https://doi.org/10.1016/j.jclepro.2016.08.101>
- Chiarini, A. (2014). Sustainable manufacturing-greening processes using specific lean production tools: An empirical observation from European motorcycle component manufacturers. *Journal of Cleaner Production*, 85, 226-233.
- Chien, M. K., & Shih, L. M. (2007). An empirical study of the implementation of green supply chain management practices in the electrical and electronic industry and their relation to organization performance. *International Journal of Environmental Science and Technology*, 4(3), 383-394.
- Danarahmanto, P. A., Primiana, I., Azis, Y., & Kaltum, U. (2020). The sustainable performance of the digital start-up company based on customer participation, innovation, and business model. *Business: Theory and Practice*, 21(1), 115-124.
- Dev, N. K., Shankar, R., & Qaiser, F. H. (2020). Industry 4.0 and circular economy: Operational excellence for sustainable reverse supply chain performance. *Resources, Conservation and Recycling*, 153, Article 104583.
- Diekola, A. M. (2016). *The moderating effect of environmental regulation and policy on the relationship between total quality management (TQM) and organizational performance in the Malaysian food and beverage companies* (Master Thesis). Universiti Utara Malaysia, Malaysia. <http://etd.uum.edu.my/6578/>
- Dora, M., Kumar, M., Van Goubergen, D., Molnar, A., & Gellynck, X. (2013). Food quality management system: Reviewing assessment strategies and a feasibility study for European food small and medium-sized enterprises. *Food Control*, 31(2), 607-616. <https://doi.org/10.1016/j.foodcont.2012.12.006>
- Dües, C. M., Tan, K. H., & Lim, M. (2013). Green as the new Lean: How to use Lean practices as a catalyst to greening your supply chain. *Journal of Cleaner Production*, 40, 93-100. <https://doi.org/10.1016/j.jclepro.2011.12.023>.
- Dunphy, D. (2011). Chapter 1 conceptualizing sustainability: The business opportunity. In G. Eweje & M. Perry (Eds.), *Business and sustainability: Concepts, strategies and changes* (pp. 3-24). Emerald Group Publishing Limited. [https://doi.org/10.1108/s2043-9059\(2011\)0000003009](https://doi.org/10.1108/s2043-9059(2011)0000003009)

- Ellram, L. M., Tate, W., & Carter, C. R. (2008). Applying 3DCE to environmentally responsible manufacturing practices. *Journal of Cleaner Production*, 16(15), 1620-1631. <https://doi.org/10.1016/j.jclepro.2008.04.017>
- Eltayeb, T. K., Zailani, S., & Ramayah, T. (2011). Green supply chain initiatives among certified companies in Malaysia and environmental sustainability: Investigating the outcomes. *Resources, Conservation and Recycling*, 55(5), 495-506. <https://doi.org/10.1016/j.resconrec.2010.09.003>
- Escrig-Tena, A. B. (2004). TQM as a competitive factor. *International Journal of Quality & Reliability Management*, 21(6), 612-637. <https://doi.org/10.1108/02656710410542034>
- Fatorachian, H., & Kazemi, H. (2018). A critical investigation of Industry 4.0 in manufacturing: Theoretical operationalisation framework. *Production Planning & Control*, 29(8), 633-644. <https://doi.org/10.1080/09537287.2018.1424960>
- FMM. (2017). *Member Directory, Federation of Malaysian Manufacturers, Selangor*. Federation of Malaysian Manufacturers.
- Foerstl, K., Azadegan, A., Leppelt, T., & Hartmann, E. (2015). Drivers of supplier sustainability: Moving beyond compliance to commitment. *Journal of Supply Chain Management*, 51(1), 67-92. <https://doi.org/10.1111/jscm.12067>
- Fotopoulos, C. V., & Psomas, E. L. (2010). The structural relationships between TQM factors and organizational performance. *The TQM Journal*, 22(5), 539-552. <https://doi.org/10.1108/17542731011072874>
- Glover, J. L., Champion, D., Daniels, K. J., & Dainty, A. J. D. (2014). An institutional theory perspective on sustainable practices across the dairy supply chain. *International Journal of Production Economics*, 152, 102-111. <https://doi.org/10.1016/j.ijpe.2013.12.027>
- Green, K. W., Zelbst, P. J., Meacham, J., & Bhadauria, V. S. (2012). Green supply chain management practices: Impact on performance. *Supply Chain Management: An International Journal*, 17(3), 290-305. <https://doi.org/10.1108/13598541211227126>
- Guan, Y. H., Cheng, H. F., & Ye, Y. (2010). Performance evaluation of sustainable supply chain based on AHP and fuzzy comprehensive evaluation. In *Applied Mechanics and Materials* (Vol. 26, pp. 1004-1007). Trans Tech Publications Ltd. <https://doi.org/10.4028/www.scientific.net/amm.26-28.1004>
- Haigh, N., & Hoffman, A. J. (2014). The new heretics: Hybrid organizations and the challenges they present to corporate sustainability. *Organization & Environment*, 27(3), 223-241. <https://doi.org/10.1177/1086026614545345>
- Hallam, C. R., & Contreras, C. (2016). The interrelation of Lean and green manufacturing Practices: A case of push or pull in implementation. In *2016 Portland International Conference on Management of Engineering and Technology (PICMET)* (pp. 1815-1823). IEEE Publishing.
- Hassan, M. G., Akanmu, M. D., & Yusoff, R. Z. (2018). Technological integration and sustainable performance in manufacturing firms. *International Journal of Technology*, 9(8), 1639-1650. <https://doi.org/10.14716/ijtech.v9i8.2747>
- Herrero, S. G., Saldaña, M. A. M., del Campo, M. A. M., & Ritzel, D. O. (2002). From the traditional concept of safety management to safety integrated with quality. *Journal of Safety Research*, 33(1), 1-20. [https://doi.org/10.1016/s0022-4375\(02\)00008-7](https://doi.org/10.1016/s0022-4375(02)00008-7)

- Hofmann, H., Busse, C., Bode, C., & Henke, M. (2014). Sustainability-related supply chain risks: Conceptualization and management. *Business Strategy and the Environment*, 23(3), 160-172.
- Iranmanesh, M., Zailani, S., Hyun, S. S., Ali, M. H., & Kim, K. (2019). Impact of lean manufacturing practices on firms' sustainable performance: Lean culture as a moderator. *Sustainability*, 11(4), Article 1112. <https://doi.org/10.3390/su11041112>
- Jakhar, S. K., Rathore, H., & Mangla, S. K. (2018). Is lean synergistic with sustainable supply chain? An empirical investigation from emerging economy. *Resources, Conservation and Recycling*, 139, 262-269.
- Joo, J., & Shin, M. (2017). Building sustainable business ecosystems through customer participation: A lesson from South Korean cases. *Asia Pacific Management Review*, 23(1), 1-11. <https://doi.org/10.1016/j.apmr.2017.01.001>
- Kamble, S. S., Gunasekaran, A., & Gawankar, S. A. (2018a). Sustainable Industry 4.0 framework: A systematic literature review identifying the current trends and future perspectives. *Process Safety and Environmental Protection*, 117, 408-425. <https://doi.org/10.1016/j.psep.2018.05.009>.
- Kamble, S. S., Gunasekaran, A., & Sharma, R. (2018b). Analysis of the driving and dependence power of barriers to adopt Industry 4.0 in Indian manufacturing industry. *Computers in Industry*, 101, 107-119. <https://doi.org/10.1016/j.compind.2018.06.004>
- Kamble, S. S., Gunasekaran, A., & Gawankar, S. A. (2020). Achieving sustainable performance in a data-driven agriculture supply chain: A review for research and applications. *International Journal of Production Economics*, 219, 179-194. <https://doi.org/10.1016/j.ijpe.2019.05.022>
- Kolberg, D., & D. Zühlke (2015). Lean automation enabled by Industry 4.0 technologies. *IFAC-PapersOnLine*, 48, 1870-1875. <https://doi.org/10.1016/j.ifacol.2015.06.359>
- Konig, G., Silva, C. A., & Mhlanga, N. (2013). *Enabling environments for agribusiness and agro-industries development*. National Center for Agricultural Research and Documentation.
- Kovilage, M. P. (2018, August 12-13). Influence of lean and green paradigms on supply chain performance: An interpretive structural modelling approach. In *International Conference on Multidisciplinary Researches*. Maldives National University, Maldives.
- Kovilage, M. P. (2020). Influence of lean-green practices on organizational sustainable performance. *Journal of Asian Business and Economic Studies*, 28(2), 121-142. <https://doi.org/10.1108/jabes-11-2019-0115>
- Krause, D. R., Scannell, T. V., & Calantone, R. J. (2000). A structural analysis of the effectiveness of buying firms' strategies to improve supplier performance. *Decision Sciences*, 31(1), 33-55. <https://doi.org/10.1111/j.1540-5915.2000.tb00923.x>
- Kumar, M., Antony, J., Singh, R. K., Tiwari, M. K., & Perry, D. (2006). Implementing the lean sigma framework in an Indian SME: A case study. *Production Planning & Control*, 17(4), 407-423. <https://doi.org/10.1080/09537280500483350>
- Laureani, A., & Antony, J. (2017). Leadership characteristics for lean six sigma. *Total Quality Management & Business Excellence*, 28(3-4), 405-426. <https://doi.org/10.1080/14783363.2015.1090291>
- Longoni, A., & Cagliano, R. (2015). Cross-functional executive involvement and worker involvement in lean manufacturing and sustainability alignment. *International Journal of Operations & Production Management*, 35(9), 1332-1358. <https://doi.org/10.1108/ijopm-02-2015-0113>

- Martínez-Jurado, P. J., & Moyano-Fuentes, J. (2014). Lean management, supply chain management and sustainability: A literature review. *Journal of Cleaner Production*, *85*, 134-150. <https://doi.org/10.1016/j.jclepro.2013.09.042>
- Meudt, T., Metternich, J., & Abele, E. (2017). Value stream mapping 4.0: Holistic examination of value stream and information logistics in production. *CIRP Annals*, *66*(1), 413-416. <https://doi.org/10.1016/j.cirp.2017.04.005>
- MyCC. (2019). *Strategic plan for competition advocacy & communication*. Malaysia Competition Commission. www.Mycc.gov.my
- Neuman, R. P., & Cavanagh, R. (2000). *The six sigma way: How GE, Motorola, and other top companies are honing their performance*. McGraw Hill Professional.
- Nordin, N., Deros, B. M., & Wahab, D. A. (2014). Lean manufacturing implementation in Malaysian automotive industry: An exploratory study. *Operations and Supply Chain Management: An International Journal*, *4*(1), 21-30. <https://doi.org/10.31387/oscm090053>
- Panwar, A., Nepal, B., Jain, R., Rathore, A. P. S., & Lyons, A. (2017). Understanding the linkages between lean practices and performance improvements in Indian process industries. *Industrial Management & Data Systems*, *117*(2), 346-364. <https://doi.org/10.1108/imds-01-2016-0035>
- Pei, Y. L., Amekudzi, A. A., Meyer, M. D., Barrella, E. M., & Ross, C. L. (2010). Performance measurement frameworks and development of effective sustainable transport strategies and indicators. *Transportation Research Record: Journal of the Transportation Research Board*, *2163*(1), 73-80. <https://doi.org/10.3141/2163-08>
- Sagandira, C., Nqeketo, S., Mhlana, K., Sonti, T., Watts, P., & Gaqa, S. (2022). Towards 4th industrial revolution efficient and sustainable continuous flow manufacturing of active pharmaceutical ingredients. *Reaction Chemistry & Engineering*, *7*(2), 214-244. <https://doi.org/10.1039/D1RE00483B>
- Saleh, A. S., & Ndubisi, N. O. (2006). An evaluation of SME development in Malaysia. *International Review of Business Research Papers*, *2*(1), 1-14.
- Salim, H. K., Padfield, R., Lee, C. T., Syayuti, K., Papargyropoulou, E., & Tham, M. H. (2018). An investigation of the drivers, barriers, and incentives for environmental management systems in the Malaysian food and beverage industry. *Clean Technologies and Environmental Policy*, *20*(3), 529-538. <https://doi.org/10.1007/s10098-017-1436-8>
- Sancha, C., Longoni, A., & Giménez, C. (2015). Sustainable supplier development practices: Drivers and enablers in a global context. *Journal of Purchasing and Supply Management*, *21*(2), 95-102. <https://doi.org/10.1016/j.pursup.2014.12.004>
- Sanders, A., Elangeswaran, C., & Wulfsberg, J. (2016). Industry 4.0 implies lean manufacturing: Research activities in industry 4.0 function as enablers for lean manufacturing. *Journal of Industrial Engineering and Management*, *9*(3), 811-833. <https://doi.org/10.3926/jiem.1940>
- Shah, R., & Ward, P. T. (2002). Lean manufacturing: Context, practice bundles, and performance. *Journal of Operations Management*, *21*(2), 129-149. [https://doi.org/10.1016/S0272-6963\(02\)00108-0](https://doi.org/10.1016/S0272-6963(02)00108-0)
- Shah, R., & Ward, P. T. (2007). Defining and developing measures of lean production. *Journal of Operations Management*, *25*(4), 785-805.

- Simpson, D., Power, D., & Samson, D. (2007). Greening the automotive supply chain: A relationship perspective. *International Journal of Operations & Production Management*, 27(1), 28-48. <https://doi.org/10.1108/01443570710714529>
- Snee, R. D. (2010). Lean six sigma – getting better all the time. *International Journal of Lean Six Sigma*, 1(1), 9-29. <https://doi.org/10.1108/20401461011033130>
- Sousa, R., & Voss, C. A. (2008). Contingency research in operations management practices. *Journal of Operations Management*, 26(6), 697-713. <https://doi.org/10.1016/j.jom.2008.06.001>
- Thoben, K. D., Veigt, M., Lappe, D., Franke, M., Kück, M., Kolberg, D., Fahl, I., Zimmerling, R., Schlick, J., Stephan, P., & Guth, P. (2014, June 4). Towards networking logistics resources to enable a demand-driven material supply for lean production systems-basic concept and potential of a cyber-physical logistics system. In *7th International Scientific Symposium on Logistics* (pp. 42-69). Cologne, Germany.
- Tortorella, G. L., & Fettermann, D. (2018). Implementation of Industry 4.0 and lean production in Brazilian manufacturing companies. *International Journal of Production Research*, 56(8), 2975-2987. <https://doi.org/10.1080/00207543.2017.1391420>.
- Vachon, S. (2007). Green supply chain practices and the selection of environmental technologies. *International Journal of Production Research*, 45(18-19), 4357-4379. <https://doi.org/10.1080/00207540701440303>
- Vachon, S., & Klassen, R. D. (2006). Green project partnership in the supply chain: The case of the package printing industry. *Journal of Cleaner Production*, 14(6-7), 661-671. <https://doi.org/10.1016/j.jclepro.2005.07.014>
- Womack, J. P., Jones, D. T., & Roos, D. (2007). *The machine that changed the world: The story of lean production - Toyota's secret weapon in the global car wars that is now revolutionizing world industry*. Free Press.
- Yang, C., Lan, S., Shen, W., Huang, G. Q., Wang, X., & Lin, T. (2017). Towards product customization and personalization in IoT-enabled cloud manufacturing. *Cluster Computing*, 20(2), 1717-1730. <https://doi.org/10.1007/s10586-017-0767-x>.
- Yusuf, Y., Gunasekaran, A., & Dan, G. (2007). Implementation of TQM in China and organisation performance: An empirical investigation. *Total Quality Management & Business Excellence*, 18(5), 509-530. <https://doi.org/10.1080/14783360701239982>
- Zelbst, P. J., Green Jr, K. W., Sower, V. E., & Abshire, R. D. (2014). Impact of RFID and information sharing on JIT, TQM and operational performance. *Management Research Review*, 37(11), 970-989. <https://doi.org/10.1108/mrr-10-2014-273>
- Zhu, Q., Geng, Y., & Lai, K. (2010). Circular economy practices among Chinese manufacturers varying in environmental-oriented supply chain cooperation and the performance implications. *Journal of Environmental Management*, 91(6), 1324-1331. <https://doi.org/10.1016/j.jenvman.2010.02.013>
- Zhu, Q., Sarkis, J., & Lai, K. (2012). Green supply chain management innovation diffusion and its relationship to organizational improvement: An ecological modernization perspective. *Journal of Engineering and Technology Management*, 29(1), 168-185. <https://doi.org/10.1016/j.jengtecman.2011.09.012>
- Zikmund, W. G., Babin, B. J., Carr, J. C., & Griffin, M. (2010). *Business research methods* (8th Ed.). Nelson Education, Ltd.



Importance of Transfer of Technology Skills and Human Resource Development Skills in Work Performance of Extension Agent in Sarawak Cocoa Industry

Nur Syahirah Abd Halim^{1*}, Salim Hassan¹ and Ramle Kasin²

¹Faculty of Agriculture, Universiti Putra Malaysia, 43400 UPM, Serdang, Selangor, Malaysia

²Wisma SEDCO Locked Bag 211, 88999 Kota Kinabalu, Sabah, Malaysia

ABSTRACT

Smallholders monopolized the cocoa industry in Sarawak, and it has the biggest cultivated area compared to Sabah and Peninsular Malaysia. Despite possessing a big, cultivated area, the production of cocoa beans in Sarawak still does not meet the expectation set by the Malaysian Cocoa Board (MCB). Extension agents play an important role in transferring technology to smallholders; thus, extension agents should be competent in performing the duty. Transfer of technology (ToT) skills and human resource development (HRD) skills are two primary skills that have been proven to be important in determining the work performance of extension agents. Thus, this study determines the relationship between ToT skills, HRD skills, and the work performance of extension agents in the Sarawak cocoa industry. Stratified random sampling has been employed in this research with 148 respondents to evaluate the performance of extension agents. The data were analyzed using descriptive, correlational, and regression analysis. This research showed that all the skills of ToT and HRD have a positive relationship with work performance. Regression analysis showed that decision-making, social, and technical skills have a significant value of <0.05 . The improvement work performance of extension agents in ToT and HRD skills will aid the production of cocoa beans in Sarawak to be improved as expected by

MCB. Smallholders will have more access to knowledge, technology, and information related to the cocoa industry, so there is a chance to increase the production of cocoa beans in the region.

ARTICLE INFO

Article history:

Received: 30 September 2021

Accepted: 11 February 2022

Published: 25 May 2022

DOI: <https://doi.org/10.47836/pjst.30.3.30>

E-mail addresses:

syiraahmy@gmail.com (Nur Syahirah Abd Halim)

salimhassan@upm.edu.my (Salim Hassan)

ramlekasin@gmail.com (Ramle Kasin)

*Corresponding author

Keywords: Competency, extension, HRD, ToT, work Performance

INTRODUCTION

Cocoa is one of Malaysia's commodity crops apart from rubber and oil palms. In Malaysia, the most covered area of cocoa plantation is in East Malaysia, which is Sabah and Sarawak. The area covered by Sabah and Sarawak is 6,881 hectares and 6,772 hectares, respectively (Malaysian Cocoa Board, 2017). Malaysia used to be one of the largest producers of cocoa beans globally. However, due to several factors such as poor world cocoa prices, competition of land use for rubber and oil, climate change, and pest and disease, the production of cocoa beans in Malaysia decreased significantly. As a result, the global supply and demand for cocoa beans fluctuated between 2010 and 2017 (ICCO, 2019). According to ICCO (2019), there was a surplus of production of cocoa beans in 2011, 2012, 2015, 2017, and 2018 while there was a deficit of production in 2013, 2014, and 2016. For the cocoa industry in Malaysia, supply and demand have been in constant deficit from the year 2000 until 2016. As a result of the increase in the demand for cocoa beans, the production of cocoa beans has decreased; thus, this situation is very worrisome. The production of cocoa beans decreased from 70,262 tonnes in the year 2000 to 1,757 tonnes in 2016 in Malaysia, whereas in the case of Sarawak, the cocoa beans production decreased from 3,710 tonnes in 2000 to 272 tonnes in 2016 (Malaysian Cocoa Board, 2017).

In Sarawak, smallholders are the main sector that is involved in cocoa. Since 2009, the cocoa cultivated area in Sarawak has been bigger than Peninsular Malaysia and Sabah, despite all the cultivated areas being smallholders (Malaysian Cocoa Board, 2017). This research focused on Sarawak because smallholders are dominant farmers compared to Sabah and West Malaysia. Smallholders rely on extension agents to receive new technology, information, and knowledge related to the cocoa plantation. Extension agents are the ones that educate farmers for the benefit of technology adoption. Fadzim et al. (2016) stated that farmers need to access all the technology and relevant knowledge on cocoa farming for better production. Therefore, focusing on developing knowledge and skill for cocoa farmers with the help of extension agents is the primary objective in improving the local production of cocoa beans.

Malaysian Cocoa Board (MCB) is the agency managing the cocoa plantation and has introduced several extension services to overcome the situation. The extension agents of MCB carried out their duty under the coordination of the Technology Transfer and Extension Division. This division is responsible for transferring new technology developed by the research and development division. Extension agents must possess hard skills, such as technical skills, and soft skills, such as leadership skills. These abilities have aided extension agents in performing their duty effectively in every situation and helped the technology dissemination process to be successful. According to Kasin (2012), extension agents of MCB has the responsibility to motivate cocoa farmers to identify the problems and solutions through the adoption of technology being disseminated, to serve as a link

between the MCB researcher and cocoa farmers, and lastly, to persuade cocoa farmers to adopt the new technology that has been transferred.

MCB has introduced several extension programs to the farmers. However, they still have failed to increase the production of cocoa beans. The MCB targeted yield to be achieved set to be 1.5 tons/ha/yr, but the current average production is only 0.5 tons/ha/yr, and the gaps can be seen to be over 50% and create a lot of challenges (Malaysian Cocoa Board, 2017). Apart from external problems that cannot be controlled, such as climate change and world cocoa price, competencies of the extension agents in Sarawak that are disseminating the technology could be a problem. The performance of extension agents in technology transfer is crucial because it can facilitate the process of technology and knowledge transfer so the farmers can increase the productivity of a farm (Suvedi & Kaplowitz, 2016; Danso-Abbeam et al., 2018).

Murni et al. (2019) stated that extension agents need to possess transfer of technology (ToT) skills, as these skills are the basic skills in technology dissemination. The ToT skills mentioned are technical skills, delivering skills, and evaluating skills. Furthermore, Isah et al. (2019) also mentioned that these ToT skills influence the performances of extension agents when executing their duty. Isah et al. (2019) added that human resource development (HRD) skills, such as leadership skills, decision-making skills, and social skills, help stimulate extension agents' performances in technology and knowledge transfer. Organizations with employees with inefficient HRD skills will affect the entire organization's performance (Mengal & Habib, 2016). Therefore, extension agents of MCB in Sarawak must possess ToT skills and HRD skills to disseminate the technology successfully.

Agricultural extension services in Malaysia only concentrate on developing and improving ToT skills (Shah et al., 2013). It is not common to find research on HRD skills and work performance; thus, this shows a gap between ToT skills, HRD skills, and work performance. Specific ToT skills and HRD skills are needed for the performance of extension agents to aid in an increase in agriculture productivity (Issahaku, 2014). Research by Isah et al. (2019) and Motoloni et al. (2017) has proved that extension agents need specific ToT and HRD skills to transfer technology to the farmers successfully. Thus, this study examined the relationship between ToT skills, HRD skills, and work performance of extension agents MCB in Sarawak based on the perception of cocoa farmers.

This study aims to determine extension agents' skills related to ToT, HRD, and work performance to determine the relationship between ToT and HRD with work performance. The last objective is to identify which skills contribute to the work performance of the extension agents based on the perception of cocoa farmers.

LITERATURE REVIEW

Competency is the ability to perform tasks effectively and efficiently, and it is important in organizations because it can be a key to a successful organization. Competency does not only involve knowledge and skill but also depends on how to fulfill complex demands (Raychen & Salganik, 2001). The Iceberg Model of Spencer and Spencer (1993) showed that competencies required by individuals in any field of work are knowledge, skill, self-concepts, traits, and motive. The model of the iceberg was applied in this research because this model describes competencies required by extension agents of MCB in Sarawak. Knowledge refers to individuals' information and learning, such as the agricultural extension agent of MCB in Sarawak knows all related cocoa technology. Skill refers to the individual ability to perform their task, such as the agricultural extension agent of MCB in Sarawak skill in transferring technology. Self-concept refers to an individual's attitude, such as interaction skills between extension agents and cocoa farmers. Traits refer to the physical characteristic and reactions towards any situation. For example, extension agents of MCB in Sarawak need to have good leadership in building the trust between cocoa farmers. The last characteristic is motives, which refer to the emotion or desire to complete the task. This characteristic is important to extension agents as they are responsible for delivering the technology to the cocoa farmers. All characteristics are equally important to give out the perfect performance for the extension agent of MCB in Sarawak. Lack of knowledge and skill related to the technology will delay the process of technology transfer (Scheer et al., 2011; Efstathiades et al., 2000). Overall, competency includes knowledge, skill, traits, abilities, and behavior that need to be regularly assessed so that individuals can perform work effectively (Davis, 2015; Suvedi & Kaplowitz, 2016).

In many organizations, an individual's work performance is important in ensuring the productivity performance of organizations (Shaffril & Uli, 2010). For an organization to be productive all year long, the performance of the employee and employer needs to be assessed to make sure they can deliver their task successfully (Loper, 2016). In the agriculture industry, numerous research was conducted to evaluate the work performance of extension agents. The performance of extension agents influences crop production's productivity because the crop's production can be increased with new technology adopted by farmers through technology delivered by extension agents. Bahua (2013) reported that improvement of performance extension agents showed significant increases in farmers' participation in maize planting activity.

Transfer of technology (ToT) is defined as a process of delivering the technology and knowledge for a client's adoption (Powers & McDougal, 2005). ToT is an essential skill that extension agents require. In making sure technology can be transferred to the farmers smoothly, extension agents need to have excellent technical skills as these skills reflect the performance of extension agents. A study by Wasihun et al. (2013) found that the technical

skills of extension agents in Ethiopia were poor, and it reflected the work performance of extension agents in technology dissemination. Similar to Günsel et al. (2018), who proved that the work performance of extension agents influences the performance in transferring technology. According to environmental changes extension agents must regularly keep their knowledge and skills up to date. It enables them to transfer the technology to the cocoa farmers. Besides technical skills, delivering skills play an important role in technology transfer. According to Alhassan (2013), technology transfer includes an effective delivery method in persuading farmers to receive and adopt new technologies. The effectiveness and success of technology transferred to the farmer result from the service delivered by extension agents. Transfer of technology results is often used to evaluate the performance of technology transferred by extension agents to the farmers to improve performance as the effect of technology adoption (Yoo & Yang, 2015). Evaluation skills of extension agents are skills used to measure work performance. Ability extension agents to evaluate farmers' improvement in knowledge and skill based on technology adoption are important in technology transfer (Waroonkun, 2007). Extension agents of MCB in Sarawak should have sufficient and up-to-date knowledge and skills concerning the delivery of cocoa technology and evaluating cocoa technology adopted by farmers.

Human resource development (HRD) usually relates to an individual's soft skills, and it is defined as the combination of training and career development within organizations for organizational growth and effectiveness (Salleh & Sulaiman, 2016). Two organizations that offer the same services were differentiated in the quality of human resources (Sharma & Maheshwari, 2013). Thus, human resource development in organizations must be elevated to another level for efficient production. HRD in agriculture functions as a tool to aid the farmers in making their own decisions for crop production. Extension agents need to have strong HRD skills as these skills facilitate the smooth process of transferring technology to the farmers (Kesti, 2012). Therefore, the enhancement of HRD in extension agents is the priority for agricultural extension services.

However, the HRD skills of extension agents were not widely evaluated in Malaysia compared to ToT skills. Performance extension agents in HRD need to be discovered widely in ensuring the agricultural extension services can sustain and be successful in the foreseeable future (Rahim, 2010). Performance of extension agents on HRD can be reflected based on leadership skills, assisting farmers in making sound decisions, and social skills that are known to be related to the HRD improvement for extension agents (Rosnita et al., 2017). Martin and Suwanto (2019) found that the work performance of extension agents was influenced by communication skills, critical thinking skills, and decision-making skills. Varner (2011) determined that social interaction, knowledge and technology delivery, and leadership, contribute prominently to work performance. In order to ensure the process of technology dissemination is successful, extension agents of MCB in Sarawak are required to exhibit HRD skills, such as leadership skills, decision-making skills, and social skills.

The literature review findings indicate that skills in ToT and HRD in extension agents play a significant role in technology adoption by cocoa farmers. Cocoa farmers need an extension agent who can decide to adopt or reject new technologies. Furthermore, the literature review proved that skills in ToT and HRD influenced the work performance of extension agents in delivering technology to the farmers. Therefore, extension agents must possess skills of ToT and HRD as it was apparent that guidance from extension agents can improve crop production.

METHODOLOGY

This study employed descriptive correlational research to describe and explain the importance of data collected and discover the relationship between the dependent and independent variables. In this research, the dependent variable is the work performance of extension agents, while the independent variables are ToT skills and HRD skills. This research is based on the model of the iceberg by Spencer, and Spencer (1993), where skills under ToT, which are technical, delivering, and evaluating skills, represent knowledge and skill, while skills under HRD, which are leadership skills, decision-making skills, and social skills represent self-concepts, trait, and motives. As highlighted by Spencer and Spencer (1993), knowledge, skill, self-concepts, traits, and motives influence the work performance of individuals in completing their tasks. The iceberg model adequately explains the relationship between ToT skills, HRD skills, and work performance of extension agents of MCB in Sarawak. In this research, there are six hypotheses developed. The following hypothesis was tested.

H1: There is a significant relationship between technical skills and work performance of extension agent MCB in Sarawak

H2: There is a significant relationship between delivering skills and work performance of extension agent MCB in Sarawak

H3: There is a significant relationship between evaluating skills and work performance of extension agent MCB in Sarawak

H4: There is a significant relationship between leadership skills and work performance of extension agent MCB in Sarawak

H5: There is a significant relationship between decision-making skills and work performance of extension agent MCB in Sarawak

H6: There is a significant relationship between social skills and work performance of the extension agent MCB in Sarawak

The study's target population was from the Kota Samarahan and Betong regional offices because most productive cocoa farmers are under the management of these two regional offices. Sebuyau, Sri Aman, Asajaya and Padawan are under management of Kota Samarahan regional office while Engkilili is under Betong regional office of the cocoa board. Therefore, the study population was the productive cocoa farmers in Sarawak with 5–7 years of experience in the cocoa plantation. They have received the cocoa technology transferred by extension agents such as pruning, fertilization, pest and disease control, and processing of cocoa beans technologies. This technology was transferred to farmers when the cocoa trees were matured, which takes a minimum of 4 years. Cocoa farmers who had just started to plant cocoa were excluded from this research because they had not yet received the technology measured in this research. The productive cocoa farmers must have experience attending basic and intensive training provided by MCB.

The population for the study was 249 productive cocoa farmers in Sarawak. The study's sample size was determined using table from Krejcie and Morgan (1970). The size of this study is 179 respondents (Table 1). One hundred forty-eight respondents answered the questionnaire, but only 129 questionnaires can be used for analysis, and the other 19 cannot be used because of the unfilled questionnaire.

Table 1
Number of respondents

Region Office	Population	Number of samples	Number of respondents
Kota Samarahan	191	127	119
Betong	58	52	29
Total	249	179	148

This study was carried out using quantitative research methods where the participant answered the structured questions in a questionnaire. The questionnaire in this study is based on the research by Motoloni et al. (2017) as he conducted his research on the work performance of extension agents of MCB in Peninsular Malaysia in terms of technical skills, delivering skills, evaluating skills, leadership skills, decision-making skills, and social skills. In this research, measurement of performance extension agents is based on pruning technology, fertilization technology, pest and disease technology, and processing of cocoa beans technology. This study was conducted in Sarawak, where smallholders monopolized the cocoa industry. The data was collected with the help of the MCB officer. They helped gather all the participants in one place to collect the data successfully. The data collecting session was held in August 2017.

The collected data were analyzed descriptive statistics for the frequency and percentages of the respondents as age, educational level, race, income, clone, and cocoa planted area. The correlational analysis evaluated the relationship between ToT and HRD with work performance. The most contributing variables towards the work performance were determined using multiple regression analysis. This study analyzed all the data using Statistical Packages for Social Science (SPSS) version 22.0.

RESULT

Respondent Profile

Based on the findings, 89.1% of respondents were males, with 10.9% female respondents. The age of the respondents shows that 35.7% were over 61 years old, ages between 51 to 60 were 34.9%, 23 (17.8%) respondents were between 41–50 years old, 13 (10.1%) respondents were aged between 31–40 and 1.6% of respondents were less than 30. Also, 62.8% of farmers have less than RM1000 income, 34.1% realized income range between RM1000–RM1999, while 0.8% of farmers have income between RM2000–RM2999 and 1.6% have an income range of RM3000–RM3999 and 0.8% earned income of RM4000, respectively. About 53% of farmers were Iban, 43% were Malay, 10.1% were Bidayuh, and Chinese farmers were 3.1%. There were 58.1% of farmers cultivate cocoa on a full-time basis, while 41.9% of farmers cultivate cocoa part-time. Most farmers (97%) completed primary school, while 25% and 7% had only completed secondary school (25%) and certificate.

Farm Profile

For years of planting, 75.2% within 2010–2006, 6.2% were 2005–2001, and 2.3% were at/before 2000. Of most farmers, 69% used less than three clones on their farms. 29.5% of farmers planted 3–5 clones/farm, and only 1.6% of farmers used more than five clones in their farmland. Data showed that most farmers 83.7% have 1–3 hectares of cocoa plantation, 15.5% of farmers have less than 1 hectare, and 0.8% of farmers have 3.1–5 hectares area.

Level of Extension Agents in Transfer of Technology (ToT) Skills, Human Resource Development (HRD) Skills, and Work Performance

The level of ToT skills, HRD skills, and work performance can be measured based on the mean level. The mean level was divided into three categories; low, medium, and high, as referred to in the study by Hassan and Abdullah (2015) and Demba (2017). Range of mean between 1–2.669 category as low, 2.67–4.339, category as a medium, and 4.34–6 as high.

Technical Skill. This skill was evaluated by the cocoa farmers based on the ability and knowledge of extension agents in cocoa technology. 89.1% of farmers evaluated extension agents as having high technical skills, while the remaining farmers (10.9%) said that extension agents have moderate skills in cocoa technology. The mean and standard deviation of technical skill is $M = 5.03$, $SD = 0.541$ (Table 2). From the results, it means that extension agents of MCB had sufficient knowledge of technical skills of cocoa to be transferred to the farmers.

Table 2
Level of technical skill

Level	Frequency	Percentage	Mean	Std. Deviation
Low (1–2.669)	0	0	5.03	0.541
Moderate (2.67–4.339)	14	10.9		
High (4.34–6)	115	89.1		

Delivering Skill. Cocoa farmers evaluate extension agents' ability to deliver the technology to them by showing the proper method of the cocoa technology. For technology delivering skill, 86% of farmers evaluated the extension as having high skill, 13.2% evaluated moderate skill, and 0.8% evaluated the low skill level. The mean and standard deviation of technology delivering skills is $M = 4.99$, $SD = 0.638$ (Table 3). Therefore, the competency of extension agents in delivering technology is high, which means the technology was successfully delivered to farmers.

Table 3
Level of technology delivering skill

Level	Frequency	Percentage	Mean	Std. Deviation
Low (1–2.669)	1	0.8	4.99	0.638
Moderate (2.67–4.339)	17	13.2		
High (4.34–6)	111	86.0		

Evaluating Skill. Evaluating skills were evaluated to determine the ability of extension agents to evaluate farmers' understanding of the cocoa technology that has been transferred. Most of the farmers (84.5%) assessed those extension agents have a high level of skill in evaluating cocoa technology, and another 15.5% assessed that extension agents have a moderate level of skill. Technology evaluation skills' mean level and standard deviation

are $M = 4.89$, $SD = 0.545$ (Table 4). Data show that extension agents have high knowledge and skill in evaluating the effectiveness of the technology used by farmers.

Table 4
Level of technology evaluation skill

Level	Frequency	Percentage	Mean	Std. Deviation
Low (1–2.669)	0	0	4.89	0.545
Moderate (2.67–4.339)	20	15.5		
High (4.34–6)	109	84.5		

Leadership Skill. Extension agents have a high level of leadership skills as evaluated by 80.6% of farmers, and another 19.4% evaluate extension agents as having moderate skills. The leadership skill’s mean level and standard deviation are $M = 4.92$, $SD = 0.658$ (Table 5). Therefore, the capabilities of extension agents to empower the farmers to become leaders in the local institutions are high as extension agents’ skills are high in leadership.

Table 5
Level of leadership skill

Level	Frequency	Percentage	Mean	Std. Deviation
Low (1–2.669)	0	0	4.92	0.658
Moderate (2.67–4.339)	25	19.4		
High (4.34–6)	104	80.6		

Help Decision Making Skill. Data shows that the level of extension agents in help deciding is high, as evaluated by 89.1% of the farmers, and the remaining farmers, which are 10.9%, evaluate extension as a moderate skill. The mean level and standard deviation of help-making decision skills are $M = 4.93$, $SD = 0.585$ (Table 6). Skill in the decision-making of extension agents is high, as most respondents evaluated. It means that cocoa farmers can decide on their own with the help of extension agents.

Table 6

Level of decision-making skill

Level	Frequency	Percentage	Mean	Std. Deviation
Low (1–2.669)	0	0	4.93	0.585
Moderate (2.67–4.339)	14	10.9		
High (4.34–6)	115	89.1		

Social Skill. The last HRD sub-variable is a social skill. The result showed that 76.7% of respondents agree that extension agents have a high-level skill, 21.7% agree on moderate, and 1.6% say that extension agents have a low social skill level. The social skills' mean level and standard deviation are $M = 4.73$, $SD = 0.753$ (Table 7). About three-quarters of respondents agreed that extension agents involve their local festivals and unofficial invitations by the farmers.

Table 7

Level of social skill

Level	Frequency	Percentage	Mean	Std. Deviation
Low (1–2.669)	2	1.6	4.73	0.753
Moderate (2.67–4.339)	28	21.7		
High (4.34–6)	99	76.7		

Work Performance. The work performance of the extension agents was also evaluated by the respondents (farmers). Table 8 shows the level of work performance of extension agents where 87.6% of respondents evaluate extension agents of MCB as a high level of work performance, and the other 12.4% evaluate moderate skill. The mean and standard deviation for the work performance is $M = 4.91$, $SD = 0.649$. From the results, the extension agents have improved the farmers' productivity, as the level of work performance evaluated is high.

Table 8

Level of work performance

Level	Frequency	Percentage	Mean	Std. Deviation
Low (1–2.669)	0	0	4.91	0.649
Moderate (2.67–4.339)	16	12.4		
High (4.34–6)	113	87.6		

The mean level of competency of extension agents in ToT and HRD is averagely high, and this result is supported by Motoloni et al. (2017). Therefore, it can be interpreted as extension agents of MCB have performed their task with broad knowledge and skills in technical skills, technology delivery skills, technology evaluation skills, leadership skills, decision-making skills, and social skills.

Relationship of Transfer of Technology and Human Resource Development with Work Performance

The Pearson correlation coefficient determined the relationship of extension agents’ ToT and HRD with work performance. The strength of the relationship is measured according to Guilford’s (1973) Rule of Thumb. Results showed a positive and strong relationship between ToT ($r = 0.730$) and HRD ($r = 0.842$) with work performance, as shown in Table 9. This result aligns with Sail (2010) and Motoloni et al. (2017), who indicated that ToT and HRD have a positive and strong relationship toward work performance.

Table 9
Relationship between ToT and HRD with work performance

Variables	ToT	HRD	WP
ToT	1	.780	.730
HRD		1	.842
Work Performance			1

The relationship of sub-variables in ToT and HRD was also analyzed, and findings show that all the sub-variables have a positive relationship with work performed. The sub-variables that represent ToT are technical skills that have a strong and positive relationship ($r = 0.748$), technology delivery skills that have a moderate and positive relationship ($r = 0.689$), and technology evaluation skills moderate and positive relationship ($r = 0.481$) (Table 10). Also, HRD variables; leadership skill has a moderate and positive relationship ($r = 0.646$), decision making has a strong and positive relationship ($r = 0.821$), and social skill has a strong and positive relationship ($r = 0.792$) as tabulated in Table 10.

Table 10
Relationship between ToT and HRD skills with work performance

Skills	X1	X2	X3	X4	X5	X6	Y
Technical skill (X1)	1	.749	.536	.672	.680	.629	.748
Delivering technology skill (X2)		1	.670	.710	.717	.578	.689
Evaluating technology skills (X3)			1	.509	.589	.447	.481
Leadership skill (X4)				1	.713	.603	.646
Help to make decision skills (X5)					1	.782	.821
Social skill (X6)						1	.792
Work performance (Y)							1

Skills Contributed to The Performance of Extension Agents

Regression analysis was conducted to determine which factors contribute to the work performance of the extension agents in MCB Sarawak based on the perception of productive cocoa farmers. Results show that three skills contributed to the work performance of MCB extension agents. The skills are significant as their p-value < 0.05. Therefore, decision-making skills, social skills, and technical skills are significant (Table 6). The analysis shows that the highest Beta values are the decision-making skills (0.389), followed by social skills (0.313) and technical skills (0.281), as in Table 11.

Table 11
Estimate coefficients for extension agents' performance model

Variables	Unstandardized Coefficients		Standardized Coefficient	t	p-values
	B	Std. Error	Beta		
Technical skill	.337	.084	.281	4.014	.000
Delivering technology skill	.107	.081	.105	1.320	.189
Evaluating technology skill	-.107	.069	-.090	-1.538	.127
Leadership skill	-.037	.066	-.037	-.555	.580
Help to make decision skill	.432	.084	.389	4.616	.000
Social skill	.270	.060	.313	4.485	.000

Three skills that contribute to the work performance, technical skills, represent ToT, and the other two, decision-making skills and leadership skills, represent HRD. This result shows that HRD skills contributed more to MCB extension performance than ToT skills.

DISCUSSION

The result of level skills of ToT and HRD are in line with previous research by Murni et al. (2019), Motoloni et al. (2017), and Sail (2010). The mean level of all skills is high as perceived by the extension agents. Transferring the technology to the farmers depends on the ability of extension agents with higher skills and knowledge to satisfy the cocoa farmers' needs (Varner, 2011). Olagunju et al. (2019) proved that ToT and HRD skills are important in developing the work performance of extension agents to perform their duty effectively.

The result of correlation analysis showed that all skills in ToT and HRD have a significant positive relationship with the work performance of extension agents. This result was in line with the research by Isah et al. (2019), Murni et al. (2019), and Motoloni et al. (2017). Help in decision-making skills has the strongest relationship with the work performance of MCB extension agents in Sarawak. Help in decision-making skills is a vital skill that extension agents need to possess as this skill will make extension agents more trustworthy by cocoa farmers for technology adoption. A study by Mariano et al. (2012), Asfaw et al. (2012), and Baloch and Thapa (2016) proved that agents that help farmers in making decisions increase the chances of new technology adoption by farmers. While help in decision-making skills has the strongest relationship with work performance, evaluating skills has the weakest relationship with the work performance of extension agent MCB in Sarawak. Evaluation skills of extension agents need to be improved as it is particularly important to determine the level of performance of extension agents (Lamn & Israel, 2011). Suvedi and Stoep (2016) proposed that agricultural organizations need to make investments to strengthen the evaluation skills of the extension agents and subsequently improve their work performance. Improving evaluation skills will aid future research by evaluating previous technology and programs to determine the improvement of the area in cocoa beans production for innovation to work on.

Two HRD skills (help in decision-making skills and social skills) and one ToT skill (technical skill) contribute to the work performance of extension agents MCB in Sarawak, which is significant at 0.05. The predictive power for the three skills is 0.772, which means that these three skills had about 77% of the variation in the work performance of extension agents. This result was in line with the research by Motoloni et al. (2017), with the same skills showing the contribution to the work performance of extension agents in Peninsular Malaysia. However, the study by Motoloni et al. (2017) showed that leadership skills contribute to the work performance of extension agents in Peninsular Malaysia, which was contrasted with the result in this research. It shows that extension agents of MCB in Sarawak lack leadership skills, and they need to attend a course on improving them. Moreover, delivery skills and evaluation skills are insignificant as the p-value is more than 0.05. Therefore, these three skills did not significantly contribute to the work performance of the extension agents. It might be due to a lack of exposure to proper delivery

methods technology and evaluation method of technology and programs. Therefore, MCB needs to invest in developing extension agents' ToT and HRD skills, as it will help them perform their tasks successfully. Producing cocoa beans can be improved by improving performance extension agents in transfer technology. Upon adopting new cocoa technology, cocoa farmers will seek help and knowledge from extension agents; therefore, extension agents need to have good skills in ToT and HRD for better work performance (Olagunju et al., 2019).

CONCLUSION

This research aims to determine how extension agents improve their work performance in ToT and HRD among the cocoa farmers' community. This research studies relationship between ToT skills, HRD skills, and work performance of extension agent MCB in Sarawak based on the perception of cocoa farmers. The relationship between ToT skills (technical skill, delivery skill, and evaluating skill) and HRD skills (leadership skill, help in decision-making skills, and social skills) with work performance was evaluated, and all the skill shows a significant positive relationship with the work performance of extension agent MCB in Sarawak. Of all the six skills, help in decision-making skills, social skills, and technical skills of extension agent MCB in Sarawak has a significant contribution to the work performed.

The implication of this study is focusing on the importance of identifying skills in ToT and HRD that contributes to the work performance of extension agent MCB in Sarawak. This study provides insights on how important technical skills, delivering skills, evaluating skills, leadership skills, help decision-making skills, and social skills are in developing the performance of extension agents in transferring the technology to the cocoa farmers. This study will create awareness among extension agents to excel in ToT and HRD skills to ensure they disseminate the cocoa technology successfully. These six skills should be ingrained in training programs introduced by agriculture organizations, especially the Malaysian Cocoa Board, to ensure sustainable production of cocoa beans in the future. Most importantly, the empowerment of extension agents in all six skills needs to be enhanced by providing training programs introduced by agriculture organizations, especially the Malaysian Cocoa Board, to increase the production of cocoa beans. Research in the relationship between work performance and ToT skills in agriculture is common. However, research on the HRD skills of extension agents was not extensive. This research can be a revelation for other agriculture institutions to evaluate the performance of extension agents in ToT and HRD skills together.

Qualitative research can be conducted to find what other factors contribute to the work performance of extension agents from MCB in Sarawak. A comparison between the work performance of extension agents in Peninsular Malaysia and Sarawak also can be

conducted for future research. The limitation of this study emanated from the evaluation of the work performance of extension agents comes only from productive cocoa farmers. In future research, the study sample can be more diverse to represent the entire community of cocoa farmers.

ACKNOWLEDGEMENT

The author wants to acknowledge the staff from the Malaysian Cocoa Board in Sarawak that has been so helpful in completing the research. The author also wants to thank Universiti Putra Malaysia for providing the funds to complete the data collection in Sarawak.

REFERENCES

- Alhassan, Z. (2013). Assessment of the potential of agricultural extension delivery on Guinea Fowl (*Numidea meleagris*) production by small scale farmers in the Upper East Region of Ghana (Master thesis). University of Ghana, Ghana. <http://ugspace.ug.edu.gh/handle/123456789/5449?show=full>
- Asfaw, S., Shiferaw, B., Simtowe, F., & Lipper, L. (2012). Impact of modern agricultural technologies on smallholder welfare: Evidence from Tanzania and Ethiopia. *Food Policy*, 37(3), 283-295. <https://doi.org/10.1016/j.foodpol.2012.02.013>
- Bahua, M. I. (2013). Factors affecting the performance of agricultural extension and their impact at behavior maize farmers in Gorontalo Province. *The Journal of Agricultural Education and Extension*, 1, 1-10.
- Baloch, M. A., & Thapa, G. B. (2016). The effect of agricultural extension services: Date farmers' cases in Balochistan, Pakistan. *Journal of the Saudi Society of Agricultural Sciences*, 17(3), 282-289. <https://doi.org/10.1016/j.jssas.2016.05.007>
- Danso-Abbeam, G., Ehiakpor, D. S., & Aidoo, R. (2018). Agricultural extension and its effects of farm productivity and income: Insight from Northern Ghana. *Agriculture & Food Security*, 7(1), 1-10. <https://doi.org/10.1186/s40066-018-0225-x>
- Davis, K. (2015). *The new extensionist: Core competencies for individuals*. Global Forum for Rural Advisory Services.
- Demba, S. (2017). Personality traits and work performance of paddy farmers in the Central River Region, Gambia (Unpublished Master thesis). Universiti Putra Malaysia, Malaysia. <http://psasir.upm.edu.my/id/eprint/68775/1/FP%202018%2048%20IR.pdf>
- Efstathiades, A., Tassou, S. A., Oxinos, G., & Antoniou, A. (2000). Advanced manufacturing technology transfer and implementation in developing countries. *Technovation*, 20(2), 93-102. [https://doi.org/10.1016/S0166-4972\(99\)00100-5](https://doi.org/10.1016/S0166-4972(99)00100-5)
- Fadzim, W. R., Aziz, M. I. A., Mat, S. H. C., & Maamor, S. (2016). Estimating the technical efficiency of smallholder cocoa farmers in Malaysia. *International Journal of Economics and Financial Issues*, 6(7S), 1-5.
- Günsel, A., Dodourova, M., Ergün, A. T., & Gerni, C. (2018). Research on effectiveness of technology transfer in technology alliances: Evidence from Turkish SMEs. *Technology Analysis and Strategic Management*, 31(3), 279-291. <https://doi.org/10.1080/09537325.2018.1495836>

- Hassan, S. & Abdullah, S. N. S. (2015). Personality traits for the majority of paddy farmers in Mada Kedah, Malaysia. *Journal of Agriculture and Life Sciences*, 2(1), 146-151.
- ICCO. (2019). *International Cocoa Organisation*. <https://www.icco.org/>
- Isah, I. A., Olagunju, O., Ismail, M. M., Hassan, S., & Man, N. (2019). Enhancing sustainable stingless beekeeping production through technology transfer and human resource development in relationship with extension agents work performance among Malaysian beekeepers. *Asian Journal of Agricultural Extension, Economics & Sociology*, 30(2), 1-12.
- Issahaku, A. (2014). Perceived Competencies of Agriculture Extension Workers in Extension Services Delivery in Northern Region of Ghana: Perspective from Literature. *Developing Country Studies*, 4(15), Article 107.
- Kasin, P. R. (2012). *Contribution of group dynamics factors to technology adoption among Malaysia cocoa farmers' clusters* (Unpublished Doctoral dissertation). Universiti Putra Malaysia, Malaysia. <http://psasir.upm.edu.my/id/eprint/48724/>
- Kesti, M. (2012). Organization human resources development connection to business performance. *Procedia Economics and Finance*, 2, 257-264.. <https://doi.org/10.1037/e582902013-002>
- Krejcie, R. V., & Morgan, D. W. (1970). Determining sample size for research activities. *Educational and Psychological Measurement*, 30, 607-610.
- Lamm, A. J. & Israel, G. D. (2011). An organizational approach to understanding evaluation in extension. *Journal of Agricultural Education*, 52(4),136-149.
- Loper, J. R. (2016). *Relationship between information technology skills and performance evaluation scores of Mississippi State University Extension Service agents* (Doctoral Dissertation). Mississippi State University, USA. <https://search.proquest.com/openview/cedb0a2947b9a02b7f187206ee2caa53/1?pq-origsite=gscholar&cbl=18750&diss=y>
- Malaysian Cocoa Board. (2017). *Statistics*. Malaysian Cocoa Board. <https://www.koko.gov.my/lkm/loader.cfm?page=10>
- Mariano, M. J., Villano, R., & Fleming, E. (2012). Factors influencing farmers' adoption of modern rice technologies and good management practices in the Philippines. *Agricultural Systems*, 110, 41-53. <https://doi.org/10.1016/j.agsy.2012.03.010>
- Martin, H. & Suwanto, A. S. (2019). Analysis of determinant performance of agricultural extension agents in Lebak District, Banten Province of Indonesia. *Russian Journal of Agricultural and Socio-Economic*, 8(92).
- Mengal, A. A., & Habib, S. (2016). Human resource development for an effective agriculture extension tool: An empirical study of Baluchistan province. *International Journal of Agricultural Extension*, 04(01), 71-77.
- Motoloni, M. M. M., Hassan, S., Olagunju, O., & Kasin, R. (2017). ToT and HRD competencies and its relationship to extension agents' performance among cocoa smallholders. *IOSR Journal of Agriculture and Veterinary Science*, 10(12), 14-21.
- Murni, A. M. P., Salim, H., & Ramle, K. (2019). Transfer of technology and its relationship towards work performance among extension agents in Malaysian Cocoa Board (East Malaysia). *IOSR Journal of Agriculture and Veterinary Science*, 12(3), 41-47.

- Olagunju, O. O., Hassan, S., Samad, M. Y. A., & Kasin, R. (2019). Transfer of technology skills, human resource development skills and extension agents' work performance: The perception of cocoa growers in Malaysia. *International Journal of Scientific & Technology Research*, 8(9), 299-307.
- Powers, J. B. & McDougall, P. (2005). Policy orientation effects on performance with licensing to start-ups and small companies. *Policy Research*, 34, 1028-1042.
- Rahim, M. S. (2010). Human resource development and transfer of technology competencies and their relationships to extension agents' job performance. *Academica*, 79, 127-137.
- Rosnita, R., Yulida, R., Dewi, N., Arifudin, A., & Andriani, Y. (2017). The Performance of Agricultural Extension Workers on Empowerment and Independent Smallholder Farmer in Riau Province, Indonesia. *International Journal of Agriculture System*, 5(1), 69-83. <http://dx.doi.org/10.20956/ijas.v5i1.1173>
- Rychen, D. S., & Salganik, L. H. (2001). *The definition and selection of key competencies*. Horefe & Huber Publisher.
- Sail, M. R. (2010). Human resource development and transfer of technology competencies and their relationships to extension agents' job performance. *Academica* 79, 127-137.
- Salleh, K. M., & Sulaiman, N. L. (2016). Competencies among human resource development practitioners according to disciplines and levels in Malaysian organizations. *International Journal of Applied Business and Economic Research*, 14(10), 6567-6578.
- Scheer, S., Cochran, G., Harder, A., & Place, N. (2011). Competency modeling in extension education: Integrating an academic extension education model with an extension human resource management model. *Journal of Agricultural Education*, 52(3), 64-74. <https://doi.org/10.5032/jae.2011.03064>
- Shaffril, H. A. M., & Uli, J. (2010). The influence of socio-demographic factors on work performance among employees of government agriculture agencies in Malaysia. *The Journal of International Social Research*, 3(10), 459-469.
- Shah, J. A., Asmuni, A., & Ismail, A. (2013). Roles of extension agents towards agricultural practice in Malaysia. *International Journal on Advanced Science, Engineering and Information Technology*, 3(1), 59-63.
- Sharma, J. K., & Maheshwari, R. (2013). Human resource development and its technique. *International Journal of Educational Research and Technology*, 4(2), 85-87.
- Spencer, L., & Spencer, S. (1993). *Competence at work: Model for superior performance*. John Wiley & Sons
- Suvedi, M., & Kaplowitz, M. (2016). *Core competency handbook: What every extension worker should know*. USAID-MEAS. <http://dev.meas.illinois.edu/wp>
- Suvedi, M., & Stoep, G. V. (2016). *Improving the monitoring and evaluation of agricultural extension programs*. USAID-MEAS. <https://meas.illinois.edu/wp>
- Varner, D. L. (2011). *A phenomenological study of millennial generation cooperative extension educators' development of core competencies* (Doctoral dissertation). University of Nebraska-Lincoln, USA. <http://digitalcommons.unl.edu/aglediss/27>
- Waroonkun, T. (2007). *Modelling international technology transfer in Thai construction projects* (Unpublished Doctoral Thesis). Griffith University, Australia. <https://research-repository.griffith.edu.au/bitstream/handle/10072/366192/02Whole.pdf?sequence=1>

- Wasihun, B. N., Kwarteng, J. A. & Okorley, E. L. (2013). Professional and technical competencies of extension agents as perceived by male and female farmers and the extension agents themselves: The need for data source triangulation. *Journal of Agriculture and Biodiversity Research*, 2(1), 11-16.
- Yoo, K. H., & Yang, Y. S. (2015). Technology-transfer through international network formation: Revisiting the role of cultural variation. *Management Studies*, 3(2), 98-109. <https://doi.org/10.17265/2328-2185/2015.0304.004>



REFEREES FOR THE PERTANIKA JOURNAL OF SCIENCE & TECHNOLOGY

Vol. 30 (3) Jul. 2022

The Editorial Board of the Pertanika Journal of Science and Technology wishes to thank the following:

Abdul Azim Abd Ghani
(UPM, Malaysia)

Chieng Buong Woei
(UPNM, Malaysia)

Mailin Mission
(UMS, Malaysia)

Abdulrazak Yahya Saleh Al-Hababi
(UNIMAS, Malaysia)

Chua Han Bing
(Curtin University, Malaysia)

Manousakis Nikolaos
(UNIWA, Greece)

Adeel Arshad
(University of Nottingham, UK)

Chuah Cheng Hock
(UM, Malaysia)

Maryati Md Dasor
(UiTM, Malaysia)

Ahmad Khusairi Azemi
(USM, Malaysia)

Fouad Hussain M.H Al-Bayaty
(UiTM, Malaysia)

Mohamad Hidayat Jamal
(UTM, Malaysia)

Ahmad Ramli Mohd Yahya
(USM, Malaysia)

Galuh Yuliani
(UPI, Indonesia)

Mohamad Najib Mat Pa
(USM, Malaysia)

Ahmad Sufriil Azlan Mohamed
(USM, Malaysia)

Ghufran Redzwan
(UM, Malaysia)

Mohamed Abd Rahman
(IIUM, Malaysia)

Amir Izzwan Zamri
(UMT, Malaysia)

Hasanudin
(Universitas Sriwijaya, Indonesia)

Mohd Bijarimi Mat Piah
(UMP, Malaysia)

Amirreza Talaiekhazani
(JIT, Iran)

Jamilah Hanum Abdul Khaiyom
(IIUM, Malaysia)

Mohd Shahrul Nizam Mohd Danuri
(KUIS, Malaysia)

Andrew R. Barron
(Swansea University, UK)

Kek Sie Long
(UTHM, Malaysia)

Mohd Yusoff Yahaya
(UiTM, Malaysia)

Aslina Baharum
(UMS, Malaysia)

Lee Hui-Shan
(UTAR, Malaysia)

Muzzneena Ahmad Mustapha
(UKM, Malaysia)

Aweng Eh Rak
(UMK, Malaysia)

Leow Soo Kar
(Sunway University, Malaysia)

Nik Norsyahariati Nik Daud
(UPM, Malaysia)

Ayu Haslija Abu Bakar
(UCSI University, Malaysia)

Lim Chin Wai
(UNITEN, Malaysia)

Nik Raihan Nik Yusoff
(UMK, Malaysia)

Badronnisa Yusuf
(UPM, Malaysia)

Lim Soh Fong
(UNIMAS, Malaysia)

Noor Hisyam Noor Mohamed
(UNIMAS, Malaysia)

Che Zulzikrami Azner Abidin
(UniMAP, Malaysia)

Mahadimenakbar Mohd. Dawood
(UMS, Malaysia)

Nor Faiza Mohd Tohit
(IIUM, Malaysia)

Nor Hamdan Mohamad
Yahaya
(UKM, Malaysia)

Noramalina Abdullah
(USM, Malaysia)

Norashikin Mohd Fauzi
(UMK, Malaysia)

Nurul Asyikin Yahya
(UKM, Malaysia)

Rasha Thabit Mohammed
(ARUC, Iraq)

Rohazila Mohamad Hanafiah
(USIM, Malaysia)

Roslaini Abd Majid
(UPM, Malaysia)

Sarina Sulaiman
(IIUM, Malaysia)

Sebastian Terence
(KITS, India)

Shahrul Azmi Mohd Yusof
(UUM, Malaysia)

Shanmughasundaram
Palanisamy
(KCE, India)

Shariza Jamek
(UMP, Malaysia)

Sheila Devi Sukumaran
(UCSI University, Malaysia)

Siow Chun Lim
(MMU, Malaysia)

Siti Mahani Marjugi
(UPM, Malaysia)

Syaza Azhari
(USIM, Malaysia)

Syuhada Mohd Tahir
(UiTM, Malaysia)

Tee Tuan Poy
(UPM, Malaysia)

Teo Pao Ter
(UMK, Malaysia)

Viv Djanat Prasita
(Universitas Hang Tuah, Indonesia)

Vivien Jong
(UiTM, Malaysia)

Wan Azizun Wan Adnan
(UPM, Malaysia)

Yap Wei Boon
(UKM, Malaysia)

Zalisham Jali
(USIM, Malaysia)

Zuraini Dahari
(USM, Malaysia)

ARUC – Al Rasheed University College
IIUM – International Islamic University Malaysia
JIT – Jami Institute of Technology
KCE – Karpagam College of Engineering
KITS – Karunya Institute of Technology and Sciences
KUIS – Kolej Universiti Islam Antarabangsa Selangor
MMU – Multimedia University Malaysia
UiTM – Universiti Teknologi MARA
UKM – Universiti Kebangsaan Malaysia
UM – Universiti Malaya
UMK – Universiti Malaysia Kelantan
UMP – Universiti Malaysia Pahang
UMS – Universiti Malaysia Sabah

UMT – Universiti Malaysia Terengganu
UniMAP – Universiti Malaysia Perlis
UNIMAS – Universiti Malaysia Sarawak
UNIWA – University of West Attica
UNITEN – Universiti Tenaga Nasional
UPI – Universitas Pendidikan Indonesia
UPM – Universiti Putra Malaysia
UPNM – Universiti Pertahanan Nasional Malaysia
USIM – Universiti Sains Islam Malaysia
USM – Universiti Sains Malaysia
UTAR – Universiti Tunku Abdul Rahman
UTHM – Universiti Tun Hussein Onn Malaysia
UUM – Universiti Utara Malaysia

While every effort has been made to include a complete list of referees for the period stated above, however if any name(s) have been omitted unintentionally or spelt incorrectly, please notify the Chief Executive Editor, *Pertanika* Journals at executive_editor.pertanika@upm.edu.my

Any inclusion or exclusion of name(s) on this page does not commit the *Pertanika* Editorial Office, nor the UPM Press or the university to provide any liability for whatsoever reason.

Pertanika Journal of Science & Technology

Our goal is to bring high-quality research to the widest possible audience

INSTRUCTIONS TO AUTHORS

(REGULAR ISSUE)

(Manuscript Preparation & Submission Guide)

Revised: November 2020

Please read the *Pertanika* guidelines and follow these instructions carefully. The Chief Executive Editor reserves the right to return manuscripts that are not prepared in accordance with these guidelines.

MANUSCRIPT PREPARATION Manuscript Types

Pertanika accepts submission of mainly 4 types of manuscripts

- that have not been published elsewhere (including proceedings)
- that are not currently being submitted to other journals

1. Regular article

Regular article is a full-length original empirical investigation, consisting of introduction, methods, results, and discussion. Original research work should present new and significant findings that contribute to the advancement of the research area. *Analysis and Discussion* must be supported with relevant references.

Size: Generally, each manuscript is **not to exceed 6000 words** (excluding the abstract, references, tables, and/or figures), a maximum of **80 references**, and **an abstract of less than 250 words**.

2. Review article

A review article reports a critical evaluation of materials about current research that has already been published by organising, integrating, and evaluating previously published materials. It summarises the status of knowledge and outlines future directions of research within the journal scope. A review article should aim to provide systemic overviews, evaluations, and interpretations of research in a given field. Re-analyses as meta-analysis and systemic reviews are encouraged.

Size: Generally, it is expected **not to exceed 6000 words** (excluding the abstract, references, tables, and/or figures), a maximum of **80 references**, and **an abstract of less than 250 words**.

3. Short communications

Each article should be timely and brief. It is suitable for the publication of significant technical advances and maybe used to:

- (a) reports new developments, significant advances and novel aspects of experimental and theoretical methods and techniques which are relevant for scientific investigations within the journal scope;
- (b) reports/discuss on significant matters of policy and perspective related to the science of the journal, including 'personal' commentary;
- (c) disseminates information and data on topical events of significant scientific and/or social interest within the scope of the journal.

Size: It is limited to **3000 words** and have a maximum of **3 figures and/or tables, from 8 to 20 references, and an abstract length not exceeding 100 words**. The information must be in short but complete form and it is not intended to publish preliminary results or to be a reduced version of a regular paper.

4. Others

Brief reports, case studies, comments, concept papers, letters to the editor, and replies on previously published articles may be considered.

Language Accuracy

Pertanika emphasises on the linguistic accuracy of every manuscript published. Articles can be written in **English** or **Bahasa Malaysia** and they must be competently written and presented in clear and concise grammatical English/Bahasa Malaysia. Contributors are strongly advised to have the manuscript checked by a colleague with ample experience in writing English manuscripts or a competent English language editor. For articles in Bahasa Malaysia, the title, abstract and keywords should be written in both English and Bahasa Malaysia.

Author(s) **may be required to provide a certificate** confirming that their manuscripts have been adequately edited. **All editing costs must be borne by the authors.**

Linguistically hopeless manuscripts will be rejected straightaway (e.g., when the language is so poor that one cannot be sure of what the authors are really trying to say). This process, taken by authors before submission, will greatly facilitate reviewing, and thus, publication.

MANUSCRIPT FORMAT

The paper should be submitted in **one-column format** with 1.5 line spacing throughout. Authors are advised to use Times New Roman 12-point font and *MS Word* format.

1. Manuscript Structure

The manuscripts, in general, should be organised in the following order:

Page 1: Running title

This page should **only** contain the running title of your paper. The running title is an abbreviated title used as the running head on every page of the manuscript. The running title **should not exceed 60 characters, counting letters and spaces.**

Page 2: Author(s) and Corresponding author's information

General information: This page should contain the **full title** of your paper **not exceeding 25 words**, with the name of all the authors, institutions and corresponding author's name, institution and full address (Street address, telephone number (including extension), handphone number, and e-mail address) for editorial correspondence. **The corresponding author must be clearly indicated with a superscripted asterisk symbol (*).**

Authors' name: The names of the authors should be named **in full without academic titles.** For Asian (Chinese, Korean, Japanese, Vietnamese), please write first name and middle name before surname (family name). The last name in the sequence is considered the surname.

Authors' addresses: Multiple authors with different addresses must indicate their respective addresses separately by superscript numbers.

Tables/figures list: A list of the number of **black and white/colour figures and tables** should also be indicated on this page. See **"5. Figures & Photographs"** for details.

Example (page 2):

Fast and Robust Diagnostic Technique for the Detection of High Leverage Points

Habshah Midi^{1,2*}, Hasan Talib Hendi¹, Jayanthi Arasan² and Hassan Uraibi³

¹*Institute for Mathematical Research, Universiti Putra Malaysia, 43400 UPM, Serdang, Selangor, Malaysia*

²*Department of Mathematics, Faculty of Science, Universiti Putra Malaysia, 43400 UPM, Serdang, Selangor, Malaysia*

³*Department of Statistics, University of Al-Qadisiyah, 88 -Al-Qadisiyah -Al-Diwaniyah, Iraq*

E-mail addresses

habshah@upm.edu.my (Habshah Midi)

h.applied.t88@gmail.com (Hasan Talib Hendi)

jayanthi@upm.edu.my (Jayanthi Arasan)

hssn.sami1@gmail.com (Hassan Uraibi)

*Corresponding author

List of Table/Figure: Table 1.

Figure 1.

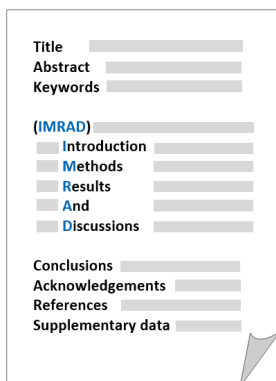
Page 3: Abstract

This page should **repeat** the **full title** of your paper with only the **Abstract**, usually in one paragraph and **Keywords**.

Keywords: *Not more than 8 keywords in alphabetical order must be provided to describe the content of the manuscript.*

Page 4: Text

A regular paper should be prepared with the headings *Introduction, Materials and Methods, Results and Discussions, Conclusions, Acknowledgements, References, and Supplementary data* (if any) in this order. The literature review may be part of or separated from the *Introduction*.



MAKE YOUR ARTICLES AS CONCISE AS POSSIBLE

Most scientific papers are prepared according to a format called IMRAD. The term represents the first letters of the words Introduction, Materials and Methods, Results, And, Discussion. It indicates a pattern or format rather than a complete list of headings or components of research papers; the missing parts of a paper are: Title, Authors, Keywords, Abstract, Conclusions, and References. Additionally, some papers include Acknowledgments and Appendices.

The Introduction explains the scope and objective of the study in the light of current knowledge on the subject; the Materials and Methods describes how the study was conducted; the Results section reports what was found in the study; and the Discussion section explains meaning and significance of the results and provides suggestions for future directions of research. The manuscript must be prepared according to the Journal's instructions to authors.

2. Levels of Heading

Level of heading	Format
1 st	LEFT, BOLD, UPPERCASE
2 nd	Flush left, Bold, Capitalise each word
3 rd	Bold, Capitalise each word, ending with .
4 th	Bold italic, Capitalise each word, ending with .

3. Equations and Formulae

These must be set up clearly and should be typed double-spaced. Numbers identifying equations should be in square brackets and placed on the right margin of the text.

4. Tables

- All tables should be prepared in a form consistent with recent issues of *Pertanika* and should be numbered consecutively with Roman numerals (Table 1, Table 2).
- A brief title should be provided, which should be shown at the top of each table (APA format):

Example:

Table 1

PVY infected Nicotiana tabacum plants optical density in ELISA

- Explanatory material should be given in the table legends and footnotes.
- Each table should be prepared on a new page, embedded in the manuscript.
- Authors are advised to keep backup files of all tables.

**** Please submit all tables in Microsoft word format only, because tables submitted as image data cannot be edited for publication and are usually in low-resolution.**

5. Figures & Photographs

- Submit an original figure or photograph.
- Line drawings must be clear, with a high black and white contrast.
- Each figure or photograph should be prepared on a new page, embedded in the manuscript for reviewing to keep the file of the manuscript under 5 MB.
- These should be numbered consecutively with Roman numerals (Figure 1, Figure 2).
- Provide a brief title, which should be shown at the bottom of each table (**APA format**):

Example: Figure 1. PVY-infected in vitro callus of Nicotiana tabacum

- If a figure has been previously published, acknowledge the original source, and submit written permission from the copyright holder to reproduce the material.
- Authors are advised to keep backup files of all figures.

**** Figures or photographs must also be submitted separately as TIFF or JPEG, because figures or photographs submitted in low-resolution embedded in the manuscript cannot be accepted for publication. For electronic figures, create your figures using applications that are capable of preparing high-resolution TIFF files.**

6. Acknowledgement

Any individuals and entities who have contributed to the research should be acknowledged appropriately.

7. References

References begin on their own page and are listed in alphabetical order by the first author's last name. Only references cited within the text should be included. All references should be in 12-point font and double-spaced. If a Digital Object Identifier (DOI) is listed on a print or electronic source, it is required to include the DOI in the reference list. Use Crossref to find a DOI using author and title information.

NOTE: When formatting your references, please follow the **APA-reference style** (7th edition) (refer to the examples). Ensure that the references are strictly in the journal's prescribed style, failing which your article will **not be accepted for peer-review**. You may refer to the *Publication Manual of the American Psychological Association* (<https://apastyle.apa.org/>) for further details.

Examples of reference style are given below:

Books		
	Insertion in text	In reference list
Book/E-Book with 1-2 authors	<p>Information prominent' (the author's name is within parentheses):</p> <p>... (Staron, 2020)</p> <p>... (Darus & Rasdi, 2019)</p> <p>... Or</p> <p>'Author prominent' (the author's name is outside the parentheses):</p> <p>(Starron, 2020)...</p> <p>Darus and Rasdi (2019) ...</p>	<p>Staron, M. (2020). <i>Action research in software engineering</i>. Springer International Publishing. https://doi.org/10.1007/978-3-030-32610-4</p> <p>Darus, A., & Rasdi, I. (2019). <i>Introduction to occupational health a workbook</i>. UPM Press.</p>
Book/E-Book with 3 or more authors	<p><i>For all in-text references, list only the first author's family name and followed by 'et al.'</i></p> <p>Information prominent' (the author's name is within parentheses):</p> <p>... (Yusof et al., 2020)</p> <p>... Or</p> <p>'Author prominent' (the author's name is outside the parentheses):</p> <p>Yusof et al. (2020) ...</p>	<p>Yusof, N. A., Azmi, U. Z. M., Ariffin, N., & Rahman, S. F. A. (2020). <i>Biosensors and chemical sensors: A practical approach</i>. UPM Press.</p>
Book/E-Book with more than 20 authors		<p>For books with more than 20 authors, please follow the guidelines for journal articles with more than 20 authors.</p>
Chapter in an edited Book/E-Book	<p>Inform ation pr ominent' (the author 's name is within parentheses):</p> <p>... (Mainzer, 2020) ...</p> <p>... (Tang et al., 2020) ...</p> <p>Or</p> <p>'Author prominent' (the author's name is outside the parentheses):</p> <p>Mainzer (2020) ...</p> <p>Tang et al. (2020) ...</p>	<p>Mainzer, K. (2020). Logical thinking becomes automatic. In K. Mainzer (Ed.), <i>Artificial intelligence-When do machines take over?</i> (pp. 15-45). Springer. https://doi.org/10.1007/978-3-662-59717-0_3</p> <p>Tang, W., Khavarian, M., Yousefi, A., & Cui, H. (2020). Properties of self-compacting concrete with recycled concrete aggregates. In R. Siddique (Ed.), <i>Self-Compacting Concrete: Materials, Properties, and Applications</i> (pp. 219-248). Woodhead Publishing. https://doi.org/10.1016/B978-0-12-817369-5.00009-X</p>

	Insertion in text	In reference list
Editor	<p>Information prominent' (the author's name is within parentheses): ... (Kesharwani, 2020) (Lanza et al., 2020) ... Or 'Author prominent' (the author's name is outside the parentheses): Kesharwani (2020) ... Lanza et al. (2020) ...</p>	<p>Kesharwani, P. (Ed.). (2020). <i>Nanotechnology based approaches for tuberculosis treatment</i>. Academic Press.</p> <p>Lanza, R., Langer, R., Vacanti, J. P., & Atala, A. (Eds.). (2020). <i>Principles of tissue engineering</i>. Academic press. https://doi.org/10.1016/C2018-0-03818-9</p>
Several works by the same author in the same year	<p>Information prominent' (the author's name is within parentheses): ... (Aggarwal & Aggarwal, 2020a, 2020b) ... Or 'Author prominent' (the author's name is outside the parentheses): Aggarwal & Aggarwal (2020a, 2020b) ...</p>	<p>Aggarwal, P., & Aggarwal, Y. (2020a). Strength properties of SCC. In R. Siddique (Ed.), <i>Self-Compacting Concrete: Materials, Properties, and Applications</i> (p. 83-115). Woodhead Publishing. doi: https://doi.org/10.1016/B978-0-12-817369-5.00004-0</p> <p>Aggarwal, P., & Aggarwal, Y. (2020b). Carbonation and corrosion of SCC. In R. Siddique (Ed.), <i>Self-Compacting Concrete: Materials, Properties, and Applications</i> (p. 147-193). Woodhead Publishing. doi: https://doi.org/10.1016/B978-0-12-817369-5.00007-6</p>
Journals		
Journal article with 1-2 authors	<p>Information prominent' (the author's name is within parentheses): ... (Laan & Fox, 2019) ... Or 'Author prominent' (the author's name is outside the parentheses): Laan and Fox (2019) ...</p>	<p>Laan, E., & Fox, J. W. (2019). An experimental test of the effects of dispersal and the paradox of enrichment on metapopulation persistence. <i>Oikos</i>, 129(1), 49-58. https://doi.org/10.1111/oik.06552</p>
Journal article with 3 or more authors	<p><i>For all in-text references, list only the first author's family name and followed by 'et al.'</i> Information prominent' (the author's name is within parentheses): ... (Midi et al., 2020) (Shagufta et al., 2017) ... Or 'Author prominent' (the author's name is outside the parentheses): Midi et al. (2020) ... Shagufta et al. (2017) ...</p>	<p>Midi, H., Hendi, H. T., Arasan, J., & Uraibi, H. (2020). Fast and Robust Diagnostic Technique for the Detection of High Leverage Points. <i>Pertanika Journal of Science & Technology</i>, 28(4), 1203-1220.</p> <p>Shagufta, B., Sivakumar, M., Kumar, S., Agarwal, R. K., Bhilegaonkar, K. N., Kumar, A., & Dubal, Z. B. (2017). Antimicrobial resistance and typing of Salmonella isolated from street vended foods and associated environment. <i>Journal of Food Science and Technology</i>, 54(8), 2532-2539. doi: https://doi.org/10.1007/s13197-017-2698-1</p>
Journal article with more than 20	<p>Information prominent' (the author's name is within parentheses): ... (Wiskunde et al., 2019) ... Or 'Author prominent' (the author's name is outside the parentheses): Wiskunde et al. (2019) ...</p>	<p>Wiskunde, B., Arslan, M., Fischer, P., Nowak, L., Van den Berg, O., Coetzee, L., Juárez, U., Riyaziyyat, E., Wang, C., Zhang, I., Li, P., Yang, R., Kumar, B., Xu, A., Martinez, R., McIntosh, V., Ibáñez, L. M., Mäkinen, G., Virtanen, E., ... Kovács, A. (2019). Indie pop rocks mathematics: Twenty One Pilots, Nicolas Bourbaki, and the empty set. <i>Journal of Improbable Mathematics</i>, 27(1), 1935-1968. https://doi.org/10.0000/3mp7y-537</p>
Journal article with an article number	<p>Information prominent' (the author's name is within parentheses): ... (Roe et al., 2020) ... Or 'Author prominent' (the author's name is outside the parentheses): Roe et al. (2020) ...</p>	<p>Roe, E. T., Bies, A. J., Montgomery, R. D., Watterson, W. J., Parris, B., Boydston, C. R., Sereno, M. E., & Taylor, R. P. (2020). Fractal solar panels: Optimizing aesthetic and electrical performances. <i>Plos One</i>, 15(3), Article e0229945. https://doi.org/10.1371/journal.pone.0229945</p>
Journal article with missing information	<p>Information prominent' (the author's name is within parentheses): ... (Alfirevic et al., 2017) (Hayat et al., 2020) (Fan et al., 2020) ...</p>	<p>Missing volume number Alfirevic, Z., Stampalija, T., & Dowswell, T. (2017). Fetal and umbilical Doppler ultrasound in high-risk pregnancies (review). <i>Cochrane Database of Systematic Reviews</i>, (6), 1-163. https://doi.org/10.1002/14651858.CD007529.pub4. Copyright</p>

	Insertion in text	In reference list
Journal article with missing information	Or 'Author prominent' (the author's name is outside the parentheses): Alfirevic et al. (2017) ... Hayat et al. (2020) ... Fan et al. (2020) ...	Missing issue number Hayat, A., Shaishta, N., Mane, S. K. B., Hayat, A., Khan, J., Rehman, A. U., & Li, T. (2020). Molecular engineering of polymeric carbon nitride based Donor-Acceptor conjugated copolymers for enhanced photocatalytic full water splitting. <i>Journal of colloid and interface science</i> , 560, 743-754. https://doi.org/10.1016/j.jcis.2019.10.088 Missing page or article number Fan, R. G., Wang, Y. B., Luo, M., Zhang, Y. Q., & Zhu, C. P. (2020). SEIR-Based COVID-19 Transmission Model and Inflection Point Prediction Analysis. <i>Dianzi Keji Daxue Xuebao/Journal of the University of Electronic Science and Technology of China</i> , 49(3). https://doi.org/10.12178/1001-0548.9_2020029
Several works by the same author in the same year	Information prominent' (the author's name is within parentheses): ... (Chee et al., 2019a, 2019b) ... Or 'Author prominent' (the author's name is outside the parentheses): Chee et al. (2019a, 2019b) ...	Chee, S. S., Jawaid, M., Sultan, M. T. H., Alothman, O. Y., & Abdullah, L. C. (2019a). Accelerated weathering and soil burial effects on colour, biodegradability and thermal properties of bamboo/kenaf/epoxy hybrid composites. <i>Polymer Testing</i> , 79, Article 106054. https://doi.org/10.1016/j.polymeresting.2019.106054 Chee, S. S., Jawaid, M., Sultan, M. T. H., Alothman, O. Y., & Abdullah, L. C. (2019b). Evaluation of the hybridization effect on the thermal and thermo-oxidative stability of bamboo/kenaf/epoxy hybrid composites. <i>Journal of Thermal Analysis and Calorimetry</i> , 137(1), 55-63. https://doi.org/10.1007/s10973-018-7918-z
Newspaper		
Newspaper article – with an author	... (Shamshuddin, 2019) ... Or ... Shamshuddin (2019) ...	Shamshuddin, J. (2019, September 23). Lynas plant waste residue can be used to boost oil palm growth? <i>New Straits Times</i> . https://www.nst.com.my/opinion/letters/2019/09/523930/lynas-plant-waste-residue-can-be-used-boost-oil-palm-growth
Newspaper article – without an author	("Zoonotic viruses," 2017). OR "Zoonotic viruses" (2017) ... Use a shortened title (or full title if it is short) in Headline Case enclosed in double quotation marks.	Zoonotic viruses like swine flu are ticking time bombs, say experts. (2020, July 4). <i>New Straits Times</i> , 3.
Dissertation/Thesis		
Published Dissertation or Thesis References	... (Rivera, 2016) ... Or ... Rivera (2016) ...	Rivera, C. (2016). <i>Disaster risk management and climate change adaptation in urban contexts: Integration and challenges</i> [Doctoral dissertation, Lund University]. Lund University Publications. https://lup.lub.lu.se/search/ws/files/5471705/8570923.pdf
Unpublished Dissertation or Thesis References	... (Brooks, 2014) ... Or ... Brooks (2014) ...	Brooks, J. D. (2015). <i>Bamboo as a strengthening agent in concrete beams for medium height structures</i> [Unpublished Doctoral dissertation]. The University of Washington.
Conference/Seminar Papers		
Conference proceedings published in a journal	... (Duckworth et al., 2019) ... Or Duckworth et al. (2019) ...	Duckworth, A. L., Quirk, A., Gallop, R., Hoyle, R. H., Kelly, D. R., & Matthews, M. D. (2019). Cognitive and noncognitive predictors of success. <i>Proceedings of the National Academy of Sciences, USA</i> , 116(47), 23499-23504. https://doi.org/10.1073/pnas.1910510116
Conference proceedings published as a book chapter	... (Bedenel et al., 2019) ... Or Bedenel et al. (2019) ...	Bedenel, A. L., Jourdan, L., & Biernacki, C. (2019). Probability estimation by an adapted genetic algorithm in web insurance. In R. Battiti, M. Brunato, I. Kotsireas, & P. Pardalos (Eds.), <i>Lecture notes in computer science: Vol. 11353. Learning and intelligent optimization</i> (pp. 225-240). Springer. https://doi.org/10.1007/978-3-030-05348-2_21

	Insertion in text	In reference list
Online	... (Gu et al., 2018) ... Or Gu et al. (2018) ...	Gu, X., Yu, J., Han, Y., Han, M., & Wei, L. (2019, July 12-14). <i>Vehicle lane change decision model based on random forest</i> . [Paper presentation]. 2019 IEEE International Conference on Power, Intelligent Computing and Systems (ICPICS), Shenyang, China. https://doi.org/10.1109/ICPICS47731.2019.8942520
Government Publications		
Government as author	First in-text reference: Spell out the full name with the abbreviation of the body. ... National Cancer Institute (2019) ... Or ... (National Cancer Institute, 2019) ... Subsequent in-text reference: ... NCI (2019) ... Or ... (NCI, 2019) ...	National Cancer Institute. (2019). <i>Taking time: Support for people with cancer</i> (NIH Publication No. 18-2059). U.S. Department of Health and Human Services, National Institutes of Health. https://www.cancer.gov/publications/patient-education/takingtime.pdf

8. General Guidelines

Abbreviations: Define alphabetically, other than abbreviations that can be used without definition. Words or phrases that are abbreviated in the *Introduction* and following text should be written out in full the first time that they appear in the text, with each abbreviated form in parenthesis. Include the common name or scientific name, or both, of animal and plant materials.

Authors' Affiliation: The primary affiliation for each author should be the institution where the majority of their work was done. If an author has subsequently moved to another institution, the current address may also be stated in the footer.

Co-Authors: The commonly accepted guideline for authorship is that one must have substantially contributed to the development of the paper and share accountability for the results. Researchers should decide who will be an author and what order they will be listed depending upon their order of importance to the study. Other contributions should be cited in the manuscript's *Acknowledgements*.

Similarity Index: All articles received must undergo the initial screening for originality before being sent for peer review. *Pertanika* does not accept any article with a similarity index exceeding **20%**.

Copyright Permissions: Authors should seek necessary permissions for quotations, artwork, boxes or tables taken from other publications or other freely available sources on the Internet before submission to *Pertanika*. The *Acknowledgement* must be given to the original source in the illustration legend, in a table footnote, or at the end of the quotation.

Footnotes: Current addresses of authors if different from heading may be inserted here.

Page Numbering: Every page of the manuscript, including the title page, references, and tables should be numbered.

Spelling: The journal uses American or British spelling and authors may follow the latest edition of the Oxford Advanced Learner's Dictionary for British spellings. Each manuscript should follow one type of spelling only.

SUBMISSION OF MANUSCRIPTS

All submissions must be made electronically using the **ScholarOne™ online submission system**, a web-based portal by Clarivate Analytics. For more information, go to our web page and click "**Online Submission (ScholarOne™)**".

Submission Checklist

1. MANUSCRIPT:

Ensure your manuscript has followed the *Pertanika* style particularly the first-4-pages as explained earlier. The article should be written in a good academic style and provide an accurate and succinct description of the contents ensuring that grammar and spelling errors have been corrected before submission. It should also not exceed the suggested length.

2. DECLARATION FORM:

Author has to sign a declaration form. In signing the form, authors declare that the work submitted for publication is original, previously unpublished, and not under consideration for any publication elsewhere.

Author has to agree to pay the publishing fee once the paper is accepted for publication in Pertanika.

3. COVER LETTER:

In Step 6 of the ScholarOne system, author is asked to upload a cover letter in *Pertanika* format. Please ignore this instruction and replace the cover letter with the **Declaration Form**.

Note:

COPYRIGHT FORM: Author will be asked to sign a copyright form when the paper is accepted. In signing the form, it is assumed that authors have obtained permission to use any copyrighted or previously published material. All authors must read and agree to the conditions outlined in the form and must sign the form or agree that the corresponding author can sign on their behalf. Articles cannot be published until a signed form (original pen-to-paper signature) has been received.

Visit our Journal's website for more details at <http://www.pertanika.upm.edu.my/>.

ACCESS TO PUBLISHED MATERIALS

Under the journal's open access initiative, authors can choose to download free material (via PDF link) from any of the journal issues from *Pertanika*'s website. Under "**Browse Journals**" you will see a link, "*Regular Issue*", "*Special Issue*" or "*Archives*". Here you will get access to all current and back-issues from 1978 onwards. No hard copy of journals or offprints are printed.

Visit our Journal's website at:

http://www.pertanika.upm.edu.my/regular_issues.php for "Regular Issue"

http://www.pertanika.upm.edu.my/cspecial_issues.php for "Special Issue"

http://www.pertanika.upm.edu.my/journal_archives.php for "Archives"

PUBLICATION CHARGE

Upon acceptance of a manuscript, a processing fee of RM 750 / USD 250 will be imposed on authors; RM 750 for any corresponding author affiliated to an institution in Malaysia; USD 250 for any corresponding author affiliated to an institution outside Malaysia. Payment must be made online at <https://paygate.upm.edu.my/action.do?do=>

Any queries may be directed to the **Chief Executive Editor's** office via email to executive_editor.pertanika@upm.edu.my

- The Effectiveness of Workplace Health Promotion Programme in Improving Sickness Absenteeism, Medical Cost Claims and Work Engagement Among Manufacturing Workers in Malaysia: A Randomised Control Trial
Ahmad Fairuz Mohamed, Marzuki Isahak, Mohd Zaki Awg Isa and Rusli Nordin 2225
- Facies Mapping of the Holocene Carbonate Complexes in Kepulauan Seribu Java Basin, Indonesia Using Satellite-Derived Data Set
Shafiqah Amir, Haylay Tsegab, Grisel Jimenez Soto and Ali Imran Azman 2253
- Hybrid Lean Practices Integrated with IR 4.0 and Sustainability in Malaysia Food and Beverages Companies: Conceptual Framework and Hypothesis Development
Muslim Diekola Akanmu and Norshahrizan Nordin 2271
- Importance of Transfer of Technology Skills and Human Resource Development Skills in Work Performance of Extension Agent in Sarawak Cocoa Industry
Nur Syahirah Abd Halim, Salim Hassan and Ramle Kasin 2295

Thermal Performances of Hybrid Pin Fin with Connector Heat Sink Under Natural Convection <i>Rosnadiyah Bahsan, Muhammad Aniq Asyraf Mohd Zamri, Alhassan Salami Tijani, Jeeventh Kubenthiran, Sajith Thottathil Abdulrahman and Ibrahim Kolawole Muritala</i>	2077
Evaluation of Factors Affecting Microbial Growth Inhibition and Optimization Using Pineapple Leaves Juice <i>Norazwina Zainol, Amirah Ya'acob, Putri Nurul Yasmin Mohd Ridza, Siti Hatijah Mortan and Kamaliah Abdul Samad</i>	2097
<i>Short Communication</i> Canarium odontophyllum Miq. (Dabai) Leaf Phytoextracts and Their Medicinal Properties <i>Muhammad Wahizul Haswan Abdul Aziz, Siti Fathiah Masre, Dayang Fredalina Basri and Ahmad Rohi Ghazali</i>	2115
Synthesis, Characterisation, and Electrochemical Impedance Spectroscopy Study of Green and Sustainable Polyurethane Acrylate from Jatropha Oil Using a Three Step Process <i>Kai Ling Chai, Min Min Aung, Hong Ngee Lim, Ikhwan Syafiq Mohd Noor, Luqman Chuah Abdullah and Hiroshi Uyama</i>	2127
<i>Review Article</i> A Review on Soil Erodibility Studies in Malaysia <i>Adnan Derahman, Mohd Fairuz Bachok, Muhamad Fuad Shukor, Farah Wahida Mohd Latib and Rohaya Alias</i>	2139
<i>Review Article</i> Classification of Fault Prediction: A Mapping Study <i>Sasha Farhana Shamsul Anwar, Marshima Mohd Rosli and Nur Atiqah Sia Abdullah</i>	2157
Effect of Khat Chewing on Gingival Health of Patients with Fixed Orthodontic Appliances: A Controlled-Clinical Trial <i>Ahmed Taher Al-Haj, Rami Ishaq, Anas Shamala, Mohammed Al-Wesabi, Khalid Aldhorae, Mohammed Sultan Alakhali and Mohammed Al-Labani</i>	2173
Statistical Analysis of Dry Grinding of Mica in Planetary Mill <i>Ku Esyra Hani Ku Ishak, Shafinaz Saad, Syed Fuad Saiyid Hashim and Hashim Hussin</i>	2191
Water Quality Assessment of Surface Water at the Urban Area of An Giang Province, Vietnam <i>Khanh Tran Thien Nguyen, Chi Thi Dao Vo, An Thuy Ngo, Nghi Thanh Doan, Luyen Phuc Huynh and Dung Huynh Thuy Tran</i>	2205

Experimental Investigations on Scour Volume Upstream of a Slit Weir <i>Naeem Zaer Nkad, Thamer Ahmad Mohammad and Haider Mohammed Hammoodi</i>	1927
Removal of Remazol Yellow Using SnO ₂ -Co Photocatalyst <i>Muhammad Said, Fahma Riyanti, Poedji Loekitowati Hariani, Sastriani and Widya Twiny Rizki</i>	1949
<i>Review Article</i>	
The Compilation Records of Fireflies (Coleoptera: Lampyridae) Diversity and Distribution and Display Trees Throughout Malaysia <i>Nurhafizul Abu Seri and Azimah Abd Rahman</i>	1963
<i>Review Article</i>	
Trends of Filtration and Adsorption Technology Using Biomaterials from Agricultural Wastes: A Bibliometric Analysis <i>Awang Nasrizal Awang Ali, Jason Lowell Jitolis, Juferi Idris, Ismail Saad and Nurmin Bolong</i>	1989
Validity and Reliability of Typhoid Risk Factors Questionnaire (TRFQ) in Gombe Metropolis, Gombe State, Nigeria <i>Umar Abdullahi Tawfiq, Shamarina Shohaimi, Noor Hisham Mohd Nadzir, Syafinaz Amin Nordin, Abdul Hafiz Ab Rahman and Nader Salari</i>	2007
Leaching of Electric Arc Furnace Slag for Selective Recovery of Iron: Effect of Temperature, H ₂ SO ₄ /HCl Acid, and Oxidant Concentration <i>Faizatul Syazwani Zulkifili, Hawaiah Imam Maarof, Norhaslinda Nasuha and Siti Wahidah Puasa</i>	2023
A Hybrid Technique for Analysis of Low-Frequency Oscillation in Power System <i>Abhinav Pathak and Ratnesh Gupta</i>	2033
<i>Review Article</i>	
Mechanical Properties of Natural Fibre Reinforced Geopolymer Composites: A Review <i>Noor Abbas Al-Ghazali, Farah Nora Aznieta Abdul Aziz, Khalina Abdan and Noor Azline Mohd Nasir</i>	2053
<i>Case Study</i>	
An Unusual Cause of Tenosynovitis by Group B <i>Streptococcus</i> in the Immunocompromised Patient: A Case Report <i>AbdulRahman Muthanna, Nur Afiza Aziz, Mohd Nasir Mohd Desa, Nurul Diana Dzaraly, Nurul Hana Zainal Baharin, Mohammad Noor Amal Azmai and Syafinaz Amin-Nordin</i>	2071

Pertanika Journal of Science & Technology

Vol. 30 (3) Jul. 2022

Content

Foreword <i>Chief Executive Editor</i>	i
Modeling and Molecular Dynamics of Aquaporin from an Antarctic <i>Pseudomonas</i> sp. Strain AMS3 <i>Muhairil Sulong Tuah, Wahhida Latip, Ainur Yasmin Ahmad Ridzwan, Samyuktha Balakrishnan, Raja Noor Zaliha Raja Abd. Rahman, Noor Dina Muhd Noor and Mohd Shukuri Mohamad Ali</i>	1755
Mathematical Models for Predicting the Mechanical Properties of Poly(Lactic Acid) for Load-Bearing Applications <i>Abraham Aworinde, Titus Ajewole, Olakunle Olukayode and Joseph Dirisu</i>	1771
Assessment of the Grid Safety Values for Substation Grounding Grid Design Parameters in Vertical Two-Layer Soil Structure <i>Navinesshani Permal, Miszaina Osman, Azrul Mohd Ariffin and Mohd Zainal Abidin Ab Kadir</i>	1789
<i>Review Article</i>	
External Skeletal Fixator to Stabilize the Orthopedic Conditions in Avian Species: A Systematic Review of Case Reports and Case Series <i>Hossein Taiyari and Jalila Abu</i>	1815
Spectral Gradient Method with Log-determinant Norm for Solving Non- Linear System of Equations <i>Yeong Lin Koay, Hong Seng Sim, Yong Kheng Goh and Sing Yee Chua</i>	1841
Esterification of Acetin Production from By-Products of Biodiesel Industry Using Heterogeneous Catalysts Based on Wetland Commodities <i>Hesty Heryani, Abdul Ghofur and Nursiah Chairunnisa</i>	1861
DFT-Based Reversible Watermarking Method for Image Ownership Protection <i>Ansam Osamah Abdulmajeed and Sundus Abdulmuttalib Mohamed</i>	1883
Vulnerability of Saudi Private Sector Organisations to Cyber Threats and Methods to Reduce the Vulnerability <i>Emad Shafie</i>	1909



Pertanika Editorial Office, Journal Division,
Putra Science Park,
1st Floor, IDEA Tower II,
UPM-MTDC Center,
Universiti Putra Malaysia,
43400 UPM Serdang,
Selangor Darul Ehsan
Malaysia

<http://www.pertanika.upm.edu.my>
Email: executive_editor@upm.edu.my
Tel. No.: +603- 9769 1622

PENERBIT
UPM
UNIVERSITI PUTRA MALAYSIA
PRESS

<http://www.penerbit.upm.edu.my>
Email: penerbit@upm.edu.my
Tel. No.: +603- 9769 8851

